THÈSE

Pour obtenir le grade de

DOCTEUR DE L'UNIVERSITÉ GRENOBLE ALPES

École doctorale : ISCE - Ingénierie pour la Santé la Cognition et l'Environnement
Spécialité : BIS - Biotechnologie, instrumentation, signal et imagerie pour la biologie, la médecine et l'environnement
Unité de recherche : IAB : Epigenetics, Environment, Cell Plasticity, Cancer (UGA / Inserm U1209 / CNRS UMR 5309)

Caractérisation de la fonction de la protéine CCDC146 dans la spermiogenèse et la fertilité masculine

Characterization of CCDC146 protein function in spermiogenesis and male fertility

Présentée par :

Jana MURONOVA

Direction de thèse :

Pierre RAY Professeur des Univ. - Praticien hosp., Université Grenoble Alpes	Directeur de thèse
Christophe ARNOULT DIRECTEUR DE RECHERCHE, CNRS Délégation Alpes	Co-directeur de thèse
Corinne LOEUILLET CRCN, CNRS	Co-encadrante de thèse

Rapporteurs :

CARSTEN JANKE
Directeur de recherche, CNRS DELEGATION PARIS CENTRE
MICHAEL MITCHELL
Directeur de recherche, INSERM PACA - CORSE

Thèse soutenue publiquement le **24 avril 2023**, devant le jury composé de :

PIERRE RAY Professeur des Univ. - Praticien hosp., UNIVERSITE GRENOBLE ALPES	Directeur de thèse
CHRISTOPHE ARNOULT Directeur de recherche, CNRS DELEGATION ALPES	Co-directeur de thèse
CHARLES COUTTON Professeur des Univ. - Praticien hosp., UNIVERSITE GRENOBLE ALPES	Président
MELANIE BONHIVERS Directeur de recherche, CNRS DELEGATION AQUITAINE	Examinatrice
CARSTEN JANKE Directeur de recherche, CNRS DELEGATION PARIS CENTRE	Rapporteur
MICHAEL MITCHELL Directeur de recherche, INSERM PACA - CORSE	Rapporteur

ABSTRACT

Infertility is a global health problem that is estimated to touch 9% of couples and the male factor alone or in conjunction with the female factor accounts for approximately 50% of cases. Spermatogenesis is a highly complex process, and it involves hundreds to thousands of genes that contribute to proper sperm formation. Identification of new genes involved in male fertility has been on the rise in the recent years due to an increased use of massive parallel sequencing technologies, especially of whole-exome sequencing (WES). Identification and functional characterization of these genes is important for our fundamental comprehension of spermatogenesis as well as for improving medical diagnostic, counselling, and infertility treatment.

This work addresses multiple factors that can affect male fertility and focuses on a particular type of asthenoteratozoospermia called the multiple morphological abnormalities of the sperm flagella (MMAF) syndrome. Biallelic mutations in the Coiled-coil domain-containing 146 (*CCDC146*) gene were identified in two patients from our cohort of 167 infertile men affected by the MMAF syndrome. The primary objective of the thesis was to validate the candidate gene on a mouse model, and then to characterize the function of CCDC146 in male fertility. Male *Ccdc146* knock-out (KO) mice were infertile, reproduced the MMAF phenotype and had low sperm concentration and showed an absence of sperm motility, confirming the involvement of CCDC146 in the MMAF syndrome. Next, we showed that CCDC146 is present in the axoneme of human and mouse spermatozoa. Expansion microscopy and biochemistry experiments suggested that CCDC146 could be located in the lumen of axonemal microtubule doublets and could be a microtubule inner protein (MIP). We showed that CCDC146 plays a role(s) during spermiogenesis where its absence leads to defects in axoneme assembly, manchette formation, aberrant head-shaping, and duplicated centrioles that are often abnormally distant from the nucleus. These defects during spermiogenesis are at the origin of the MMAF phenotype, oligoasthenoteratozoospermia, and consequent infertility. In somatic cells, CCDC146 was associated with the centrosome throughout the cell cycle, and localized to spindle microtubules, the midzone and the midbody during mitosis. Due to its multiple microtubule-related localizations and because its absence mostly affected microtubule-based structures, we hypothesized that CCDC146 could be a microtubule-associated protein (MAP).

Next, we have shown that an accumulation of rare heterozygous variants in MMAF-associated genes important for proper axoneme assembly (*Ccdc146*, *Armc2*, *Cfap43*, and *Cfap44*) leads to a progressive degradation of sperm head morphology and has an impact on sperm motility. These results suggested that oligogenic inheritance, the presence of specific gene variants in functionally interconnected genes, could explain some cases of idiopathic male infertility.

Finally, we discussed several aspects of the sperm epigenome, including the impact of non-coding RNAs on sperm formation and embryo development, and their potential roles in inter- and transgenerational inheritance that could mediate the adaptation of the progeny to the environment.

RESUME

L'infertilité est un problème majeur de santé publique, qui touche environ 9 % de couples. Un facteur masculin seul ou associé à un facteur féminin est trouvé dans environ 50 % des cas. La spermatogenèse est un processus très complexe qui implique des centaines, voire des milliers de gènes qui contribuent au développement des spermatozoïdes. L'identification de nouveaux gènes impliqués dans la fertilité masculine a augmenté ces dernières années en raison d'une utilisation accrue des technologies de séquençage parallèle massif, en particulier du séquençage de l'exome entier (WES). L'identification et la caractérisation fonctionnelle de ces gènes sont importantes pour notre compréhension fondamentale de la spermatogenèse ainsi que pour l'amélioration du diagnostic médical, du conseil et du traitement de l'infertilité.

Ce travail aborde plusieurs facteurs impactant la fertilité masculine et se concentre sur un type particulier d'asthénotératozoospermie appelé syndrome des anomalies morphologiques multiples du flagelle (MMAF). Notre équipe a identifié des mutations biallélіques dans le gène Coiled-coil domain-containing 146 (*CCDC146*) chez deux patients d'une cohorte de 167 hommes infertiles atteints du syndrome MMAF. L'objectif principal de ma thèse était de valider l'implication de ce gène candidat dans le syndrome MMAF sur un modèle murin, puis de caractériser la fonction de la protéine CCDC146 dans la fertilité masculine. Les souris mâles mutées pour *Ccdc146* (KO) sont infertiles, atteintes par le phénotype MMAF, et l'absence de la protéine provoque une forte diminution de la concentration des spermatozoïdes ainsi qu'une absence de motilité, confirmant l'implication de CCDC146 dans le syndrome MMAF. Ensuite, nous avons montré que CCDC146 est présente dans l'axonème des spermatozoïdes humains et murins. Des expériences de microscopie d'expansion et de biochimie ont suggéré que CCDC146 pourrait être située dans la lumière des doublets de microtubules anoxémiques et pourrait être une protéine interne des microtubules (MIP). Nous avons aussi montré que CCDC146 joue un ou plusieurs rôles au cours de la spermiogenèse où son absence entraîne des défauts d'assemblage de l'axonème et de la manchette, provoque la formation de têtes anormales, ainsi que la présence de centrioles surnuméraires qui sont souvent anormalement éloignés du noyau du spermatozoïde. Ces défauts de la spermiogenèse sont à l'origine du phénotype MMAF, de l'oligoasthénotératozoospermie et, par conséquent de l'infertilité observée. Dans les cellules somatiques, CCDC146 était associée au centrosome quel que soit la phase du cycle cellulaire et est localisée dans les microtubules du

fuseau mitotique, dans le sillon de division, ainsi que dans le corps central au cours de la mitose. En raison de ces multiples localisations liées aux microtubules, et parce que son absence affecte principalement les structures à base de microtubules, nous avons émis l'hypothèse que CCDC146 pourrait être une protéine associée aux microtubules (MAP).

Ensuite, nous avons montré qu'une accumulation de variants hétérozygotes rares dans des gènes associés avec le phénotype MMAF et importants pour l'assemblage des axonèmes (*Ccdc146*, *Armc2*, *Cfap43* et *Cfap44*), conduit à une dégradation progressive de la morphologie de la tête des spermatozoïdes et impacte la motilité des spermatozoïdes. Ces résultats suggèrent que l'hérédité oligogénique, la présence de variants spécifiques de gènes fonctionnellement interconnectés, peut expliquer certains cas idiopathiques d'infertilité masculine.

Enfin, nous avons discuté de plusieurs aspects de l'épigénome du sperme, y compris de l'impact des ARN non-codants sur la formation des spermatozoïdes et le développement de l'embryon, et leurs rôles potentiels dans l'héritage inter- et transgénérationnel, qui pourraient servir de médiateur à l'adaptation de la descendance à l’environnement.

TABLE OF CONTENTS

LIST OF TABLES

LIST OF FIGURES

LIST OF ABBREVIATIONS

A

$A_{aligned}$ – Spermatogonia type A aligned (mouse)
A_{dark} – Spermatogonia type A dark (human)
A_{paired} – Spermatogonia type A paired (mouse)
A_{pale} – Spermatogonia type A pale (human)
A_S – Spermatogonial stem cell type A single (mouse)
AAA - ATPases associated with diverse cellular activities (protein family)
ADP – Adenosine diphosphate
AKAP – cAMP-dependent protein kinase anchoring proteins
ARMC – Armadillo Repeat Containing (protein family)
ART – Assisted-reproductive technologies
ATP – Adenosine triphosphate

B

C

CA – Central apparatus
CCDC – Coiled-coil domain containing (protein family)
CFAP – Cilia and flagella associated protein (protein family)
CP – Central pair (of microtubules)

D

DC – Distal centriole
DNA – Deoxyribonucleic acid
DNAH - Dynein heavy chain (protein family)
DRC – Dynein Regulatory Complex Subunit

E

EB proteins – (Microtubule) end-binding proteins
Endo-siRNA – Endogenous interfering RNAs

F

FS – Fibrous sheath

G

GDP – Guanosine diphosphate
GTP – Guanosine triphosphate

H

HTCA – Head-tail coupling apparatus

I

ICSI – Intracytoplasmic sperm injection
IDA – Inner dynein arm
IF – Immunofluorescence
IFT – Intraflagellar transport
IMT – Intramanchette transport
INM – Inner nuclear membrane
IVF – *In vitro* fertilization

J

K

KASH – Klarsicht/Anc1/Syne1 homology domain-containing

L

LINC complex – Linker of nucleoskeleton and cytoskeleton complex

M

MAP – Microtubule-associated proteins
MiRNA – Micro RNA
MIP – Microtubule inner proteins
MMAF – Multiple morphological abnormalities of the sperm flagella
MT - Microtubule

N

N-DRC – Nexin-dynein regulatory complex
ncRNA – Non-coding RNA

O

ODA – Outer dynein arm
ODF – Outer dense fiber
OLIDA – Oligogenic Disease Database
ONM – Outer nuclear membrane

P

PC – Proximal centriole
PCD – Primary ciliary dyskinesia
Pi-RNA – Piwi-interacting RNA
PKA – cAMP-dependent protein kinase
PLCζ - Phospholipase C zeta
PTMs – Post-translational modifications

Q

R

Rab – Ras-related protein

RNA – Ribonucleic acid
RNAi – RNA interference
RS – Radial spoke

S

SC – Segmented/ striated column
SNARE – Soluble N-ethylmaleimide-sensitive factor attachment proteins receptor
Stage MI – Metaphase I during meiosis
SUN – Sad1/UNc84 homology domain-containing protein

T

tRFs – Transfer RNA-derived fragments
TUBB8 – Tubulin Beta 8 Class VIII

U

V

W

WES – Whole-exome sequencing
WHO – World Health Organization

X

Y

γ-TuRC – γ-tubulin ring complex

Z

INTRODUCTION

CHAPTER 1: THE SPERMATOZOON

Mammalian spermatozoa are highly specialized germ cells with a unique objective: to fertilize an egg. But first, these germ cells must undergo remarkably complex morphological, chemical, and functional changes.

Spermatozoa are formed during the complex process of spermatogenesis that occurs in the testis. They gain their typical slender shape and assemble flagella during the last step of spermatogenesis called spermiogenesis. Morphologically, spermatozoa can be divided into three main parts: the sperm head, the connecting piece, and the flagellum. The sperm head contains a very condensed nucleus that carries the haploid genetic material of the male. The connecting piece links the sperm head to the tail. Finally, the flagellum works as a propulsive engine, allowing the sperm to move through the female genital tract and the protective layers of the egg. In contrast to somatic cells, spermatozoa are believed to be transcriptionally and translationally silent. Cytoplasmic organelles transform during spermatogenesis: the Golgi apparatus gives rise to the acrosome, centrioles become the connection between the sperm head and flagellum, and mitochondria reposition along the sperm axoneme and participate in energy production and sperm motility.

Although sperm morphology is similar among vertebrate species, slight differences can be observed. In this work, we will primarily discuss the differences in spermatogenesis of humans and mice. For instance, sperm heads are 1.6 times longer and flagella are approximately 2.5 times longer in mice than in humans (Figure 1). The mouse head is also larger and has a hooked shape whereas the human sperm head has an oval shape (Gu et al. 2019; Inaba 2011).

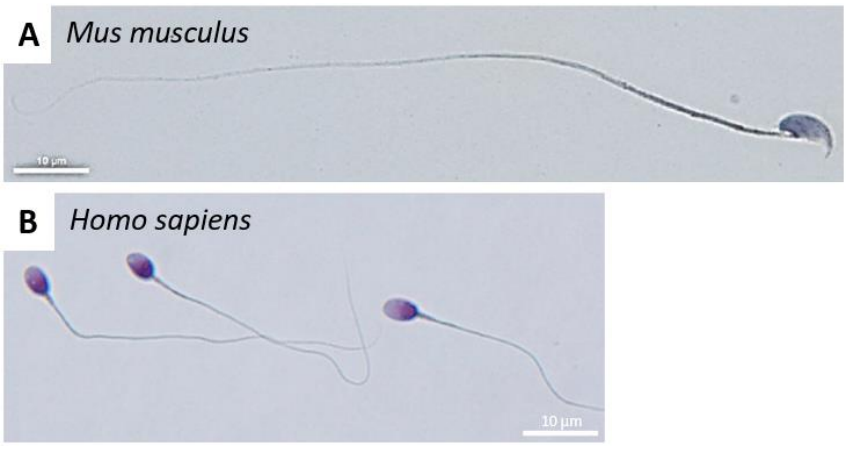

Figure 1: Differences in sperm morphology and size between mouse (A) and human (B) spermatozoa. *Adapted from Coutton et al., 2019.*

1 THE SPERM HEAD

1.1 THE NUCLEUS

The sperm head contains two major structures: the nucleus and the acrosome. The nucleus is the largest structure of the sperm head and contains highly condensed chromosomes. The compaction is established by the replacement of histones by protamines during spermiogenesis that results in the absence of transcription in mature spermatozoa (Steger 1999).

Nuclear chromatin remodelling occurs during spermiogenesis (Figure 2). The histone-to-protamine transition is facilitated by the replacement of somatic histones with histone variants and by histone post-translational modifications (PTMs). Histones are gradually replaced by transition proteins and then by protamines which facilitate high chromatin compaction (T. Wang et al. 2019; Moritz and Hammoud 2022). Mature spermatozoa retain only a small percentage of histones in their genome, around 1% in mice (Balhorn, Gledhill, and Wyrobek 1977) and 15% in humans (Gatewood et al. 1990).

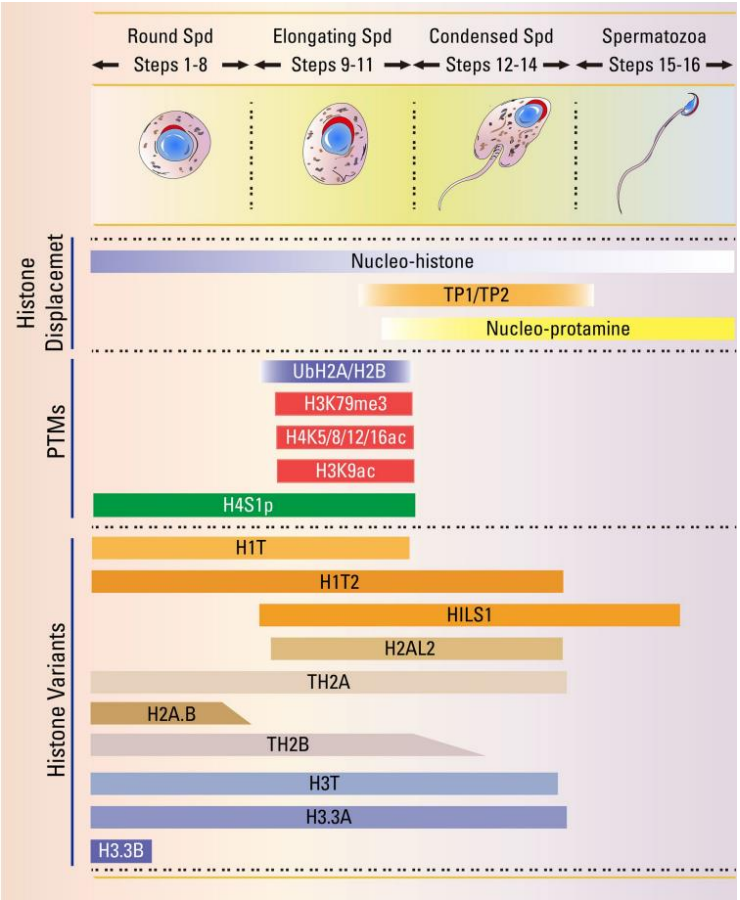

Figure 2: Histone-to-protamine transition during spermiogenesis is highly regulated. *The replacement of somatic histones by transition proteins (TP), and subsequently by protamines, is modulated by somatic and testis-specific histone variants and histone post-translation modifications (PTMs) of somatic histones and histone variants. Abbreviations: spermatid (Spd). From Wang et al. 2019.*

The nucleus is enclosed in a cytoskeletal capsule called the "perinuclear theca" that fills most of the cytoplasmic space of the sperm head. It is apically sandwiched between the acrosome and the nuclear envelope, and caudally between the nuclear envelope and the cell plasma membrane (postacrosomal segment) (Darszon et al. 2005) (Figure 3). The perinuclear theca is important for maintaining the architecture of the sperm nucleus. It is composed of spermatid-specific cytosolic and nuclear proteins, including a factor important for oocyte activation, the phospholipase C zeta (PLCζ) (Escoffier et al. 2015). A major basic protein called Calicin appears to be an organizing center of the structure and interacts with itself and other perinuclear theca components, participating in the formation of a bridge between the inner acrosomal membrane (interacting with e.g. Spaca1) and the nuclear envelope (e.g. Dpy19l2) (X.-Z. Zhang et al. 2022).

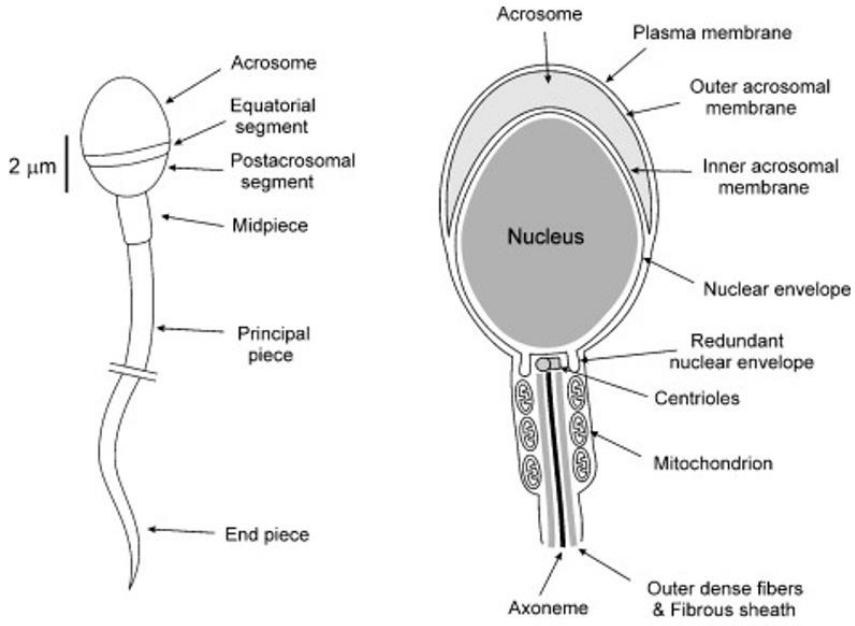

Figure 3: Structure of a human spermatozoon. *From Darszon et al., 2005.*

1.2 THE ACROSOME

The acrosome is a large and flat granule resembling a cap that covers the anterior part of the nucleus (Figure 3) (Zanetti and Mayorga 2009). It is positioned between the plasma membrane and the nuclear envelope. The acrosome starts to form after meiosis when germ cells enter the round spermatid stage and is completed at the end of spermiogenesis (L.D. Russell et al. 1990).

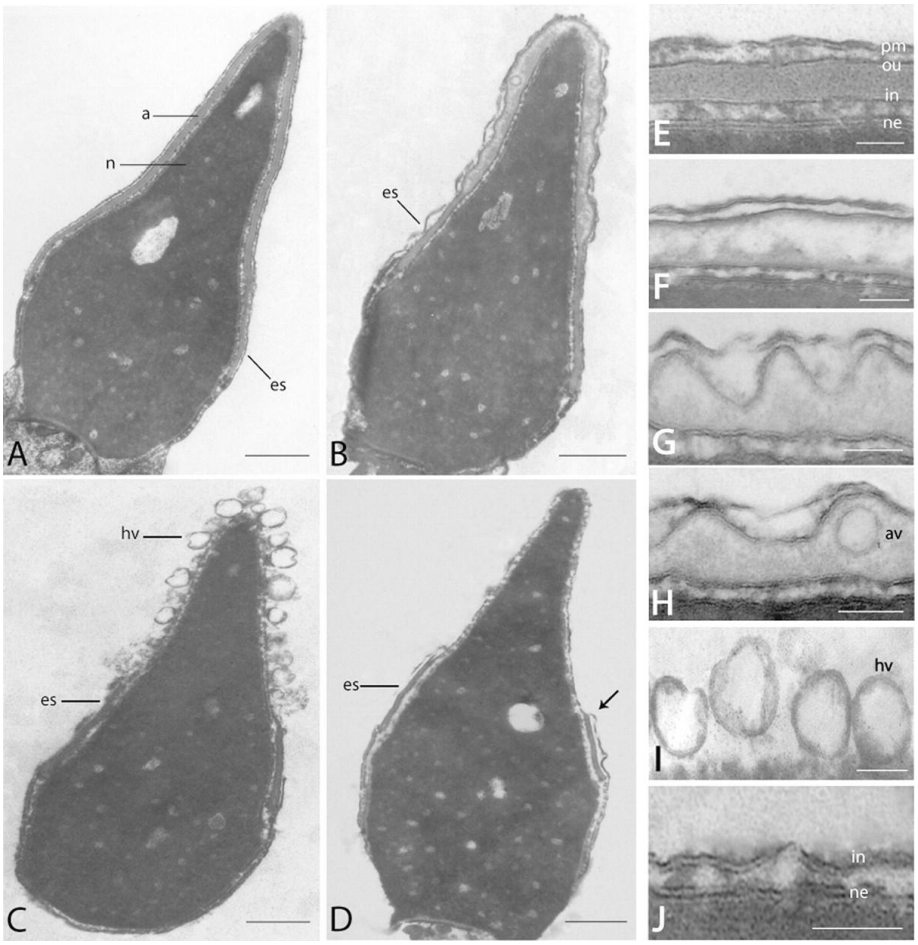

Figure 4: Morphological changes occurring during the acrosomal reaction in human spermatozoa (A-D). *(A, E) Unreacted sperm with an intact acrosome. The acrosome becomes swollen (B, F). (C, H, I) Pores start to appear in the plasma membrane and outer acrosomal membrane, leading to the formation of hybrid vesicles (hv) containing both membranes and their exocytosis. (D, J) A sperm with a completed acrosomal reaction. The equatorial segment remains unaltered. Arrow shows the continuity between the plasma membrane and the inner acrosomal membrane. Scale bars = 550 nm (A-D), 100 nm (E-J). Abbreviations: acrosome (a), intra-acrosomal vesicle (av), nucleus (n), equatorial segment (es), hybrid vesicle (hv), plasma membrane (pm), outer acrosome membrane (ou), inner acrosome membrane (in), nuclear envelope (ne). Adapted from Zanetti and Mayorga 2009.*

The acrosome contains hydrolytic and proteolytic enzymes. Upon stimulation, the outer membrane fuses with the plasma membrane of the sperm head and the acrosome undergoes exocytosis, gradually releasing these enzymes during a process called the acrosome reaction (Figure 4) (K.-S. Kim, Foster, and Gerton 2001). The exact location where the acrosome reaction occurs within the female reproductive tract (at the zona pellucida, in the vicinity of the egg, or before) and the role of acrosomal enzymes (penetration of the cumulus oophorus, sperm-egg binding, and sperm entry) are still subject to debate and might be species-specific. It is generally accepted that the acrosome is important for successful fertilization, and the inner acrosomal membrane participates in sperm-egg binding and fusion (Yoshinaga and Toshimori 2003; Ikawa et al. 2010; Gupta 2021; Wolkowicz et al. 2008).

To be able to initiate the acrosome reaction, the sperm must first undergo capacitation (Austin 1952). Capacitation involves changes in the sperm plasma membrane (e.g. membrane fluidity and cholesterol movement), intracellular pH, cytoplasmic alkalinization, activation of membrane ion channels, and changes in membrane potential (Puga Molina et al. 2018). In the female genital tract (or under capacitating conditions *in vitro*), sperm become hyperactivated that leads to changes in their motility patterns. Even-though mammalian ejaculated sperm are motile, hyperactivated sperm move with greater amplitude and propulsion by creating an asymmetric beating pattern that helps them traverse the viscous environment in the oviduct and penetrate an egg's zona pellucida and the cumulus oophorus (Suarez 2008). An essential part of hyperactivation is the rise in flagellar Ca^{2+} that is predominantly incorporated from the extracellular space through the CatSper channel that are present in the plasma membrane of the flagellar principal piece (Ren et al. 2001; Rahban and Nef 2020).

2 THE SPERM FLAGELLUM

The sperm flagellum serves as the propulsive engine of the male germ cell. The main structure of the flagellum is the axoneme and it spans the entire length of the flagellum (Figure 5) (Dunleavy et al. 2019; Linck, Chemes, and Albertini 2016). The axoneme is surrounded by various peri-axonemal structures (mitochondrial sheath, outer dense fibers, fibrous sheath) that define three main parts of the flagellum: the midpiece, the principal piece and the end piece. All peri-axonemal structures are only present in spermatozoa but not in cilia.

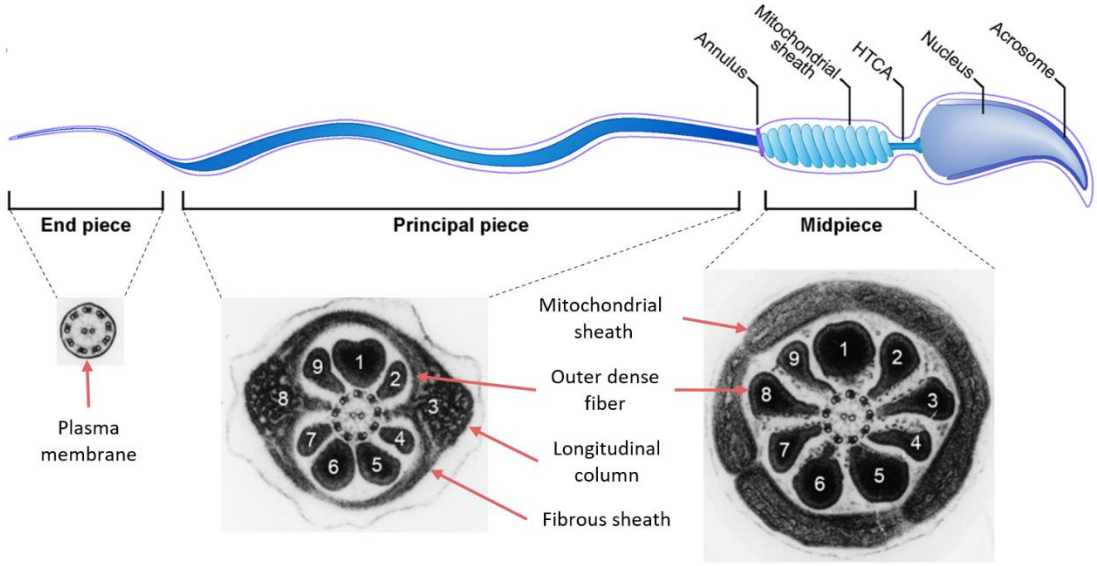

Figure 5: Schematic representations of a mammalian spermatozoon showing inner structural components. *Outer dense fibers are numbered. Adapted from Dunleavy et al. 2019, electron micrographs were adapted from Linck, Chemes, and Albertini 2016.*

2.1 THE AXONEME

The axoneme is a microtubule-based structure. Microtubules (MT) are major components of the cytoskeleton and are essential for mitosis, protein trafficking, cell motility, and maintenance of cell shape. They are composed of α- and β-tubulin heterodimers that polymerize into long, polarized protofilaments which in turn arrange laterally to form hollow tubes of ~25 nm in diameter (Goodson and Jonasson 2018). Microtubules are however not completely hollow and can contain proteins that are termed microtubule inner proteins (MIP).

The sperm axoneme is composed of two singlet microtubules in the center, the central pair, that are radially surrounded by nine MT doublets termed outer microtubule doublets (the 9+2 arrangement) (Figure 6). Each outer MT doublet contains an A- and a B-tubule. In mammalian cells, a single MT generally contains 13 protofilaments that can be seen in the A-tubule of outer MTs whereas the B-tubule is not complete and only contains 10 protofilaments. The central pair is also composed of singlet MTs and each contains 13 protofilaments.

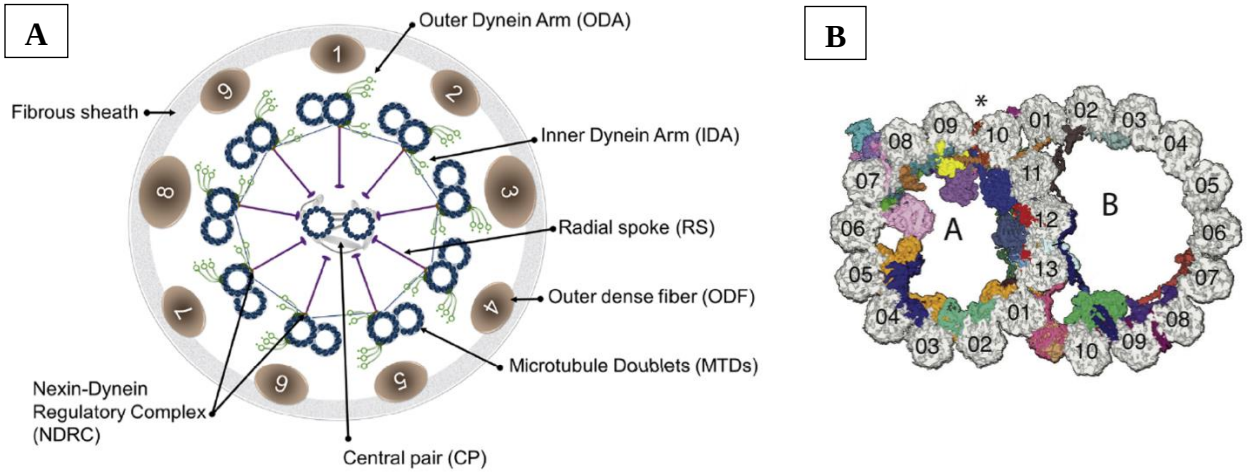

Figure 6: Schematic illustration of the inner structure of a mammalian spermatozoon. *(A) Cross-section of a flagellum of the principal piece showing the axoneme and peri-axonemal structures. ODFs are numbered. The central pair is surrounded by projections (grey). From Touré et al. 2021. (B) Structure of outer microtubule doublets showing 13 protofilaments in the A-tubule and 10 protofilaments in the B-tubule. The seam (asterisk) determines the location of the B-tubule nucleation. Colored structures represent different microtubule inner proteins (MIPs) bound to the microtubule lumen. Adapted from Ma et al., 2019.*

2.1.1 The central apparatus

The central apparatus (CA) is composed of the central pair, two singlet MTs denoted C1 and C2, that are each surrounded by a set of proteins termed "asymmetric projections" (Figure 7). In the mouse, C1 and C2 are each surrounded by five different projection proteins termed C1a, C1b, C1c, C1d, C1e and C2a, C2b, C2c, C2d, C2e. Projections repeat in a periodical manner along the length of the axoneme (Leung 2021).

The central apparatus plays an important role in the generation and regulation of ciliary and flagellar movement (Loreng and Smith 2017). All motile cilia and flagella, except for nodal cilia,

contain the 9+2 structure whereas immobile primary cilia have a 9+0 configuration (Smith and Lefebvre 1997; Samsel et al. 2021; Girardet et al. 2019; Odate et al. 2016).

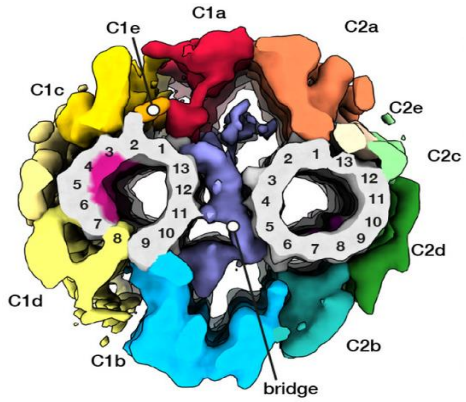

Figure 7: Diagram of a central apparatus from a mouse sperm axoneme. *Microtubule singlet C1 is on the left and C2 on the right. Each microtubule contains 13 tubulin protofilaments (numbered). Microtubule inner proteins are in pink. The central pair is surrounded by projection proteins (C1a-e, C2a-e) and connected by a bridge. From Leung et al. 2021.*

The overall architecture of the central apparatus is similar in spermatozoa between pigs (*S. scrofa*), horses (*E. caballus*) and mice (*M. musculus*) and resembles the CA in flagella from C*hlamydomonas* and sea urchin sperm. The differences between mammalian species are in their MIPs (Leung 2021) that will be discussed in *Chapter 3: Microtubules and related structures, subchapter 7: Microtubule inner proteins*. C1 and C2 are interconnected through a complex network called the bridge and through some of the projections (Carbajal-González et al. 2013).

So far, 66 proteins have been identified as components of the central pair in the *Chlamydomonas* (Adams et al. 1981; L. Zhao et al. 2019). Out of these proteins, 13 have homologues in humans and mice, and 10 of them have been linked to male infertility and abnormal sperm morphology: CFAP54 (McKenzie et al. 2015), CFAP69 (Dong et al. 2018), CFAP221/ Pcdp1 (L. Lee et al. 2008), DLEC1 (Okitsu et al. 2020), Hydin (Oura et al. 2019), LRGUK-1 (Y. Liu et al. 2015), SPEF2 (Sironen et al. 2011), SPAG6 (Sapiro et al. 2002), SPAG16L (Zhibing Zhang et al. 2006), and SPAG17 (Kazarian et al. 2018). The absence of SPEF2, CFAP54, CFAP221, SPAG6 was also associated with primary ciliary dyskinesia (PCD) and/ or hydrocephaly. PCD is an autosomal recessive genetic condition with symptoms caused by malfunction of motile cilia, often involving recurrent respiratory infections (Sironen et al. 2020). Some of these proteins, including SPEF2, LRGUK-1, and SPAG17, were also shown to interact with intraflagellar (IFT) and intramanchette (IMT) transport-related proteins and their absence was associated with an abnormal manchette and aberrant head shape. These aspects will be discussed in more detail in *Chapter 2: Spermatogenesis, subchapter 7: Axoneme formation.*

2.1.2 Radial spokes

Radial spokes, 40 nm-long multiprotein T-shaped structures, provide a link between the central pair and outer MT doublets (Figure 8). They protrude from the A-tubule and transiently interact with the CA projections through electrostatic interactions (Gui, Ma, et al. 2021). They are composed of three parts: the head, the neck, and the stalk. The head faces the central pair and the elongated stalk is anchored to the A-tubule of the outer MT doublets (Pigino et al. 2011). The stalk extensively interacts with the inner dynein arms (IDAs) that are also present on the outer MT doublets. Radial spokes are mechanochemical transducers and contribute to the regulation of dynein activity and are thus crucial for sperm and cilia motility (Lin et al. 2014; Xin Zhang et al. 2021).

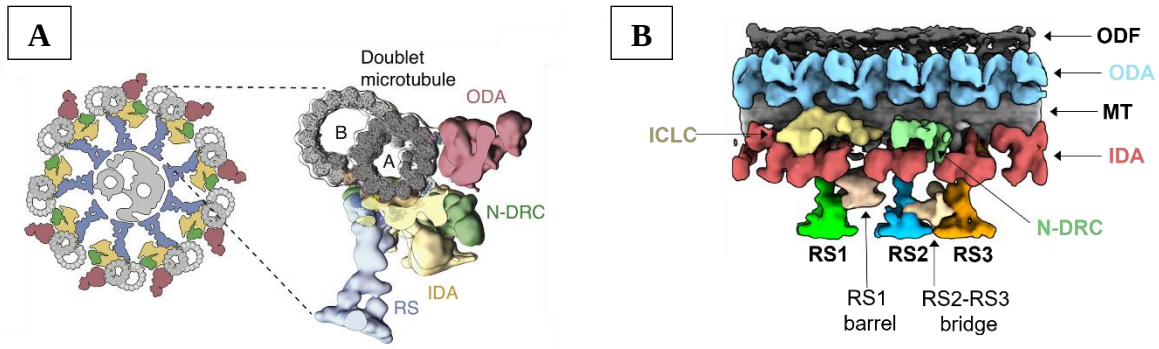

Figure 8: Association of outer microtubule doublets with radial spokes, outer dynein arms (ODA), inner dynein arms (IDA), and the nexin-dynein regulatory complex (N-DRC). *(A) Radial spokes are anchored to the A-tubule of outer MT doublets and interact with IDAs at their stalk. From Ma et al. 2019. (B) Structure of the 96 nm mouse axoneme from the principal piece decorated with regulatory structures. Radial spokes 2 and 3 are connected by the RS2-RS3 bridge. Abbreviations: outer dense fiber (ODF), microtubule (MT), intermediate chain/light chain of the I1 dynein (ICLC), radial spoke (RS). From Leung et al. 2021.*

Three types of radial spokes (R1, R2, R3) are present in mammalian axonemes but they were mostly studied in unicellular organisms (*Chlamydomonas*, *Tetrahymena*) and in sea urchin sperm. The *Chlamydomonas* only has the RS1 and RS2 and a very small RS3 that is not linked to the CP. The RS3 also structurally differs from RS1 and RS2 which have similar structures (Lin et al. 2012; Z. Chen et al. 2023). Radial spokes repeat in doublets (e.g. *Chlamydomonas*) or triplets (e.g. mammals) in a 96 nm interval along the long axis of the outer doublets. In a recent study, Chen *et al.* showed that mouse and human sperm axonemes contain additional densities, a barrel between RS1 and RS2, a RS2-RS3 cross-linker and an RS3 scaffold. These structures are missing from

both human respiratory cilia and unicellular model organisms. They were also asymmetrically distributed between doublets and were less prominent in some human doublets compared to the mouse (Z. Chen et al. 2023) (Figure 9).

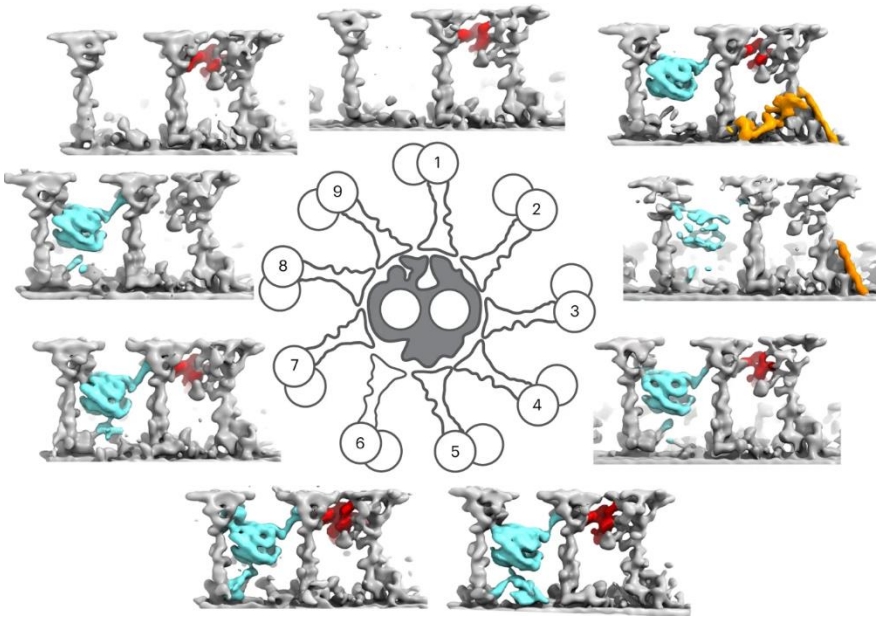

Figure 9: Asymmetric distribution of newly identified radial spoke-associated structures in mouse sperm axonemes. *Common features of radial spokes are in grey. The barrel (cyan) is absent from microtubule doublets 1 and 9, the RS2-RS3 cross-linker (red) is absent in doublets 3 and 8, and the RS3 scaffold is only present in doublets 2 and 3. From Chen et al., 2023.*

Radial spokes are composed of at least 23 different proteins in the *Chlamydomonas* (Piperno, Huang, and Luck 1977; Piperno et al. 1981; P. Yang et al. 2001) out of which 15 have homologues in mammals (Yogo 2022). The absence of *Rsph6*a and *Lrrc23* was associated with male infertility in mice but cilia were not affected (Abbasi et al. 2018; Xin Zhang et al. 2021). *Rsph6*a-deficient mice had short and immotile flagella with strong defects in the mitochondrial and fibrous sheaths, and an abnormal head morphology. The assembly of the flagellum and manchette removal were delayed. *Lrrc23*-deficient mice seemed to have sperm flagella with normal length, but their motility was severely decreased, possibly due to a frequent absence of radial spokes in the axoneme. The absence of radial spoke proteins *RSPH1* (Kott et al. 2013), *RSPH3* (Jeanson et al. 2015), *RSPH4A* and *RSPH9* (Castleman et al. 2009) was associated with PCD PCD in humans.

2.1.3 The nexin-dynein regulatory complex

The nexin-dynein regulatory complex (N-DRC) is a thin filament that connects the A-tubule of one doublet to the B-tubule of the neighbouring doublet (Heuser et al. 2009) (Figure 8). It is present on the doublets every 96 nm (Heuser et al. 2009). The N-DRC is believed to maintain an optimal alignment of MT doublets and help regulate their sliding, thus participating in ciliary and flagellar motility (Bower et al. 2013). Structurally, the N-DRC in mouse sperm flagella has additional densities compared to the N-DRC in human respiratory cilia, and the form of these densities varies between MT doublets (Z. Chen et al. 2023) (Figure 10).

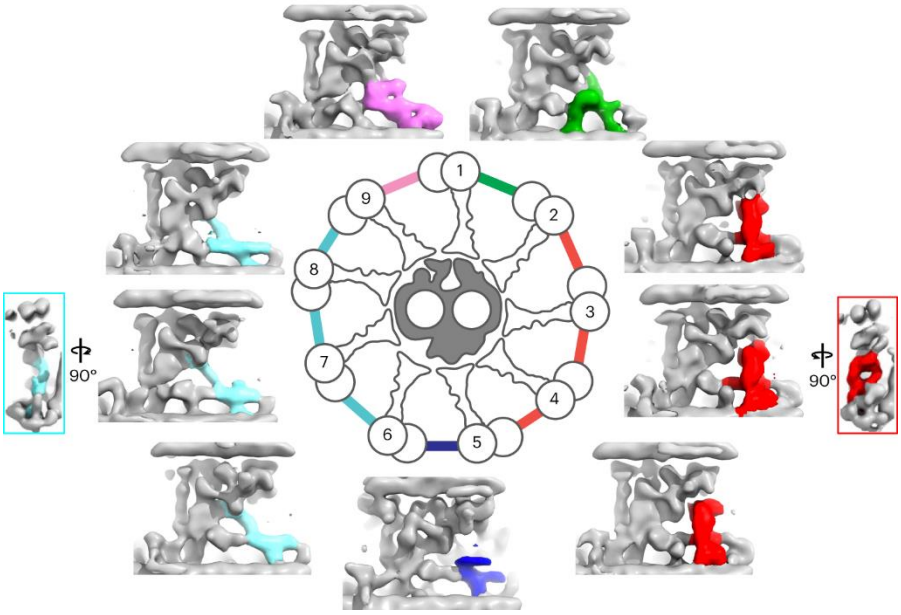

Figure 10: Asymmetric distribution of newly identified N-DRC features in mouse sperm axonemes. *Common structure of N-DRCs between microtubule doublets are in grey. Unique features of the N-DRC are colored based on structural similarities in between microtubule doublets. From Chen et al., 2023.*

Mutations in *Ccdc164/ Drc1* (J. Zhang et al. 2021), *Lrrc48/ Drc3* (Ha et al. 2016), *Tcte1/ Drc5* (Castaneda et al. 2017), *Drc7* (Morohoshi et al. 2020), *Iqcg/ Drc9* (R.-K. Li et al. 2014) were associated with male infertility in mice. The absence of CCDC164/ DRC1 in mice led to severe flagellar defects, including short and coiled flagella (J. Zhang et al. 2021). This syndrome is termed multiple morphological abnormalities of the sperm flagella (MMAF) (Ben Khelifa et al. 2014) and will be discussed in *Chapter 4: Infertility, subchapter 4.1: Multiple morphological abnormalities of the sperm flagella*. Mutations in *CCDC164/ DRC1* (Morimoto et al. 2019), *CCDC65/ DRC2* (Horani et al. 2013), *Lrrc48/ Drc3 (Ha et al. 2016),* and *Gas8/ GAS8/ DRC4* (Olbrich et al. 2015)

were also associated with PCD. Moreover, a mutation in another N-DRC component, *Fbxl13/ Drc6,* did not lead to any defects in cilia not flagella (Morohoshi et al. 2020). Some components of the N-DRC appear to be more important for the function and/or assembly of either cilia or flagella.

2.1.4 Inner and outer dynein arms

Dyneins are ATP-dependent microtubule motor proteins. They move along MTs toward the MT minus end. Two types of dyneins exist, cytoplasmic and axonemal dynein. They share some structural similarities, however their functions are different.

Cytoplasmic dynein-1 travels along MTs and participates in intracellular transport, delivering cargo such as protein, organelles, and mRNA to different locations in most eukaryotic cells, and also participates in mitosis (Torisawa and Kimura 2020). Cytoplasmic dynein-2 interacts with the intraflagellar transport (IFT) machinery that is required for the assembly of cilia and flagella. The dynein-2-IFT complex is involved in retrograde transport, from the tip of the cilium/ flagellum to the base (Pazour, Wilkerson, and Witman 1998; Hou and Witman 2015). On the other hand, axonemal dyneins are structural components of the axoneme. Their role is to power the beating of motile cilia and flagella and propagation the binding along the length of the axoneme (Roberts 2018).

Structurally, dyneins are large multisubunit complexes (Figure 11). Dynein subunits are classified according to their mass into heavy (∼520 kD), intermediate (∼70 –140 kD), light intermediate (∼53–59 kD), and light (∼10–30 kD) chains (Pfister et al. 2006). The light intermediate chains are only present in complexes with cytoplasmic dynein. The heavy chains have several important roles. At the N-terminal domain, they contain the "tail domain" that contains binding sites for adaptor proteins such as the HOOK protein family. The adaptors mediate interactions between dynein and their cargo. The tail domain is also associated with the intermediate, light intermediate, and light chains. At the C-terminal, the heavy chain contains six AAA ATPase domains that constitute the "motor domain" of the complex. The stalk is composed of two antiparallel coiled-coil domains and a MT-binding domain in between them (Braschi et al. 2022; Schiavo et al. 2013).

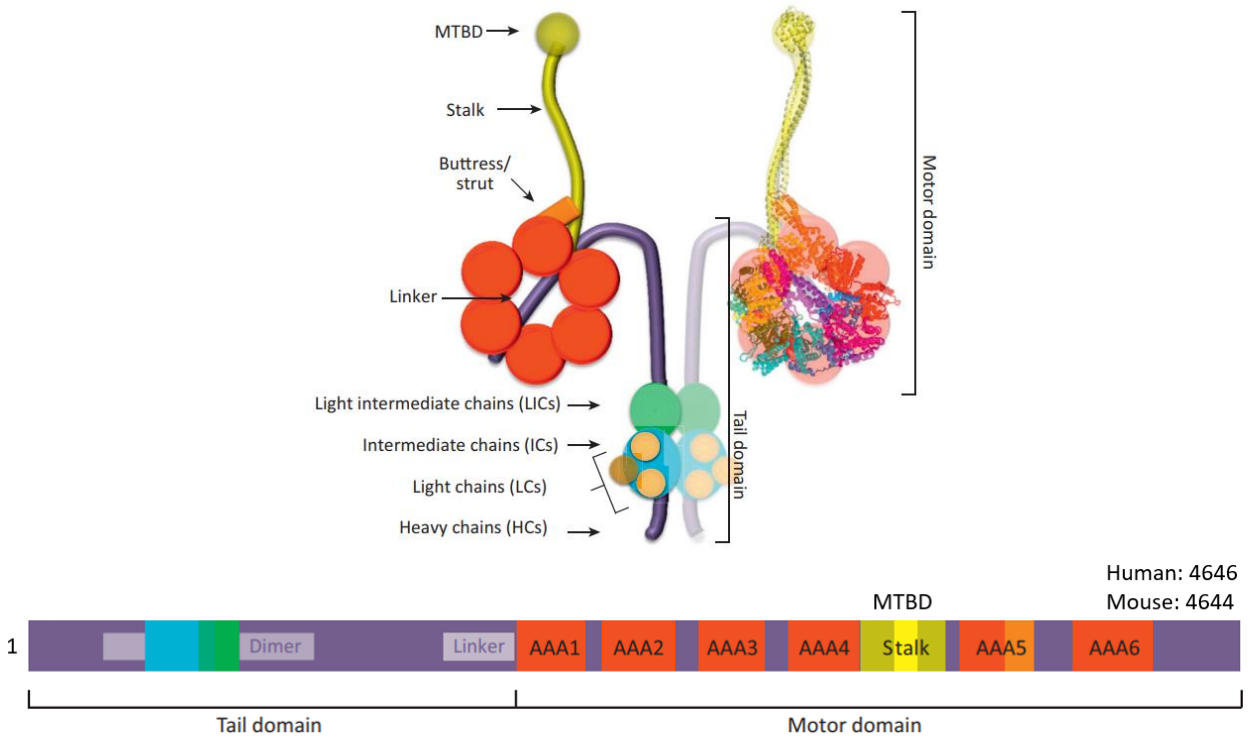

Figure 11: Structure of the cytoplasmic dynein complex with two heavy chains. *(A) The core of the complex is the heavy chain dimer (dark purple) and its associated subunits. The motor domain contains a stalk (yellow) with a microtubule-binding domain (MTBD) and six AAA ATPase domains (red circles), the buttress (orange), and the linker region. HCs are associated with light intermediate chains (LICs) (green), intermediate chains (ICs) (cyan), and light chains (LCs) (light yellow). (B) Protein domain composition of cytoplasmic dynein. Number of amino acids in human and mouse cytoplasmic dynein heavy chain are shown. From Schiavo et al. 2013.*

Axonemal dyneins are known as the inner and outer dynein arms (IDAs, ODAs) (Figure 12). IDAs and ODAs are permanently attached to the A-tubules of outer MT doublets and transiently interact with the B-tubule of the adjacent doublets in an ATP-dependent manner. The interaction is mediated by their intermediate chains. In this way, they regulate the sliding of MT doublets relative to each other. This coordinated motion of MT sliding along the length of the flagellum creates bending that is propagated along the flagellum and is seen as flagellar/ ciliary beating. ODAs regulate the frequency of ciliary waveforms whereas IDAs influence the amplitude (Brokaw and Kamiya 1987; Kamiya and Yagi 2014).

Moreover, IDA and ODA differ in composition, function, and periodicity. Most of our understanding of IDA and ODA structure and composition comes from studies in the *Chlamydomonas*, and mouse and human structures are not available yet. Mammalian cytoplasmic

dynein is composed of two identical heavy chains and several smaller subunits, whereas axonemal dynein consists of non-identical heavy chains. Each ODA contains two (metazoans) or three (*Chlamydomonas*, *Tetrahymena*) heavy chains (α, β, γ), two intermediate and about ten light chains. IDAs are more divergent than ODA. They contain one heterodimer (dynein f) and six monomeric (a, b, c, d, e, and g) dyneins. The dynein f isoform contains two heavy chains called α et β, 3 intermediate chains and 5 light chains. Monomeric isotypes contain one heavy chain, one intermediate, and one light chain (Bui et al. 2008; Goodenough and Heuser 1985; Movassagh et al. 2010; Walton, Wu, and Brown 2021) (Figure 12).

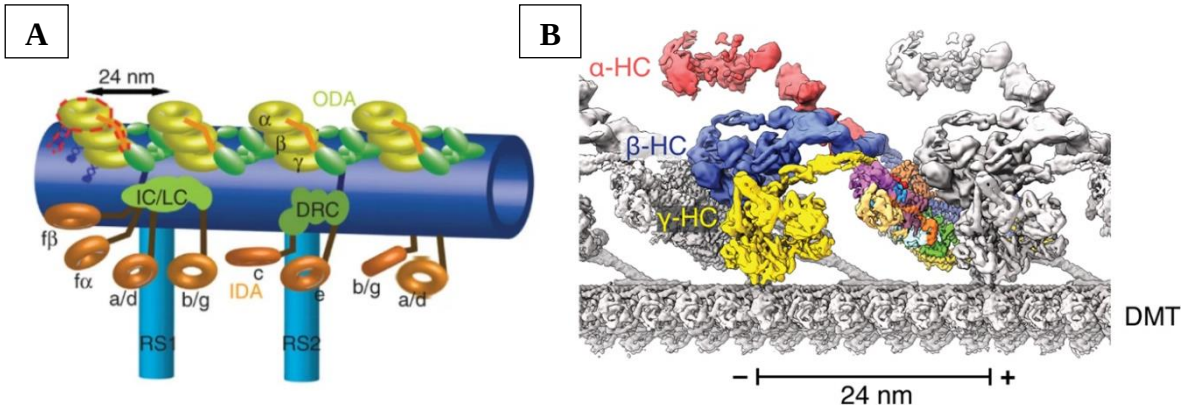

Figure 12: Schematic representation of IDA and ODA (A) and a structure of the ODAs (B). *(A) Illustration of IDA (orange), ODA (yellow, green) and radial spokes (light blue) connected to the A-tubule of outer MT doublets (dark blue) in Chlamydomonas flagella. The IDA contain seven different heavy chains in the Chlamydomonas. Dynein f forms a heterodimer with two heavy chains (fα, fβ), and others are monomeric (dynein a, b, c, d, e, and g). (B) Structure of the ODA axonemal dynein bound to the A-tubule of outer MT doublets from the Chlamydomonas. A single ODA contains three dynein heavy chains (α, β, γ) with motor domains on the right and the tail domains connected to the MT. Abbreviations: IC/LC of dynein f and the dynein regulatory complex (DRC). (A) from Movassagh et al. 2010 and (B) from Walton, Wu, and Brown 2021.*

ODAs repeat every 24 nm and are attached to the A-tubule through a docking complex (Nicastro, McIntosh, and Baumeister 2005), whereas IDAs repeat with a 96-nm periodicity (Nicastro et al. 2006).

In humans, mutations in genes coding for IDA and ODA proteins, including *DNAH1* (Ben Khelifa et al. 2014), *DNAH2* (Hwang et al. 2021), *DNAH8* (C. Liu et al. 2020), *DNAH10* (Tu et al. 2021), and *DNAH17* (Yanwei Sha, Wei, Ding, Mei, et al. 2020) were associated with male infertility,

absence of sperm motility and MMAF. Mutations in *DNAH5* (Hornef et al. 2006) and *DNAH11* (Knowles et al. 2012; Schultz et al. 2020) were shown to cause PCD.

2.1.5 Molecular rulers

The aforementioned axonemal components (N-DRC, radial spokes, IDA, ODA) are regularly spaced along MT doublets. Binding of proteins to the MT doublets show a periodicity of 8-nm multiples (8, 16, 24, 48, and 96 nm) that correspond to the length of a α-β-tubulin heterodimer which is 8 nm (Ma et al. 2019). Within each 96 nm axonemal repeat, four ODAs bind with 24 nm periodicity, along with one unit of 7 IDAs, radial spokes (RS1, RS2, and the remnants of RS3), and one N-DRC (Figure 13).

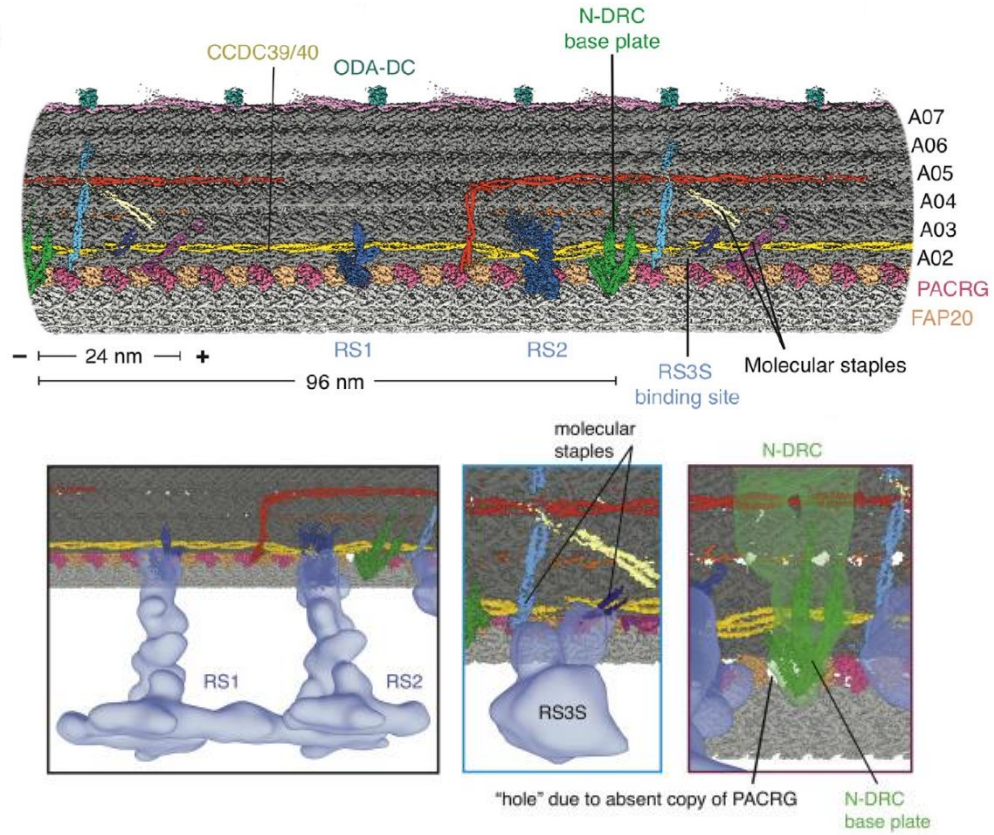

Figure 13: Relative position of molecular rulers and axonemal complexes within the 96-nm repeat of the A-tubule. *The surface of the A-tubule is decorated with several long coiled-coil proteins, particularly the CCDC39/40 complex (yellow), an L-shape protein (red) and molecular staples (various colors). CCDC39/40 is believed to be a molecular ruler that determines binding sites and periodicities of axonemal complexes. Below are zoomed images showing the location of these proteins around radial spokes and the N-DRC. PACRG and FAP20 are MIPs protruding from the MT lumen and are responsible for the stability of the doublet. A02-7 stand for numbers of tubulin protofilaments. Based on Chlamydomonas axonemes. From Ma et al., 2019.*

Oda *et al.* in *Chlamydomonas* showed the presence of a molecular ruler that determines the 96-nm spacing of axonemal components (RSs, IDAs, and N-DRCs) (Oda et al. 2014). This molecular ruler corresponds to a 96-nm long coiled-coil complex of CCDC39 and CCDC40, called FAP59/FAP172 in *Chlamydomonas*, that is present between protofilaments A02 and A03 (Figure 13; yellow). The CCDC39/40 complex is believed to determine the binding sites of these axonemal components on the surface of the A-tubule. The absence of either CCDC39 or CCDC40 leads to identical phenotypes in humans, including the loss of IDA and disorganization of axonemal structures in cilia and flagella, MMAF, PCD, and male subfertility or infertility (Blanchon et al. 2012; Antony et al. 2013; D. Chen et al. 2021).

Several long coiled-coil proteins are present on the external surface of the A-tubule while few are bound to the surface of the B-tubule in *Chlamydomonas* (Ma et al. 2019; Gui, Ma, et al. 2021) (Figure 13). Several unidentified coiled-coils were shown to interact with the CCDC39/40 complex at the A-tubule and were called "molecular staples." They bind across the CCDC39/40 complex and laterally interact with neighbouring protofilaments, which suggests that they could help maintain the complex in place. A long, L-shaped coiled-coil (red) is present in the cleft between protofilaments A02 and A05, then turns perpendicularly and crosses the complex at protofilaments A02-3. Authors suggested that it might determine the periodic docking of IDAs to protofilaments A03 and A04 (Ma et al. 2019).

Repeating protein structures are also present in the lumen of MT doublets (Figure 14). Microtubule inner proteins (MIPs) are present in both the A- and the B-tubule and form lateral and longitudinal interactions with tubulin protofilaments. MIPs with similar periodicities (8, 16, or 48 nm) interact together to form interconnected networks. They are believed to help establish and maintain the architecture of MT doublets and provide stability to MTs to withstand mechanical stress during ciliary/ flagellar beating. MIPs and their function will be discussed in more detail in *Chapter 3: Microtubules and related structures, subchapter 7: Microtubule inner proteins.*

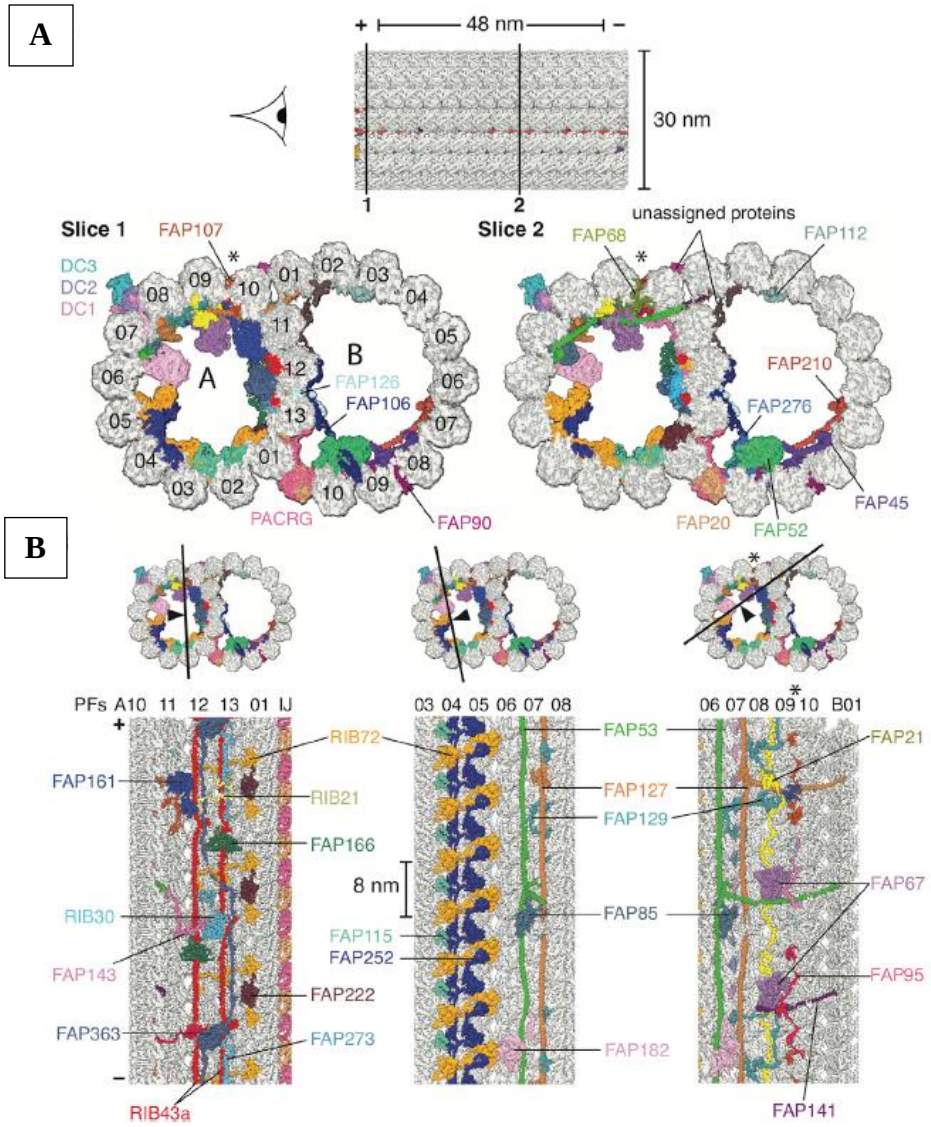

Figure 14: Microtubule inner proteins (MIPs) decorate the lumen of Chlamydomonas axonemal MT doublets in a periodic manner. *(A) Two cross-sections of the 48-nm repeat reveal numerous differentially colored MIPs. (B) Longitudinal sections through 3 different sections of the A-tubule show periodically repeating MIPs in the lumen. From Ma et al., 2019.*

2.2 THE MIDPIECE

The midpiece is characterized by an axoneme surrounded by nine outer dense fibers (ODFs) and by helically arranged mitochondria forming the mitochondrial sheath. The ODFs are arranged on the outside of the mitochondrial sheath (Figure 15).

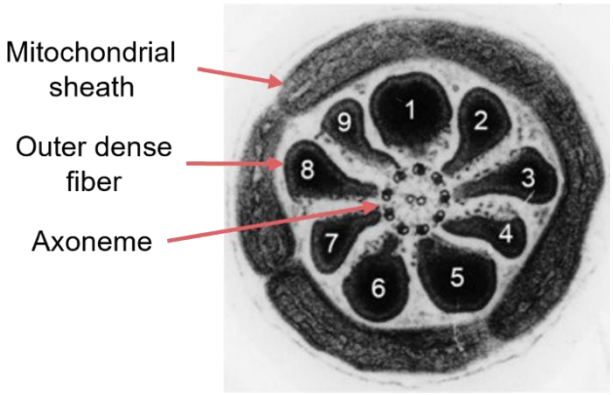

Figure 15: Structure of a mammalian midpiece. *Outer dense fibers are numbered. Adapted from Linck, Chemes, and Albertini 2016.*

2.2.1 The mitochondrial sheath

Mitochondria are known sources of energy in somatic cells, however sperm metabolism and the source of energy for sperm movement has been a matter of debate. Both oxidative phosphorylation in mitochondria and glycolysis appear to contribute to sperm motility in mammals. While glycolysis appears to be the main source, these observations may be species-dependent (Freitas, Vijayaraghavan, and Fardilha 2017; Losano et al. 2018).

2.2.2 The annulus

The midpiece and principal piece are separated into distinct membrane domains by a ring-like cytoskeletal structure called the annulus (Figure 16) (Shen et al. 2017; Korneev et al. 2021). The function and protein composition of the annulus are not fully understood. It is believed to serve as a protein diffusion barrier and is important for a correct organization of the midpiece. Its known components are members of the septin family (SEPT 1, 2, 4, 6, 7, 12) whose absence was linked to abnormal sperm morphology, motility defects and male infertility (Kwitny, Klaus, and Hunnicutt 2010; Touré et al. 2021; Shen et al. 2017; Kissel et al. 2005).

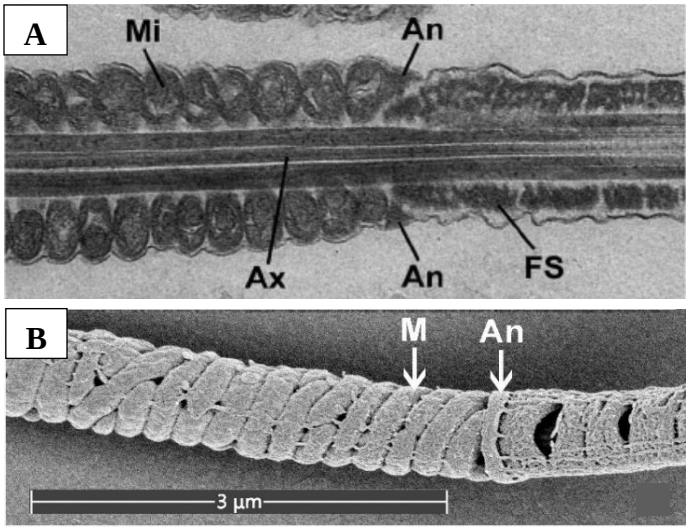

Figure 16: Electron microscopy images of a mouse sperm midpiece showing helically arranged mitochondria and the annulus. *Mitochondria are absent from the principal piece and the axoneme is surrounded by the fibrous sheath. Abbreviations: mitochondrion (Mi/ M), axoneme (Ax), annulus (An), fibrous sheath (FS). (A) From Shen et al. 2017. (B) From Korneev et al. 2021.*

2.3 THE PRINCIPAL PIECE

In the principal piece, the mitochondrial sheath is no longer present. The axoneme in the principal piece is surrounded by seven ODFs that extend from the midpiece. Two ODFs, numbers 3 and 8, are replaced by longitudinal columns. The ODFs are surrounded by the fibrous sheath (FS) (Figure 17).

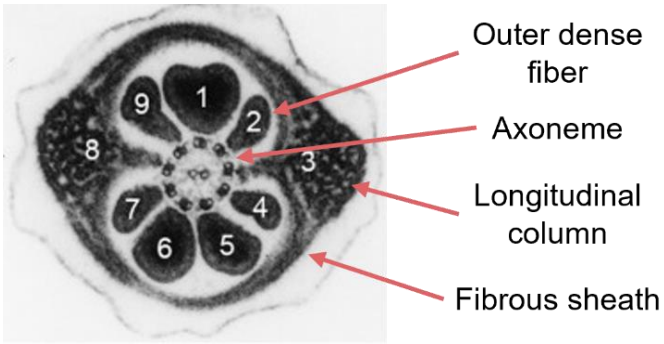

Figure 17: Structure of a mammalian principal piece. *Outer dense fibers and longitudinal columns are numbered. Adapted from Linck, Chemes, and Albertini 2016.*

2.3.1 Outer dense fibers

ODFs are keratin-like filaments (Abraham L. Kierszenbaum 2002a). They provide elasticity, structural integrity, and shear resistance to the flagellum. They are anchored at the base of the flagellum. ODFs have a strong connection to the outer MT doublets and each individual ODF is associated with one outer MT doublet in the midpiece and in the principal piece (Olson and Sammons 1980; Mari S Lehti and Sironen 2017; Lindemann and Lesich 2016) (Figure 15, Figure 17).

ODFs contain at least 14 proteins including coiled-coil proteins ODF1, ODF2, ODF3 (also called Shippo 1) (Egydio de Carvalho et al. 2002), ODF4 (also called Oppo1) (Nakamura et al. 2002), PMFBP1 (also called Stap, first identified as ODF3) (Ohuchi et al. 2001; Petersen et al. 2002), SPAG5 (Fitzgerald, Oko, and van der Hoorn 2006), tektin Tekt4 (Iida et al. 2006), TPX-1 (O'Bryan et al. 2001), VDAC2 and VDAC3 (Hinsch et al. 2004).

ODF proteins are present at multiple locations in the cell other than the ODFs. ODF1 (also known as ODF27) and ODF2 (also known as ODF84) interact, and together with PMFBP1 are present at the connecting piece (Schalles et al. 1998; Fuxi Zhu et al. 2018). ODF2 localizes to centrioles and basal bodies in somatic cells (Schweizer and Hoyer-Fender 2009; Kashihara et al. 2019). Tektins are alpha-helical coiled-coil proteins are associated with axonemal and centriolar microtubules (Amos 2008) and Tektin5 is a MIP in cilia of bovine trachea cells (Gui, Farley, et al. 2021).

Mutations in *ODF1* (P. Yang et al. 2001; Hoyer-Fender 2022), *ODF2* (Z.-J. Zhu et al. 2022; Ito et al. 2019), and *PMFBP1* (Yan-Wei Sha, Wang, Xu, et al. 2019; Fuxi Zhu et al. 2018), *Tekt2* (Tanaka et al. 2004) lead to infertility in humans and/ or mice. ODF1, ODF2 and PMFBP1 appear to be important for a proper connection of the sperm head and flagellum because their absence leads to acephalic spermatozoa, and malformed ODFs and the mitochondrial sheath. The absence of *ODF2* was associated with MMAF in humans.

2.3.2 The fibrous sheath

The FS is formed of two long longitudinal columns connected to ODFs 3 and 8 in the anterior part of the principal piece. The columns are interlinked by semicircumferential ribs. The FS columns replace the ODFs in the middle and posterior part of the principal piece where they become associated with MT doublets 3 and 8. The size of the columns decreases towards the endpiece (Fawcett 1975; Eddy, Toshimori, and O'Brien 2003) (Figure 17).

Along with ODFs, the fibrous sheath (FS) has a structural role in providing stability to the flagellum by restraining flagellar bending. It also serves as a platform for glycolytic enzymes and signaling molecules that provide a localized source of ATP for sperm motility (Eddy, Toshimori, and O'Brien 2003; Miki et al. 2002; Krisfalusi et al. 2006; Nakamura et al. 2002). More than 20 FS proteins have been detected (Mari S Lehti and Sironen 2017). The major constituents of the FS are cAMP-dependent protein kinase (PKA) anchoring proteins (AKAP) AKAP3 and AKAP4.

AKAP3 is important for the formation of the FS and incorporates AKAP4 in later stages where it is important for the completion of the FS assembly (Brown et al. 2003). Mutations in *AKAP3* (C. Liu et al. 2022) and *AKAP4* (Miki et al. 2002; G. Zhang et al. 2021), as well as in another FS component, *FSIP2* (Martinez et al. 2018; W. Liu et al. 2019), were associated with male infertility. The absence of AKAP3 and FSIP2 caused disruptions of the fibrous sheath and MMAF.

2.4 THE ENDPIECE

Finally, the endpiece, also called the terminal piece, is only formed by an axoneme that is enclosed by a plasma membrane (Figure 18). At the end of the flagellum, the 9+2 arrangement is lost, and axonemal doublets become singlets. This zone is referred to as the singlet region. Both singlet A-tubules and B-tubules can extend to the tip in humans. The singlets were shown to appear in humans and in mice in two different ways: by splitting of the doublets into two singlets or by the abrupt termination of the B-tubule (Zabeo, Croft, and Höög 2019; Leung et al. 2021).

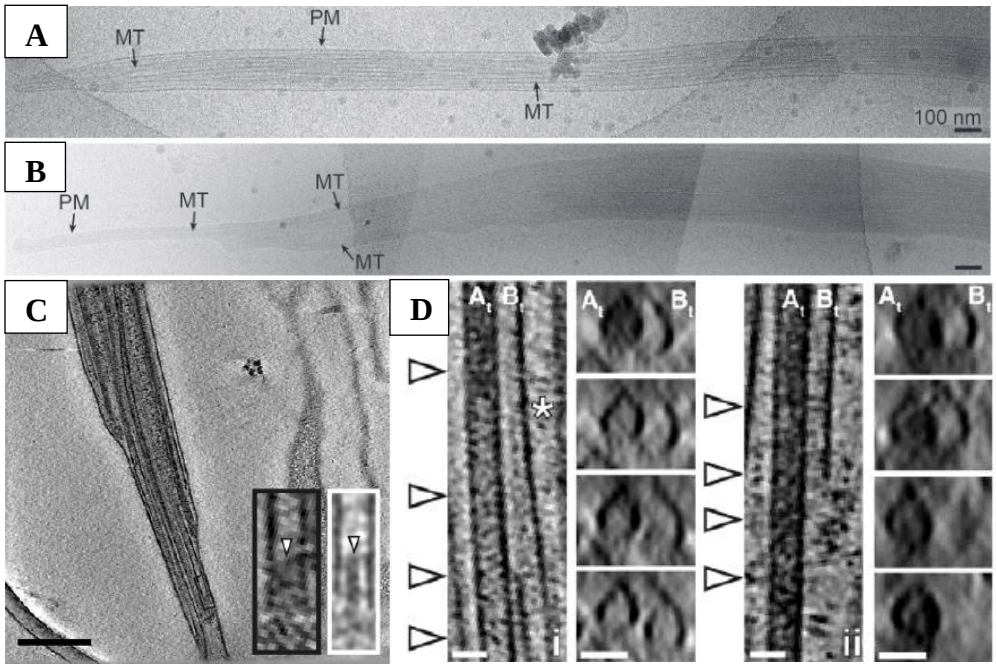

Figure 18: Cryo-electron tomography of human (A, B) and mouse (C, D) axonemal endpieces showing the singlet zones. *(A, B) Human endpieces showed high morphological heterogeneity. Abbreviations: microtubule (MT), plasma membrane (PM). From Zabeo, Croft, and Höög 2019. (C) Mouse singlet zone with insets showing a plug in the microtubule lumen (arrowhead). (D) Splitting of microtubule doublets in mouse sperm show separating an A- (A_t) and a B-tubule (B_t) into two singlets (left, panel i), and a B-tubule ending abruptly while the A-tubule continues to extend (right, panel ii). Scale bars: C = 250 nm, D = 25 nm. From Leung et al. 2021.*

Endpiece MTs were also capped by a plug that was extending ~30 nm into the MT lumen, suggesting a possible stabilizing structure that could prevent MTs from depolymerizing. A similar plug was also observed in pigs and horses (Leung et al. 2021).

2.5 THE CONNECTING PIECE

The connecting piece, also called head-tail coupling apparatus (HTCA) or sperm neck, provides a link between the sperm head and the flagellum. It contains a centriole pair composed of a proximal (PC) and a distal centriole (DC), and associated structures including the base plate, capitulum, and segmented columns also called striated or cross-striated columns. The PC is positioned below the nucleus, and the DC is positioned further away from the nucleus and gives rise to the sperm flagellum. The general architecture of the HTCA appears to be conserved among mammals even-though the precise shape and dimensions vary (Leung et al. 2021; Woolley and Fawcett 1973).

The HTCA shows a marked left–right and dorsoventral asymmetry (Figure 19, Figure 20). The HTCA and the sperm nucleus are connected at the basal plate, a local electron-dense thickening of the nuclear membrane. The caudal pole of the nucleus where the HTCA docks is called the implantation fossa. The basal plate is connected to the capitulum through numerous fine bridging filaments that are oriented perpendicular to the two surfaces. The capitulum is a thin electron-dense fibrous structure that lies between two lighter sections. Below the capitulum is a cylindrical niche that encloses the proximal centriole (PC). The PC is oriented with its distal end in the direction of the flattening of the sperm head. The distal centriole (DC) is oriented perpendicular to the PC and is prolonged by the axonemal microtubules. One or both centrioles are lost from mature spermatozoa in many species (see below). The presumably empty space where the DC has been, is referred to as the vault. The capitulum fuses caudally with the segmented columns (SC) that have a banded appearance and follow a conserved pattern of light and dark bands with a conserved periodicity. The SCs form nine cross-striated columns that create a chamber englobing the centrioles. The SCs gradually separate into nine SCs and fuse with the nine ODFs in the midpiece (Fawcett and Phillips 1969; Tapia Contreras and Hoyer-Fender 2021).

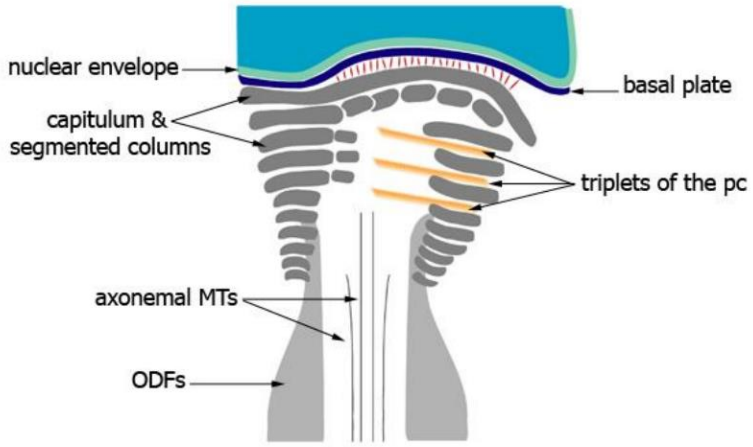

Figure 19: Structural elements of a mammalian HTCA. *Abbreviations: proximal centriole (pc), microtubules (MTs), outer dense fibers (ODFs). From Tapia Contreras and Hoyer-Fender 2021.*

The structure of the HTCA in mature spermatozoa varies among different species. For a long time, it was believed that sperm centrioles and their associated pericentriolar material partially or fully disintegrate in a process called centrosome reduction. Centriole disintegration was shown to begin during spermiogenesis and it is completed during the transit through the epididymis. Rodents (mice, rats, hamsters) lose both centrioles, whereas humans, bulls, pigs, and sheep retain the PC while the DC degenerates. The DC leaves an empty vault with remnants of microtubules that protrude from the sperm flagellum (Woolley and Fawcett 1973; Manandhar et al. 1999; Fawcett and Phillips 1969; Avidor-Reiss et al. 2015).

While still true for many species, recent work by Fishman *et al.* in 2018 showed that human and bull spermatozoa retain an atypical DC (Figure 20) (Fishman et al. 2018). The atypical DC is highly remodelled and shows modifications in the composition and location of centrosomal proteins. It is composed of splayed microtubules that extend from the axoneme, surround the vault, and form an inverted cone facing the sperm nucleus. On the outside, the atypical DC is surrounded by SCs, ODFs and mitochondria. Splayed microtubules of the atypical DC were also observed in pigs and horses (Leung et al. 2021).

Mouse spermatozoa do not have recognizable centrioles. However, some centriolar MTs of the PC were shown to remain, suggesting an incomplete degeneration (Figure 20C). A pair of singlet MTs was shown to extend beyond the axoneme into the vault.

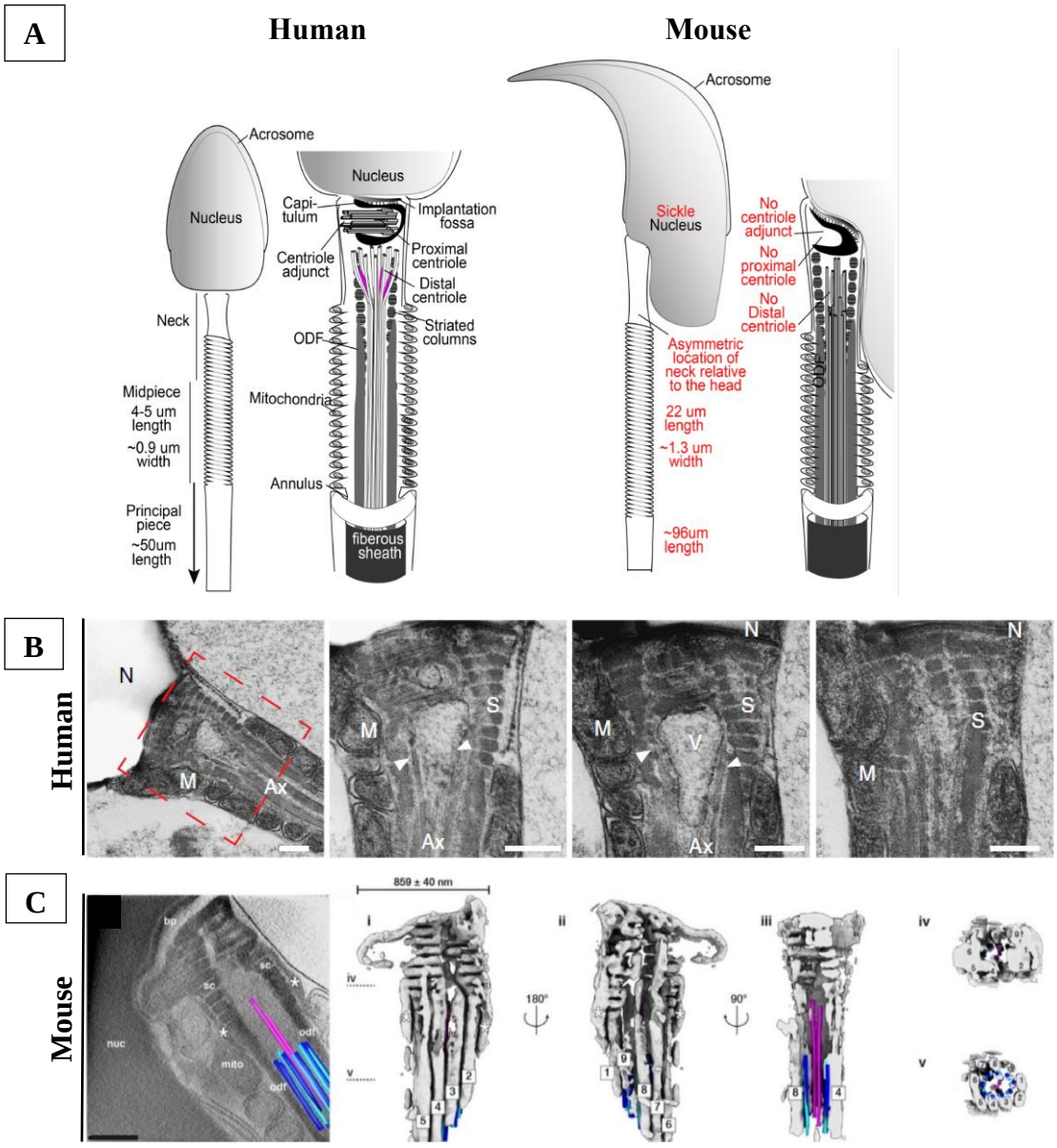

Figure 20: Comparison of the human and mouse connecting piece. *(A) Schematic description of the HTCA in human (left) and mouse (right) showing morphological differences, a proximal and an atypical distal centriole in humans and the absence of both centrioles in the mouse. From Avidor-Reiss et al. 2019. (B) Longitudinal sections of the HTCA in human showing the splayed microtubules of the atypical distal centriole that surround the electron light vault (V). Images were taken using electron microscopy with high-pressure freezing. Scale bar = 200 nm. Abbreviation: nucleus (N), axoneme (Ax), striated column (S), mitochondrion (M). From Fishman et al. 2018. (C) Longitudinal section and 3D reconstructions of mouse sperm HTCA. View from the top (iv) and bottom (v). Microtubule doublets (A-tubule in light blue, B-tubulin in dark blue), singlets (pink). Images were obtained using cryo-electron tomography. Abbreviations: basal plate (bp), striated column (sc), nucleus (nuc), mitochondrion (mito), outer dense fiber (odf). Scale bar = 250 nm. From Leung et al., 2021.*

CHAPTER 2: SPERMATOGENESIS

1 DESCRIPTION OF THE SEMINIFEROUS EPITHELIUM

Testes are organs in the scrotum whose two major functions are: the production of male hormones and the formation of spermatozoa. The testis is filled with a well-organized network of hundreds of coiled lobes called seminiferous tubules where spermatogenesis occurs.

Seminiferous tubules are surrounded by connective tissue that contains nerve fibers and blood and lymphatic vessels (Figure 21) (Varuzhanyan and Chan 2020). In the mouse, lymphatic vessels do not penetrate the entire organ (Svingen et al. 2012). Major cell types in the connective tissue include Leydig cells, fibroblasts, lymphocytes, and macrophages. Leydig cells are important hormonal regulators of spermatogenesis. They produce androgens including testosterone, and influence the production of growth factors and steroid hormones (Zhou et al. 2019).

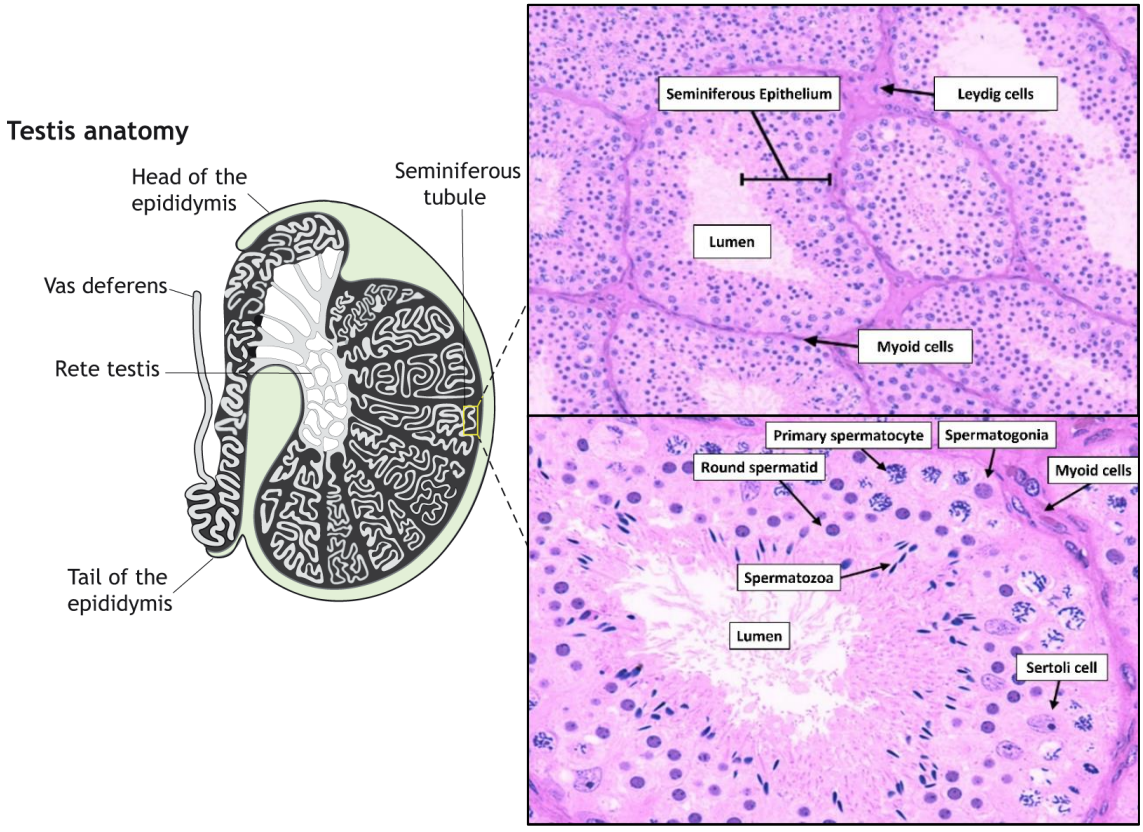

Figure 21: Organization of the testis and the seminiferous epithelium in the mouse. *Testis anatomy adapted from Varuzhanyan and Chan 2020, right images adapted from http://medcell.med.yale.edu/systems_cell_biology/male_reproductive_system_lab.php.*

Immune cells protect the developing germ cells from microbial infections and from systemic immune attacks (L. Zhao et al. 2019).

The seminiferous tubules are separated from the connective tissue by a basement membrane that contains extracellular matrix proteins and peritubular myoid cells. Myoid cells are contractile smooth muscle cells found on the periphery of seminiferous tubules. They are involved in the transport of spermatozoa in the tubule and in the movement of testicular fluid. One layer of myoid cells is present in rodents (mice, rats, hamsters) whereas humans have 5-7 layers (Maekawa, Kamimura, and Nagano 1996).

The epithelium of seminiferous tubules is composed of somatic Sertoli cells and of germ cells at different stages of differentiation. Less mature cells are on the periphery and maturing cells arrange radially towards the centre of the tubule. The most mature germ cells in the testis are testicular spermatozoa that were released into the lumen of seminiferous tubules *via* a process called spermiation. They subsequently travel to the rete testis and through efferent ducts to mature in the epididymis. The sperm then move through the vas deferens and are released through the urethra in the middle of the penis.

Sertoli cells are the somatic cells that reside among germ cells within seminiferous tubules. They are polarised and irregular cells that span from the basement membrane to the tubule lumen. They have highly complex and dynamic structure and function (Figure 22, Figure 23) (Wong and Russell 1983; França et al. 2016; Vogl, Weis, and Pfeiffer 1995). Their long cytoplasmic processes envelop multiple generations of developing germ cells, and nurture and position them throughout their differentiation.

Sertoli cells form many intercellular bridges with adjacent Sertoli cells and germ cells. These tight junctions, along with Sertoli's ectoplasmic specializations, desmosomes, and gap junctions, contribute to the formation of the blood-testis barrier which divides the seminiferous epithelium into the basal and the adluminal compartments. The basal compartment contains spermatogonia and preleptotene spermatocytes, whereas primary and secondary spermatocytes, and round and elongated spermatids reside in the adluminal compartment. The function of the blood-testis barrier is to create an immunopriviledged environment for the developing germ cells (Mruk and Cheng 2015).

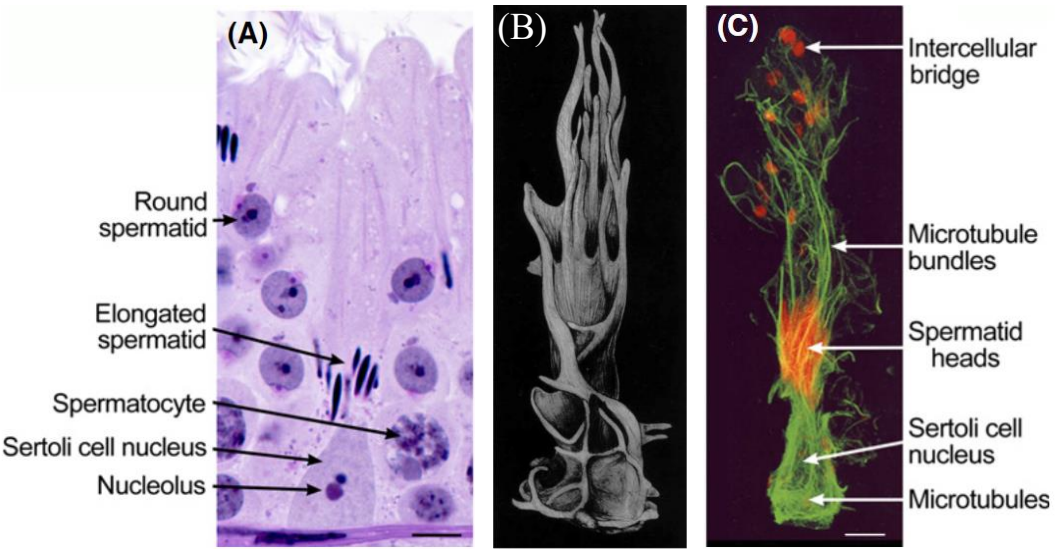

Figure 22: Sertoli cell morphology. *(A) Mouse seminiferous epithelium observed with light microscopy. A large Sertoli cell nucleus is positioned adjacent to the basement membrane. The Sertoli cell is in intimate contact with developing germ cell: pachytene spermatocytes are adjacent to the Sertoli cell cytoplasm and elongating spermatids are located deep inside the crypts of Sertoli cell cytoplasm. Scale bar = 12 µm. (B) 3D model of a rat Sertoli cell forming crypts where elongating spermatids are embedded. From V. Wong and Russell 1983. (C) Immunofluorescence microscopy of an isolated Sertoli cell showing tubulin (green) and F-actin (red). Actin stains intercellular bridges and ectoplasmic specializations. Numerous junctions are associated with elongating spermatid heads. Scale bar = 10 µm. From França et al. 2016, based on Vogl et al., 1995.*

Early spermatids attach to Sertoli cell crypts and become increasingly more embedded inside them as they elongate (Figure 23). Sertoli cells form ectoplasmic specializations, testis-specific and actin-based tight junctions that form with maturing spermatids. They localize close to the developing acrosome at the moment when the cell polarizes, and the acrosome comes in contact with the plasma membrane. Sertoli cells orient and transport elongating spermatids within the seminiferous epithelium toward the lumen. They exert forces on the sperm nucleus during spermatid elongation. During the last stages of spermatid elongation, actin-filament related structures called tubulobulbar complex form between Sertoli cells and the maturing spermatids, and participate in the removal of excess cytoplasm and disengagement of mature spermatids from the epithelium during spermiation (Hess and Vogl 2015; França et al. 2016; Liying Wang et al. 2022).

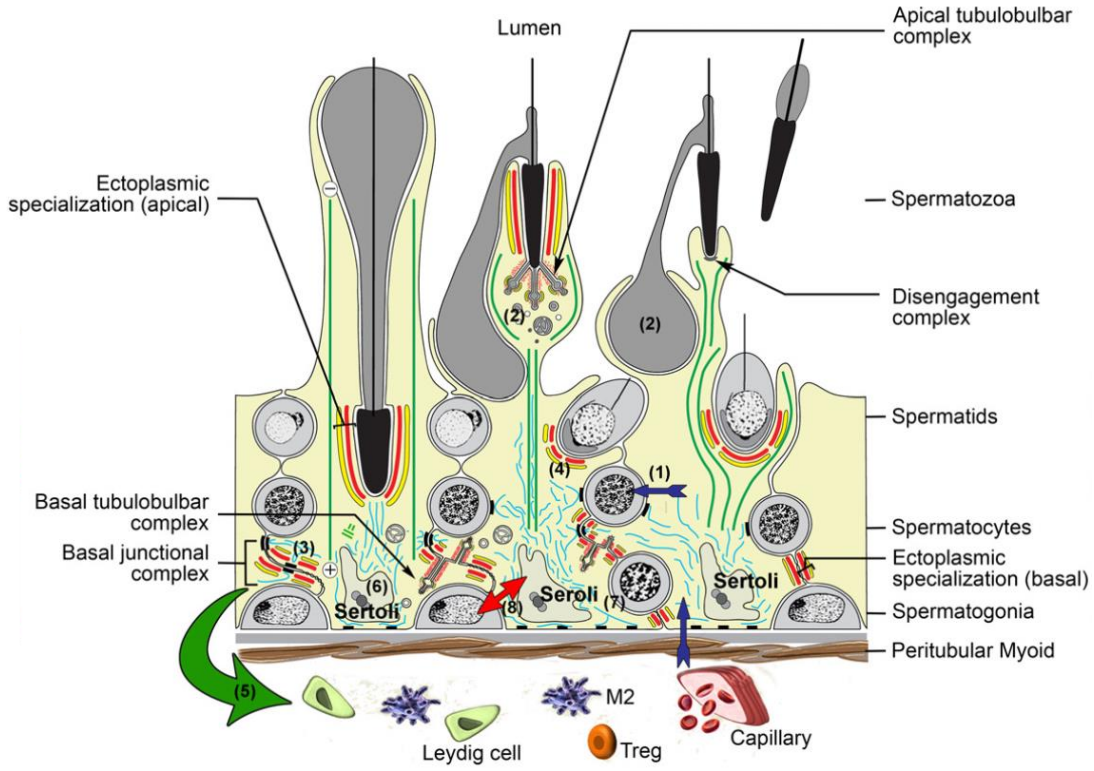

Figure 23: Schematic drawing of Sertoli cell interactions with germ cells and key functions of Sertoli cells. *(1) Sertoli cells provide micronutrients across junctional complexes, (2) phagocyte waste and leftover cytoplasm of elongated spermatids, (3) maintain the blood-testis barrier through intercellular bridges that sequesters most of autoimmunogenic germ cells to the adluminal compartment, (4) adhere to and communicate with germ cells, (5) inhibit immune reactions by secreting immunoregulatory factors to regulate the immune response and maintain immune privilege, (6) initiate and respond to endocrine signaling pathways, (7) initiate and regulate the cycle of the seminiferous epithelium (see chapter 2: Spermatogenesis, subchapter 2.3.1), (8) maintain stem cell homeostasis. From França et al. 2016, based on Hess and Vogl 2015.*

2 STAGES OF SPERMATOGENESIS

Spermatogenesis is a highly complex and well-coordinated process. It occurs in a continuous manner throughout the reproductive lifetime and leads to the production of millions of spermatozoa per day. This process is regulated through the interplay of hormones and tight interactions between germ cells and supporting somatic cells (Griswold 2016).

Spermatogenesis occurs in three phases: the multiplication phase, meiosis, and spermiogenesis (Figure 24). It is estimated to last approximately 74 days in humans (Heller and Clermont 1964) and 34.5 days in mice (Oakberg 1956b).

The multiplication phase includes multiple divisions and differentiation of spermatogonial stem cells that give rise to primary spermatocytes committed to meiosis. Diploid spermatocytes undergo two meiotic divisions, with no intervening DNA synthesis, and produce haploid round spermatids. During spermiogenesis, round spermatids undergo important cytological and morphological changes including chromatin condensation, nuclear shaping, and the formation of the acrosome and the sperm tail, leading to the formation of testicular spermatozoa that are released into the lumen of seminiferous tubules.

2.1 THE MULTIPLICATION PHASE

Spermatogonia are located on the periphery of the seminiferous epithelium and adhere to the basement membrane. Stem cells are very rare cells and represent only 0.03% of all male germ cells in the mouse (Tagelenbosch and de Rooij 1993). More spermatogonial subtypes are present in mice than in humans (Boitani et al. 2016). The different populations in both species can be distinguished based on their size and morphology, molecular markers and specific gene expression profiles (von Kopylow and Spiess 2017; T. Zhang et al. 2014; Boitani et al. 2016).

Spermatogonial stem cells (A_S) regularly divide and either self-renew by mitosis to maintain a stem cell population or begin the differentiation pathway to eventually produce spermatozoa (Figure 24). In mice, a division of the A_S can give rise to two A_S or to a pair of spermatogonia (A_{paired}) that stay interconnected by an intracytoplasmic bridge. Intercellular bridges result from incomplete cytokinesis and allow "cytoplasmic sharing" of signalling molecules. Intercellular bridges are formed in all subsequent divisions and persist between cells from the same generation (Niedenberger et al. 2018; Greenbaum et al. 2011). These cells divide by mitosis to produce a long chain of 8 or 16 spermatogonia ($A_{aligned}$). One A_S will produce 16 $A_{aligned}$ spermatogonia. The A_S, A_{paired}, and $A_{aligned}$ represent a pool of "undifferentiated spermatogonia".

The $A_{aligned}$ spermatogonia can differentiate into A_1 spermatogonia that represent the "differentiating spermatogonia." They subsequently divided by mitosis several times to produce type B spermatogonia (A_1 -> A_2 -> A_3 -> A_4 -> Intermediate spermatogonia -> B).

In humans and monkeys, there are three distinct populations of spermatogonia: dark type A (A_{dark}), pale type A (A_{pale}), and type B. Type A spermatogonia are believed to be the counterpart of mouse undifferentiated spermatogonia. A_{dark} and some of the A_{pale} spermatogonia appear to be the stem

cell population at different stages of the cell cycle. They undergo 1-2 amplifying divisions before they differentiate into type B spermatogonia, which represent the "differentiated spermatogonia".

Type B spermatogonia in both species are committed to enter meiosis. They divide to produce primary spermatocytes that undergo DNA duplication and enter meiosis (Fayomi and Orwig 2018; Boitani et al. 2016).

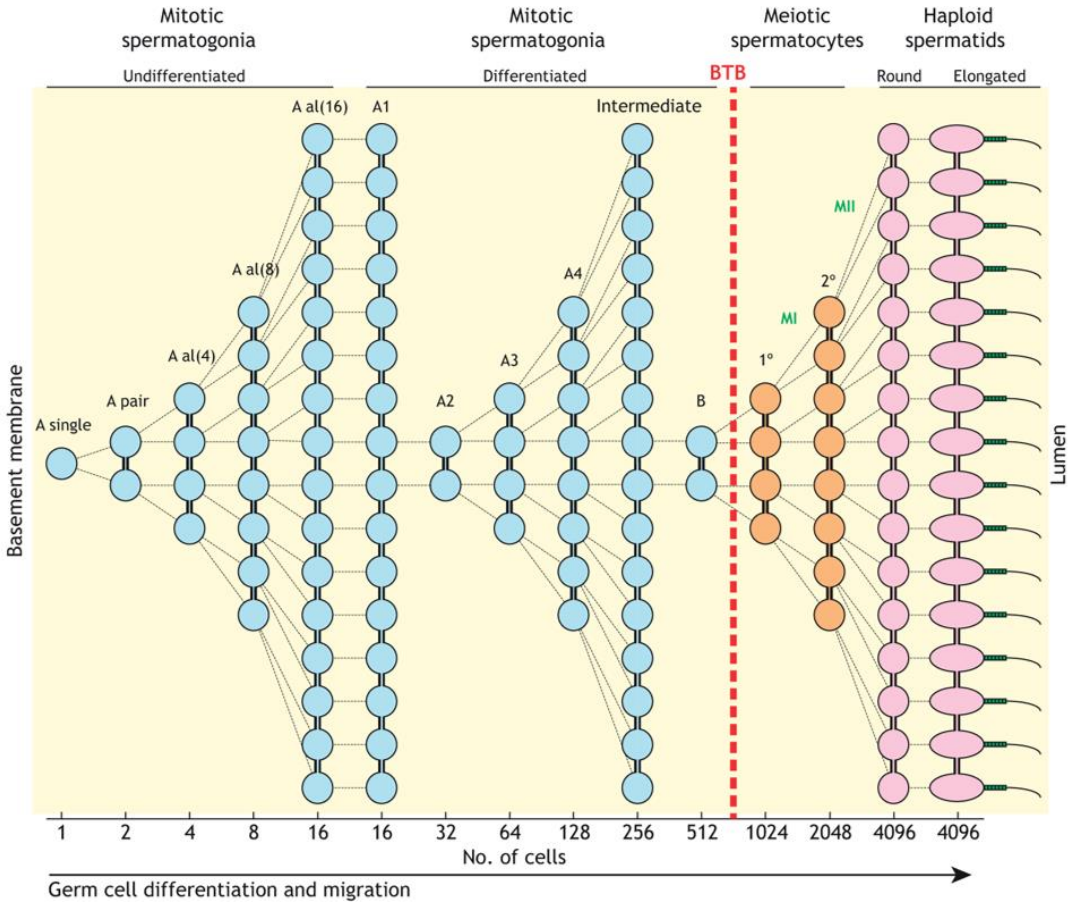

Figure 24: Schematic illustration of mouse spermatogenesis. *One A_1 spermatogonium can give rise to up to 128 spermatozoa. Abbreviations: blood-testis barrier (BTB). From Varuzhanyan and Chan 2020.*

2.2 MEIOSIS OR MATURATION PHASE

The meiosis phase is also known as the maturation phase. Meiosis I is "reductive" and is characterized by the separation of homologous chromosome pairs. It begins with an extended prophase I that can be divided into 5 phases: leptotene, zygotene, pachytene, diplotene, and diakinesis. Chromatin begins to condense (leptotene), homologous chromosomes start to

physically pair along their length and a synapsis forms (zygotene). Homologous chromosomes remain connected due to a proteinaceous structure called the "synaptonemal complex" (Figure 25).

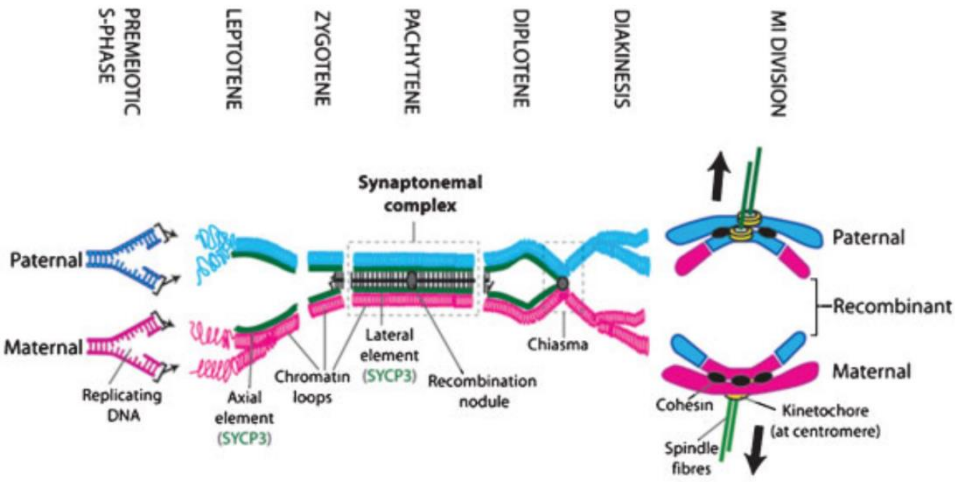

Figure 25: Schematic illustration of the assembly and dissociation of the synaptonemal complex in prophase I of meiosis I. *The DNA has been duplicated during pre-meiotic S-phase and each chromosome consists of two sister chromatids. A conserved scaffold called the axial element assembles between sister chromatids, organizes chromatin into linear arrays of loops and recruits the recombination machinery (leptotene). Axial elements of homologous chromosomes pair to form the lateral elements of the synaptonemal complex (zygotene). Autosomal homologous chromosomes have fully synapsed (pachytene), and the recombination machinery allows the formation of crossovers. Chiasmata constitute DNA links between the homologues where DNA recombined. The synaptonemal complex disassembles and axial elements separate (diplotene). The disassembly is immediately followed by DNA condensation and first meiotic division. From Burgoyne, Mahadevaiah, and Turner 2007.*

The synapsis enables recombination between non-sister chromatids of homologous chromosomes that occurs during the pachytene stage. The synaptonemal complex begins to disassemble during the diplotene stage and is completely lost in diakinesis. Homologous chromosomes only remain connected at chiasmata, locations where recombination occurred. These connections remain until metaphase I to ensure that homologs remain paired. The meiotic spindle begins to form during diakinesis, primary spermatocytes divide and give rise to secondary spermatocytes that can enter meiosis II. Meiosis II is "equational" and leads to the separation of sister chromatids to produce haploid spermatids (Cohen, Pollack, and Pollard 2006; Handel and Schimenti 2010; Jan et al. 2012; Bolcun-Filas and Handel 2018).

2.3 SPERMIOGENESIS

Spermiogenesis is the differentiation phase of spermatogenesis, and no cell division occurs in this phase. Round spermatids undergo complex cytodifferentiation including an elongation and flattening of the sperm head, chromatin condensation due to the histone-protamine exchange, and the assembly of the flagellum.

2.3.1 The cycle of the seminiferous epithelium and stages of spermiogenesis

The organization of the seminiferous epithelium slightly varies between humans and mice. Here, we will focus on the description in the mouse that will serve for the comprehension of the thesis.

The seminiferous epithelium is well-organized in time and space and undergoes a repetitious series of changes. Cross-sections of seminiferous tubules revealed that germ cells at specific stages of development are always found together. These groupings are called "cellular associations" (Oakberg 1956a). This is because the kinetic of spermatogenesis is very precise and spermatogenic stem cells divide in regular intervals (Clermont 1972). The number of cellular associations is limited but contains all the stages of spermatogenesis. One "cycle of the seminiferous epithelium" represents one cycle of spermatogenesis, from spermatogonia to testicular spermatozoa, that occurs over time in a given point of the tubule (Leblond and Clermont 1952). In the mouse, one cycle lasts 8.6 days and spermatogenesis requires 4 cycles to complete, therefore the length of spermatogenesis was estimated at 34.5 days (Oakberg 1956b) (Figure 26) (Sugimoto, Nabeshima, and Yoshida 2012).

In the mouse, Oakberg identified 12 distinct cellular associations that are referred to as stages. The 12 stages correspond to one cycle of the seminiferous epithelium (Oakberg 1956a). Based on morphological changes, however, spermiogenesis can be divided into 16 steps. Stages are denoted by Roman numerals (I-XII) while steps use Arabic numerals (1-16). The completion of spermatogenesis is longer than the 12 stages. The first 12 steps of spermatid development follow the 12 stages of spermiogenesis and then step 13 continues into stage I. Spermiogenesis is completed at step 16 and stage VIII of the following cycle. Hence, stages I-VIII contain two generations of spermatids in different stages of differentiation (Figure 27).

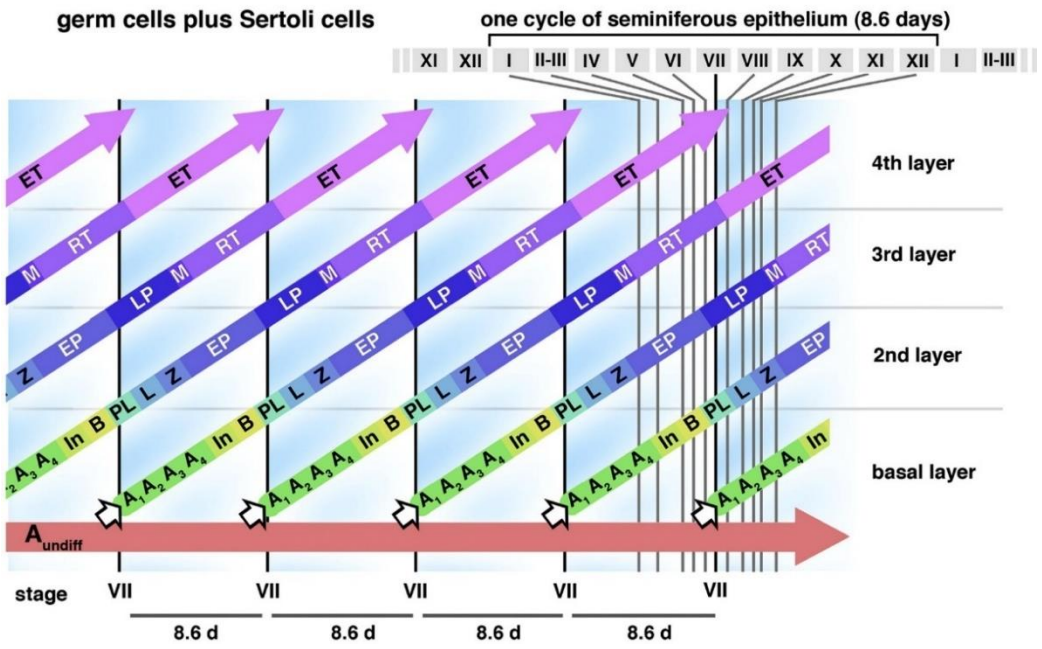

Figure 26: Schematic representation of the cycle of the seminiferous epithelium in the mouse. *Abbreviations: spermatogonia (A1–A4, Intermediate (In), type B), primary spermatocytes (preleptotene (PL), leptotene (L), zygotene (Z), early pachytene (EP), late pachytene (LP), diplotene (D)), meiotic divisions and secondary spermatocytes (M), round spermatids (RT) and elongated spermatids (ET). From Sugimoto, Nabeshima, and Yoshida 2012.*

The stages and steps of spermiogenesis can be primarily distinguished based on the spreading of the spermatid acrosome and based on the types of cells (cellular associations) that are present, their localization and orientation within the tubule (Oakberg 1956a; L.D. Russell et al. 1990; Ahmed and de Rooij 2009; Meistrich and Hess 2013). A useful binary decisional tree to distinguish different stages was published by Meistrich & Hess (Meistrich and Hess 2013) and Nakata *et al.* described the different stages using fluorescence microscopy as well as histochemistry (Nakata et al. 2015).

Based on the development of the acrosome, we can distinguish: the initiation or Golgi phase (steps 1-3), cap phase (steps 4-7), acrosomal phase (steps 8-12), and maturation phase (steps 13-16).

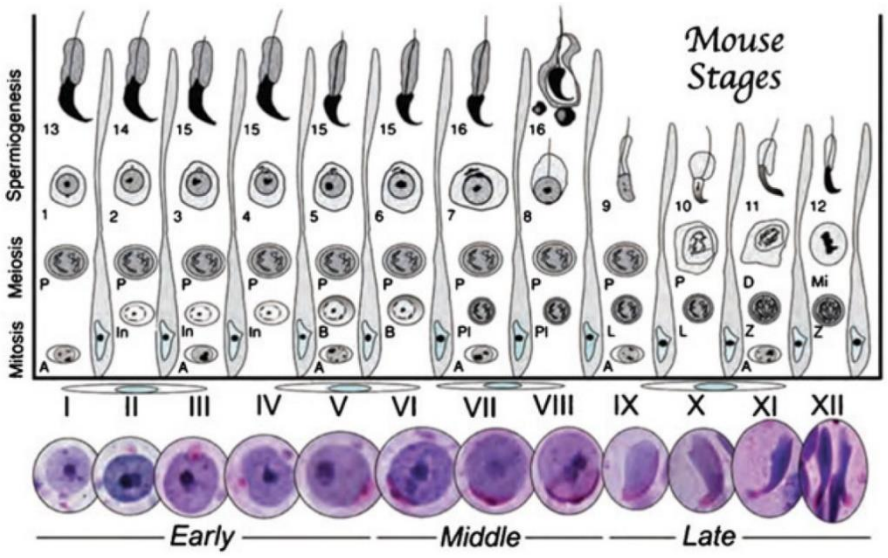

Figure 27: Spermatogenesis stages in mouse development. *The distribution of 16 steps of spermiogenesis during 12 stages of spermatogenesis. From Meistrich and Hess 2013.*

2.3.2 The initiation or Golgi phase

The initiation/ Golgi phase (steps 1-3, stages I-III) is characterized by the formation of the acrosomal vesicle (Figure 28). Newly formed step 1 spermatids are round, 30-40% smaller than secondary spermatocytes, and their nucleus is less condensed and positioned in the center of the cell. The Golgi apparatus is positioned close to the nucleus. Small proacrosomal vesicles derived from the *trans*-Golgi compartment and from the endocytic pathway accumulate near the nuclear membrane. These vesicles contain "granules" composed of acrosomal proteins. The proacrosomal vesicles fuse together and their granular contents accumulates (step 2). A single, large acrosomal vesicle forms, comes in contact with the nucleus and becomes embedded into an indentation in the nuclear envelope (step 3). The acrosomal vesicle remains rounded.

Correct orientation of the Golgi apparatus towards the developing acrosome is essential for acrosome formation and requires an intact microtubule network (Elkis et al. 2015; Moreno, Palomino, and Schatten 2006). Vesicle transport from the Golgi to the acrosome is mediated along microtubule and F-actin tracks (A.L. Kierszenbaum, Rivkin, and Tres 2003).

In step 1 spermatids, a pair of centrioles migrates to the periphery of the cell and an axoneme begins to form from the distal centriole.

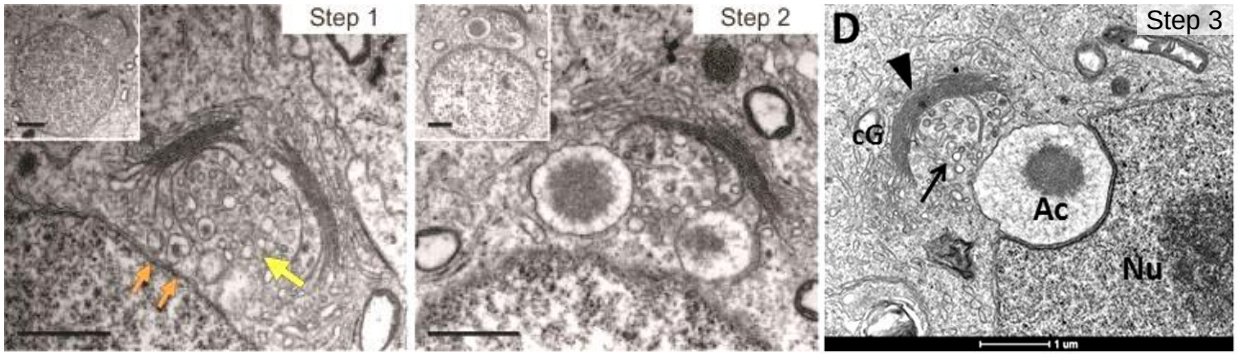

Figure 28: The initiation/ Golgi phase in mouse spermatids showing the formation of the proacrosomal vesicle and its attachment to the nuclear envelope. *In step 1 spermatid, the yellow arrow shows pro-acrosomal vesicles containing pro-acrosomal granules, and their adherence location, the acroplaxome, is shown by orange arrows. Abbreviations: nucleus (Nu), cis-Golgi (cG), acrosome (Ac). Scale bar = 1 µm. Step 1-2 are from Pleuger et al. 2020 and step 3 is from Elkis et al. 2015.*

2.3.3 The cap phase

During the cap phase (steps 4-7, stages IV-VII), the acrosomal vesicle continues to incorporate more proacrosomal vesicles and begins to flatten over the nucleus (Figure 29). The acrosomal granule within the vesicle moves toward the nucleus and contacts the inner acrosomal membrane in the center of the acrosome (step 4). The vesicle flattens (step 5) and gradually begins to spread over the nucleus to form a cap. It covers 1/3rd of the nucleus (step 6), then spreads further to cover up to 1/2 of the nucleus (step 7).

The developing acrosome is anchored to the nucleus through a cytoskeletal attachment plate called the acroplaxome. It is believed to secure the acrosome in place during spermatid elongation and facilitate its spreading over the nucleus. Proacrosomal vesicles adhere to the acroplaxome during acrosome biogenesis. The acroplaxome is particularly composed of F-actin and keratin 5. Keratin 5 is present in the inner acrosomal membrane and interacts with intermediate filaments in the nuclear envelope. The structure is present in mouse, rat, and human spermatids (Abraham L. Kierszenbaum, Rivkin, and Tres 2003; Abraham L. Kierszenbaum and Tres 2004). The acroplaxome also participates in the docking of the acrosomal granule in the center of the acrosome which is important for the symmetrical development of the acrosome (Zakrzewski et al. 2020).

In step 5 spermatids, the centriole pair with an attached axoneme migrate from the periphery to the caudal nuclear pole and begin to assemble the connecting piece.

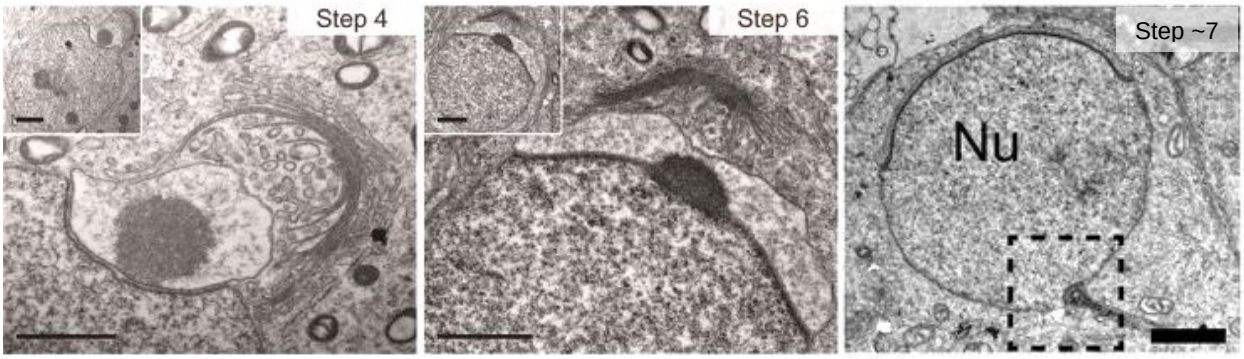

Figure 29: The cap phase showing a growth of the proacrosomal vesicle and its spreading over the spermatid nucleus. *Nucleus (Nu). Scale bar = 1 µm in steps 4 & 6, = 5 µm in step 7-8. Images of step 4, 6 spermatids are from Pleuger et al. 2020 and step 7 from Shang et al. 2017.*

2.3.4 The acrosomal phase

The acrosomal phase (step 8-12, stages VIII-XII) is characterized by the elongation and shaping of the nucleus (Figure 30). Until this moment, the nucleus was positioned in the center of the cell. In step 8, the nucleus with the acrosome make contact with the cell plasma membrane and the spermatid reorients with the acrosome facing the basement membrane of the seminiferous tubule. The Golgi apparatus, that was previously positioned close to the developing acrosome, has moved to the caudal pole of the cell. The acrosome spreads and covers 1/3rd of the nucleus. The manchette, a transient microtubule-based structure forms in step 8 spermatids. It is anchored in the perinuclear ring and surrounds the posterior 2/3^{rds} of the nucleus. The role of the manchette in spermatid elongation and head-shaping, and in protein trafficking will be discussed below and in *Chapter 8: Nuclear remodelling and intramanchette transport*. The nucleus slightly loses its round symmetry and begins to elongate.

During the following steps (step 9-15), the nucleus continues to elongate and flatten, and slowly takes on the slender, hooked form with a dominant apex of a mature spermatozoon (Figure 30). The acrosome spreads over the rounded dorsal surface of the elongating spermatid. The manchette descends the nucleus in a zipper-like manner (step 8-13) and is surrounded on both sides by flattened cisterns of the endoplasmic reticulum.

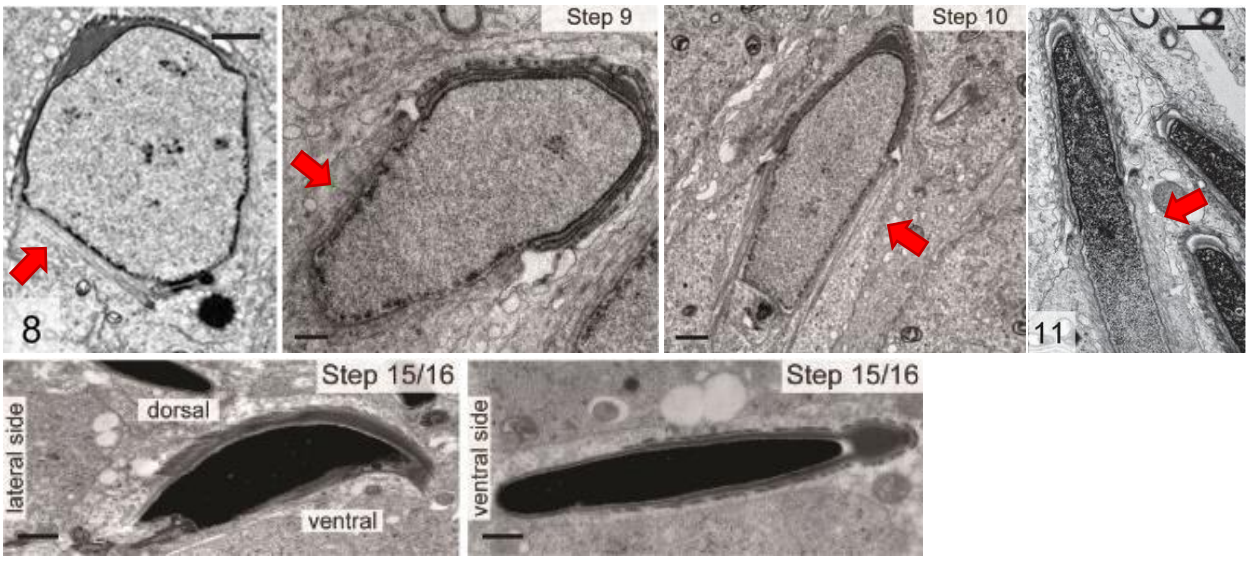

Figure 30: The acrosomal phase in the mouse. *Green arrows show the position of the manchette. Scale bar = 1 µm. The step 8 spermatid has already assembled a manchette. Nuclear condensation in the ~11 step spermatid has begun and continues from the tip of the head towards the flagellum. Step 8 and 11 spermatids are from Crapster et al. 2020 and other images were adapted from Pleuger et al. 2020.*

The histone-to-protamine exchange is believed to start at step 10, the histones disappear by step 12, and transition proteins are replaced by protamines by step 15 (Rathke et al. 2014).

The annulus begins to form as an accumulation of dense material that encircles the junction between the distal centriole and the axoneme. The exact timing of annulus formation is not clear, however it is usually first described at the moment when the PC has already docked to the nucleus (~ step 5-9) (Dooher and Bennett 1973; Fawcett, Eddy, and Phillips 1970). An annulus protein septin SEPT4, that is present at the annulus in mature spermatozoa, appears at the neck region at step 9 spermatids (Guan, Kinoshita, and Yuan 2009).

2.3.5 The maturation phase

During the maturation phase (step 12 or 13-16, stages XII-VIII), nuclear condensation takes place in a gradual manner (step 12-14), the manchette disassembles (step 13-14), and the nucleus of the elongated spermatid reaches the appearance of a mature spermatozoon (step 14-15) (Figure 30, Figure 31). The annulus migrates caudally (step 15), and mitochondria, scattered in the cytoplasm, arrange in a helical manner along the axoneme to form the sperm midpiece (step 15) (Figure 31, Figure 32).

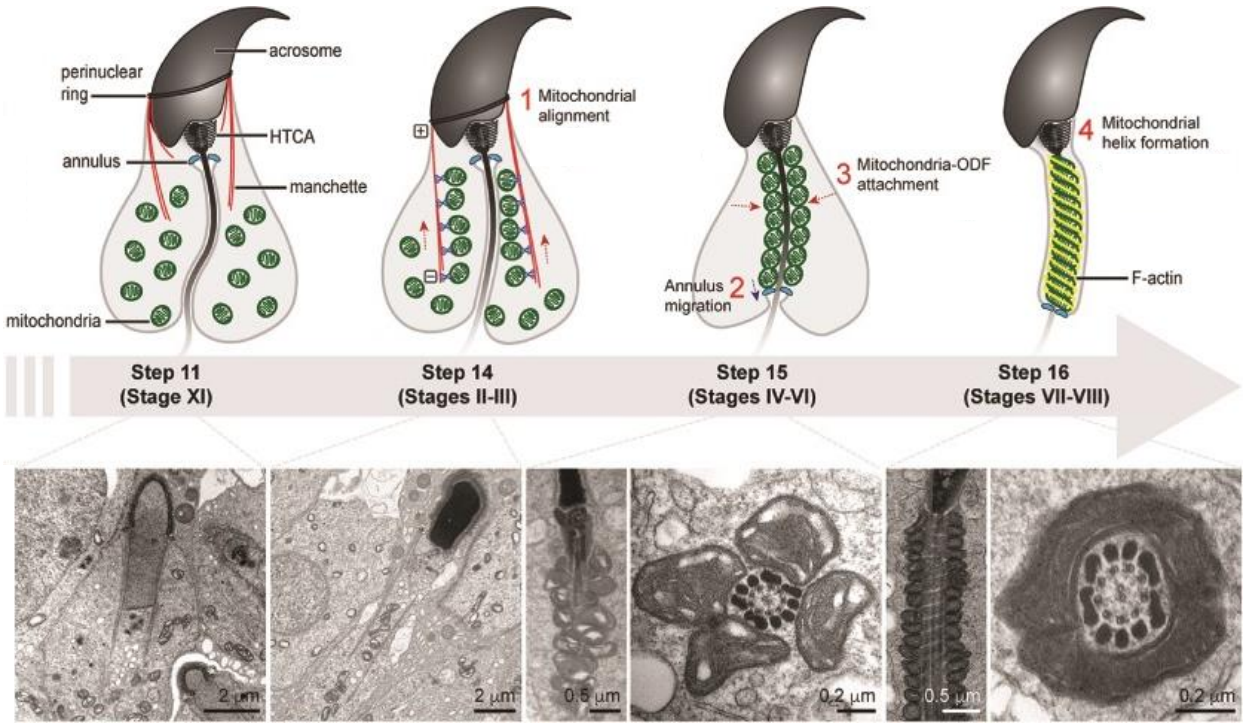

Figure 31: A proposed model for spermatid elongation and the assembly of the mitochondrial sheath. *See text for explanation. Adapted from Pleuger et al. 2020.*

Formation of the mitochondrial sheath is not fully understood. Mitochondria need to be transported from the cytoplasm to the spermatid flagellum and then restructured and arranged into a left-handed helix around the ODFs (Figure 31, Figure 32) (Otani et al. 1988; Ho and Wey 2007). The relocation of mitochondria might be mediated along manchette MTs *via* the plus-end-directed motor KLC3 (Pleuger et al. 2020; Dunleavy et al. 2019). The kinesin light chain 3 (KLC3) is highly expressed during this phase of spermiogenesis and has been shown to interact with ODFs and with mitochondria either directly or *via* an adapter. Similar to dynein, conventional kinesin is a homodimer and consists of two heavy chains and two light chains. Each heavy chain contains a motor domain and a MT-binding domain at the head, a coiled-coil stalk, and a cargo-binding domain at the C-terminal tail. The light chain interacts with the heavy chains near the C-terminus (Woehlke and Schliwa 2000). At the cell periphery, mitochondria are associated with dynein and kinesin (Figure 31, step 11). KLC3 is thought to disrupt their interaction with kinesin that could lead to a dynein-mediated movement of mitochondria towards the flagellum (step 14). At the midpiece, KLC3 associated with mitochondria could mediate their interaction with ODFs (Ying Zhang et al. 2012). Consistent with the hypothesis that mitochondrial migration is mediated along

manchette MTs is the fact that defects in the manchette are also associated with a disorganized mitochondrial sheath (Dunleavy et al. 2019; Pleuger et al. 2020). In mice, F-actin forms a double helix in the midpiece that accompanies mitochondria (Gervasi et al. 2018). The local arrangement of mitochondria into the helix might be mediated by myosin, an actin motor protein, along actin tracks. Myosin was shown to interact with mitochondria in somatic and male germ cells in non-mammalian species (Y.-R. Li and Yang 2016).

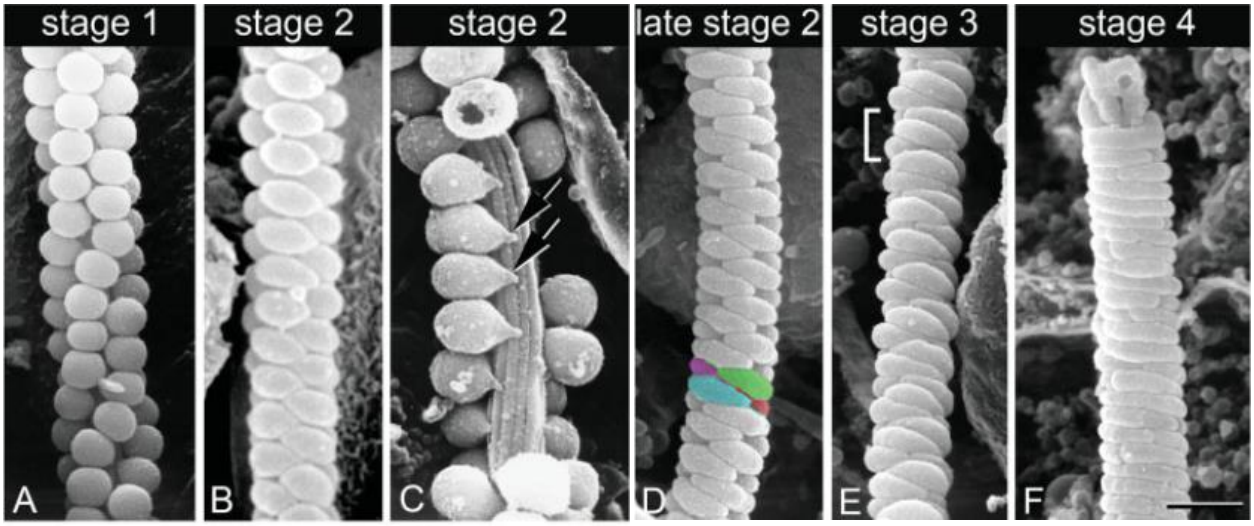

Figure 32: Assembly of the mitochondrial sheath during step 15 in mouse spermiogenesis. *The assembly can be divided into 4 stages. At stage 1 (A), spherical mitochondria are regularly attached around the ODFs of the midpiece and form four dextral longitudinal arrays. At stage 2 (B-D), mitochondria laterally elongate along the ODFs. Mitochondrial pairs from opposing arrays connect and form a ring-like structure. (C) Arrows show the attachment point of elongating mitochondria to the ODFs. Some mitochondria were lost during sample preparation, leaving empty gaps. At stage 3 (E), mitochondria continue to elongate and slide past each other at the contact points, forming a double helical structure. At stage 4 (F), mitochondria become rod-shaped and join end-to-end. Scale bar = 1 µm. From Ho and Wey 2007.*

Finally, at the end of the maturation phase, mature elongated spermatids can be released into the lumen of seminiferous tubules *via* spermiation (step 16).

The descriptions were based on mouse histological observations of Oakberg and Fawcett, electron microscopy by Dooher & Bennett and excellent electron microscopy pictures and a comprehensive review by Russel *et al.* (Oakberg 1956a; Fawcett, Eddy, and Phillips 1970; Fawcett and Phillips 1969; Dooher and Bennett 1973; L.D. Russell et al. 1990).

3 THE FIRST WAVE OF SPERMATOGENESIS

The first round of spermatogenesis is termed the "first wave" and leads to the formation of the first generation of spermatozoa from spermatogonia. In the mouse, it starts early after birth (Figure 33) (Ibtisham et al. 2017). By postnatal day 6, the seminiferous epithelium only contains two types of cells: Sertoli cells and primitive type A spermatogonia. Type A and B spermatogonia are present on postnatal day 8, preleptotene spermatocytes appear on day 8, leptotene spermatocytes on day 10, and zygotene spermatocytes are first observed on day 12. Primary spermatocytes differentiate into early pachytene stage by day 14 and reach the late pachytene stage on day 18. The onset of spermiogenesis and the appearance of round spermatids occurs on days 20-21. Spermatid elongation continues until postnatal days 30-35 when testicular spermatozoa can be observed (Bellve et al. 1977). This study was done on CD-1 mice. Others, based on B6C3F$_1$/J mice, mention the appearance of round spermatids already at day 18 and elongated spermatids at day 30 (Janca, Jost, and Evenson 1986).

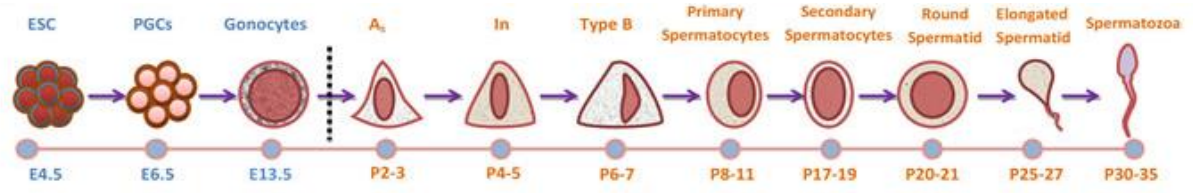

Figure 33: Developmental timeline of male germ cells in the mouse. *Successful fertilization leads to the formation of a zygote that develops into a blastocyst containing embryonic stem cells (ESC) in the inner cell mass. Primordial germ cells (PGCs) appear shortly before gastrulation, migrate to the fetal gonad where they differentiate into prospermatogonia/ gonocytes and become arrested in seminiferous tubules until after birth. Gonocytes undergo spermatogenesis and give rise to spermatozoa at puberty. From Ibtisham et al. 2017.*

4 DEVELOPMENT OF THE CONNECTING PIECE

Development of the connecting piece, flagellum assembly and head-shaping are interlinked processes that will be described below. Overall, the description of the developing connecting piece is primarily based on the observations of Fawcett and Phillips in spermatids of various rodent species, including the mouse (Fawcett and Phillips 1969). The authors made similar observations between the different species and the above text should also apply to the development of mouse spermatids.

4.1 CENTRIOLE DEVELOPMENT

Until the round spermatid stage, germ cells have somatic-like centrioles composed of a mother (distal) and a daughter (proximal) centriole surrounded by pericentriolar material. The structure and function of centrioles is also discussed in *Chapter 3: Microtubules and associated structures, subchapter 6: Microtubule-based structures*. Centrioles in these germ cells participate in mitotic and meiotic cell division (Avidor-Reiss and Fishman 2019). A recent study showed for the first time, that the mother centriole can also form primary cilia in mouse meiotic cells, in late leptotene to zygotene spermatocytes. A group of interconnected spermatocytes were shown to share a single primary cilium. The authors hypothesized that spermatocytes within one group share signalling and sensory information from the environment. Primary cilia were not observed in later stages of meiosis (López-Jiménez et al. 2022).

In early spermatids (step 1), the centriole pair transforms into a basal body. The centriole pair migrates from the Golgi region to the periphery of the cell where the distal centriole (DC) orients perpendicularly to the cell membrane, docks, and a simple (9+2) axoneme starts to assemble from the DC. The exact mechanism driving the attachment of the DC to the plasma membrane in spermatids is unknown. Since the flagellum is a modified motile cilium, this process might be similar to ciliogenesis. Mammalian spermatids are believed to use the extracellular pathway of ciliogenesis where the distal centriole docks directly to the plasma membrane, instead of a ciliary vesicle in the cytoplasm (intracellular pathway) (Figure 34) (Avidor-Reiss, Ha, and Basiri 2017; Sorokin 1962; Labat-de-Hoz et al. 2021a). The distal (mother), but not the proximal (daughter) centriole, has distal and subdistal appendages that are essential for cilia formation and function. More details about centriole structure can be found in *Chapter 3: Microtubules and related*

structures, subchapter 6: Microtubule-based structures. Distal appendages are important for anchoring ciliary vesicles in the intracellular pathway (N. A. Hall and Hehnly 2021), docking to the plasma membrane (Tanos et al. 2013), and they are also the assembly points for the recruitment of IFT trains (Deane et al. 2001), while subdistal appendages anchor microtubules and position centrioles and cilia within the cell (Delgehyr, Sillibourne, and Bornens 2005; Mazo et al. 2016; Tateishi et al. 2013).

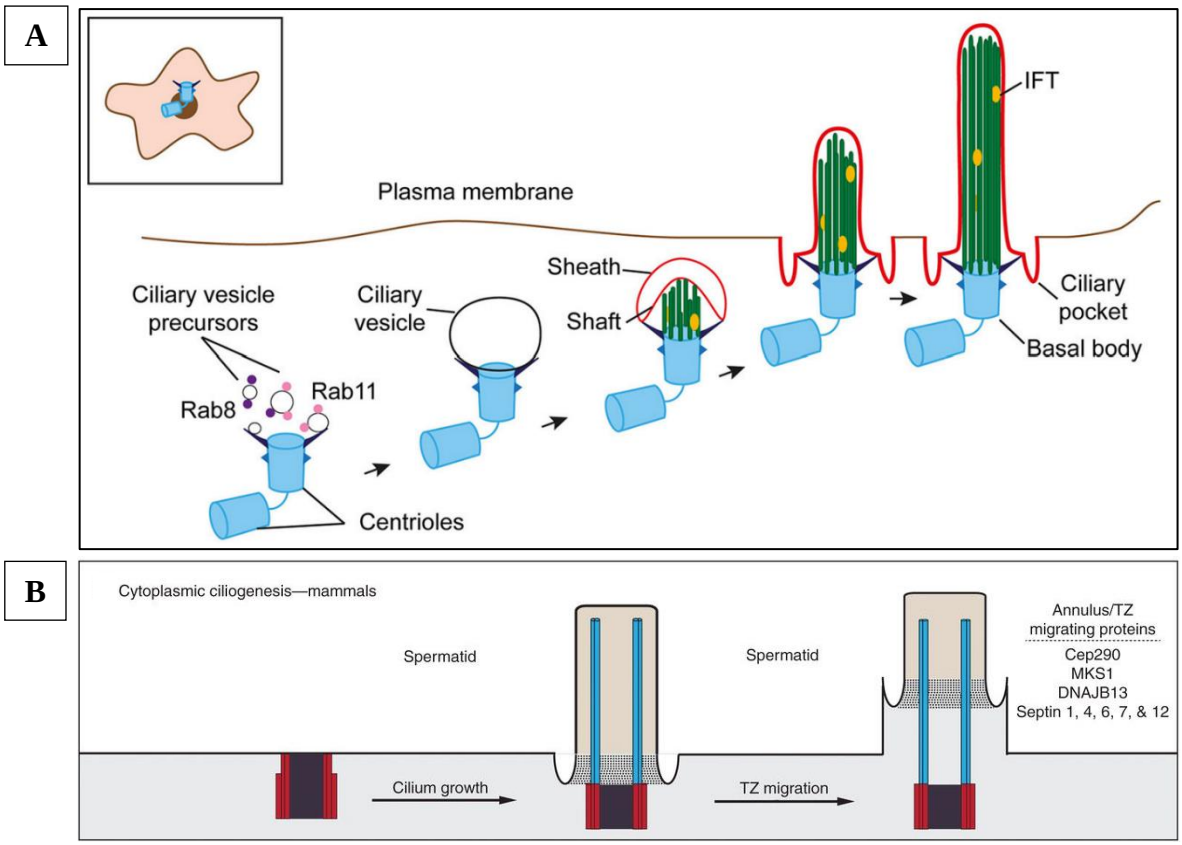

Figure 34: Model of mammalian ciliogenesis. *(A) During the intracellular route of primary ciliogenesis, small vesicles fuse to form a large ciliary vesicle at distal appendages of the mother centriole. An axoneme begins to form intracellularly and deforms the ciliary vesicle to create an inner membrane (shaft) and an outer membrane (sheath). The growing cilium becomes exposed in the plasma membrane. The sheath forms the ciliary pocket and the shaft gives rise to the ciliary membrane. (B) In mammalian spermatids, the axoneme fully forms within a compartmentalized cilium. A part of the axoneme that will become the midpiece becomes exposed to the cytoplasm as the annulus and the transition zone migrate along the axoneme. Proteins involved in this process are indicated. (A) from Avidor-Reiss, Ha, and Basiri 2017, (B) from Labat-de-Hoz et al. 2021a.*

Following the anchoring to the plasma membrane, possibly *via* distal appendages, the axoneme develops in a compartment separated from the rest of the cytoplasm by a specialized gatekeeping

complex called the "transition zone" (Avidor-Reiss, Ha, and Basiri 2017). In cilia, the transition zone forms a membrane diffusion barrier that selectively regulates the movement of proteins between the cytoplasm and the ciliary compartment (Takao et al. 2017; Nachury 2018; Park and Leroux 2022). In male germ cells, the transition zone is synonymous with the annulus (Kwitny, Klaus, and Hunnicutt 2010; Avidor-Reiss, Ha, and Basiri 2017).

First morphological changes in centrioles start to occur when the centriole pair is still at the periphery of the cell (Figure 35). A thin density starts to appear parallel to the long edge of the proximal centriole, and this site will become the future anchoring point of the centriole pair to the nucleus. One of the striated columns begins to form between the end of the proximal and parallel to the distal centriole. Later, in step 5 spermatids, the centriole pair with the membrane-bound axoneme starts to migrate toward the nucleus, invaginates the cell and the PC anchors to the caudal pole of the nucleus, forming the implantation fossa. The nuclear envelop locally indents and thickens to form the basal plate.

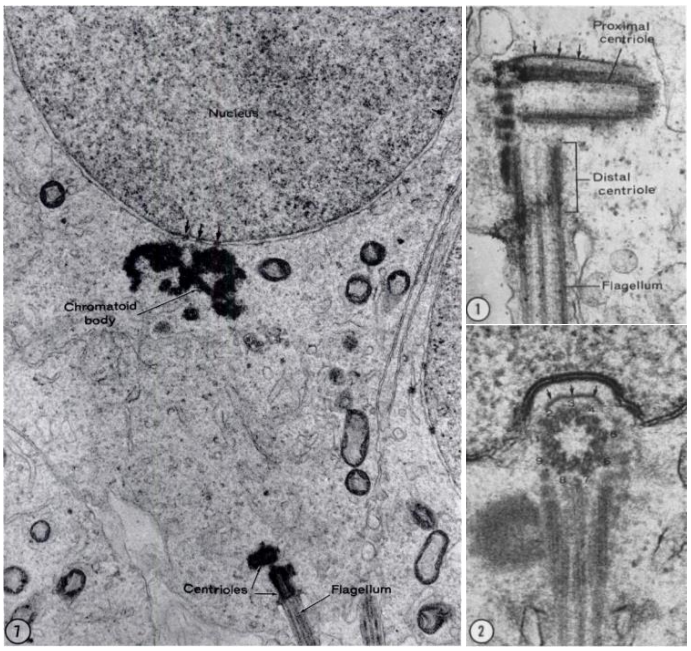

Figure 35: Migration and maturation of the centriole pair. *A flagellum has formed from the distal centriole at the periphery of the cell and the centriole pair hasn't migrated to the nucleus yet (left, right top). The centriole begins its transformation into the HTCA at the cell periphery (right, top). The centriole pair has migrated and became anchored to the nucleus (right, bottom). Arrows show an accumulation of a thin density that will likely participate in the centriole-nucleus connection (right). The images on the right are from chinchilla spermatids. The image on the left is from Fawcett, Eddy, and Phillips 1970 and images on the right are from Fawcett and Phillips 1969.*

As the spermatid continues to differentiate, the proximal centriole starts to progressively increase in length to form the centriolar adjunct (Figure 36). This structure disappears abruptly and completely in late stages of spermiogenesis. The adjunct has a similar structure to centrioles as it is composed of nine triplets of microtubules, however MTs are closer together and the walls of the B- and C-tubules do not fuse with the walls of the following subunits. The tip of the adjunct is

capped with fibrous material and was suggested to form a MT aster in mouse spermatids (Manandhar et al. 1998; 1999). The role of the adjunct is unknown. A MT array appears to emanate from the centriolar adjunct during spermatid elongation, suggesting its possible involvement in manchette nucleation (Manandhar et al. 1998; M S Lehti and Sironen 2016). Another study suggested that, based on its position relative to the nucleus, it might regulate the flattening direction of the spermatid head (Kojima 1994). In humans, only a fraction of mature spermatozoa retains the centriolar adjunct and its presence is more prevalent in men with idiopathic infertility than in fertile men (Garanina et al. 2019).

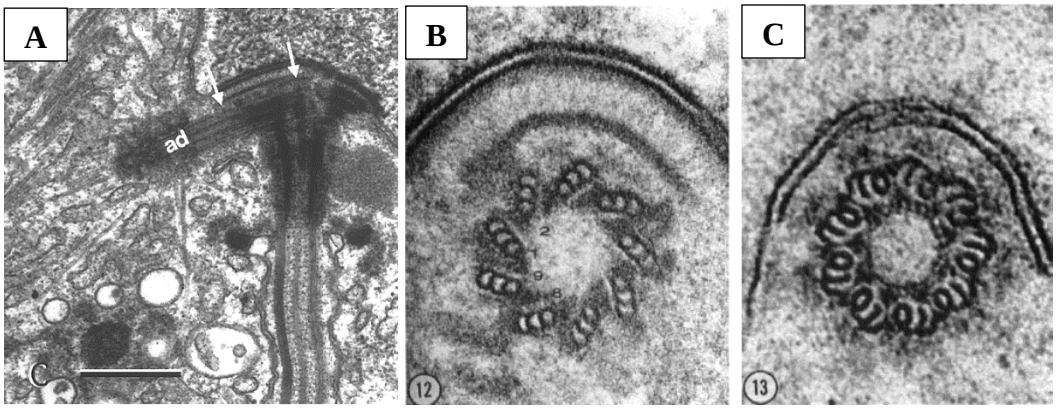

Figure 36: The centriolar adjunct forms from the proximal centriole in an elongating spermatid. *A cross-section of the proximal centriole (B) and the adjunct (C) shows differences in the shape of microtubule triplets. (A) Material accumulates at the end of the centriolar adjunct. Microtubules appear to emanate from the adjunct. (A) from the mouse, (B) from a Chinese hamster spermatid and (C) from a chinchilla spermatid. (A) from Manandhar et al. 1998, (B) and (C) from Fawcett and Phillips 1969.*

During nuclear condensation, both centrioles begin to organize material that is necessary for the formation of a mature HTCA (Figure 37). Dense material starts to accumulate between MT triplets in the wall of the proximal centriole. The material extends outward in different directions to form the future capitulum and striated columns. As the spermatid reaches maturity, a large amount of material accumulates beneath the capitulum. The proximal centriole becomes completely embedded in this material until the centriolar structure becomes hardly identifiable. Moreover, a mass of granular material also accumulates next to the distal centriole throughout HTCA formation. The origin of the material accumulating in centrioles is unknown. The distal centriole also undergoes profound morphological changes during chromatin condensation. Dense material begins to accumulate between the triplets of the distal centriole and gradually increases the spaces between them. The walls of the distal centrioles are no longer parallel but bow outward and the

centriole widens. The matrix gradually extends from the distal centriole and forms the distal portions of the striated columns. Moreover, the central MT pair extends through the cavity of the distal centriole and contacts the wall of the proximal centriole. Due to the separation of the microtubule triplets, the distal centriole loses its structural identity and becomes unrecognizable in mature mouse spermatids (Figure 20).

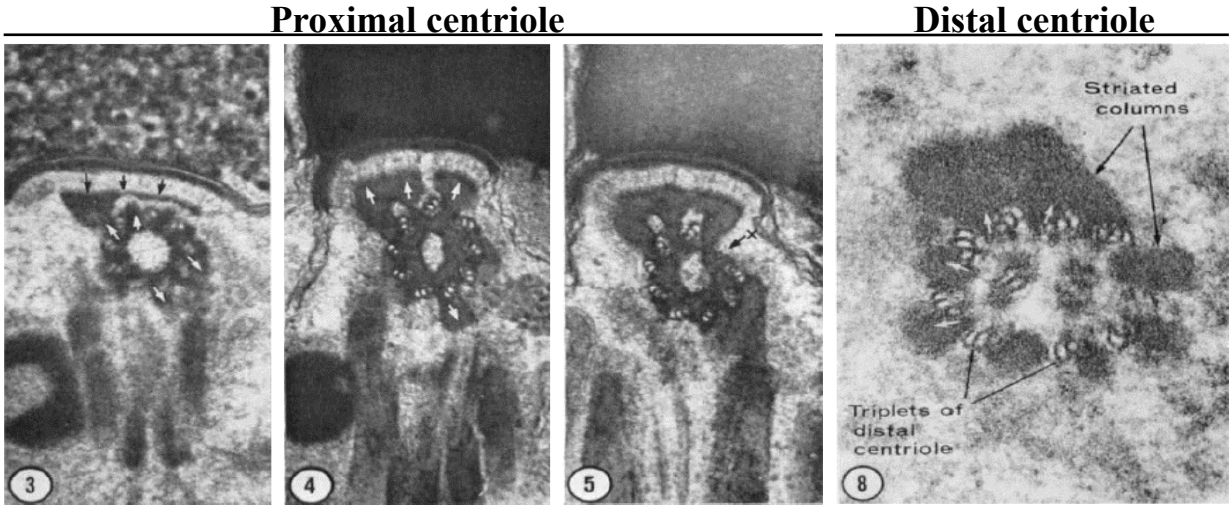

Figure 37: Accumulation of dense material between microtubule triplets of the proximal and distal centrioles. *Images of the proximal centriole show the direction of the incoming material, that will give rise to the capitulum and striated columns. Images of the proximal centriole are from chinchilla spermatids, the distal centriole from a Chinese hamster. From Fawcett and Phillips 1969.*

4.2 ANNULUS DEVELOPMENT

The annulus migrates from the centriole region to the junction between the midpiece and the principal piece (step 15). During this process, a part of the axoneme is exposed to the spermatid cytoplasm. Spherical mitochondria, that were previously distributed in the cytoplasm, start to alight around the axoneme, and progressively change their shape during mitochondrial compaction to form a tight helical conformation, as was discussed previously in *Chapter 2: Spermatogenesis, subchapter 2.3.5 The maturation phase* (Figure 39, Figure 32).

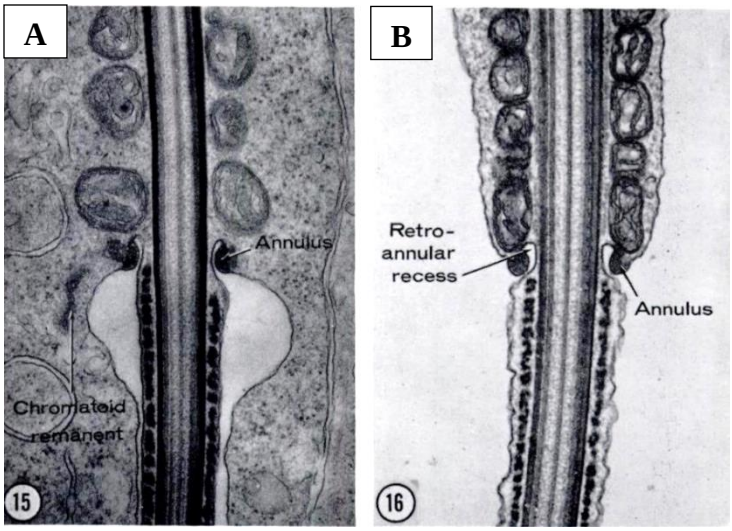

Figure 38: Junctional region between the midpiece and the principal piece during the last stages of spermatid elongation in chinchilla. *The annulus has migrated from the HTCA region to the junction with the principal piece. Mitochondria are starting to assemble along the axoneme (step 15), and cytoplasm has been reduced by Sertoli cells in a more mature spermatid (step 16). From Fawcett, Eddy, and Phillips 1970.*

4.3 DEVELOPMENT OF PERI-AXONEMAL STRUCTURES

Peri-axonemal accessory elements develop during the latest stages of spermiogenesis (Figure 39). The outer dense fibers (ODFs) assemble as very thin filaments along outer MT doublets in the whole flagellum. As they continue to grow in thickness, they separate from MT doublets into independent fibers. Their growth follows a base-to-tip gradient and therefore the diameter of the fibers gradually narrows towards the tip of the flagellum. The striated columns and ODFs fuse in mature spermatids.

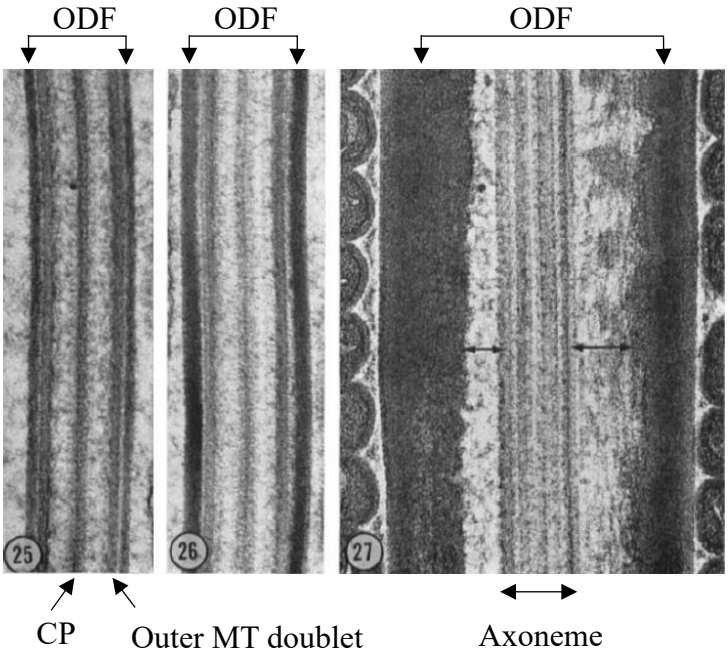

Figure 39: Successive stages in the development of outer dense fibers. *From a Chinese hamster spermatid. Abbreviations: central pair (CP), outer dense fibers (ODF), microtubule (MT). Adapted from Fawcett and Phillips 1969.*

5 THE LINC COMPLEX

To maintain a correct spermatid development, the acrosome, the manchette and the HTCA need to be tightly associated with the remodelling nucleus. This connection is believed to be mediated by the LInker of Nucleoskeleton and Cytoskeleton (LINC) complex that is present in the nuclear envelope. It contains two protein families: SUN (Sad1/UNc84 homology domain-containing) and KASH (Klarsicht/Anc1/Syne1 homology domain-containing) proteins. SUN proteins localize to the inner nuclear membrane (INM), whereas KASH proteins are present in the outer nuclear membrane (ONM), thus forming a complex that spans across the nuclear envelope and connect the nuclear cytoskeleton with cytoplasmic structures (Figure 40).

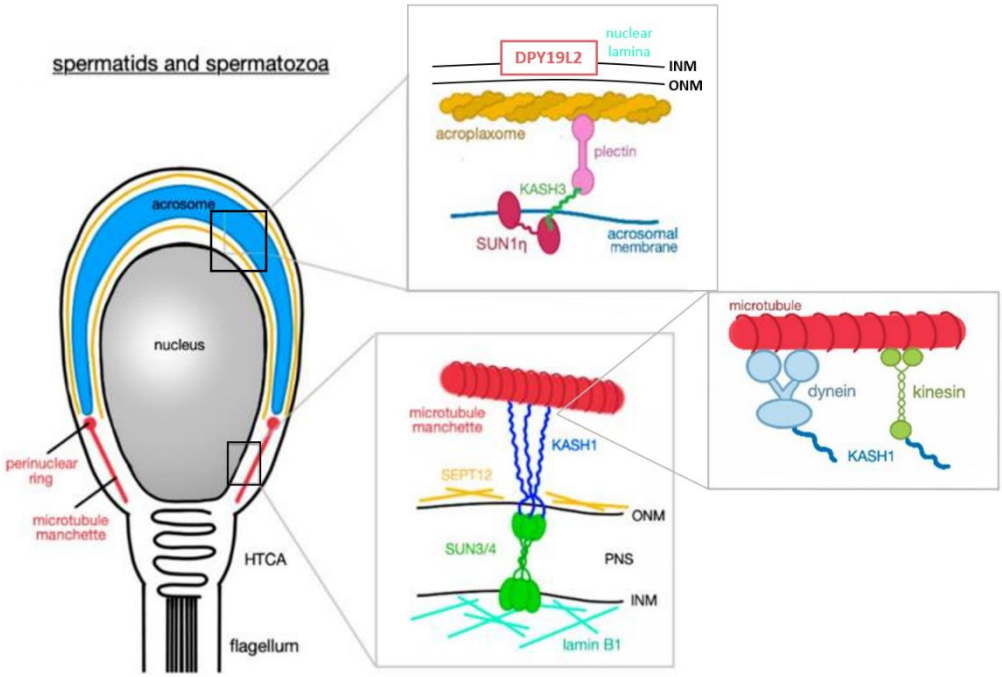

Figure 40: The complexes mediating the connection of the acrosome and the manchette to the nucleus. *The LINC complex is also present between the HTCA and the nucleus (not shown), see the next chapter. Abbreviations: inner nuclear membrane (INN), outer nuclear membrane (ONM), perinuclear space (PNS), head-tail coupling apparatus (HTCA). See the text for more details. Adapted from Kmonickova et al. 2020.*

Humans and mice have five SUN proteins (SUN1-5) and five KASH proteins (KASH1-4 also called nesprin1-4 or Syne-1-4, and KASH5). SUN3, 4 and 5 are only expressed in the testis. Various combinations of interacting SUN and KASH proteins exist and are associated with different structures and functions (Kmonickova et al. 2020; Pereira et al. 2019; Manfrevola et al.

2021). The LINC complex plays a role during meiotic prophase I in spermatocytes, where a complex of SUN1/2 and KASH5 participate in chromosome pairing and meiotic progression (Ding et al. 2007; Horn et al. 2013). A complex between SUN1η, an isoform of SUN1, and KASH3/Nesprin3 was proposed to form a link between the acroplaxome and the acrosomal membrane. SUN1η does not localize to the INM, instead it is associated with the acrosomal membrane, recruits KASH3/Nesprin3, that in turn interacts with plectin that is a components of the acroplaxome (Figure 40, Figure 41) (Morgan et al. 2011; Göb et al. 2010; Kmonickova et al. 2020).

Another important protein for the anchoring of the acrosome to the nucleus is DPY19L2 (Figure 40). It is a transmembrane protein specifically expressed in spermatids. DPY19L2 localizes to the INM facing the acrosomal vesicle and anchors the acroplaxome to the dense nuclear lamina (Pierre et al. 2012). Both the nuclear lamina and the junction between the nuclear envelope and the acroplaxome are destabilized in the absence of DPY19L2 which leads to the detachment of the acrosome during spermiogenesis. The manchette fails to correctly attach to the nucleus and spermatozoa have round heads. The absence of DPY19L2 was therefore associated with male infertility in humans and mice and is responsible for the majority of cases of globozoospermia in humans, a case of round-headed spermatozoa (Yassine, Escoffier, Martinez, et al. 2015; F. Zhu et al. 2013). DPY19L2 was proposed to cooperate with the LINC complex in acrosome anchoring, however this hypothesis was not scientifically proven (Beurois et al. 2020).

The protein complexes that maintain the connection between the manchette and the nuclear envelope are poorly known and might be also mediated by the LINC complex. SUN3 in the INM is believed to interact with KASH1/ Nesprin1 in the ONM. Their localization follows the manchette during spermatid elongation (Göb et al. 2010). KASH1/ Nesprin1 can interact with microtubules through either a dynein-dynactin complex or the KIF3B subunit of kinesin II (Fan and Beck 2004; Xiaochang Zhang et al. 2009). SUN4, also called SPAG4, was shown to interact with the SUN3:KASH1 complex in mouse spermatids and localizes to the manchette. In the absence of SUN3 and SUN4, the manchette fails to form which leads to male infertility and a globozoospermia-like phenotype (Q. Gao et al. 2020; Calvi et al. 2015; Pasch et al. 2015).

SUN5, also called SPAGAL, and KASH3, also called Nesprin3, were shown to be essential for a proper connection between the nucleus and the HTCA at the implantation fossa (Figure 41).

During spermatogenesis, SUN5/SPAGAL localizes to multiple compartments until it is relocates to the HTCA (Yassine, Escoffier, Nahed, et al. 2015). The absence of SUN5/SPAG4L disrupts the development of the HTCA and leads to decapitated spermatozoa (Shang et al. 2017; Fuxi Zhu et al. 2016; Shang et al. 2018). In this mutant, the HTCA is only partially bound to the nucleus in round spermatids and breaks off during spermatid elongation, leading to decapitated spermatozoa. The axoneme, however, appears to form normally. KASH3/ Nesprin3 is necessary to attach the centrosome to the nuclear envelope in somatic cells (Wilhelmsen et al. 2005; Morgan et al. 2011) and interacts with SUN5 at the HTCA (Yunfei Zhang et al. 2021). SUN5/SPAG4L and KASH3/Nesprin3 appear to be two components of the LINC complex at the HTCA.

6 COMPONENTS OF THE CONNECTING PIECE

A strong connection between the nucleus, the HTCA and the flagellum is essential for sperm motility and therefore for fertility. A complete loss of this connection, a separation between the sperm head and flagellum, leads to the acephalic spermatozoa syndrome and male infertility (Yu Wang et al. 2022; B. Wu et al. 2020; Tapia Contreras and Hoyer-Fender 2021). Whole-exome sequencing among patients with the acephalic spermatozoa syndrome led to the discovery of multiple protein essential for correct development of the HTCA (Tapia Contreras and Hoyer-Fender 2021). Perhaps not surprisingly, many of these proteins were also associated with the centrosome in somatic cells (Centrin 1, CEP128, ODF1, ODF2, CCDC42, Centrobin, and Azi/ Cep131), although several others are testis-specific (PMFBP1, SUN4/SPAG4, SUN5/SPAG4L2, OAZ3, SPATA6, SPAG6, TSGA10, Speriolin). Sperm decapitation was observed at different places of the HTCA, e.g. between the nuclear envelope and the basal plate, between the basal plate and the capitulum, between centrioles, and after the distal centriole. The specific breaking points were used to deduce the localization of the different proteins. A summary of important HTCA proteins and their location within the HTCA is shown in Figure 41.

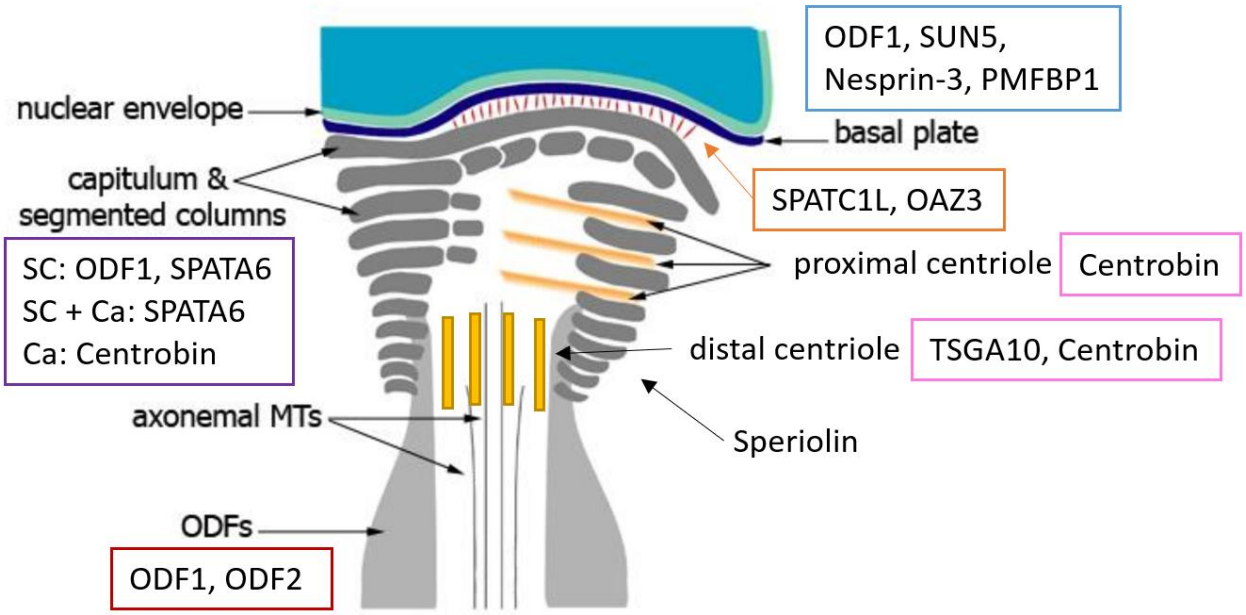

Figure 41: Distribution of proteins localizing to different HTCA components in spermatids. *The nuclear envelope/ basal plate (blue), connection between the basal plate and the capitulum (orange), proximal or distal centrioles (pink), capitulum (Ca) and/ or segmented columns (SC) (purple), outer dense fibers (ODF; red). Speriolin is located on the outside of segmented columns. Image adapted from Tapia Contreras and Hoyer-Fender 2021.*

The absence of centriolar proteins CEP128 (Xueguang Zhang et al. 2022) and Centrin 1 (Avasthi et al. 2013) leads to male infertility. The absence of Centrin 1 in the mouse leads to a separation of the HTCA from the nucleus without decapitation, short and malformed flagella, and malformed heads. CEP128 interacts with ODF2 to form the subdistal appendages of the centriole (Kashihara et al. 2019). Mutations in CEP128 lead to abnormalities of the HTCA, with missing or incomplete proximal and distal centrioles, and striated columns, and to malformed flagella in humans and mice. The basal plate appeared almost normal (Xueguang Zhang et al. 2022).

ODF1 and ODF2/ cenexin proteins localize to ODFs, the capitulum, striated columns and the basal plate (Schalles et al. 1998). Mutations in ODF1 (K. Yang et al. 2012; Hoyer-Fender 2022) and ODF2 (Z.-J. Zhu et al. 2022; Ito et al. 2019) lead to sperm decapitation and disorganization of the flagellum. Heterozygous ODF1 spermatozoa show an enlarged distance between the capitulum and the basal plate.

ODF1 and ODF2 interact with CCDC42, a coiled-coil domain containing proteins that localises to the HTCA and also to the manchette and the sperm tail (Tapia Contreras and Hoyer-Fender 2019).

Its absence leads to HTCA multiplication, decapitation, abnormal manchette and sperm head shape, and the lack of flagellated sperm (Pasek et al. 2016).

SUN5 also interacts with Centlein (Ying Zhang et al. 2021) in the HTCA that in turn binds ODF3/ PMFBP1 (Yan-Wei Sha, Wang, Xu, et al. 2019; Fuxi Zhu et al. 2018), and this protein complex participates in the anchoring of the basal plate to the nuclear envelope. The absence of these proteins leads to decapitated spermatozoa.

At least two proteins are important for a tight link between the basal plate and the capitulum: SPATC1L (J. Kim et al. 2018; Y.-Z. Li et al. 2022) and OAZ3 (Tokuhiro et al. 2009).

Other proteins involved in the formation or maintenance of the HTCA include SPATA6 (S. Yuan et al. 2015), SPAG6 (Sapiro et al. 2002), PRSS21 (Netzel-Arnett et al. 2009), and centrosome-associated proteins Centrobin (Liška et al. 2009), Azi/ Cep131 (E. A. Hall et al. 2013), manchette and HTCA protein azh/HOOK1 (Mochida, Tres, and Kierszenbaum 1999; Mendoza-Lujambio 2002), TSGA10 that also interacts with ODF2 and PMFBP1 (Y.-W. Sha et al. 2018) and Speriolin (Goto, O'Brien, and Eddy 2010).

7 AXONEME FORMATION

Axoneme formation has been mostly studied in motile *Chlamydomonas* flagella and in non-motile primary cilia where it relies on intraflagellar transport (IFT). IFT is also essential for sperm axoneme formation during spermiogenesis in mammals (San Agustin, Pazour, and Witman 2015; Mari S Lehti and Sironen 2017; Pleuger et al. 2020).

IFT particles, also called trains, mediate bidirectional protein trafficking in and out of cilia or flagella, delivering their cargo to the growing tip (Figure 42) (W.-L. Wang, Tu, and Tan 2020). IFT proteins serve as adaptors between motor proteins, kinesin and dynein, and cargo proteins (Nakayama and Katoh 2020).

IFT trains can be divided into 2 multisubunit complexes: IFT complex A (IFT-A) and IFT complex B (IFT-B). IFT-B is composed of 16 subunits. It binds kinesin-2 motor protein that mediates transport in the anterograde direction, from the base to the distal tip towards the MT plus end. One of its most important cargos is the αβ-tubulin heterodimer that is the building block of the axoneme

(Bhogaraju et al. 2013). IFT-A contains 6 subunits and binds dynein-2 that moves in the retrograde direction, from the tip of the cilium towards the base and the MT minus end.

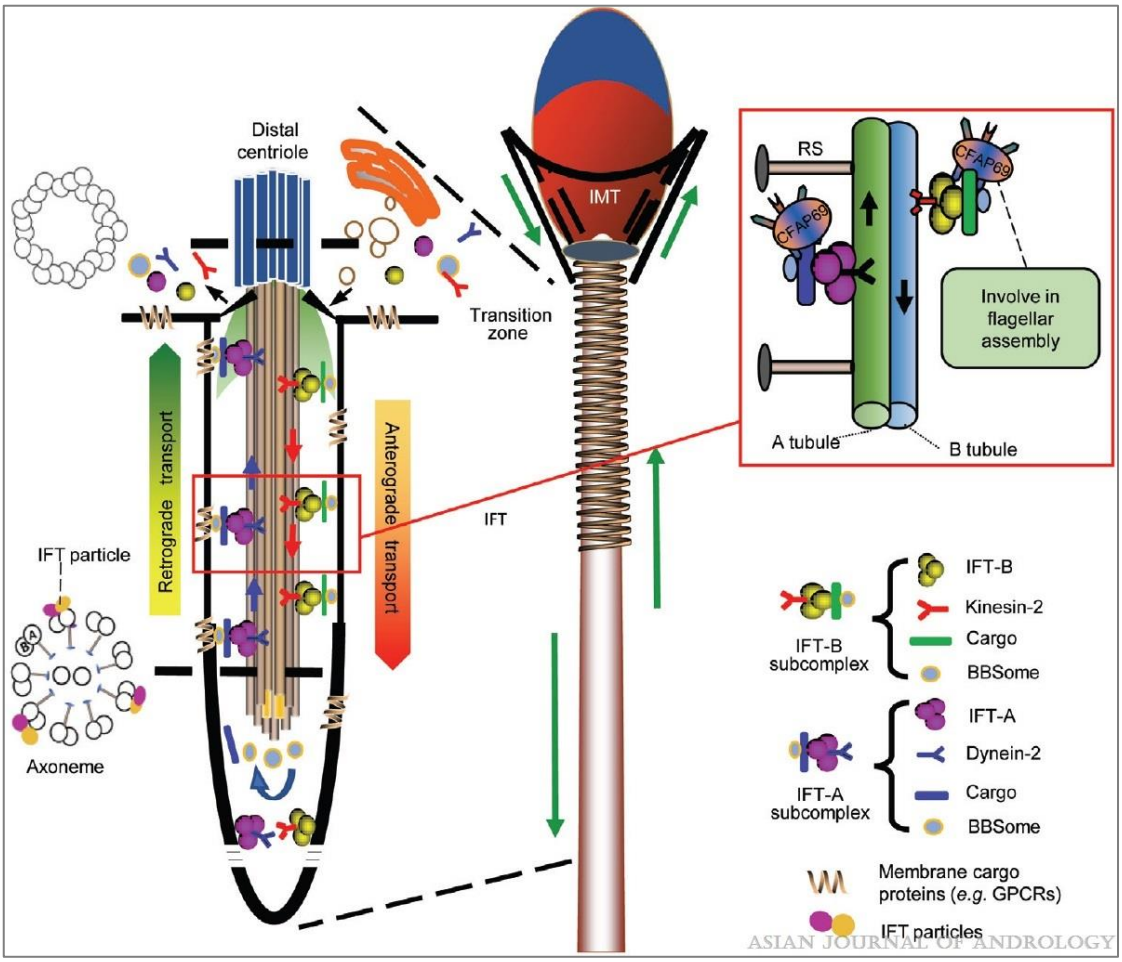

Figure 42: Intraflagellar and intramanchette transport in mammalian spermatids. *From W.-L. Wang, Tu, and Tan 2020.*

Studies in the *Chlamydomonas* showed that the IFT-B train loads the IFT-A motor proteins and cargo at the basal body, before they pass the transition zone. At the axoneme tip, the trains subsequently reorganize and return to the basal body by retrograde transport (van den Hoek et al. 2022; Prevo, Scholey, and Peterman 2017). In the *Chlamydomonas*, the transport of tubulin appears to be both mediated by diffusion as well as by IFT (Van De Weghe et al. 2020; Craft et al. 2015; Luo et al. 2017), and the building blocks of the axoneme, including dynein arms and preassembled radial-spoke complexes, are transported *via* the IFT machinery (Pleuger et al. 2020; Qin et al. 2004; Ishikawa et al. 2014; Hou et al. 2007). A similar mechanism might be present in mammals.

8 NUCLEAR REMODELLING AND INTRAMANCHETTE TRANSPORT

8.1 FORMATION OF THE MANCHETTE AND SHAPING OF THE SPERMATID HEAD

The spermatid nucleus undergoes extensive compaction and elongation during spermiogenesis. The manchette, a transient microtubule-based structure, appears in step 8 round spermatids. It plays important roles in head shaping and intra-manchette transport (IMT) of proteins (M S Lehti and Sironen 2016; Dunleavy et al. 2019) (Figure 43).

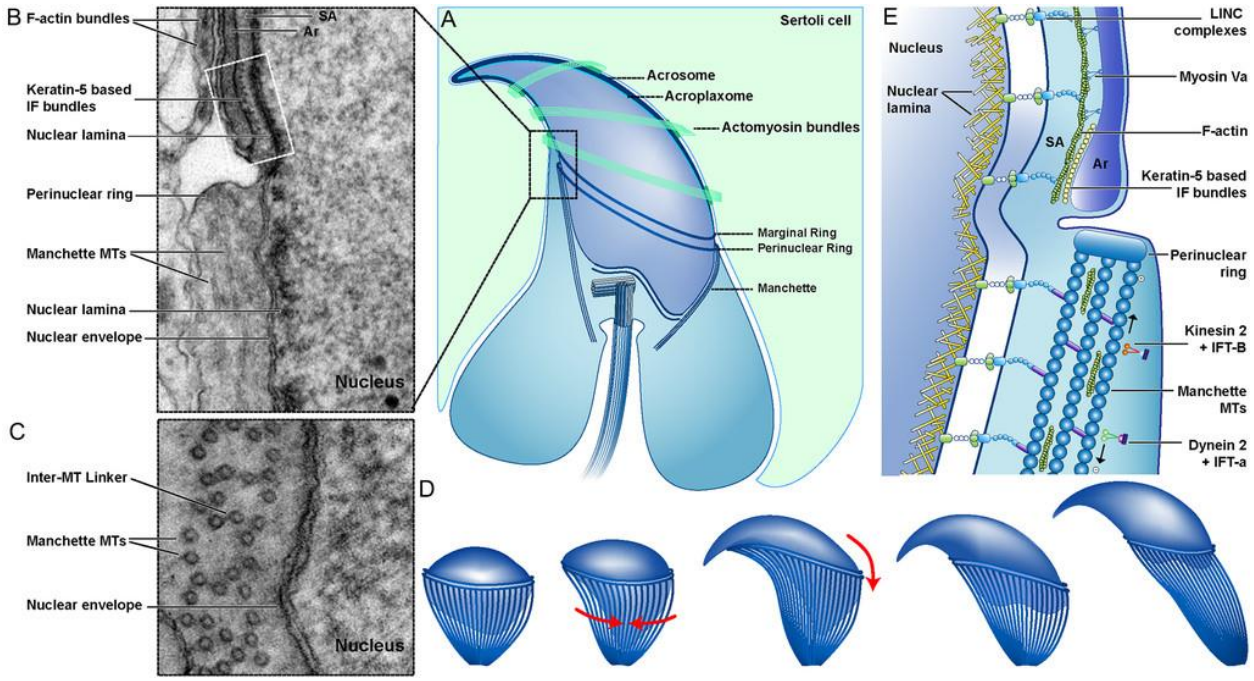

Figure 43: Nuclear remodeling in elongating spermatids is believed to be driven by endogenous forces provided by the manchette and the acroplaxome, and exogenous forces from the actomyosin bundles present in the surrounding Sertoli cell (A). *An electron micrograph (B) and a schematic representation (E) of the acrosome-acroplaxome and the manchette. The acrosome (Ar) is anchored to the nucleus via the acroplaxome containing Keratin-5 intermediate filaments, F-actin, Myosin Va, and the LINC complex. F-actin bundles of the Sertoli ectoplasmic specializations can be seen on the left of the acrosome. The manchette is anchored in the perinuclear ring and parallel microtubules descend along the nucleus toward the cytoplasm (B). Microtubule motors dynein 2 and kinesin 2, along with the IFT complex transport cargos along the manchette (E). The manchette and the acrosome-acroplaxome are separated by a groove (B). A transverse section of the manchette (C) and a schematic representation of the zipper-like descend of the manchette that shapes the spermatid nucleus (D). From Dunleavy et al. 2019.*

The structure is maintained in many mammalian species including humans (Courtens et al. 1981). It is composed of up to 1000 parallel interconnected MT filaments that are arranged in long rays and form a sleeve around the sperm nucleus. The manchette is anchored with MT plus-ends in a perinuclear ring below the acrosome and projects into the spermatid cytoplasm. MT number and length increase during early spermiogenesis, attain the maximum number as chromatin condensation becomes apparent (~step 12), and subsequently disappear in a gradual manner (step 13-14) before the formation of the midpiece. The length of MTs growing into the cytoplasm is regulated by MT severing enzymes including the Katanin complex and KATNAL2 (O'Donnell et al. 2012; Dunleavy et al. 2017). During spermatid elongation, the manchette descends in a zipper-like movement toward the flagellum and its movement coincides with the expansion of the acrosome (Rattner and Brinkley 1972). It is believed that the manchette exerts mechanical constrictive forces onto the nucleus by forming progressive connections with the nuclear envelope as it descends toward the flagellum (Lonnie D. Russell et al. 1991). However, the exact mechanism of function of the manchette remains to be resolved. The manchette is believed to connected to the nucleus through the LINC complex, as was discussed previously in *Chapter 2: Spermatogenesis, subchapter 5: The LINC complex*. The manchette also contains actin filaments and associated motor proteins, myosin, that participate in IMT (Abraham L. Kierszenbaum and Tres 2004).

The location of the manchette's nucleation site and assembly mechanism remain debated. Lehti and Sironen showed that manchette microtubules might be nucleated from the centrosome, possibly at the centriolar adjunct (Figure 44) (M S Lehti and Sironen 2016). In early round spermatids (step 7-8), microtubules first start to appear around the basal body, and then start to grow toward the acrosomal region, as was shown by microtubule co-staining with a MT plus-end tracking protein EB3. Subsequently, MTs are anchored to the perinuclear ring (step 8-9) and detach from the centrosomal region. EB3 staining remains at the perinuclear ring as the manchette descends the nucleus and until it clears at spermatid step 14. In the mouse, the centriolar adjunct contains γ-tubulin, a known MT nucleator. A MT array linked to the manchette is also associated with the centriolar adjunct during spermatid elongation, supporting this hypothesis (Manandhar et al. 1998; Fouquet 1998).

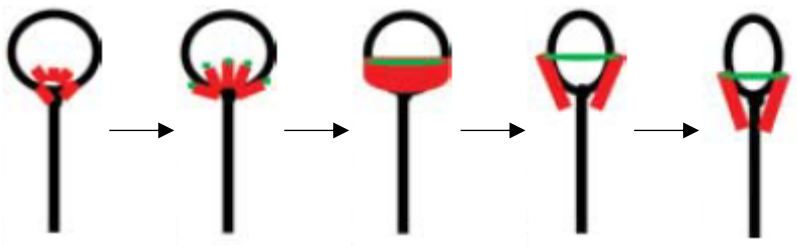

Figure 44: Illustration of proposed mechanism of manchette nucleation. *Microtubule plus-end tracking protein EB3 is in green, microtubules in red. Adapted from M S Lehti and Sironen 2016.*

Other possibilities for manchette nucleation sites exist but, overall, further research is needed to elucidate this question. The manchette could be also nucleated at the perinuclear ring. New short MTs appear around and over the nucleus in round spermatids (step 7) and increase in size until a fully formed manchette becomes recognizable (step 9) (Moreno and Schatten 2000). On the hand, the perinuclear ring does not contain γ-tubulin. MTs could be also nucleated from existing MTs or from other sites in the cytoplasm.

8.2 NUCLEOCYTOPLASMIC TRANSPORT

The manchette is involved in nucleocytoplasmic transport (Abraham L. Kierszenbaum 2002b; Abraham L. Kierszenbaum and Tres 2004). Protein trafficking in and out of the nucleus might be mediated by Ran GTPases present on manchette MTs and might direct proteins for disposal by the ubiquitin–proteosome system (M S Lehti and Sironen 2016). Mutations in a ubiquitin-conjugating enzyme mHR6B show male infertility, head invaginations and an accumulation of unknown material in the head, an ectopic manchette and an abnormal distribution of periaxonemal structures (Escalier et al. 2003).

8.3 INTRAMANCHETTE TRANSPORT

The manchette serves as a platform for vesicle trafficking along manchette microtubules (Figure 45). IMT is important for the transport of proteins required for the assembly of the axoneme, axonemal accessory structures, the perinuclear theca, and it may also be important for the strengthening of the HTCA (M S Lehti and Sironen 2016; Pleuger et al. 2020). The manchette is anchored at the perinuclear ring below the acrosome, extends into cytoplasmic lobes where protein translation occurs and is present close to the HTCA where the transition zone regulates protein

entry into the compartmentalized axoneme. It is therefore perfectly positioned for protein trafficking between the different spermatid cellular compartments.

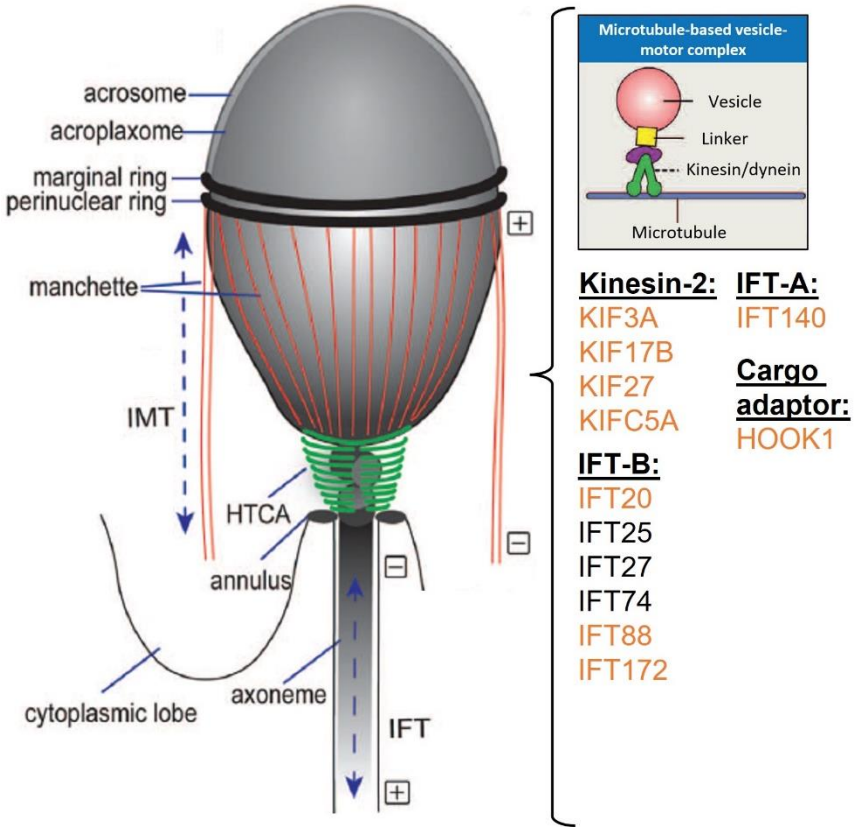

Figure 45: Schematic overview intramanchette transport (IMT). *Manchette microtubules are anchored with their plus-end at the perinuclear ring, and their minus-ends extend into the spermatid cytoplasm. Bidirectional vesicle transport along manchette microtubules is mediated by kinesin towards the microtubule plus-ends (anterograde transport; IFT-B) and by dynein motors towards the minus-ends (retrograde transport; IFT-A). Cargo adaptors/ linkers (IFT proteins, HOOK1) mediate the connection between microtubule motors and cargo vesicles. Proteins labeled in orange were localized to the manchette, the absence of the others influences manchette structure suggesting their presence in the structure. Spermatid schema adapted from Pleuger et al. 2020, an insert of microtubule-based vesicle-motor complex is from A.L. Kierszenbaum, Rivkin, and Tres 2003.*

The mechanism of intramanchette transport (IMT) resembles intraflagellar transport (IFT) (Figure 45). It is carried out by MT motor proteins, kinesin and dynein, that mediate cargo movement along MT tracks, and by myosin that moves along F-actin tracks and might mediate short-distance transport (A.L. Kierszenbaum, Rivkin, and Tres 2003; Hayasaka et al. 2008; Zakrzewski et al. 2017). IFT proteins serve as adaptors between the molecular motors that bind microtubules and the cargo. Several kinesin-2 proteins and proteins belonging to the IFT-B and IFT-A machinery

were detected in the manchette. Kinesin-2 proteins include KIF3A (Mari S. Lehti, Kotaja, and Sironen 2013), KIF17B (Saade et al. 2007), KIF27 (Nozawa et al. 2014), and KIFC5A (Navolanic and Sperry 2000); IFT-B proteins include IFT20 (Sironen et al. 2011; Zhengang Zhang et al. 2016), IFT25 (H. Liu et al. 2017), IFT74 (Shi et al. 2019), IFT88 (Abraham L. Kierszenbaum and Tres 2004; San Agustin, Pazour, and Witman 2015), and IFT172 (S. Zhang et al. 2020); and IFT-A protein IFT140 (Yong Zhang et al. 2018; X. Wang et al. 2019).

During spermatogenesis, defects in proteins involved with IMT and IFT are generally associated with male infertility, low sperm count, and decreased motility due short and disrupted or absent flagella. The manchette can be abnormally elongated or ectopic, leading to abnormal head shapes. Both the axoneme and/or the accessory structures are disrupted, highlighting the importance of IMT for the development of the flagellum. However, the exact contribution of each mechanism to the development of the flagellum, whether it is IFT or IMT, is hard to determine since multiple IFT proteins are implicated in both mechanisms.

The absence of other proteins, including centrosome-associated CEP131, Centrobin, CCDC42; MT organizers E-MAP-115 and LRGUK1; and MT-severing protein KATNB1, was also shown to negatively impact manchette establishment, head shaping and flagellum assembly (M S Lehti and Sironen 2016; Pasek et al. 2016). MT-motors, adaptors, cargo proteins, and microtubule-associated proteins all seem to play roles during IMT and IFT.

Moreover, formation of the acrosome, the manchette, HTCA, and flagellum formation appear to be linked processes since multiple proteins have been shown to localize these sites during spermiogenesis. For instance, intraflagellar transport proteins IFT88 and IFT20 localize to the cytosolic side of pro-acrosomal vesicles from the *trans*-Golgi, participate in protein transport in the manchette, and relocate to the HTCA during spermatid differentiation. IFT88 is also present in the flagellum (Abraham L. Kierszenbaum et al. 2011; Sironen et al. 2011). A similar pattern was observed for KIF3A that localizes to the manchette, the HTCA and the axoneme of elongating spermatids (Mari S. Lehti, Kotaja, and Sironen 2013). These observations show that protein trafficking, whether it is associated with the Golgi, the acrosome, HTCA, the manchette or IFT, is essential for correct sperm formation and the cytoskeleton plays a great role during spermiogenesis. Mutation in one or multiple associated proteins leads to a deregulation of the system and a cascade of defects, showing the specificity and fragility of the system.

Spermiogenesis is an incredibly complex process, and its complete regulatory network remains to be fully understood.

CHAPTER 3: MICROTUBULES AND RELATED STRUCTURES

1 INTRODUCTION

The cytoskeleton is a complex and highly dynamic network of interlinked filaments. Together with actin and intermediate filaments, microtubules form one of the three classes of cytoskeletal elements. MTs are conserved in all eukaryotic organisms and implicated in many essential cellular processes including cell division, maintenance of cell shape and polarity, cell migration, organelle organization, and protein trafficking. They also serve as the backbone of cilia and flagella (Goodson and Jonasson 2018).

MTs also play a central role in all steps of spermatogenesis, as was shown in the previous chapters: in the formation of the mitotic and meiotic spindles, in the cytoskeleton of Sertoli cells, in the sperm axoneme, and manchette head-shaping and protein trafficking (Dunleavy et al. 2019; Gadadhar, Hirschmugl, and Janke 2023).

In this chapter, we will discuss MT structure and regulation by tubulin isotypes and post-translational modifications (PTMs), by microtubule-associated proteins (MAPs) and microtubule inner proteins (MIPs). We will also discuss MT-associated structures including the centrosome, the mitotic spindle, and the midbody.

2 MICROTUBULE STRUCTURE AND NUCLEATION

Microtubules are hollow tubes formed of α- and β-tubulin heterodimers. They have a ~25 nm-wide outer diameter, and a 17 nm-wide interior diameter. Their number and length in metazoan cells are highly variable, ranging from less than 1 µm to more than 100 µm. Tubulin heterodimers are stacked to form protofilaments that assemble laterally to create sheets. The sheets are rolled into a tube and the boundary where the sheet connects is called a "seam". Most microtubules *in vivo* form a left-handed helix formed of 13 protofilaments that can be recognized by an offset at the seam of 1.5 dimers. The resulting microtubule is polar, with a fast-growing "plus end" that exposes β-

tubulin and a slow-growing "minus end" that exposes α-tubulin. Heterodimers can associate to or dissociate from both ends of the MT (Figure 46) (Goodson and Jonasson 2018).

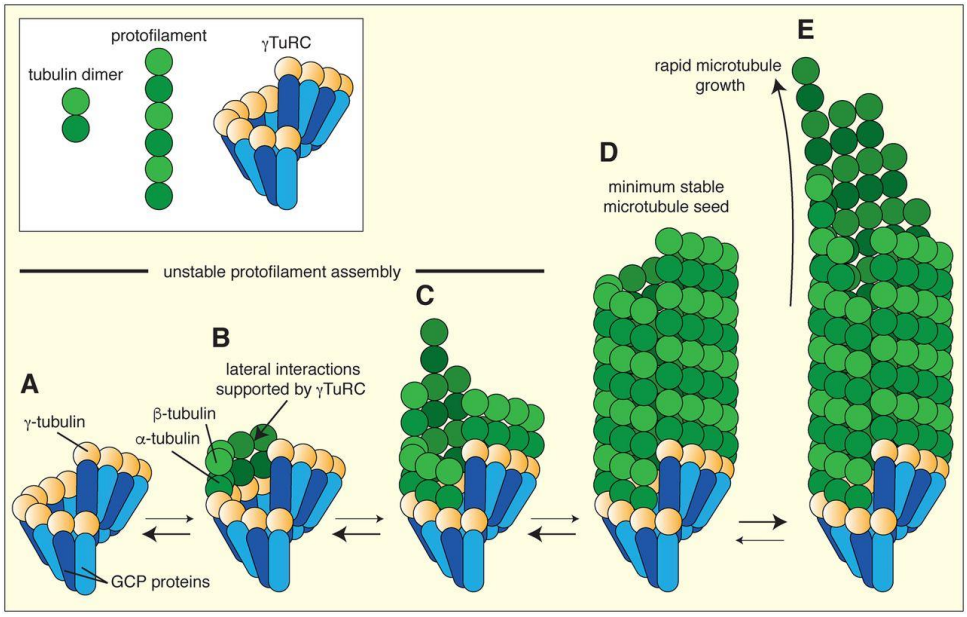

Figure 46: Illustration of microtubule nucleation from a mammalian γ-tubulin ring complex (γ-TuRC). *(A) The base of the complex is formed of 13 GCP (GCP2-6) proteins that are arranged in a cone-shaped structure. Each GCP protein is bound to a γ-tubulin molecule. The lumen of the complex contains a structure called the "lumenal bridge" and contains unknown densities and an actin-like protein, that could help stabilize the structure. (B) Tubulin αβ dimers bind to γ-tubulin that is thought to promote lateral interaction of tubulin dimers as they grow and form filaments. (C, D) Assembly passes through an unstable stage, until the size of the structure has reached a sufficient size, referred to as a "microtubule seed". (E) Once the stable MT seed has formed, MT assembly becomes favorable, and the MT grows rapidly. From Tovey and Conduit 2018.*

Microtubules exist in a state of "dynamic instability" (Mitchison and Kirschner 1984), in which MT ends randomly transition between periods of depolymerization and growth. The transition from growth to depolymerization is called a "catastrophe" and the opposite is called a "rescue". Microtubule nucleation is GTP-dependent. Microtubules assemble from soluble GTP-bound tubulin, and GTP becomes hydrolysed to GDP as tubulin dimers are incorporated into the lattice. The MT plus-end is therefore capped by GTP-tubulin, whereas the rest of the filament contains GDP-tubulin. The GTP cap stabilizes the filament, and its disappearance leads to MT shrinkage. Microtubule nucleation and polymerization are tightly regulated in time and space by numerous MT-binding factors to ensure the correct formation of MT networks (Akhmanova and Kapitein 2022; Roostalu and Surrey 2017; Tovey and Conduit 2018).

Although microtubules can form spontaneously from highly concentrated α-β-tubulin, microtubule *de novo* nucleation is more efficient in the presence of a specialized nucleation machinery called the "γ-tubulin ring complex (γ-TuRC)" (Figure 46). An essential component of the complex is γ-tubulin which is considered to be a universal MT nucleator (Oakley and Oakley 1989). The complex serves as a template for MT assembly and caps MTs at the minus-ends to prevent their depolymerization. Tubulin dimers begin to assemble, and the MT grows from their plus-end. The complexes are recruited to specific sites called microtubule-organizing centers (MTOCs). The major MTOC in mammalian cells is the centrosome, however other structures such as the Golgi apparatus, the cell nucleus, and mitochondria can act as MTOCs and anchor and nucleate microtubules. Microtubules can also branch and nucleate from other microtubules (J. Wu and Akhmanova 2017; Goodson and Jonasson 2018; Wieczorek et al. 2020; Tovey and Conduit 2018; Thawani and Petry 2021; Consolati et al. 2020).

3 THE TUBULIN CODE

Microtubules are implicated in many essential cellular processes and form the backbone of various very different structures (e.g., an axoneme and the mitotic spindle). How can nearly identical microtubules perform such diverse functions? This question led to the concept of the "tubulin code". It states that microtubule function can be finely regulated by a combination of tubulin isotypes and post-translational modifications (PTMs). The tubulin code also mediates and regulates interactions with numerous microtubule-associated proteins (MAP) that influence MT dynamics (Figure 47) (Verhey and Gaertig 2007; Janke and Magiera 2020; Nsamba and Gupta 2022). Consequently, is it very difficult to identify the role and properties of every component.

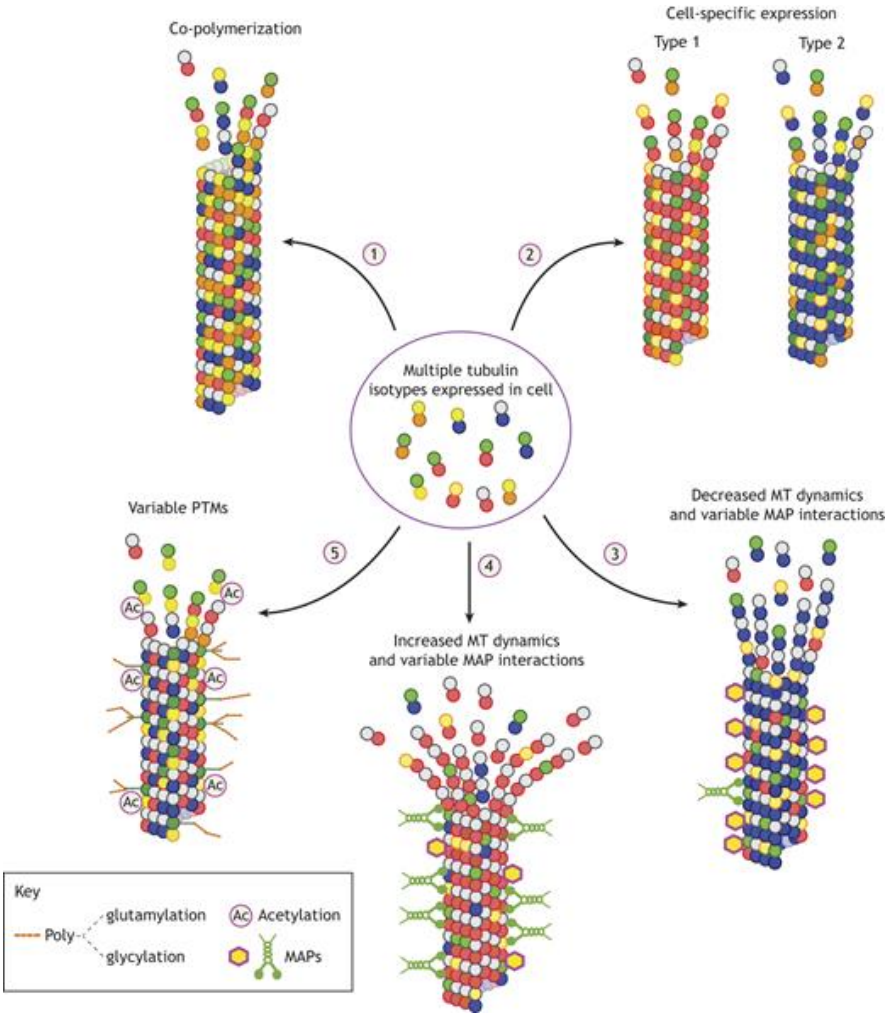

Figure 47: Illustration of microtubule diversity. *(1) Tubulin isotypes (different colors) co-polymerize with αβ dimers producing MTs with distinct composition and function. (2) Tubulin isotypes can be expressed in a cell-specific manner (2), modulate MT dynamics through divers MAP interactions (3, 4), and can be decorated by distinct PTMs that can have influence on MT properties (5). From Nsamba and Gupta 2022.*

3.1 TUBULIN ISOTYPES

Microtubule composition shows a great diversity (Figure 47). Humans have 8 α-tubulin genes and 8 isoforms, and 9 β-tubulin genes and 7 isoforms (Roll-Mecak 2015; 2019). The roles, spaciotemporal expression patterns, and mechanistic properties of tubulin isoforms vary among different cell types. Some eukaryotic cells express few isoforms while others express multiple isoforms and thus create a large variety of αβ-tubulin heterodimers. Less common isotypes probably evolved in specific organisms with novel microtubule functions (Janke and Magiera

2020). For instance, isoforms are specifically associated with cell types and tissues, such as platelets (Schwer et al. 2001) and brain neuronal and non-neuronal cells (Burgoyne et al. 1988; Hausrat et al. 2021). In human reproduction, *TUBB8* (Tubulin Beta 8 Class VIII) is responsible for the production of β-tubulin, a major component of the meiotic spindle (Feng et al. 2016). Absent in mature spermatozoa, TUBB8 is highly expressed in oocytes and during the very early stages of embryonic development. Its absence is associated with highly abnormal spindle formation and meiotic arrest, often at the MI (meiosis I) stage and leading to infertility. Moreover, mutations in *TUBB4B*, a β-tubulin subtype, are responsible for distinct PCD and ciliopathy phenotypes in humans (Mechaussier et al. 2022). The different variants differentially influenced MT dynamics leading to the disruption of cilia and centrosomes, and failed axoneme formation. Male *Tubb4b* mice were infertile.

As was discussed before, γ-tubulin is an important microtubule nucleator. Other tubulin isotypes present in mammals also include delta (δ-) tubulin and epsilon (ε-) tubulin (Stathatos et al. 2021). In human and mouse somatic cells, both δ- and ε-tubulin are present at the centrosome, but their localization differs from each other and from γ-tubulin. While δ-tubulin partially co-localizes with both centrioles and γ-tubulin, it is most prominent between the centrioles. The pattern of ε-tubulin localization is different and appears to be dependent on the cell cycle. It associates with the older centriole after centriole duplication and concentrates on both centrioles over time. It is also present in the midbody between dividing cells (Chang and Stearns 2000). Both are required for the stabilization of MTs in basal bodies and in cilia/ flagella of unicellular organisms and mouse and human cell cultures (Stathatos et al. 2021).

Tubulin isotypes are also involved in mouse spermatogenesis. The long isoform of δ-tubulin is present in intercellular bridges between germ cells from the spermatocyte stage to the elongated spermatid stage and as components of the perinuclear ring of the manchette and its precursor (Kato, Nagata, and Todokoro 2004). It is also present in the flagellum of testicular and epididymal spermatozoa (Smrzka, Delgehyr, and Bornens 2000). Both are present at the centrioles in elongating spermatids, and ε-tubulin localizes to manchette MTs. They co-localize with the MT-severing protein KATNAL2 at the base of the spermatid nucleus (δ-tubulin) or the manchette and pericentriolar region (ε-tubulin). KATNAL2 does not sever α- and β-tubulin, however it is essential for regulating spermatid cytoskeleton. Its absence leads to male infertility, centriole

multiplication, manchette defects, acrosome detachment, and sperm lack an axoneme (Dunleavy et al. 2017). The functional role of both tubulin isotypes in spermatogenesis has not been tested, however they were proposed to stabilize MTs at the manchette and centrioles during spermiogenesis (Stathatos et al. 2021).

3.2 TUBULIN POST-TRANSLATIONAL MODIFICATIONS

The negatively charged MT surface is a key site for motor proteins, MAPs and PTMs (Figure 48). Tubulin heterodimers consist of a globular "body" and α- and β- C-terminal tails. The tubulin "body" is involved in tubulin-tubulin interactions and forms the core structure of microtubules. The MT exterior is decorated by the C-terminal tails, also called E-hooks, that consist of 10-12 protruding residues of α-tubulin and 16-22 residues of β-tubulin. The tails are disordered, flexible and negatively charged due to the presence of glutamate and aspartate residues, and they convey the negative charge to the MT surface (Goodson and Jonasson 2018; Roll-Mecak 2015).

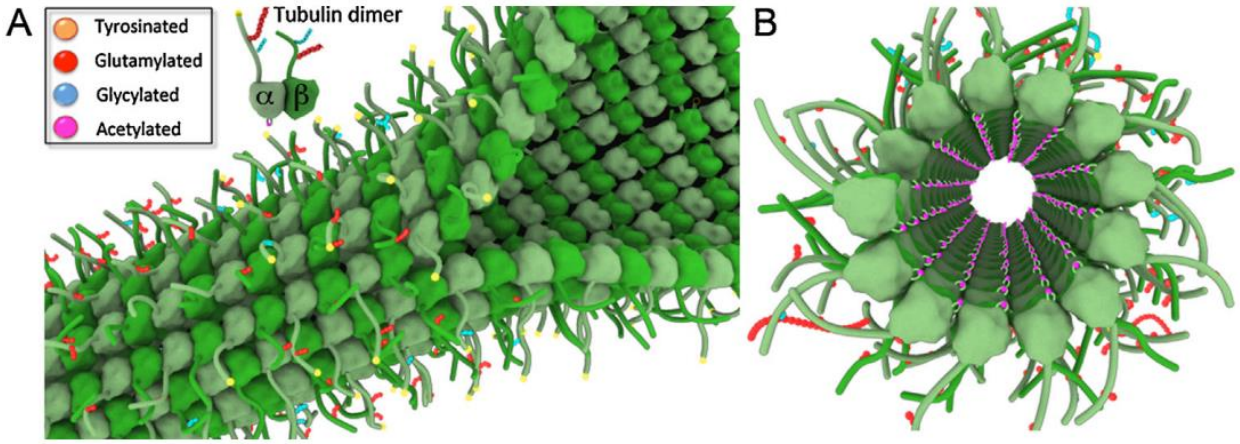

Figure 48: Illustration of a microtubule showing the C-terminal tails of tubulin dimers. *Several post-translational modifications can be added onto the tails. PTMs of α-tubulin include acetylation, tyrosination, detyrosination, polyglutamylation and polyglycylation, and β-tubulin can be modified by polyglutamylation and polyglycylation. Microtubule inner proteins are not shown inside the microtubule (B). From Roll-Mecak 2015.*

Microtubules are subjected to several types of PTMs including acetylation, phosphorylation, detyrosination/tyrosination, (poly)glutamylation, (poly)glycylation, and polyamination, that fine-tune their properties and functions (Roll-Mecak 2015; Janke and Magiera 2020). These modifications also play roles in the regulation of cilia and flagella. Spermatogenesis appears to be

mainly influenced by glutamylation and glycylation, where they regulate sperm motility, flagellum assembly, centriole number regulation and are important for a strong HTCA (Figure 49).

Glutamylation is essential for cilia/ flagella and for sperm development (Ikegami et al. 2010; Gadadhar, Hirschmugl, and Janke 2023). It is mediated by glutamic acid ligases from the TTLL family that conjugate one or multiple glutamate residues onto the α- and β-tubulin C-terminal tails on the MT surface. Glutamylation is mainly present on the B-tubule of outer MT doubles in *Tetrahymena*. The B-tubule is the side of force generation by dynein arms. The absence of glutamic acid ligases led to severe defects in ciliary/ flagellar motility in *Tetrahymena* and *Chlamydomonas* suggesting that polyglutamylation levels control dynein activity and therefore ciliary beating (Suryavanshi et al. 2010; Kubo et al. 2010; Janke and Magiera 2020).

In mice, mutations in *Ttll5* (G.-S. Lee et al. 2013), *Ttll1* (Vogel et al. 2010), *PGs1*/ ROSA22 (Campbell et al. 2002), and *Ttll9* (Konno et al. 2016) led to decreased male fertility. *Ttll5* knock-out animals showed irregular axoneme formation with a missing MT doublet 4, detached heads and tails, coiled flagella and decreased sperm concentration and motility leading to subfertility/ infertility phenotypes. In humans, mutations in *Ttll5* cause retinal dystrophy and infertility in some cases (Smirnov et al. 2021; Bedoni et al. 2016). TTLL5 glutamylates α-tubulin and can be found on centrioles in rat photoreceptor cells, human fibroblasts, and the HTCA in human spermatozoa (Bedoni et al. 2016). The absence of *Ttll1* led to a MMAF-like phenotype and PCD. The absence of *PGs1*/ ROSA22, a polyglutamylase subunit 1 that forms a complex with TTLL1, also led to male infertility due to defects in axoneme formation accompanied by changes in intermate behaviour and loss of body fat (Campbell et al. 2002). Knock-out *Ttll9* spermatozoa had shortened MT doublet 7 and a reduction of polyglutamylation on doublet 5, detached sperm heads and tails, and aberrant flagellar beating causing reduced motility (Konno et al. 2016).

Tubulin deglutamylases CCP1 and CCP5 from the CCP family (H.-Y. Wu, Wei, and Morgan 2017; Giordano et al. 2019) were also shown to be important for male fertility, proper axoneme formation and head-shaping. Mutations in *Ccp1* also led to neuronal degeneration. Spermatids lacking CCP5 accumulated polyglutamylated tubulin, had an abnormal manchette and supernumerary and detached centrioles, and failed to evacuate excess cytoplasm (Giordano et al. 2019).

Polyglycylation in mammals is catalyzed by TTLL3, TTLL8 and TTLL10 and consists of an addition of a chain of glycine residues onto a glutamate present in the tail of both tubulins. A

double knock-out *Ttll3-Ttll8* mice are subfertile and showed perturbed conformation of dynein arms, and an asymmetric flagellar beat that resulted in decreased sperm motility (Gadadhar et al. 2021).

Tubulin in sperm flagella is highly acetylated. Absence of an α-tubulin acetyltransferase αTAT1 decreased acetylation in multiple tissues, and in cilia, flagella, and axons. Male mice lacking αTAT1 were subfertile and had a reduced number of spermatozoa, the length of their flagella was decreased, and sperm motility was reduced, however no severe flagellar defects were observed (Kalebic et al. 2013).

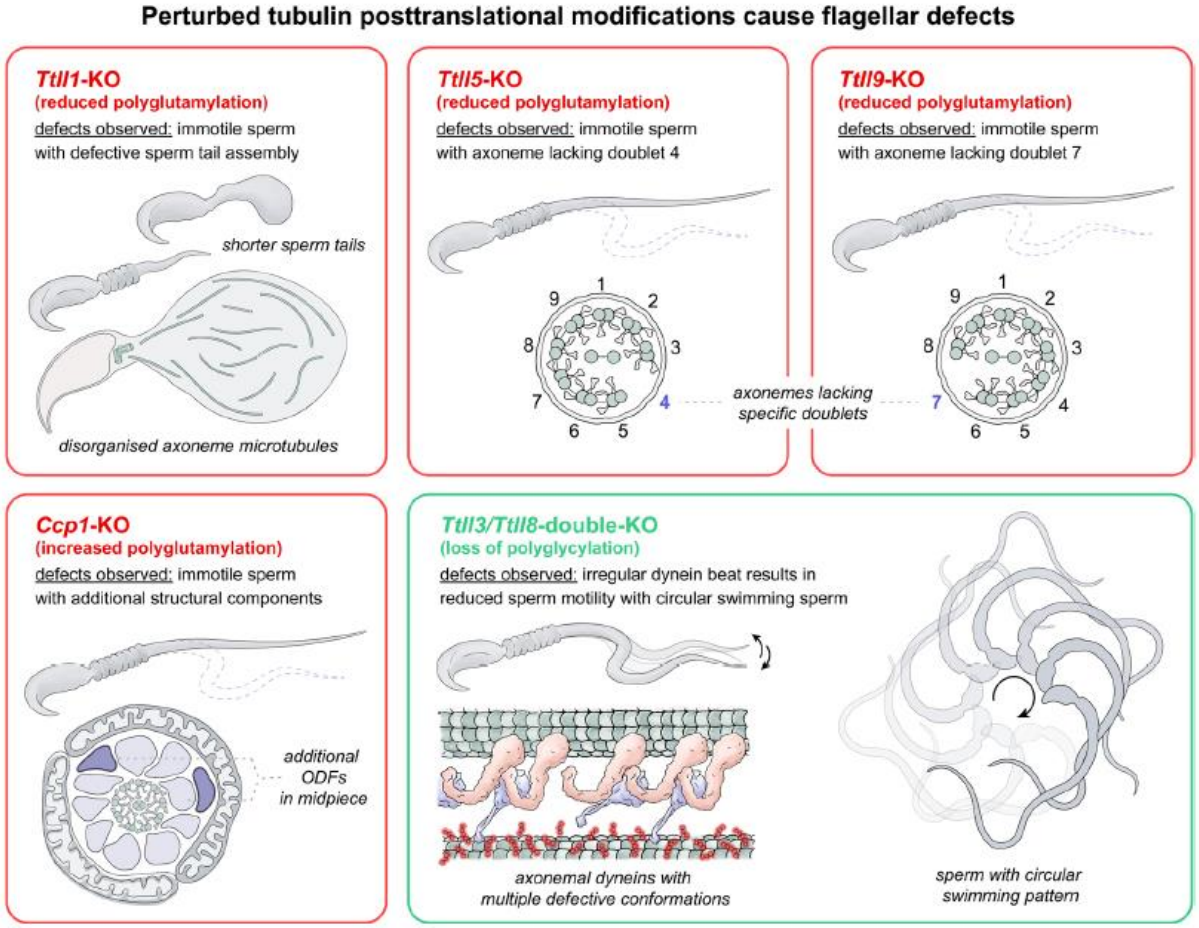

Figure 49: A summary illustration of flagellar defects caused by the absence of enzymes mediating post-translational modifications. *From Gadadhar, Hirschmugl, and Janke 2023.*

4 MICROTUBULE-ASSOCIATED PROTEINS

Microtubule-associated proteins (MAP) include all proteins that interact with microtubules. MAPs can be divided into groups based on their function such as microtubule stabilizers and destabilizers, motor proteins, capping proteins, and microtubule nucleators. However, the group names appear to differ among reviews, and some MAPs are involved in multiple activities and therefore belong to more than one group (Figure 50).

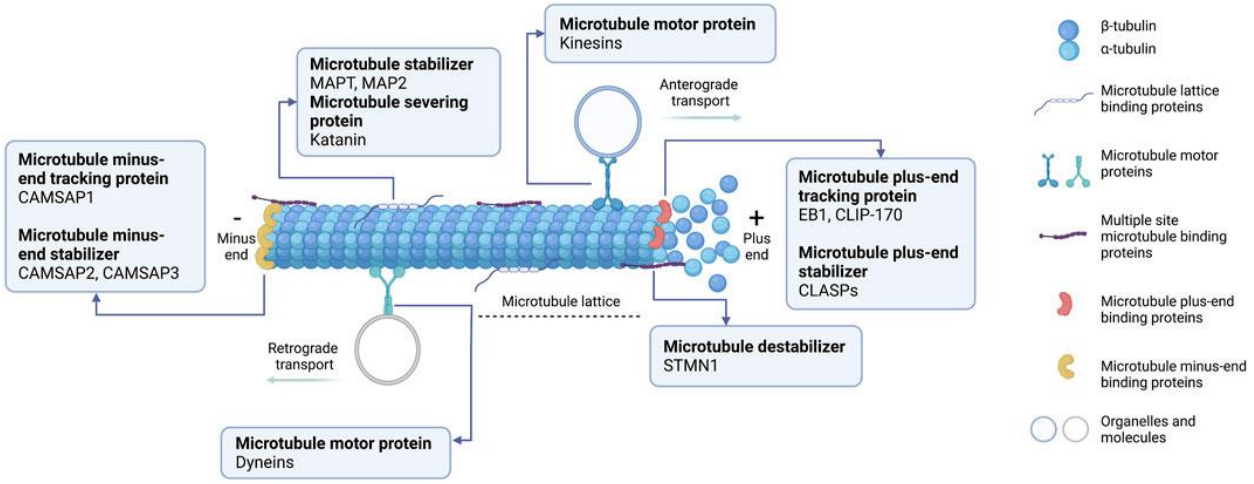

Figure 50: Schematic representation of microtubule-associated proteins (MAPs). *From Wattanathamsan and Pongrakhananon 2022.*

MAPs enable microtubules to perform their numerous functions. They promote MT nucleation, influence MT structure by cross-linking protofilaments, organize the MT network, and cross-link MTs with other cytoskeletal components such as actin. Ultimately, they stabilize the MTs structure by preventing catastrophe, promoting rescue or both. They also influence intracellular transport and modulate the activity of MT-severing enzymes katanin, spastin, and fidgetin. In turn, the action of MAPs is also regulated by PTMs such as phosphorylation (Ramkumar, Jong, and Ori-McKenney 2018). MAPs are well studied in the brain and deregulation of several MAPs was shown to lead to neurodegeneration and neurodevelopmental defects (Goodson and Jonasson 2018; Bodakuntla et al. 2019; Yipeng Wang and Mandelkow 2016). Deregulation of MAPs was also shown in many types of cancer and appears to contribute to cancer aggressiveness by altering MT dynamics in cell migration and invasion (Wattanathamsan and Pongrakhananon 2022).

In cells, dynamic instability of MT tips allows them to explore the cell's cytoplasm and search for intracellular structures (Gudimchuk and McIntosh 2021). They bind to organelles such as mitochondria and the endoplasmic reticulum, and to chromosomes during interphase and cell division, respectively, and mediate their transport throughout the cell *via* minus end-directed motors (Figure 51A, B) (Kanfer et al. 2017). Microtubules can be also cross-linked with actin filaments. End-binding proteins (EB proteins) that are present on the growing MT tip can create a platform and recruit actin-binding adaptor and regulatory proteins, and mediate the nucleation of actin filaments from MT tips (Figure 51C) (Henty-Ridilla et al. 2016). Proteins found at the MT tips as well as motor proteins are MAPs.

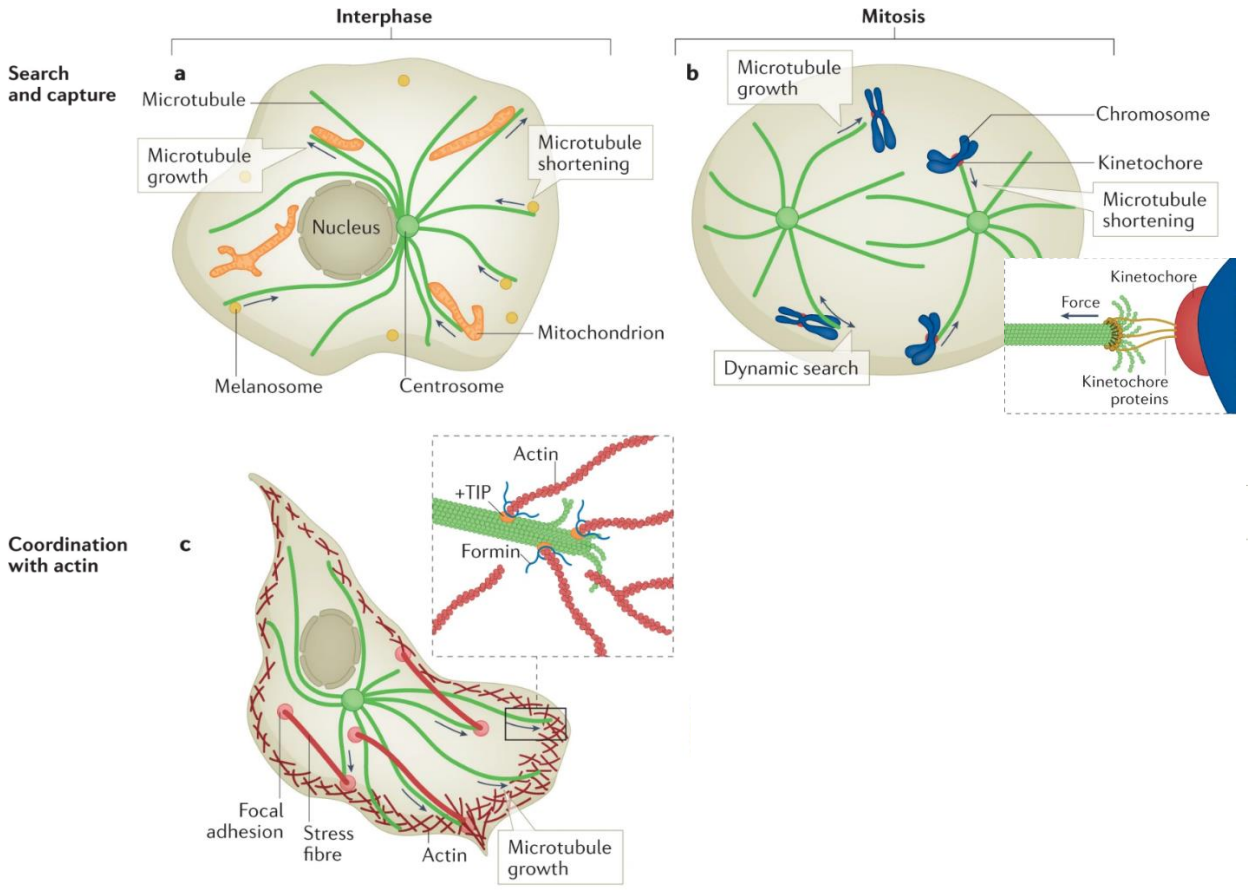

Figure 51: Microtubule dynamics during interphase and mitosis. *(a, b) Dynamic microtubules search and capture of membrane-bound organelles such as mitochondria and melanosomes by microtubule tips during interphase (a) and of chromosomes during mitosis (b). (b) Microtubule tips interact with the kinetochore and use pulling forces to transport chromosomes. (c) Growing microtubules can create a hub where plus-tip interacting proteins (+TIP) recruit actin-interacting proteins, such as formin, to catalyse actin microfilament growth. From Gudimchuk and McIntosh 2021.*

In the testis, Sertoli cells have a very complex cytoskeleton that stretches across the entire seminiferous epithelium (Figure 52).

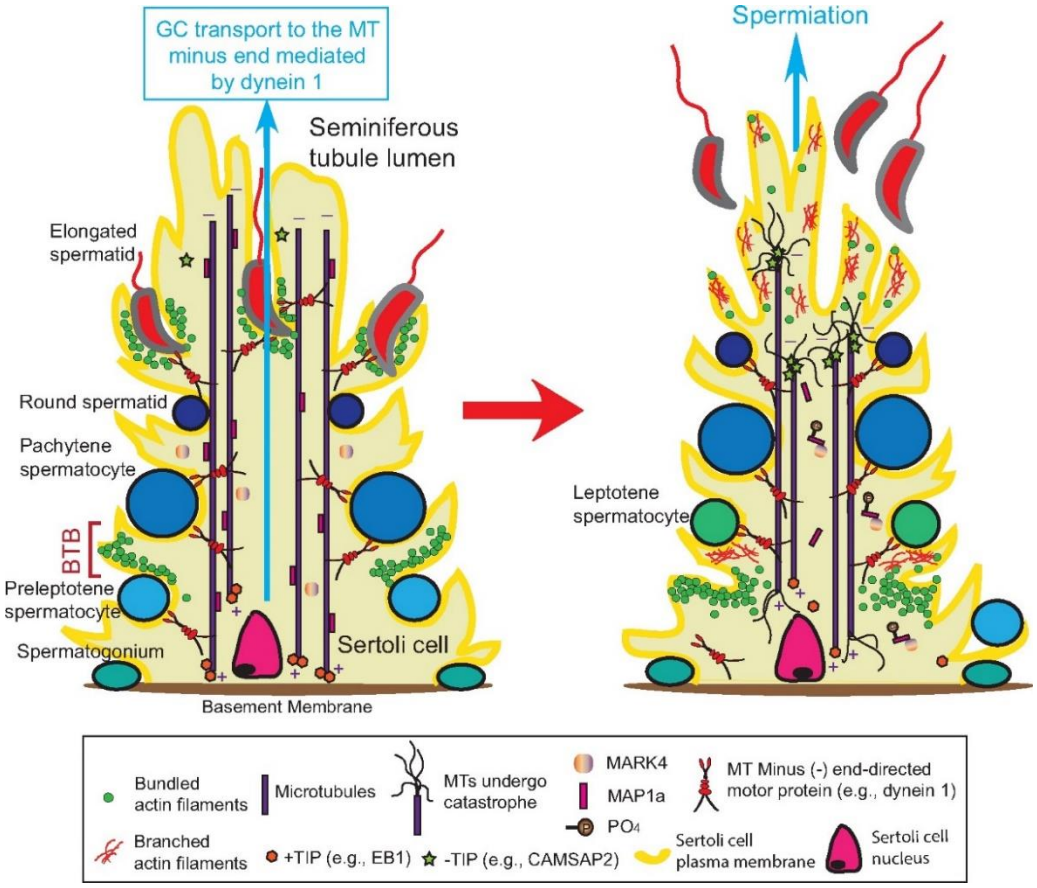

Figure 52: Model of the dynamic microtubule (MT) cytoskeleton and germ cell transport in the seminiferous epithelium. *Microtubules in Sertoli cell cytoplasm are polarized and stretch across the entire seminiferous epithelium. (Left) MTs are stabilized at their ends by +TIP and -TIP end-tracking proteins. Germ cells (GC) are transported by minus end motor proteins along MT tracks towards the tubule lumen. Actin filaments are present in apical ectoplasmic specializations and in tight junctions of the blood-testis barrier (BTB). (Right) Binding of calmodulin-regulated spectrin-associated protein (CAMSAP2) to the MT minus end triggers MT catastrophe that, along with the degeneration of ectoplasmic specializations, supports spermiation. From L. Wang et al. 2020.*

Microtubules and F-actin mediate Sertoli-Sertoli and Sertoli-germ cells interactions and participate in protein trafficking and germ cell transport across the seminiferous epithelium (Tang, Lee, and Cheng 2016). Sertoli cell MTs form stalk-like structures that lay perpendicular to the basement membrane and span the entire epithelium. The MT plus end is located near the basement membrane and the minus end is oriented towards the seminiferous tubule lumen (Redenbach and Vogl 1991; Redenbach and Boekelheide 1994). Important vesicle transport along actin tracks is mediated by

myosin VIIa, and along MT tracks by kinesin to the MT plus end, and by cytoplasmic dynein towards the minus end (Wen et al. 2019; 2018). During spermatogenesis, spermatocytes are transported across the blood-testis barrier (Mruk and Cheng 2015) and elongating spermatids, embedded Sertoli cell crypts, move up and down the adluminal compartment. It is believed that MT motors including dynein 1 and kinesin KIF15 mediate this transport (Wen et al. 2016; Tang, Lee, and Cheng 2016; Lingling Wang et al. 2020). MAP stabilizers and growing end-binding (EB1) and minus end-binding proteins (CAMSAP2) mediate MT and actin integrity in the seminiferous epithelium, and regulate the blood-testis barrier (Tang et al. 2015; Mao et al. 2019; Mao, Ge, and Cheng 2020).

5 MICROTUBULE INNER PROTEINS

Microtubule inner proteins (MIPs) were first recognized as periodic densities in the lumen of microtubule doublets in *Chlamydomonas* flagella by cryo-electron tomography (Nicastro et al. 2006; 2011). Most studies are based on unicellular organisms and the sea urchin, however recent studies also showed MIPs in mammalian cilia and flagella (Z. Chen et al. 2023; Leung et al. 2021; Kiesel et al. 2020; Gui, Farley, et al. 2021). MIPs are present in MT singlets and doublets, in both A- and B-tubules. Their composition varies among species and cell types (Leung et al. 2021; Z. Chen et al. 2023). Figure 53 shows MIPs densities in axonemal outer MT doublets and in the central apparatus of the mouse.

MIPs specifically bind α- or β-tubulin and form lateral and longitudinal interactions with each other and cross multiple tubulin protofilaments. They can be divided into 3 classes: globular MIPs that protrude into the MT lumen, filamentous MIPs that are present at clefts between protofilaments and contain a single helix, and extended MIPs that lack secondary structures (Ma et al. 2019; Leung et al. 2021; Ichikawa et al. 2017). As was mentioned previously in *Chapter 1: The spermatozoon, subchapter 2.1.5 Molecular rulers,* MIPs with similar periodicities (8, 16, 48 nm) cluster together and form interconnected networks. Filamentous MIPs have a 48-nm periodicity, whereas globular and extended MIPs repeat every 8, 16, or 48 nm.

As was shown in the *Chlamydomonas,* MIPs appear to have several functions (Ma et al. 2019). MIPs were shown in the MT lumen, at the junction between the A- and the B-tubule, and many were protruding to the outside of the doublets through openings between adjacent protofilaments.

At these sites, they can be in contact with ODA proteins. These MIPs are believed to create novel protein binding sites and thus dictate the correct position of axonemal structures on the axoneme.

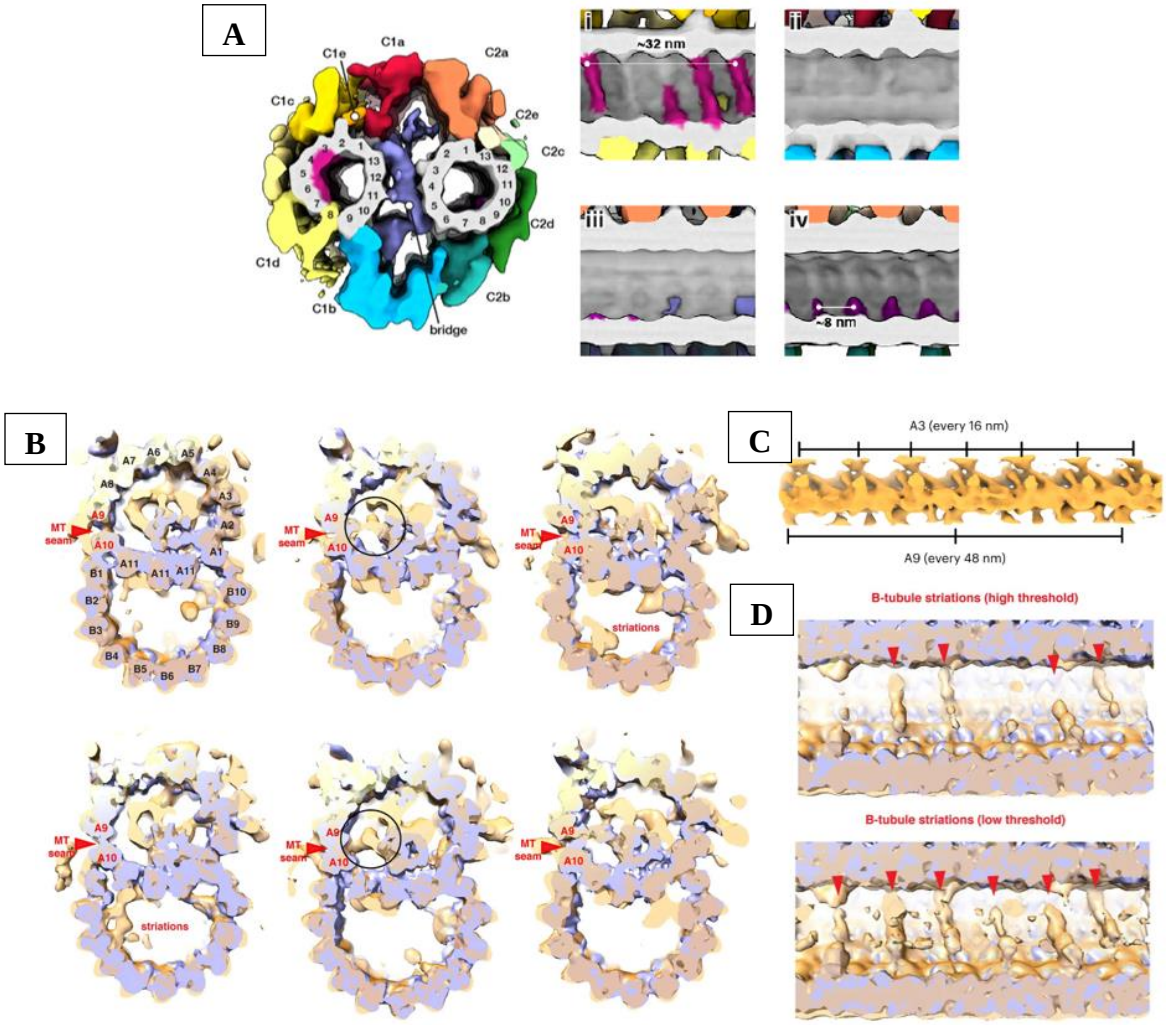

Figure 53: MIPs in the mouse sperm axoneme. *(A) Views of the lumen of the microtubules C1 (i, ii) and C2 (iii, iv) of the central apparatus. Images i and iii represent the left side of the lumen, and images ii and iv correspond to the right side. Microtubules are shown in grey and individual MIPs are in pink and violet. MIPs are of unknown function. From Leung et al. 2021. (B) Six cross-sections of outer microtubule doublets of the 48-nm repeat of doublet. The mouse sperm axoneme structure (orange) is compared with bovine trachea cilia (blue) from Gui et al. 2021, showing differences in MIP densities. An additional density is located close to A9-A10 protofilaments (circled). Longitudinal view of the MIP densities present in the A-tubule (C) and in the B-tubule (D). (C) The MIP densities connect with the protofilament A3 every 16 nm, and with the protofilament A9 with a 48 nm periodicity. (D) Images with high and low acceptance threshold. Striations repeat every 8 nm. From Chen et al. 2023.*

MIPs can also influence the angle between tubulin protofilaments and thus affect the structure of microtubule doublets (Ichikawa et al. 2017). Moreover, MIPs are generally believed to confer stability to microtubules so that they withstand ciliary/ flagellar beating (Owa et al. 2019; Ma et al. 2019) Their lateral and longitudinal interactions with the tubulin lattice are believed to prevent depolymerization of MT doublets.

Around 33 MIPs have been identified in the *Chlamydomonas* and some of their orthologues were studied in humans. Mutations in these proteins were associated with laterality abnormalities, *situs inversus*, recurrent respiratory infections, PCD, and male infertility (Ma et al. 2019). The function and identity of most mammalian MIPs is unknown.

6 MICROTUBULE-BASED STRUCTURES

6.1 THE CENTROSOME

The centrosome contains two distinct structures: a pair of barrel-shaped centrioles connected by a linker and a surrounding proteinaceous matrix called the pericentriolar material (PCM) (Figure 54) (Doxsey 2001).

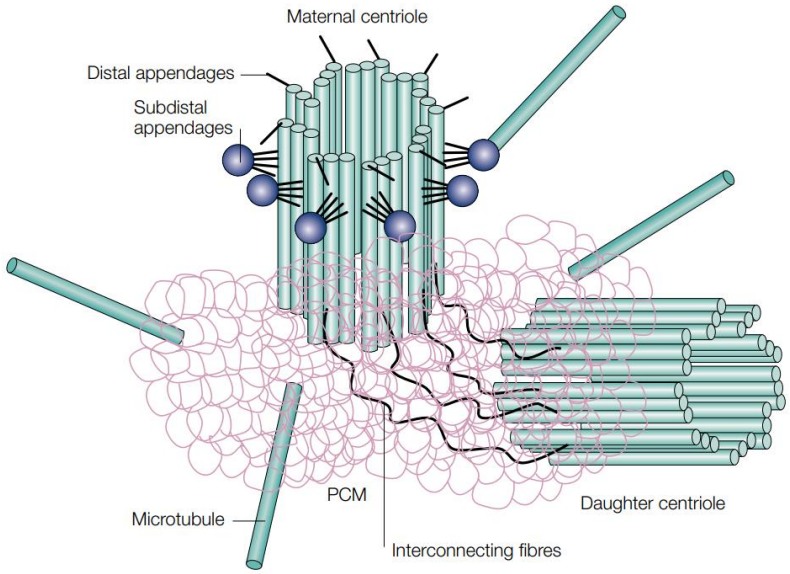

Figure 54: Model of a centrosome. *The centrosome is composed of a mother (maternal) centriole and a daughter centriole connected by interconnecting fibers or a linker. The centrioles are surrounded by pericentriolar material (PCM) that is responsible for microtubule nucleation and anchoring. From Doxsey 2001.*

The centrosome is a non-membrane bound organelle that constitutes the major MTOC of most animal cells. Except for plants and some mammalian embryos (Hamada 2014; Howe and fitzharris 2013; Zenker et al. 2017), the centrosome is essential for cell division where it forms the poles of the mitotic/ meiotic spindle and nucleates and anchors the microtubule network of the spindle. Its deregulation can lead to incorrect cell division and cancer (LoMastro and Holland 2019). As was already discussed before, centrioles are also essential for the formation of cilia and flagella.

6.1.1 Centriolar structure

Mammalian centrioles are typically 450-500 nm in height and 200-250 nm in outer diameter (Figure 55). The centriole pair contains a mother centriole, also called the distal centriole, and the daughter centriole also known as the proximal centriole. The terms "distal" and "proximal" refer to their position relative to the nucleus in spermatids. The mother centriole gave rise to the daughter centriole in the previous cell cycle (Nigg and Holland 2018). The two centrioles are connected *via* a centriolar linker.

Centrioles are MT-based and are thus also polarized structures along their long axis. The centriole is nucleated at its proximal end, then follows the central region, and an axoneme can assemble at the centriolar distal end. Centrioles are formed of 9 triplets of interconnected microtubules that are radially arranged at the periphery. The MT triplets are called the A-, B- and C-tubule. The A-microtubule contains 13 tubulin protofilaments, whereas the B- and C-tubules are incomplete, and each contains 10 protofilaments. The A-tubule is connected to the C-tubule of the next triplet *via* an A-C linker (Klena et al. 2020). In human centrioles, MT triplets are present at the proximal end and change to doublets towards the distal end, at about 50% of their length, by discontinuing the C-tubule (Gönczy 2012; Vasquez-Limeta and Loncarek 2021; Le Guennec et al. 2020).

A helical inner scaffold is present in the central region of the centriole (Figure 55). It lines the lumen and maintains cohesion between MT triplets. The inner scaffold contains several known centriolar proteins including Centrin, POC5, POC1B, and FAM161A (LeGuennec et al. 2021; Klena et al. 2020; Le Guennec et al. 2020).

The mother centriole's distal end is decorated by distal and subdistal appendages that are essential for ciliogenesis (Figure 55). Their shape and number varies between cells and is dependent on the laboratory preparation (Uzbekov and Alieva 2018). Subdistal appendages contain six proteins

including ODF2, CEP128, and Centriolin. The distal appendage anchor ciliary vesicles (N. A. Hall and Hehnly 2021), mediate docking of the mother/ distal centriole to the cell plasma membrane (Tanos et al. 2013), and serve as assembly points for the recruitment of IFT trains (Deane et al. 2001). Subdistal appendages anchor MTs and position centrioles with cilia within the cell (Delgehyr, Sillibourne, and Bornens 2005; Mazo et al. 2016; Tateishi et al. 2013).

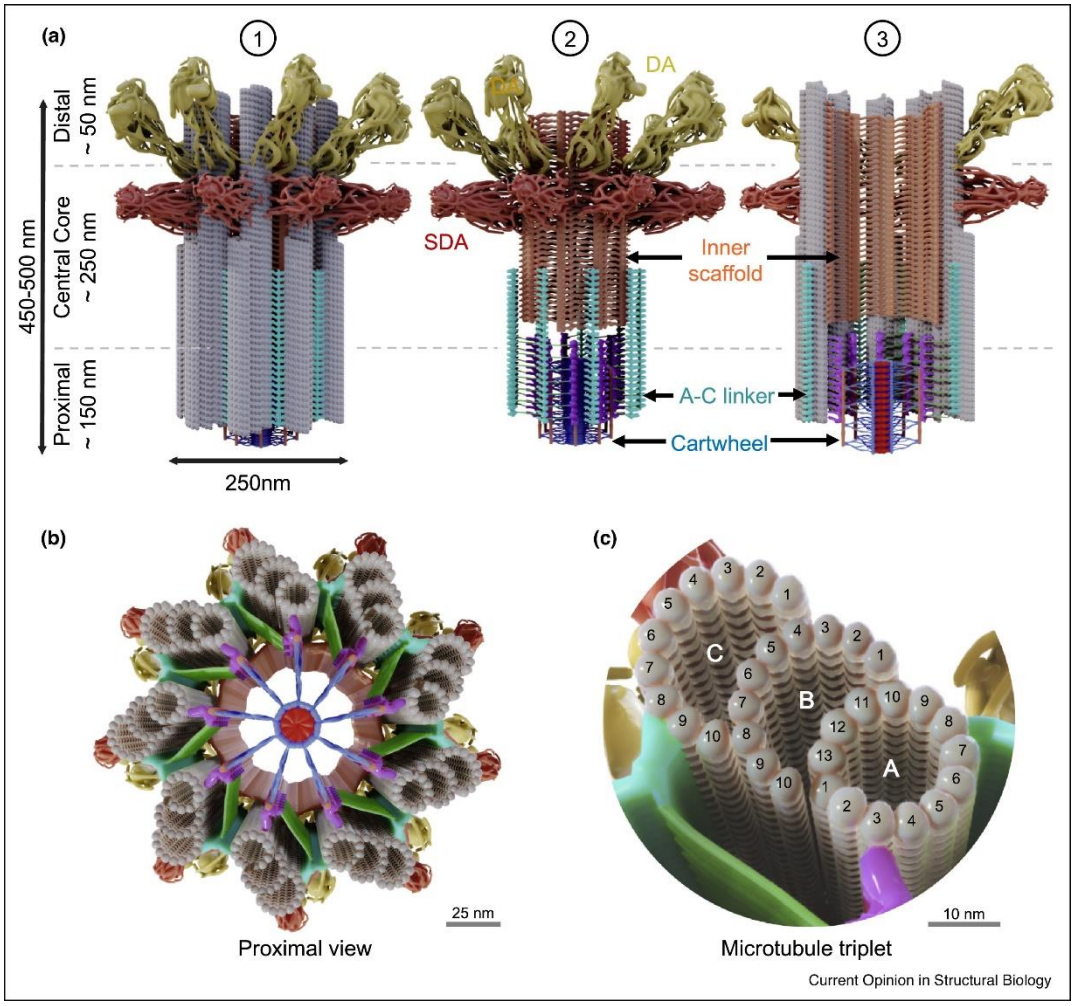

Figure 55: Model of centriolar structure. *(a) A complete model of a centriole divided into the proximal, central, and distal region Microtubules are shown in grey (1). Model without microtubules showing non-microtubule structural features (2). Cross-section of a centriole showing the inner structure (3). (b) View of a centriole from the proximal side. (c) Microtubule triplets of the centriole showing numbered protofilaments. Abbreviations: subdistal appendages (SDA), distal appendages (DA). From LeGuennec et al. 2021.*

6.1.2 Centriolar tubulin code

Centriolar microtubules are very stable and grow slowly, about 30000 times slower than cytoplasmic microtubules (Guichard, Laporte, and Hamel 2023). Centriolar MTs are not only associated with α- and β-tubulin, but also with δ- and ε-tubulin isotypes in rodents, humans and unicellular organisms (Stathatos et al. 2021). They also carry PTMs including acetylation, glutamylation, and detyrosination. Acetylation is one of the best known PTM of centrioles and predominantly occurs on lysine 40 residue (K40) of both α- and β-tubulins. It is the only tubulin PTMs found in the MT lumen. It is mediated by the tubulin acetyl transferase αTAT1 whose absence increases MT resistance against depolymerization and leads to male subfertility in mice (Kalebic et al. 2013). Acetylation decorates most of the MT wall in mature centrioles and appears gradually from the proximal to the distal end during centriole formation (Sahabandu et al. 2019). Its exact role in centrioles is unknown, however it is believed to convey mechanical resistance and stability to MTs (Janke and Montagnac 2017). Glutamylation occurs on centriolar and mitotic spindle MTs. Polyglutamylation of centriolar MTs occurs on both α- and β-tubulin in contrast with cytoplasmic MTs where the PTM is associated with β-tubulin (Bobinnec et al. 1998). It is essential for centriole maturation and MT stability and might also strengthen interactions between the centriole and the PCM (Guichard, Laporte, and Hamel 2023). Tubulin tyrosination has also been observed on centriolar MTs during the whole cell cycle except for mitosis (Balashova, Lokhov, and Bystrevskaya 2009), however its role in centrioles has not been investigated.

6.1.3 Pericentriolar material

The pericentriolar material (PCM) was for long believed to be an amorphous cloud surrounding the centrioles. Instead, the PCM has an organized architecture (Figure 56) (Mennella et al. 2014; Fry et al. 2017). It is organized into annular concentric layers around the centrosome, ranging from 200 to 500 nm in diameter. The primary function of the PCM is to nucleate and anchor microtubules. Tubulin dimers concentrate at the centrosome and MT nucleation is mediated by γ-TURCs that become embedded in the PCM. Major constituents of the PCM, including pericentrin and Cep152 contain many coiled-coil domains and provide a scaffold for protein-protein interactions with centriolar regulators, including proteins involved in centriole duplication.

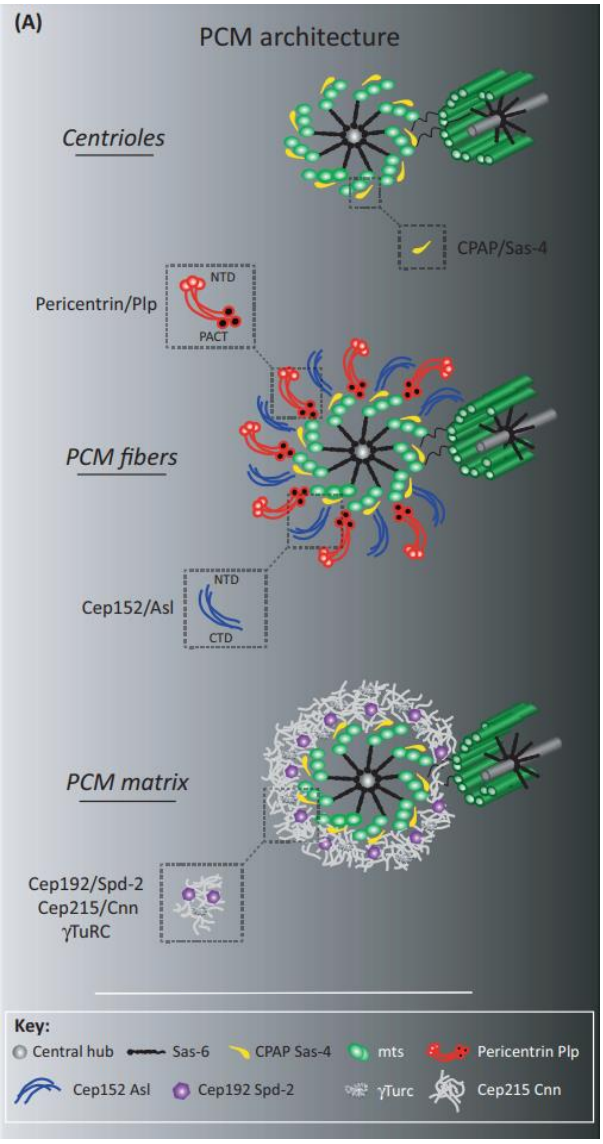

Figure 56: Schematic representation of an interphase centrosome showing the PCM architecture. *Three layers of centrosome architecture show: a pair of centrioles, and two layers of PCM proteins. The proximal layer includes PCM fibers comprised of pericentrin/ pericentrin-like protein (PLP) and Cep152/Asl, elongated coiled-coil proteins with their C-termini close to the centriole wall and N-termini projected outward to the periphery. Pericentrin/PLP can extend from the centriole wall more than 150 nm in human cells. The proximal layer is likely attached to the centriole wall by proteins involved in centriole duplication including CPAP/Sas-4 (Cizmecioglu et al. 2010). The second layer, the PCM matrix, is comprised of Cep215/centrosomin (Cnn), γ-tubulin, and Cep192/Spd-2 molecules that are homogenously organized around the centriole wall. They form a matrix that can extend to the N-terminus region of pericentrin/PLP and Cep152/Asl. Abbreviations: microtubules (mts), N-terminal or C-terminal domain (NTD, CDT). From Mennella et al. 2014.*

6.1.4 Centriole duplication

Most cells have a single MTOC composed of a pair of centrioles. Centrioles duplicate once per cell cycle to assure that both daughter cells inherit one centriole pair (Figure 57). During the G1 phase, the centriole pair is connected *via* a linker also called a "tether". The mother centriole contains both distal and subdistal appendages. Duplication occurs during the G1/S phase parallel to DNA duplication. Each centriole assembles a procentriole that forms perpendicularly from the wall of the older centrioles. The proximal part of the procentriole's lumen contains a scaffolding structure called the "cartwheel" that will interact with a γ-TURC-like structure and give rise to a new centriole that continues to elongate throughout the G2 phase. In late G2, the older centriole is associated with PCM and the procentriole lacks the ability to recruit PCM. The PCM greatly

expands during the G2/M transition in preparation for mitotic spindle formation. During the M phase, the older centrioles separate, and each new pair is positioned at one pole of the mitotic spindle. Each pair will be inherited by one daughter cell. The distal and subdistal appendages might be transiently modified or disassembled during the M phase and will be acquired by the new mother centriole (Nigg and Holland 2018; Gönczy 2012; Guichard, Hamel, and Gönczy 2018). The cartwheel is important for centriole formation but disappears in mature centrioles in human cells (Paintrand et al. 1992; Guichard, Hamel, and Gönczy 2018).

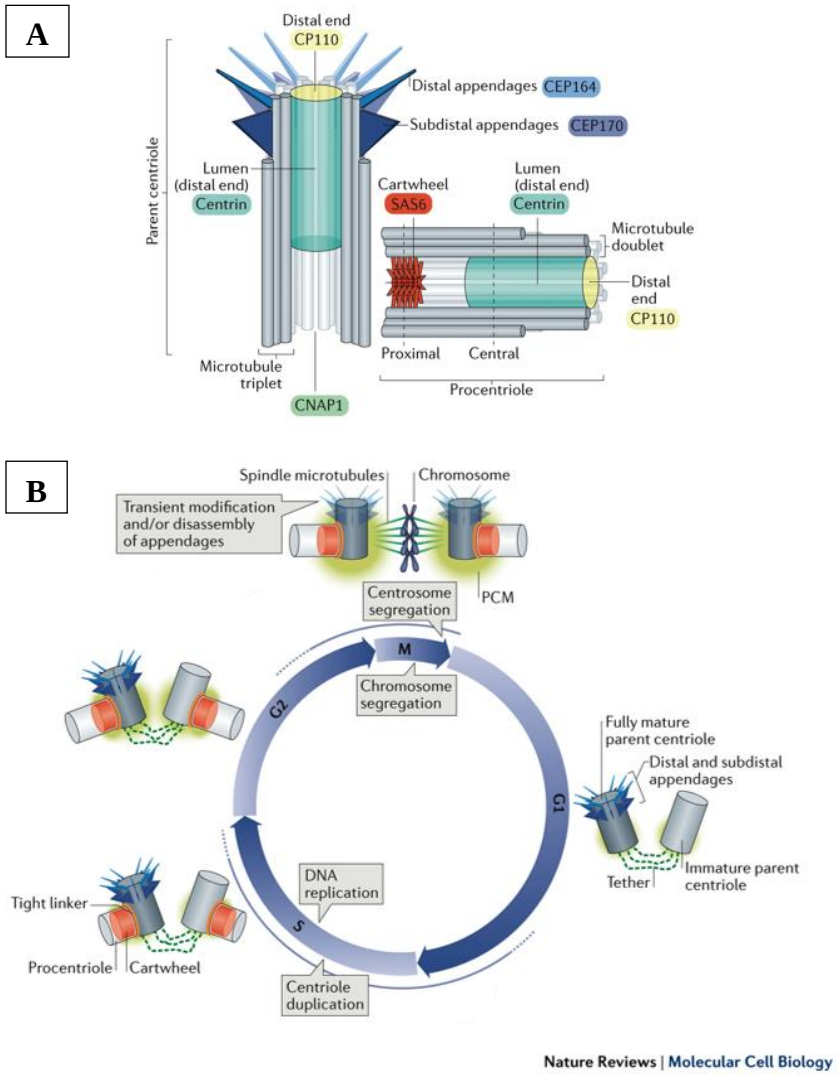

Figure 57: Centriole duplication during the cell cycle. *(A) Structure of a mature centriole and an associated procentriole. (B) Centriolar duplication is coordinated with DNA duplication and cell division. Major proteins associated with every structure and process are shown. See text for description. Adapted from Nigg and Holland 2018.*

6.1.5 Centriolar satellites

Centriolar satellites are small membrane-less cytoplasmic granules that concentrate around the centrosome. Satellites form a very complex interconnected network. They move along microtubules, participate in protein trafficking, and in the regulation of protein contents and availability around the centrosome (Figure 58). They are highly dynamic and their number and composition changes in response to stimuli and cell stress (Prosser and Pelletier 2020; Odabasi, Batman, and Firat-Karalar 2020).

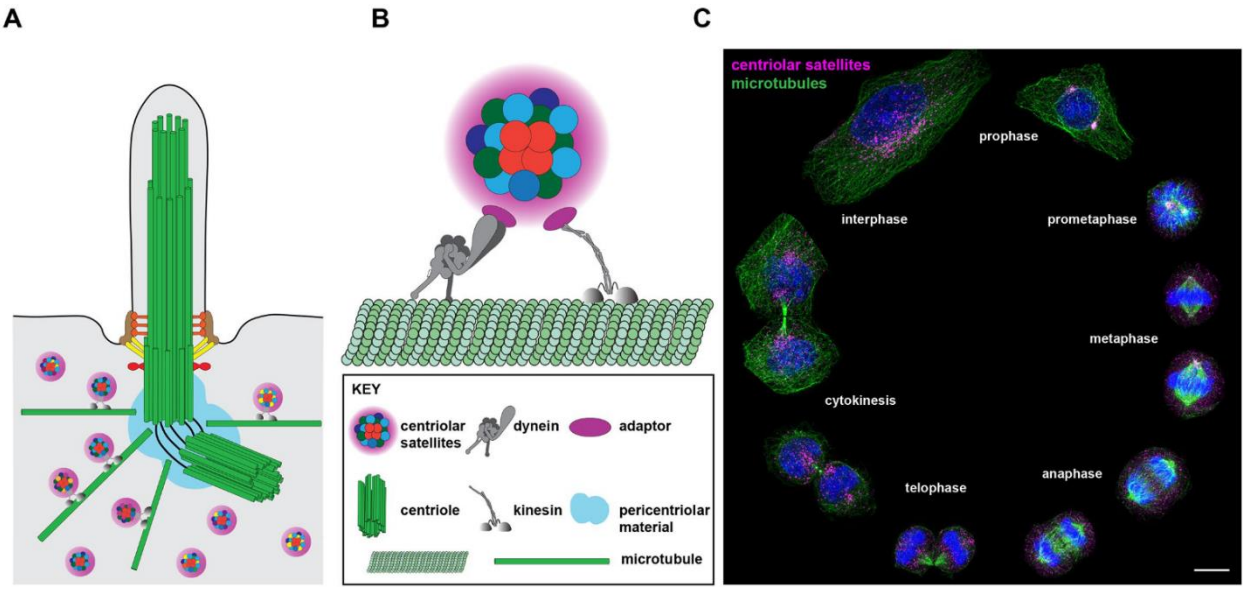

Figure 58: The structure and distribution of centriolar satellites during the cell cycle. *(A) Satellites move along microtubule tracks, concentrate around the centrosome/ basal body, and participate in the regulation of ciliogenesis. (B) Centriolar satellites are membrane-less macromolecular complexes that interact with centrosomal proteins, MAPs, and enzymes such as kinases and ubiquitin ligases. Their interaction with microtubule motor proteins is mediated by adaptor proteins. (C) Dynamic distribution of centriolar satellites based on PCM1 (pink) during the cell cycle. Microtubules are labeled in green, and DNA in blue. Satellites appear as dots and concentrate around the centrosome in interphase, at spindle poles during prophase and prometaphase, and are dissolved during the rest of mitosis, and reappear during cytokinesis. Some centriolar satellites were shown to persist at the centrosome during mitosis (Kim et al. 2004; Batman, Deretic, and Firat-Karalar 2022). From Odabasi, Batman, and Firat-Karalar 2020.*

Satellites were first identified as 70-100 nm electron-dense granules (Bernhard and de Harven 1960; Bessis and Breton-Gorius 1958; de-Thé 1964). Proteomic studies showed that satellites share similar protein composition as the centrosome (Gheiratmand et al. 2019; Quarantotti et al. 2019). So far, 65 satellites have been identified and observed at satellites by cellular co-localization

studies (Prosser and Pelletier 2020). Pericentriolar Material 1 protein (PCM1) was the first identified centriolar satellite and is believed to be essential for the assembly of all or the majority centriolar satellites (Kubo et al. 2010; Dammermann and Merdes 2002). PCM1 has long been used as a marker of satellites, and many satellite proteins have been identified through proteomics studies based on co-immunoprecipitation with PCM1 (Gupta 2021; Gheiratmand et al. 2019; Quarantotti et al. 2019). New studies showed that some protein interactions persist in the absence of PCM1 and that PCM1 might be absent from some populations of satellites (Gheiratmand et al. 2019).

Lack of certain centriolar satellites has been associated with ciliopathies and, in some cases, with male infertility, including mutations in *Pcm1* and *Azi1/Cep131* (Lopes et al. 2011; E. A. Hall et al. 2013; 2022). A knockout of *Pcm1* in mice was associated with prenatal mortality, and the surviving individuals suffered from dwarfism, male infertility, ciliogenesis defects, hydrocephaly, and cerebellar hypoplasia. Sperm numbers were highly reduced, immotile, and showed an abnormal manchette and defects of the HTCA and in axoneme formation. The authors proposed that during ciliogenesis, PCM1 removes cap proteins CP110 and CEP97 from the mother centriole, a step important for subsequent steps in ciliogenesis, including centriole binding to preciliary vesicles, formation of the transition zone, and recruitment of the IFT machinery (E. A. Hall et al. 2022). A similar ciliary mechanism might be involved in sperm formation and explain the observed defects. The absence of *Azi1/Cep131*, another centriolar satellite important for ciliogenesis, was shown in mice to lead to isolated infertility without ciliopathies, with an abnormal ectopic manchette with impaired IMT and PTMs, axoneme malformation, and misaligned HTCA (E. A. Hall et al. 2013). To conclude, centriolar satellites also appear to be involved in spermatogenesis, even-though their involvement is still poorly known.

6.2 THE MITOTIC SPINDLE, THE MIDZONE AND THE MIDBODY

The bipolar mitotic spindle is another microtubule-based structure. During mitosis, spindle MTs can be nucleated by the kinetochore, however the centrosome appears to be the main nucleator of the spindle. Prior mitosis, the interphase MT network disassembles, the centriole pair duplicates during the S/G2 phase and the PCM rapidly expands around each mother centriole in preparation for nucleation of spindle MTs (Figure 57) (Hoffmann 2021). During the mitotic prophase, the two centriole pairs/ centrosomes separate, and each migrates to the opposite pole of the cell. In prometaphase, MTs are nucleated from the centrosomes, start to search for the chromosomes with their growing tips, and orient them at the metaphase plate (Figure 51, Figure 59).

The mitotic spindle is formed of three types of microtubules: kinetochore MTs (k-fibers), astral MTs and non-kinetochore MTs (Figure 59) (Prosser and Pelletier 2017; Glotzer 2009). K-fibers are attached to chromosomes *via* the kinetochore and mediate their movement. Their MT minus-ends are embedded in the centrosome and the plus-ends are connected to the kinetochore. Astral MTs emanate from each spindle pole and interact with the cell cortex, a thin layer of actin cytoskeleton that is associated with the plasma membrane and plays key roles in cell mechanics (Svitkina 2020). This interaction is important for spindle positioning (Grill and Hyman 2005). Non-kinetochore MTs extend from each pole and help stabilize the structure.

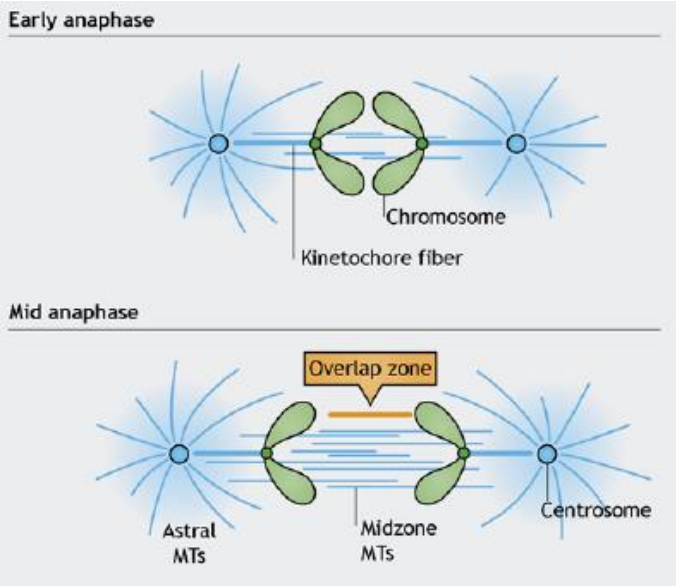

Figure 59: Schematic illustration of three types of microtubules (MTs) present at the mitotic spindle. *Kinetochore microtubules connect the chromosome to the spindle poles, astral microtubules emanate from the poles to the periphery, and non-kinetochore (midzone) microtubules localize to the midzone/ central spindle. From Glotzer 2009.*

Chromosome segregation begins during early anaphase (Figure 60). The minus-ends of non-kinetochore MTs are anchored at the centrosome, and their plus-ends localize in a region between the segregating chromosomes. As anaphase progresses, they lose their interaction with the spindle poles. These MTs overlap and bundle between the segregating chromosomes, and form a structure called the "midzone". Some authors define the midzone as the entire region between the two poles, and the zone where the MTs overlap is referred to as the "central spindle" (Glotzer 2009). Others refer to the central spindle as the midzone (Wadsworth 2021), and we will use this definition here. MTs that occupy the central spindle/ midzone will be called "midzone microtubules", and others have also used names including interchromosomal, interpolar, and interzonal microtubules. As anaphase progresses, midzone MTs become progressively more bundled and show a well-defined zone of overlap.

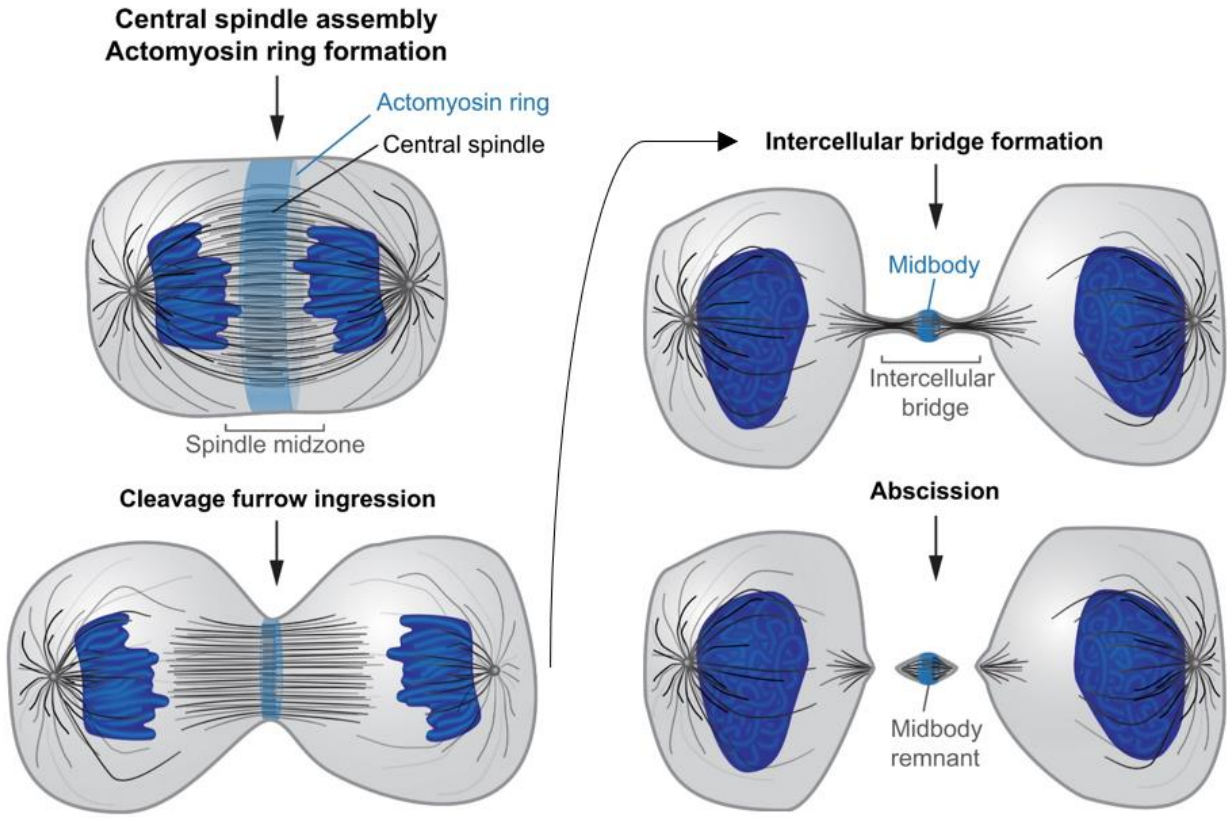

Figure 60: Schematic illustration of the midzone/ central spindle assembly, midbody formation and abscission in mammalian cells. *Adapted from Mierzwa and Gerlich 2014.*

A recent study in human cells and *C. elegans* also showed that during later stages of anaphase, midzone microtubules are no longer connected to the centrosomes and some of them are connected to chromosomes. Laser ablation of these MTs blocked chromosome from migrating towards the spindle poles, suggesting a role of the midzone in this process (C.-H. Yu et al. 2019). Some authors also claimed that midzone microtubules originate from the chromosome region and not from the centrosomes, and they are nucleated from existing microtubules (Uehara and Goshima 2010).

The assembly of the midzone is mediated by MAP complexes including MT plus-end-tracking proteins that accelerate MT assembly, proteins involved in MT bundling, several kinesin motor proteins, and mitotic kinases. In telophase, an actomyosin contractile ring compacts the midzone and the two daughter cells become connected by a cytoplasmic bridge. In the center of the cytoplasmic bridge is the compacted midzone called the "midbody". The midbody is essential for cytokinesis and concentrates proteins in a spaciotemporal manner to regulate abscission. Some of its components come from the midzone and the contractile ring, while others are delivered in endocytic and Golgi-derived vesicles.

The intercellular bridge becomes a site for a dynamic accumulation and fusion of intracellular vesicles that are targeted here from both daughter cells (Figure 61). Vesicles are delivered along MTs or actin by molecular motors kinesin, dynein, and myosin. They are docked to a target membrane by tethering complexes, such as exocyst, and become inserted into it by SNARE proteins (Soluble N-ethylmaleimide-sensitive factor Attachment Proteins REceptor). These processes are regulated by several Arf and Rab family GTPases, e.g., Rab8, Rab11, Rab35. These GTPases are associated with endosomal vesicles that are transported to and from the intercellular bridge, accumulate at the midbody in later stages, and are required for proper abscission.

First, the intercellular bridge filled with MTs progressively diminishes in diameter and becomes locally constricted at the site of abscission, called the "secondary constriction" side that is positioned next to the midbody. Then, F-actin cytoskeleton and local microtubules are cleared from the abscission site, allowing the recruitment of the ESCRT-III (endosomal sorting complexes required for transport) complex. It interacts with MT severing proteins such as spastin, and mediate membrane remodelling and fusion in a zone that lacks actin and microtubules, likely triggering abscission (Figure 61) (Halcrow et al. 2022; Frémont and Echard 2018; C.-T. Chen, Hehnly, and

Doxsey 2012; Mierzwa and Gerlich 2014; Glotzer 2009; Wadsworth 2021; Lakshmi, Nair, and Manna 2018; Prosser and Pelletier 2017; Echard 2012).

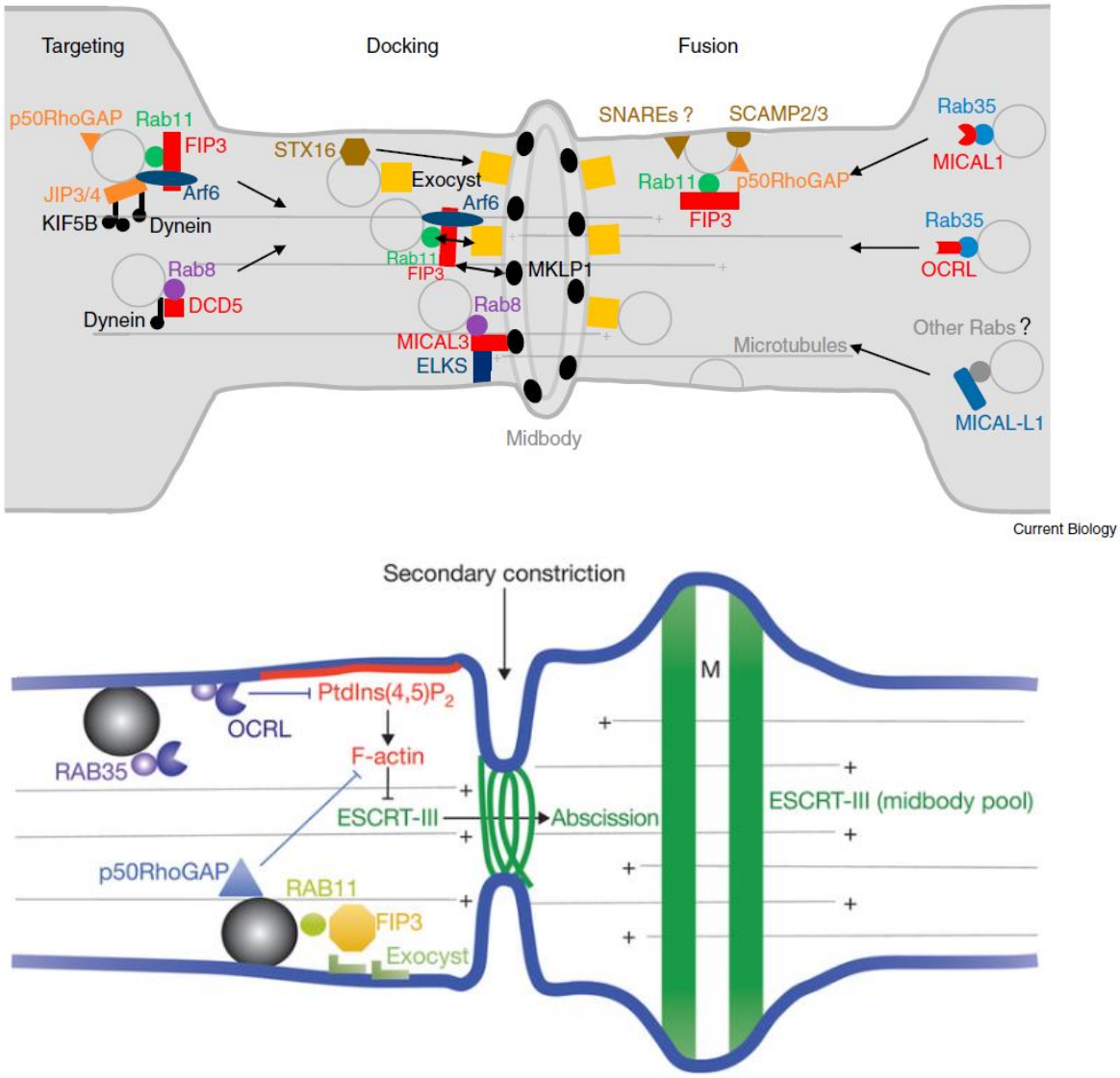

Figure 61: Vesicle and membrane traffic at the midbody during cytokinesis. *Secretory vesicles derived from the Golgi and the endocytic pathway are transported by dynein and kinesin motors along microtubules (e.g., KIF5B) in a bidirectional manner. The vesicles are associated with Rab and Art GTPase families whose effectors are labeled in red. Vesicles are docked to the target plasma membrane by the exocyst, and their fusion with the target membrane is mediated by SNARE proteins. MKLP1 is a kinesin that localizes the exocyst and other docking complexes at the center of the intercellular bridge. Rab11 and Rab35 along with MICAL and OCRL participate in F-actin depolymerization at the midbody that is important for abscission and allows the recruitment of the ESCRT-III machinery. Cytokinesis is highly complex and only a part of these processes and proteins is depicted on this figure. Top figure is from Frémont and Echard 2018, bottom figure was adapted from Echard 2012.*

Cell division in animal cells is also highly regulated by membrane composition of phosphoinositides, that refer to phosphatidylinositol and its seven derivatives (Cauvin and Echard 2015). They regulate cell shape and orientation of the mitotic spindle, participate in the stability of the intercellular bridge where they recruit cytoskeleton binding proteins and force generators. Hydrolysis of these lipids and their specific concentrations in the plasma membrane are also important for correct cytokinesis, including membrane traffic and abscission.

Disruption of the highly complex and interconnected protein trafficking system during the cytokinesis might result in cell death. However, an incomplete abscission is also normal in some cell types and it is widespread across eukaryotes (Chaigne and Brunet 2022). For instance, they are common in male germ cells including human and mouse spermatogonial stem cells (Niedenberger et al. 2018; Greenbaum et al. 2011).

Following abscission, the midbody membrane can be cleaved on both sides and the midbody remnant can be released into the extracellular space or can be inherited by one of the daughter cells if the cleavage only occurs on one side of the intercellular bridge (Figure 62) (Bernabé-Rubio et al. 2016; Ott 2016; Labat-de-Hoz et al. 2021b). When inherited, the midbody remnant moves along the apical surface of the daughter cell towards the proximal centriole that was docked to the plasma membrane. When the remnant comes close, the centrosome starts to assemble a primary cilium. The remnant is believed to provide factors involved in primary ciliogenesis (e.g., IFT proteins, Rab8, signalling proteins) that are present in the resting arm of the intercellular bridge, and feed the centrosome with cellular membranes to build the primary cilium.

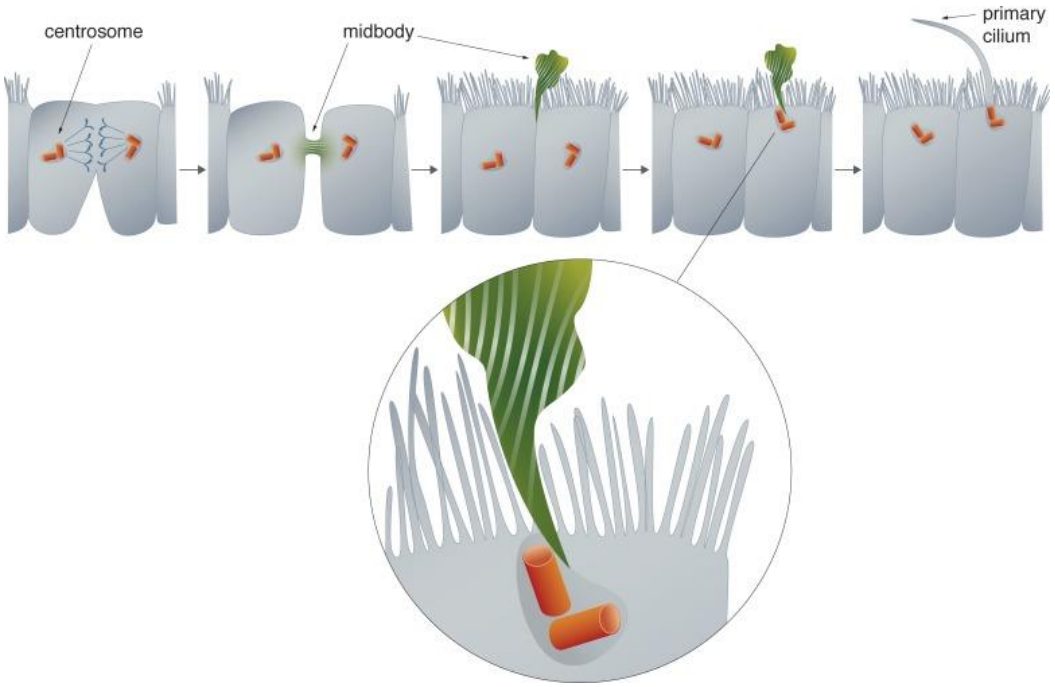

Figure 62: Inheritance of midbody remnant licenses primary ciliogenesis in epithelial cells. *After cytokinesis, the midbody cleaved at one side of the intercytoplasmic bridge is inherited by one of the daughter cells. The midbody remnant moves along the apical surface toward the centrosome that was relocated to the plasma membrane, concentrates ciliary machinery and it participates in primary ciliogenesis. From Ott 2016.*

CHAPTER 4: INFERTILITY

1 INTRODUCTION

The majority of adults have a desire to be parents. Not all couples will, however, spontaneously achieve a pregnancy due to fertility issues of one or both partners. Infertility is a disease of the male or female reproductive system that is defined by the World Health Organization (WHO) as "the inability to achieve a pregnancy after 12 months or more of regular unprotected intercourse" (WHO, 2022). Millions of people around the world have fertility problems and the infertility rates are on the rise (Minhas et al. 2021). While the precise numbers are hard to obtain, it was estimated that a median of 9% of couples are suffering from infertility worldwide (Boivin et al. 2007). Infertility and childlessness are psychologically difficult for many couples and can have severe social consequences, particularly in developing countries (Ombelet et al. 2008).

2 MALE INFERTILITY

Male infertility, solely or in conjunction with the female factor, accounts for 50% of all infertility cases (Agarwal et al. 2015). It is a complex multifactorial pathology that may be congenital or acquired due to illnesses, injuries, lifestyle choices or exposure to environmental pollutants and toxins (Kumar and Singh 2022). Male infertility can be divided into three major categories: ductal obstruction or dysfunctions, hormonal (hypothalamic-pituitary axis) disorders, and spermatogenic quantitative and/ or qualitative defects (Tournaye, Krausz, and Oates 2017).

Potential male fertility is routinely estimated based on medical and reproductive history, physical examination, and standardized semen analysis guidelines published by the WHO (World Health Organization 2010; 2021). A confirmed finding of a semen abnormality can lead to a second-line investigation including a microbial, endocrine, and imaging assessment and a third-line investigation with genetic testing and testicular histology/ cytology (Ferlin and Foresta 2020).

Semen analysis can provide an invaluable first insight into a man's fertility potential. Sperm parameters include semen volume, pH, viscosity, and sperm concentration, motility, vitality, and morphology (

Table 1). Disturbances of spermatogenesis can lead to a decrease in sperm concentration (oligozoospermia) or to a complete absence of spermatozoa in the ejaculate (azoospermia). Spermatozoa can bear one or several morphological defects (teratozoospermia) that can affect the sperm head, midpiece, or tail. Abnormalities in sperm flagella often lead to a decrease or absence of sperm motility (asthenozoospermia) (Tournaye, Krausz, and Oates 2017; Ferlin and Foresta 2020). These phenotypes can appear alone or in combinations, with oligo-astheno-teratozoospermia being one of the most common phenotypes that bears both qualitative and quantitative sperm defects (Jungwirth et al. 2012). Reference values for some of these parameters were adjusted in the 2021 WHO 6th edition and terms describing sperm anomalies (e.g., "asthenozoospermia", "teratozoospermia", *etc.*) have been removed. Authors argued that these reference thresholds alone are meaningless and multiple criteria must be considered together to establish a diagnosis for male infertility (Boitrelle et al. 2021; World Health Organization 2010; 2021).

Further biochemical and molecular examinations, including acrosome integrity, the measurement of seminal reactive oxygen species, and sperm DNA fragmentation, could increase the predictivity of fertility potential, however standardized methods and randomized controlled trials are currently missing (Minhas et al. 2021; Ferlin and Foresta 2020).

Pathological semen quality	
Oligozoospermia	Sperm concentration <15x10^6 / mL
Azoospermia	No spermatozoa in the ejaculate
Asthenozoospermia	<42% total motility <30% progressive motility
Teratozoospermia	<4% morphologically normal spermatozoa
Oligo-astheno-teratozoospermia	Disturbance of sperm concentration, motility, and morphology
Cryptozoospermia	Spermatozoa absent from fresh preparation but observed in a centrifuged pellet
Aspermia	No ejaculate
Leucospermia	>1x10^6 ml leukocytes in the ejaculate

Table 1: Nomenclature for anomalies associated with pathological semen quality in humans. *Reference values are given according to men in couples who achieved natural conception within one year of unprotected sexual intercourse. According to World Health Organization 2010; 2021.*

3 GENETICS OF MALE INFERTILITY

Genetic factors are highly associated with male infertility (Vincent et al. 2002). It is estimated that they account for at least 15% of all cases (Tournaye, Krausz, and Oates 2017) and could be present in 30% of infertile men with oligozoospermia or non-obstructive azoospermia (Tüttelmann et al. 2011). They include chromosome abnormalities (sex chromosome aneuploidy, structural chromosome aberrations, copy number variations), including the Klinefelter syndrome, 46,XX male syndrome, Robertsonian translocation, and Y chromosome deletions, and loss-of-function mutations in single genes (Ferlin et al. 2019; Krausz and Riera-Escamilla 2018). Genetic anomalies were inversely correlated with sperm concentration, meaning that the likelihood of genetic anomalies increases with a decreasing sperm count (Krausz and Riera-Escamilla 2018; Pylyp et al. 2013). Genetic screening of infertile patients in the clinic can therefore be beneficial for better diagnosis and subsequent treatment, and should be especially considered during patient counselling for assisted reproductive technologies (ART) (Ferlin et al. 2019).

Male fertility is a complex disease with heterogenous phenotypes, that might be in part explained by a large quantity of genes that are associated with spermatogenesis. The human genome contains approximately 20000 protein-coding genes that in size represent about 2% of the whole genome. Major combined studies of protein expression and RNA sequencing that were behind the human protein atlas revealed that the testis has the highest number of tissue-enriched genes, with more than 1000 genes showing an at least 5-fold higher expression in the testis than in other tissues (Figure 63) (Uhlen et al. 2010; Uhlén et al. 2015; Djureinovic et al. 2014). Approximately 77% (~15400) of all protein-coding genes were expressed in the testis and the majority of them (80%) were also expressed in all other tissues, suggesting that they have "house-keeping" roles such as cell growth and basic metabolism. Out of the resulting 20% (>3000 genes), 1124 genes were shown to be highly (n=364) and moderately (n=760) enriched in the testis, and a large proportion of them are thought to be involved in spermatogenesis. At the moment however, the function of many of these proteins remains poorly characterized (Djureinovic et al. 2014) and around 30-40% of cases of male infertility remain idiopathic (Krausz and Riera-Escamilla 2018; Kothandaraman et al. 2016).

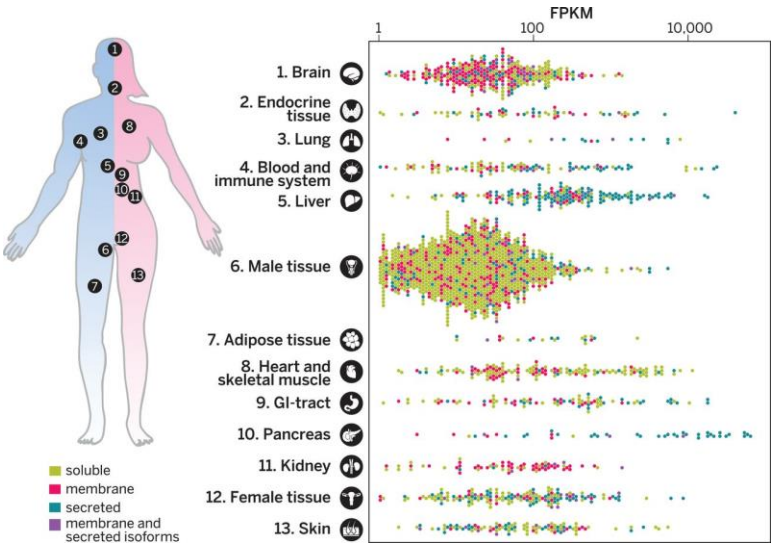

Figure 63: The testis contains the most tissue-enriched proteins in humans. *The study was based on RNA and protein expression studies among 12 other human tissues. FPKM corresponds to mRNA levels. From Uhlen et al., 2015.*

3.1 IDENTIFICATION OF NEW PATHOLOGICAL VARIANTS

The identification of new genes linked to male infertility has been on the rise in the recent years. Approximately 4 genes per year were identified in the period between 2000-2016, and 10 per year in the period of 2017-2019, yielding a 150% increase (Houston et al. 2021). Identification of new genes involved in diseases and cellular processes has been revolutionized by the development of massive parallel sequencing, including whole-genome and whole-exoneme sequencing, that are significantly faster and less laborious than previous technologies.

The search for genetic causes is a part of the diagnostic work-up when other causes of infertility, such as ductal obstruction, absence of the vas deferens, and chromosomal anomalies, have been eliminated and is primarily used for men with severe oligozoospermia or azoospermia (Krausz and Riera-Escamilla 2018; Z.-E. Kherraf et al. 2022). These phenotypes are rare and severe, which suggests a monogenic homozygous mutation could be the cause of the phenotype (Condò 2022; Mitchell et al. 2017). Studies of consanguineous families facilitated the search for homozygous or hemizygous loss-of-function mutations in humans. Rare recessive mutations are predicted to be present in every population, however the union of close relatives significantly increases chances of achieving homozygosity at any genetic locus in the offspring (Erzurumluoglu et al. 2016; Clavijo 2020; Carr et al. 2013). Another option is the recruitment of genetically unrelated patients presenting an identical phenotype which might increase the chances of finding genes implicated in the pathology (Okutman et al. 2018).

Whole-exome sequencing (WES) is frequently used for the identification of causal biallelic mutations. It is used to sequence all coding regions and their flanking regulatory regions including the splice junctions and 3' and 5' untranslated region sequences (Robay et al. 2018). In brief, patient DNA is sequenced and compared to a reference genome, and candidate variants are filtered through an informatics pipeline. The candidate gene should be predominantly or exclusively expressed in the testis, their allelic frequency in the general population should be rare (<1%) and absent from control individuals. The variant should also have a high impact at the protein level causing a loss-of-function (Okutman et al. 2018; Z.-E. Kherraf et al. 2022).

Once a candidate gene has been identified, infertility studies, as is also the case for other pathology studies, frequently use animal models to functionally validate the candidate pathogenic variant. The CRISPR/Cas9 technology has been particularly used for the generation of knock-out mouse models (Z.-E. Kherraf et al. 2018) that have been greatly used in recent infertility studies (Hwang et al. 2021; Kherraf et al. 2017). Other models such as *C. elegans*, zebrafish and *Drosophila melanogaster*, and knock-out models of ciliated and flagellated unicellular organisms including *Trypanosoma*, *Chlamydomonas*, and *Tetrahymena* have also been used to study genes involved in reproduction and fertility (Charles Coutton et al. 2018; Xavier et al. 2021).

4 TERATOZOOSPERMIA

In the following part, we will focus on a subtype of male fertility called teratozoospermia. As was mentioned before, teratozoospermia refers to sperm bearing one or several morphological anomalies of the head, midpiece, or tail. The resulting phenotypes can be very heterogenous: only some or all spermatozoa might be affected, and the abnormal spermatozoa might bear one or a combination of multiple defects (Coutton et al. 2015). The main types of teratozoospermia can be divided into two categories. First, defects can be primary affecting the sperm head, which include globozoospermia, macrozoospermia, and acephalic spermatozoa, and second, flagellum-associated defects, which are referred to as the multiple morphological abnormalities of the flagella (MMAF) syndrome.

Sperm macrocephaly or macrozoospermia (prevalence of <1% in infertile men), globozoospermia (<0.05-0.1%) (Fesahat, Henkel, and Agarwal 2020), and the acephalic spermatozoa syndrome (unknown prevalence) are rare and severe forms of teratozoospermia. Macrozoospermia sperm are

often aneuploid or polyploid, and have irregular, large heads, a variable number of tails, and low to no motility (Nistal, Paniagua, and Herruzo 1978; Chianese et al. 2015). Globozoospermia is characterized by round-headed spermatozoa that have altered genome packaging and DNA damage, and no acrosome (Yassine, Escoffier, Martinez, et al. 2015). These spermatozoa have difficulties to activate and fertilize an oocyte due to missing enzymes in the acrosome, such as phospholipase Cζ (Escoffier et al. 2015). The acephalic spermatozoa syndrome is defined as semen composed of mostly headless spermatozoa with the separation mostly occurring between the nucleus and the centriolar region (Mazaheri Moghaddam et al. 2021). The MMAF syndrome was the focus of the thesis and will be described in the next chapter.

4.1 MULTIPLE MORPHOLOGICAL ABNORMALITIES OF THE SPERM FLAGELLA

The MMAF syndrome is characterized by a heterogenous phenotype with several types of flagellar defects, including short, coiled, bent, irregular or missing flagella (Figure 64) (Ben Khelifa et al. 2014). Flagellar defects have a severe negative effect on sperm motility, with sperm showing reduced motility or no motility at all, and their phenotype is therefore defined as astheno-terato-zoospermia. At the ultrastructural level, the axonemal defects can be due to missing, multiplicated or disorganized axonemal and peri-axonemal components. Sperm heads can be often seen attached to cytoplasmic bags containing unassembled axonemal and peri-axonemal components (Touré et al. 2021). Even-though the MMAF phenotype is typically associated with flagellar defects, mutations in some MMAF genes can have an impact to variable degrees on sperm head morphology (Charles Coutton et al. 2018; Hwang et al. 2021).

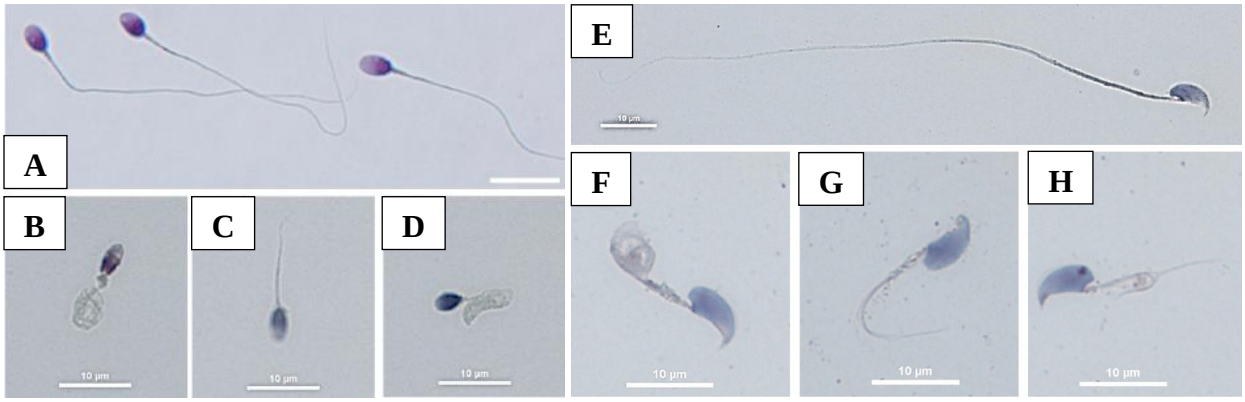

Figure 64: Human (B-D) and mouse (F-H) spermatozoa with multiple morphological abnormalities of the flagella (MMAF) as compared to healthy human (A) and mouse (E) individuals. *MMAF spermatozoa correspond to mutations in Armc2. Adapted from Coutton et al. 2019.*

The term MMAF was established in 2014 during the discovery of the gene *DNAH1* that encodes an axonemal heavy chain of IDAs (Ben Khelifa et al. 2014). Similar phenotypes were previously described as "dysplasia of the fibrous sheath", "short tails" and "stump tails" (C. Coutton et al. 2015).

The number of genes linked to the MMAF phenotype has been rising drastically (Figure 65) (Touré et al. 2021; J. Wang, Wang, et al. 2022). Only 5 genes were confidently linked with the disease in 2018 (Houston et al. 2021), and now more 40 genes have been associated with MMAF or are listed as candidate genes in humans and/ or in mice.

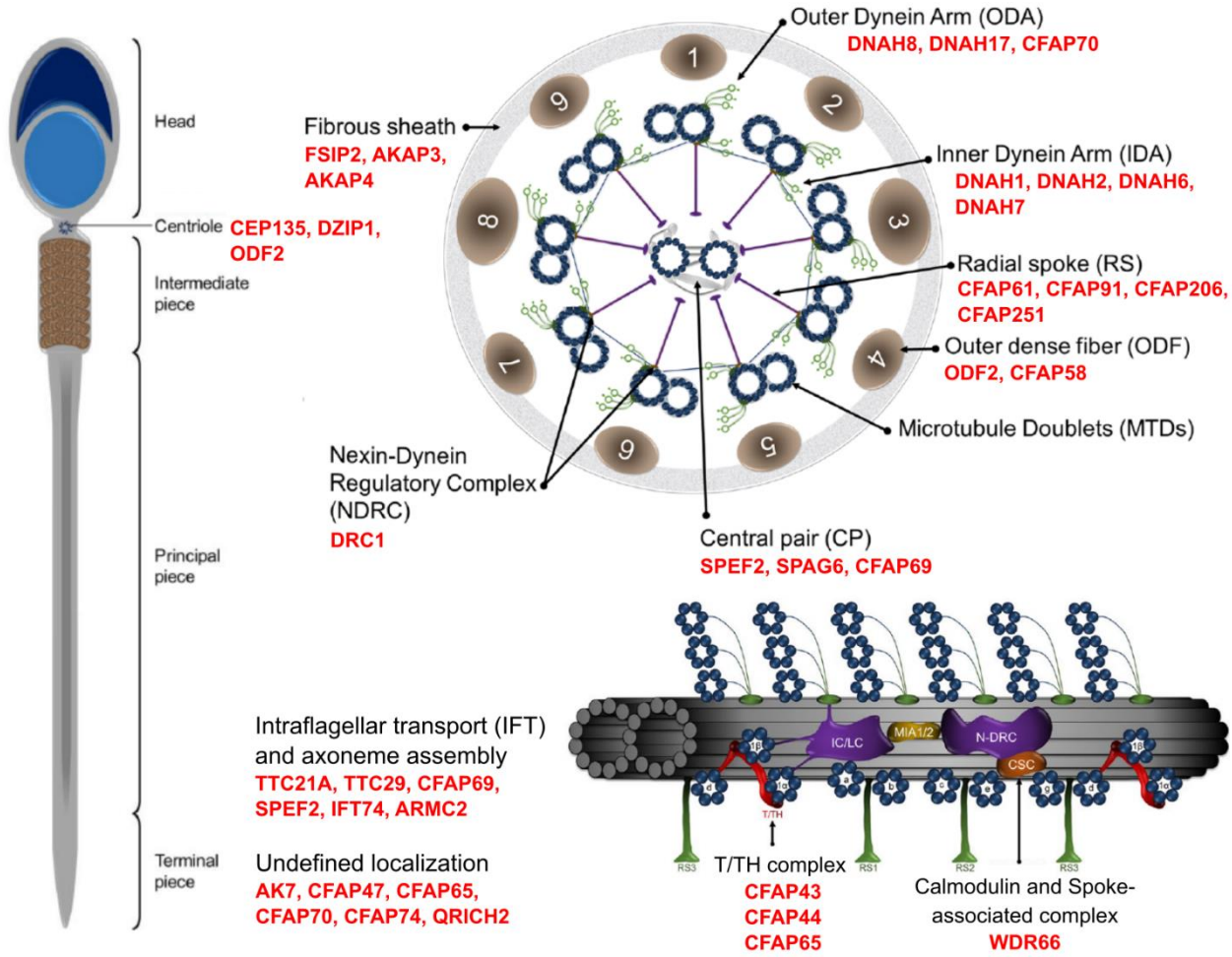

Figure 65: Location of proteins associated with MMAF in the sperm flagellum. *The tether/ tether head (T/TH) complex links the motor domains of the regulatory I1 dynein to the microtubule A-tubule. Protein localization was based on Touré et al. 2021 and J. Wang, Wang, et al. 2022, illustrations were adapted from Touré et al. 2021.*

Male infertility and disorganized flagella are often observed in individuals suffering from primary ciliary dyskinesia (PCD). PCD is a multisystemic genetic disease that causes malfunction of motile airway cilia and is associated with chronic nasal discharge and wet cough, recurrent respiratory and ear infections, pulmonary disease, and *situs inversus* (Sironen et al. 2020).

5 ASSISTED-REPRODUCTIVE TECHNOLOGIES

Couples suffering from infertility might look for assisted reproductive technologies (ART) that could help them in achieving pregnancy. Couples might use different techniques that are most appropriate for their situation, including intrauterine insemination (IUI), *in vitro* fertilization (IVF) or intracytoplasmic sperm injection (ICSI).

To increase the number of oocytes and improve the outcome of IVF and ICSI, both procedures require a hormonal ovarian stimulation that is followed by a surgical retrieval of ovulated oocytes from the ovaries. In conventional IVF, the oocytes are co-incubated overnight with sperm in a culture dish. The sperm are allowed to naturally fertilize the oocyte by passing the protective extracellular layer of the oocyte called the zona pellucida (Figure 66). In contrast, ICSI has originally been developed for severe cases of male infertility where the sperm quantity and quality were not compatible with neither natural conception nor conventional IVF (Palermo 1992). During this procedure, a spermatozoon is directly injected into the ooplasm of an egg. In both cases, the fertilized eggs are cultured for 2-6 days and then usually a single embryo is transferred into the uterus and/ or the embryos are cryopreserved.

Selection of an embryo with the highest quality is very challenging. Prior to implantation, the embryos might be subjected to invasive or non-invasive preimplantation genetic testing. Current invasive techniques rely on a biopsy of one or several cells from the embryo that are subsequently tested for chromosome abnormalities or severe inherited conditions that might be deleterious for its viability. Less invasive approaches enabling a genetic analysis are technically difficult and still in development (Leaver and Wells 2020). Without genetic testing, the embryo to be transferred is primarily selected based on several morphologic parameters (Greco et al. 2020). One of the non-invasive techniques includes a time-lapse imaging for embryo morphokinetic parameters such as cell shape and number, as well as the timing of polar body extrusion and divisions that can be predictive of embryo quality (Milewski and Ajduk 2017).

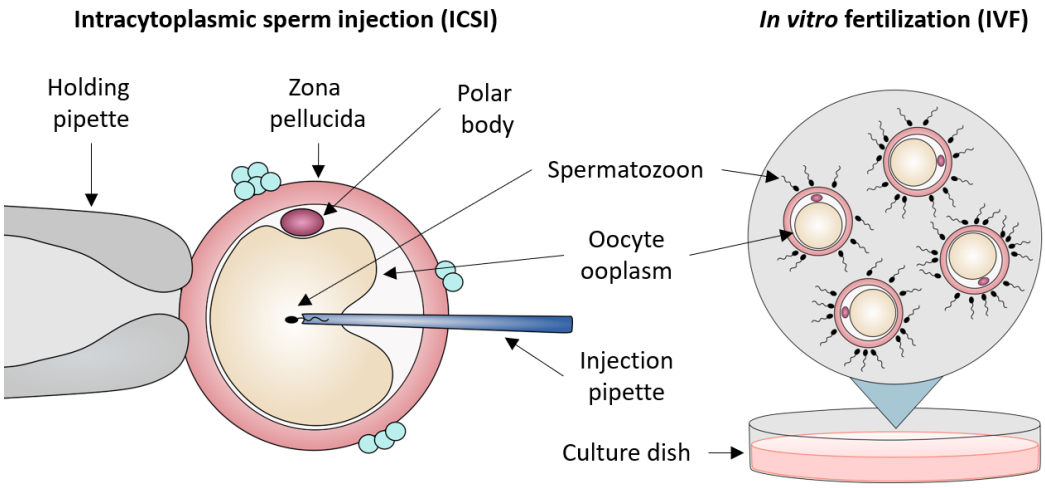

Figure 66: An illustration of assisted-reproductive technology methods including intracytoplasmic sperm injection (ICSI) and conventional in vitro fertilization (IVF). *During ICSI, the oocyte is maintained in place by the holding pipette while the injection pipette passes through the zona pellucida and the oocyte membrane to inject a single spermatozoon into the oocyte's ooplasm. During conventional IVF, oocytes are incubated overnight with numerous spermatozoa to stimulate a natural fertilization.*

ART is an essential tool for conception in severe cases of male infertility. ICSI is mandatory in complete asthenozoospermia (no sperm motility) and globozoospermia. In case of azoospermia (absence of sperm in the ejaculate), testicular or epididymal sperm extraction can be performed if spermatogenesis is not completely abolished. In other cases of male infertility, the use of IVF was shown to be equally effective as ICSI, however the success of IVF and ICSI are highly dependent on the cause of infertility and the consequent sperm quality (Esteves et al. 2018; Touré et al. 2021).

Taken together, infertility is a global issue that touches hundreds of thousands of couples worldwide. Male fertility alone or in conjunction with the female factor accounts for approximately half of the cases and is often associated with a genetic cause. Advances in high-throughput sequencing allowed the identification of many monogenic causes of male infertility, particularly in the MMAF syndrome, that lead to qualitative and quantitative sperm defects. The introduction of ICSI allowed individuals with severe cases of spermatogenic defects to father their own children that highlights the need for genetic testing and diagnosis to predict the ICSI outcome and to avoid the transmission of genetic abnormalities to the newborns.

THESIS OBJECTIVES

The general objective of the thesis was the identification and characterization of novel causes of male infertility. We focused on the Multiple morphological abnormalities of the flagella (MMAF) syndrome that is associated with severe flagellar defects and consequent low sperm motility. Our laboratory recruited 167 patients with MMAF and, following whole-exome sequencing, have already identified biallelic deleterious variants in 22 genes among 83 subjects.

Among these individuals, three men harbored a biallelic mutation in the gene *CCDC146* that stands for Coiled-coil domain-containing protein 146. The primary objective of the thesis was to characterize the role of CCDC146 in male infertility. To elucidate this question, we used a mouse knock-out and a tagged model and localized the protein in germ and somatic cells.

The underlying cause of male infertility cannot be identified in about 30-50% cases. Current screening methods primarily focus on identifying rare, deleterious and biallelic pathogenic variants. We wondered whether oligogenic heterozygosity could explain some cases of idiopathic infertility. We used mice that were heterozygous for one to four MMAF genes (*Ccdc146, Armc2, Cfap43,* and *Cfap44*) and observed if the accumulation of these heterozygous mutations influenced male fertility, in particular sperm morphology, motility, and concentration.

The final minor objective of the thesis was a participation in writing a review article that discusses epigenetic factors, especially non-coding RNAs, that influence sperm development and that can be transmitted and have an intergeneration and transgenerational effect on the progeny.

RESULTS

ARTICLE 1

"Lack of CCDC146, a ubiquitous centriole and microtubule-associated protein, leads to non-syndromic male infertility in human and mouse"

Jana Muroňová[1,2,3,†], Zine-Eddine Kherraf[1,2,3,4,†], Elsa Giordani[1,2,3], Simon Eckert[5], Caroline Cazin[1,2,3,4], Amir Amiri-Yekta[1,2,3,4], Emeline Lambert[1,2,3], Geneviève Chevalier[1,2,3], Guillaume Martinez[1,2,3,6], Yasmine Neirijnck[7], Francoise Kühne[7], Lydia Wehrli[7], Nikolai Klena[8,9], Virginie Hamel[8], Jessica Escoffier[1,2,3], Paul Guichard[8], Charles Coutton[1,2,3,6], Selima Fourati Ben Mustapha[10], Mahmoud Kharouf[10], Raoudha Zouari[10], Nicolas Thierry-Mieg[11], Serge Nef[7], Stefan Geimer[5], Corinne Loeuillet[1,2,3], Pierre Ray[1,2,3,4,‡], Christophe Arnoult[1,2,3,‡,*]

[1] Institute for Advanced Biosciences (IAB), INSERM 1209,
[2] Institute for Advanced Biosciences (IAB), CNRS UMR 5309
[3] Institute for Advanced Biosciences (IAB), Université Grenoble Alpes
[4] UM GI-DPI, CHU Grenoble Alpes, F-38000 Grenoble, France
[5] Cell Biology/ Electron Microscopy, University of Bayreuth, 95440 Bayreuth, Germany
[6] UM de Génétique Chromosomique, Hôpital Couple-Enfant, CHU Grenoble Alpes, F-38000 Grenoble, France
[7] Department of Genetic Medicine and Development, University of Geneva Medical School, Geneva 1211, Switzerland
[8] University of Geneva, Department of Molecular and Cellular Biology, Sciences III, Geneva, Switzerland
[9] Present address: Human Technopole, 20157 Milan, Italy
[10] Polyclinique les Jasmins, Centre d'Aide Médicale à la Procréation, Centre Urbain Nord, 1003 Tunis, Tunisia
[11] Laboratoire TIMC/MAGe, CNRS UMR 5525, Pavillon Taillefer, Faculté de Medecine, 38700 La Tronche, France

†These authors contributed equally to this work
‡These authors contributed equally to this work as senior authors

*Correspondence: christophe.arnoult@univ-grenoble-alpes.fr or PRay@chu-grenoble.fr

Article accepted by *Elife* (2023)

DOI: 10.1101/2023.02.27.530236

Contribution: This study was the principal project of the thesis. Concerning my experimental contribution to the project, I performed all the experiments that allowed the description of the reproductive phenotype of the Ccdc146 knock-out mouse (figures 2, 3, 13, supplementary figure 3), I described the localization of the protein in somatic and germ cells (fig. 4, 5, 7, 8, 11, sup 4, sup 5), except for expansion microscopy, and I analysed and described images obtained by electron microscopy (fig. 11, 12, 14, sup 10, sup 11). I participated in the writing of the manuscript and assembled a majority of the figures. I also participated in discussions and result analysis of other experiments that were performed for the project.

Summary:

The objective of this project was to characterize the role of the Coiled-coil domain containing protein 146 (CCDC146) in male fertility. Loss-of-function mutations in *CCDC146* were detected in two male patients affected by the MMAF syndrome. A mouse knock-out (KO) model reproduced the human MMAF phenotype and allowed us to show that CCDC146 plays a role(s) during spermiogenesis where it is important for correct manchette establishment, axoneme assembly, centriole number regulation and stable HTCA attachment to the head. In somatic cells, CCDC146 concentrated at and around both centrioles throughout the cell cycle. During mitosis, a part of CCDC146 dynamically relocated along microtubules to the midzone and the midbody. CCDC146 was present in mouse and human sperm flagella but not in primary cilia and its absence was not associated with ciliopathies. Due to its localization and impact on microtubule-based structures, we propose that CCDC146 is a microtubule-associated protein (MAP).

The following part termed “Introduction” will provide a bibliographic background of the project and will show some details that will be complementary with the research article presented afterwards.

Introduction:

A cohort of 167 MMAF-affected male individuals was analyzed by WES to identify biallelic monogenic mutations that might be at the origin of the patients' phenotype. The individuals seeking consultations for infertility were recruited in North Africa (83), Iran (52), and France (32). Their phenotype included severe asthenozoospermia and several flagellar abnormalities (coiled, short, absent, or irregular) in >5% of their spermatozoa (Coutton et al. 2019). Among these individuals, two harboured a biallelic mutation in the gene *CCDC146* that stands for Coiled-coil domain-containing protein 146, also known as KIAA1505 and MBO2. Unfortunately, no raw patient data were available to us. Two patients underwent successful ICSI treatments with correct fecundation rates. One patient had 3 ICSI, 2 biochemical pregnancies and 1 birth, and another had 2 ICSI, 2 births and 3 babies (unpublished data).

The *CCDC146* gene is located on chromosome 7 in humans and contains 19 exons whereas in the mouse it is present on chromosome 5 and has 20 exons ("National Center for Biotechnology Information" n.d.). The genes encode a protein containing 955 amino acids (112.8 kDa) in humans and 977 amino acids (115 kDa). The protein orthologues show 76.44% identity. Both human and mouse CCDC146 proteins contain a disordered N-terminal region and five coiled-coil domains (Figure 67) (The UniProt Consortium et al. 2021).

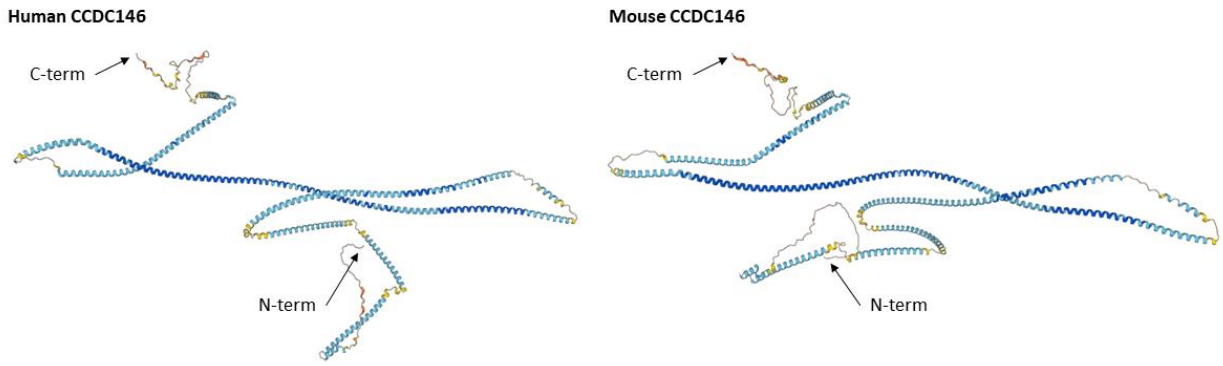

Figure 67: Predicted protein structure of human (left) and mouse (right) CCDC146. *The C-terminal and N-terminal residues are shown. The structure was predicted by AlphaFold based on the accession numbers of full-length proteins: human (Q8IYE0), mouse (E9Q9F7). The colors represent the confidence level of the predicted model, on a scale of 0 to 100. Dark blue regions correspond to a very high accuracy of the model (per-residue confidence score (pLDDT) > 90), light blue to confident (90 > pLDDT > 70), yellow to low confidence (70 > pLDDT > 50) and orange regions were predicted with very low confidence (pLDDT < 50) (Jumper 2021; Varadi 2021).*

Based on the predicted structures by AlphaFold (Jumper et al. 2021; Varadi et al. 2022), the human and mouse CCDC146 proteins appear to have similar backbone structures, possibly with an additional disordered region at the C-terminal. The disordered N-terminal regions contain acidic residues in both species (The UniProt Consortium et al. 2021).

Coiled-coil domains are protein structures comprised of two or more adjacent α-helices that are twisted around each other to form a supercoil. They are ubiquitous motifs and expressed in a wide variety of tissues and have functional roles in most physiological processes as well as in cancer. They serve as molecular rulers and spacers (e.g., CCDC39 and CCDC40), mediate vesicle tethering (e.g., Golgins), and participate in mitosis (e.g., Ndc80 that binds kinetochores to spindle microtubules). They also influence the architecture and stability of centrioles and are common proteins of the pericentriolar material (Priyanka and Yenugu 2021; Truebestein and Leonard 2016; Woodruff, Wueseke, and Hyman 2014). As of 2021, 22 coiled-coil domain-containing proteins have been shown to be involved in male reproduction and their function is summarized in Table 2 (Priyanka and Yenugu 2021).

Name	Function
CCDC9	Regulation of sperm motility and spermiogenesis
CCDC33	Role as an important peroxisomal protein in spermatogenesis
CCDC38	Aids in spermatogenesis
CCDC39	Structural arrangement and activity of cilia and flagella
CCDC42	Forms head-to-tail coupling apparatus and aids in sperm tail formation. Localized expression in the manchette of spermatids
CCDC62	Enhances estrogen receptor expression in prostate cancer. Polymorphism associated with Parkinson's disease. Cancer/testis antigen
CCDC63	Regulates length of sperm flagellum
CCDC70	Regulator of spermatogenesis and epididymis sperm maturation
CCDC73	Shows testis-enriched expression in mice and helps in fertility
CCDC78	Role in motor function and epididymis sperm maturation
CCDC83	An effective testis antigen to diagnose colon cancer
CCDC87	Role in sperm function and male fertility
CCDC108	Role in mitochondrial oxidation-reduction reaction and also in the subfertility of roosters
CCDC112	Marker for pachytene and diplotene spermatocytes
CCDC113	Primary cilium formation in mammalian sperm
CCDC135	Helps in sperm motility
CCDC136	Crucial in acrosome formation and fertilization. Acts as a negative regulator of Wnt/β-catenin signaling pathway
CCDC147	Cilia-flagella-associated protein
CCDC151	Crucial factor for ciliary and flagellar motility. Mutations associated with Kartagener syndrome
CCDC172	Localizes to the mid-piece of rat spermatozoa and interacts with Tektin 2 protein
CCDC181	Binding to microtubule and interacts with Hook1 protein in sperm
CCDC189	Sperm motility and fertilization

Table 2: Functional roles of coiled-coil domain-containing (CCDC) proteins in spermatogenesis. *From Priyanka and Yenugu 2021.*

CCDC146 is conserved in many organisms including primates and other mammals, some birds, fish, and reptiles (Ensembl – Gene tree), and in unicellular organisms such as *Chlamydomonas* and *Trypanosoma* ("National Center for Biotechnology Information" n.d.). In both humans and mice, Ccdc146 is present in male reproductive tissues (testis, epididymis), in the airway epithelium (trachea, nasal epithelium, lung), in the skeletal and heart muscles, and in the oviduct (Hruz et al. 2008)**.** Consequently, the protein appears to be particularly associated with tissues containing cilia and/or flagella.

During spermatogenesis, RNA-seq studies show that CCDC146 is particularly expressed at the spermatocyte and spermatid stage in both humans and mice (Figure 68) (Gan et al. 2013; Green et al. 2018; M. Wang et al. 2018; Moretti et al. 2016).

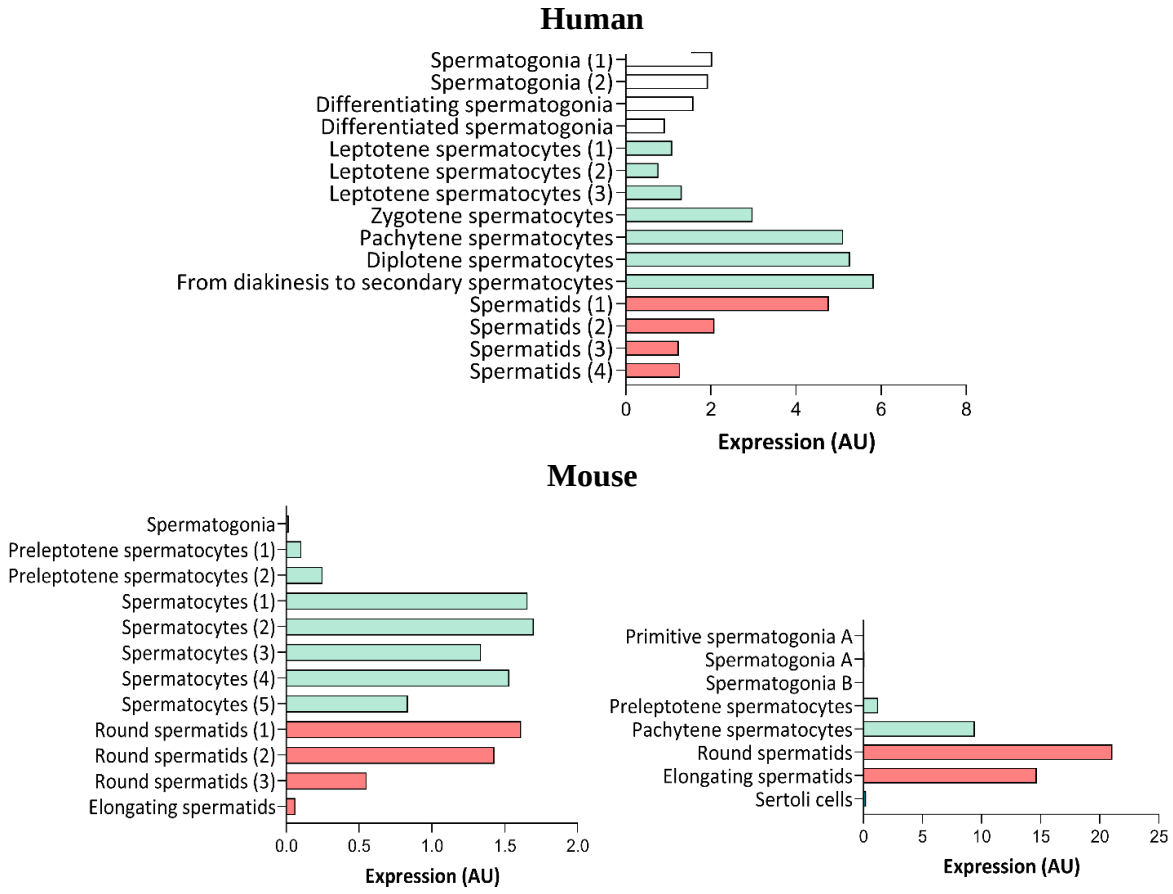

Figure 68: Expression of Ccdc146 in spermatogenic cells based on RNA-sequencing studies in humans and mice. *The data from human and mice (left) were grouped based on differing expression profiles within each cell type. Human data are from Wang et al., 2018; mouse data on the left are from Green et al., 2018 and data on the right are from Gan et al., 2013 reanalyzed using the last version of the mouse genome (mm10) in Moretti et al., 2016. Artificial units (AU).*

The exact function of CCDC146 is unknown. The first mention of CCDC146 comes from studies of its orthologue MBO2 (Coiled-coil flagellar protein) in the green algae *Chlamydomonas reinhardtii*. The MBO2 protein also contains five coiled-coil domains, a disordered C-terminal region and shares a 29% identity with human CCDC146 ("BLAST | UniProt" n.d.). The alga moves by using its two flagella to propel forwards by an asymmetric "ciliary" waveform whereas in the backward movement, it uses a symmetrical "flagellar" waveform. Mutations in the *MBO2* gene resulted in an alteration of this cell motility and the cells could move backwards only (MBO) using the "flagellar" waveform (Tam and Lefebvre 2002; Segal et al. 1984). The protein was localized along the length of the axoneme and to the basal body at the base of the axoneme, further supporting its possible role in sperm motility (Figure 69A).

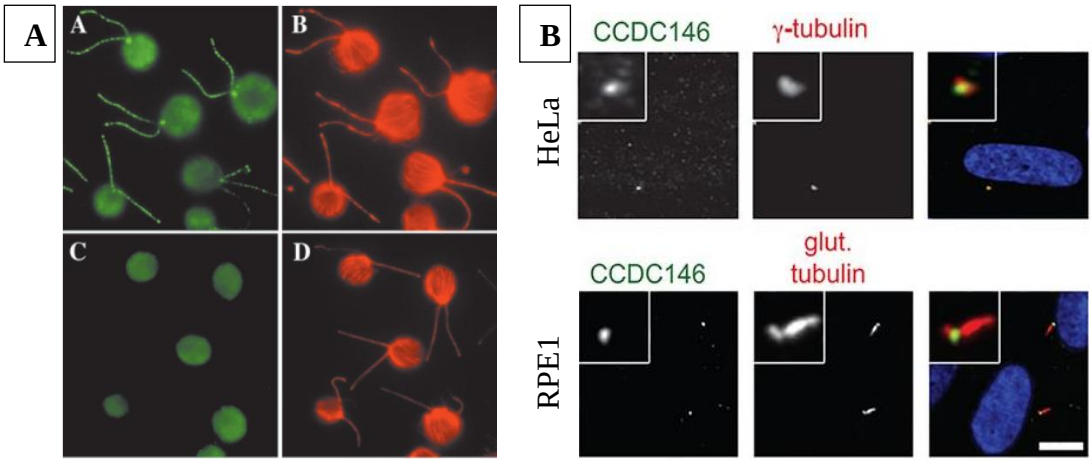

Figure 69: Immunofluorescence localization of MBO2 in the green algae Chlamydomonas (left-A) and of its human orthologue CCDC146 in human HeLa and RPE1 cells (right-B). *(A) Knock-out strains were rescued by a MBO2-HA gene construct (A, B) or a control construct (C, D) showing the localization of MBO2-HA at the axonemes and at the basal body. From Tam & Lefebvre, 2002. (B) CCDC146 (green) co-localizes at the centrosome with γ-tubulin (red) in HeLa cells (top) and is present at the basal body of the primary cilium stained for polyglutamylated tubulin (bottom). DNA is stained in blue. From Firat-Karalar et al., 2014.*

The MBO2 mutant cells were missing projections in the lumen of the B-tubules of the outer microtubule doublets 5 and 6, called beak-like projections (Tam and Lefebvre 2002), whose composition remains unknown (Dutcher 2020). The localization of the protein in the axoneme was not disturbed in mutants missing structural components of the axoneme, including radial spokes, central pair microtubules, outer dynein arms, and some inner arm dyneins, suggesting that it is localized elsewhere but its precise localization remains unknown. The authors also noted a

difficulty in extracting the protein from the axoneme, suggesting that it might be tightly associated with microtubule doublets even-though the absence of MBO2 did not significantly alter MT structure (Tam and Lefebvre 2002). The protein also localized around the basal body, even in the absence of MBO1 that is necessary for its assembly into the flagellum, suggesting that MBO2 may be involved in intraflagellar transport (IFT) whose proteins, cargo and IFT proteins are thought to concentrate at the basal body to assemble into trains and binding cargoes for transport (Hibbard et al. 2021).

The aforementioned localization of MBO2 at the basal body was interesting in the light of a study by Firat-Karalar *et al.* who analyzed the centriolar proteome of bovine spermatozoa by mass spectrometry and identified CCDC146 as one of its components (Firat-Karalar et al. 2014). They further showed that CCDC146 also localizes to the basal body of primary cilia in RPE1 (human Retinal Pigment Epithelium) cells and to the mother centriole in HeLa cells through co-localization with γ-tubulin (Figure 69B) and CEP164 (not shown).

Almeida *et al.* further supported the localization of CCDC146 at the centrosome in HeLa cells and showed that host CCDC146 can be recruited to the periphery of the inclusion membrane in cells infected by *Chlamydia trachomatis* (Almeida et al. 2018). *C. trachomatis* is an obligate intracellular bacterium that multiplies inside the host cells in a membrane bound vacuole known as the inclusion vacuole, which plays a role in mediating *Chlamydia*-host cell interactions. They showed that CCDC146 might be recruited from the centrosome to the inclusion vacuole by bacterial proteins, however, the functional and physiological relevance of the recruitment was not studied further.

A genome-wide association study in patients with type 2 diabetes by Ustinova *et al.* tried to associate particular gene expression with major diabetes complications such as diabetic neuropathy, nephropathy, mascovascular complications, and ophthalmic complications (Ustinova et al. 2021). CCDC146 was significantly associated with macrovacsular complications along with other genes and solely associated with a greater risk of ophthalmic complications. Both types of complications might be associated with cilia, considering that the eyes contain many cell types with specialized primary cilia including the photoreceptor neuron cells capable of recognizing light and converting it into an electric signal (Wheway, Parry, and Johnson 2014). Similarly, ciliary signaling is involved in satiety signaling of the hypothalamus and in other tissues involved in the

metabolism, such as the pancreatic islets (Volta and Gerdes 2017). However, these links remain hypothetical and the role of CCDC146 in these systems was not studied.

CCDC146 was also detected as a neoantigen, along with 10 others, present in breast cancer cells, particularly in patients with lymph node metastasis. The authors suggested that a neoantigen-targeting vaccine against CCDC146 and other aforementioned neoantigens could be a promising treatment option (Z. Wang et al. 2019).

A paralogue of CCDC146 called CFAP58 (Cilia- And Flagella-Associated Protein 58), also known as CCDC147 (Coiled-Coil Domain-Containing Protein 147), is primarily expressed in the testis, contains two contains 2 coiled-coil regions, and shares a 23.18% protein identity with human CCDC146. It is present in both humans and mice (The UniProt Consortium et al. 2021; Cunningham et al. 2022a). The absence of CFAP58 was associated with the MMAF syndrome and male infertility in humans and mice (He et al. 2020). The mutations in men were in the protein's coiled-coil domains. In the mouse, sperm concentration was severely decreased and no motility was observed. The protein localized to the entire flagellum with an accumulation at the mitochondrial sheath in control sperm (He et al. 2020). CFAP58 had a similar localization to the ODF2 protein, a mother centriole protein and is important for the elongation of the mouse sperm midpiece (Z.-Z. Li et al. 2020). The authors suggested that CFAP58 could be involved in outer dense fiber (ODF) transport during flagellum formation.

Based on the aforementioned data, CCDC146 appears to be associated with the centrosome and flagella, with a possible role during spermiogenesis due to its increased expression in spermatids. Since it was identified in infertile MMAF patients, we wanted to characterize its role in male reproduction and our investigation is presented in the following article.

Lack of CCDC146, a ubiquitous centriole and microtubule-associated protein, leads to non-syndromic male infertility in human and mouse

Abstract

Genetic mutations are a recurrent cause of male infertility. Multiple morphological abnormalities of the flagellum (MMAF) syndrome is a heterogeneous genetic disease, with which more than 50 genes have been linked. Nevertheless, for 50% of patients with this condition, no genetic cause is identified. From a study of a cohort of 167 MMAF patients, pathogenic biallelic mutations were identified in the *CCDC146* gene in two patients. This gene encodes a poorly characterized centrosomal protein which we studied in detail here. First, protein localization was studied in two cell lines. We confirmed the centrosomal localization in somatic cells and showed that the protein also presents multiple microtubule-related localizations during mitotic division, suggesting that it is a microtubule-associated protein (MAP). To better understand the function of the protein at the sperm level, and the molecular pathogenesis of infertility associated with *CCDC146* mutations, two genetically modified mouse models were created: a *Ccdc146* knock-out (KO) and a knock-in (KI) expressing a HA-tagged CCDC146 protein. KO male mice were completely infertile, and sperm exhibited a phenotype identical to our two MMAF patient's phenotype with *CCDC146* mutations. No other pathology was observed, and the animals were viable. CCDC146 expression starts during late spermiogenesis, at the time of flagellum biogenesis. In the spermatozoon, the protein is conserved but is not localized to centrioles, unlike in somatic cells, rather it is present in the axoneme at the level of microtubule doublets. Expansion microscopy associated with the use of the detergent sarkosyl to solubilize microtubule doublets, provided evidence that the protein could be a microtubule inner protein (MIP). At the subcellular level, the absence of CCDC146 affected the formation, localization and morphology of all microtubule-based organelles such as the manchette, the head–tail coupling apparatus (HTCA), and the axoneme. Through this study, we have characterized a new genetic cause of infertility, identified a new factor in the formation and/or structure of the sperm axoneme, and demonstrated that the CCDC146 protein plays several cellular roles, depending on the cell type and the stages in the cell cycle.

Introduction

Infertility is a major health concern, affecting approximately 50 million couples worldwide [1], or

12.5% of women and 10% of men. It is defined by the World Health Organization (WHO) as the "failure to achieve a pregnancy after 12 months or more of regular unprotected sexual intercourse". In almost all countries, infertile couples have access to assisted reproductive technology (ART) to try to conceive a baby, and there are now 5 million people born as a result of ART. Despite this success, almost half of the couples seeking medical support for infertility fails to successfully conceive and bear a child by the end of their medical care. The main reason for these failures is that one member of the couple produces gametes that are unable to support fertilization and/or embryonic development. Indeed, ART does not specifically treat or even try to elucidate the underlying causes of a couple's infertility, rather it tries to bypass the observed defects. Consequently, when defects in the gametes cannot be circumvented by the techniques currently proposed, ART fails. To really treat infertility, a first step would be to gain a better understanding of the problems with gametogenesis for each patient. This type of approach should increase the likelihood of adopting the best strategy for affected patients, and if necessary, should guide the development of innovative therapies.

Male infertility has several causes, such as infectious diseases, anatomical defects, or a genetic deficiency. Genetic defects play a major role in male infertility, with over 4000 genes thought to be involved in sperm production, of which more than 2000 are testis-enriched and almost exclusively involved in spermatogenesis [2]. Mutations in any of these genes can negatively affect spermatogenesis and produce one of many described sperm disorders. The characterization and identification of the molecular bases of male infertility is thus a real challenge. Nevertheless, thanks to the emergence of massively parallel sequencing technologies, such as whole exome sequencing (WES) and whole genome sequencing (WGS), the identification of genetic defects has been greatly facilitated in recent years. As a consequence, remarkable progress has been made in the characterization of numerous human genetic diseases, including male infertility.

Today, more than 120 genes are associated with all types of male infertility [3], including quantitative and qualitative sperm defects. Qualitative spermatogenesis defects impacting sperm morphology, also known as "teratozoospermia"[4, 5], are a heterogeneous group of abnormalities covering a wide range of sperm phenotypes. Among these phenotypes, some relate to the morphology of the flagellum. These defects are usually not uniform, and patients' sperm show a wide range of flagellar morphologies such as short and/or coiled and/or irregularly sized flagella.

Due to this heterogeneity, this phenotype is now referred to as multiple morphological abnormalities of the sperm flagellum (MMAF)[5]. Sperm from these patients are generally immotile, and patients are sterile.

Given the number of proteins present in the flagellum and necessary for its formation and functioning, many genes have already been linked to the MMAF phenotype. Study of the MMAF phenotype in humans has allowed the identification of around 50 genes [6] coding for proteins involved in axonemal organization, present in the structures surrounding the axoneme – such as the outer dense fibers and the fibrous sheath – and involved in intra-flagellar transport (IFT). Moreover, some genes have been identified from mouse models, and their human orthologs are very good gene candidates for MMAF, even if no patient has yet been identified with mutations in these genes. Finally, based on the remarkable structural similarity of the axonemal structure of motile cilia and flagella, some MMAF genes were initially identified in the context of primary ciliary dyskinesia (PCD). However, this structural similarity does not necessarily imply a molecular similarity, and only around half (10 of the 22 PCD-related genes identified so far [7]) are effectively associated with male infertility. However, in most cases, the number of patients is very low, and the details of the sperm tail phenotype are unknown [7].

We have recruited 167 patients with MMAF. Following whole exome sequencing, biallelic deleterious variants in 22 genes were identified in 83 subjects. The genes identified are *AK7*[8], *ARMC2* [9], *CFAP206* [10], *CCDC34* [11], *CFAP251* [12], *CFAP43* and *CFAP44* [13], *CFAP47* [14], *CFAP61* [15], *CFAP65* [16], *CFAP69* [17], *CFAP70* [18], *CFAP91* [19], *CFAP206* [10], *DNAH1* [20], *DNAH8* [21], *FSIP2* [22], *IFT74* [23], *QRICH2* [24], *SPEF2* [25], *TTC21A* [26] and *TTC29* [27]. Despite this success, a molecular diagnosis is obtained in half of the patients (49.7%) with this sperm phenotype, suggesting that novel candidate genes remain to be identified. We have pursued our effort with this cohort to identify further mutations that could explain the patient MMAF phenotype. As such, we have identified biallelic truncating mutations in *CCDC146* in two unrelated infertile patients displaying MMAF. *CCDC146* is known to code for a centrosomal protein when heterogeneously expressed in HeLa cells [28, 29], but minimal information is available on its distribution within the cell, or its function when naturally present. Moreover, this gene has never been associated with any human disease.

The centrosome, located adjacent to the nucleus, is a microtubule-based structure composed of a

pair of orthogonally-oriented centrioles surrounded by the pericentriolar material (PCM). The centrosome is the major microtubule-organizing center (MTOC) in animal cells, and as such regulates the microtubule organization within the cell. Therefore, it controls intracellular organization and intracellular transport, and consequently regulates cell shape, cell polarity, and cell migration. The centrosome is also crucial for cell division as it controls the assembly of the mitotic/meiotic spindle, ensuring correct segregation of sister chromatids in each of the daughter cells [30]. The importance of this organelle is highlighted by the fact that 3% (579 proteins) of all known human proteins have been experimentally detected in the centrosome (https://www.proteinatlas.org/humanproteome/subcellular/centrosome). Centrioles also play essential roles in spermatogenesis and particularly during spermiogenesis. In round spermatids, the centriole pair docks to the cell membrane, whereas the distal centriole serves as the basal body initiating assembly of the axoneme. The proximal centriole then tightly attaches to the sperm nucleus and gradually develops the head-to-tail coupling apparatus (HTCA), linking the sperm head to the flagellum [31]. In human and bovine sperm, the proximal centriole is retained and the distal centriole is remodeled to produce an 'atypical' centriole [32]; in contrast, in rodents, both centrioles are degenerated during epididymal maturation [33]. Despite the number of proteins making up the centrosome, and its importance in sperm differentiation and flagellum formation, very few centrosomal proteins have been linked to MMAF in humans – so far only CEP135 [34], CEP128 [35] and DZIP1 [36]. Moreover, some major axonemal proteins with an accessory location in the centrosome, such as CFAP58 [37] and ODF2 [38, 39], have also been reported to be involved in MMAF syndrome. Other centrosomal proteins lead to MMAF in mice, including CEP131 [40] and CCDC42 [41]. The discovery that MMAF in humans is linked to CCDC146, known so far as a centrosomal protein, adds to our knowledge of proteins important for axoneme biogenesis.

In this manuscript, we first evaluated the localization of endogenous CCDC146 during the cell cycle in two types of cell cultures, immortalized cells and primary human foreskin fibroblasts. To validate the candidate gene and improve our knowledge of the corresponding protein, we also generated two mouse models. The first one was a *Ccdc146* knock-out (KO) model that served to study the impact of the protein's depletion on the general phenotype, and in particular on the male reproductive function using several optical and electron microscopy techniques. The second model was a HA-tagged CCDC146 model, which was used to study the localization of the protein in

different cell types. Data from these genetically modified mouse models were confirmed in human sperm cells.

Results

1/ WES identifies *CCDC146* as a gene involved in MMAF

We performed whole exome sequencing (WES) to investigate a highly-selected cohort of 167 MMAF patients previously described in [9]. The WES data was analyzed using an open-source bioinformatics pipeline developed in-house, as previously described [42]. From these data, we identified two patients with homozygous truncating variants in the *CCDC146* (coiled-coil domain containing 146) gene, NM_020879.3 (Figure 1A). No other candidate variants reported to be

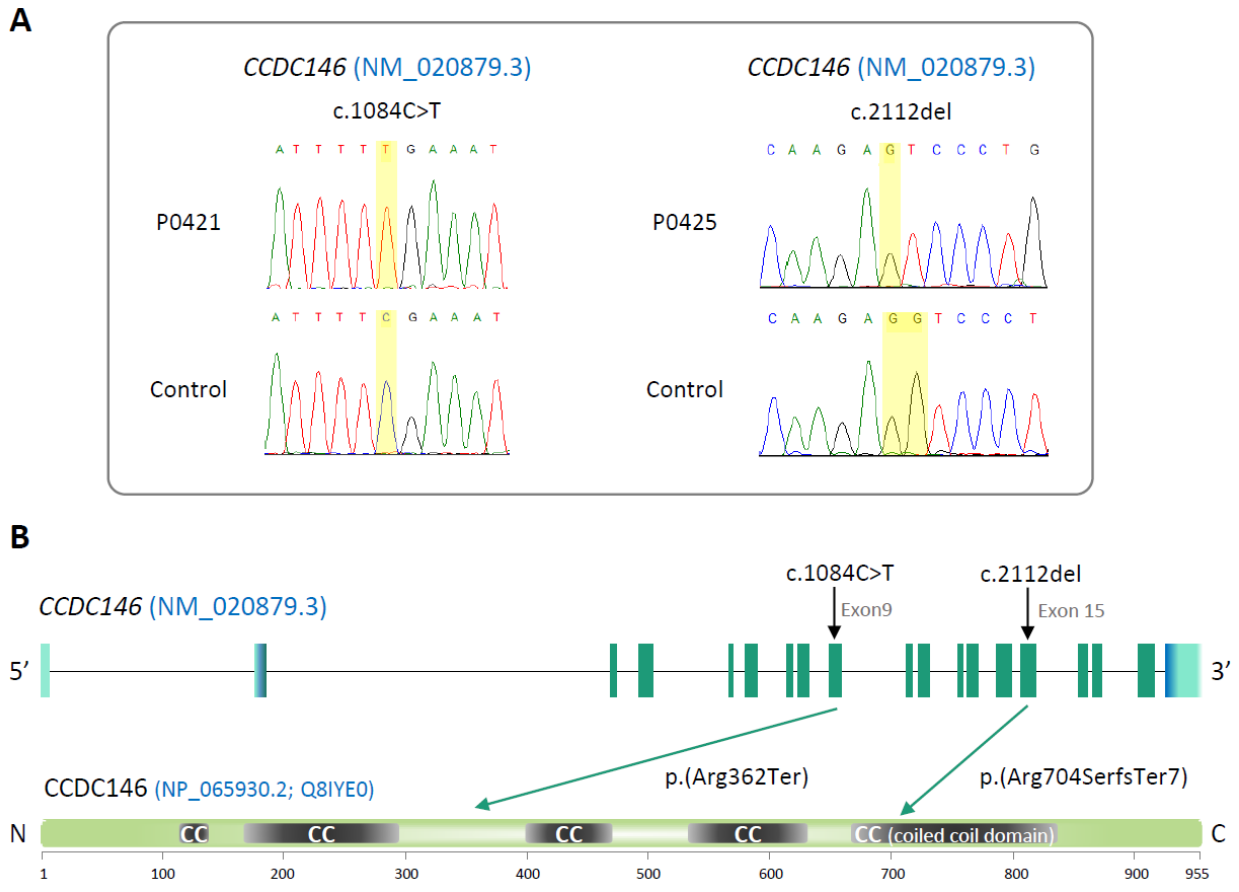

Figure 1: Identification of two CCDC146 gene variants in MMAF patients. (A) Position of the observed variants in both probands. Electropherograms indicating the homozygous state of the identified variant: variant c.1084C>T is a nonsense mutation, and c. c.2112Del is a single-nucleotide deletion predicted to induce a translational frameshift. (B) Structure of the canonical CCDC146 gene transcript showing the position of the variants and their impact on translation. Variants are annotated according to HGVS recommendations.

associated with male infertility was detected in these patients. This gene is highly transcribed in both human and mouse testes (Supp Figure 1). The first identified mutation is located in exon 9/19 and corresponds to c.1084C>T, the second is located in exon 15/19 and corresponds to c.2112Del (Figure 1B). The c.1084C>T variant is a nonsense mutation, whereas the single-nucleotide deletion c.2112Del is predicted to induce a translational frameshift. Both mutations were predicted to produce premature stop codons: p.(Arg362Ter) and p.(Arg704serfsTer7), respectively, leading either to the complete absence of the protein, or to the production of a truncated and non-functional protein. The two mutations are therefore most likely deleterious (Figure 1B). Both variants were absent in our control cohort and their minor allele frequencies (MAF), according to the gnomAD v3 database, were $6.984x10^{-5}$ and 0 respectively. The presence of these variants and their homozygous state were verified by Sanger sequencing, as illustrated in Figure 1. Taken together, these elements strongly suggest that mutations in the *CCDC146* gene could be responsible for the infertility of these two patients and the MMAF phenotype.

2/ *Ccdc146* knock-out mouse model confirms that lack of CCDC146 is associated with MMAF

To validate the hypothesis that CCDC146 deficiency leads to MMAF and male infertility, we produced by CRISPR/Cas9 two mouse lines carrying each a frameshift mutation in *Ccdc146* (ENSMUST00000115245) (Supp Figure 2). We analyzed the reproductive phenotype of the edited animals from the F2 generation and found that homozygous males were infertile and reproduced the MMAF phenotype like the two patients carrying the homozygous variants in the orthologous gene. Based on these findings, we restricted our study to a strain with a 4-bp deletion in exon 2 (c.164_167delTTCG).

The KO mice were viable without apparent defects. The reproductive phenotypes of male and female mice were explored. WT and heterozygous animals and KO females were fertile, whereas KO males were completely infertile (Figure 2A). This infertility is associated with a 90% decrease in epididymal sperm concentration (from ~30 to ~3 million) (Figure 2B) and an almost complete absence of motility (Figure 2C). Closer examination revealed sperm morphology to be strongly altered, with a typical MMAF phenotype and marked defects in head morphology (Figure 2E) indicative of significantly impaired spermiogenesis. In addition, testicle weight relative to whole body weight was significantly lower (Figure 2D), suggesting a germ cell rarefaction in the

seminiferous epithelia due to high apoptosis level. A study of spermatogenic cell viability by TUNEL assay confirmed this hypothesis, with a significant increase in the number of positive cells in *Ccdc146* KO animals (Supp Figure 3).

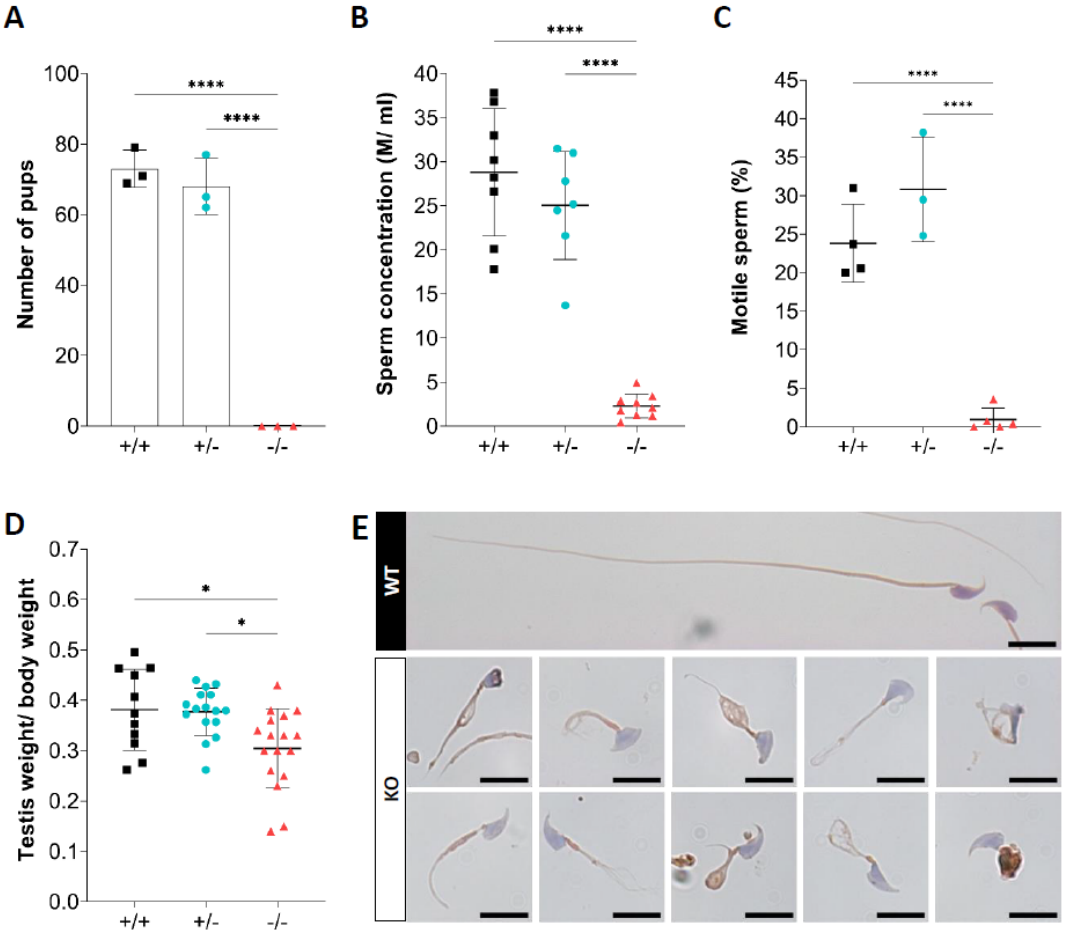

Figure 2: Ccdc146 KO mice are infertile and KO sperm exhibit a typical "multiple morphological abnormalities of the flagellum (MMAF)" phenotype. (A) Number of pups produced by wild-type (+/+, WT), CCDC146 heterozygote (+/-) and CCDC146 knock-out (-/-, KO) males (3 males per genotype) after mating with fertile WT females (2 females per male) over a period of three months. (B) Sperm concentration and (C) sperm mobility. (D) Comparison of testis weights (mg). (E) Illustration of WT and KO sperm morphologies stained with Papanicolaou and observed under optic microscopy. Statistical comparisons were based on ordinary one-way ANOVA tests (**** $p<0.0001$; *** $p<0.001$, ** $p<0.01$, * $p<0.05$). Scale bar of images: 10 µm.

Comparative histological studies (Figure 3) showed that on sections of spermatogenic tubules, structural and shape defects were present from the elongating spermatid stage in KO mice, with almost complete disappearance of the flagella in the lumen. At the epididymal level, transverse sections of the epididymal tubules from KO males contained almost no spermatozoa, and the tubules were filled with an acellular substance.

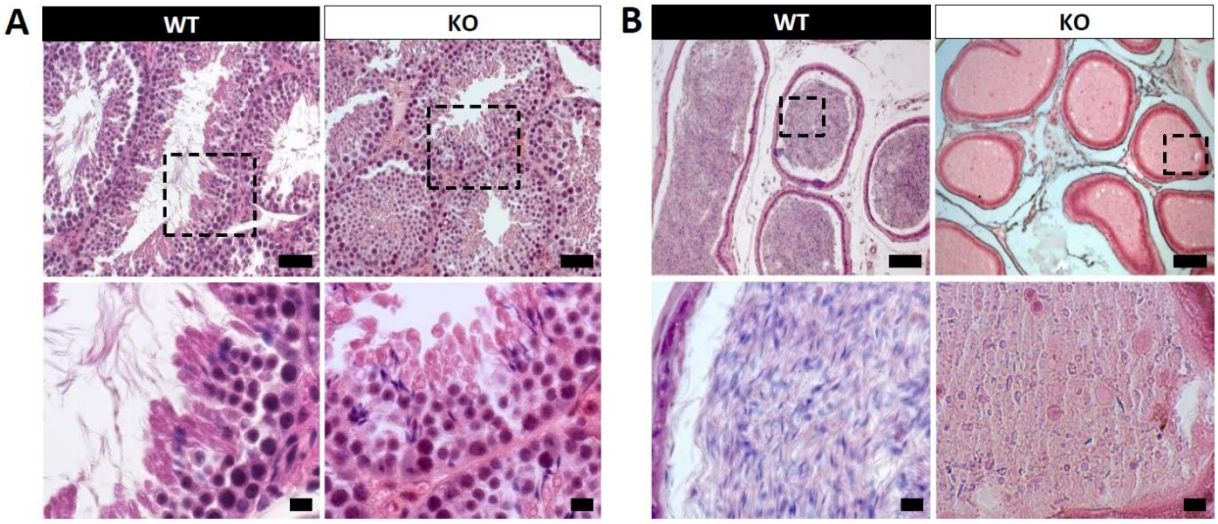

Figure 3: Histological evidence that spermiogenesis is disrupted in Ccdc146 KO males and leads to a strong decrease in sperm concentration in the epididymis. (A) Transversal sections of WT and KO testis stained with hematoxylin and eosin. The upper images show the sections at low magnification (scale bars: 50 µm) and the lower images are an enlargement of the dotted square (scale bars: 10 µm). In the KO, spermatid nuclei were very elongated and no flagella were visible within the seminiferous tubule lumen. (B) Transversal sections of WT and KO epididymis stained with hematoxylin and eosin. Despite similar epididymis section diameters in WT and KO testes, KO lumen were filled with round cells and contained few spermatozoa with abnormally shaped heads and flagella. The upper images show the sections at low magnification (scale bars 50 µm) and the lower images are an enlargement of the dotted square (scale bars: 10 µm).

3/ *Ccdc146* codes for a centriolar protein

CCDC146 has been described as a centriolar protein in immortalized HeLa cells [28, 29]. To confirm this localization, we performed immunofluorescence experiments in HEK-293T cells (Figure 4). First, we focused on the centrosome. In HEK-293T cells, using an antibody recognizing centrin (anti-centrin Ab) as a centriole marker and an anti-CCDC146 Ab, CCDC146 was shown to colocalize with centrioles. However, the signal was not strictly localized to centrioles, as peri-centriolar labeling was clearly visible. As this labeling pattern suggests the presence of centriolar satellite proteins, we next performed co-labeling with an antibody recognizing PCM1, a canonical centriolar satellite marker [43]. Once again, the colocalization was only partial (Supp Figure 4). Based on these observations, CCDC146 has a unique localization profile that may indicate specific functions.

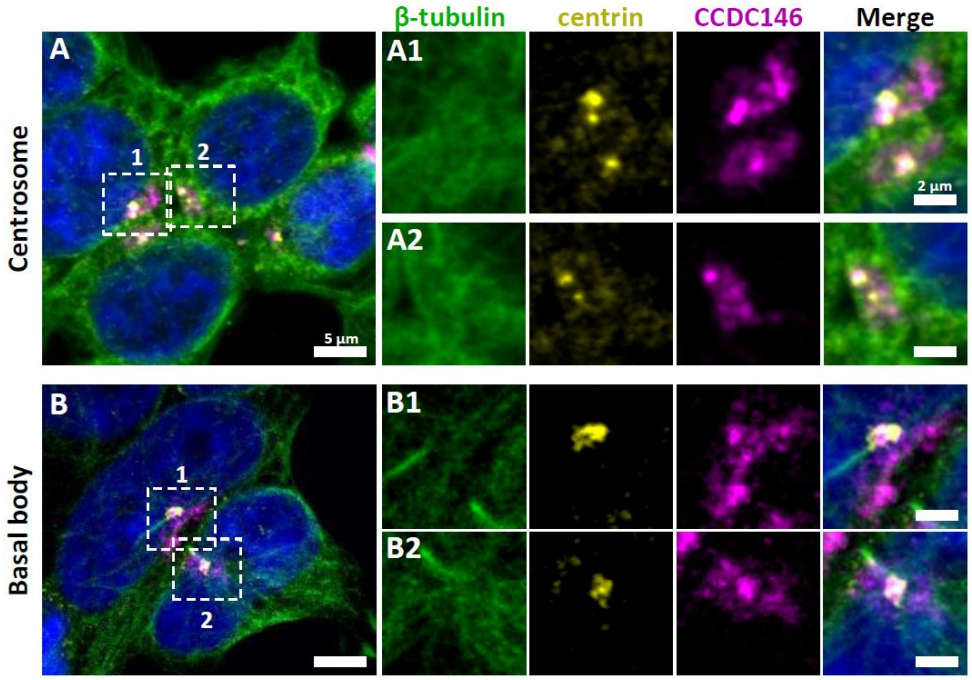

Figure 4: CCDC146 has a centriolar and pericentriolar localization in interphase somatic HEK-293T cells. HEK-293T cells were immunolabeled for β-tubulin (green), centrin (yellow) and CCDC146 (magenta). DNA was stained with Hoechst (blue). (A) CCDC146 localized to centrioles and/ or to the pericentriolar material in interphase cells. The centrosomes of two cells are shown enlarged in A1 and A2. (B) In serum starved cells with primary cilia, CCDC146 localizes to the basal body of primary cilia. The basal body of two cells are shown enlarged in B1 and B2. CCDC146 is also present as dotted signal resembling the pattern for centriolar satellite proteins. Scale bars on zoomed images: 2 µm.

4/ CCDC146 co-localizes with multiple tubulin-based organelles

Interestingly, our immunofluorescence experiments revealed that CCDC146 labeling was not strictly limited to centrosomes – other tubulin-containing cellular substructures were also labeled, particularly structures emerging during cell division (Figure 5). Thus, the mitotic spindle was labeled at its base and at its ends. The co-labeling intensified in the midzone during chromatid separation. Finally, the separation structure between the two cells, the midbody, was also strongly stained. As HEK-293T cells are an immortalized cell line, we therefore verified that this labeling pattern was not due to an aberrant expression profile and that it also reflected the situation in primary cell lines. Identical labeling profiles were observed in freshly prepared Human foreskin fibroblasts (HFF cells) (Supp Figure 5).

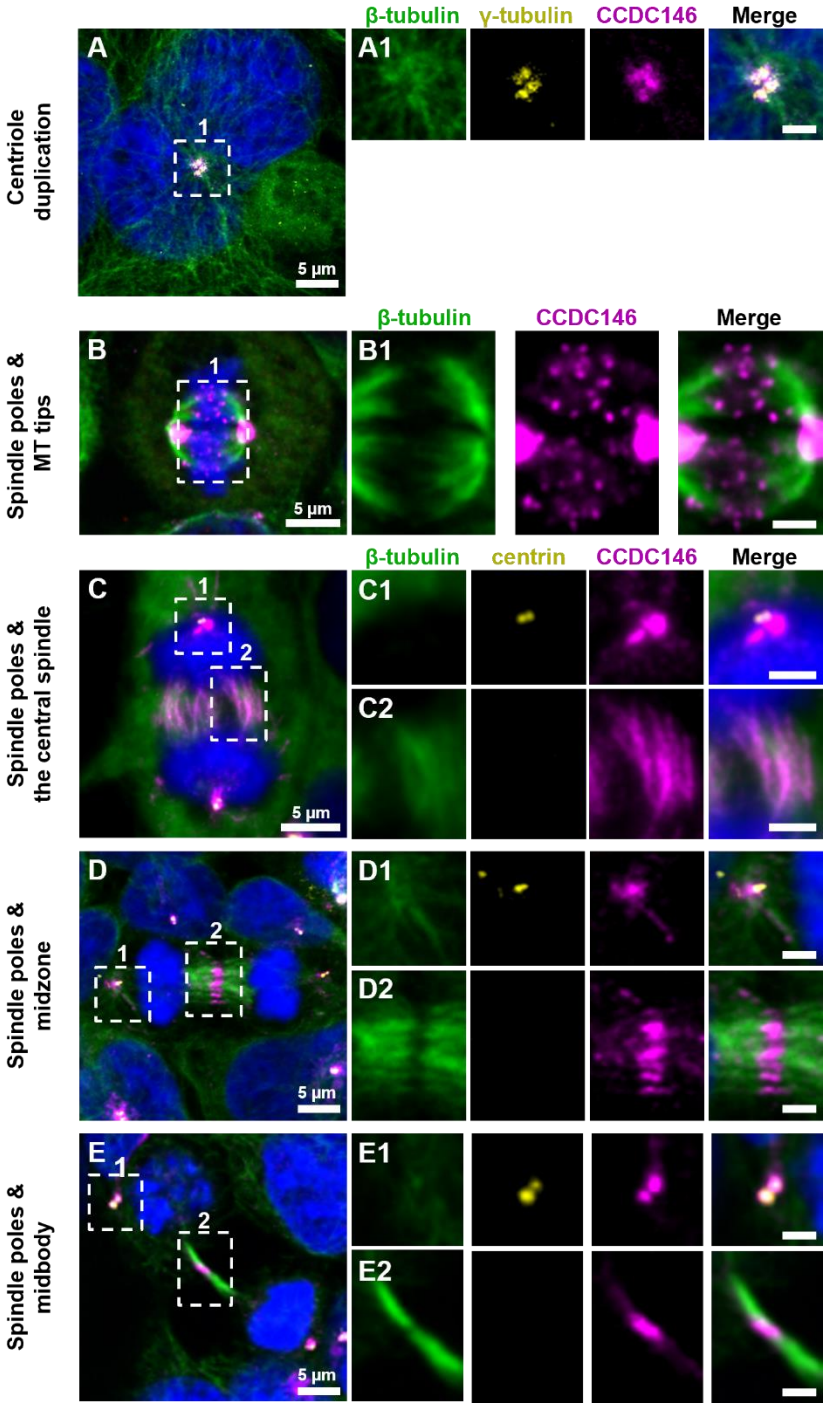

Figure 5: CCDC146 is a microtubule-associated protein (MAP) associated with microtubule-based structures throughout the cell cycle. HEK-293T cells were immunolabeled with anti-β-tubulin (green), anti-centrin (yellow), and anti- CCDC146 (magenta) Abs. DNA was stained with Hoechst (blue). In synchronized HEK-293T cells, CCDC146 is observed associated with (A) mother centrioles and their corresponding procentrioles during centriole duplication. (B) In non-synchronized cells, CCDC146 is observed associated with microtubule tips during metaphase, (C) the central spindle during (C) anaphase and (D) telophase, and (E) the midbody during cytokinesis. Images on the right show the enlargement of the dotted square in the left image. Scale bar of zoomed images: 2 µm.

5/ Expression profile of CCDC146 during the first wave of spermatogenesis in mouse

From our immunofluorescence analysis of somatic cell lines, it was clear that CCDC146 expression is associated with the cell cycle. In the testis, a wide variety of cell types co-exist, including both somatic and germline cells. The germline cells can be further subcategorized into a wide variety of cells, some engaged in proliferation (spermatogonia), others in meiosis (spermatocytes), or in differentiation (spermatids). To better understand the role of CCDC146 in spermatogenesis, and thus how its absence leads to sperm death and malformation, we initially studied its expression during the first wave of spermatogenesis [44] and sought to detect the protein in testis extracts at several postnatal timepoints and in the mature epididymal spermatozoon. Results from this study should shed light on when CCDC146 is required for sperm formation. Surprisingly, RT-PCR failed to detect *Ccdc146* transcripts in proliferating spermatogonia on day 9 after birth (Figure 6A). Transcription of *Ccdc146* started on day 18, concomitantly with the initiation of meiosis 2. Expression peaked on day 26, during the differentiation of spermatids. We also wished to explore the expression of the protein. To overcome a lack of specific antibodies recognizing mouse CCDC146, a transgenic mouse was created: (hemagglutinin) sequence was inserted by the CRISPR/Cas9 system into the coding sequence of the *Ccdc146* gene between the two first codons to produce a tagged protein at the N-terminus domain (Supp Figure 6). This insertion induced no phenotypic changes, and both female and male mice were viable with normal fertility. Tag insertion was validated by Western blotting (WB) (Figure 6B). The theoretical MW of the tagged protein is around 116.2 kDa (115.1 + 1.1); the observed MW was slightly higher, suggesting some post-translational modifications. Using these mice, testicular extracts from several postnatal timepoints and from epididymal spermatozoa were analyzed (Figure 6B). In accordance with RT-PCR experiments, bands corresponding to HA-tagged CCDC146 were detectable at D26 and 35, and in epididymal sperm (Figure 6C). The protein is therefore present during spermatid differentiation and conserved in mature sperm. The absence of the protein during spermatogonia proliferation suggests a new function for CCDC146 in sperm cells.

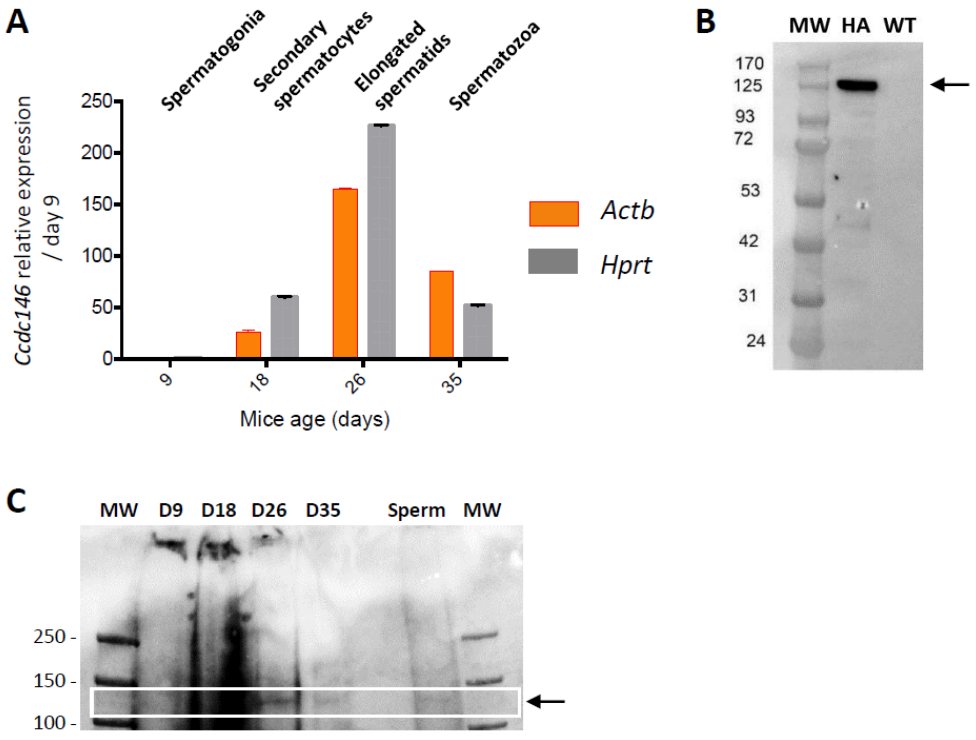

Figure 6: CCDC146 is expressed in late spermatocyte and in spermatids; CCDC146 protein is present in spermatids and in epididymal spermatozoa in mouse. (A) mRNA expression levels of Ccdc146 relative to *Actb* and *Hprt* in CCDC146-HA mouse pups' testes. Extremely low expression was detected at day 9, corresponding to testes containing spermatogonia and Sertoli cells only. Ccdc146 expression was observed from postnatal day 18 (formation of secondary spermatocytes), peaked at day 26 (formation of elongated spermatids), and subsequently decreased from day 35 (formation of spermatozoa), suggesting that Ccdc146 is particularly expressed in elongated spermatids during spermatogenesis. (B) Western blot of HA-tagged and WT sperm showing the specific band (arrow) corresponding to HA-tagged CCDC146 (CCDC146-HA) in epididymal whole sperm. (C) Western blot of HA-tagged testis extracts at different postnatal days. The presence of HA-tagged CCDC146 was revealed by an anti-HA Ab. Faint bands at the expected molecular weight are observed at D26, D35 and in epididymal sperm.

6/ In sperm, CCDC146 is present in the flagellum, not in the centriole

To attempt to elucidate the function of CCDC146 in sperm cells, we next studied its localization by IF in human and murine spermatozoa. We focused successively on the anterior segment (head, neck and beginning of the intermediate piece) of the sperm and then on the flagellum. In humans, the spermatozoon retains its two centrioles [32], and they are observable in the neck, as shown by anti-centrin and anti-tubulin labeling (Figure 7A1-3). No colocalization of the CCDC146 label with centrin was observed on human sperm centrioles, suggesting that the protein is not present in

or around this structure. However, two unexpected labeling events were observed: sub-acrosomal labeling and labeling of the midpiece. At the flagellum level, faint staining was observed along the whole length (Figure 7A4).

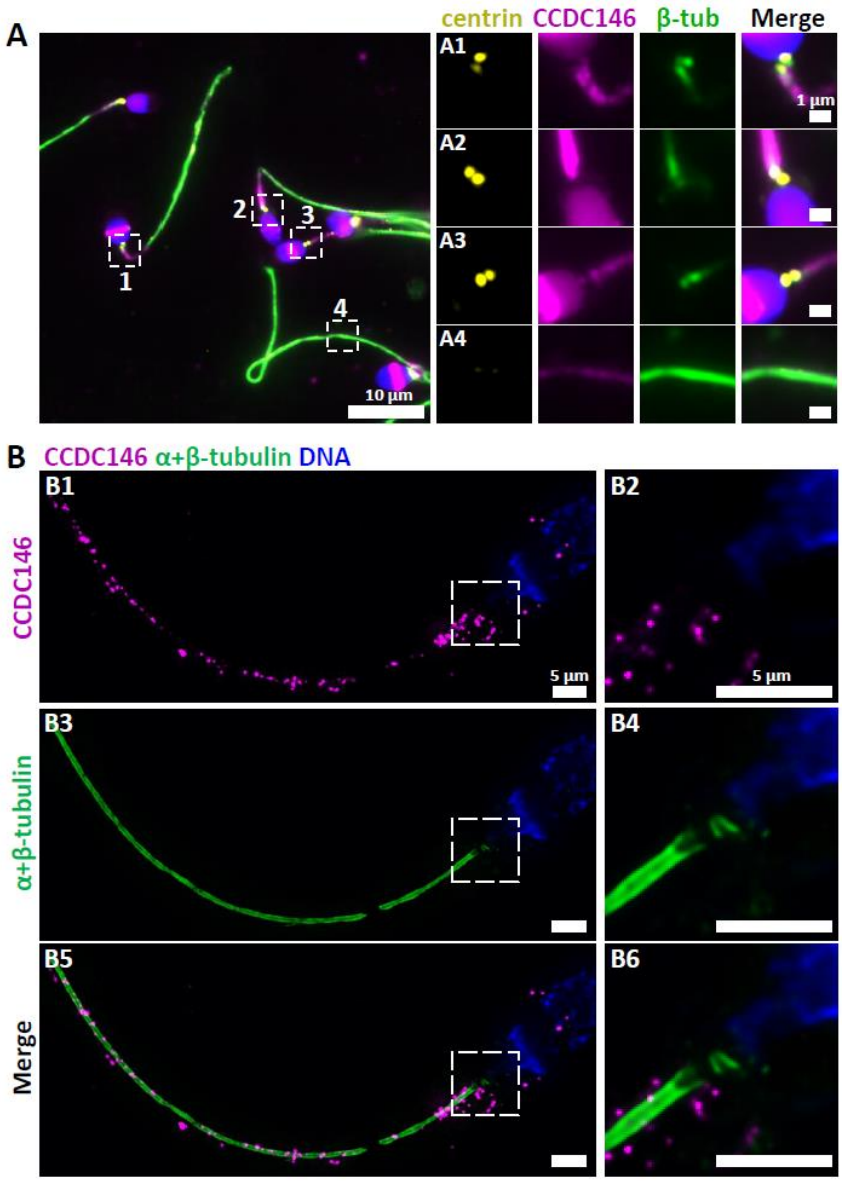

Figure 7: CCDC146 localizes to the flagellum but not to the centrioles of ejaculated human spermatozoa. (A) Human ejaculated sperm were immunolabeled with Abs recognizing centrin (yellow), CCDC146 (magenta), and β-tubulin (green). DNA was stained with Hoechst (blue). (A1-A3) enlargement of dotted square focused on sperm neck: no colocalization between CCDC146 and centrin. (A4) A faint signal for CCDC146 is present along the length of the sperm flagellum. Scale bar of zoomed images: 1 µm. (B) Human ejaculated sperm observed by expansion microscopy. Sperm were immunolabeled with anti-CCDC146 (magenta) and anti-β-tubulin (green), and DNA was stained with Hoechst (blue). B1 and B5 show strong staining for CCDC146 in the axoneme, B3 showing the localization of the axoneme through tubulin staining. B2, B4 and B6 show enlargements of the dotted square focused on the sperm neck. CCDC146 did not colocalize with the centrioles at the base of the axoneme. The CCDC146 staining observed probably corresponds to non-specific labeling of mitochondria.

To enhance resolution, ultrastructure expansion microscopy (U-ExM), an efficient method to study in detail the ultrastructure of organelles [45], was used (Figure 7B). The localization of the two centrioles was perfectly visible following anti-tubulin labeling, and was confirmed by co-labeling with an anti-POC5 Ab (Supp Figure 7). Once again, no CCDC146 labeling was observed on sperm centrioles (Figure 7B3), confirming the conventional IF results. Moreover, U-ExM unveiled that the observed CCDC146 midpiece staining (Figure 7A) seems in fact associated with isolated structures, which we hypothesize could be mitochondria, now visible by expansion (Figure 7B1). This suggests that the labeling on the midpiece observed in IF corresponds to non-specific mitochondrial labeling. This conclusion is supported by the fact that the same isolated structures were also labeled with anti-POC5 Ab (Supp Figure 7). In contrast, at the flagellum level, clear punctiform labeling was observed along the whole length of the main piece (Figure 7B1-B3), confirming that the protein is present in the sperm flagellum.

The same experiments were performed on murine epididymal spermatozoa. For this study, we used the mouse model expressing HA-tagged CCDC146 protein. It should be noted that unlike in humans, in mice, centrioles are no longer present in epididymal spermatozoa [33]. In conventional IF, using an anti-HA Ab, labeling was observed along the whole flagellum (Figure 8A). The strong HA-labeling in the midpiece was clearly non-specific, as the signal was still present when secondary antibodies were used alone (Supp Figure 8). In expansion microscopy, unexpectedly, the mouse flagellum presented breaks that most likely resulted from the expansion procedure (Figure 8B). Interestingly, strong HA-labeling was observed at the level of these breaks suggesting that CCDC146 epitopes are buried inside the axonemal structure and become accessible only on blunt or broken microtubule doublets. The same pattern was observed with three different anti-HA antibodies (Figure 8A-C). To confirm the presence of CCDC146 in the flagellum, sperm flagella were purified after mild sonication, and protein extracts were analyzed by WB (Figure 8D). In the flagella fraction, the HA Ab revealed a single band at around 120 kDa, thus confirming the flagellar localization of CCDC146 in both human and mouse sperm.

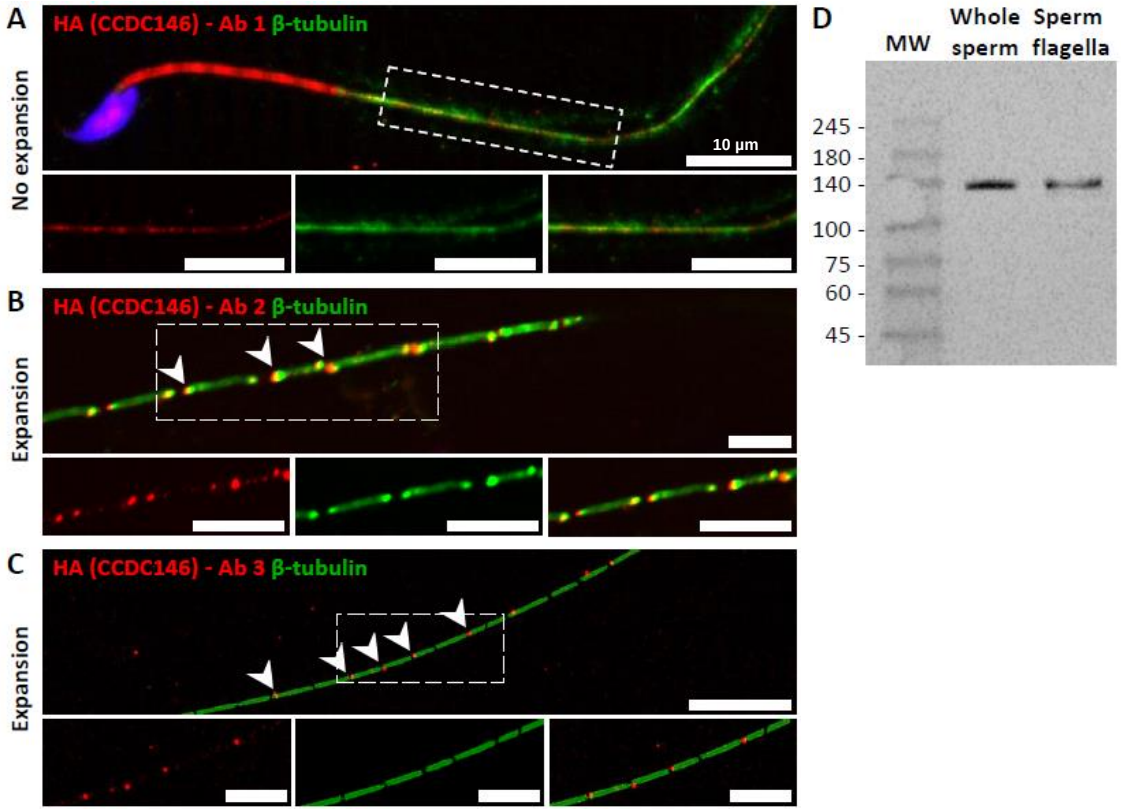

Figure 8: CCDC146 localizes to the flagellum of mouse epididymal spermatozoa. (A) Mouse epididymal spermatozoa observed with conventional IF. CCDC146-HA sperm were labeled with anti-HA #1 (red) and anti-β-tubulin (green) Abs. DNA was stained with Hoechst (blue). The upper image shows the sperm with merged immunostaining, and the lower images, the staining (red, green, and merge) observed in the principal piece of the flagellum. Scale bars: 10 µm. (B) Mouse epididymal spermatozoa observed with expansion microscopy. CCDC146-HA sperm were immunolabeled with anti-HA #2 (red) and anti-β-tubulin (green) Abs. DNA was stained with Hoechst (blue). The upper image shows the sperm with merged immunostaining. The lower images show the staining (red, green, and merge) observed in the principal piece of the flagellum. Strong punctiform signals were observed at the level of axonemal breakages induced by the expansion process. White arrows indicate the zones of the micro breaks. Scale bars: 10 µm. (C) Similar experiment performed with a third anti-HA Ab (#3). Scale bars: 10 µm. (D) Western blot of whole sperm and flagella fraction extracts. The presence of CCDC146-HA was revealed by an anti-HA Ab.

7/ CCDC146 labeling associates with microtubule doublets

We next wanted to determine whether CCDC146 staining was associated with the axoneme or accessory structures of the flagellum (outer dense fibers or fibrous sheath), and if so, whether it was associated with microtubule doublets or the central pair. To do so, we used U-ExM on human sperm and quantified the relative position of each CCDC146 dot observed (outside the axoneme, outer left and right; microtubule doublets left and right and central pair – Figure 9A-C). The distribution of localizations was summarized in two bar graphs, generated for two distinct sperm

cells. Labeling was preferentially located on the right and left doublets (Figure 9D and 9F), indicating that CCDC146 associates more with microtubule doublets. Analysis of protein distribution in mice was not easy, because signal tended to concentrate at breaks. Nevertheless, on some spermatozoa with frayed microtubule doublets., i.e. with the flagellum taking on the shape of a hair, we could find that isolated doublets carried the punctiform labeling confirming the results of analyses on human spermatozoa (Figure 9G). Taken together, these results from mouse and human sperm demonstrate that CCDC146 is an axonemal protein, probably associated with microtubule doublets.

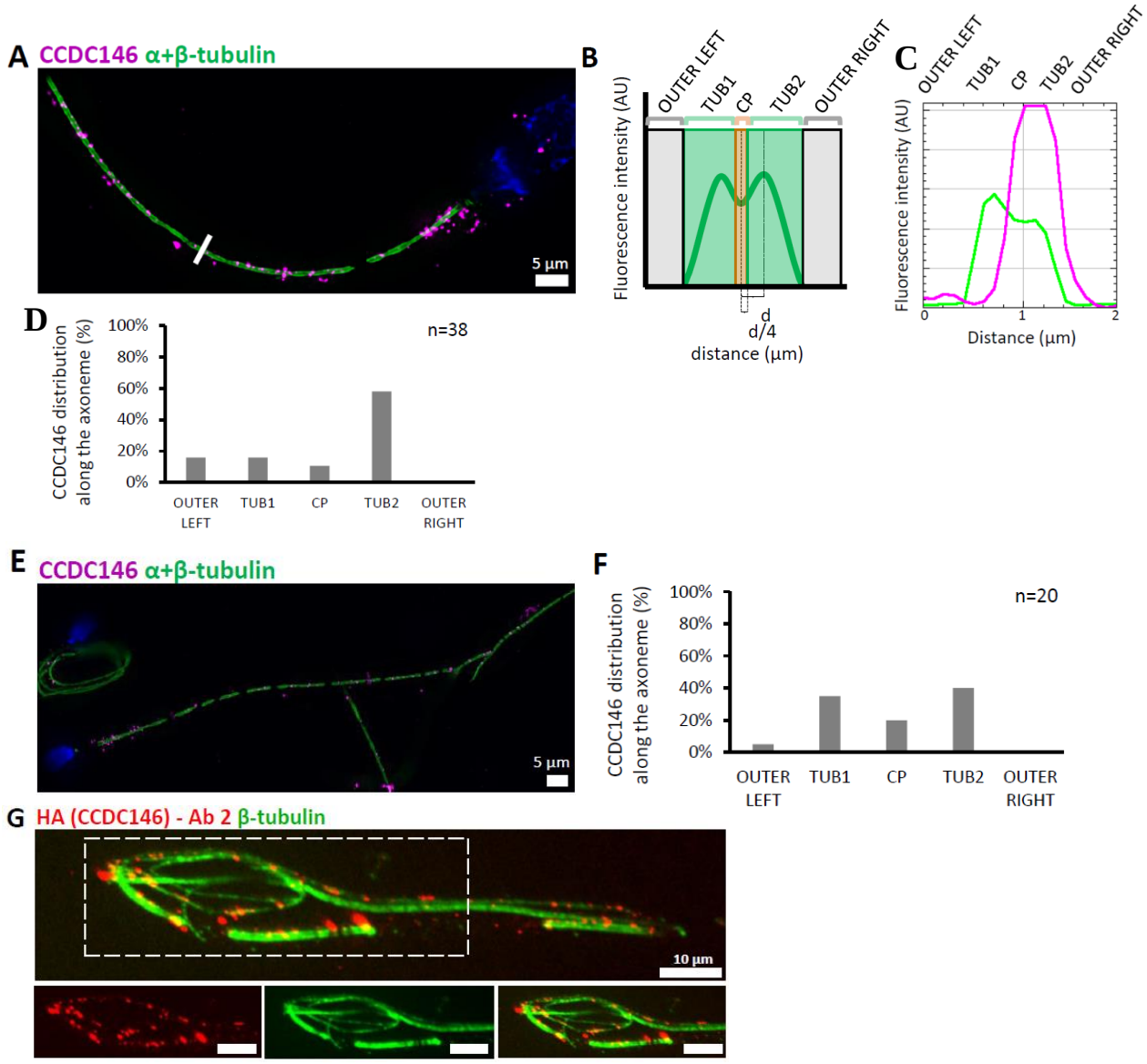

Figure 9: CCDC146 localizes to the microtubule doublets of the axoneme in human and mouse (description on the following page).

(Previous page) Figure 9: CCDC146 localizes to the microtubule doublets of the axoneme in human and mouse. (A) Sperm was double-stained with anti-tubulin Ab (green) and anti-CCDC146-Ab (magenta) and observed by expansion microscopy. (B) The position of the CCDC146 signal with respect to the tubulin signal was measured along the entire flagellum. CCDC146 signals were localized to different compartments of the axoneme by the following method: the green signal is quite characteristic with two peaks corresponding to the left and right microtubule doublet, it identifies five axonemal compartments (left outer, left doublet, central pair, right doublet, and right outer). For each CCDC146 signal (magenta dots), the flagellum was perpendicularly cut (example, white bar in A) and the tubulin and CCDC146 signals measured to assign each CCDC146 signal to a localization area. (C) Example of a measurement obtained at the right bar shown in (A). (D) Histogram showing the distribution of CCDC146 labeling in ejaculated human sperm 1, presented in (A). (E) Ejaculated human sperm double-stained with anti-tubulin Ab (green) and anti-CCDC146-Ab (magenta). (F) Histogram showing how CCDC146 labeling distributed in ejaculated human sperm 2. (G) Flagellum of a mouse epididymal spermatozoa observed with expansion microscopy. CCDC146-HA sperm were immunolabeled with anti-HA #2 (red) and anti-β-tubulin (green). The upper image shows the sperm with merged immunostaining, and the lower images, the staining (red, green, and merge) observed in the principal piece of the flagellum. Scale bars 10 µm.

8/ CCDC146 could be a Microtubule Inner Protein (MIP)

The presence of extensive labeling at axoneme breaks suggests that the antigenic site is difficult to access in an intact flagellum. We therefore hypothesized that CCDC146 could be a MIP. MIPs are generally resistant to solubilization by detergents. However, N-lauroylsarcosine (sarkosyl) can solubilize microtubule doublets, with increasing concentrations destabilizing first the A-tubule, then the B-tubule [46, 47]. Microtubule solubilization allows release of the MIPs contained within the tubules, and the method is recognized [48, 49]. To test our hypothesis that CCDC146 is a MIP, we treated spermatozoa from HA-tagged CCDC146 mice with sarkosyl and performed a WB on the supernatant (Figure 10A). The protein was effectively solubilized, leading to the appearance of bands at around 120 kDa on an SDS-PAGE gel following migration of extracts from sperm treated with 0.2% and 0.4% sarkosyl concentrations. Interestingly, a second band around 90 kDa was also immunodecorated by anti-HA antibody in the sarkosyl treated sample, a band not present in the protein extracts from WT males. The other detergents and buffers tested – RIPA, CHAPS or Tris-HCl – barely solubilized CCDC146 or led to no solubilization (Figure 10B). This result confirms the unique action of sarkosyl on CCDC146 and strengthens the hypothesis that the protein is localized in the lumen of tubules. To confirm the action of sarkosyl on the accessibility of the antigenic site, murine spermatozoa were labeled with an anti-HA antibody after treatment with sarkosyl or no treatment. CCDC146 labeling was significantly increased in the presence of sarkosyl (Figure 10C). The full image panel including secondary Ab control experiments can be found in Supp Figure 9.

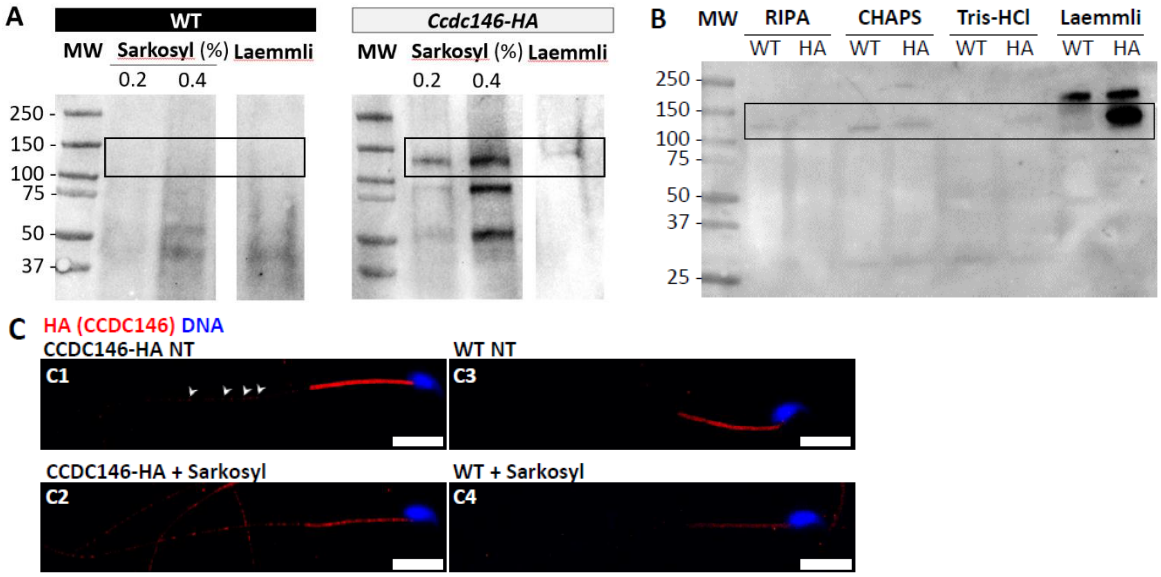

Figure 10: CCDC146 could be a microtubule inner protein in sperm: evidence from sarkosyl treatment. (A) Western blot of WT and CCDC146-HA sperm extract solubilized with N-lauroylsarcosine (sarkosyl), an anionic detergent. Sarkosyl was used at increasing concentrations (0.2 and 0.4%). The presence of CCDC146-HA was detected by an anti-HA Ab. (B) Western blot of WT and CCDC146-HA sperm extracts solubilized with alternative detergents (RIPA, CHAPS, Tris-HCl) and whole sperm extract solubilized in Laemmli. The presence of CCDC146-HA was revealed by an anti-HA Ab. (C) Epididymal CCDC146-HA sperm (C1-C2) and WT sperm (C3-C4), treated with sarkosyl (5 min, 0.2% sarkosyl) or not (NT), were immunostained to reveal the HA-tag (red) and counterstained with Hoechst (blue). (C1) Without treatment, a faint CCDC146 signal (white arrow heads) is observed along the flagellum from CCDC146-HA sperm. (C2) Treatment with sarkosyl enhanced the CCDC146-HA signal along the sperm flagellum. (C3) HA signal in WT non-treated (NT) sperm is present in the midpiece only, suggesting that this signal is not specific. (C4) The HA signal in WT sperm is not enhanced by sarkosyl treatment. Scale bars 10 µm.

9/ KO models show defects in tubulin-made organelles

To better characterize the function of CCDC146 in mouse sperm, we went on to perform a detailed morphological analysis of tubulin-made organelles by IF, and examined the morphological defects induced by the absence of CCDC146 at the subcellular level by scanning and/or transmission electron microscopy. This work was performed on immature testicular sperm and on seminiferous tubule sections from adult WT and KO males. Mouse testicular sperm were used because they still contain centrioles that become disassembled as sperm transit through the epididymis [50]. We mainly focused our analyses on the centrioles, the manchette, and the axoneme.

The connecting piece between the head and the flagellum, known as the sperm head-tail coupling apparatus (HTCA), is a complex structure containing several substructures including both centrioles, the capitulum and the segmented columns. The distal centriole is embedded in the segmented column and the axoneme emerges from the distal centriole. This structure has a specific shape when observed by scanning electron microscopy (Figure 11A). In *Ccdc146* KO sperm, the connecting piece was severely damaged (Figure 11A). In WT testicular sperm, IF experiments show that the centrioles, identified by anti-tubulin Ab, are very close to each other and adjacent to the capitulum (Figure 11B). In *Ccdc146* KO males, centriole separation was visible in numerous spermatozoa (Figure 11B3, B4), with the structures located far away from the connecting piece (Figure 11B5) or duplicated (Figure 11B6).

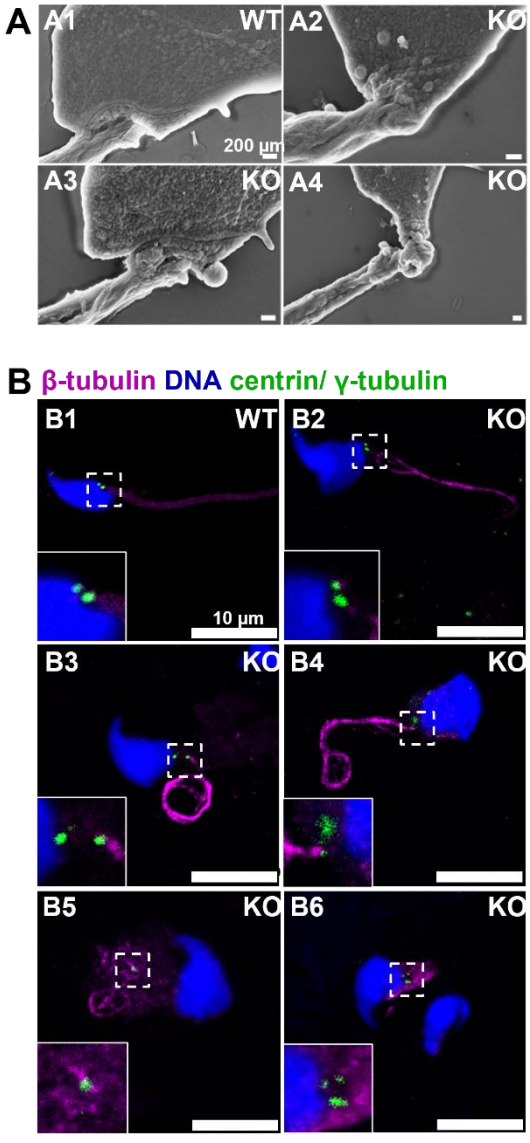

Figure 11: The absence of CCDC146 causes defects of the head-tail coupling apparatus in epididymal spermatozoa and duplication and mislocalization of centriole in testicular sperm. (A) Scanning electron microscopy of WT and Ccdc146 KO epididymal spermatozoa showed aberrant head morphologies and irregular head-tail coupling apparatus (HTCA) linking the sperm head with the flagellum. (B) Testicular spermatozoa from WT (B1) and Ccdc146 KO (B2-B6) mice immunolabeled with anti-β-tubulin (magenta) and anti-centrin (B1-B3) or anti-γ-tubulin (B4-B6) (green) Abs. Centrioles appeared to be normal (B2) in some spermatozoa, separated but partially attached to the head (B3, B4), completely detached from the sperm head (B5), or duplicated (B6).

Interestingly, the overall structure of the HTCA under construction in spermatids, observed by TEM, was conserved in *Ccdc146* KO spermatids, with the presence of both centrioles, containing nine triplets of microtubules, the proximal centriole and its adjunct, as well as accessory cytoskeletal structures, including the capitulum and the segmented columns (Figure 12AB). Remarkably, in a very large proportion of sections, no singlet or doublet of microtubules emerged from the distal KO centriole, suggesting that the process of tubulin polymerization is somehow hampered in these cells (Figure 12A). The absence of microtubules at the end of the distal centriole was confirmed by analysis of serial sections of the sperm centrioles (Figure 12C). Moreover, the defects observed in IF experiments, such as duplication, or defective attachment to the nuclear membrane, were frequently confirmed in TEM images (supp Figure 10). Such defects were not observed in WT spermatids.

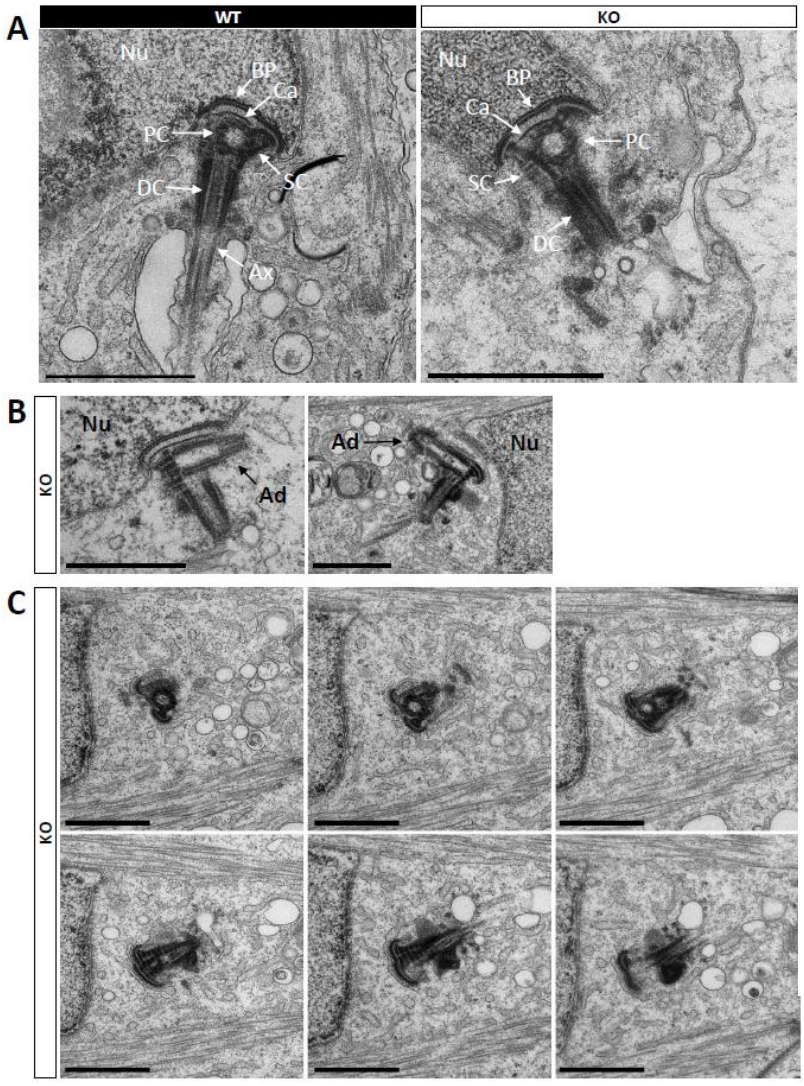

Figure 12: Absence of elongation of axonemal microtubules at the base of the distal centriole. (A) In WT spermatids, the proximal centriole (PC) is linked to the base of the compacting nucleus (Nu) through the basal plate (BP) and the capitulum (Ca), and the distal centriole (DC) is embedded in the segmented column (SC). All these sperm-specific cytoskeletal structures make up the HTCA. At the base of the distal centriole, axonemal microtubules (MT) grow. In Ccdc146 KO elongating spermatids, the overall structure of the HTCA is conserved, with the presence of the centrioles and the accessory cytoskeletal structures. However, no axonemal microtubules are visible. (B) The adjunct (Ad) of the proximal centriole is also preserved in Ccdc146 KO spermatids. (C) Serial sections of the HTCA of a Ccdc146 KO spermatid confirm the absence of axonemal microtubules at the base of the distal centriole during spermatid elongation. Scale bars: 1 µm.

Manchette formation – which occurs from the round spermatid to fully-elongated spermatid stages – was next studied by IF using b-tubulin Ab. Simultaneously, we monitored formation of the acrosome using an antibody binding to DPY19L2 (Figure 13). Initial acrosome binding at step III was not disrupted, and we observed no differences in the caudal descent of the acrosome during subsequent steps (III-VIII). The development of the manchette in between stages IX-XII was not hampered, but noticeable defects appeared indicating defective manchette organization– such as a random orientation of the spermatids and abnormal acrosome shapes. Finally, at step I, the manchette was clearly longer and wider than in WT cells, suggesting that the control of the manchette biogenesis is defective. In TEM, microtubules in the manchette were clearly visible surrounding the compacting nucleus of elongating spermatids. However, many defects such as marked asymmetry and enlargement were visible (Figure 14). The manchette normally anchors on the perinuclear ring, which is itself localized just below the marginal edge of the acrosome and separated by the groove belt [51]. In KO spermatids, the perinuclear ring was no longer localized in the vicinity of the acrosome and was often spread into the cytoplasm, providing a large nucleation structure for the manchette (Figure 14 D-F, red arrows), which explains its width and irregularity.

(Next page) Figure 13: Analysis of stages of spermatogenesis by IF reveals acrosome formation and manchette elongation defects. Cross sections of WT and Ccdc146 KO testes showing different stages of mouse spermatogenesis (I, VII-XII). Stages were determined by double immunostaining for β-tubulin (red) and DPY19l2 (green; acrosome localization), and DNA was stained with Hoechst (blue). (A) Very few mature spermatozoa lined the lumen at stage VII-VIII in the KO. Cell orientations appear random from stage IX-X in the KO and the tubules contain more advanced spermatid stages. The acrosome of elongating KO spermatids had become abnormal by stage XII, and the manchette of elongated spermatids at stage I was longer in the KO compared with the WT. (B) Typical spermatids from stages I-XII, showing details of acrosome formation and manchette elongation. Scale bars stages VII-VIII 20 µm, scale bars IX-X, XII and I: 10 µm.

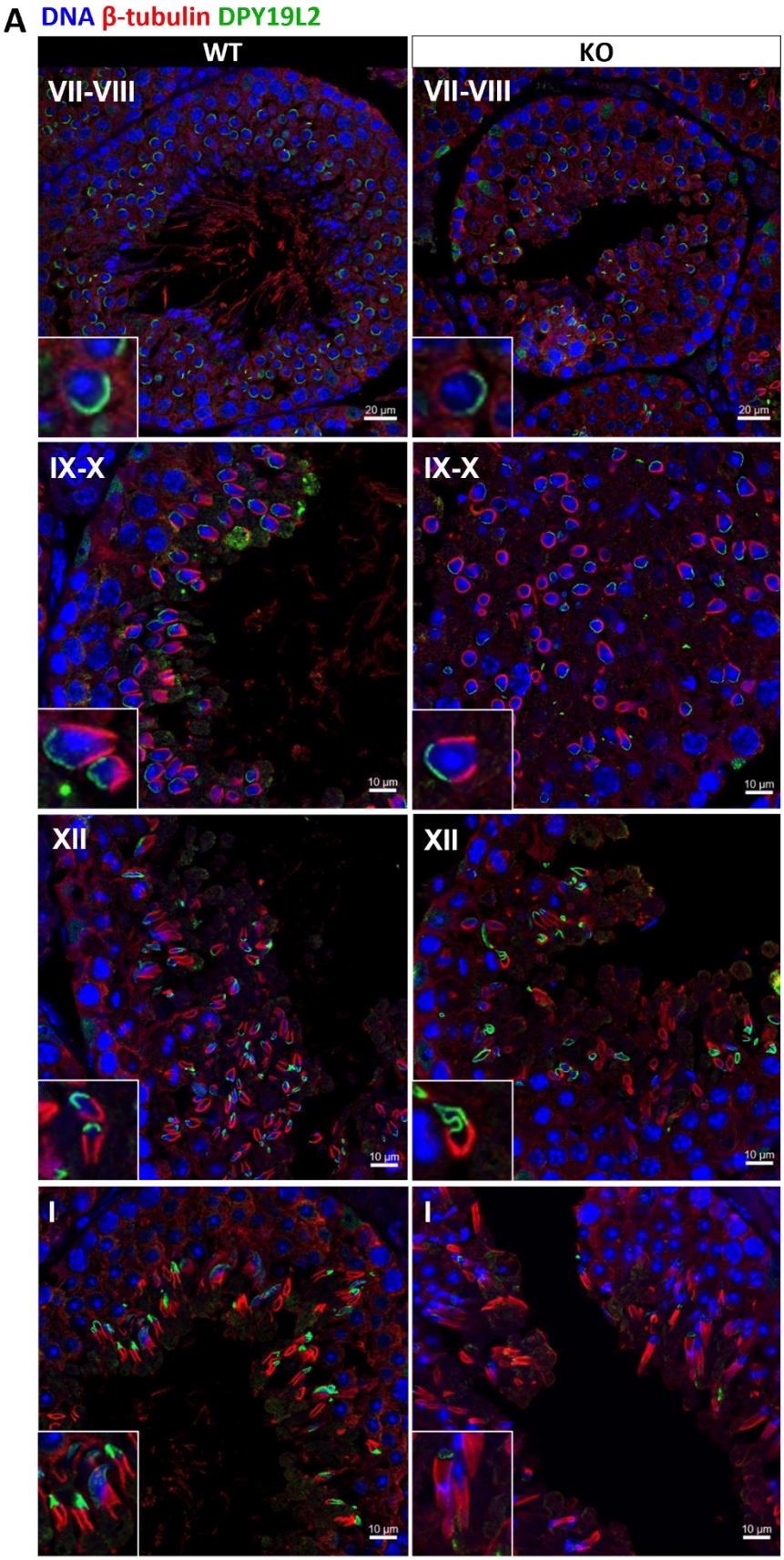
A
DNA β-tubulin DPY19L2
WT
KO
VII-VIII
VII-VIII
IX-X
IX-X
XII
XII
I
I
20 µm
20 µm
10 µm
10 µm
10 µm
10 µm
10 µm
10 µm

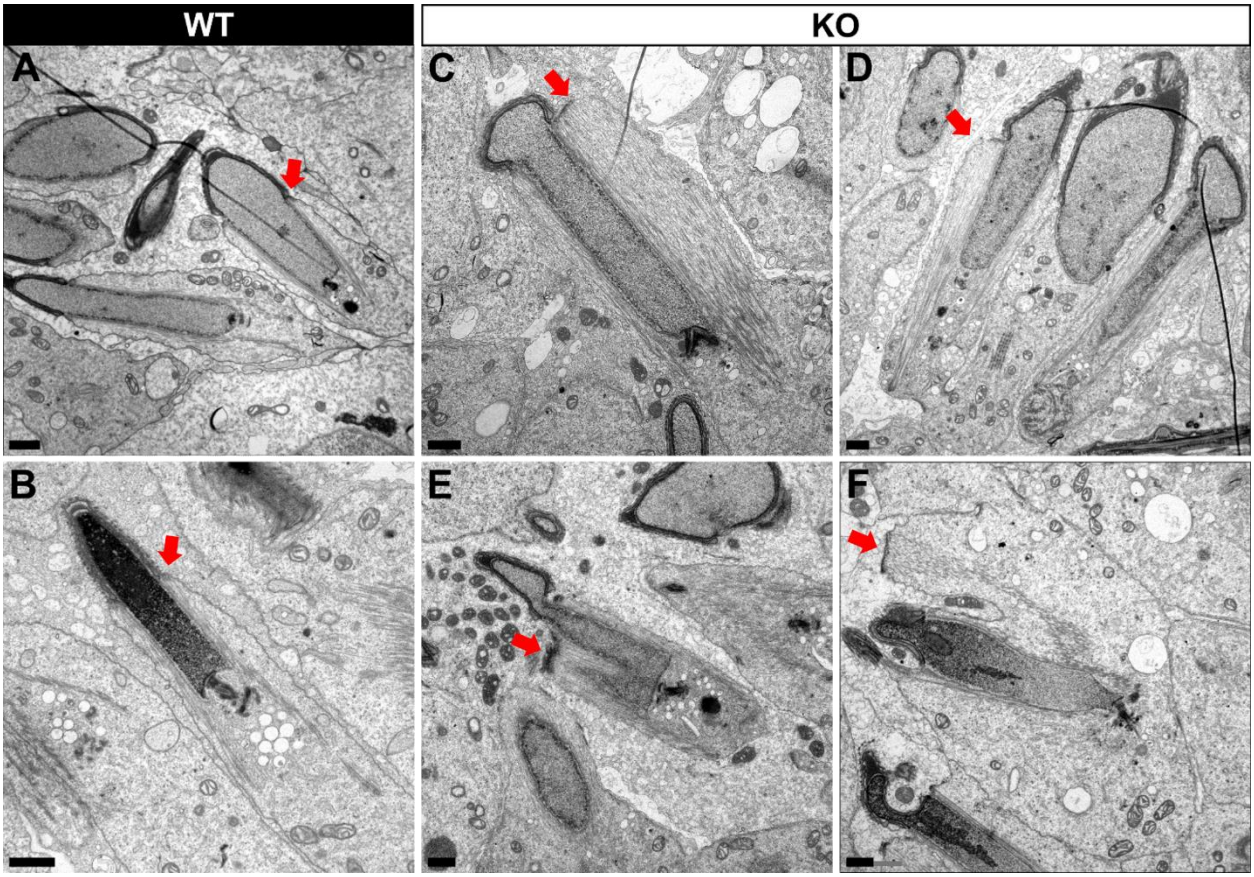

Figure 14: TEM of elongating spermatids from Ccdc146 KO male shows ultrastructural defects of the manchette. (A, B) Ultrastructural analysis of the manchette in WT elongating spermatids shows the normal thin perinuclear ring, anchored below the acrosome and allowing a narrow array of microtubules to anchor. (C-F) In elongating spermatids from CCDC146 KO animals, the perinuclear ring was abnormally broad, usually located on one side of the spermatid (red arrows), creating an asymmetric and wide bundle of microtubules. The resulting manchette was wider and often longer than in WT animals. (E, F) The tubulin nucleation location was sometimes ectopic in the KO and coincided with irregularly shaped sperm heads. Scale bar: 1 µm.

Numerous defects were also observed in the axoneme. These axoneme defects were generally similar to the defects observed in other MMAF mouse models, with disorganization of the axoneme structure (Figure 15A) accompanied by fragmentation of the dense fibers and their random arrangement in cell masses anchored to the sperm head (Figure 15C). The absence of emerging singlet or doublet microtubules at the base of the distal centriole leads to a complete disorganization of the flagellum and the presence of notably dense fiber rings devoid of internal tubulin elements (Figure 15BC).

Finally, the shape of the nucleus presented numerous abnormalities (Supp Figure 11). The emergence of head defects was concomitant to the implantation of the manchette, with no defects observed on round spermatids at stages III-VIII. Unexpectedly, a distortion was created in the

center of the nucleus at the anterior pole, causing the formation of a bilobed compacted nucleus (Supp Figure 13E-G) containing visible vacuoles.

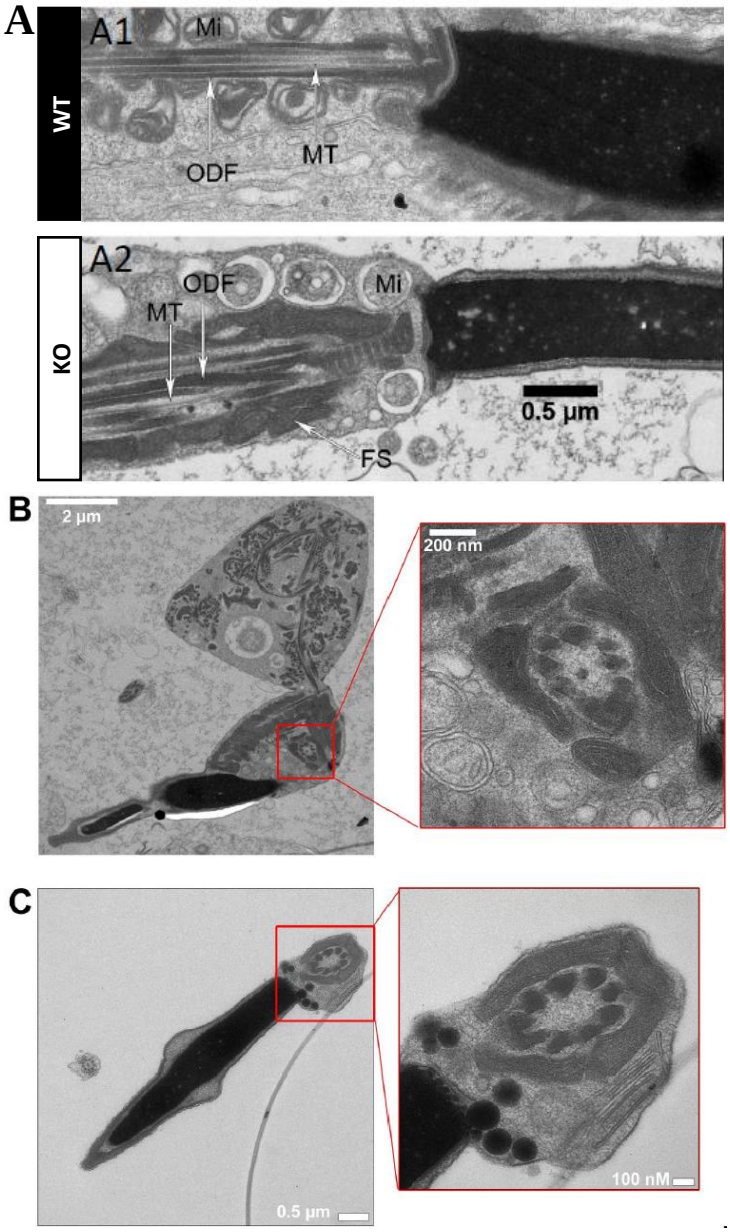

Figure 15: The axonemes of Ccdc146 KO spermatids present multiple defects visible under TEM. (A1) A longitudinal section of a WT flagellum shows a typical structure of the principal piece, with outer dense fibers (ODF) at the periphery, microtubules (MT) in the center, and mitochondria (Mi) aligned along the flagellum. (B1) A longitudinal section of a Ccdc146 KO flagellum shows a disorganized midpiece, with altered mitochondria, the presence of an amorphous fibrous sheath (FS) and altered microtubules. (B) Longitudinal section of a Ccdc146 KO sperm showing dispersed and non-assembled flagellar material in a cytoplasmic mass. The right-hand image is the enlargement of the red square, showing the presence of an external ring of mitochondria surrounding an outer dense fiber ring devoid of microtubular material. (C) Longitudinal section of another Ccdc146 KO sperm showing a similar abnormal midpiece structure. The right-hand image is the enlargement of the red square, showing the presence of an external ring of mitochondria surrounding an outer dense fiber ring devoid of microtubular material.

Discussion

This study allowed us to identify and validate the involvement of a new candidate gene in male infertility, *CCDC146*. This gene was first described in mice by our team earlier this year, in the context of a research project on the different types of genetic causes of sperm abnormalities in mouse [52]. However, no data other than the sperm phenotype (MMAF) was presented in this

initial report. In this paper, we present for the first time the evidence of the presence of mutations in humans and a description of the localization of the protein in somatic and germ cells. We also examined the lesion spectrum at the subcellular level, to obtain a detailed view of the molecular pathogenesis associated with defects in this gene.

1/ Genetic complexity of MMAF

It is essential to characterize all genes involved in male infertility. Therefore, the characterization of a new gene involved in MMAF syndrome is not just "one more gene". First, it further confirms that MMAF syndrome is a heterogeneous recessive genetic disease, currently associated with defects in more than 50 genes. Second, it helps direct the diagnostic strategy to be directed during genome-wide searches. The type of profiling required for MMAF is very different from that performed for instance for cystic fibrosis, where one mutation is responsible for more than 50% of cases. Third, the discovery of all genes involved in MMAF is important in the context of oligogenic heterozygous inheritance of sperm abnormalities in human [52]. Indeed, a homozygous deleterious mutation is found in only half of all MMAF patients, suggesting that other modes of inheritance must be involved. Only by establishing an extended list of genes linked to MMAF will it be possible to determine whether oligogenic heterozygous inheritance is a relevant cause of this syndrome in humans. Finally, some of the genes involved in MMAF syndrome are also involved in ciliary diseases [7]. By further exploring MMAF-type infertility, we can hope to enhance our understanding of another underlying pathology. Although the vast majority of patients with PCD are diagnosed before 5 years of age [53], one study showed that in a cohort of 240 adults with a mean age of 36 years (36 ± 13) presenting with chronic productive cough and recurrent chest infections, PCD was identified for the first time in 10% of patients [54]. This result suggests that infertility diagnosis can occur before PCD diagnosis, and consequently that infertility management might improve PCD diagnosis and care.

2/ Functional complexity of CCDC146

The results presented in this report show striking differences in localization of CCDC146 between somatic and germ cells. Our results show that the protein displays several subcellular localizations, which vary according to the cell cycle, and the cell nature. In somatic cells, the protein is mostly associated with the centrosome and other microtubular structures – in particular the mitotic spindle – at the end of microtubules and at the level of the kinetochore and the midbody. These

observations identify CCDC146 as a microtubule-associated protein (MAP). In contrast, in spermatozoa, IF images indicate that CCDC146 is an axonemal protein that could be localized in the microtubule doublets. Moreover, the CCDC146 signal was enhanced when sperm were treated with the sarkosyl detergent, used to identify microtubule inner proteins (MIP). Finally, expansion microscopy revealed a strong signal in mouse sperm at the point of axoneme rupture. Taken together, these elements suggest that CCDC146 may be a MIP. Despite its broad cellular distribution, the association of CCDC146 with tubulin-dependent structures is remarkable. However, centrosomal and axonemal localizations in somatic and germ cells, respectively, have also been reported for CFAP58 [37, 55], thus the re-use of centrosomal proteins in the sperm flagellar axoneme is not unheard of. In addition, 80% of all proteins identified as centrosomal are found in multiple localizations (https://www.proteinatlas.org/humanproteome/subcellular/centrosome). The ability of a protein to home to several locations depending on its cellular environment has been widely described, in particular for MAP. The different localizations are linked to the presence of distinct binding sites on the protein. For example, MAP6 binds and stabilizes microtubules, through Mc modules, and associates with membranes and neuroreceptors through palmitoylated cysteines. MAP6 can also localize in the microtubule lumen, in its role as MIP, thanks to its Mn modules. Finally, in addition to its associations with subcellular compartments and receptors, the presence of proline-rich domains (PRD) in the MAP6 sequence, allows it to bind to SH3-domain-containing proteins, and thus triggering activation of signaling pathways [56]. Another example of a protein with multiple localizations is CFAP21, which is a MIP but also a cytosolic calcium sensor. In the latter capacity, CFAP21 modulates the interaction of STIM1 and ORAI1 upon depletion of calcium stores [57, 58]. These examples illustrate the complexity of function of some multiple-domain proteins.

The fact that CCDC146 can localize to multiple subcellular compartments suggests that it also contains several domains. Interestingly, a PF05557 motif (Pfam mitotic checkpoint protein, https://www.ebi.ac.uk/interpro/protein/UniProt/E9Q9F7/) has been identified in the mouse CCDC146 sequence between amino acids 130 and 162. Proteins belonging to the “mitotic spindle checkpoint” monitor correct attachment of the bipolar spindle to the kinetochores. The presence of this motif likely explains the ability of CCDC146 to localize to cell cycle-dependent subcellular compartments containing tubulin. However, the most important structural motifs identified in CCDC146 are the coiled-coil domains. Although coiled-coils play a structural role in a variety of

protein interactions, their presence in CCDC146 remains mysterious, and how they contribute to its function remains to be elucidated. Nevertheless, this motif is compatible with a MIP function for this protein, since several MIP proteins including CCDC11 (FAP53), CCDC19 (FAP45), and CCDC173 (FAP210) are coiled-coil proteins [57]. It is worth noting that the ortholog of *CCDC146* in *Chlamydomonas*, *MBO2*, codes for a protein required for the beak-like projections of doublets 5 and 6, located inside the lumen of the tubule B [59], in the proximal part of the *Chlamydomonas* flagellum. Although no beak-like projections are present in the mammalian axoneme, the location inside the tubule seems to be evolutionarily conserved. A more recent study of MBO2 showed that the protein is also present all along the flagellum of *Chlamydomonas* and is tightly associated with microtubule doublets [60]. These observations support our results showing association of CCDC146 with this axonemal structure.

The results presented here also show a striking difference in the phenotype induced by the lack of the protein in somatic and male germ cells. This protein is essential for spermatogenesis, and its absence leads to immotile non-functional sperm and to complete infertility in both humans and mice. Conversely, both patients and *Ccdc146* KO mice seem to be healthy and present no other conditions such as primary ciliary dyskinesia (PCD). CCDC146, despite its wide expression profile in many tissues therefore seems to be dispensable except during spermatogenesis. Nevertheless, because this protein is localized on the tips of the spindle and may be involved in mitotic checkpoints, its absence may lead to late proliferative disorders. This hypothesis is supported by the fact that *CCDC146* is reported to be down-regulated in thyroid cancer [61]. The link between infertility and risk of cancer was recently underlined, with mutations found in genes like *FANCM* [62]. Therefore, it would be interesting to monitor aging in *Ccdc146* KO mice and to study their life expectancy and cancer rates compared to WT mice.

3/ Absence of CCDC146 in sperm centriole

Several proteomics studies of the sperm centriole identified CCDC146 as a centrosome-associated protein in bovine sperm [28, 63], a species where centrioles are present in ejaculated sperm. Using a different methodological approach, based on IF with conventional and expansion microscopy, we observed no CCDC146 signal in centrioles from testicular mouse and ejaculated human sperm. The same result was obtained with two different types of antibodies: with human sperm, we used a commercial anti-CCDC146 Ab, whereas with mouse sperm we used several anti-HA antibodies.

The same IF approach allowed us to clearly identify the sperm centrosome using a number of antibodies such as anti-POC5 and anti-beta tubulin, ruling out a possible failure of our IF protocol. It is worth noting that centrosomal proteins were isolated from whole flagella using several strategies including sequential use of multiple detergents, and that the centrosomal proteins were purified in the last fractions. These results indicate that CCDC146 is in fact barely soluble in conventional buffers, which could explain why it is co-purified with the centrosomal fraction in proteomics studies.

4/ TEM reveals that lack of CCDC146 severely impacts microtubule-based organelles

No morphological defects were observed before the elongating spermatid stage, and in round spermatids, the acrosome started to spread on the nucleus in a normal way (Figure 13). Morphological defects appeared clearly from the onset of spermatid elongation. This result indicates that the protein is only necessary for late spermiogenesis, from the phase corresponding to flagellum biogenesis. All the organelles composed mainly of tubulin were strongly affected by the absence of the protein.

The manchette structure in elongating *Ccdc146* KO spermatids was asymmetric, abnormally broad, and ectopic, leading to the formation of aberrantly shaped sperm heads. So far, manchette defects have been associated with defects in intra-flagellar transport (IFT), and intra-manchette transport (IMT) [64]. CCDC146 was only localized to the sperm axoneme by IF, and no signal was observed in the manchette, suggesting that CCDC146 is probably not involved in the transport machinery. Moreover, our results indicated that the manchette was remarkably long in elongated spermatids. A similar phenotype was observed in Katanin80-deficient animals [65]. Katanin80 is a microtubule-severing enzyme that is important for manchette reduction. Interestingly, the absence of WDR62, a scaffold protein involved in centriole duplication, leads to defective katanin80 expression, and the presence of elongated manchettes in mice [66]. In combination with our results, this detail suggests that the manchette's structure and its reduction are influenced by centrosomal proteins, possibly through katanin defects. The precise molecular link between CCDC146 and manchette assembly and reduction remains to be identified.

The HTCA was also aberrant in *Ccdc146* KO spermatids. Centrioles in elongating spermatids were frequently displaced from their implantation fossa at the nuclear envelope. We observed some correctly lodged centrioles in round spermatids; however, we are unable to determine with

certainty whether the majority of centrioles failed to correctly attach or whether they detached from the nuclear envelope during spermatid elongation. Defects in cohesion of the HTCA have been associated with the acephalic spermatozoa syndrome, and were shown to involve a number of proteins such as SUN5, SPATA6 and ODF1 [4, 67-69]. Here, we did not observe any sperm decapitation, suggesting that CCDC146 is involved in a different pathway controlling the HTCA. Moreover, elongating *Ccdc146* KO spermatids displayed supernumerary centrioles. Abnormal centriole numbers have also been reported in the absence of a few other centrosome-associated proteins including DZIP1 [36] and CCDC42 [41], and of microtubule-regulating proteins such as katanin like-2 [70] and tubulin deglutamylase CCP5 [71].

Studies of the spermiogenesis defects observed in different models deficient for centrosomal proteins show some common features such as abnormal manchette and duplicated centrosomes. The absence of these proteins does not appear to be directly responsible for these defects, rather it seems to modify the expression of microtubule regulatory proteins such as katanins [65, 66, 70]. These modifications could explain the pleiotropic effect of the absence of CCDC146 on microtubule-based organelles.

In conclusion, by characterizing the genetic causes of human infertility, we not only improve the diagnosis and prognosis of these pathologies but also pave the way for the discovery of new players in spermatogenesis. We are constantly adding to the number of proteins present in the flagella of the mammalian spermatozoa that are necessary for its construction and functioning. This study showed that CCDC146, a protein previously described as a centrosomal protein in somatic and germ cells, localizes in spermatozoa's axonemal microtubule doublets. The presence of CCDC146 in somatic cells' centrosomes gives weight to the idea of a centrosome with a dynamic composition, allowing it to fulfill its multitude of functions throughout all the phases of cellular life.

Supplementary figures

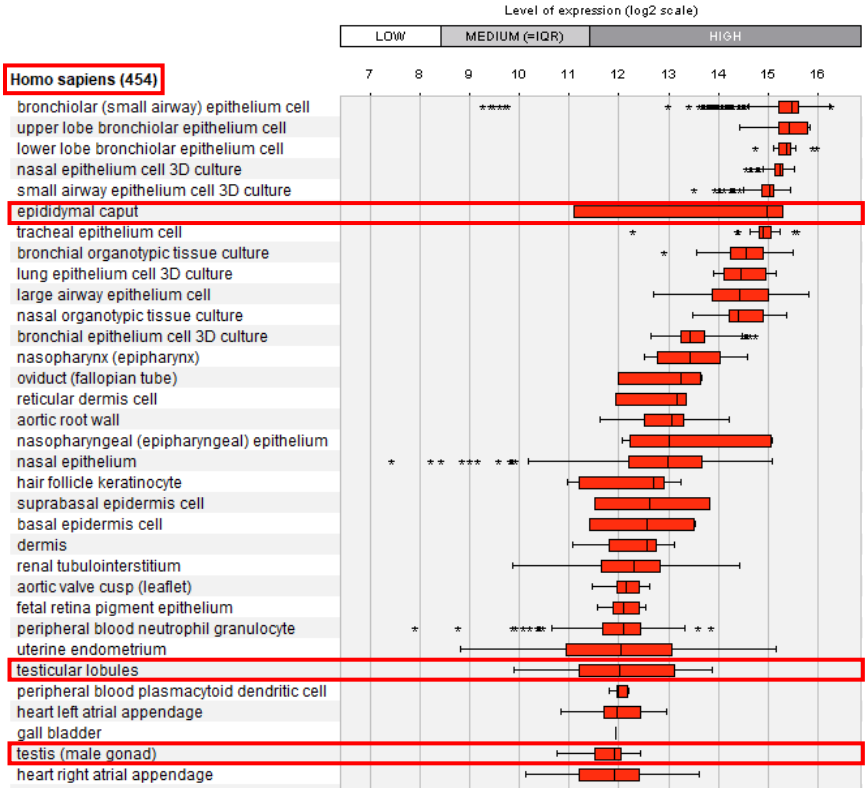

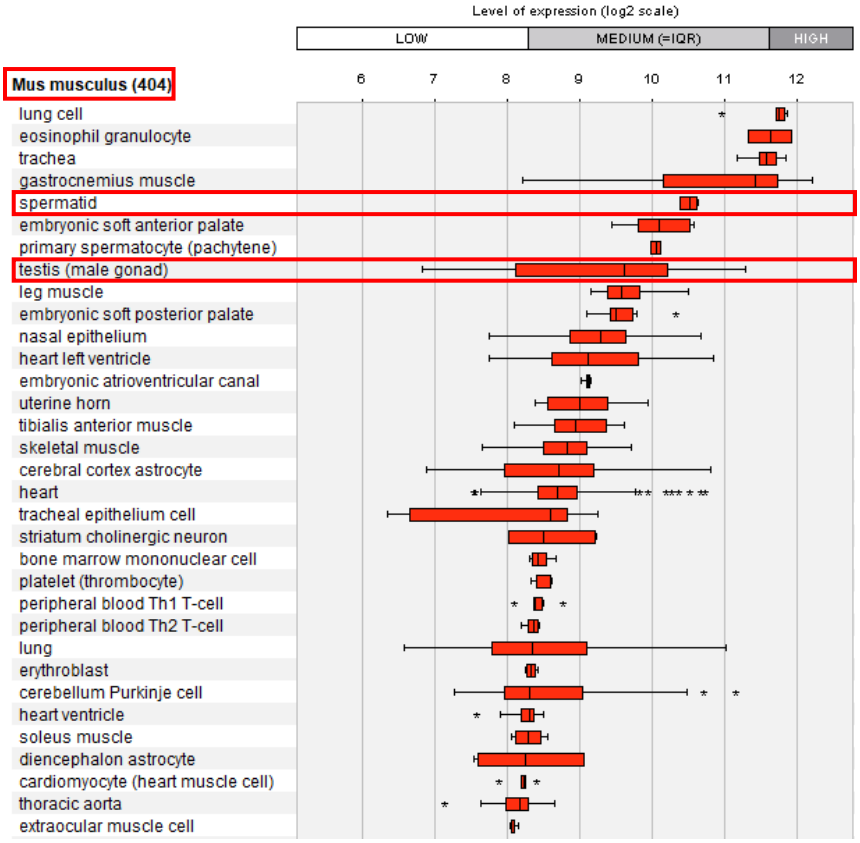

(Previous page) Supplementary figure 1: Relative mRNA expression levels for human and mouse CCDC146 transcripts. (A) CCDC146 mRNA levels measured in different tissues/cells in humans using Affymetrix microarrays (data available from the Genevestigator database, https://genevestigator.com). Red rectangles highlight the high expression level in male reproductive organs. (B) Similar data for mice. Data were generated with Genevestigator (Hruz T, Laule O, Szabo G, Wessendorp F, Bleuler S, Oertle L, Widmayer P, Gruissem W and P Zimmermann (2008) Genevestigator V3: a reference expression database for the meta-analysis of transcriptomes. Advances in Bioinformatics 2008, 420747).

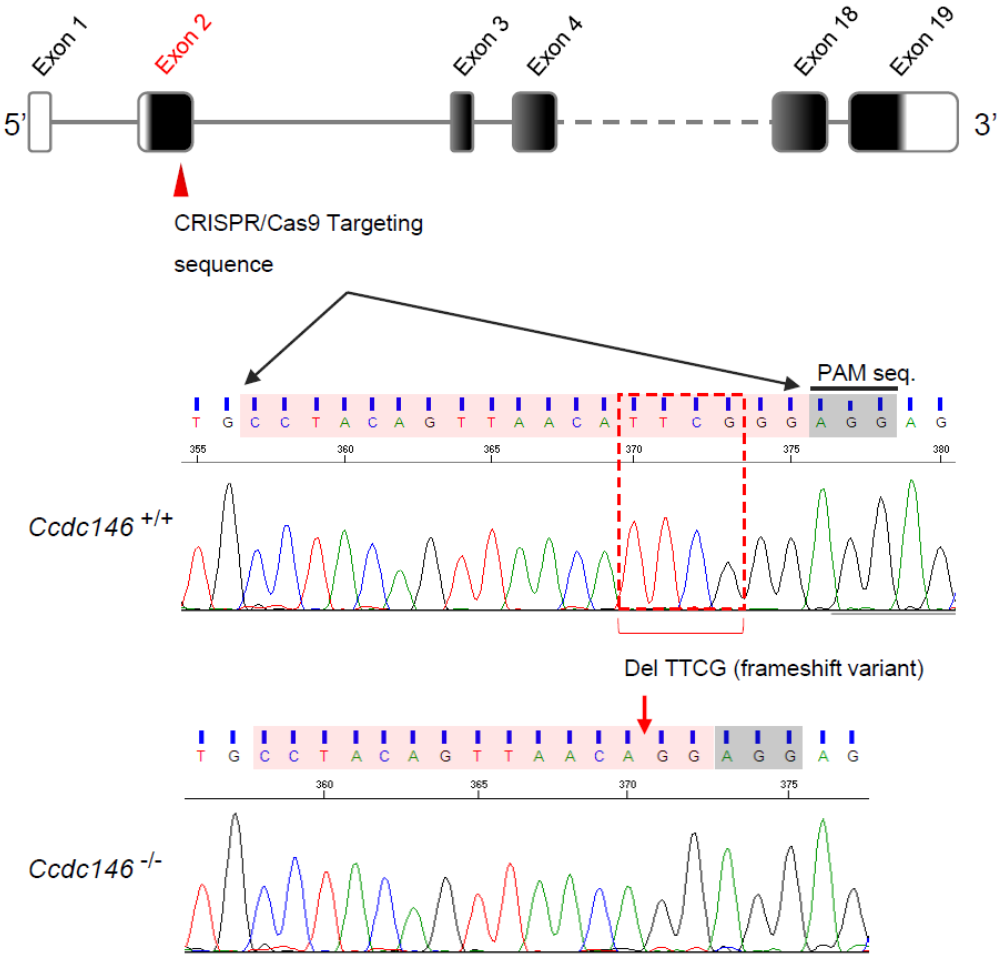

Supplementary figure 2: Molecular strategy used to generate Ccdc146 KO mice by CRISPR/Cas9. The exonic structure of mouse Ccdc146 is shown and the coding sequence indicated in black. Exon 2, the first coding sequence, was targeted by an RNA guide (5'-CCT ACA GTT AAC ATT CGG G-3) and the Cas9 induced a deletion of four nucleotides upstream the PAM sequence, as indicated by the red box. Electropherogram presenting the WT and the homozygote deletion are shown.

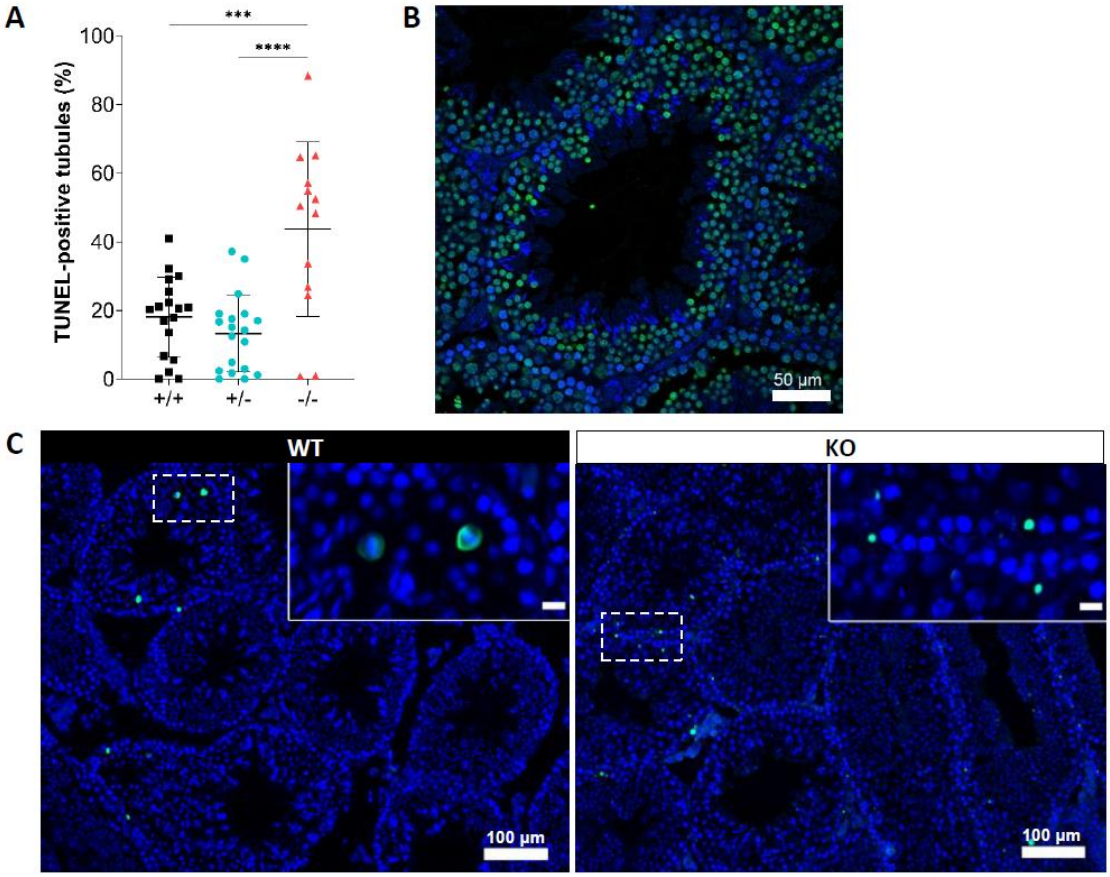

Supplementary figure 3: Increased levels of apoptosis in testes from Ccdc146 KO mice. The TUNEL assay was used to visualize double-strand DNA breaks, as an indication of the level of apoptosis during WT and KO spermatogenesis. (A) Comparison of the % of tubules per testis cross-section containing at least one TUNEL-positive cell in WT, heterozygote, and Ccdc146 KO animals. Number of sections counted per genotype n=13-20, 3 different mice per genotype. (B) The majority of TUNEL-positive cells in the WT corresponded to pachytene cells undergoing meiosis (B, WT zoomed image) whereas the localization of TUNEL-positive cells in KO was more scattered. (C) Control testis section treated with H_20_2. Statistical comparisons according to ordinary one-way ANOVA test (**** $p<0.0001$; *** $p<0.001$, ** $p<0.01$, * $p<0.05$). Scale bar of zoomed images 50 µm.

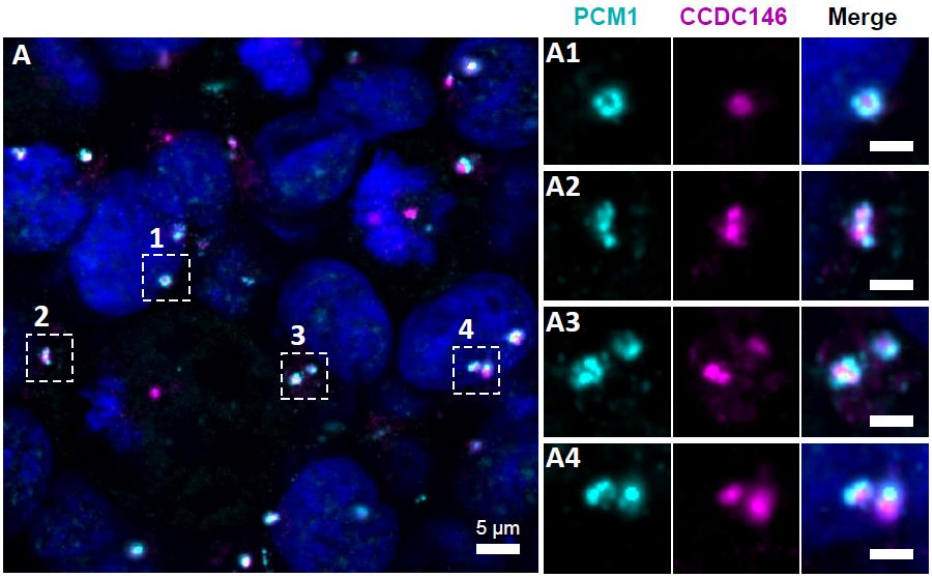

Supplementary figure 4: CCDC146 does not colocalize with the centriolar satellite marker PCM1. (A) HEK-293T cells were double immunolabeled for PCM1 (cyan) and CCDC146 (magenta). (A1-A4) Images on the right show the enlargement of the dotted squares in the left image. PCM1 surrounds the CCDC146 signal, but no colocalization is observed, suggesting that CCDC146 is not a centriolar satellite protein. DNA was stained with Hoechst (blue). Scale bars on zoomed images represent 2 µm.

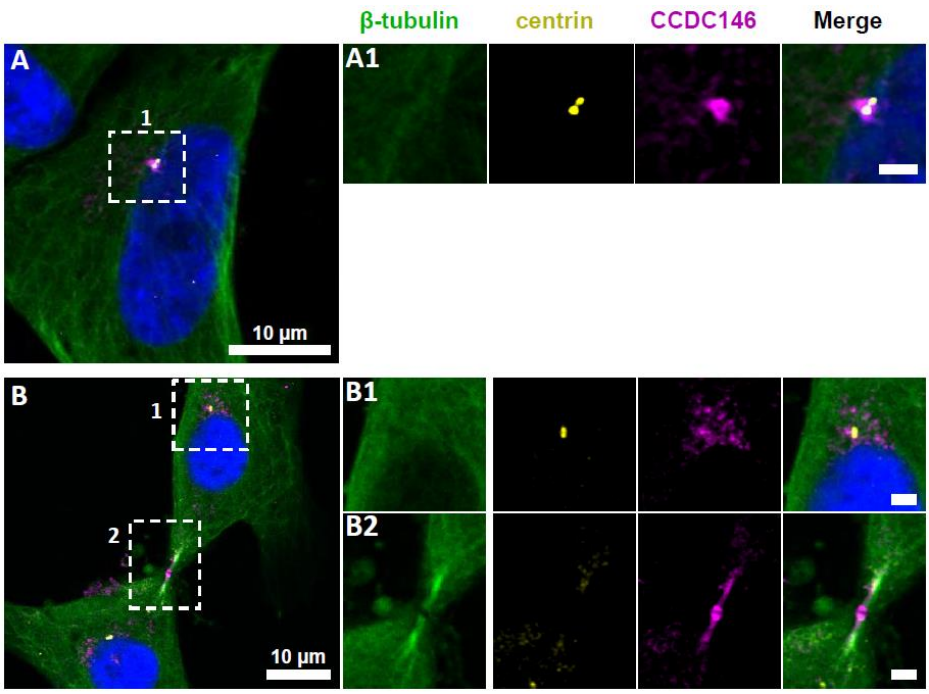

Supplementary figure 5: CCDC146 shows a similar localization to the centrosome and to the midbody in primary HFF cells. (A) Primary human foreskin fibroblast (HFF) cells were triple immunolabeled with anti-β-tubulin (green), anti-centrin (yellow, showing the centrioles) and anti-CCDC146 (magenta). (A1) The right-hand images show the enlargement of the dotted squares in the left-hand image. CCDC146 localized to and around the centrioles. (B) similar staining showing co-labeling of the midbody during cytokinesis by anti-CCDC146 Abs (B2). Scale bar of zoomed images 2 µm.

Ccdc146 : Knock-in Edits

Transcript: ENSMUST00000115245.7 (GRCm38.p6)

Guide RNA design

TACTTTAGAACTGTGAAAAATGG (in red, the start codon in exon 2/19)

HA Tag sequence

Coding sequence (5'-3') : TAC CCA TAC GAT GTT CCA GAT TAC GCT

Amino-acid sequence (N-C ter) : Y P Y D V P D Y A

Strand	Sequence	PAM	On-target score	Off-target score
+	TACTTTAGAACTGTGAAAAA	TGG	27.9	29.0

1) Tag insertion :

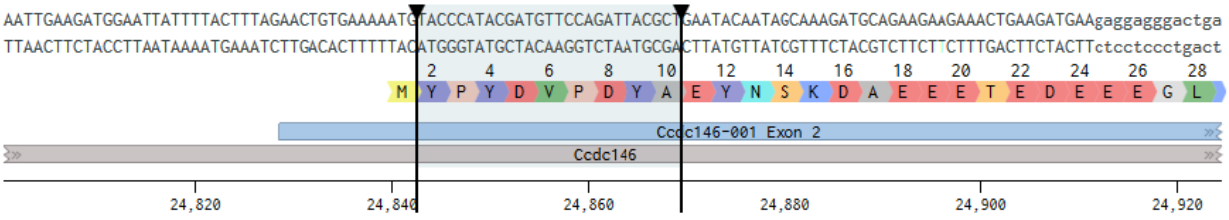

Supplementary figure 6: Molecular strategy used to generate HA-tagged CCDC146 mice by CRISPR/Cas9. The reference CCDC146 mouse transcript is ENSMUST00000115245.7 (GRCm38.p6). Exon 2, the first coding sequence, was targeted by an RNA guide (5'- TAC TTT AGA ACT GTG AAA AAT GG -3'). We used a single-stranded DNA (ssDNA) template to insert the HA sequence (5'-TAC CCA TAC GAT GTT CCA GAT TAC GCT-3') upstream of the PAM sequence.

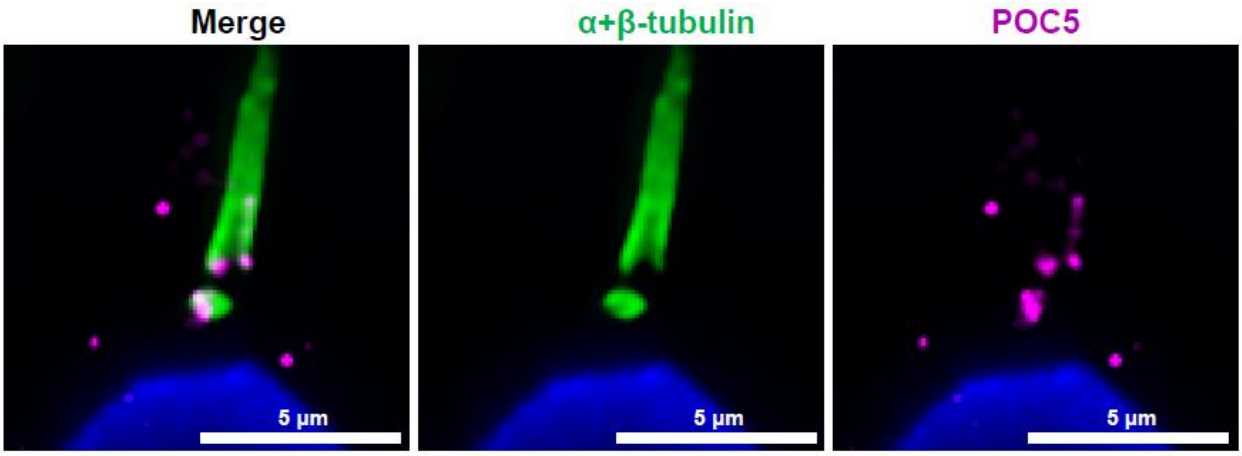

Supplementary figure 7: Centrioles are identified by anti-POC5 Abs in expanded human ejaculated spermatozoa. Human control sperm were co-stained, after expansion, with anti- α+β-tubulin (green) and anti-POC5 (magenta) Abs. The centrosomal protein POC5 locates to centrioles at the base of the axoneme. Scale bars 5 µm.

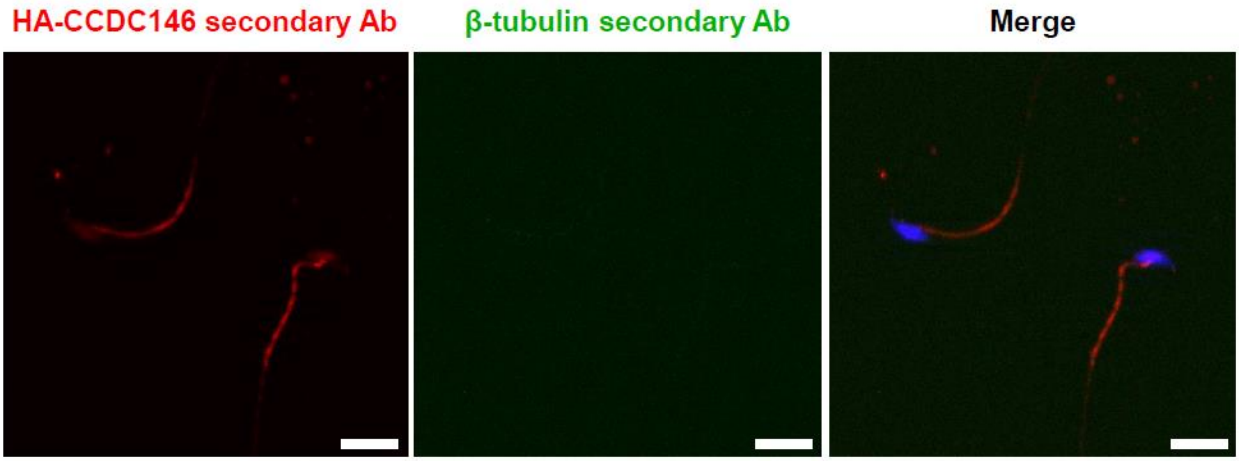

Supplementary figure 8: Non-specific midpiece staining in mouse sperm by rabbit secondary antibody. Mouse sperm were stained with secondary antibodies only. Scale bars 10 µm.

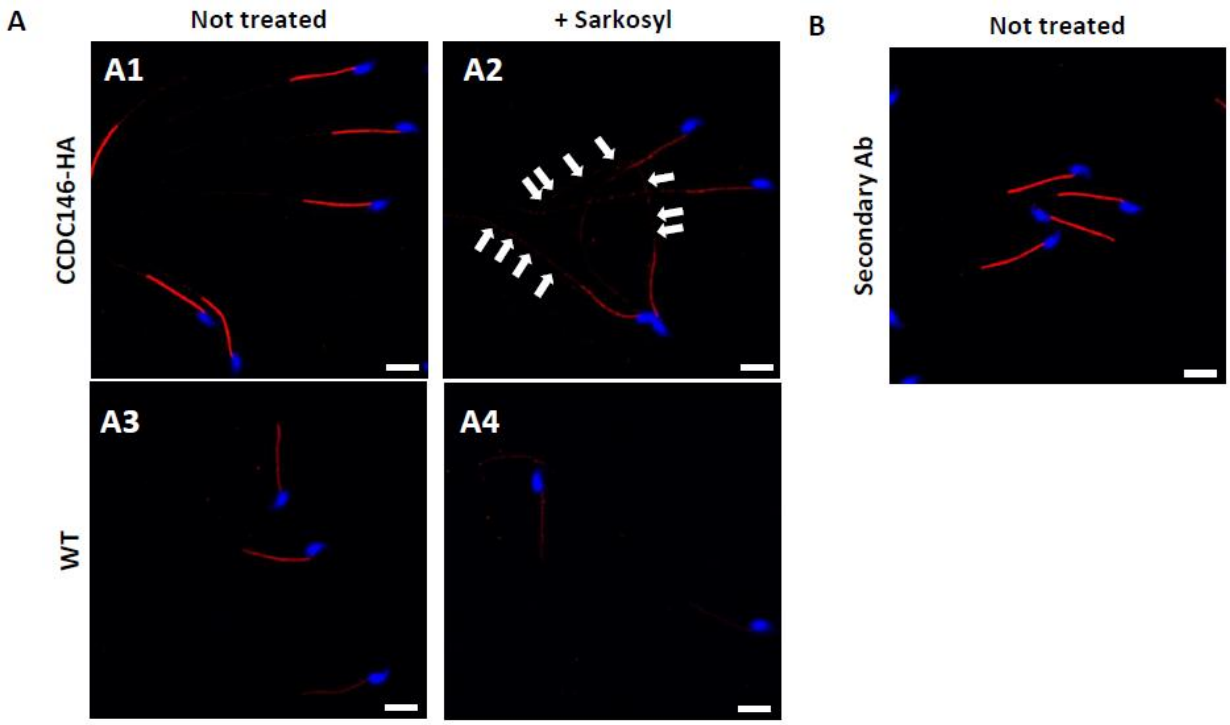

Supplementary figure 9: Sperm sarkosyl treatment corroborates the presence of CCDC146 along the mouse flagellum. CCDC146-HA sperm (A1-A2) and epididymal WT (A3-A4) not treated or treated (5 min, 0.2% sarkosyl), were immunostained with anti-HA Ab (red) and counterstained with Hoechst (blue). (A1) Without treatment, a faint CCDC146-HA signal was observed along the CCDC146-HA principal piece. The strong staining in the midpiece is not specific (see panel B) (A2) After treatment with sarkosyl, the CCDC146-HA signal along the sperm principal piece was enhanced (white arrows), whereas the signal in the midpiece decreased. (A3) WT untreated (NT) sperm exhibited almost no CCDC146-HA signal in the principal piece. The midpiece is however strongly stained (not specific see panel B) (A4) The HA signal is not enhanced in WT principal piece by sarkosyl treatment, suggesting that the enhanced signal observed with sarkosyl on CCDC146-HA sperm is specific. (B) CCDC146-HA sperm were immunolabeled with secondary antibody only. Strong staining is observed on the midpiece, confirming its non-specific nature. Scale bars: 10 μm.

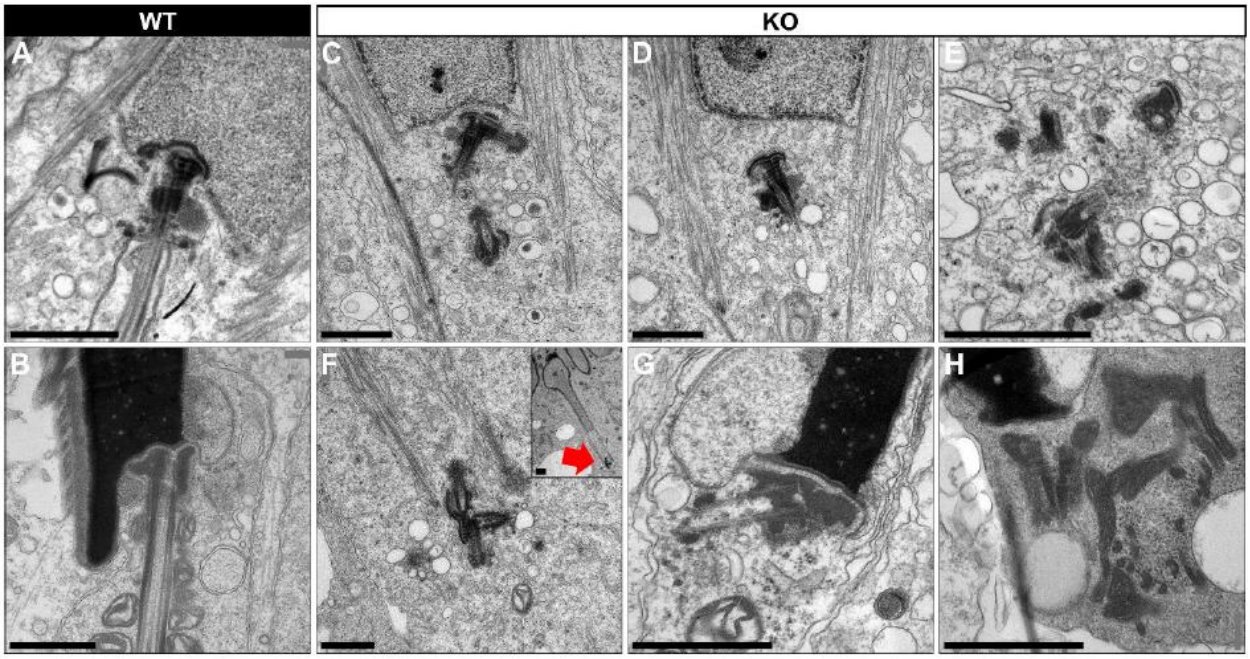

Supplementary figure 10: Lack of CCDC146 causes centriole duplication and mislocalization in Ccdc146 KO spermatids. Ultrastructural analysis of centrioles in adult mouse WT (A, B) and Ccdc146 KO (C-H) testis sections. (A) In WT spermatids, the proximal centriole is linked to the base of the compacting nucleus through the basal plate and the capitulum, and the distal centriole is embedded in the segmented column. These sperm-specific cytoskeletal structures make up the head-to-tail coupling apparatus (HTCA). (B) In WT elongated spermatids, the different components of the axonemal structures (microtubules and ODF) were visible downstream the distal centriole. (C) In Ccdc146 KO elongating spermatids, the overall structure of the HTCA was conserved, with the presence of the centrioles and the accessory cytoskeletal structures. However, the HTCAs were often duplicated (C, E, F) and separated from their usual nuclear attachment site (C-F, H), and sometimes misplaced far away from the nucleus (F), likely preventing axoneme elongation. (F) The arrow indicates the misplaced centrioles at the end of the manchette. (G, H) In elongated spermatids with condensed nucleus, malformed and detached centrioles with poorly assembled or missing flagella compared to the WT (B) can be seen. Scale bars: 1 μm.

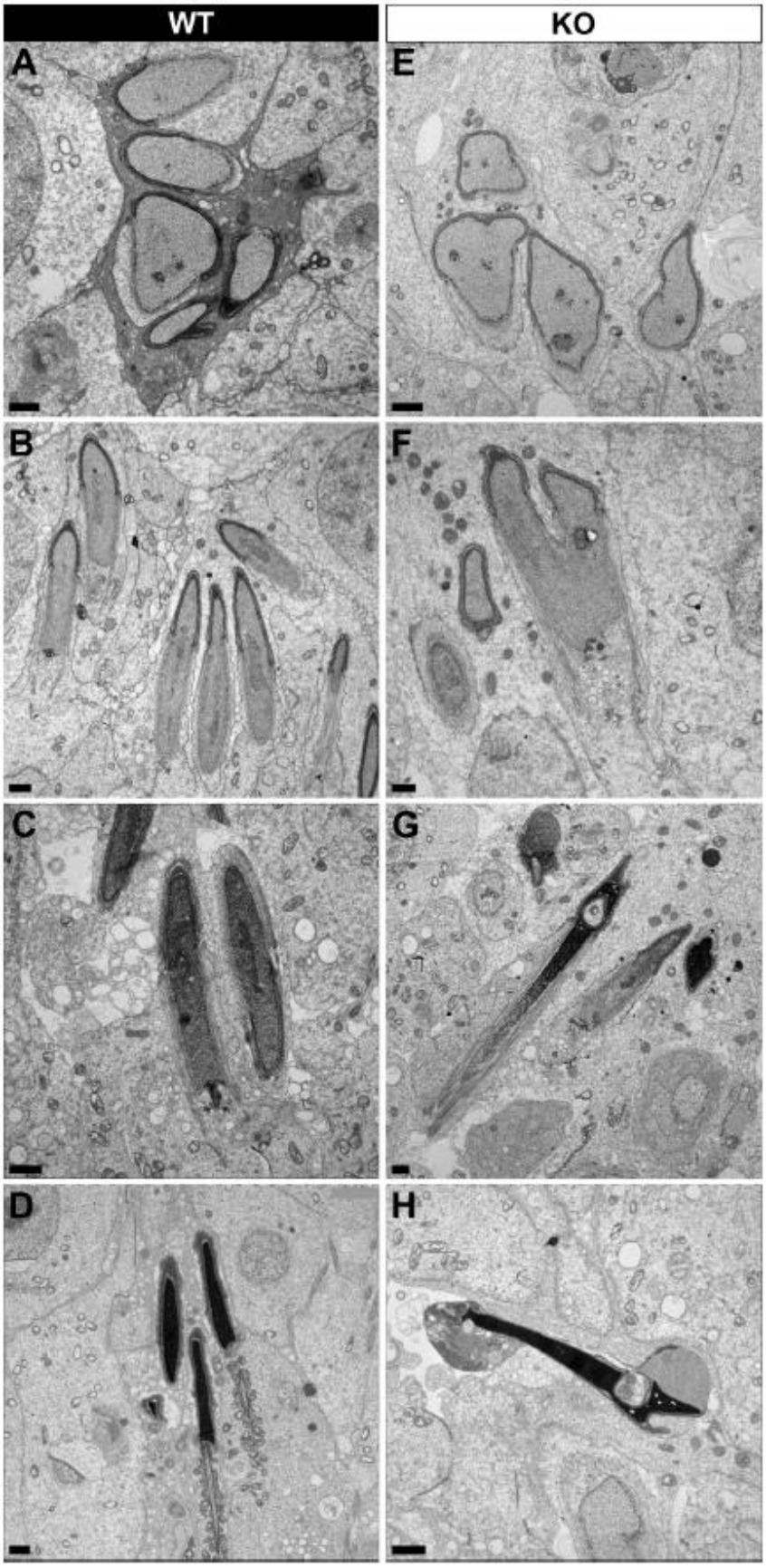
WT
KO
A
E
B
F
C
G
D
H

(Previous page) Supplementary figure 11: Spermatid head shape is aberrant in the absence of CCDC146. Comparative ultrastructural analysis of the spermatid head in WT (A-D) and Ccdc146 KO (E-H) testis sections. (A, E) Spermatid nuclei at the beginning of elongation. KO spermatid nuclei showing nuclear membrane invaginations and irregular shape that were not present in the WT. The acrosome in the KO sperm appeared intact. (B, F) Spermatid nuclei in elongating spermatids. Whereas nucleus elongation is symmetric in the WT, in the CCDC146-KO, more pronounced head invaginations are observed. (C, G) Elongated spermatids. Although nuclear condensation appeared normal in both WT and KO nuclei, vacuolization is observed in KO nucleus. (D, H) Elongated KO spermatids showed malformed elongated nuclear shapes with frequent invaginations and poorly assembled flagella (H) compared to the WT (D). Scale bars: 1 μm.

Material and methods

Human subjects and controls

We analyzed WES data from a cohort of 167 MMAF individuals previously established by our team [9]. All individuals presented with a typical MMAF phenotype characterized by severe asthenozoospermia (total sperm motility below 10%) with at least three of the following flagellar abnormalities present in >5% of the spermatozoa: short, absent, coiled, bent or irregular flagella. All individuals had a normal somatic karyotype (46,XY) with normal bilateral testicular size, normal hormone levels and secondary sexual characteristics. Sperm analyses were carried out in the source laboratories during routine biological examination of the individuals according to World Health Organization (WHO) guidelines [72]. Informed and written consents were obtained from all the individuals participating in the study and institutional approval was given by the local medical ethical committee (CHU Grenoble Alpes institutional review board). Samples were stored in the Fertithèque collection declared to the French Ministry of health (DC-2015-2580) and the French Data Protection Authority (DR-2016-392).

Sanger sequencing

CCDC146 single nucleotide variants identified by exome sequencing were validated by Sanger sequencing as previously described [9]. PCR primers used for each individual are listed in Table supplementary 1.

Cell culture

HEK-293T (Human Embryonic Kidney) and HFF (Human Foreskin Fibroblasts) cells were grown in D10 consisting in DMEM with GlutaMAX (Dulbecco's Modified Eagle's Medium, Sigma Aldrich) supplemented with 10% heat-inactivated fetal bovine serum (FBS, Life Technologies)

and 10% of penicillin-streptomycin (Sigma Aldrich) in a 5% CO_2 humidified atmosphere at 37 °C. HEK-293T cells were divided twice weekly by 1/10 dilution. HFFs cells were divided 1/5 one time a week.

Ethics statement

Breeding and experimental procedures were carried out in accordance with national and international laws relating to laboratory animal welfare and experimentation (EEC Council Directive 2010/63/EU, September 2010). Experiments were performed under the supervision of C.L. (agreement 38 10 38) in the Plateforme de Haute Technologie Animale (PHTA) animal care facility (agreement C3851610006 delivered by the Direction Départementale de la Protection des Populations) and were approved by the ethics committee of the PHTA and by the French government (APAFlS#7128-2016100609382341.v2).

Generation of *Ccdc146* KO and *HA-tagged CCDC146* mice

Ccdc146 KO mice were generated using the CRISPR/Cas9 technology as previously described [52]. Briefly, to maximize the chances of generating deleterious mutations, two gRNAs located in two distinct coding exons located at the beginning of the targeted gene were used. For each gene, the two gRNAs (5'-CCT ACA GTT AAC ATT CGG G-3' and 5'-GGG AGT ACA ATA TTC AGT AC-3'), respectively targeting exons 2 and 4, were inserted into two distinct plasmids, each plasmid also contained the Cas9 sequence (Supp Figure 2). The Cas9 gene was controlled by a CMV promoter and the gRNA and its RNA scaffold by a U6 promoter. Full plasmids (pSpCas9 BB-2A-GFP (PX458)) containing the specific sgRNA were ordered from Genescript (https://www.genscript.com/crispr-synthetic-sgrna.html). Both plasmids were co-injected into the zygotes' pronuclei at a concentration of 2.5 ng/mL. Plasmids were directly injected as delivered by the supplier, without in vitro production and purification of Cas9 proteins and sgRNA.

Ccdc146-HA knock-in mice were also generated by CRISPR/Cas9. Twenty-seven nucleotides encoding the HA (hemagglutinin) tag (5'-TAC CCA TAC GAT GTT CCA GAT TAC GCT TAG-3') were inserted immediately after the start codon of Ccdc146. One plasmid containing one sgRNA (5'-TAC TTT AGA ACT GTG AAA AA-3') and Cas9 was injected (5 ng/µL) with a single-stranded DNA (150 nucleotides, 50 ng/µl) as a template for the homology directed repair (HDR) Appendix figure 6. PCR primers used for genotyping are listed in Table supplementary 1.

Transgenic CCDC146 strains were bred in the Grenoble university animal platform (HTAG) and housed under specific-pathogen-free conditions. Animals were euthanized by cervical dislocation at the indicated ages.

Phenotypic analysis of *Ccdc146* KO mice

Fertility test – Three adult males of each genotype were housed individually with two fertile WT B6D2 females for 12 weeks. The date of birth and the number of pups were recorded.

Sperm analysis – Epididymal sperm were obtained by making small incisions in the mouse caudae epididymides placed in 1 mL of warm M2 medium (Sigma Aldrich), and the sperm were allowed to swim up for 10 min at 37 °C. Sperm samples (10 µL) were used for Computer-assisted semen analysis (CASA, Hamilton Thorn Research, Beverley, MA, USA) using a 100-µm-deep analysis chamber (Leja Products B.V., Nieuw-Vennep, the Netherlands). A minimum of 100 motile sperm was recorded in each assay. The remaining sperm samples were washed in 1X phosphate buffered saline (PBS, Life technologies), 10 µL were spread onto slides pre-coated with 0.1% poly-L-lysine (Epredia), fixed in 70% ethanol (Sigma Aldrich) for 1 h at room temperature (RT) and submitted to a papanicolaou staining (WHO laboratory manual) to assess sperm morphology. Images were obtained using a Zeiss AxioImager M2 fitted with a 40X objective (color camera AxioCam MRc) and analyzed using ZEN (Carl Zeiss, version 3.4).

Testis and epididymides histology

Testis and epididymides samples from 8-16-week-old mice were fixed for 24 h in PBS/4% PFA (Electron Microscopy Sciences), dehydrated in a graded ethanol series, embedded in paraffin wax, sectioned at 5 µm and placed onto Superfrost slides (Fischer scientific). For both, slides were deparaffinated and rehydrated prior to use. Tissue morphology and structure were observed after coloration by Mayer's hematoxylin and eosin phloxine B (WHO protocols) using a Zeiss AxioImager M2 (color camera AxioCam MRc).

Terminal deoxynucleotidyl transferase dUTP nick-end labeling (TUNEL) assay on testes

Testes samples from three adult individuals for each genotype were analyzed. Apoptotic cells in testis sections were identified using the Click-iT™ Plus TUNEL Assay kit (Invitrogen) in line with the manufacturer's instructions. DNA strand breaks for the positive control were induced by DNase

I treatment. Each slide contained up to eight testis sections. DNA was stained with Hoechst (2 µg/mL). Images were acquired and reconstituted using a Zeiss Axioscan Z1 slide scanner and analyzed by Fiji [73]. The total number of seminiferous tubules and the number of tubules containing at least one TUNEL-positive cell were counted in each testis section.

Conventional Immunofluorescence (IF)

Somatic Cells – HEK-293T or HFFs (10 000 cells) were grown on 10-mm coverslips previously coated with poly-D-lysine (0.1 mg/mL, 1 h, 37 °C, Gibco) placed in a well on a 24-well plate. After 24 h, cells were directly fixed with ice-cold methanol (Sigma Aldrich) for 10 min. After washing twice in PBS, non-specific sites were blocked with PBS/5% FBS/5% NGS (normal goat serum, Life technologies) for 1 h at RT. After washing three times in PBS/1% FBS, primary antibody was added in PBS/1% FBS and incubated overnight at 4 °C. Coverslips were washed three times in PBS/1% FBS before adding secondary antibody in PBS/1% FBS and incubating for 2 h at RT. After washing three times in PBS, nuclei were stained with 2 µg/mL Hoechst 33342 in PBS (Sigma Aldrich). Coverslips were once again washed three times in PBS, then carefully placed on Superfrost slides (cells facing the slide) and sealed with nail polish.

Spermatogenic cells – Seminiferous tubules were isolated from mouse testes (8–16 weeks old). After removing of the tunica albuginea, the testes were incubated at 37 °C for 1 h in 3 mL of a solution containing (mM): NaCl (150), KCl (5), CaCl2 (2), MgCl2 (1), NaH2PO4 (1), $NaHCO_3$ (12), D-glucose (11), Na-lactate (6), HEPES (10) pH 7.4, and collagenase type IA (1 mg/mL – Sigma Aldrich). Tubules were rinsed twice in collagenase-free medium and cut into 2-mm sections. Spermatogenic cells were obtained by manual trituration and filtered through a 100-µm filter. The isolated cells were centrifuged (10 min, 500 g), resuspended in 500 µL PBS and 50 µL was spread onto slides pre-coated with 0.1% poly-L-lysine (Epredia) and allowed to dry. Dried samples were fixed for 5 min in PBS/4% PFA. After washing twice in PBS, slides were placed in PBS/0.1% Triton/5% BSA (Euromedex) for 90 min at RT. Following two washes in PBS, the primary antibody was added in PBS/1% BSA overnight at 4 °C. After washing three times in PBS/1% BSA, secondary antibody was added in PBS/1% BSA for 2 h at RT. After washing three times in PBS, nuclei were stained with 2 µg/mL Hoechst 33342 in PBS (Sigma Aldrich) and slides were mounted with DAKO mounting media (Agilent).

Testis sections – After deparaffination and rehydration, testis sections were subjected to heat antigen retrieval for 20 min at 95 °C in a citrate-based solution at pH 6.0 (VectorLabs). Tissues were then permeabilized in PBS/0.1% Triton X-100 for 20 min at RT. After washing three times in PBS (5 min each), slides were incubated with blocking solution (PBS/10% BSA) for 30 min at RT. Following three washes in PBS, slides were incubated with primary antibodies in PBS/0.1% Tween/5% BSA overnight at 4 °C. Slides were washed three times in PBS before applying secondary antibodies in blocking solution and incubating for 2 h at RT. After washing in PBS, nuclei were stained with 2 µg/mL Hoechst 33342 in PBS (Sigma Aldrich) for 5 min at RT. Slides were washed once again in PBS before mounting with DAKO mounting media (Agilent).

Spermatozoa (conventional protocol) - Mouse spermatozoa were recovered from the caudae epididymides. After their incision, sperm were allowed to swim in 1 mL of PBS for 10 min at 37 °C. They were washed twice with 1 mL of PBS 1X at 500 g for 5 min, and 10 µL of each sample was smeared onto slides pre-coated with 0.1% poly-L-lysine (Epredia). Sperm were fixed in PBS/4% PFA for 45 s, washed twice in PBS and permeabilized in PBS/0.1% Triton for 15 min at RT. After incubation in PBS/0.1% Triton/2% NGS for 2 h at RT, primary antibody was added in PBS/0.1% Triton/2% NGS overnight at 4 °C. After washing three times in PBS/0.1% Triton, the secondary antibody was applied in PBS/0.1% Triton/2% NGS for 90 min at RT. Slides were washed three times in PBS before staining nuclei with 2 µg/mL Hoechst 33342 in PBS (Sigma Aldrich). Slides were washed once in PBS before mounting with DAKO mounting media (Agilent).

For human spermatozoa, the protocol was based on that of Fishman *et al.* [32]. Straws were thawed at RT for 10 min and resuspended in PBS. Sperm were washed twice in 1 mL of PBS (10 min, 400 g), 50 µL was spread onto slides pre-coated with 0.1% poly-L-lysine and left to dry. Dry slides were fixed in 100% ice-cold methanol for 2 min and washed twice in PBS. Cells were permeabilized in PBS/3% Triton X-100 (PBS-Tx) for 1 h at RT. Slides were then placed in PBS-Tx/1% BSA (PBS-Tx-B) for 30 min at RT. Immunofluorescence was performed as for mouse spermatozoa. Sperm were then incubated with primary antibodies in PBS-Tx-B overnight at 4 °C. After washing three times in PBS-Tx-B for 5 min each, slides were incubated with secondary antibodies for 1 h at RT in PBS-Tx-B. After washing three times in PBS, nuclei were stained with

2 µg/mL Hoechst 33342 in PBS (Sigma Aldrich) and slides were mounted with DAKO mounting media (Agilent).

Spermatozoa (sarkosyl protocol) - Mouse sperm from caudae epididymides or human sperm from 250-µL straws were collected in 1 mL PBS 1X, washed by centrifugation for 5 min at 500 g and then resuspended in 1 mL PBS 1X. Sperm cells were spread onto slides pre-coated with 0.1% poly-L-lysine (Epredia), treated or not for 5 min with 0.2% sarkosyl (Sigma) in Tris-HCl 1 mM, pH7.5 at RT and then fixed in PBS/4% PFA for 45 s at RT. After washing twice for 5 min with PBS, sperm were permeabilized with PBS/0.1% Triton X-100 (Sigma Aldrich) for 15 min at RT and unspecific sites were blocked with PBS/0.1% Triton X-100/2% NGS for 30 min at RT. Then, sperm were incubated overnight at 4 °C with primary antibodies diluted in PBS/0.1% Triton X-100/2% NGS. Slides were washed three times with PBS/0.1% Triton X-100 before incubating with secondary antibody diluted in PBS/0.1% Triton X-100/2% NGS for 90 min at RT. Finally, sperm were washed three times in PBS/0.1% Triton X-100, adding 2 µg/mL Hoechst 33342 (Sigma Aldrich) during the last wash to counterstain nuclei. Slides were mounted with DAKO mounting media (Agilent). Confocal microscopy was performed on a Zeiss LSM 710 or NIKON eclipse A1R/Ti2 using a 63x oil objective.

Image acquisition – For all immunofluorescence experiments, images were acquired using a 63X oil objective on a multimodal confocal Zeiss LSM 710 or Zeiss AxioObserver Z1 equipped with ApoTome and AxioCam MRm. Images were processed using Fiji [73] and Zeiss ZEN (Carl Zeiss, version 3.4). Figures for cultured cells were arranged using QuickFigures [74].

Expansion microscopy (U-ExM)

Coverslips used for either sample loading (12 mm) or image acquisition (24 mm) were first washed with absolute ethanol and dried. They were then coated with poly-D-lysine (0.1 mg/mL) for 1 h at 37 °C and washed three times with ddH2O before use. Sperm from cauda epididymides or human sperm from straws were washed twice in PBS. $1x10^6$ sperm cells were spun onto 12-mm coverslips for 3 min at 300 g. Crosslinking was performed in 1 mL of PBS/1.4% formaldehyde/2% acrylamide (ThermoFisher) for 5 h at 37 °C in a wet incubator. Cells were embedded in a gel by placing a 35-µL drop of a monomer solution consisting of PBS/19% sodium acrylate/10% acrylamide/0.1% N,N'-methylenbisacrylamide/0.2% TEMED/0.2% APS (ThermoFisher) on parafilm and carefully placing coverslips on the drop, with sperm facing the gelling solution.

Gelation proceeded in two steps: 5 min on ice followed by 1 h at 37 °C. Coverslips with attached gels were transferred into a 6-well plate for incubation in 5 mL of denaturation buffer (200 mM SDS, 200 mM NaCl, 50 mM Tris in ddH2O, pH 9) for 20 min at RT until gels detached. Then, gels were transferred to a 1.5-mL microtube filled with fresh denaturation buffer and incubated for 90 min at 95 °C. Gels were carefully removed with tweezers and placed in beakers filled with 10 mL ddH2O to cause expansion. The water was exchanged at least twice every 30 min. Finally, gels were incubated in 10 mL of ddH2O overnight at RT. The following day, a 5-mm piece of gel was cut out with a punch. To remove excess water, gels were placed in 10 mL PBS for 15 min, the buffer was changed, and incubation repeated once. Subsequently, gels were transferred to a 24-well plate and incubated with 300 µL of primary antibody diluted in PBS/2% BSA at 37 °C for 3 h with vigorous shaking. After three washes for 10 min in PBS/0.1% Tween 20 (PBS-T) under agitation, gels were incubated with 300 µL of secondary antibody in PBS/2% BSA at 37 °C for 3 h with vigorous shaking. Finally, gels were washed three times in PBS-T for 10 min with agitation. Hoechst 33342 (2 µg/mL) was added during the last wash. The expansion resolution was between 4X and 4.2X depending on sodium acrylate purity. For image acquisition, gels were placed in beakers filled with 10 mL ddH2O. Water was exchanged at least twice every 30 min, and then expanded gels were mounted on 24-mm round poly-D-lysine-coated coverslips, placed in a 36-mm metallic chamber for imaging. Confocal microscopy was performed using either a Zeiss LSM 710 using a 63x oil objective or widefield was performed using a Leica THUNDER widefield fluorescence microscope, using a 63x oil objective and small volume computational clearing. (Guichard / Hamel lab, Geneva).

Ccdc146 **expression**

Testis from CCDC146-HA pups were collected at days 9, 18, 26 and 35 after birth and directly cryopreserved at -80 °C before RNA extraction. RNA was extracted as follow. Frozen testes were placed in RLT buffer (Qiagen)/1% β-mercaptoethanol (Sigma), cut in small pieces and lysis performed for 30 min at RT. After addition of 10 volumes of TRIzol (5 min, RT, ThermoFisher) and 1 volume of chloroform (2 min, RT, Sigma Aldrich), the aqueous phase was recovered after centrifugation at 12 000 g, 15 min, 4 °C. RNA was precipitated by the addition of one volume of isopropanol (Sigma) and of glycogen (20 mg/mL, ThermoFisher) as a carrier, tube was placed overnight at -20 °C. The day after, after centrifugation (15 min, 12 000 g, 4 °C), RNA pellet was

washed with ethanol 80%, air-dried and resuspended in 30 □l of ultrapure RNAse free water (Gibco). RNA concentrations were determined by using the Qubit RNA assay kit (ThermoFisher). 800 ng of total RNA were used to perform the RT step using the iScript cDNA synthesis kit (Bio-Rad) in a total volume of 20 mL. Gene expression was assessed by qPCR (1 mL of undiluted cDNA in a final volume of 20 mL with the appropriate amount of primers, see table 1) using the SsoAdvanced Universal SYBR Green Supermix (Bio-Rad). The qPCR program used was 94 °C 15 min, (94 °C 30 s, 58 °C 30 s, 72 °C 30 s) x40 followed by a melt curve analysis (58 °C 0.05 s, 58–95 °C 0.5-°C increment 2–5 s/step). Gene expression was calculated using the $2^{-\Delta\Delta CT}$ method. Results are expressed relative to *Ccdc146* expression on day 9.

	Forward primer		Reverse primer	
Genes	Sequence	Concentration (nM)	Sequence	Concentration (nM)
Ccdc146	5'-TGCTGCATGACGCCGTGATG-3'	750	5'-GGAGACCTCCGTGGAGAATGCTTC-3'	500
Hprt	5'-CCTAATCATTATGCCGAGGATTTGG-3'	500	5'-TCCCATCTCCTTCATGACATCTCG-3'	250
Actb	5'-CTTCTTTGCAGCTCCTTCGTTGC-3'	250	5'-AGCCGTTGTCGACGACCAGC-3'	250

CCDC146 detection by WB

Protein extraction from the testis – Testis from pups were recovered at days 9, 18, 26 and 35 after birth. After removing the albuginea, they were homogenized in 2X Laemmli buffer (Bio-Rad) using a Dounce homogenizer, and heated at 95 °C for 10 min. The supernatant was recovered after centrifugation (15 000 g, 10 min, 4 °C), 5% b mercapto-ethanol was added (Sigma), and tubes were once again incubated at 95 °C for 10 min. After cooling, the supernatant was stored at -20 °C until use.

Protein extraction from sperm head and sperm flagella – Spermatozoa from a CCDC146-HA male (9 weeks old) were isolated from both epididymis in 1 mL PBS and washed twice with PBS by centrifugation at RT (5 min, 500 g). Half of the sperm were incubated with 1X protease inhibitor cocktail (mini Complete EDTA-free tablet, Roche Diagnostic), incubated for 15 min on ice and

sonicated. Separated flagella were isolated by centrifugation (600 g, 20 min, 4 °C) in a Percoll gradient. Percoll concentrations used were 100%, 80%, 60%, 34%, 26%, 23%, and sperm flagella were isolated from the 60% fraction. Samples were washed with PBS by centrifugation (500 g, 10 min, 4 °C). Whole sperm or sperm flagella were incubated in 2X Laemmli buffer (Bio-Rad), heated at 95 °C for 10 min and centrifuged (15 000 g, 10 min, 4 °C). The supernatants were incubated with 5% β-mercaptoethanol, boiled (95 °C, 10 min), cooled down and placed at -20 °C until use.

Proteins extraction from total sperm – CCDC146-HA sperm were recovered from caudae epididymides in 1 mL PBS and washed twice in 1 mL PBS by centrifugation 500 g, 5 min. Lysis was then performed for 2 h at 4 °C on wheel in either Chaps buffer (10 mM Chaps / 10 mM HEPES / 137 mM NaCl / 10% Glycerol), in RIPA Buffer (Pierce IP Lysis buffer, ThermoFisher), in Tris 10 mM / HCl 1 M buffer or in Tris 10 mM / HCl 1 M / 0.2 to 0.8% sarkosyl buffer. After centrifugation 15 000 g, 4 °C, 15 min, the supernatants were recovered and 5% of β-mercaptoethanol added. After boiling (95 °C, 10 min), the samples were cooled down and placed at -20 °C until use.

Western blot – Protein lysates were fractionated on 5-12% SDS-PAGE precast gels (Bio-Rad) and transferred onto Trans-Blot Turbo Mini 0.2 µm PVDF membranes using the Trans-Blot Turbo Transfer System (Bio-Rad) and the appropriate program. Membranes were then blocked in PBS/5% milk/0.1% Tween 20 (PBS-T) for 2 h at RT before incubating with the primary antibody in PBS-T overnight at 4 °C with agitation. Membranes were then washed three times for 5 min in PBS-T and incubated with the secondary HRP-antibody in PBS-T for 1 h at RT. After three washes (PBS-T, 10 min), the membrane was revealed by chemiluminescence using the Clarity ECL substrate (Bio-Rad) and images were acquired on a Chemidoc apparatus (Bio-Rad).

Transmission electron microscopy

Transmission electron microscopy was performed by Dr. Stefan Geimer at the University of Bayreuth as follows. Testis from adult mice were fixed in PBS/4% paraformaldehyde (PFA). They were then decapsulated from the tunica albuginea and the seminiferous tubules were divided into three to four pieces using a razor blade (Gillette Super Sliver). The seminiferous tubules were incubated for 60 min at RT in fixation buffer (100 mM HEPES pH7.4, 4 mM CaCl2, 2.5% glutaraldehyde, 2% PFA, all from Sigma Aldrich) and then the buffer was exchanged with fresh

fixation buffer and the samples left overnight fixed at 4 °C. After washing three times for 10 min in 100 mM HEPES pH 7.4, 4 mM CaCl2, samples were post-fixed in 1% osmium tetroxide (Carl Roth, Karlsruhe, DE) in distilled water for 120 min at 4 °C. After three additional 10-min washes in distilled water, the tissue pieces were embedded in 1.5% DifcoTM Agar noble (Becton, Dickinson and Company, Sparks, MD, US) and dehydrated using increasing concentrations of ethanol. The samples were then embedded in glycidyl ether 100 (formerly Epon 812; Serva, Heidelberg, Germany) using propylene oxide as an intermediate solvent according to the standard procedure. Ultrathin sections (60-80 nm) were cut with a diamond knife (type ultra 35°; Diatome, Biel, CH) on the EM UC6 ultramicrotome (Leica Microsystems, Wetzlar, Germany) and mounted on single-slot pioloform-coated copper grids (Plano, Wetzlar, Germany). Finally, sections were stained with uranyl acetate and lead citrate [75]. To obtain different section planes within a sample, serial sections (60-80 nm) were made using the same method. The sectioned and contrasted samples were analyzed under a JEM-2100 transmission electron microscope (JEOL, Tokyo, JP) at an acceleration voltage of 80 kV. Images were acquired using a 4080 x 4080 charge-coupled device camera (UltraScan 4000 - Gatan, Pleasanton, CA, US) and Gatan Digital Micrograph software. The brightness and contrast of images were adjusted using the ImageJ program.

Scanning electron microscopy

The two epididymides of mature males were recovered in 1 mL of 0.1 M sodium cacodylate buffer (pH 7.4, Electron Microscopy Sciences) and the sperm were allowed to swim for 15 min at 37 °C. After centrifugation for 10 min, 400 g, RT, the supernatant was discarded and the pellet resuspended in primary fixating buffer (2% glutaraldehyde/0.1 M sodium cacodylate buffer, pH 7.4, Electron Microscopy Sciences) for 30 min at 4 °C. After washing three times in 0.1 M sodium cacodylate buffer (400 g, 10 min), the pellet was submitted to post fixation using 1% Osmium tetroxide 2% (OsO4, Electron Microscopy Sciences) in 0.1 M sodium cacodylate buffer for 30 min at 4 °C. Fixed cells were washed three times in 0.1 M sodium cacodylate buffer (400 g, 5 min), the sample was then placed on a coverslip and treated with Alcian blue 1% (Electron Microscopy Sciences) to improve attachment. The sample was then dehydrated in graded ethanol series: 50%, 70%, 80%, 90%, 96% and 100% (10 min, once each). Final dehydration was performed for 10 min in a v/v solution of 100% ethanol/100% Hexamethyldisilazane (HMDS) followed by 10 min in 100% HMDS. Samples were left to dry overnight before performing metallization. Samples were

analyzed using a Zeiss Ultra 55 microscope at the C.M.T.C. – Consortium des Moyens Technologiques Communs (Material characterization platform), Grenoble INP.

Statistical analysis

The statistics related to the reproductive phenotypes were automatically calculated by GraphPad Prism 8 and 9. Statistical differences were assessed by applying an unpaired t test and one-way ANOVA. Histograms show mean ± standard deviation, and p-values were considered significant when inferior to 0.05.

Antibodies

Primary antibodies				
Target	**Host species**	**Reference**		**Dilution**
CCDC146	Rabbit	Atlas Antibodies	HPA020082	IF: 1/200 U-ExM: 1/200
Centrin, 20H5	Mouse	Merck	04-1624	IF: 1/200
γ-tubulin	Mouse	Santa Cruz Biotechnology	sc-17787	IF: 1/500
β-tubulin	Guinea pig	Geneva Antibody Facility	AA344-GP	IF: 1/500
β-tubulin	Rabbit	Cell Signaling Technology	2128	IF: 1/100
PCM1 (G-6)	Mouse	Santa Cruz Biotechnology	sc-398365	IF: 1/200
α-tubulin	Mouse	Geneva Antibody Facility	AA-345	U-ExM: 1/250
β-tubulin *			AA-344	IF: 1/500
POC5	Rabbit	Bethyl	A303-341A	IF: 1/250 U-ExM: 1/200
High Affinity (HA)	Rat	Roche	11867423001	IF: 1/400 U-ExM: 1/400 WB: 1/2500
High Affinity (HA)	Rabbit	Cell Signaling Technology	3724	U-ExM: 1/100
High Affinity (HA)	Rabbit	Sigma Aldrich	H6908	U-ExM: 1/200
Dpy19L2	Rabbit	**		IF: 1/100

Target	**Fluorophore**	**Reference**		**Dilution**
Goat anti-Rabbit	Alexa Fluor 488	Jackson ImmunoResearch	111-545-144	IF: 1/800 U-ExM: 1/250
Goat anti-Mouse	DyLight 549	Jackson ImmunoResearch	115-505-062	IF: 1/400
Goat anti-Guinea Pig	Alexa Fluor 647	Invitrogen	A-21450	IF: 1/800
Goat anti-Rabbit	Alexa Fluor 568	Life Technologies	A11036	U-ExM: 1/250

Goat anti-Mouse	Alexa Fluor 488	Life Technologies	A11029	U-ExM: 1/250
Goat anti-Rat	Alexa Fluor 549	Jackson ImmunoResearch	112-505-175	IF: 1/800
Goat Anti-Rat	HRP conjugate	Merck	AP136P	1/10 000

*α-tubulin and β-tubulin were used together and noted as α+β-tubulin

**Dpy19l2 antibodies are polyclonal antibodies produced in rabbit that were raised against RSKLREGSSDRPQSSC and CTGQARRRWSAATMEP peptides corresponding to amino acids 6-21 and 21-36 of the N-terminus of mouse Dpy19l2, as described in [76].

Acknowledgments

This work was supported by INSERM, CNRS, Université Grenoble Alpes, the French Agence Nationale pour la Recherche (ANR) grants ‘‘MAS-Flagella’’ (ANR-19-CE17-0014), and “FLAGELOME” (ANR-19-CE17-0014) to P.F.R., the Direction Générale de l’Offre de Soin (DGHOS) for the program PRTS 2014 to P.F.R., the Fondation Maladies Rares (FMR)- grant ‘‘Whole genome sequencing of subjects with Flagellar Growth Defects (FGD)’’ financed by for the program Séquençage à haut débit 2012 to P.F.R.and the European Research Council (ERC) ACCENT Starting Grant 715289 to P.G.

References

1. Boivin, J., et al., *International estimates of infertility prevalence and treatment-seeking: potential need and demand for infertility medical care.* Hum.Reprod., 2007. **22**(6): p. 1506-1512.
2. Uhlén, M., et al., *Transcriptomics resources of human tissues and organs.* Mol Syst Biol, 2016. **12**(4): p. 862.
3. Houston, B.J., et al., *A systematic review of the validated monogenic causes of human male infertility: 2020 update and a discussion of emerging gene-disease relationships.* Hum Reprod Update, 2021. **28**(1): p. 15-29.
4. Beurois, J., et al., *Genetics of teratozoospermia: Back to the head.* Best Pract Res Clin Endocrinol Metab, 2020. **34**(6): p. 101473.
5. Touré, A., et al., *The genetic architecture of morphological abnormalities of the sperm tail.* Hum Genet, 2021. **140**(1): p. 21-42.
6. Wang, J., et al., *Clinical detection, diagnosis and treatment of morphological abnormalities of sperm flagella: A review of literature.* Front Genet, 2022. **13**: p. 1034951.
7. Sironen, A., et al., *Sperm defects in primary ciliary dyskinesia and related causes of male infertility.* Cell Mol Life Sci, 2020. **77**(11): p. 2029-2048.
8. Lores, P., et al., *Homozygous missense mutation L673P in adenylate kinase 7 (AK7) leads to primary male infertility and multiple morphological anomalies of the flagella but not to primary ciliary dyskinesia.* Hum Mol Genet, 2018.
9. Coutton, C., et al., *Bi-allelic Mutations in ARMC2 Lead to Severe Astheno-Teratozoospermia Due to Sperm Flagellum Malformations in Humans and Mice.* Am J Hum Genet, 2019. **104**(2): p. 331-340.
10. Shen, Q., et al., *Bi-allelic truncating variants in CFAP206 cause male infertility in human and mouse.* Hum Genet, 2021. **140**(9): p. 1367-1377.
11. Cong, J., et al., *Homozygous mutations in CCDC34 cause male infertility with oligoasthenoteratozoospermia in humans and mice.* J Med Genet, 2022. **59**(7): p. 710-718.
12. Kherraf, Z.E., et al., *A Homozygous Ancestral SVA-Insertion-Mediated Deletion in WDR66 Induces Multiple Morphological Abnormalities of the Sperm Flagellum and Male Infertility.* Am J Hum Genet, 2018. **103**(3): p. 400-412.
13. Coutton, C., et al., *Mutations in CFAP43 and CFAP44 cause male infertility and flagellum defects in Trypanosoma and human.* Nat Commun, 2018. **9**(1): p. 686.
14. Liu, C., et al., *Deleterious variants in X-linked CFAP47 induce asthenoteratozoospermia and primary male infertility.* Am J Hum Genet, 2021. **108**(2): p. 309-323.
15. Liu, S., et al., *CFAP61 is required for sperm flagellum formation and male fertility in human and mouse.* Development, 2021. **148**(23).
16. Li, W., et al., *Biallelic mutations in CFAP65 cause male infertility with multiple morphological abnormalities of the sperm flagella in humans and mice.* J Med Genet, 2020. **57**(2): p. 89-95.
17. Dong, F.N., et al., *Absence of CFAP69 Causes Male Infertility due to Multiple Morphological Abnormalities of the Flagella in Human and Mouse.* Am J Hum Genet, 2018. **102**(4): p. 636-648.
18. Beurois, J., et al., *CFAP70 mutations lead to male infertility due to severe astheno-teratozoospermia. A case report.* Hum Reprod, 2019. **34**(10): p. 2071-2079.

19. Martinez, G., et al., *Biallelic variants in MAATS1 encoding CFAP91, a calmodulin-associated and spoke-associated complex protein, cause severe astheno-teratozoospermia and male infertility.* J Med Genet, 2020. **57**(10): p. 708-716.
20. Ben Khelifa, M., et al., *Mutations in DNAH1, which encodes an inner arm heavy chain dynein, lead to male infertility from multiple morphological abnormalities of the sperm flagella.* American Journal of Human Genetics, 2014. **94**(1): p. 95-104.
21. Liu, C., et al., *Bi-allelic DNAH8 Variants Lead to Multiple Morphological Abnormalities of the Sperm Flagella and Primary Male Infertility.* Am J Hum Genet, 2020. **107**(2): p. 330-341.
22. Martinez, G., et al., *Whole-exome sequencing identifies mutations in FSIP2 as a recurrent cause of multiple morphological abnormalities of the sperm flagella.* Hum Reprod, 2018. **33**(10): p. 1973-1984.
23. Lorès, P., et al., *A missense mutation in IFT74, encoding for an essential component for intraflagellar transport of Tubulin, causes asthenozoospermia and male infertility without clinical signs of Bardet-Biedl syndrome.* Hum Genet, 2021. **140**(7): p. 1031-1043.
24. Kherraf, Z.E., et al., *Whole exome sequencing of men with multiple morphological abnormalities of the sperm flagella reveals novel homozygous QRICH2 mutations.* Clin Genet, 2019. **96**(5): p. 394-401.
25. Liu, C., et al., *Homozygous mutations in SPEF2 induce multiple morphological abnormalities of the sperm flagella and male infertility.* J Med Genet, 2020. **57**(1): p. 31-37.
26. Liu, W., et al., *Bi-allelic Mutations in TTC21A Induce Asthenoteratospermia in Humans and Mice.* Am J Hum Genet, 2019. **104**(4): p. 738-748.
27. Lorès, P., et al., *Mutations in TTC29, Encoding an Evolutionarily Conserved Axonemal Protein, Result in Asthenozoospermia and Male Infertility.* Am J Hum Genet, 2019. **105**(6): p. 1148-1167.
28. Firat-Karalar, E.N., et al., *Proteomic analysis of mammalian sperm cells identifies new components of the centrosome.* J Cell Sci, 2014. **127**(Pt 19): p. 4128-4133.
29. Almeida, F., et al., *The Human Centrosomal Protein CCDC146 Binds Chlamydia trachomatis Inclusion Membrane Protein CT288 and Is Recruited to the Periphery of the Chlamydia-Containing Vacuole.* Front Cell Infect Microbiol, 2018. **8**(article 254).
30. Blanco-Ameijeiras, J., P. Lozano-Fernández, and E. Martí, *Centrosome maturation - in tune with the cell cycle.* J Cell Sci, 2022. **135**(2/jcs.259395).
31. Wu, B., et al., *The coupling apparatus of the sperm head and tail†.* Biol Reprod, 2020. **102**(5): p. 988-998.
32. Fishman, E.L., et al., *A novel atypical sperm centriole is functional during human fertilization.* Nat Commun, 2018. **9**(1): p. 2210.
33. Manandhar, G., et al., *Centrosome reduction during mouse spermiogenesis.* Dev Biol, 1998. **203**(2): p. 424-434.
34. Sha, Y.W., et al., *A homozygous CEP135 mutation is associated with multiple morphological abnormalities of the sperm flagella (MMAF).* Gene, 2017. **633**: p. 48-53.
35. Zhang, X., et al., *CEP128 is involved in spermatogenesis in humans and mice.* Nat Commun, 2022. **13**(1): p. 1395.
36. Lv, M., et al., *Homozygous mutations in DZIP1 can induce asthenoteratospermia with severe MMAF.* J Med Genet, 2020. **57**(7): p. 445-453.

37. Sha, Y., et al., *Biallelic mutations of CFAP58 are associated with multiple morphological abnormalities of the sperm flagella.* Clin Genet, 2021. **99**(3): p. 443-448.
38. Zhu, Z.J., et al., *Novel mutation in ODF2 causes multiple morphological abnormalities of the sperm flagella in an infertile male.* Asian J Androl, 2022. **24**(5): p. 463-472.
39. Nakagawa, Y., et al., *Outer dense fiber 2 is a widespread centrosome scaffold component preferentially associated with mother centrioles: its identification from isolated centrosomes.* Mol Biol Cell, 2001. **12**(6): p. 1687-1697.
40. Hall, E.A., et al., *Acute versus chronic loss of mammalian Azi1/Cep131 results in distinct ciliary phenotypes.* PLoS Genet, 2013. **9**(12): p. e1003928.
41. Pasek, R.C., et al., *Coiled-coil domain containing 42 (Ccdc42) is necessary for proper sperm development and male fertility in the mouse.* Dev Biol, 2016. **412**(2): p. 208-18.
42. Kherraf, Z.E., et al., *Whole-exome sequencing improves the diagnosis and care of men with non-obstructive azoospermia.* Am J Hum Genet, 2022. **109**(3): p. 508-517.
43. Odabasi, E., U. Batman, and E.N. Firat-Karalar, *Unraveling the mysteries of centriolar satellites: time to rewrite the textbooks about the centrosome/cilium complex.* Mol Biol Cell, 2020. **31**(9): p. 866-872.
44. Zindy, F., et al., *Control of spermatogenesis in mice by the cyclin D-dependent kinase inhibitors p18(Ink4c) and p19(Ink4d).* Mol Cell Biol, 2001. **21**(9): p. 3244-55.
45. Gambarotto, D., et al., *Imaging cellular ultrastructures using expansion microscopy (U-ExM).* Nat Methods, 2019. **16**(1): p. 71-74.
46. Yanagisawa, H.A., et al., *FAP20 is an inner junction protein of doublet microtubules essential for both the planar asymmetrical waveform and stability of flagella in Chlamydomonas.* Mol Biol Cell, 2014. **25**(9): p. 1472-83.
47. Witman, G.B., et al., *Chlamydomonas flagella. I. Isolation and electrophoretic analysis of microtubules, matrix, membranes, and mastigonemes.* J Cell Biol, 1972. **54**(3): p. 507-39.
48. Linck, R.W., *Flagellar doublet microtubules: fractionation of minor components and alpha-tubulin from specific regions of the A-tubule.* J Cell Sci, 1976. **20**(2): p. 405-39.
49. Kirima, J. and K. Oiwa, *Flagellar-associated Protein FAP85 Is a Microtubule Inner Protein That Stabilizes Microtubules.* Cell Struct Funct, 2018. **43**(1): p. 1-14.
50. Simerly, C., et al., *Post-Testicular Sperm Maturation: Centriole Pairs, Found in Upper Epididymis, are Destroyed Prior to Sperm's Release at Ejaculation.* Sci Rep, 2016. **6**: p. 31816.
51. Kierszenbaum, A.L., et al., *The acroplaxome is the docking site of Golgi-derived myosin Va/Rab27a/b- containing proacrosomal vesicles in wild-type and Hrb mutant mouse spermatids.* Biol.Reprod., 2004. **70**(5): p. 1400-1410.
52. Martinez, G., et al., *Oligogenic heterozygous inheritance of sperm abnormalities in mouse.* Elife, 2022. **11**.
53. Collins, S.A., W.T. Walker, and J.S. Lucas, *Genetic Testing in the Diagnosis of Primary Ciliary Dyskinesia: State-of-the-Art and Future Perspectives.* J Clin Med, 2014. **3**(2): p. 491-503.
54. Shoemark, A., L. Ozerovitch, and R. Wilson, *Aetiology in adult patients with bronchiectasis.* Respir Med, 2007. **101**(6): p. 1163-70.
55. Li, Z.Z., et al., *The novel testicular enrichment protein Cfap58 is required for Notch-associated ciliogenesis.* Biosci Rep, 2020. **40**(1).
56. Cuveillier, C., et al., *Beyond Neuronal Microtubule Stabilization: MAP6 and CRMPS, Two Converging Stories.* Front Mol Neurosci, 2021. **14**: p. 665693.

57. Ma, M., et al., *Structure of the Decorated Ciliary Doublet Microtubule.* Cell, 2019. **179**(4): p. 909-922.e12.
58. Jardin, I., et al., *SARAF and EFHB Modulate Store-Operated Ca(2+) Entry and Are Required for Cell Proliferation, Migration and Viability in Breast Cancer Cells.* Cancers (Basel), 2021. **13**(16).
59. Segal, R.A., et al., *Mutant strains of Chlamydomonas reinhardtii that move backwards only.* J Cell Biol, 1984. **98**(6): p. 2026-34.
60. Tam, L.W. and P.A. Lefebvre, *The Chlamydomonas MBO2 locus encodes a conserved coiled-coil protein important for flagellar waveform conversion.* Cell Motil Cytoskeleton, 2002. **51**(4): p. 197-212.
61. Shi, Z., et al., *Potential Novel Modules and Hub Genes as Prognostic Candidates of Thyroid Cancer by Weighted Gene Co-Expression Network Analysis.* Int J Gen Med, 2021. **14**: p. 9433-9444.
62. Kasak, L., et al., *Bi-allelic Recessive Loss-of-Function Variants in FANCM Cause Non-obstructive Azoospermia.* Am J Hum Genet, 2018. **103**(2): p. 200-212.
63. Amargant, F., et al., *The human sperm basal body is a complex centrosome important for embryo preimplantation development.* Mol Hum Reprod, 2021. **27**(11:gaab062).
64. Lehti, M.S. and A. Sironen, *Formation and function of the manchette and flagellum during spermatogenesis.* Reproduction, 2016. **151**(4): p. R43-54.
65. O'Donnell, L., et al., *An essential role for katanin p80 and microtubule severing in male gamete production.* PLoS Genet, 2012. **8**(5): p. e1002698.
66. Ho, U.Y., et al., *WDR62 is required for centriole duplication in spermatogenesis and manchette removal in spermiogenesis.* Commun Biol, 2021. **4**(1): p. 645.
67. Zhu, F., et al., *Biallelic SUN5 Mutations Cause Autosomal-Recessive Acephalic Spermatozoa Syndrome.* Am J Hum Genet, 2016. **99**(4): p. 942-949.
68. Yuan, S., et al., *Spata6 is required for normal assembly of the sperm connecting piece and tight head-tail conjunction.* Proc.Natl.Acad.Sci.U.S.A, 2015. **112**(5): p. E430-E439.
69. Hoyer-Fender, S., *Development of the Connecting Piece in ODF1-Deficient Mouse Spermatids.* Int J Mol Sci, 2022. **23**(18:10280).
70. Dunleavy, J.E.M., et al., *Katanin-like 2 (KATNAL2) functions in multiple aspects of haploid male germ cell development in the mouse.* PLoS Genet, 2017. **13**(11): p. e1007078.
71. Giordano, T., et al., *Loss of the deglutamylase CCP5 perturbs multiple steps of spermatogenesis and leads to male infertility.* J Cell Sci, 2019. **132**(3).
72. Wang, Y., et al., *Variability in the morphologic assessment of human sperm: use of the strict criteria recommended by the World Health Organization in 2010.* Fertil Steril, 2014. **101**(4): p. 945-9.
73. Schindelin, J., et al., *Fiji: an open-source platform for biological-image analysis.* Nat Methods, 2012. **9**(7): p. 676-82.
74. Mazo, G., *QuickFigures: A toolkit and ImageJ PlugIn to quickly transform microscope images into scientific figures.* PLoS One, 2021. **16**(11): p. e0240280.
75. Reynolds, E.S., *The use of lead citrate at high pH as an electron-opaque stain in electron microscopy.* J Cell Biol, 1963. **17**(1): p. 208-12.
76. Pierre, V., et al., *Absence of Dpy19l2, a new inner nuclear membrane protein, causes globozoospermia in mice by preventing the anchoring of the acrosome to the nucleus.* Development, 2012. **139**(16): p. 2955-65.

ARTICLE 2

"Oligogenic heterozygous inheritance of sperm abnormalities in mouse"

Guillaume Martinez, Charles Coutton, Corinne Loeuillet, Caroline Cazin, **Jana Muroňová**, Magalie Boguenet, Emeline Lambert, Magali Dhellemmes, Geneviève Chevalier, Jean-Pascal Hograindleur, Charline Vilpreux, Yasmine Neirijnck, Zine-Eddine Kherraf, Jessica Escoffier, Serge Nef, Pierre F Ray, Christophe Arnoult

Published article in *Elife* (2022)

DOI: 10.7554/eLife.75373

Contribution:

I prepared a part of the samples that were used in the project and participated in discussions and analysis of the results.

Summary:

Spermatogenesis is a highly complex process, and it involves hundreds to thousands of genes that contribute to proper sperm formation. Identification of new genes involved in male fertility has been on the rise in the recent years due to an increased use of massive parallel sequencing technologies, especially of whole-exome sequencing (WES). In about half of patients affected by the multiple morphological abnormalities of the sperm flagella (MMAF) syndrome, a biallelic pathogenic variant in a single gene cannot be identified using WES. We hypothesized whether some of these cases could involve oligogenic inheritance, an accumulation of rare variants in two or more distinct but functionally linked genes.

Here, we used heterozygote mouse strains harbouring one to four loss-of-function mutations in MMAF-related genes: *Ccdc146, Armc2, Cfap43* and *Cfap44* (Charles Coutton et al. 2019; 2018). Mutations in these genes lead to MMAF, asthenozoospermia, and consequent male infertility in humans and mice. These genes are autosomal recessive. ARMC2 is a cargo adapter required for the IFT of radial spokes in the *Chlamydomonas* (K. F. Lechtreck et al. 2022). Both CFAP43 and CFAP44 are flagellar components, and CFAP43 is involved in intra-manchette transport (IMT)

(Yu et al. 2021). CCDC146 has been shown to be a centriolar protein in bovine spermatozoa (Firat-Karalar et al. 2014) and its localization and potential functions were discussed above.

The aim of the study was to observe whether the accumulation of up to four heterozygous truncating mutations would affect overall fertility and sperm parameters including motility and head and flagellar morphology in mice.

The accumulation of heterozygous mutations led to a progressive increase in head morphological defects (430% with four mutations compared to the control). This wasn't the case for flagellar abnormalities and overall motility, however the quality of movement was compromised. The presence of 4 mutations did not affect sperm concentration, nor overall fertility and mice produced a similar number of pups as the control.

To conclude, this study shows that haploinsufficiency and oligogenic heterozygosity can lead to spermatogenesis defects in mice and could be explored in humans where it could potentially explain some cases of male unexplained infertility.

RESEARCH ARTICLE

Oligogenic heterozygous inheritance of sperm abnormalities in mouse

Guillaume Martinez[1,2]*, Charles Coutton[1,2], Corinne Loeuillet[1], Caroline Cazin[1,3], Jana Muroňová[1], Magalie Boguenet[1], Emeline Lambert[1], Magali Dhellemmes[1], Geneviève Chevalier[1], Jean-Pascal Hograindleur[1], Charline Vilpreux[1], Yasmine Neirijnck[4], Zine-Eddine Kherraf[1,3], Jessica Escoffier[1], Serge Nef[4], Pierre F Ray[1,3], Christophe Arnoult[1,5]*

[1]Institute for Advanced Biosciences, INSERM, CNRS, Université Grenoble Alpes, Grenoble, France; [2]UM de Génétique Chromosomique, Hôpital Couple-Enfant, CHU Grenoble Alpes, Grenoble, France; [3]UM GI-DPI, CHU Grenoble Alpes, Grenoble, France; [4]Department of Genetic Medicine and Development, University of Geneva Medical School, Genève, Switzerland; [5]Station de Primatologie, UPS 846, CNRS, Rousset, France

Abstract Male infertility is an important health concern that is expected to have a major genetic etiology. Although high-throughput sequencing has linked gene defects to more than 50% of rare and severe sperm anomalies, less than 20% of common and moderate forms are explained. We hypothesized that this low success rate could at least be partly due to oligogenic defects – the accumulation of several rare heterozygous variants in distinct, but functionally connected, genes. Here, we compared fertility and sperm parameters in male mice harboring one to four heterozygous truncating mutations of genes linked to multiple morphological anomalies of the flagellum (MMAF) syndrome. Results indicated progressively deteriorating sperm morphology and motility with increasing numbers of heterozygous mutations. This first evidence of oligogenic inheritance in failed spermatogenesis strongly suggests that oligogenic heterozygosity could explain a significant proportion of asthenoteratozoospermia cases. The findings presented pave the way to further studies in mice and man.

***For correspondence:** gmartinez@chu-grenoble.fr (GM); christophe.arnoult@univ-grenoble-alpes.fr (CA)

Competing interest: The authors declare that no competing interests exist.

Funding: See page 18

Received: 08 November 2021
Preprinted: 16 November 2021
Accepted: 07 April 2022
Published: 22 April 2022

Reviewing Editor: Jean-Ju Chung, Yale University, United States

Editor's evaluation

This study provides insights into the detrimental effect of accumulative heterozygous mutations on sperm abnormalities. By breeding a series of knockout strains known to cause multiple flagellar defects, the authors demonstrated that such variations at two (digenic) or more loci (oligogenic) can contribute to sperm abnormalities in the head. These findings are significant in that they implicate oligogenic inheritance as a possible cause of unexplained male infertility.

Introduction

Infertility is a major health concern affecting 15% of couples of reproductive-age worldwide (***Mascarenhas et al., 2012***; ***Boivin et al., 2007***). The infertility burden has increased globally for both genders in the past 30 years (***Sun et al., 2019***), and now affects approximately 50 million couples worldwide (***Datta et al., 2016***). Infertility is broadly treated by assisted reproductive technologies (ART), and today the number of individuals who were conceived by ART is close to 0.1% of the total world population, with over 8 million children already born following in vitro fertilization (IVF). Currently, ART is estimated to account for 1–6% of births in most countries (***Faddy et al., 2018***), with over 2.5 million

cycles performed every year, resulting in over 500,000 births worldwide annually (**Fauser, 2019**). Despite this undeniable success, almost half the couples who seeks medical assistance for infertility fail to achieve successful pregnancy, and nearly 40% of infertile couples worldwide are simply diagnosed with unexplained or idiopathic infertility (**Sadeghi, 2015**). In the clinical context, few efforts are currently being made to understand and specifically address the underlying causes of a couple's infertility because ART can often successfully rescue fertility even without a molecular diagnosis. Nevertheless, this absence of identification of the causes of infertility means that we lack alternative treatments for couples for whom current therapies are unsuccessful. Consequently, it is essential to improve the molecular diagnosis of infertility.

Human male infertility is a clinically heterogeneous condition with a complex etiology, in which genetic defects play a significant role. It is estimated that half of idiopathic cases of male infertility could be attributed to an as-yet unidentified genetic defect (**Krausz, 2011**). However, characterization of the molecular causes of male infertility represents a significant challenge, as over 4000 genes are thought to be involved in sperm production (**Jan et al., 2017**). Over the past decade, significant progress has been made in gene identification thanks to the emergence of next-generation sequencing (NGS), and in functional gene validation thanks to new gene-editing techniques such as CRISPR/Cas9. NGS provides an inexpensive and rapid genetic approach through which to discover novel disease-associated genes (**Fernandez-Marmiesse et al., 2018**). It has proven to be a highly powerful tool in the research and diagnosis context of male infertility (**Xavier et al., 2021**; **Krausz and Riera-Escamilla, 2018**). In addition, validation of newly-identified variants through functional experiments has greatly benefited from the ability to generate mouse knock-out models using CRISPR technology (**Kherraf et al., 2018**) and the use of novel model organisms like *Trypanosoma brucei* to study specific phenotypes, such as multiple morphological abnormalities of the [sperm] flagella (MMAF) syndrome (**Coutton et al., 2018**; **Lorès et al., 2019**; **Martinez et al., 2020**). These developments have resulted in a diagnostic yield, based on known genetic causes, explaining about 50% of cases of rare qualitative sperm defects like globozoospermia, acephalic, or MMAF syndromes (**Beurois et al., 2020**; **Touré et al., 2021**). In contrast, the diagnostic yield for quantitative sperm abnormalities such as oligozoospermia or azoospermia remains below 20%, even though these are the most common forms of male infertility (**Krausz, 2011**; **Krausz and Riera-Escamilla, 2018**; **Tüttelmann et al., 2018**). To improve these low diagnostic yields, international consortia have been created to attempt to identify very low-frequency variants (https://gemini.conradlab.org/ and https://www.imigc.org/). In addition, several groups have started to assemble cohorts of patient-parent trios, aiming to identify de novo mutations causing male infertility as well as providing insight into dominant maternal inheritance (**Xavier et al., 2021**; **Veltman and Brunner, 2012**; **McRae, 2017**). Phenotypic heterogeneity and apparent incomplete penetrance were observed for some genetic alterations involved in male infertility (**Vogt, 2005**; **Röpke et al., 2013**; **Kherraf et al., 2017**). These observations are difficult to reconcile with a model of Mendelian inheritance. We thus raised the possibility that the low diagnostic yield is partly due to the complex etiology of infertility, and hypothesized that some of the unsolved cases are due to oligogenic events, that is, accumulation of several rare hypomorphic variants in distinct, functionally connected genes, and in particular to oligogenic heterozygosity. The molecular basis of oligogenicity is poorly understood. The main hypotheses are that two or more mutant proteins may act at different levels in the same intracellular pathway and could quantitatively contribute to its progressive dysfunction. When a critical threshold is reached, the disease phenotype would emerge. Alternatively, the mutant nonfunctional proteins produced may be part of the same multiprotein complex, and the presence of numerous pathogenic variants would increase the chance of the complex becoming compromised – leading to a progressive collapse of its cellular function (**Kousi and Katsanis, 2015**).

Here, we addressed the oligogenic heterozygosity hypothesis in male infertility using four specially-generated MMAF knock-out (KO) mouse models with autosomal recessive inheritance (**Coutton et al., 2018**; **Coutton et al., 2019**). Following extensive cross-breeding of our KO mouse lines, we produced lines harboring between one and four heterozygous truncating mutations. We assessed and compared fertility for these lines, analyzing both quantitative and qualitative sperm parameters, and performed a fine analysis of sperm nuclear morphology for all strains. Using this strategy, we were able to describe new genetic inheritance of sperm deficiencies.

Results

Selection and characterization of individual MMAF mouse lines

To generate mice carrying up to four heterozygous truncating mutations, we first selected four lines carrying mutations in genes inducing a MMAF phenotype, namely *Cfap43*, *Cfap44*, *Armc2*, and *Ccdc146*. Three of these lines were already available and previously reported by our laboratory: a strain with a 4 bp deletion in exon 21 (delAAGG) for Cfap43 (**Coutton et al., 2018**), a strain with a 7 bp insertion in exon 3 (InsTCAGATA) for *Cfap44* (**Coutton et al., 2018**), and a strain with a one-nucleotide duplication in exon 4 (DupT) for Armc2 (**Coutton et al., 2019**), inducing a translational frameshift that leads to the production of a truncated protein. We generated the fourth strain using CRISPR-Cas9 technology as described in the Materials and methods section, inducing a 4 bp deletion in exon 2 (delTTCG) of the *Ccdc146* gene (**Appendix 1—figure 1A**). A study describing how this mutation in the *Ccdc146* gene affects spermatogenesis is currently under review elsewhere (for the reviewers only, we provide the complete phenotype for the Ccdc146 KO mouse strain, demonstrating its role in MMAF syndrome in mice).

We first confirmed the MMAF phenotypes for all four strains. Sperm from all homozygous KO male mice displayed more than 95% morphological abnormalities of the flagellum including coiled, bent, irregular, short or/and absent flagella (**Figures 1–4**). We then analyzed sperm morphology (head and flagellum) in heterozygous animals by optical microscopy. The four strains fell into two categories. For the two strains targeting *Cfap43* and *Cfap44*, *Cfap43*$^{+/-}$, or *Cfap44*$^{+/-}$ +/- males had higher rates (+ 4% and + 12.75%) of abnormalities than wild-type mice (**Figures 1A and 2A**; *Cfap43*: t = −2.79, df = 6.13, p-value = 0.03; *Cfap44*: t = −8.80, df = 6.14, p-value = 0.0001). These results were in accordance with previous observations (**Coutton et al., 2018**). In contrast, for strains harboring heterozygous mutations in *Armc2* and *Ccdc146*, no significant differences were observed with respect to wild-type males (**Figures 3A and 4A**).

Because head morphology defects may be subtle and difficult to detect by visual observation, we applied a newly-developed method, involving the use of Nuclear Morphology Analysis Software (NMAS) (**Skinner et al., 2019**). The method is described in detail in the Materials and methods section. The nuclear morphologies of sperm from each genotype (WT, heterozygotes, and homozygotes) were characterized. For all corresponding wild-type strains, shape modeling gave extremely similar consensus and angle profiles for nuclei, highlighting the common genetic background of the KO animals (**Appendix 1—figure 2**). For heterozygous *Cfap43*$^{+/-}$, *Cfap44*$^{+/-}$, and *Ccdc146*$^{+/-}$ +/-, the angle profiles were very similar to WT profiles (**Figures 1B, 2B and 4B**). In contrast, *Armc2*$^{+/-}$ +/- showed a slightly modified angle profile (–6° at position 365 and +6° at position 435) compared to the WT profile, due to a narrower caudal base inducing a more pronounced caudal bulge and a reduced dorsal angle (**Figure 3B**). When the profiles for all heterozygous males were compared, a very similar nuclear morphology with nearly identical angle and variability profiles was found, apart from for *Armc2*$^{+/-}$, which had slightly more variability (IQR *Armc2*$^{+/-}$ +/- than other curves with +10 IQR in position 350 and +5 IQR in position 450) than the other lines despite a similar angle profile (**Appendix 1—figure 3**).

We also compared these profiles with those of the corresponding KO mice, which displayed very unique and specific patterns (**Figures 1B–4B**). Briefly, *Cfap43*$^{-/-}$ and *Cfap44*$^{-/-}$ angle profiles both displayed a flattening from the ventral angle to the dorsal angle leading to their characteristic 'pepper' shape. The lines for both profiles merged over the majority of regions such as the under-hook concavity and the acrosomal curve, and showed intermediate impairment, greater than that observed in the *Armc2*$^{-/-}$ line and less than that observed in the *Ccdc146*$^{-/-}$ line. The angle profile for *Armc2*$^{-/-}$ mice was similar to that of wild-type mice at the tip, dorsal angle, and acrosomal curve, as these regions do not appear to be affected by the mutation. Under-hook concavity, ventral angle, and tail socket regions were slightly affected, although less than in other lineages. In contrast to the other lineages, the caudal base was markedly shortened, with a significant flattening observed. For the *Ccdc146*$^{-/-}$ line, with the exception of the ventral-vertical region, which was unaffected in any lineage, all regions of the angle profile were strongly impacted. The dorsal angle was completely absorbed into the acrosomal curve, and the under-hook concavity, ventral angle and caudal bulge regions were flattened. The tail socket region even displayed an inverted angular profile compared to the other lineages. Overall, the profile of *Ccdc146*$^{-/-}$ showed considerable variability, and complete remodeling of the angle profile with, among other changes, total inversion of the curve at position 330–400, corresponding to complete disappearance of the tail socket. Comparison of the profiles for KO

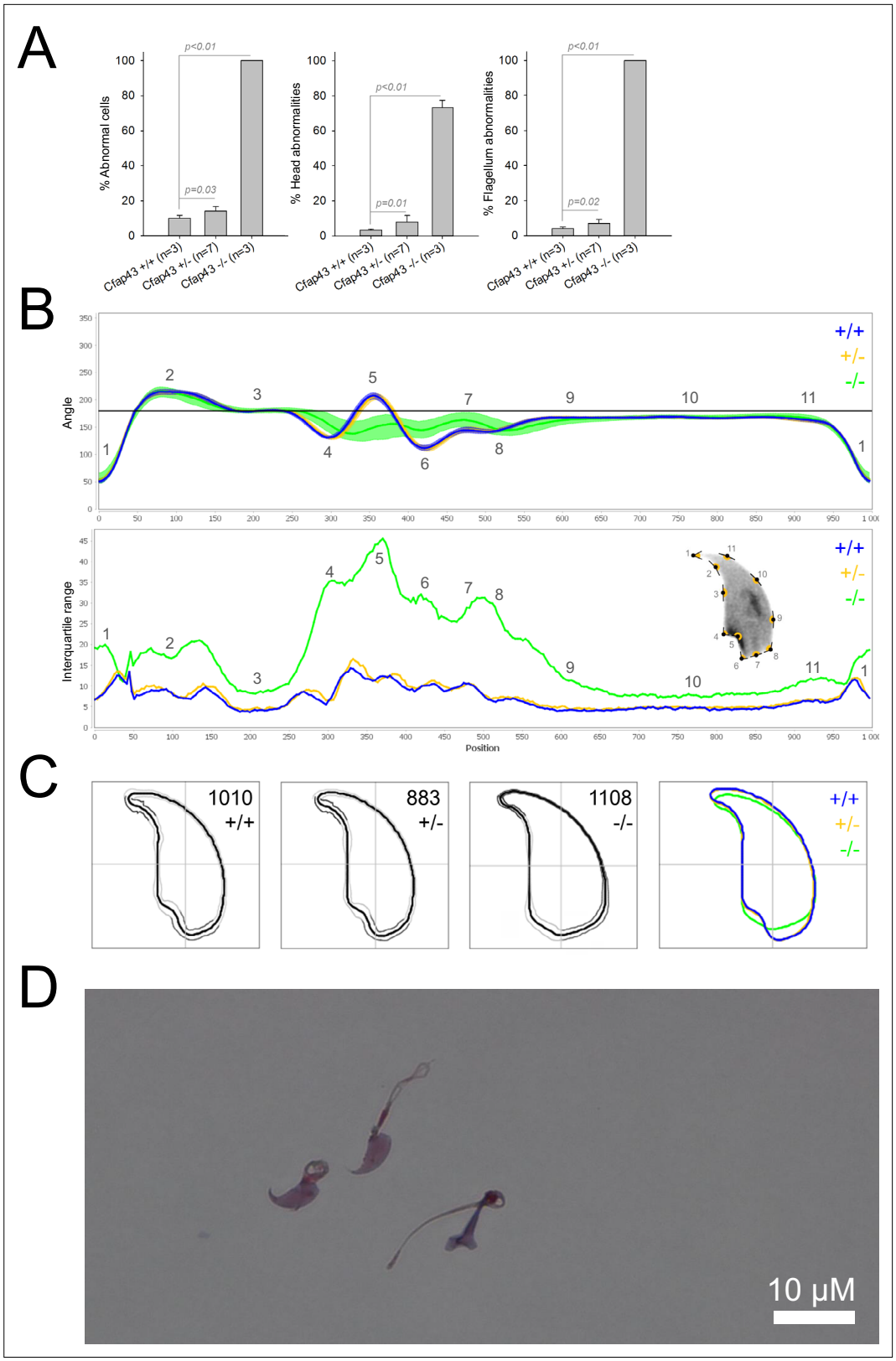

Figure 1. Sperm morphology analysis for the *Cfap43* mouse strain.
(**A**) Histogram showing proportions of morphological anomalies (mean ± SD) for each *Cfap43* genotype observed by light microscopy. Statistical significance was assessed by applying an unpaired Welch *t*-test; p-values are indicated. (**B**) Angle profiles (top) and variability profiles (bottom) from *Cfap43*$^{+/+}$ (blue), *Cfap43*$^{+/-}$ (yellow), and

Figure 1 continued on next page

Figure 1 continued

Cfap43$^{-/-}$ (green) mice. The x axis represents an index of the percentage of the total perimeter as measured counterclockwise from the apex of the sperm hook. The y axis, corresponding to the angle profile, represents the interior angle measured across a sliding window centered on each index location. The y axis, corresponding to the variability profile, represents the Interquartile Range (IQR) value (the difference between the 75th and 25th percentiles). Specific regions of the nuclei are mapped on the profile and the graphical representation (from ***Skinner et al., 2019***) with: 1-tip; 2-under-hook concavity; 3-vertical; 4-ventral angle; 5-tail socket; 6-caudal bulge; 7-caudal base; 8-dorsal angle; 9–11-acrosomal curve. (**C**) Consensus nuclear outlines for each genotype alongside a merged consensus nucleus (blue = *Cfap43*$^{+/+}$, yellow = *Cfap43*$^{+/-}$, green = *Cfap43*$^{-/-}$). The numbers assigned to each consensus outline correspond to the number of nuclei processed per condition. (**D**) Optical microscopy analysis showing a representative MMAF phenotype for *Cfap43* KO mice (scale bar, 10 µm).

sperm (***Appendix 1—figure 4***) showed that *Cfap43*$^{-/-}$ and *Cfap44*$^{-/-}$ mice displayed similar alterations (general enlargement of the head, rounding of the base at the expense of the flagellum insertion, etc.) resulting in close consensus; the other two lines were quite distinct. Although it was the most affected heterozygous line, *Armc2*$^{-/-}$ mice displayed the mildest alterations to nuclear morphology and variability of the four lines. KO animals nonetheless retained specific patterns, including modification of the hook curve and a specific slope of the base profile. Finally, *Ccdc146*$^{-/-}$ mice displayed extremely severe alterations, with almost all of their nuclei presenting a triangular shape (***Figure 4C–D***). In line with previous studies (***Coutton et al., 2018***; ***Lorès et al., 2019***; ***Coutton et al., 2019***; ***Hwang et al., 2021***), these results demonstrate that absence of MMAF genes not only affects sperm flagellum biogenesis but can also have an impact on sperm head morphology.

From these extensively characterized lines, we then proceeded to generate mice harboring multiple mutations.

Impact of accumulation of heterozygous mutations

All mice harboring between one and four heterozygous truncating mutations were generated by standard cross-breeding of the four lines. A considerable number of generations were produced over several years. Due to time and financial constraints, only one combination of multiple heterozygous lines was created and analyzed. Double heterozygotes were obtained by crossing *Cfap43* and *Cfap44* KO mouse lines. Triple heterozygous animals were mutated for *Cfap43*, *Cfap44*, and *Armc2*; and the quadruple heterozygous line also had the *Ccdc146* mutation (***Figure 5***).

The accumulation of heterozygous mutations on the four selected genes involved in MMAF syndromes induced qualitative spermatogenesis defects (illustrated in ***Appendix 1—figure 5***), with progressive increased numbers of morphological anomalies (from 9.81% ± 2.48% for control mice to 42.33% ± 3.78% for mice bearing four mutations, a 430% increase. ***Figure 5A***), in particular defects of the head (from 6.56% ± 2.30% for control mice to 40.33% ± 3.78% for mice bearing four mutations, a 615% increase. ***Figure 5B***). Males harboring one mutation exhibited a significant increase in flagellar abnormalities (***Figure 5C***; see also 6 C). However, flagellar anomalies were not amplified as the number of mutated genes increased (t = −2.78, df = 2.41, p-value = 0.08, for control versus four mutations. ***Figure 5C***). Nevertheless, accumulation of mutations had a negative impact on sperm motility parameters (illustrated in ***Videos 1–5***). Although the decrease of the overall percentage of motile cells is not significant with increasing numbers of mutations (from 38.55 ± 11.50 µm/s for control to 29.13 ± 6.02 µm/s for mice bearing four mutations, t = 1.48, df = 4.78, p-value = 0.20. ***Figure 5D***), the quality of sperm movement was strongly affected (***Figure 5E–F***). Thus, for sperm bearing two mutations, the average sperm velocity and straight-line velocity were halved (–44.6% and –46.1% respectively) compared to control mice (VAP: 92.31 ± 23.38–51.16 ± 16.59 µm/s,; VSL: 81.52 ± 20.84–43.96 ± 13.75 µm/s), and the decreasing trend continued as mutations accumulated (41.18 ± 10.27 and 33.43 ± 8.62 µm/s for VAP and VSL of mice bearing four mutations, that is –55.4% and –59% versus control mice). It is worth noting that the deterioration of the morphological phenotype with the addition of new heterozygous mutations occurs even though the *Ccdc146* and *Armc2* heterozygous mutations alone had no impact on the sperm phenotype observed by optical microscopy (***Figures 3A and 4A***).

From the crosses performed to generate multi-heterozygous animals, other combinations of heterozygous mutations were obtained. The sperm parameters of the corresponding animals were also

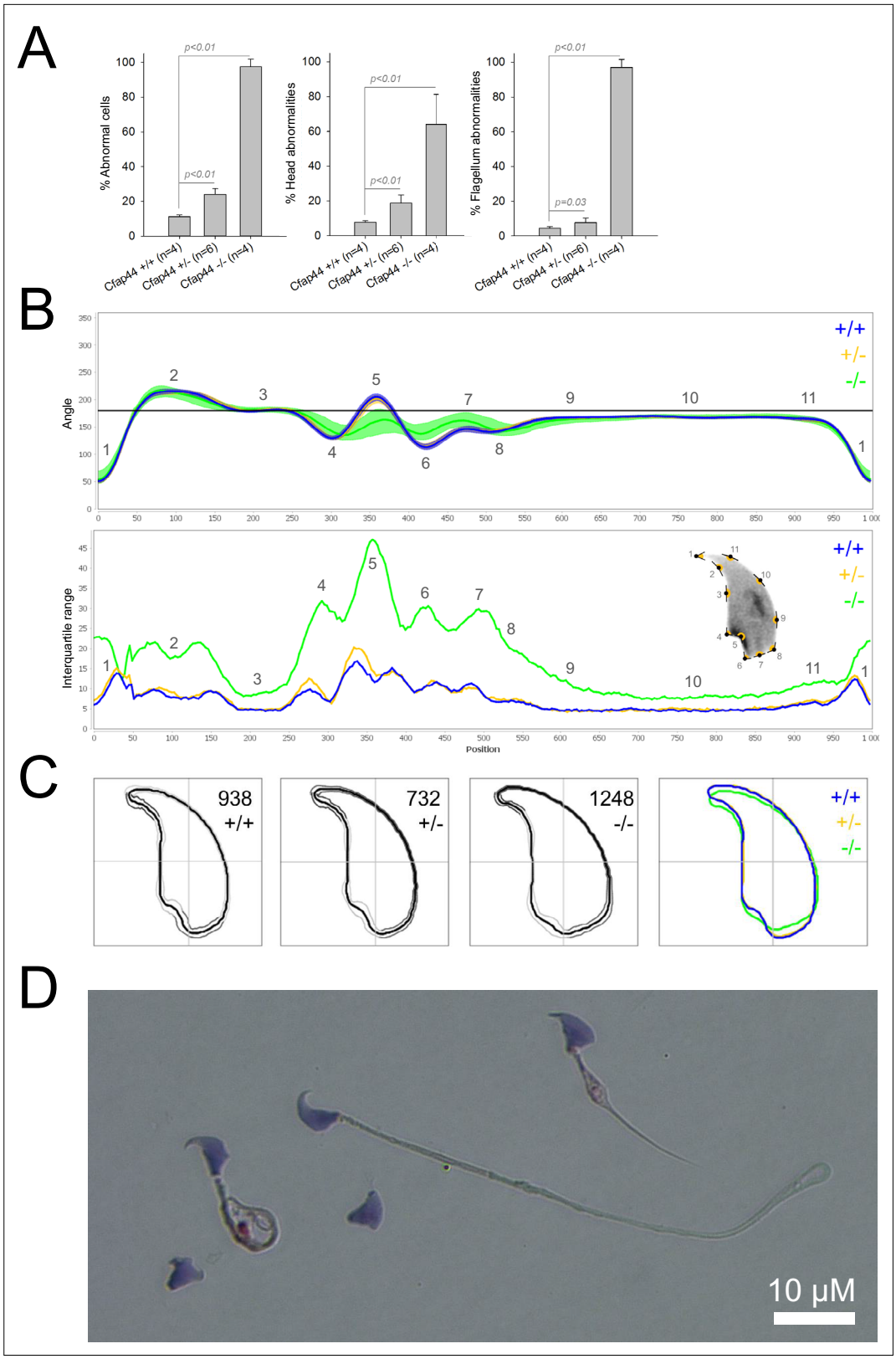

Figure 2. Sperm morphology analysis for the *Cfap44* mouse strain.
(**A**) Histogram showing proportions of morphological anomalies (mean ± SD) for each *Cfap44* genotype. Statistical significance was assessed by applying an unpaired Welch *t*-test; p-values are indicated. (**B**) Angle profiles (top) and variability profiles (bottom) for *Cfap44*$^{+/+}$ (blue), *Cfap44*$^{+/-}$ (yellow), and *Cfap44*$^{-/-}$ (green) mice. The x axis represents

Figure 2 continued on next page

Figure 2 continued

an index of the percentage of the total perimeter, as measured counterclockwise from the apex of the sperm hook. The y axis corresponding to the angle profile is the interior angle measured across a sliding window centered on each index location. The y axis corresponding to the variability profile represents the Interquartile Range (IQR) value (the difference between the 75th and 25th percentiles). Specific regions of the nuclei are mapped on the profile and the graphical representation (from ***Skinner et al., 2019***) with: 1-tip; 2-under-hook concavity; 3-vertical; 4-ventral angle; 5-tail socket; 6-caudal bulge; 7-caudal base; 8-dorsal angle; 9–11-acrosomal curve. (**C**) Consensus nuclear outlines for each genotype alongside a merged consensus nucleus (blue = *Cfap44*$^{+/+}$, yellow = *Cfap44*$^{+/-}$, green = *Cfap44*$^{-/-}$). The numbers assigned to each consensus outline correspond to the number of nuclei processed per condition. (**D**) Optical microscopy analysis showing a representative MMAF phenotype for *Cfap44* KO mice (scale bar, 10 µm).

phenotyped. Interestingly, rates of morphological defect (***Figure 6A–C***, red dots) and motility parameters (***Figure 6D–F***, red dots) were very similar whatever the gene combinations. Taken together, these results show that it is not the specific combination of heterozygous mutations that leads to altered sperm morphology and sperm motility parameters, but rather their accumulation.

Despite a marked alteration of spermatocytograms, accumulation of mutations did not have a significant effect on quantitative spermatogenesis defects. For example, sperm production – represented by testis weight and sperm concentration – and overall fertility of the animals – based on the number of pups per litter and interval between litters – were not affected, whatever the combination and number of mutations (testis weight: t = −0.80, df = 2.33, p-value = 0.49; sperm concentration: t = −0.89, df = 5.68, p-value = 0.40; time/litter: t = 0.70, df = 25.98, p-value = 0.48; pups/litter: t = 0.80, df = 34.68, p-value = 0.42; for control versus mice bearing four mutations. ***Figure 7***).

As for mouse lines bearing single mutations, we then used NMAS to help characterize head anomalies in multi-heterozygote mutated lines. Our results indicated a striking progressive deterioration in sperm head morphology as mutations accumulated (***Figure 8***). Each additional mutation progressively and significantly increased the variability and severity of the morphological defects observed in the nucleus, negatively influencing angle and consensus profiles (perimeter and max feret progressively decline from 49.12 ± 0.07 and 19.01 ± 0.03 µm to 44.23 ± 0.21 and 16.41 ± 0.11 µm between mice bearing one and four mutations for example). This negative effect was cumulative, and if a threshold or plateau effect exists, it was not reached upon accumulation of four mutations.

To extend our analysis, we then used the software to analyze sperm sub-populations by performing unbiased nuclear morphology categorization. Clustering based on angle profiles revealed a total of ten sub-groups of nuclei shape, which matched with the usual shapes of normal and abnormal mouse sperm, defined more than 30 years ago (***Krzanowska, 1981***). Mutation-accumulation progressively increased the frequency of all abnormal shapes and decreased the frequency of normal forms. The most unstructured forms were associated with the highest number of mutations (***Appendix 1—figure 6***).

Discussion

The aim of this study was to determine whether the accumulation of several rare heterozygous variants in functionally connected genes affected fertility and sperm parameters in mice. Our results clearly demonstrated that spermatogenesis failure can arise from oligogenic heterozygosity in mice. Males bearing increased numbers of heterozygote mutations in genes involved in MMAF syndrome exhibited altered spermatocytogram, with significant increase of proportion of abnormal sperm and decreased sperm motility. Both defective sperm motility and abnormal sperm head morphology could negatively impact fertility. Concerning sperm motility, it has been clearly shown that the percentage of conception depends on the total number of motile sperm within the semen (***Publicover and Barratt, 2011***). Sperm motility is indeed a key parameter for fertilization, which occurs deeply in the mammalian female tract. Motility is necessary not only for the sperm to reach the oocyte in the oviduct, but sperm motility is also required for the sperm to cross the protective layers of the oocytes and is essential for gamete fusion (***Ravaux et al., 2016***). Concerning abnormal head morphology, there are numerous reports of a significant correlation between morphology and infertility and it is accepted that any increase in any sperm abnormality should be regarded as a possible cause of decreased fertility, and that precise analyses of sperm abnormalities is a useful approach for diagnosis or research

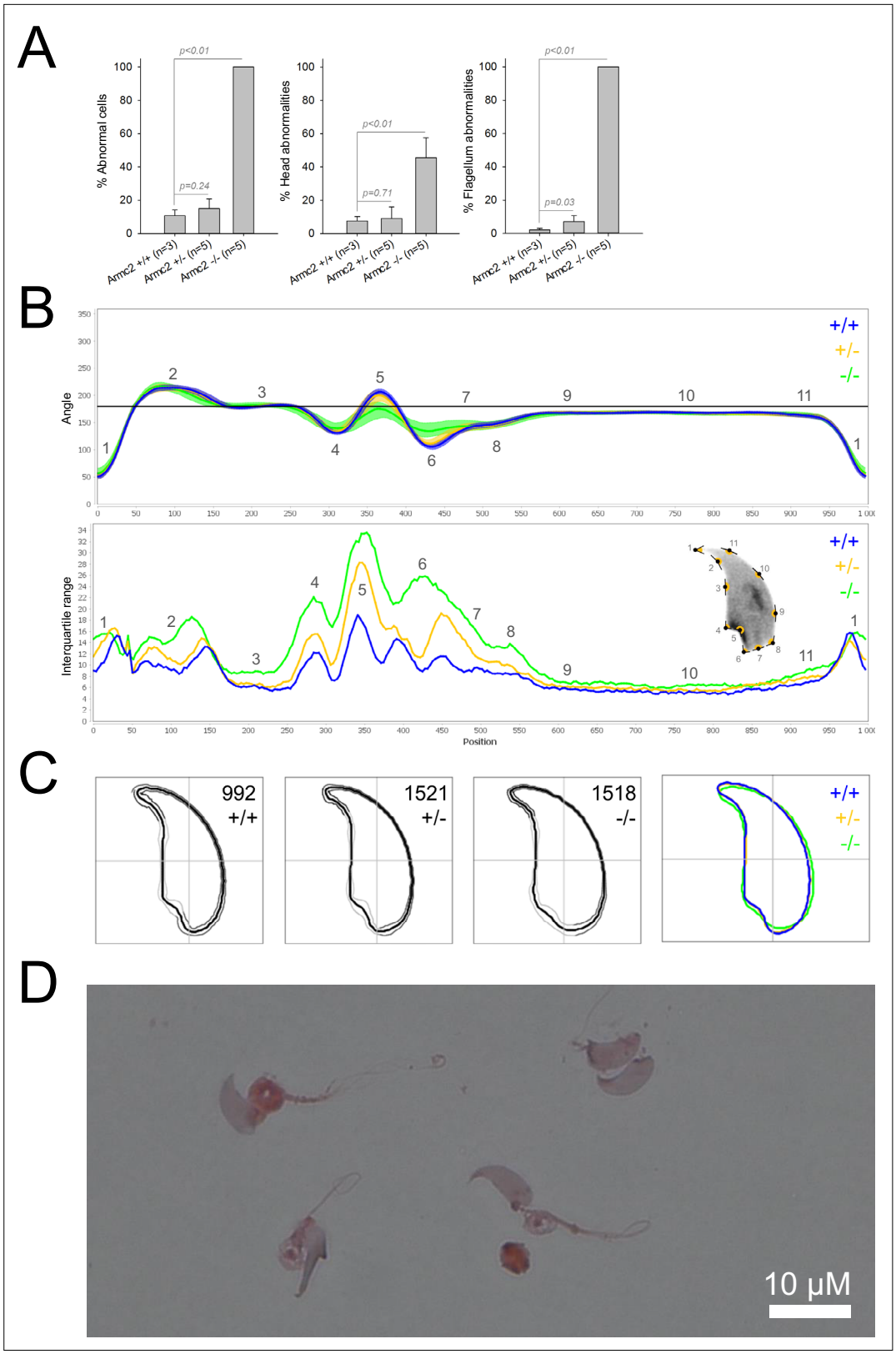

Figure 3. Sperm morphology analysis for the *Armc2* mouse strain.
(**A**) Histogram showing proportions of morphological anomalies (mean ± SD) for each *Armc2* genotype. Statistical significance was assessed by applying an unpaired Welch *t*-test; p-values are indicated. (**B**) Angle profiles (top) and variability profiles (bottom) for *Armc2*$^{+/+}$ (blue), *Armc2*$^{+/-}$ (yellow), and *Armc2*$^{-/-}$ (green) mice. The x axis represents

Figure 3 continued on next page

Figure 3 continued

an index of the percentage of the total perimeter, as measured counterclockwise from the apex of the sperm hook. The y axis corresponding to the angle profile represents the interior angle measured across a sliding window centered on each index location. The y axis corresponding to the variability profile represents the Interquartile Range (IQR) value (the difference between the 75th and 25th percentiles). Specific regions of the nuclei are mapped on the profile and the graphical representation (from ***Skinner et al., 2019***) with: 1-tip; 2-under-hook concavity; 3-vertical; 4-ventral angle; 5-tail socket; 6-caudal bulge; 7-caudal base; 8-dorsal angle; 9–11-acrosomal curve. (**C**) Consensus nuclear outlines for each genotype alongside a merged consensus nucleus (blue = *Armc2*$^{+/+}$, yellow = *Armc2*$^{+/-}$, green = *Armc2*$^{-/-}$). The numbers assigned to each consensus outline correspond to the number of nuclei processed per condition. (**D**) Optical microscopy analysis showing a representative MMAF phenotype for *Armc2* KO mice (scale bar, 10 µm).

purposes (***Andrade-Rocha, 2001***; ***Chemes and Rawe, 2003***; ***Menkveld et al., 2011***; ***Auger et al., 2016***). These findings are supported by the World Health Organization which concludes in its report that 'categorizing all abnormal forms of spermatozoa may be of diagnostic or research benefit'.

However, despite significant sperm parameter alterations, we did not observe here effect on male fertility, suggesting that the threshold leading to the partial/complete collapse of the male reproductive function was not reached. This concept of threshold is strongly associated with oligogenicity. It is defined by the number of mutations within the same multiprotein complex or intracellular pathway beyond which a disease phenotype will be observed (***Dipple and McCabe, 2000***). In this study, we induced mutations in four genes coding for proteins participating in flagella formation and function. Although we did observe a negative cumulative burden, we did not reach the complex or system threshold that would lead to the emergence of a dichotomous severe infertility phenotype. This may be related to the fact that the mouse model has proved limitations to decipher the function of the proteins involved in sperm physiology and to assess the impact of their lack on fertilization. These limitations are the housing conditions, the mating protocol and the very high fertility of this model. For instance, concerning the housing conditions, the function of MAGE cancer testis antigens to protect the male germline is revealed only when males are subjected to an environmental stress (***Fon Tacer et al., 2019***). For mating protocol, the phenotyping is performed in particular conditions where mutated males are mated with wild-type females, without competition and in breeding conditions masking complex phenotypes. An example of such a limitation of classical reproductive phenotyping has been emphasized in the study on the importance of the Pkdrej protein in sperm capacitation (***Sutton et al., 2008***). Another remarkable exemple is the phenotype of Enkurin KO mice, with variable impact on litter size, despite the function of the protein in flagellum beating (***Jungnickel et al., 2018***). Overall, the highly significant increase of sperm defects (decrease of sperm motility and increase of head morphological defects) induced by the accumulation of deficient proteins shown in this study would probably impact male fertility in more challenging conditions in mouse. Moreover, the mouse model has much higher fertility than human. Human spermatogenesis is clearly less efficient than that of mice and the level of male infertility is around 15% whereas is less than 1% in mice. It is therefore to be expected that the various defects we noticed in this study will impact more severely human sperm fertilizing competence.

A similar mutational burden in humans, known to have the highest number of sperm defect among primates (***Martinez and Garcia, 2020***), could, however, be sufficient to reach the threshold for fertility collapse. It is worth noting that the probability of accumulating this type of heterozygous mutations in testis is considerable, because (i) thousands of genes are necessary to achieve spermatogenesis (***Jan et al., 2017***), (ii) expression of most spermatogenesis-associated genes is restricted to or strongly enriched in the testis (***Uhlén et al., 2016***), and consequently (iii) the risk of life-threatening impact of mutations is limited.

Moreover, mutant gene products retaining some residual function could be influenced by additional systemic perturbation (see review in ***Vander Borght and Wyns, 2018***) that would lead to system collapse. For instance, environmental factors commonly responsible for milder alterations to spermatogenesis could play an important role by severely aggravating the genetic burden on the system. This type of multi-factorial input could explain the phenotypic continuum observed in patients with idiopathic infertility.

In this article, we showed that the haplo-insufficiency of several genes involved in flagellum biogenesis and associated with MMAF syndrome leads to head defects. When one thinks of MMAF patients,

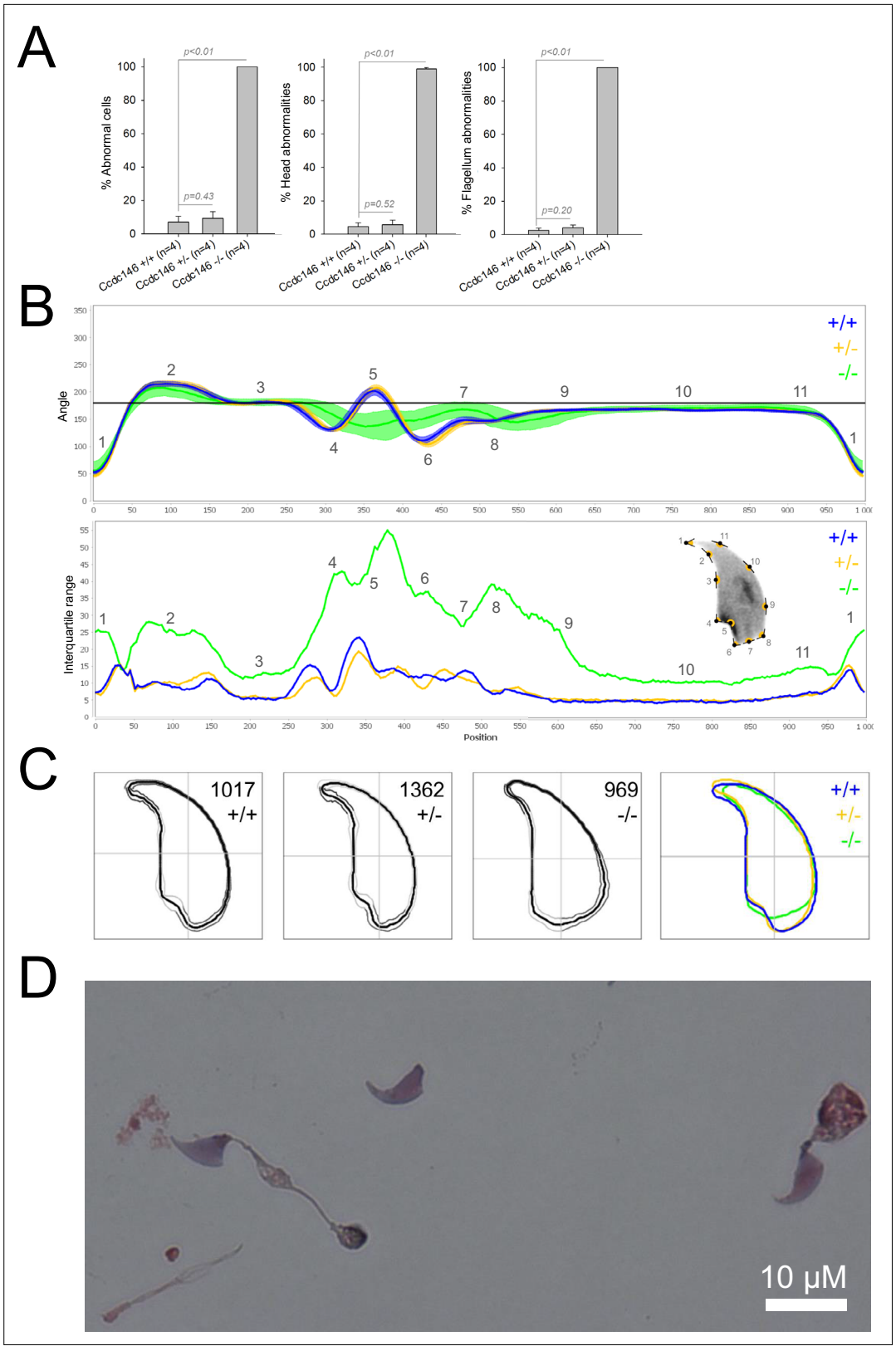

Figure 4. Sperm morphology analysis for the *Ccdc146* mouse strain.
(**A**) Histogram showing proportions of morphological anomalies (mean ± SD) for each *Ccdc146* genotype. Statistical significance was assessed by applying an unpaired Welch *t*-test; *p*-values are indicated. (**B**) Angle profiles (top) and variability profiles (bottom) for *Ccdc146*$^{+/+}$ (blue), *Ccdc146*$^{+/-}$ (yellow) and *Ccdc146*$^{-/-}$ (green)

Figure 4 continued on next page

Figure 4 continued

mice. The x axis represents an index of the percentage of the total perimeter as measured counterclockwise from the apex of the sperm hook. The y axis corresponding to the angle profile is the interior angle measured across a sliding window centered on each index location. The y axis corresponding to the variability profile represents the Interquartile Range (IQR) (the difference between the 75th and 25th percentiles). Specific regions of the nuclei are mapped on the profile and the graphical representation (from ***Skinner et al., 2019***) with: 1-tip; 2-under-hook concavity; 3-vertical; 4-ventral angle; 5-tail socket; 6-caudal bulge; 7-caudal base; 8-dorsal angle; 9–11-acrosomal curve. (**C**) Consensus nuclear outlines for each genotype alongside a merged consensus nucleus (blue = *Ccdc146*$^{+/+}$, yellow = *Ccdc146*$^{+/-}$, green = *Ccdc146*$^{-/-}$). The numbers assigned to each consensus outline correspond to the number of nuclei processed per condition. (**D**) Optical microscopy analysis showing a typical MMAF phenotype for *Ccdc146* KO mice (scale bar, 10 µm).

one immediately visualizes flagellar defects. However, the phenotype is more complex and head defects have been associated with the flagellar phenotype since the first publications (***Coutton et al., 2018***; ***Dong et al., 2018***). This is particularly the case for CFAP43/44 described in this report showing that the complete lack of these genes in KO males also strongly alters head patterning (***Coutton et al., 2018***). These head defects can actually be explained by the molecular function of the genes studied: CFAP43 is involved in intra-manchette transport (***Yu et al., 2021***) and it has been previously shown through the study of several genes such as Azh (***Mendoza-Lujambio et al., 2002***), Clip170 (***Akhmanova et al., 2005***), Rim-bp3 (***Zhou et al., 2009***), or Azil (***Hall et al., 2013***), that manchette modifications impact the head shape of the sperm. The implication of ARMC2 in intraflagellar transport

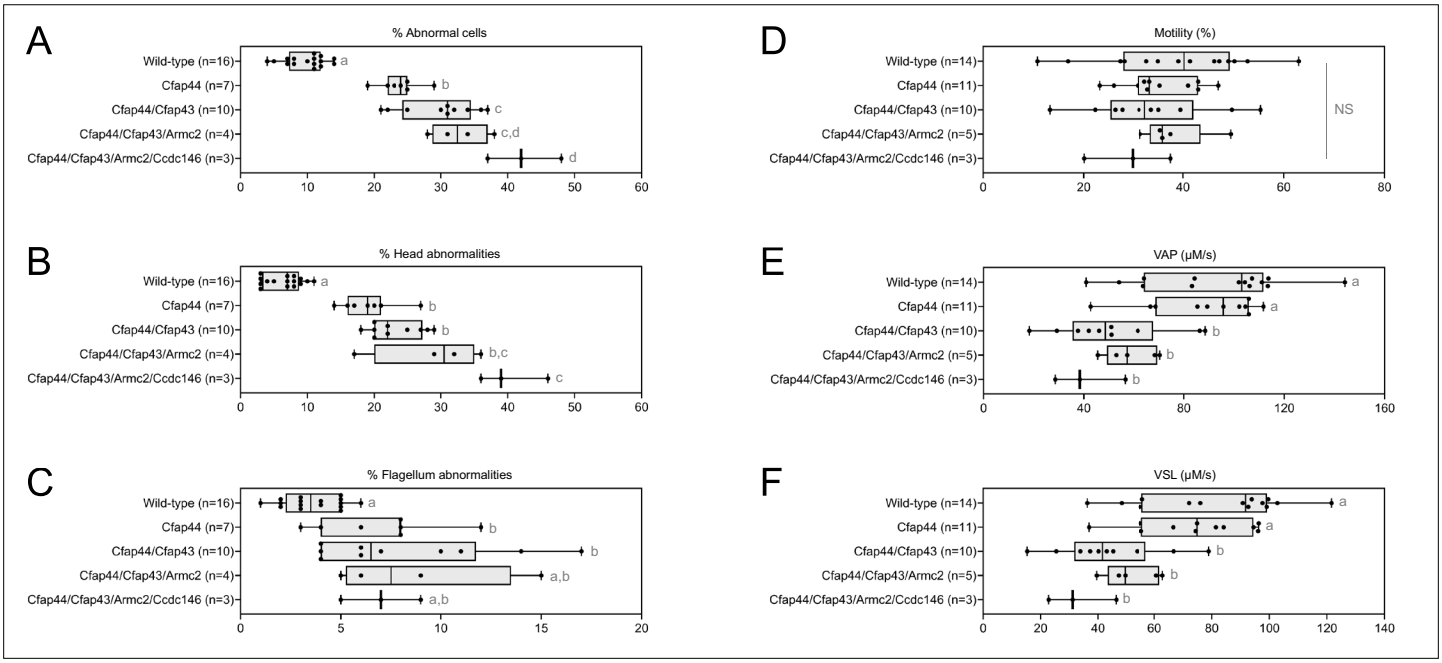

Figure 5. Increasing the number of heterozygous mutated genes involved in the MMAF syndrome has a drastic effect on sperm morphology and motility. (**A**) Sperm morphological defects, (**B**) head defects, (**C**) flagellum defects, showing only slight impact. Increasing the number of heterozygous gene mutations had little effect on (**D**) Percentage of motile sperm, but considerably reduced sperm motility parameters including (**E**) average path velocity (VAP), and (**F**) curvilinear velocity (VCL). All data are presented simultaneously as box-plot and individual datapoints. Statistical significance was assessed using an unpaired Welch *t*-test. Each group was compared individually with all other groups one by one. For each histogram, plots sharing different small letters represent statistically significantly differences between the groups ($p < 0.05$), and plots with a common letter do not present statistically significantly differences between the groups ($p > 0.05$). The corresponding statistical data can be found in ***Figure 5—source data 2–3*** and raw data can be found in ***Figure 5—source data 1***.

The online version of this article includes the following source data for figure 5:

Source data 1. Raw data of ***Figure 5***.

Source data 2. Statistical data linked to the Welch t-tests performed in ***Figure 5D–F***.

Source data 3. Statistical data linked to the Welch t-tests performed in ***Figure 5A–C***.

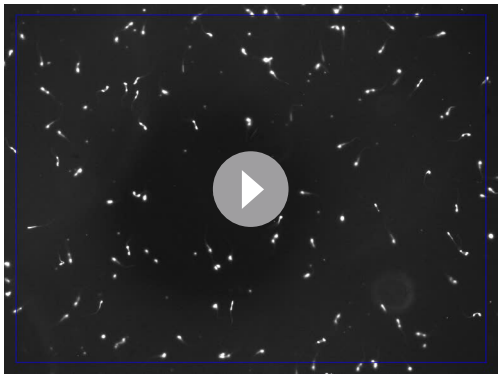

Video 1. Representative video of living sperm cells from wild-type mouse provided by Computer Assisted Sperm Analysis device. Sperm were introduced into a Leja slide (100 µm thick) and maintained at 37 °C during recording.
https://elifesciences.org/articles/75373/figures#video1

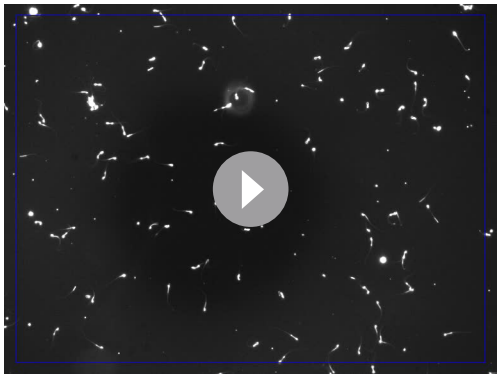

Video 3. Representative video of living sperm cells from mouse bearing two heterozygous mutation provided by Computer Assisted Sperm Analysis device. Sperm were introduced into a Leja slide (100 µm thick) and maintained at 37 °C during recording.
https://elifesciences.org/articles/75373/figures#video3

has also recently been shown (***Lechtreck et al., 2022***) and several previous reports associated sperm head malformations with IFT genes, like IFT20 (***Zhang et al., 2016***), IFT25 (***Liu et al., 2017***), IFT27 (***Zhang et al., 2017***), or IFT88 (***San Agustin et al., 2015***). Finally, CCDC146 was described as a centriolar proteins (***Firat-Karalar et al., 2014***) and other centriolar proteins are known to induce sperm head defects (***Hwang et al., 2021***). If the significant increase in head defects can be easily explained, we do not know why flagellar defects increase simultaneously very little.

As descriptions of animal reproductive phenotypes are becoming increasingly sophisticated and standardized (***Houston et al., 2021***), emerging tools such as the software used in this study to analyze nuclear morphology should be used to extensively study reproductive phenotypes, including studies of MMAF syndromes, to accurately document head defects.

For the first time, we were able to objectively document defects linked to MMAF using NMAS. This original method allows objective comparison of the impact of mutations on sperm head morphology. We found for *Cfap43*$^{-/-}$ and *Cfap44*$^{-/-}$ mice that sperm heads predominantly displayed a 'pepper' shape – characterized by a broadening of the base (median widths of body were 3.44 ± 0.09 µm and 3.93 ± 0.09 µm for *Cfap43*$^{-/-}$ and *Cfap44*$^{-/-}$ respectively, versus 2.95 ± 0.06 µm and 3.09 ± 0.12 µm for *Armc2*$^{-/-}$ and *ccdc146*$^{-/-}$ mice, respectively) and that the flagellum insertion notch had a reduced

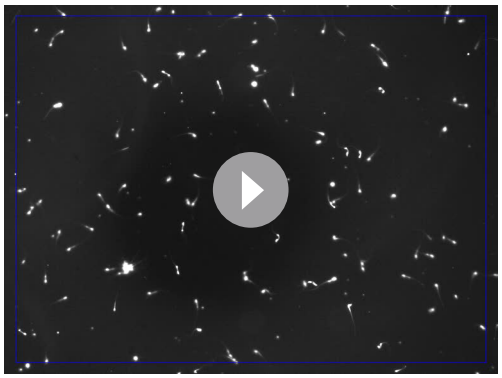

Video 2. Representative video of living sperm cells from mouse bearing one heterozygous mutation provided by Computer Assisted Sperm Analysis device. Sperm were introduced into a Leja slide (100 µm thick) and maintained at 37 °C during recording.
https://elifesciences.org/articles/75373/figures#video2

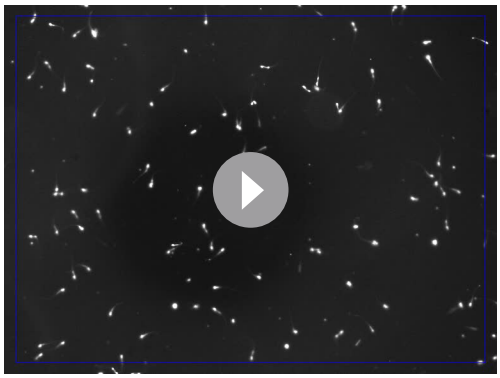

Video 4. Representative video of living sperm cells from mouse bearing three heterozygous mutation provided by Computer Assisted Sperm Analysis device. Sperm were introduced into a Leja slide (100 µm thick) and maintained at 37°C during recording.
https://elifesciences.org/articles/75373/figures#video4

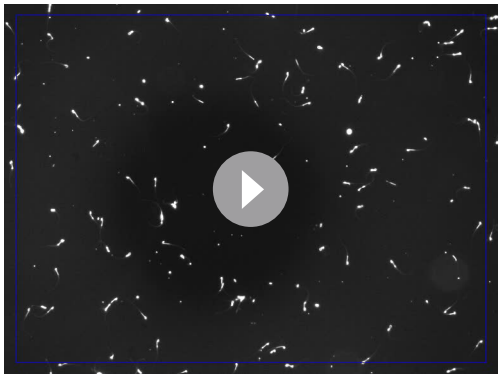

Video 5. Representative video of living sperm cells from mouse bearing four heterozygous mutation provided by Computer Assisted Sperm Analysis device. Sperm were introduced into a Leja slide (100 µm thick) and maintained at 37 °C during recording.
https://elifesciences.org/articles/75373/figures#video5

size. *Armc2*$^{-/-}$ sperm show moderate enlargement extending along the entire length of the head, including the hook (length of hook increase from 7.55 ± 0.03 µm to 8.23 ± 0.05 µm between *Armc2*$^{+/+}$ and *Armc2*$^{-/-}$ mice), and an increase in circularity (increase from 0.55 to 0.61 between *Armc2*$^{+/+}$ and *Armc2*$^{-/-}$ mice) resulting in a more rounded appearance. *Ccdc146*$^{-/-}$ sperm presented a total disorganization of the base with complete erasure of the flagellum insertion notch, and an overall decrease in size (mean area decrease from 111.86 ± 0.41 µm² to 96.78 ± 1.08 µm² between *ccdc146*$^{+/+}$ and *ccdc146*$^{-/-}$ mice), resulting in heads with a triangular aspect characteristic of the 'claw' shape. It is worth to note that the effect on sperm head shape was gene-dependent, with a milder effect observed for *Armc2* and a stronger effect observed for *Cfap43*, *Cfap44*, and *Ccd146*. This result was notable as the flagellum phenotype of *Armc2* is as severe as that observed with mutation of the other genes. Consequently, sperm head defects are not due to failed flagellum biogenesis. Thus, compared to the other proteins, Armc2 may be less involved in functions other than flagellum biogenesis. It should be noted that NMAS analysis is complementary to the human visual analysis made from optical microscopy and does not replace it because the nature of the detected defects is slightly different. Indeed, the software can detect fine nuclear shape anomalies that are undetectable to the human eye and thus reveals morphological variations that are not retained visually by the experimenter. In this study, NMAS revealed a head morphology variation of *Armc2*$^{+/-}$ versus *Armc2*$^{+/+}$ sperm (***Figure 3B***) that had not been detected by visual analysis (***Figure 3A***). On the other hand, NMAS does not identify some abnormalities evidenced by light microscopy stains such as acrosome or flagellum insertion defects. For instance, this was illustrated by the similarity of the nuclear profiles observed between *Cfap43*$^{+/-}$, *Cfap44*$^{+/-}$ and their wild-type counterparts (+/-), while abnormalities were clearly detected by light microscopy (***Figures 1A and 2A***). To summarize, we believe that NMAS will bring as much to the study of morphological defects of the head as CASA has brought to the study of defects of sperm motility.

Among the proteins encoded by previously identified MMAF genes, some belong to complexes involved in intraflagellar transport (***Liu et al., 2019a***; ***Liu et al., 2019b***; ***Chung et al., 2014***), protein degradation (***Shen et al., 2019***) or unknown processes (***Coutton et al., 2019***; ***Lorès et al., 2018***) that could affect head formation, and subsequently sperm DNA. As there is a strong relationship between cytoskeletal and chromosomal effects, the question of the potential impact of the accumulation of mutations on sperm chromatin organization arises. Another interesting question would be to investigate whether the damaged heads correspond to those carrying the mutated alleles. Future studies will be eagerly awaited to elucidate the molecular basis of oligogenicity in male infertility. Therefore, we recommend that head morphology should not be overlooked when studying MMAF syndromes, despite an obvious focus on flagellum anomalies.Despite a strong focus on sperm head defects, we also showed that sperm motility was altered in the presence of ≥2 heterozygote mutations. Thus, the function of the flagellum is affected, and an absence of morphological defects should therefore not be considered synonymous with absence of functional defects. More importantly, these results support the hypothesis that idiopathic human asthenozoospermia may be due to an accumulation of heterozygous mutations in genes known to be involved in flagellum biogenesis.

To date, the inheritance pattern of isolated male infertility was only known to be Mendelian – that is, based on a single locus – and the possibility of oligogenic inheritance had not been explored. In contrast, an oligogenic etiology for female infertility has been proposed to be associated with primary ovarian insufficiency (POI) by several groups, in particular due to the identification of heterozygous mutations in several genes associated with POI (***Patiño et al., 2017***). Oligogenic inheritance has also previously been suggested in another reproductive disorder: congenital hypogonadotropic

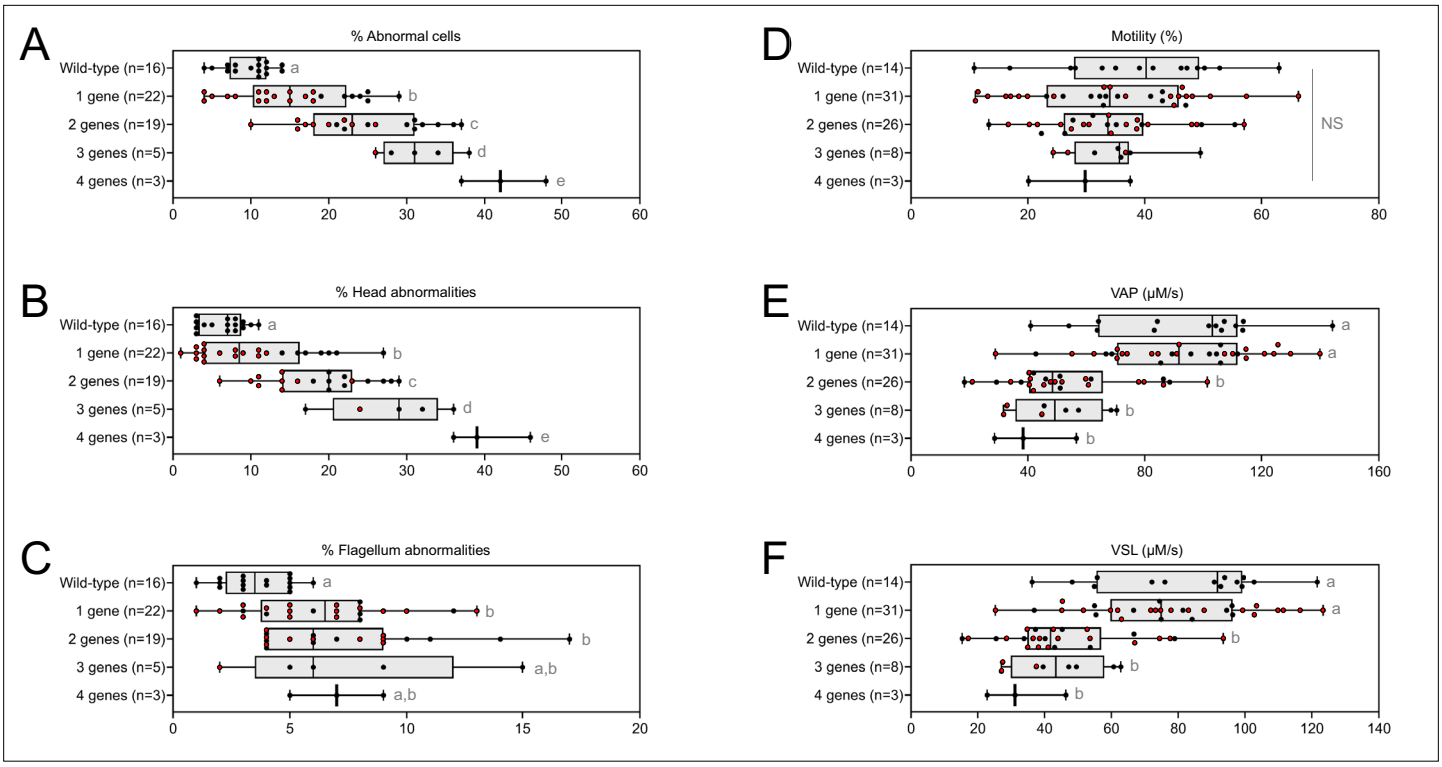

Figure 6. Very similar head morphology defects and decreased motility parameters, whatever the combination of mutated genes. Black dots correspond to the different combinations (2 = *Cfap43* and *Cfap44*; 3 = *Cfap43*, *Cfap44* and *Armc2*; 4 = *Cfap43*, *Cfap44*, *Armc2* and *Ccdc146*) of mutations presented in ***Figure 5***; red dots correspond to alternative combinations obtained with the same four genes. The range of (**A**) sperm morphological defects, (**B**) head anomalies, and (**C**) flagellum defects was similar for black and red dots. Likewise, (**D**) percentage of motile sperm, (**E**) average path velocity (VAP) and (**F**) curvilinear velocity (VCL), showed similar ranges for black and red dots. All data are presented simultaneously as box-plot and individual datapoints. Statistical significance was assessed using unpaired Welch *t*-test. Each group was compared individually with all other groups one by one. For each histogram, plots sharing different small letters represent statistically significantly differences between the groups ($p < 0.05$), and plots with a common letter do not present statistically significantly differences between the groups ($p > 0.05$). Statistical significance of differences between means calculated for all black and red dots were also assessed by applying an unpaired Welch *t*-test and the corresponding statistical data can be found in ***Figure 6—source data 2–3*** and raw data can be found in ***Figure 6—source data 1***.

The online version of this article includes the following source data for figure 6:

Source data 1. Raw data and genotypes of ***Figure 6***.

Source data 2. Statistical data linked to the Welch t-tests performed in ***Figure 6D–F***.

Source data 3. Statistical data linked to the Welch t-tests performed in ***Figure 6A–C***.

hypogonadism (***Pitteloud et al., 2007***), as well as in several non-reproductive disorders (***Li et al., 2017***). Our results demonstrate that oligogenic inheritance may be linked to both male and female human infertility, and should therefore also be accurately measured when investigating male infertility.

In conclusion, in this article, we report the first evidence of oligogenic inheritance in altered spermatogenesis, leading to teratoasthenozoospermia. This mode of inheritance is crucial as oligogenic events could be behind the difficulties encountered by a significant proportion of infertile couples, for whom the current diagnosis is the somewhat unsatisfactory 'unexplained' or 'idiopathic' infertility. Our study was conducted in a context of teratozoospermia, a qualitative disorder of spermatogenesis. It paves the way for further studies on other male infertility disorders, including quantitative disorders, such as oligozoospermia or azoospermia for which the diagnostic yield remains very low. Current genetic tests to explore male infertility focus primarily on identifying low-frequency fully-penetrant monogenic defects, which are usually autosomal recessive and linked to the most severe cases of male infertility. However, investigation of oligogenic inheritance in the huge cohorts available should provide an estimate of the frequency of such events. These investigations could potentially identify new candidate genes involved in male infertility.

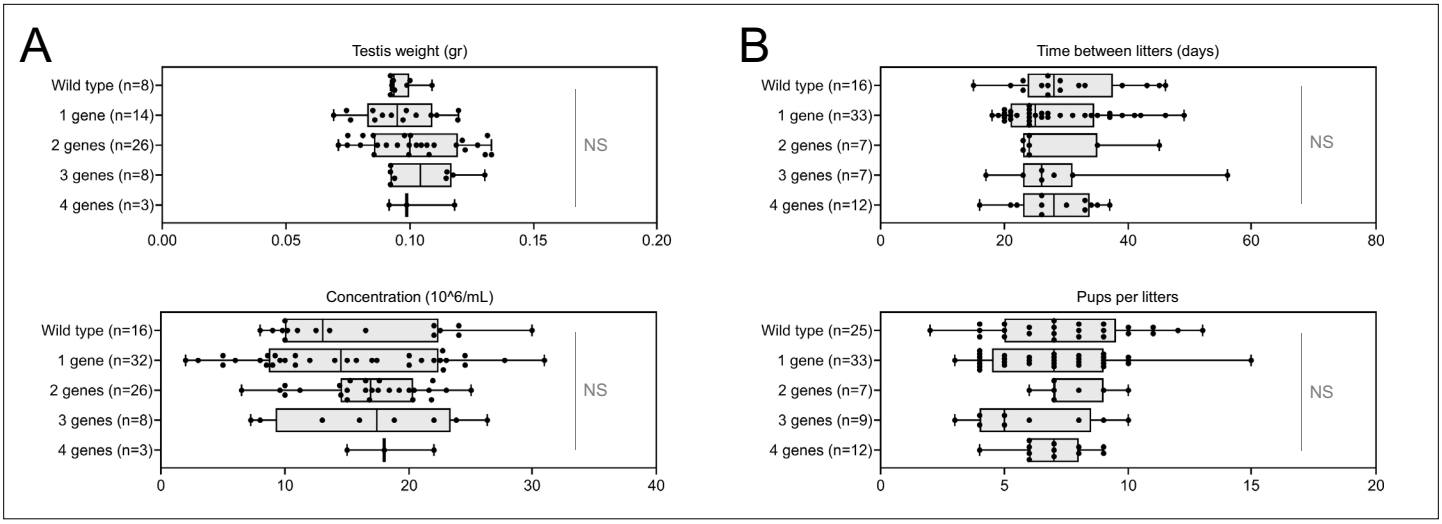

Figure 7. Increasing the number of mutated genes has little effect on overall fertility. (**A**) Sperm production data (**B**)Overall fertility of animals (measured as the interval between two litters and the number of pups per litter). All data are presented simultaneously as box-plot and individual datapoints. Statistical significance was assessed using unpaired Welch *t*-test. Each group was compared individually with all other groups one by one. For each histogram, plots sharing different small letters represent statistically significantly differences between the groups ($p < 0.05$), and plots with a common letter do not present statistically significantly differences between the groups ($p > 0.05$). The corresponding statistical data can be found in ***Figure 7—source data 2*** and raw data can be found in ***Figure 7—source data 1***.

The online version of this article includes the following source data for figure 7:

Source data 1. Raw data and genotypes of ***Figure 7***.

Source data 2. Statistical data linked to the Welch t-tests performed in ***Figure 7B***.

Source data 3. Statistical data linked to the Welch t-tests performed in ***Figure 7A***.

The discovery presented here is of major medical interest, and has implications for both clinical genetics and infertility management. First, the continuous and exponential characterization of new genes involved in infertility over the last decade offers the hope that, in the near future, an almost exhaustive list of genes and mutations involved in human infertility will be available. The identification of and screening for all known mutant alleles linked to male infertility at the heterozygous level should improve the diagnostic yield. Second, the discovery of multiple mutated genes will allow clinicians to provide more accurate genetic counselling to patients, and better guide them in their infertility journey. To improve patient management, future studies should look at potential correlations between patients' mutational burden and their intracytoplasmic sperm injection (ICSI) success, pregnancies achieved, and live birth rates. It will also be essential to assess the impact of mutational load on parameters known to influence these outcomes.

Materials and methods

Animals

Generation of *Cfap43* and *Cfap44* KO mice is described in ***Coutton et al., 2018***, generation of *Armc2* KO mice is described in ***Coutton et al., 2019***. CRISPR/Cas9 gene editing was used to produce *Ccdc146* KO mice (ENSMUST00000115245). To maximize the chances of producing deleterious mutations, two gRNAs located in two distinct coding exons positioned at the beginning of the targeted gene were used. For each gene, the two gRNAs (5'-CCT ACA GTT AAC ATT CGG G-3' and 5'-GGG AGT ACA ATA TTC AGT AC-3') targeting exons 2 and 4, respectively, were inserted into two distinct plasmids also containing the Cas9 sequence. The Cas9 gene was driven by a CMV promoter and the gRNA and its RNA scaffold by a U6 promoter. Full plasmids (pSpCas9 BB-2A-GFP (PX458)) containing the specific sgRNA were ordered from Genescript (https://www.genscript.com/crispr-cas9-protein-crRNA.html). Both plasmids were co-injected into the zygotes' pronuclei at a concentration of 2.5 ng/ml. It should be noted that the plasmids were injected as delivered by the supplier, thus avoiding the need to perform in vitro production and purification of Cas9 proteins and sgRNA. Several mutated

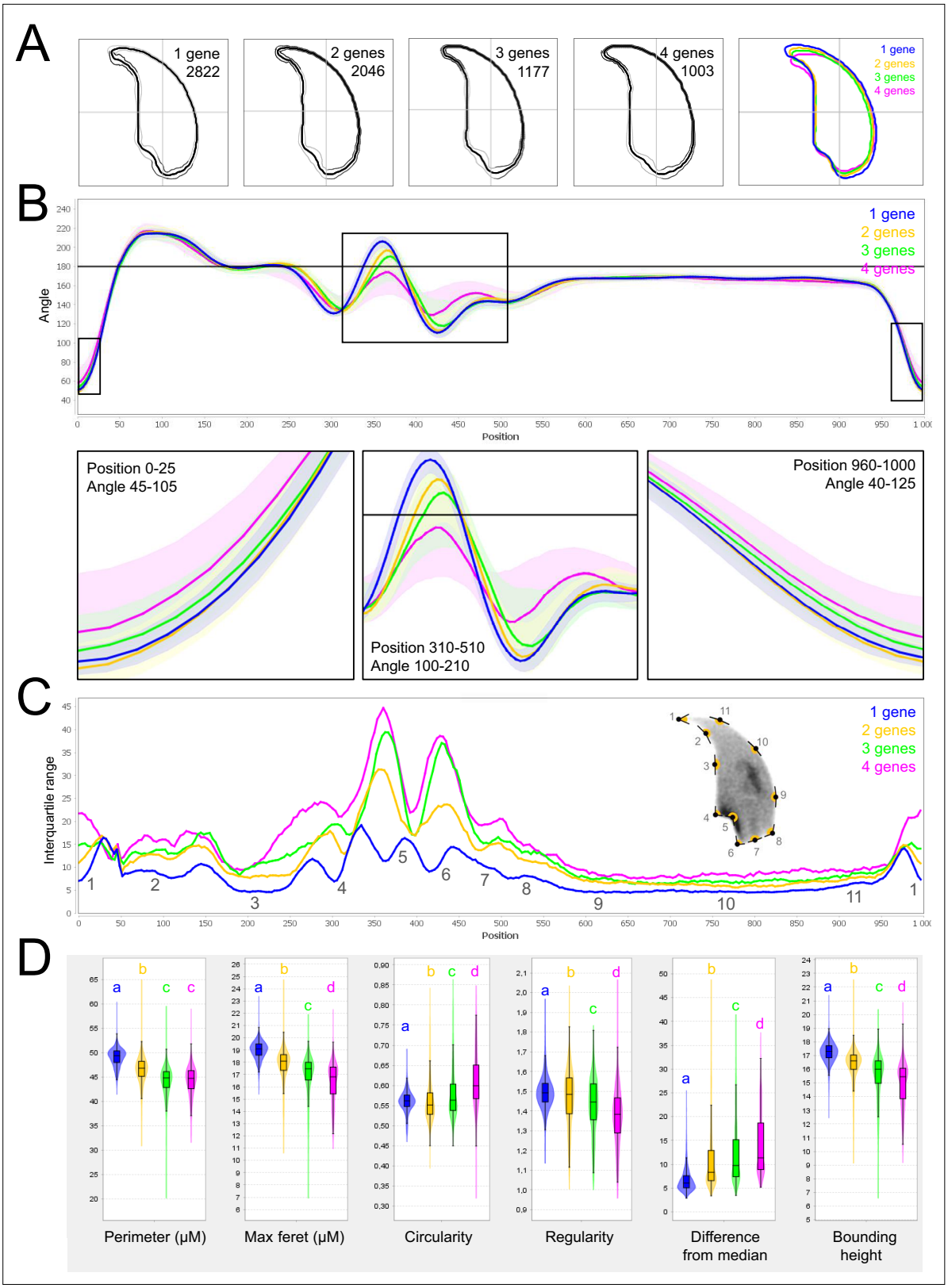

Figure 8. Fine nuclear morphology analysis of multi-mutant mice with one to four heterozygous mutations.
(**A**) Consensus nuclear outlines for each strain alongside a merged consensus nucleus (blue = one mutation, yellow = two mutations, green = three mutations and pink = four mutations). The numbers assigned to each consensus outline correspond to the number of nuclei processed per condition. (**B**) Angle profiles for each strain focusing (black boxes) on positions of specific interest. The x axis represents an index of the percentage of the total

Figure 8 continued on next page

Figure 8 continued

perimeter, as measured counterclockwise from the apex of the sperm hook. The y axis shows the interior angle measured across a sliding window centered on each index location. (**C**) Variability profiles for each strain. The x axis is the same as for the angle profile, and the y axis represents the Interquartile Range (IQR) (the difference between the 75th and 25th percentiles). Specific regions of the nuclei are mapped on the profile and the graphical representation (from ***Skinner et al., 2019***), with: 1-tip; 2-under-hook concavity; 3-vertical; 4-ventral angle; 5-tail socket; 6-caudal bulge; 7-caudal base; 8-dorsal angle; 9–11-acrosomal curve. (**D**) Violin plots of nuclear parameters for each strain. Statistical significance of differences between populations were assessed by the software, applying a Mann-Whitney U test; significantly different populations are identified by distinct letters.

animals were obtained with different insertions/deletions spanning a few nucleotides. All the mutations obtained induced a translational frameshift expected to lead to complete absence of the protein or production of a truncated protein. The reproductive phenotype of two mutated lines was analyzed; homozygous males were infertile and displayed the same MMAF phenotype. For this study, a strain with a 4 bp deletion in exon 2 was used (c.164_167delTTCG).

For each KO strain, mice were maintained in the heterozygous state, and males and females were crossed to produce animals for subsequent generations. Heterozygous and homozygous animals were selected following PCR screening, the primers used for each strain are indicated in ***Appendix 1—figure 1B***. To produce multi-heterozygous animals, homozygous females were crossed with heterozygous males.

All animal procedures were conducted according to a protocol approved by the local Ethics Committee (ComEth Grenoble No. 318), by the French government (ministry agreement number #7,128 UHTA-U1209-CA), and by the Direction Générale de la Santé (DGS) for the State of Geneva. Guide RNA, TracrRNA, ssDNA, and Cas9 were purchased from Integrated DNA Technologies. Pronuclear injection and embryo transfer were performed by the Transgenic Core facility at the Faculty of Medicine, University of Geneva. All genotypes were obtained by conventional interbreeding.

Reproductive phenotyping

All adult male mice used were between 10 and 12 weeks old. After sacrifice by cervical dislocation, the testes were isolated and weighed, and sperm from caudae epididymides were allowed to swim for 10 min at 37 °C in 1 ml of M2 medium (Sigma-Aldrich, L'Isle d'Abeau, France). The sperm concentration was measured and adjusted before CASA analysis. An aliquot of sperm suspension was immediately placed in a 100 µm deep analysis chamber (Leja Products B.V., Nieuw-Vennep, the Netherlands), and sperm motility parameters were measured at 37 °C using a sperm analyzer (Hamilton Thorn Research, Beverley, MA, USA). The settings used for analysis were: acquisition rate: 60 Hz; number of frames: 45; minimum contrast: 50; minimum cell size: 5; low static-size gate: 0.3; high static-size gate: 1.95; low static-intensity gate: 0.5; high static-intensity gate: 1.3; minimum elongation gate: 0; maximum elongation gate: 87; magnification factor: 0.7. Motile sperm were defined by an average path velocity (VAP) >1, and progressive sperm motility was defined by VAP >30 and average path straightness >70. A minimum of 200 motile spermatozoa were analyzed in each assay. Remaining sperm was rinsed with PBS-1X, centrifuged for 5 min at 500 g, spread on slides and allowed to dry at room temperature. Samples were then fixed in Ether/Ethanol 1:1 for Harris-Schorr staining (to assess overall morphology) or in 4% paraformaldehyde for DAPI staining (to assess nuclear morphology).

Morphology was visually assessed on a Nikon Eclipse 80i microscope equipped with a Nikon DS-Ri1 camera with NIS-ElementsD (version 3.1.) software by trained experimenters. At least 200 spermatozoa were counted per slide at a magnification of ×1000. Cells are classified as abnormal when they bear at least one morphological defect, either on the head or the flagellum. Normal head morphology is defined by a typical murine overall shape with a pointy kook tip, a well-defined flagellum insertion notch in continuation of a smooth central region, a prominent caudal buldge and a dorsal region without notches. Normal flagellum must be continuous, of regular size and caliber, without angulation or excessive curling. Examples of normal and abnormal morphologies are provided in ***Appendix 1—figure 7***.

Analysis of nuclear morphology

Nuclear morphology was precisely evaluated by NMAS (version 1.19.2, https://bitbucket.org/bmskinner/nuclear_morphology/wiki/Home), according to the analysis method described in ***Skinner et al., 2019***. The software processed images of DAPI-stained nuclei captured with a Zeiss Imager Z2

microscope, using a CoolCube 1 CCD camera, with a 100 x/1.4 Zeiss objective and Neon software (MetaSystems, Altlussheim, Germany). Nucleus detection settings were Kuwahara kernel: 3, and flattening threshold: 100, for preprocessing; canny low threshold: 0.5, canny high threshold: 1.5, canny kernel radius: 3, canny kernel width: 16, gap closing radius: 5, to find objects; and min area: 1 000, max area: 10 000, min circ: 0.1, max circ: 0.9, for filtering. After acquisition of images of nuclei, landmarks were automatically identified using a modification of the Zahn-Roskies transform to generate an angle profile from the internal angles measured around the periphery of the nuclei. Angles were measured at every mouse pixel around the original shape. This method combines data from every possible polygonal approximation into a single unified trace, from which landmark features can be detected (under-hook concavity, tail socket, caudal bulge and base, acrosomal curve, etc.). Angle profiles are presented as angle degrees according to the relative position of each pixel along the perimeter, and variability profiles use the interquartile range (IQR, difference between the third and first quartile) as a dispersion indicator to measure the variability of values obtained for each point. Sperm shape populations were then clustered using a hierarchical ward-distance method without reduction, based on angle profiles.

Statistical analysis

The statistics relating to nuclear morphology presented in ***Figure 8*** and ***Appendix 1—figure 4*** were automatically calculated by the Nuclear Morphology Analysis Software. This analysis relied on a Mann-Whitney U test with Bonferroni multiple testing correction. p-values were considered significant when inferior to 0.05.

All other data were treated with R software (version 3.5.2). Histograms show mean ± standard deviation, and statistical significance of differences was assessed by applying an unpaired Welch *t*-test. Statistical tests with two-tailed p-values ≤ 0.05 were considered significant.

Acknowledgements

We sincerely thank Roxane DOMINGUEZ and Aurélien SIMON for their assistance with the software and IT solutions. We are also grateful to Charlotte GUYOT and Marlène GANDULA for technical assistance.

Additional information

Funding

Funder	Grant reference number	Author
Agence Nationale de la Recherche	ANR-19-CE17-0014	Pierre F Ray Christophe Arnoult
Agence Nationale de la Recherche	ANR-21-CE17-0007	Guillaume Martinez Charles Coutton

The funders had no role in study design, data collection and interpretation, or the decision to submit the work for publication.

Author contributions

Guillaume Martinez, Investigation, Conceptualization, Funding acquisition, Methodology, Supervision, Writing - original draft, Writing - review and editing; Charles Coutton, Investigation, Conceptualization, Formal analysis, Funding acquisition, Methodology, Resources, Supervision, Writing - original draft, Writing - review and editing; Corinne Loeuillet, Caroline Cazin, Jana Muroňová, Magalie Boguenet, Emeline Lambert, Magali Dhellemmes, Geneviève Chevalier, Jean-Pascal Hograindleur, Charline Vilpreux, Yasmine Neirijnck, Zine-Eddine Kherraf, Jessica Escoffier, Funding acquisition; Serge Nef, Funding acquisition, Resources; Pierre F Ray, Investigation, Formal analysis, Methodology, Resources, Writing - original draft; Christophe Arnoult, Investigation, Conceptualization, Formal analysis, Methodology, Project administration, Resources, Supervision, Writing - original draft, Writing - review and editing

Author ORCIDs
Guillaume Martinez http://orcid.org/0000-0002-7572-9096
Jessica Escoffier http://orcid.org/0000-0001-8166-5845
Christophe Arnoult http://orcid.org/0000-0002-3753-5901

Ethics
All animal procedures were conducted according to a protocol approved by the local Ethics Committee (ComEth Grenoble No. 318), by the French government (ministry agreement number #7128 UHTA-U1209-CA), and by the Direction Générale de la Santé (DGS) for the State of Geneva.

Decision letter and Author response
Decision letter https://doi.org/10.7554/eLife.75373.sa1
Author response https://doi.org/10.7554/eLife.75373.sa2

Additional files

Supplementary files
- Transparent reporting form

Data availability
Figure 5 - Source Data 1, Figure 6 - Source Data 1 and Figure 7 - Source Data 1 contain the numerical data used to generate the figures.

References

Akhmanova A, Mausset-Bonnefont A-L, van Cappellen W, Keijzer N, Hoogenraad CC, Stepanova T, Drabek K, van der Wees J, Mommaas M, Onderwater J, van der Meulen H, Tanenbaum ME, Medema RH, Hoogerbrugge J, Vreeburg J, Uringa E-J, Grootegoed JA, Grosveld F, Galjart N. 2005. The microtubule plus-end-tracking protein CLIP-170 associates with the spermatid manchette and is essential for spermatogenesis. *Genes & Development* **19**:2501–2515. DOI: https://doi.org/10.1101/gad.344505, PMID: 16230537

Andrade-Rocha FT. 2001. Sperm parameters in men with suspected infertility Sperm characteristics, strict criteria sperm morphology analysis and hypoosmotic swelling test. *The Journal of Reproductive Medicine* **46**:577–582 PMID: 11441683.,

Auger J, Jouannet P, Eustache F. 2016. Another look at human sperm morphology. *Human Reproduction (Oxford, England)* **31**:10–23. DOI: https://doi.org/10.1093/humrep/dev251, PMID: 26472152

Beurois J, Cazin C, Kherraf ZE, Martinez G, Celse T, Touré A, Arnoult C, Ray PF, Coutton C. 2020. Genetics of teratozoospermia: Back to the head. *Best Practice & Research. Clinical Endocrinology & Metabolism* **34**:101473. DOI: https://doi.org/10.1016/j.beem.2020.101473, PMID: 33183966

Boivin J, Bunting L, Collins JA, Nygren KG. 2007. International estimates of infertility prevalence and treatment-seeking: potential need and demand for infertility medical care. *Human Reproduction (Oxford, England)* **22**:1506–1512. DOI: https://doi.org/10.1093/humrep/dem046, PMID: 17376819

Chemes EH, Rawe YV. 2003. Sperm pathology: a step beyond descriptive morphology Origin, characterization and fertility potential of abnormal sperm phenotypes in infertile men. *Human Reproduction Update* **9**:405–428. DOI: https://doi.org/10.1093/humupd/dmg034, PMID: 14640375

Chung M-I, Kwon T, Tu F, Brooks ER, Gupta R, Meyer M, Baker JC, Marcotte EM, Wallingford JB. 2014. Coordinated genomic control of ciliogenesis and cell movement by RFX2. *eLife* **3**:e01439. DOI: https://doi.org/10.7554/eLife.01439, PMID: 24424412

Coutton C, Vargas AS, Amiri-Yekta A, Kherraf Z-E, Ben Mustapha SF, Le Tanno P, Wambergue-Legrand C, Karaouzène T, Martinez G, Crouzy S, Daneshipour A, Hosseini SH, Mitchell V, Halouani L, Marrakchi O, Makni M, Latrous H, Kharouf M, Deleuze J-F, Boland A, et al. 2018. Mutations in CFAP43 and CFAP44 cause male infertility and flagellum defects in Trypanosoma and human. *Nature Communications* **9**:686. DOI: https://doi.org/10.1038/s41467-017-02792-7, PMID: 29449551

Coutton C, Martinez G, Kherraf Z-E, Amiri-Yekta A, Boguenet M, Saut A, He X, Zhang F, Cristou-Kent M, Escoffier J, Bidart M, Satre V, Conne B, Fourati Ben Mustapha S, Halouani L, Marrakchi O, Makni M, Latrous H, Kharouf M, Pernet-Gallay K, et al. 2019. Bi-allelic Mutations in ARMC2 Lead to Severe Astheno-Teratozoospermia Due to Sperm Flagellum Malformations in Humans and Mice. *American Journal of Human Genetics* **104**:331–340. DOI: https://doi.org/10.1016/j.ajhg.2018.12.013, PMID: 30686508

Datta J, Palmer MJ, Tanton C, Gibson LJ, Jones KG, Macdowall W, Glasier A, Sonnenberg P, Field N, Mercer CH, Johnson AM, Wellings K. 2016. Prevalence of infertility and help seeking among 15 000 women and men. *Human Reproduction (Oxford, England)* **31**:2108–2118. DOI: https://doi.org/10.1093/humrep/dew123, PMID: 27365525

Dipple KM, McCabe ER. 2000. Phenotypes of patients with "simple" Mendelian disorders are complex traits: thresholds, modifiers, and systems dynamics. *American Journal of Human Genetics* **66**:1729–1735. DOI: https://doi.org/10.1086/302938, PMID: 10793008

Dong FN, Amiri-Yekta A, Martinez G, Saut A, Tek J, Stouvenel L, Lorès P, Karaouzène T, Thierry-Mieg N, Satre V, Brouillet S, Daneshipour A, Hosseini SH, Bonhivers M, Gourabi H, Dulioust E, Arnoult C, Touré A, Ray PF, Zhao H, et al. 2018. Absence of CFAP69 Causes Male Infertility due to Multiple Morphological Abnormalities of the Flagella in Human and Mouse. *American Journal of Human Genetics* **102**:636–648. DOI: https://doi.org/10.1016/j.ajhg.2018.03.007, PMID: 29606301

Faddy MJ, Gosden MD, Gosden RG. 2018. A demographic projection of the contribution of assisted reproductive technologies to world population growth. *Reproductive Biomedicine Online* **36**:455–458. DOI: https://doi.org/10.1016/j.rbmo.2018.01.006, PMID: 29503211

Fauser BC. 2019. Towards the global coverage of a unified registry of IVF outcomes. *Reproductive Biomedicine Online* **38**:133–137. DOI: https://doi.org/10.1016/j.rbmo.2018.12.001, PMID: 30593441

Fernandez-Marmiesse A, Gouveia S, Couce ML. 2018. NGS Technologies as a Turning Point in Rare Disease Research , Diagnosis and Treatment. *Current Medicinal Chemistry* **25**:404–432. DOI: https://doi.org/10.2174/0929867324666170718101946, PMID: 28721829

Firat-Karalar EN, Sante J, Elliott S, Stearns T. 2014. Proteomic analysis of mammalian sperm cells identifies new components of the centrosome. *Journal of Cell Science* **127**:4128–4133. DOI: https://doi.org/10.1242/jcs.157008, PMID: 25074808

Fon Tacer K, Montoya MC, Oatley MJ, Lord T, Oatley JM, Klein J, Ravichandran R, Tillman H, Kim M, Connelly JP, Pruett-Miller SM, Bookout AL, Binshtock E, Kamiński MM, Potts PR. 2019. MAGE cancer-testis antigens protect the mammalian germline under environmental stress. *Science Advances* **5**:eaav4832. DOI: https://doi.org/10.1126/sciadv.aav4832, PMID: 31149633

Hall EA, Keighren M, Ford MJ, Davey T, Jarman AP, Smith LB, Jackson IJ, Mill P. 2013. Acute versus chronic loss of mammalian Azi1/Cep131 results in distinct ciliary phenotypes. *PLOS Genetics* **9**:e1003928. DOI: https://doi.org/10.1371/journal.pgen.1003928, PMID: 24415959

Houston BJ, Conrad DF, O'Bryan MK. 2021. A framework for high-resolution phenotyping of candidate male infertility mutants: from human to mouse. *Human Genetics* **140**:155–182. DOI: https://doi.org/10.1007/s00439-020-02159-x, PMID: 32248361

Hwang JY, Nawaz S, Choi J, Wang H, Hussain S, Nawaz M, Lopez-Giraldez F, Jeong K, Dong W, Oh JN, Bilguvar K, Mane S, Lee CK, Bystroff C, Lifton RP, Ahmad W, Chung JJ. 2021. Genetic Defects in DNAH2 Underlie Male Infertility With Multiple Morphological Abnormalities of the Sperm Flagella in Humans and Mice. *Frontiers in Cell and Developmental Biology* **9**:662903. DOI: https://doi.org/10.3389/fcell.2021.662903, PMID: 33968937

Jan SZ, Vormer TL, Jongejan A, Röling MD, Silber SJ, de Rooij DG, Hamer G, Repping S, van Pelt AMM. 2017. Unraveling transcriptome dynamics in human spermatogenesis. *Development (Cambridge, England)* **144**:3659–3673. DOI: https://doi.org/10.1242/dev.152413, PMID: 28935708

Jungnickel MK, Sutton KA, Baker MA, Cohen MG, Sanderson MJ, Florman HM. 2018. The flagellar protein Enkurin is required for mouse sperm motility and for transport through the female reproductive tract. *Biology of Reproduction* **99**:789–797. DOI: https://doi.org/10.1093/biolre/ioy105, PMID: 29733335

Kherraf Z-E, Christou-Kent M, Karaouzene T, Amiri-Yekta A, Martinez G, Vargas AS, Lambert E, Borel C, Dorphin B, Aknin-Seifer I, Mitchell MJ, Metzler-Guillemain C, Escoffier J, Nef S, Grepillat M, Thierry-Mieg N, Satre V, Bailly M, Boitrelle F, Pernet-Gallay K, et al. 2017. SPINK2 deficiency causes infertility by inducing sperm defects in heterozygotes and azoospermia in homozygotes. *EMBO Molecular Medicine* **9**:1132–1149. DOI: https://doi.org/10.15252/emmm.201607461, PMID: 28554943

Kherraf Z-E, Conne B, Amiri-Yekta A, Kent MC, Coutton C, Escoffier J, Nef S, Arnoult C, Ray PF. 2018. Creation of knock out and knock in mice by CRISPR/Cas9 to validate candidate genes for human male infertility, interest, difficulties and feasibility. *Molecular and Cellular Endocrinology* **468**:70–80. DOI: https://doi.org/10.1016/j.mce.2018.03.002, PMID: 29522859

Kousi M, Katsanis N. 2015. Genetic modifiers and oligogenic inheritance. *Cold Spring Harbor Perspectives in Medicine* **5**:a017145. DOI: https://doi.org/10.1101/cshperspect.a017145, PMID: 26033081

Krausz C. 2011. Male infertility: pathogenesis and clinical diagnosis. *Best Practice & Research. Clinical Endocrinology & Metabolism* **25**:271–285. DOI: https://doi.org/10.1016/j.beem.2010.08.006, PMID: 21397198

Krausz C, Riera-Escamilla A. 2018. Genetics of male infertility. *Nature Reviews. Urology* **15**:369–384. DOI: https://doi.org/10.1038/s41585-018-0003-3, PMID: 29622783

Krzanowska H. 1981. Sperm head abnormalities in relation to the age and strain of mice. *Journal of Reproduction and Fertility* **62**:385–392. DOI: https://doi.org/10.1530/jrf.0.0620385, PMID: 7252920

Lechtreck KF, Liu Y, Dai J, Alkhofash RA, Butler J, Alford L, Yang P. 2022. *Chlamydomonas* ARMC2/PF27 is an obligate cargo adapter for intraflagellar transport of radial spokes. *eLife* **11**:e74993. DOI: https://doi.org/10.7554/eLife.74993, PMID: 34982025

Li L, Bainbridge MN, Tan Y, Willerson JT, Marian AJA. 2017. A Potential Oligogenic Etiology of Hypertrophic Cardiomyopathy. *Circulation Research* **120**:1084–1090. DOI: https://doi.org/10.1161/CIRCRESAHA.116.310559

Liu H, Li W, Zhang Y, Zhang Z, Shang X, Zhang L, Zhang S, Li Y, Somoza AV, Delpi B, Gerton GL, Foster JA, Hess RA, Pazour GJ, Zhang Z. 2017. IFT25, an intraflagellar transporter protein dispensable for ciliogenesis in somatic cells, is essential for sperm flagella formation. *Biology of Reproduction* **96**:993–1006. DOI: https://doi.org/10.1093/biolre/iox029, PMID: 28430876

Liu W, Sha Y, Li Y, Mei L, Lin S, Huang X, Lu J, Ding L, Kong S, Lu Z. 2019a. Loss-of-function mutations in SPEF2 cause multiple morphological abnormalities of the sperm flagella (MMAF. *Journal of Medical Genetics* **56**:678–684. DOI: https://doi.org/10.1136/jmedgenet-2018-105952, PMID: 31151990

Liu W, Wu H, Wang L, Yang X, Liu C, He X, Li W, Wang J, Chen Y, Wang H, Gao Y, Tang S, Yang S, Jin L, Zhang F, Cao Y. 2019b. Homozygous loss-of-function mutations in FSIP2 cause male infertility with asthenoteratospermia. *Journal of Genetics and Genomics = Yi Chuan Xue Bao* **46**:53–56. DOI: https://doi.org/10.1016/j.jgg.2018.09.006, PMID: 30745215

Lorès P, Coutton C, El Khouri E, Stouvenel L, Givelet M, Thomas L, Rode B, Schmitt A, Louis B, Sakheli Z, Chaudhry M, Fernandez-Gonzales A, Mitsialis A, Dacheux D, Wolf J-P, Papon J-F, Gacon G, Escudier E, Arnoult C, Bonhivers M, et al. 2018. Homozygous missense mutation L673P in adenylate kinase 7 (AK7) leads to primary male infertility and multiple morphological anomalies of the flagella but not to primary ciliary dyskinesia. *Human Molecular Genetics* **27**:1196–1211. DOI: https://doi.org/10.1093/hmg/ddy034, PMID: 29365104

Lorès P, Dacheux D, Kherraf Z-E, Nsota Mbango J-F, Coutton C, Stouvenel L, Ialy-Radio C, Amiri-Yekta A, Whitfield M, Schmitt A, Cazin C, Givelet M, Ferreux L, Fourati Ben Mustapha S, Halouani L, Marrakchi O, Daneshipour A, El Khouri E, Do Cruzeiro M, Favier M, et al. 2019. Mutations in TTC29, Encoding an Evolutionarily Conserved Axonemal Protein, Result in Asthenozoospermia and Male Infertility. *American Journal of Human Genetics* **105**:1148–1167. DOI: https://doi.org/10.1016/j.ajhg.2019.10.007, PMID: 31735292

Martinez G, Beurois J, Dacheux D, Cazin C, Bidart M, Kherraf Z-E, Robinson DR, Satre V, Le Gac G, Ka C, Gourlaouen I, Fichou Y, Petre G, Dulioust E, Zouari R, Thierry-Mieg N, Touré A, Arnoult C, Bonhivers M, Ray P, et al. 2020. Biallelic variants in *MAATS1* encoding CFAP91, a calmodulin-associated and spoke-associated complex protein, cause severe astheno-teratozoospermia and male infertility. *Journal of Medical Genetics* **57**:708–716. DOI: https://doi.org/10.1136/jmedgenet-2019-106775, PMID: 32161152

Martinez G, Garcia C. 2020. Sexual selection and sperm diversity in primates. *Molecular and Cellular Endocrinology* **518**:110974. DOI: https://doi.org/10.1016/j.mce.2020.110974, PMID: 32926966

Mascarenhas MN, Flaxman SR, Boerma T, Vanderpoel S, Stevens GA. 2012. National, regional, and global trends in infertility prevalence since 1990: A systematic analysis of 277 health surveys. *PLOS Medicine* **9**:e1001356. DOI: https://doi.org/10.1371/journal.pmed.1001356, PMID: 23271957

McRae J. 2017. Prevalence and architecture of de novo mutations in developmental disorders. *Nature* **542**:433–438. DOI: https://doi.org/10.1038/nature21062, PMID: 28135719

Mendoza-Lujambio I, Burfeind P, Dixkens C, Meinhardt A, Hoyer-Fender S, Engel W, Neesen J. 2002. The Hook1 gene is non-functional in the abnormal spermatozoon head shape (azh) mutant mouse. *Human Molecular Genetics* **11**:1647–1658. DOI: https://doi.org/10.1093/hmg/11.14.1647, PMID: 12075009

Menkveld R, Holleboom CAG, Rhemrev JPT. 2011. Measurement and significance of sperm morphology. *Asian Journal of Andrology* **13**:59–68. DOI: https://doi.org/10.1038/aja.2010.67, PMID: 21076438

Patiño LC, Beau I, Carlosama C, Buitrago JC, González R, Suárez CF, Patarroyo MA, Delemer B, Young J, Binart N, Laissue P. 2017. New mutations in non-syndromic primary ovarian insufficiency patients identified via whole-exome sequencing. *Human Reproduction (Oxford, England)* **32**:1512–1520. DOI: https://doi.org/10.1093/humrep/dex089, PMID: 28505269

Pitteloud N, Quinton R, Pearce S, Raivio T, Acierno J, Dwyer A, Plummer L, Hughes V, Seminara S, Cheng Y-Z, Li W-P, Maccoll G, Eliseenkova AV, Olsen SK, Ibrahimi OA, Hayes FJ, Boepple P, Hall JE, Bouloux P, Mohammadi M, et al. 2007. Digenic mutations account for variable phenotypes in idiopathic hypogonadotropic hypogonadism. *The Journal of Clinical Investigation* **117**:457–463. DOI: https://doi.org/10.1172/JCI29884, PMID: 17235395

Publicover SJ, Barratt CLR. 2011. Sperm motility: things are moving in the lab! *Molecular Human Reproduction* **17**:453–456. DOI: https://doi.org/10.1093/molehr/gar048, PMID: 21712405

Ravaux B, Garroum N, Perez E, Willaime H, Gourier C. 2016. A specific flagellum beating mode for inducing fusion in mammalian fertilization and kinetics of sperm internalization. *Scientific Reports* **6**:31886. DOI: https://doi.org/10.1038/srep31886, PMID: 27539564

Röpke A, Tewes A-C, Gromoll J, Kliesch S, Wieacker P, Tüttelmann F. 2013. Comprehensive sequence analysis of the NR5A1 gene encoding steroidogenic factor 1 in a large group of infertile males. *European Journal of Human Genetics* **21**:1012–1015. DOI: https://doi.org/10.1038/ejhg.2012.290, PMID: 23299922

Sadeghi M. 2015. Unexplained infertility, the controversial matter in management of infertile couples. *Journal of Reproduction & Infertility* **16**:1–2.

San Agustin JT, Pazour GJ, Witman GB. 2015. Intraflagellar transport is essential for mammalian spermiogenesis but is absent in mature sperm. *Molecular Biology of the Cell* **26**:4358–4372. DOI: https://doi.org/10.1091/mbc.E15-08-0578, PMID: 26424803

Shen Y, Zhang F, Li F, Jiang X, Yang Y, Li X, Li W, Wang X, Cheng J, Liu M, Zhang X, Yuan G, Pei X, Cai K, Hu F, Sun J, Yan L, Tang L, Jiang C, Tu W, et al. 2019. Loss-of-function mutations in QRICH2 cause male infertility with multiple morphological abnormalities of the sperm flagella. *Nature Communications* **10**:433. DOI: https://doi.org/10.1038/s41467-018-08182-x, PMID: 30683861

Skinner BM, Rathje CC, Bacon J, Johnson EEP, Larson EL, Kopania EEK, Good JM, Yousafzai G, Affara NA, Ellis PJI. 2019. A high-throughput method for unbiased quantitation and categorization of nuclear morphology†. *Biology of Reproduction* **100**:1250–1260. DOI: https://doi.org/10.1093/biolre/ioz013, PMID: 30753283

Sun H, Gong T-T, Jiang Y-T, Zhang S, Zhao Y-H, Wu Q-J. 2019. Global, regional, and national prevalence and disability-adjusted life-years for infertility in 195 countries and territories, 1990-2017: results from a global

burden of disease study, 2017. *Aging* **11**:10952–10991. DOI: https://doi.org/10.18632/aging.102497, PMID: 31790362

Sutton KA, Jungnickel MK, Florman HM. 2008. A polycystin-1 controls postcopulatory reproductive selection in mice. *PNAS* **105**:8661–8666.

Touré A, Martinez G, Kherraf Z-E, Cazin C, Beurois J, Arnoult C, Ray PF, Coutton C. 2021. The genetic architecture of morphological abnormalities of the sperm tail. *Human Genetics* **140**:21–42. DOI: https://doi.org/10.1007/s00439-020-02113-x, PMID: 31950240

Tüttelmann F, Ruckert C, Röpke A. 2018. Disorders of spermatogenesis. *Medizinische Genetik* **30**:12–20. DOI: https://doi.org/10.1007/s11825-018-0181-7

Uhlén M, Hallström BM, Lindskog C, Mardinoglu A, Pontén F, Nielsen J. 2016. Transcriptomics resources of human tissues and organs. *Molecular Systems Biology* **12**:862. DOI: https://doi.org/10.15252/msb.20155865, PMID: 27044256

Vander Borght M, Wyns C. 2018. Fertility and infertility: Definition and epidemiology. *Clinical Biochemistry* **62**:2–10. DOI: https://doi.org/10.1016/j.clinbiochem.2018.03.012, PMID: 29555319

Veltman JA, Brunner HG. 2012. De novo mutations in human genetic disease. *Nature Reviews. Genetics* **13**:565–575. DOI: https://doi.org/10.1038/nrg3241, PMID: 22805709

Vogt PH. 2005. AZF deletions and Y chromosomal haplogroups: history and update based on sequence. *Human Reproduction Update* **11**:319–336. DOI: https://doi.org/10.1093/humupd/dmi017, PMID: 15890785

Xavier MJ, Salas-Huetos A, Oud MS, Aston KI, Veltman JA. 2021. Disease gene discovery in male infertility: past, present and future. *Human Genetics* **140**:7–19. DOI: https://doi.org/10.1007/s00439-020-02202-x, PMID: 32638125

Yu Y, Wang J, Zhou L, Li H, Zheng B, Yang S. 2021. CFAP43-mediated intra-manchette transport is required for sperm head shaping and flagella formation. *Zygote (Cambridge, England)* **29**:75–81. DOI: https://doi.org/10.1017/S0967199420000556, PMID: 33046149

Zhang Z, Li W, Zhang Y, Zhang L, Teves ME, Liu H, Strauss JF, Pazour GJ, Foster JA, Hess RA, Zhang Z. 2016. Intraflagellar transport protein IFT20 is essential for male fertility and spermiogenesis in mice. *Molecular Biology of the Cell* **27**:3705–3716. DOI: https://doi.org/10.1091/mbc.E16-05-0318, PMID: 27682589

Zhang Y, Liu H, Li W, Zhang Z, Shang X, Zhang D, Li Y, Zhang S, Liu J, Hess RA, Pazour GJ, Zhang Z. 2017. Intraflagellar transporter protein (IFT27), an IFT25 binding partner, is essential for male fertility and spermiogenesis in mice. *Developmental Biology* **432**:125–139. DOI: https://doi.org/10.1016/j.ydbio.2017.09.023, PMID: 28964737

Zhou J, Du Y-R, Qin W-H, Hu Y-G, Huang Y-N, Bao L, Han D, Mansouri A, Xu G-L. 2009. RIM-BP3 is a manchette-associated protein essential for spermiogenesis. *Development (Cambridge, England)* **136**:373–382. DOI: https://doi.org/10.1242/dev.030858, PMID: 19091768

Appendix 1

A

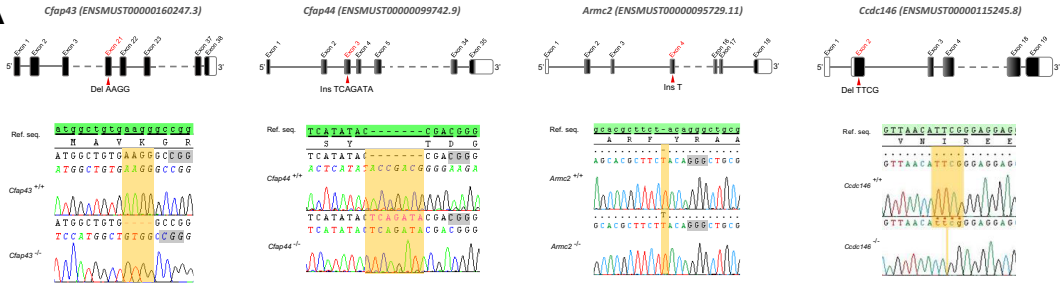

B

Primer name	Sequence (5'->3')	Tm (°C)
*Wdr52*_WT-F	ACACCACAGCTGACTCATATACC	59.87
*Wdr52*_KO-F	CCACAGCTGACTCATATACTCAGA	59.42
*Wdr52*_U-R	TGACAGTTACTGAGAGAGAGCG	59.26
*Wdr96*_WT-F	CCTTTAGAGCCCGGCCCTT	62.4
*Wdr96*_KO-F	CCTTTAGAGCCCGGCCAC	61.2
*Wdr96*_U-R	GACCGACCATAGCGTTGTCT	58.7
*Ccdc146*_Exon4-F	GCAGCTGCTCAAGTACCAAA	58.76
*Ccdc146*_Exon4-R	CCGGGGACTCACCTAGTCA	60.00
*Armc2*_WT-F	GGCCCGAGCACGCTTCTA	61.00
*Armc2*_WT-R	TTCATGTAAGAACTATCCAGGACCA	57.8
*Armc2*_KO-F	TGGGACGCAGCCCTGTAA	59.8
*Armc2*_KO-R	AACCCAAAGCTCCAGCATCTC	59.3

Appendix 1—figure 1. Genetic data associated with strains creation. (**A**) Location of mutations and electropherograms from Sanger sequencing of mutated forms of murine *Cfap43*, *Cfap44*, *Armc2*, and *Ccdc146* compared to their respective reference sequences. We confirmed a 4 bp deletion in *Cfap43* exon 21 (delAAGG), a 7 bp insertion in *Cfap44* exon 3 (InsTCAGATA), a 1 bp insertion (InsT) in *Armc2* exon 4, and a 4 bp deletion in *Ccdc146* exon 2 (delTTCG). Red arrows indicate the CRISPR/Cas9 targeting sequence, mutations are highlighted in yellow, and the gray boxes indicate the position of the protospacer-adjacent motif (PAM) sequences used during mutagenesis. (**B**) List of the primers used for PCR screening of each strain.

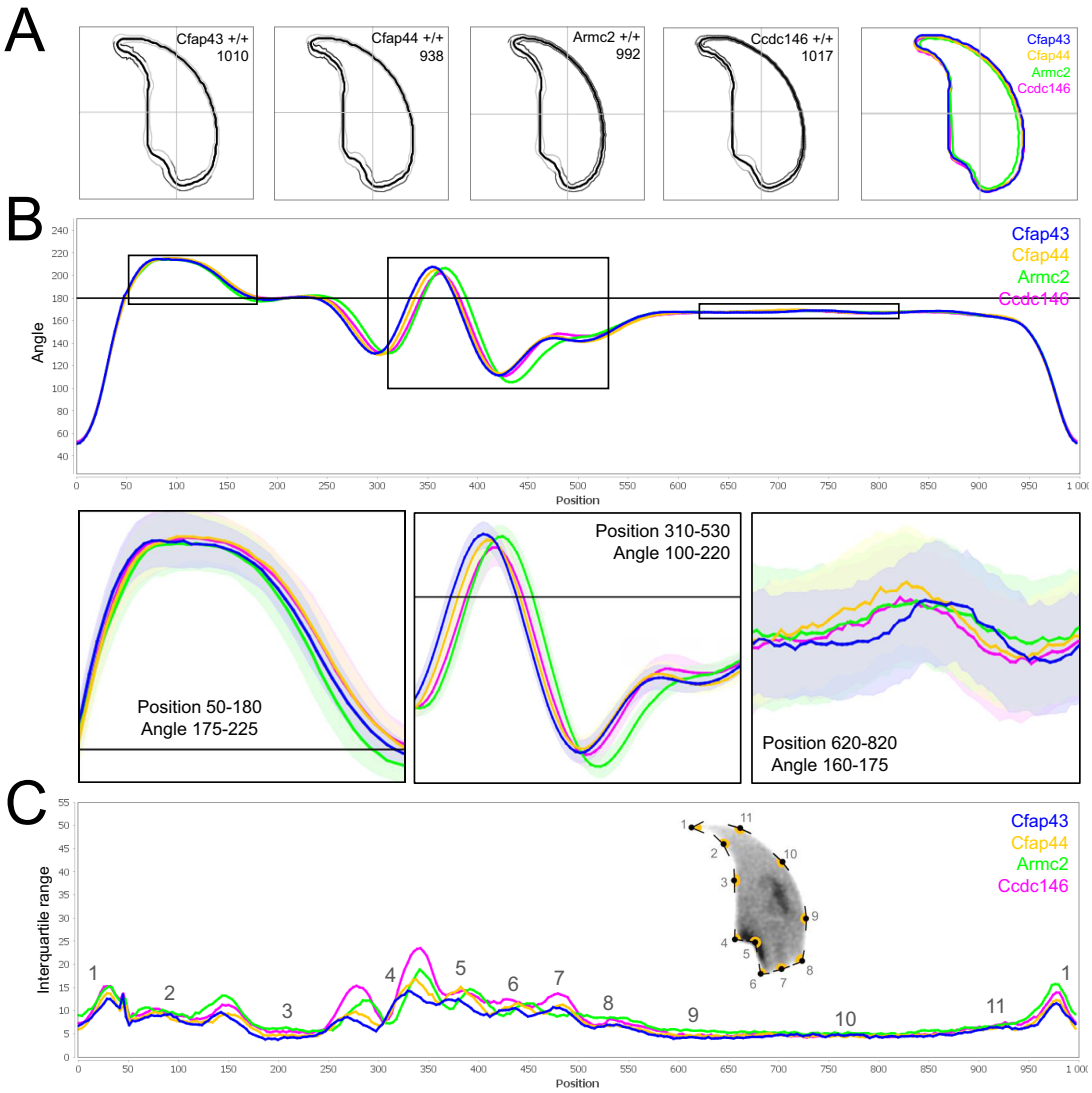

Appendix 1—figure 2. Comparison of fine nuclear morphology for wild-type animals produced from crosses of all strains studied. (**A**) Consensus nuclear outlines for each strain alongside a merged consensus nucleus (blue = *Cfap43*, yellow = *Cfap44*, green = *Armc2* and pink = *Ccdc146*). The numbers assigned to each consensus outline correspond to the number of nuclei processed per condition. (**B**) Angle profiles for each strain focusing (black boxes) on positions of specific interest. The x axis represents an index of the percentage of the total perimeter, as measured counterclockwise from the apex of the sperm hook. The y axis shows the interior angle measured across a sliding window centered on each index location (**C**) Variability profiles for each strain. The x axis is the same as for the angle profile, and the y axis represents the Interquartile Range (IQR) (the difference between the 75th and 25th percentiles). Specific regions of the nuclei are mapped on the profile and the graphical representation (from ***Skinner et al., 2019***), with: 1-tip; 2-under-hook concavity; 3-vertical; 4-ventral angle; 5-tail socket; 6-caudal bulge; 7-caudal base; 8-dorsal angle; 9–11-acrosomal curve.

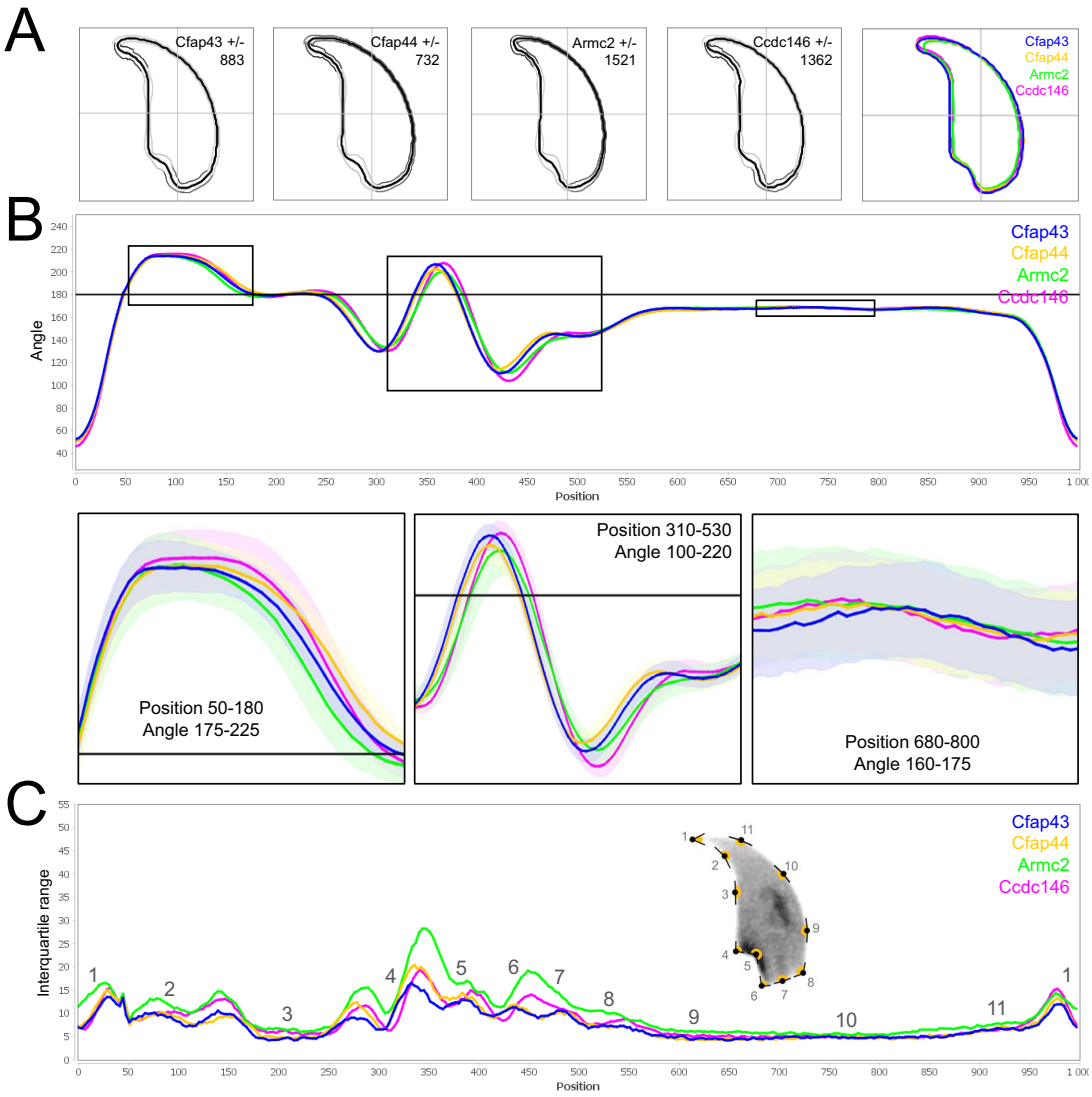

Appendix 1—figure 3. Comparison of fine nuclear morphology for heterozygous animals produced during crosses of all strains. (**A**) Consensus nuclear outlines for each strain alongside a merged consensus nucleus (blue = *Cfap43*, yellow = *Cfap44*, green = *Armc2*, and pink = *Ccdc146*). The numbers assigned to each consensus outline correspond to the number of nuclei processed per condition. (**B**) Angle profiles for each strain focusing (black boxes) on positions of specific interest. The x axis represents an index of the percentage of the total perimeter, as measured counterclockwise from the apex of the sperm hook. The y axis shows the interior angle measured across a sliding window centered on each index location (**C**) Variability profiles for each strain. The x axis is the same as for the angle profile, and the y axis represents the Interquartile Range (IQR) (the difference between the 75th and 25th percentiles). Specific regions of the nuclei are mapped on the profile and the graphical representation (from ***Skinner et al., 2019***) with: 1-tip; 2-under-hook concavity; 3-vertical; 4-ventral angle; 5-tail socket; 6-caudal bulge; 7-caudal base; 8-dorsal angle; 9–11-acrosomal curve.

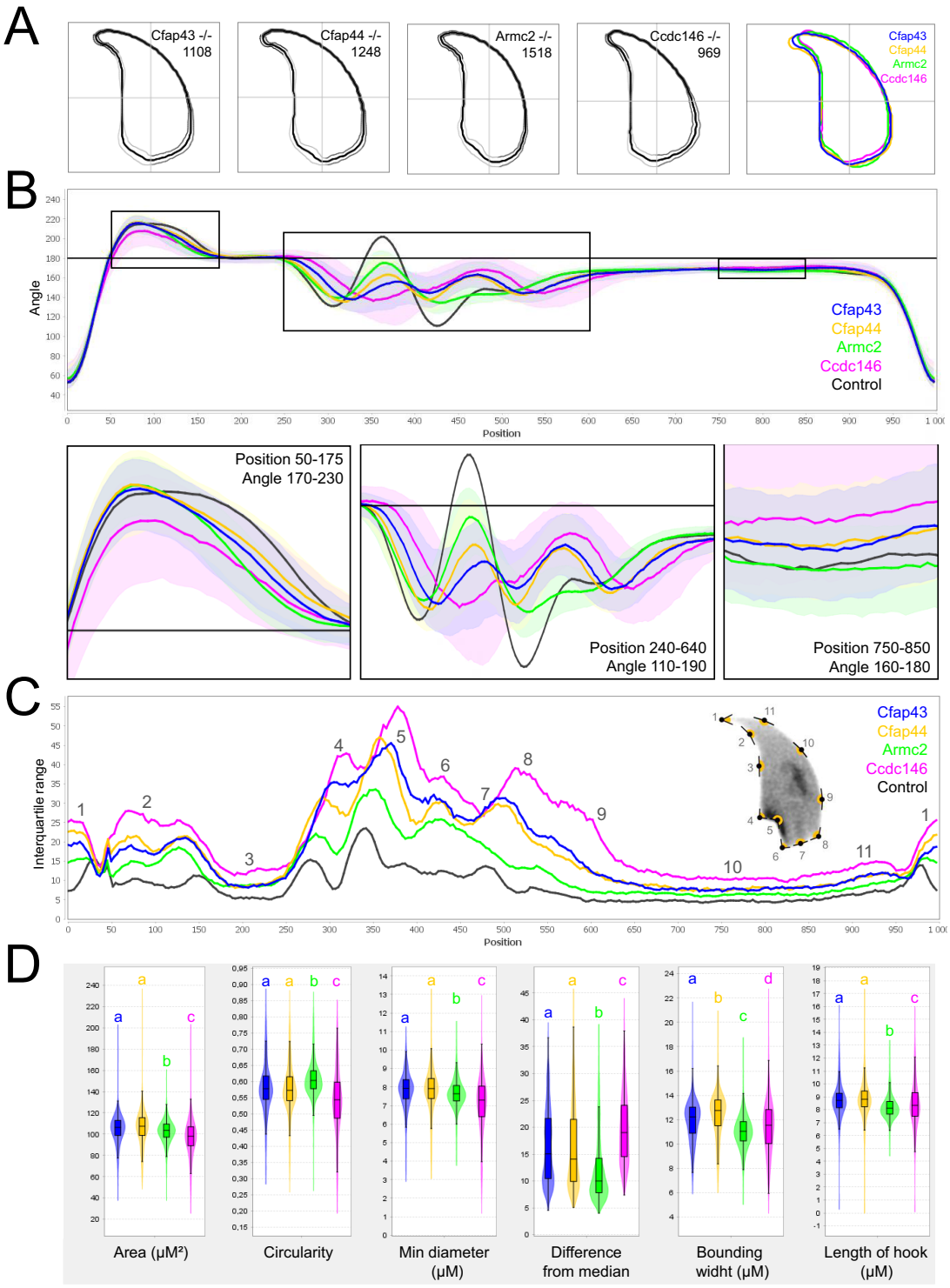

Appendix 1—figure 4. Comparison of fine nuclear morphology for sperm heads from KO and WT animals. (**A**) Consensus nuclear outlines for each KO strain alongside a merged consensus nucleus, and (far right) superimposition of the outlines of the four strains (blue = *Cfap43*, yellow = *Cfap44*, green = *Armc2*, and pink = *Ccdc146*). The numbers assigned to each consensus outline corresponds to the number of nuclei processed per condition. (**B**) Angle profiles for each strain alongside an angle profile for wild-type mice (black), focusing (black boxes) on positions of specific interest. The x axis represents an index of the percentage of the total perimeter, as measured counterclockwise from the apex of the sperm hook. The y axis corresponds to the interior angle measured across a sliding window centered on each index location (**C**) Variability profiles for each strain. The x axis

Appendix 1—figure 4 continued on next page

Appendix 1—figure 4 continued

is the same as for the angle profile, and the y axis represents the Interquartile Range (IQR) value (the difference between the 75th and 25th percentiles). Specific regions of the nuclei are mapped on the profile and the graphical representation (from ***Skinner et al., 2019***), with: 1-tip; 2-under-hook concavity; 3-vertical; 4-ventral angle; 5-tail socket; 6-caudal bulge; 7-caudal base; 8-dorsal angle; 9–11-acrosomal curve. (**D**) Violin plots presenting mean data for representative nuclear parameters associated with each gene. Statistical significance of differences between populations was assessed by the NMAS software, applying a Mann-Whitney U test. Significantly different populations are identified by distinct letters.

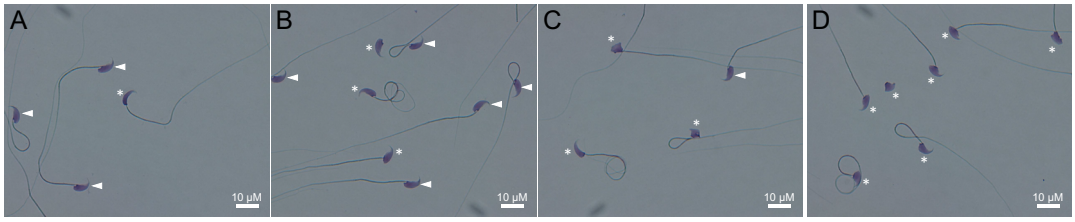

Appendix 1—figure 5. Light microscopy pictures of spermatozoa from mice bearing one mutation (**A**), two mutations (**B**), three mutations (**C**) or four mutations (**D**). Sperm with normal morphology are marked with a white arrow and those with a morphological abnormality are marked with a white asterisk.

Consensus											% abnormal cells
Head shape	Normal	Drop	Pepper	Claw	Sickle	Hammer	Cross	Cap	Lightning	Needle	
No mutation	98.33	0.53	0.00	0.82	0.07	0.18	0.00	0.00	0.00	0.07	1.67
One het. Mutation	95.55	1.48	0.11	1.83	0.30	0.34	0.11	0.04	0.04	0.19	4.45
Two het. Mutations	76.74	3.81	1.03	5.47	1.56	5.38	1.86	2.00	0.68	1.47	23.26
Three het. Mutations	66.60	6.54	3.02	5.53	1.81	6.74	2.92	2.31	1.31	3.22	33.40
Four het. mutations	44.71	3.35	6.26	8.53	3.24	7.34	10.04	4.64	3.13	8.75	55.29

Appendix 1—figure 6. Consensus and percentage distribution of the distinct sperm populations classified based on nuclear morphology and according to the number of heterozygous mutations.

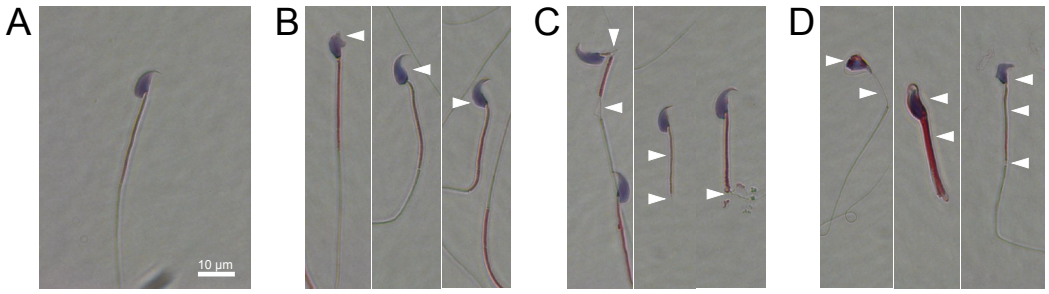

Appendix 1—figure 7. Light microscopy pictures of Harris-Schorr stained spermatozoa with (**A**) typical morphology, (**B**) head abnormalities, (**C**) flagellum abnormalities or (**D**) head and flagellum abnormalities. Defects are pointed by white arrows.

ARTICLE 3

"Paternal epigenetics: Mammalian sperm provide much more than DNA at fertilization"

Emilie Le Blévec, **Jana Muroňová**, Pierre F. Ray, Christophe Arnoult

Published review in *Molecular and Cellular Endocrinology* (2020)

DOI: 10.1016/j.mce.2020.110964

Contribution: I participated in article writing and figure preparation.

Summary:

In this review, we discuss the role of epigenetic factors during spermatogenesis and the potential roles of the epigenome and non-coding RNAs in embryo development and transgenerational inheritance. The histone-to-protamine transition during spermatogenesis includes a progressive replacement of histones by transition proteins and then by protamines. It is tightly regulated by the incorporation of histone variants and by post-translational histone modifications. Human spermatozoa are believed to retain 3-15% of histones, whose location and function remain debated (Bench et al. 1996; Samans et al. 2014). Non-coding RNAs (ncRNA) function during spermatogenesis, particularly regulating gene expression, RNA stability and decay, and transposon silencing (Gou et al. 2014; Song et al. 2011; Schuster et al. 2016). Sperm composition of ncRNAs dramatically changes during post-testicular epididymal maturation due to the incorporation of epididymosomes, vesicles that fuse with sperm during epididymal transit. The sperm especially incorporates micro RNA (miRNA) and transfer RNA-derived fragments (tRFs), and almost all piwi-interacting RNA (piRNA) are lost (U. Sharma et al. 2018; 2016). Mature spermatozoa contain numerous ncRNAs that are stored in both the nucleus and flagella, but their composition differs (U. Sharma et al. 2018). MiRNAs and small endogenous interfering RNAs (endo-siRNAs), as well as sperm mRNAs, that are present in mature spermatozoa, appear to be important for embryo development (Yue Yuan et al. 2017; Conine et al. 2018). A father's diet, (environmental, hormonal, metabolic) stress, and exercise impact the ncRNA content (miRNAs, piRNAs, and tRFs) in both the testis and spermatozoa that can have transgenerational effects and modify the progeny's susceptibility to various pathologies and disorders (Fullston et al. 2013; Ng et al. 2010;

Carone et al. 2010; de Castro Barbosa et al. 2016; Ingerslev et al. 2018; McPherson et al. 2017; da Cruz et al. 2018). Simultaneous changes were observed in DNA methylation (S. Liu et al. 2019). To conclude, spermatozoa not only bring half of the genetic material and activate the egg, but they also bear epigenetic marks and factors that are directly linked to their environment and can have intergeneration and transgenerational impact.

Molecular and Cellular Endocrinology 518 (2020) 110964

Contents lists available at ScienceDirect

Molecular and Cellular Endocrinology

journal homepage: www.elsevier.com/locate/mce

Review

Paternal epigenetics: Mammalian sperm provide much more than DNA at fertilization

Emilie Le Blévec [a,b,c], Jana Muroňová [a,b], Pierre F. Ray [a,b,d], Christophe Arnoult [a,b,*]

[a] Université Grenoble Alpes, Grenoble, F-38000, France
[b] Institute for Advanced Biosciences INSERM U1209, CNRS UMR5309, Grenoble, F-38000, France
[c] IMV Technologies, ZI N° 1 Est, L'Aigle, F-61300, France
[d] CHU de Grenoble, UM GI-DPI, Grenoble, F-38000, France

ARTICLE INFO

Keywords:
Sperm
Protamine
Sperm compaction
Epigenetic
Non-coding RNA
Embryonic development
Environmental stress

ABSTRACT

The spermatozoon is a highly differentiated cell with unique characteristics: it is mobile, thanks to its flagellum, and is very compact. The sperm cytoplasm is extremely reduced, containing no ribosomes, and therefore does not allow translation, and its nucleus contains very closed chromatin, preventing transcription. This DNA compaction is linked to the loss of nucleosomes and the replacement of histones by protamines. Based on these characteristics, sperm was considered to simply deliver paternal DNA to the oocyte. However, some parts of the sperm DNA remain organized in a nucleosomal format, and bear epigenetic information. In addition, the nucleus and the cytoplasm contain a multitude of RNAs of different types, including non-coding RNAs (ncRNAs) which also carry epigenetic information. For a long time, these RNAs were considered residues of spermatogenesis. After briefly describing the mechanisms of compaction of sperm DNA, we focus this review on the origin and function of the different ncRNAs. We present studies demonstrating the importance of these RNAs in embryonic development and transgenerational adaptation to stress. We also look at other epigenetic marks, such as DNA methylation or post-translational modifications of histones, and show that they are sensitive to environmental stress and transmissible to offspring. The post-fertilization role of certain sperm-borne proteins is also discussed.

1. Introduction

Our view of what sperm cells bring to the oocyte and its contribution to human reproduction has dramatically changed since it was first understood, and remains the subject of intense research. Sperm cells, simply called sperm, were identified in the 17th and 18th century, thanks to the development of the microscope by Dutch scientist Antoni Van Leeuwenhoek (1632–1723). Van Leeuwenhoek was the first to observe these strange moving objects within semen that he called "animalcule" (1678, communication at the London Royal Society). At that time, it was hypothesized that the head of the animalcules (sperm) contained a whole tiny human curled up inside (homunculus at this time), whose development would be assured by the female, the egg was considered to act as the placenta. Nicolaas Hartsoecker (1656–1725) was the first to propose an illustration of this hypothesis in 1694 (Hartsoecker, 1694) (Fig. 1).

We now know that this hypothesis was incorrect, but it took more than 200 years to start to decipher the contribution of sperm cells to the new living organism, and important discoveries are still being made. The fact that a spermatozoon provides half of the genetic material, and is at the origin of one of the pronuclei during fertilization was actually discovered two centuries later by several biologists between 1873 and 1883 using various animal models such as starfish (Fol, 1873), sea urchin (Hertwig, 1876) and ascaris (van Beneden, 1883). The discovery that sperm contribute half of the heredity of the embryo was discovered simultaneously 20 years later by Theodor Boveri (1862–1915) and Walter Sutton (1877–1916). In 1902–1903, they proposed that chromosomes bear hereditary factors in accordance with Mendelian laws – first described 37 years previously by the monk Augustin Mendel (1822–1884) – and that sperm provide half of the chromosomes found in the zygote. Soon after this breakthrough, Jacques Loeb (Loeb, 1913) rapidly recognized that the male gamete not only transmits the paternal characteristics to the developing embryo, but also induces development by activating the egg. A second major function of the male gamete,

* Corresponding author. "Genetics, Epigenetics and Therapies of Infertility" Team, Institute for Advanced Biosciences (IAB), INSERM 1209, CNRS UMR 5309, University Grenoble Alpes, Grenoble, France.
E-mail address: christophe.arnoult@univ-grenoble-alpes.fr (C. Arnoult).

https://doi.org/10.1016/j.mce.2020.110964
Received 8 June 2020; Received in revised form 22 July 2020; Accepted 22 July 2020
Available online 29 July 2020

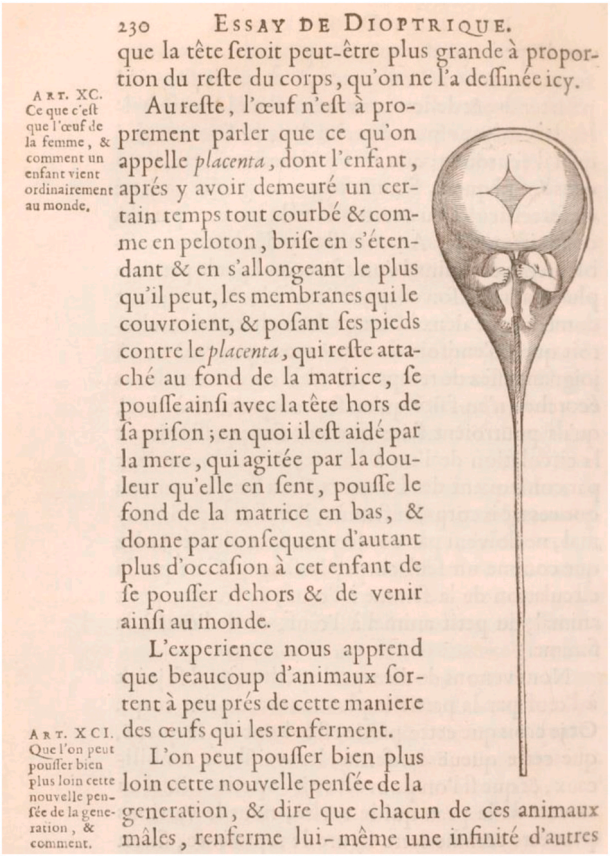
230 ESSAY DE DIOPTRIQUE.

que la tête seroit peut-être plus grande à proportion du reste du corps, qu'on ne l'a dessinée icy.

ART. XC. Ce que c'est que l'œuf de la femme, & comment un enfant vient ordinairement au monde.

Au reste, l'œuf n'est à proprement parler que ce qu'on appelle *placenta*, dont l'enfant, aprés y avoir demeuré un certain temps tout courbé & comme en peloton, brise en s'étendant & en s'allongeant le plus qu'il peut, les membranes qui le couvroient, & posant ses pieds contre le *placenta*, qui reste attaché au fond de la matrice, se pousse ainsi avec la tête hors de sa prison; en quoi il est aidé par la mere, qui agitée par la douleur qu'elle en sent, pousse le fond de la matrice en bas, & donne par consequent d'autant plus d'occasion à cet enfant de se pousser dehors & de venir ainsi au monde.

L'experience nous apprend que beaucoup d'animaux sortent à peu prés de cette maniere des œufs qui les renferment.

ART. XCI. Que l'on peut pousser bien plus loin cette nouvelle pensée de la generation, & comment.

L'on peut pousser bien plus loin cette nouvelle pensée de la generation, & dire que chacun de ces animaux mâles, renferme lui-même une infinité d'autres

Fig. 1. Illustration of the homunculus hypothesis proposed by Antoni Van Leeuwenhoek in 1678 and illustrated by Hartsoecker in 1694 (Hartsoecker, 1694). "Courtesy of The Linda Hall Library of Science, Engineering & Technology".

essential for fertilization, was then identified. The characterization of the sperm-borne factor triggering egg activation was also an epic scientific journey, and culminated in the discovery of PLCzeta (*PLCZ1*) by teams led by Karl Swann and Antony Lay in 2002 (Cox et al., 2002; Saunders et al., 2002). A description of this sperm factor is beyond the scope of this review, and for more information about this key protein, we refer readers to a recent review (Parrington et al., 2019).

For decades, the function of sperm was considered to be limited to these two roles: providing half of the hereditary material in the form of the paternal DNA, and activating the egg. In this review, we will discuss the sperm epigenome, the modifications to the genome that do not affect the DNA sequence but are capable of influencing gene expression, including non-coding RNA, DNA methylation and posttranscriptional modification of histones. We will first present the characteristics of sperm chromatin and the main elements necessary for its organization and compaction. Then, we will describe the epigenetic events occurring in the sperm, the different RNA molecules (mRNAs, regulatory non-coding RNAs) contained in sperm and their origins, and also significant sperm developmental factors including histones and proteins that are retained and transmitted. Finally, we highlight how environmental stress can alter epigenetic factors in sperm, such as DNA methylation and non-coding RNA, causing phenotypic changes in the offspring. These changes not only affect the phenotype of the F1 offspring, but also that of the following F2 generation, even though the F1 generation was not exposed to the initial environmental stress. Nevertheless, this transgenerational transmission of a new phenotype is not permanent and vanishes in most cases after the F3 generation. Readers should note that, "transgenerational transmission" is distinct from "intergenerational transmission", in that the latter only affects the F1 generation (Fig. 2).

2. Sperm DNA compaction

Sperm cells are produced during the spermatogenesis, a very complex physiological process which can be split into three successive steps: mitosis, meiosis, and spermiogenesis and involves the expression of several thousands of genes (Hess and Renato de Franca, 2008). The spermatozoon is undoubtedly the most highly differentiated cell type in mammals, with the greatest number of specific or enriched genes necessary for its biogenesis (Uhlén et al., 2016). Among the many exceptional features of this cell, its DNA organization is unique, showing a high level of compaction leading to an arrest of transcription. Sperm DNA compaction involves replacing nucleosomes by donut-shaped DNA-protamine toroids, with each toroid containing 60 kbp of DNA. This rearrangement results in a highly compact and transcriptionally inactive sperm chromatin (Steger, 1999). For a long time, the histone-to-protamine transition in mammals was considered to take place in two successive stages, with a first stage involving the replacement of histones by transition proteins, and a second stage during which transition proteins are replaced by protamines. However, discoveries in this field over the years revealed the process to be much more complex, and not as linear as it initially seemed. At the beginning of the transition, from spermatogonia to elongated spermatids, the canonical histones (H2A, H2B, H3 and H4) and the H1-linker histone undergo post-translational modifications to facilitate their progressive replacement in nucleosomes by somatic or testicle-specific variants. Each histone variant has its own expression window that is directly related to its specific role during the process of histone-to-protamine transition. The incorporation of histone variants induces chromatin instability that favors nucleosome disassembly. Moreover, post-translational modifications of the variants accentuate chromatin relaxation and allow DNA strand breaks that facilitate the progressive elimination of histone variants and their replacement by transition proteins and protamines (Rathke et al., 2014; Wang et al., 2019). Recently, it was proposed that transition proteins and protamines could be added simultaneously, rather than successively, leading to the formation of a nucleo-protamine structure (Barral et al., 2017).

2.1. Histone variants

The core canonical histones (H3, H4, H2A and H2B) can be replaced by histone variants, changing the structural and functional features of the nucleosomes. Unlike canonical histones, which are incorporated during the S-phase of the cell cycle, histone variants are synthesized and incorporated throughout the cell cycle, in particular during spermiogenesis. Many histone variants have been identified in mammals for H2A, H2B and H3 canonical histones, but none for H4. The H1-linker histone, which influences the degree of compaction of the chromatin, and whose eviction leads to decondensation, also has variants (Thoma et al., 1979). The variants are species-dependent, and human and mouse histone variants only partially overlap.

Compaction of sperm DNA is associated with intense trafficking of histone and histone variants within the nucleosome and its linker, a process that is not fully understood. Histone H1 has at least 11 variants, including the testis variants H1T, H1T2 and HILS1 (TS H1.6, TS H1.7 and TS H1.9, according to the new nomenclature) (El Kennani et al., 2017). H1T is present from the spermatocyte I stage to the elongating spermatid stage (Drabent et al., 1996). H1T maintains a relatively open chromatin configuration, which is necessary for meiotic recombination and histone replacement (Delucia et al., 1994). H1T2 is present from the round spermatid stage to the elongated spermatid stage at the apical pole of the nucleus, under the acrosome. It is required for chromatin condensation, protamine incorporation and cell restructuring (Martianov et al., 2005). HILS1, present from the elongated to the condensed spermatid stages, has a higher DNA binding capacity than other

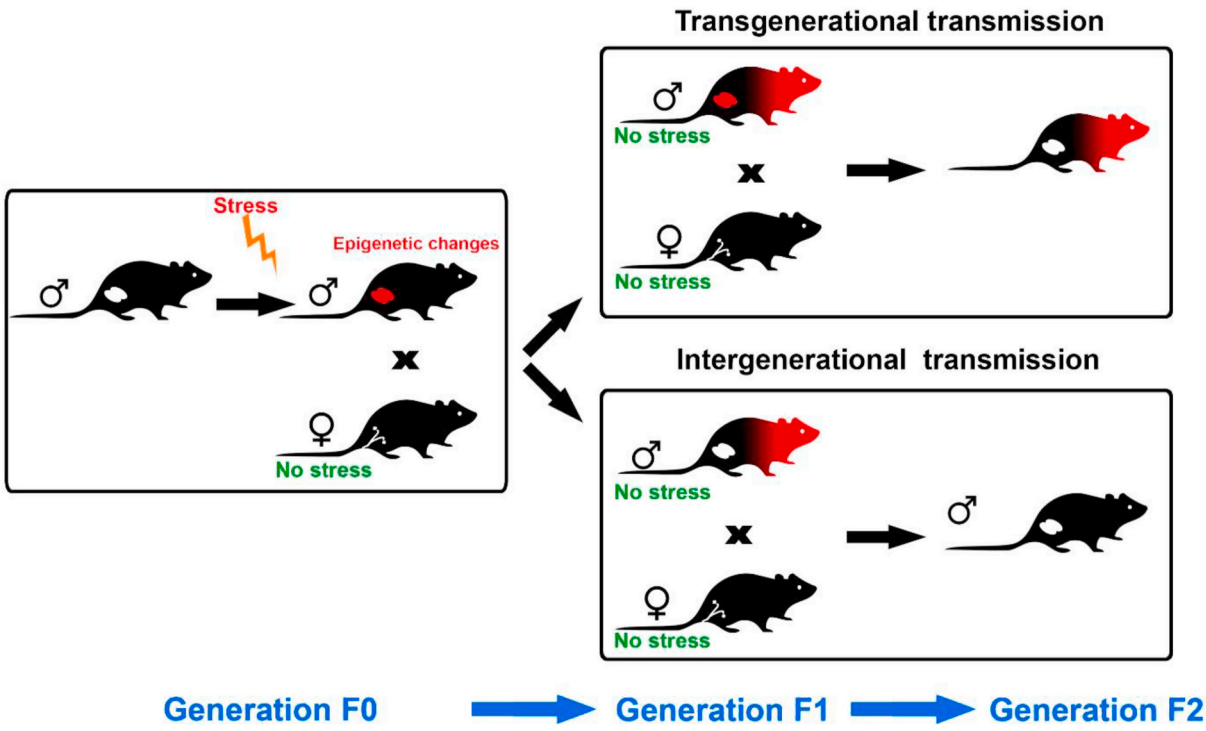

Fig. 2. Stress (Nutritional, physical, …) induces epigenetic changes in the male reproductive organs, including testes and epididymides. These epigenetic modifications lead to an alteration of epigenetic information carried by the sperm and the progeny obtained from stressed male crossed with a non-stressed female exhibits phenotypic changes dependent of the nature of the stress. Epigenetic alterations can be maintained in the male germ cells up to F3 generation, even though the subsequent generations are not exposed to the initial (F0) environmental stress, a phenomena named "transgenerational transmission". If the epigenetic alterations of the germ cells are not transmitted to the F2 generation, then the phenotypic change is named "intergenerational transmission".

histones. It could be involved in transcriptional regulation and also contribute to nuclear condensation through its interactions with transition proteins (Yan et al., 2003).

Several variants of the histone H2A (tH2A, H2A.L.1-3, H2A.B.1-3, H2AP) and the histone H2B (tH2B) have been specifically identified in mouse testis, but their specific roles have not been fully described. The histone variants tH2A and tH2B (TS H2A.1 and TS H2B.1, according to the new nomenclature) are present from the spermatogonia stage and gradually disappear during condensation of spermatid nuclei (El Kennani et al., 2017; Montellier et al., 2013; Trostle-Weige et al., 1982; van Roijen et al., 1998). They induce chromatin instability and could guide the placement of transition proteins and protamines. These variants also seem to play a role in epigenetic reprogramming (Padavattan et al., 2015). The class of histone variants H2A.L and H2B.L are present from the round spermatid stage to the elongated spermatid stage, and H2A.L.1, H2A.L.2 and H2B.L.1 are still present in the mature sperm (Govin et al., 2007). H2A.L.2 allows the chromatin to open, and could play a crucial role in the incorporation of transition proteins and protamines (Barral et al., 2017). H2A.B.3 is present from the spermatocyte I stage to the round spermatid stage (Soboleva et al., 2012). H2A.B.3 could also promote the chromatin reorganization necessary for histone-to-protamine transition, by modulating the incorporation and removal of H2A.L.2 and TP1 from chromatin (Anuar et al., 2019). It could also play a role in pre-mRNA splicing (Soboleva et al., 2017).

Histone H3 (H3.1 and H3.2) has a testicle-specific histone variant (H3t), and a testicle-enriched variant (H3.3) in mice. H3t (TS H3.4, according to the new nomenclature) is present from the spermatogonia stage to the early spermatid stage (El Kennani et al., 2017; Trostle-Weige et al., 1984). H3t could contribute to destabilizing chromatin, and play another as yet unknown role in later stages of spermiogenesis that cannot be compensated for by other members of the H3 family (Tachiwana et al., 2010; Ueda et al., 2017). H3.3 is a ubiquitous protein encoded by two genes, *H3f3a* and *H3f3b*. These genes have different nucleotide sequences, but produce the same protein. *H3f3a* transcripts are present in small amounts from the spermatogonia stage to the elongated spermatid stage, whereas *H3f3b* transcripts are only detected during the spermatocyte I stage (Bramlage et al., 1997). H3.3 allows destabilization of the chromatin, promotes transcription and plays an essential role in the histone-to-protamine transition by modulating the incorporation of TP1 and P1 in chromatin (Ahmad and Henikoff, 2002; Thakar et al., 2009; Yuen et al., 2014). Moreover, H3.3 is involved in Meiotic Sex Chromosome Inactivation (MSCI) at the pachytene stage. Sex chromosomes are located at the periphery of the nucleus in the sexual body and are inactivated during meiosis. Induction of MSCI is associated with both removal of conventional H3 and accumulation of H3.3 and γH2AX in the sexual body, suggesting that these histone variants are needed for sex chromosome condensation and silencing (Mahadevaiah et al., 2001; van der Heijden et al., 2007). The human-specific H3.5 variant is present from the spermatogonia to the spermatocyte I stages (Urahama et al., 2016). H3.5 could also be involved in chromatin destabilization. Moreover, another, as yet poorly characterized, role related to DNA synthesis has been described (Shiraishi et al., 2018; Urahama et al., 2016). Overall, this short description of the numerous histone variants involved in sperm DNA compaction highlights the complexity of the process.

2.2. *Transition proteins*

Transition proteins are basic nuclear proteins (more basic than histones and less basic than protamines) that are synthesized during the advanced stages of spermiogenesis and disappear before the final stage of spermiogenesis (Alfonso and Stephen Kistle, 1993). There are four types of transition proteins: TP1, TP2, TP3 and TP4 (or TNP1, TNP2, TNP3 and TNP4). The first two are present in all species, and are consequently the best characterized. TP1 is a 54-amino-acid protein that is highly conserved in mammals. It is rich in serine, arginine, histidine

and lysine residues (Kremling et al., 1989). TP2 is a larger protein, with 117–138 amino acids depending on the species, it is rich in the same basic amino acids as TP1, and also contains some cysteine residues (Kleene and Flynn, 1987; Schlüter et al., 1992). Its N-terminal part contains two zinc finger domains allowing it to bind to unmethylated CpG sites on DNA, whereas its C-terminal part is very basic (Baskaran and Rao, 1991; Cole and Kistler, 1987; Meetei et al., 2000). Animals lacking TP1 or TP2 produce normal sperm but have reduced fertility, demonstrating that there is some functional redundancy between TP1 and TP2. The absence of both TP1 and TP2 causes male sterility, associated with protamine defects and major DNA breaks. The cells produced are incompatible with fertilization, even by intracytoplasmic sperm injection (ICSI) (Shirley et al., 2004; Yu et al., 2000; Zhao et al, 2001, 2004). Although the two proteins can partially compensate for each other, they play unique roles in the histone-to-protamine transition. During the histone-to-protamine transition, TP1 could be involved in DNA destabilization and thus promote histone removal; it could also contribute to DNA strand break repair (Caron et al., 2001; Singh and Rao, 1987). TP2 could be necessary for stabilizing and initiating DNA condensation (Baskaran and Rao, 1990). Finally, transition proteins also carry a significant number of post-translational modifications (acetylation, phosphorylation and methylation) on their serine, lysine, and arginine residues. These modifications are inserted at specific times during nuclear condensation in spermatids and are crucial for the histone-to-protamine transition (Gupta et al., 2015).

2.3. Protamines

Protamines were first isolated and discovered in salmon sperm at the end of the 19th century by Friedrich Miescher (Miescher, 1874). There are three types of protamines: protamine 1 (P1), protamine 2 (P2) and protamine 3 (P3), but only P1 and P2 are involved in sperm DNA compaction. P1 is expressed in all vertebrates, whereas P2 is expressed only in certain mammalian species (Primates, Rodents, Lagomorphs and equine and bovine species) (Balhorn, 2007; Corzett et al., 2002; Hamilton et al., 2019b). Protamines, proteins of low molecular weight, are highly basic (more basic than histones and TPs), and containing extensive proportions of arginine (47–70% of the amino acids) and cysteine (8–16% of the amino acids) residues in placental mammals (Balhorn, 2007; Calvin, 1976; McKay et al., 1985; McKAY et al., 1986; Queralt et al., 1995). In placental mammals, P1 consists of around 50 amino acids organized in three characteristic domains. A central arginine-rich DNA binding domain, flanked on either side by short segments containing phosphorylation sites composed of serine and threonine residues, and cysteine residues necessary for the formation of inter-protamine disulfide bridges (Balhorn, 2007; McKay et al., 1985; Queralt et al., 1995). P2 contains 54 to 63 amino acids depending on the species (McKAY et al., 1986; Yelick et al., 1987). Unlike P1, a precursor to P2 is synthesized with about 100 amino acids. The mature form of P2 is obtained by cleavage, resulting in the removal of about 40% of its N-terminus (Balhorn, 2007; Carré-Eusèbe et al., 1991; Yelick et al., 1987). In humans, two mature forms of P2 have been described, P2a with 57 amino acids and P2b with 54 amino acids (McKAY et al., 1986). Both bull and boar possess the *PRM2* gene, and P2 mRNA transcripts have been detected, but no P2 protein has yet been identified in mature sperm from these animals (Ganguly et al., 2013; Maier et al., 1990; Mazrimas et al., 1986; Tobita et al., 1982). They are synthesized during the last stages of spermatogenesis to replace histones at the DNA, and highly contribute to its compaction (Rathke et al., 2014).

2.4. Organization of sperm chromatin

The presence of a large number of positively-charged amino acids in protamines, and in particular the arginine clusters, constitute zones for DNA tethering, thanks to the electrostatic bonds created by their opposing charges. These proteins therefore form very stable complexes with DNA (Balhorn, 2007; Brewer et al., 2003; DeRouchey and Rau, 2011). Protamine binding will thus neutralize the charge on the DNA molecules and allow them to pack more closely. The structural organization of the protamine-DNA interaction is still unclear, but it seems that protamines wrap around the double-stranded DNA by positioning themselves in one of the grooves of the double helix (Balhorn, 2007; Fita et al., 1983; Hud et al., 1994). P1 can bind about 11 bp of DNA, whereas the larger P2 can bind up to 15 bp, at a rate of one protamine per turn of the helix (Bench et al., 1996). Protamine binding in the DNA grooves induces curvature, resulting in the formation of a toroidal loop-like structure or “donut loop”, with each toroidal loop connecting the DNA to the nuclear matrix (Allen et al, 1993, 1997; Balhorn, 2007; Björndahl and Kvist, 2010; Hud et al., 1993; Ward, 2010). Each toroidal loop can pack up to 60 kb of DNA, and the sperm nucleus can contain up to 50, 000 toroidal loops by the end of spermiogenesis (Hud et al., 1993).

Protamines also have cysteine residues, the thiol (-SH) groups of which are oxidized to disulfide (–SS–) by nuclear glutathione peroxidase 4 (nGPx4) to form a three-dimensional network of disulfide bridges (Puglisi et al., 2012). The intra-protamine disulfide bridges stabilize the folding of different protamine domains and are essential for DNA condensation. The inter-protamine disulfide bridges, in complement, serve to increase the structural stability of the nucleoprotamines and to maintain the strained conformation of the structure, which further enhances the level of DNA compaction (Hutchison et al., 2017). The chromatin stability is proportional to the number of disulfide bridges formed, and this stabilization process is progressive, beginning in the testis and continuing as sperm transit through the epididymis (Balhorn et al., 1992; Gosálvez et al., 2011; Saowaros and Panyim, 1979; Yossefi et al., 1994).

In P2, zinc finger domains composed of cysteine and histidine residues and stabilized by zinc salt bridges contribute to the formation of P2-DNA complexes (Bench et al., 2000; Bianchi et al., 1992). In addition to its role in stabilizing the nucleoprotamine structure as effectively as disulfide bridges, zinc also prevents superstabilization by reducing the availability of free thiol groups to form disulfide bridges (Björndahl and Kvist, 2010). Zinc salt bridges are also easier to disrupt than disulfide bridges, and could allow faster decondensation of the chromatin upon oocyte fertilization (Björndahl and Kvist, 2010). This setup probably explains why species expressing only P1 have the most extensively compacted chromatin, and why species expressing more P2 are more sensitive to DNA damage (Gosálvez et al., 2011).

In addition to their structural and binding residues, protamines have serine and threonine residues which are phosphorylated immediately after protamine synthesis by SRPK1 (serine/arginine-rich protein-specific kinase-1) for P1 and Camk4 (Calcium/calmodulin-dependent protein kinase type IV) for P2 (Papoutsopoulou, 1999; Wu et al., 2000). These phosphorylation events are necessary to initially establish correct binding between the protamines and the DNA. Phosphorylation reduces the affinity of the protamines for DNA (by increasing the negative charge of protamines), to give the protamines time to position themselves optimally with respect to the DNA, thus reducing mismatching. Subsequently, the progressive dephosphorylation of protamines gradually increases the affinity of protamines for DNA and induces chromatin condensation (Green et al., 1994). Optimal positioning of protamines is essential for the appropriate formation of inter-protamine disulfide bridges (Marushige and Marushige, 1978). Other post-translational modifications of protamines have been identified and could contribute to the protamine-DNA binding or protamine removal process after fertilization, suggesting the existence of a protamine code equivalent to the histone code (Brunner et al., 2014).

During spermatogenesis, not all histones are replaced by protamines, and variable fractions of histones remain associated with DNA in the mature sperm (1–8% for mouse (Balhorn et al., 1977; Jung et al., 2017), 13% for bull (Samans et al., 2014), 3–15% for human (Bench et al., 1996; Samans et al., 2014; Tanphaichitr et al., 1978), and 25% in some marsupial species (Soon et al., 1997)). These residual histones were first

considered a defect in the replacement of histones by protamines, but it is now clear that persistent histones (canonical or variant) in mature sperm are not randomly distributed and have a role to play. Histone-enriched regions appear to be distributed either in large 10-100-kb regions corresponding to the solenoids present between toroidal loops, or in short domains dispersed throughout the genome, corresponding to stretches of DNA anchoring the toroidal loops to the nuclear matrix (Arpanahi et al., 2009; Hammoud et al., 2009; Ward, 2010). The precise location of persistent histones in the genome remains a subject of debate. Some studies found that nucleosomes are enriched at the level of hypomethylated CpG sites corresponding to promoters and genes that are important for embryogenesis (transcription factors, signaling factors, Homeobox gene clusters, globin genes, imprinted gene clusters, genes encoding microRNAs, etc.) (Arpanahi et al., 2009; Erkek et al., 2013; Gardiner-Garden et al., 1998; Hammoud et al., 2009; Royo et al., 2016; Yoshida et al., 2018). Nevertheless, other authors have reported that the nucleosomes persist at intergenic regions, regions rich in repeated sequences (telomeres, subtelomeres, centromeres, pericentromeres, LINE1 and SINE) and rRNA and SRP RNA (RNA component of Signal Recognition Particle) gene clusters (Carone et al., 2014; Hoghoughi et al., 2020; Meyer-Ficca et al., 2013; Samans et al., 2014; Sillaste et al., 2017; Zalenskaya et al., 2000). These divergent results could be due to the fact that different protocols were used to isolate histones, but could ultimately be complementary: even if the majority of persistent histones are localized in gene deserts, some of the histones are also deposited in specific regions that are important for embryonic development (Yamaguchi et al., 2018). Importantly, histones retained in sperm carry epigenetic marks that are transferred to the embryo, and they could be involved in embryonic development (Bui et al., 2011; Ihara et al., 2014; van der Heijden et al., 2008).

In summary, sperm DNA compaction is highly complex and involves a multitude of steps and molecules. Interestingly, the transition from nucleosome to nucleoprotamine does not result in total erasure of epigenetic markers, as evidenced by the presence of histones and histone variants in mature sperm. Histones are only one facet of epigenetic control over transcription/translation, and the question of the significance of other markers in paternal inheritance remains to be evaluated.

3. Paramutations in sperm and the discovery of the importance of RNA in paternal heritage

Paramutations were first described in plants as an epigenetic modification of one allele induced by crosstalk between the two alleles of the same gene, giving rise to a new phenotype for the modified allele (Chandler, 2007). Importantly, despite its name, paramutation causes changes in the expression of the affected allele without any DNA mutation. Nevertheless, the modified locus can induce a similar change in homologous sequences, and consequently this change of allelic expression is transmitted to future generations and is thus heritable. In fact, paramutation allows the transmission of heritable characteristics through epigenetic mechanisms. Paramutation was reported in mice for the Kit gene (Rassoulzadegan et al., 2006). The Kit gene, coding for a tyrosine kinase receptor, is essential for the maintenance of primordial germ cells (PGCs) in both sexes in the embryo, but it is also expressed in adult testis where it is required for DNA synthesis in differentiating spermatogonia (Rossi et al., 2000). In addition, Kit is expressed in melanocytes and is necessary for melanin expression. Kit-null animals (insertion of a lacZ cassette within the gene, Kit^{tm}) are not viable, in contrast to heterozygous animals $Kit^{+/tm}$, which have a white tail tip and white fingers (Rassoulzadegan et al., 2006). Interestingly, the authors reported that WT animals ($Kit^{+/+}$) obtained from crosses between two heterozygote animals ($Kit^{+/tm}$) or a heterozygote animal and a WT animal also had a white tail tip and white fingers, despite their full WT genotype (Fig. 3). This observation suggests that the Kit^{+} allele from the heterozygous animal has been modified (called Kit*). The white-spotted phenotype was transmitted to the F2 generation, even though no Kit^{tm} allele was present, but vanished in subsequent generations. Levels of the polyadenylated messenger RNA for Kit were generally decreased in

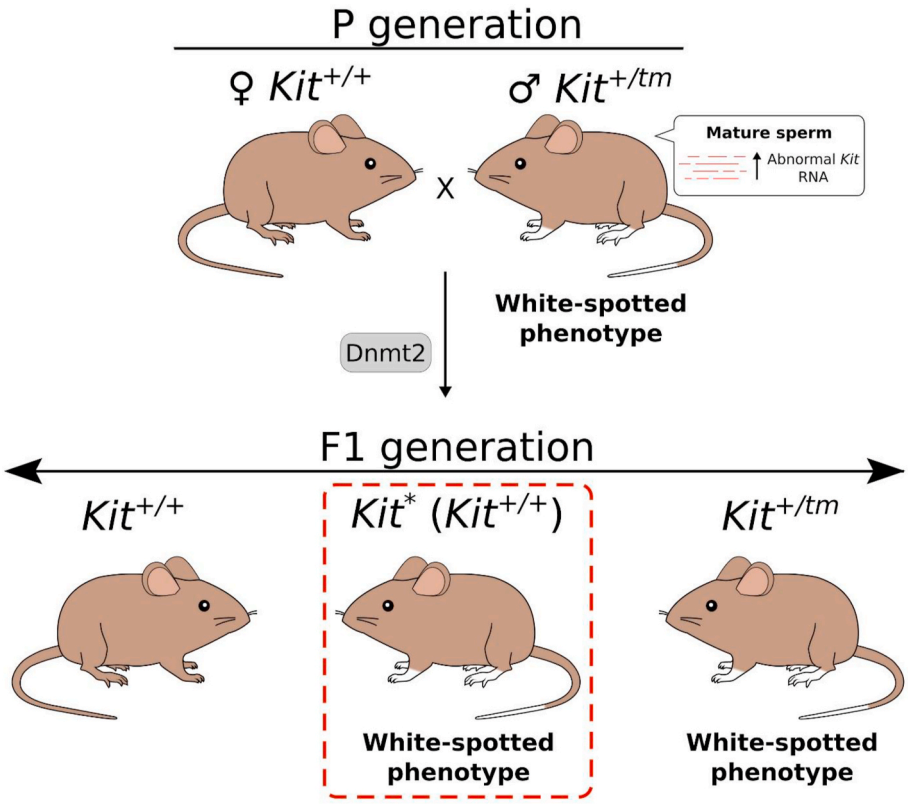

Fig. 3. Model for transgenerational inheritance of paramutated Kit. Heterozygous mice carry a wild-type (+) and a modified/inactivated Kit allele (tm), and bear a white-spotted phenotype with white fingers and white tale tips, while wild-type homozygotes have solid color. The heterozygote males produce abnormal Kit RNA from the Kit^{tm} allele, which are packaged in the sperm and delivered to the egg upon fertilization. Some resulting progeny with two wild-type alleles develop the heterozygote white-spotted phenotype (Kit*). The aberrant RNAs are transmitted to the progeny and thought to regulate expression of the wild-type allele in the zygote, thus propagating the paramutation to the progeny. The establishment and transgenerational inheritance of the paramutation also requires the expression of an RNA methyltransferase Dnmt2 (Kiani et al., 2013), but its role remains unclear. The paramutation might gradually disappear over successive generations due to the reduction in aberrant Kit RNAs.

animals with white-spotted fur and a full WT genotype (paramutated animals), but spliced fragments of the full Kit transcript with multiple sizes were strongly expressed in the testis. More surprisingly, extensive deregulation of the temporal window of Kit mRNA expression was observed, with strong expression in postmeiotic cells in heterozygous males compared to WT animals, where Kit mRNA was barely detectable. Moreover, Kit mRNA is not eliminated in the residual bodies during the sperm cytoplasmic reduction, and remains present in mature epididymal sperm, suggesting a role for Kit mRNA fragments in the transmission of the white-spotted phenotype. This role for fragmented Kit mRNA in the paramutation was demonstrated by injecting sperm mRNA extracts from heterozygous males into WT oocytes. The offspring expressed the white-spotted phenotype, in contrast to offspring from WT males. The role of fragmented Kit mRNA was also supported by the fact that an injection of 2 microRNA species (miR-221 and miR-222) targeting Kit mRNA mimicked the effect of sperm RNA injection. Importantly, animals generated from WT sperm and miRNA-injected WT oocytes could transmit the white-spotted phenotype to the F2 generation. These results allowed the authors to propose that the modified phenotype is induced by the transfer of cleaved Kit RNA molecules to embryos. These findings demonstrated that microRNA injected into the zygote can induce paramutation by altering gene expression, and thus confirmed that sperm miRNA can alter the phenotype of the progeny. This idea was supported by Grandjean and coll. (Grandjean et al., 2009), who showed that injection of miR-124 induced a large body size as a result of modification of Sox9 RNA, and Wagner and coll. (Wagner et al., 2008), who demonstrated that microinjection of miR-1 led to deregulation of the transcript Cdk9, a transcription factor, and cardiac hypertrophy in mice. In both cases, the phenotypes were transmitted to subsequent generations.

4. Sperm contains numerous messenger RNA (mRNA) and non-coding RNA (ncRNA)

The coding region of DNA represents only 2.5% of the genome. Nevertheless, most of the genome (~85%) can be transcribed as non-coding RNA (ncRNA). There are two types of ncRNAs, housekeeping RNA such as transferRNA (tRNA) and ribosomalRNA, and regulatory ncRNAs, which have many functions, including post-transcriptional regulation of mRNA. For a detailed review of the numerous classes of regulatory ncRNA and more detail on their structure and functions, we refer readers to (Hammond, 2015; Hombach and Kretz, 2016). Here, we will focus only on short ncRNAs, including Piwi-interacting RNA (piRNA), microRNA (miRNA), small interfering RNAs (endo-siRNAs), and transferRNA-derived fragments (tRFs).

Short ncRNAs can be split into two classes: those coded at specific loci in the genome, and those resulting from endonucleolytic cleavage of other types of RNA. The first class corresponds to piRNA, miRNA, and endo-siRNA. piRNA and miRNA genes, located throughout the genome, are non-coding genes which exclusively generate ncRNA. Some miRNAs are located within introns or untranslated regions (UTR) of protein coding genes. Endo-siRNAs have only been mapped to genomic areas that produce transcripts capable of forming double-stranded RNA (dsRNA) structures, such as retrotransposons or bidirectional transcription sites. tRFs, in contrast, are generated through the cleavage of transfer RNA by endonucleases such as Angiogenin, DICER, and probably some uncharacterized proteins.

During the cytoplasmic sperm compaction occurring at the end of spermiogenesis, most of the cytoplasm, including ribosomes, the endoplasmic reticulum, and the Golgi apparatus, are discarded in the residual body. Moreover, as explained above, the sperm DNA becomes highly compacted as nucleosomes are replaced by protamines, eventually resulting in closed chromatin. As a result of these changes, transcription and translation are considered to be arrested in sperm. Nevertheless, RNA was first detected in sperm over 30 years ago (Pessot et al., 1989). The more recent development of high-throughput sequencing technologies has revealed the vast diversity of RNA present, with more than 10,000 distinct transcripts identified (El Fekih et al., 2017; Selvaraju et al., 2017; Sendler et al., 2013). Various types of RNA were identified, including messenger RNAs and several classes of ncRNAs, including short and long ncRNAs (Dadoune, 2009). Moreover, RNA-seq technology identified both full and truncated RNAs, which is an interesting result when considering Kit-induced paramutation results. A multispecies sperm-borne RNA database to allow comparative annotation of all sperm RNA has been established (Schuster et al., 2016). When sperm RNAs were discovered, they were at first considered to be remnants of spermatogenesis. However, the studies showing that microinjections of RNAs into the zygote alter the heredity of the progeny over several generations (Grandjean et al., 2009; Wagner et al., 2008) stimulated a reevaluation of the role of the various endogenous sperm RNAs in embryo development and epigenetic inheritance, as explained below.

4.1. MicroRNA (miRNA) and small interfering RNAs (endo-siRNAs)

MicroRNA (miRNA) and small endogenous interfering RNAs (endo-siRNAs) are small ncRNAs characterized by transcript sizes smaller than 200 nt. Single-stranded miRNAs are generally the most abundant class of small ncRNAs, mediating gene silencing at the post-transcriptional level. Double-stranded siRNAs are key players in the RNA interference (RNAi) pathway, an alternative pathway for post-transcriptional gene silencing. Considerable light into the molecular processes governing small RNA biogenesis pathways has been shed by several teams: for miRNA, the canonical pathway involves two endoribonucleases, DROSHA in the nucleus and DICER in the cytoplasm, which sequentially generate the active, ~22-nucleotide mature miRNA from the hairpin shaped primary miRNA (Hammond, 2015) (Fig. 4). siRNA is produced from double-stranded RNA by DICER, without input from DROSHA. Both ncRNA are loaded onto the RNA-induced silencing complex (RISC), which cleaves the target complementary mRNA to induce RNA decay and gene silencing (Fig. 3). As they target the 3′ untranslated regions of mRNAs, miRNA is not very specific, and a single miRNA is predicted to induce the cleavage of hundreds of mRNAs. In contrast, siRNAs are more specific. More than 2000 distinct miRNAs have been characterized so far, targeting around 1/3 of all mRNAs.

RNA interference pathways, and particularly those involving miRNAs, are emerging as important regulators of spermatogenesis and epididymal maturation. Complete and ubiquitous deletions of DICER or DROSHA are lethal, but their deletion in germ cells only causes male and female infertility, demonstrating the importance of ncRNAs during gametogenesis. Around 600 distinct miRNAs have been described in the mouse testis (Schuster et al., 2016), and both miRNAs and siRNAs are abundantly expressed during spermatogenesis (Song et al., 2011). The nature and copy number of miRNAs changes during sperm maturation (Nixon et al., 2015); their origins and importance will be discussed below.

4.2. Transfer RNA-derived fragments (tRFs)

Transfer RNAs, key elements of the transcriptional/translational machinery, have a characteristic shape, with several domains, organized from 3′ to 5': the TψC arm, variable loop, anticodon loop and the D arm. Endonucleases can generate two types of transfer RNA-derived fragments (tRFs). In response to stress, Angiogenin cuts the anticodon loop and produces halved fragments. Other cleavage events, orchestrated by DICER, Angiogenin, and other uncharacterized enzymes near the D- or TψC-arms produce small RNA known as 5′ tRFs and 3′ tRFs, respectively (Keam and Hutvagner, 2015) (Fig. 5). Numerous functions have been attributed to tRFs. The first to be identified was a function similar to miRNA (see above), silencing gene expression by binding to the 3′ UTR of mRNAs. Other functions were since identified, such as direct regulation of translation by tRFs binding to ribosomes. Finally, tRFs can also form complexes with RNA-binding proteins such as Ybx1 to regulate

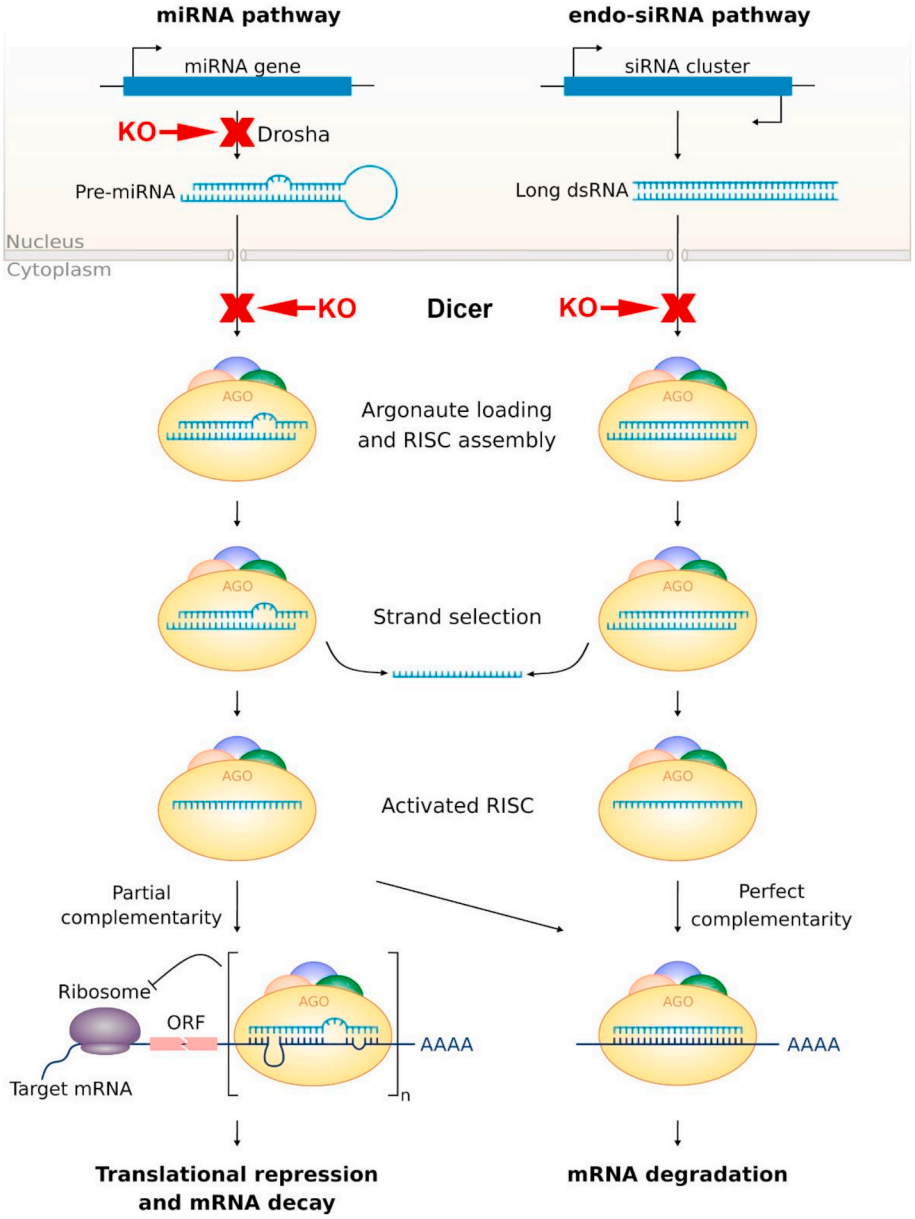

Fig. 4. The mechanism of miRNA and endo-siRNA biosynthesis and function. miRNA and endo-siRNA are involved in post-transcriptional gene silencing through translational inhibition and mRNA decay, or mRNA cleavage by Argonaute and subsequent degradation. (Adapted from (Chu and Rana, 2007; Lam et al., 2015), Chu CY, Rana TM (2007) and Clancy, S (2008)). AGO: Argonaute; endo-siRNA: endogenous small interfering RNA; miRNA: micro-RNA; pre-miRNA: precursor miRNAs; ORF: open reading frame; RISC: RNA-induced silencing complex.

RNA degradation and stability. Mature sperm from the cauda epididymis contain numerous ncRNA, and 80% of them are tRFs, mostly 5' tRFs (Peng et al., 2012; Sharma et al., 2016).

4.3. c Piwi-interacting RNA (piRNA)

Numerous transposable elements, likely derived from viruses, are found in mammalian genomes. Their movement can disrupt gene expression when transposed into exons, introns, or into 5′ or 3'-UTRs. It is thus crucial to inhibit their dissemination to preserve the integrity of the genome (Parhad and Theurkauf, 2019). Dissemination is prevented in germ cells by the expression of 22-27-nt small-ncRNA, known as piRNA, the primary function of which is transposon silencing. piRNA, located in clusters, are expressed from the pre-pachytene stage, and their production is DICER-independent (Fig. 6). The piRNA silencing pathway involves several proteins from the PIWI clade of Argonaute proteins, such as MILI, MIWI2, and MIWI. Mutations that disrupt this pathway cause transposon overexpression, leading to sterility. Interestingly, a second wave of piRNA synthesis occurs over the course of the pachytene stage, during which several hundred piRNAs with unique sequences are expressed from piRNA clusters containing few transposons and repeat sequences. The piRNAs expressed during this second wave control the expression of genes coding for proteins involved in meiosis (Goh et al., 2015), and massively eliminate the corresponding mRNAs at the elongated spermatid stage (Gou et al., 2015).

5. Origin of sperm ncRNA

Some of these RNAs appear to be deeply embedded in the sperm nucleus, since harshly purified nuclei devoid of acrosomes, plasma membrane, perinuclear theca, and nuclear envelope still contain ncRNA and mRNA (Yan et al., 2008). Due to their deep localization, they are probably produced during spermatogenesis and not discarded during sperm cytoplasm compaction. Interestingly, when these purified sperm heads were injected into artificially activated oocytes, 2-cell embryos developed, 17% of which produced live pups when re-implanted in foster mothers. Furthermore, the purification of epididymal sperm heads and flagella indicate that ncRNAs are present in both subcellular compartments, but that the composition of these ncRNAs differs between the two compartments. Whereas the heads contain mostly tRFs, the flagella

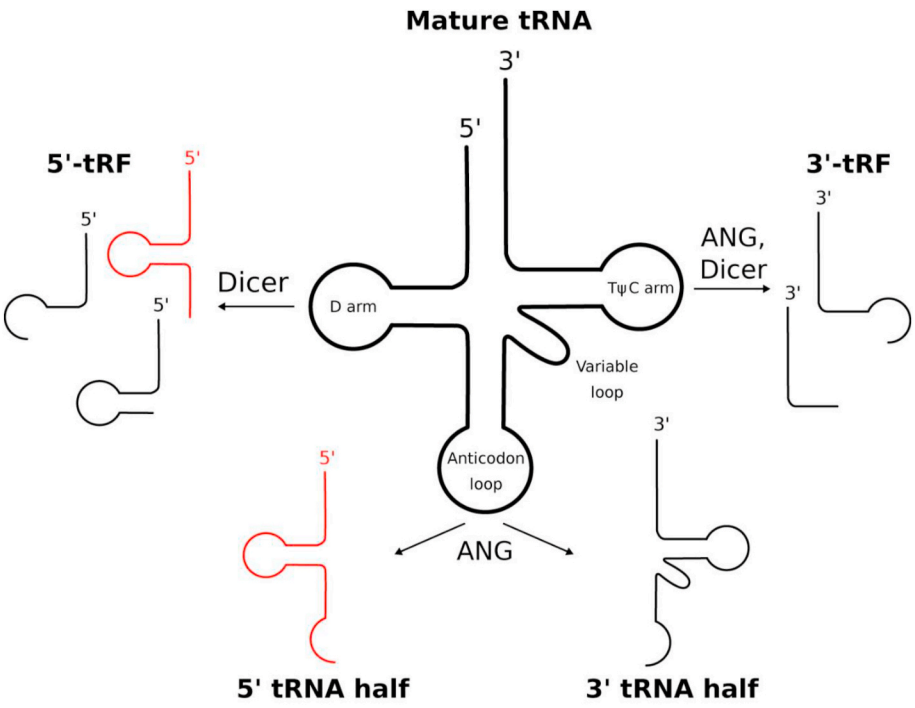

Fig. 5. tRNA fragments derived from mature tRNAs. Processing of mature tRNA can give rise to small RNA fragments. tRNA-derived fragments are shorter than tRNA halves and are produced by the action of Angiogenin and Dicer. In mammalian cells under stress, a cleavage in the anticodon loop produces tRNA halves by the action of the nuclease Angiogenin (ANG). tRNA fragments identified in mouse cauda sperm are predominantly enriched in fragments derived from the 5' ends of tRNAs (in red), as shown by (Sharma et al., 2016).

are comparatively enriched in piRNA and miRNAs (Sharma et al., 2018).

Sperm released into the lumen of the seminiferous tubules transit through the epididymis and are then stored in the cauda epididymis until ejaculation. The epididymis is separated into several functional areas. This very long epithelial tubule is composed of several cell types, including secretory cells. It is well known that during epididymal transit the composition of sperm changes dramatically, and that these changes are necessary for sperm to become competent. For instance, the lipid composition of the plasma membrane is extensively changed as a result of phospholipase A2 secretion, in addition group III sPLA2 (Sato et al., 2010) and proteins important for sperm/egg binding are inserted into the plasma membrane of the sperm as it travels (Caballero et al., 2013; Da Ros et al., 2015). Epididymal proteins are transferred to the sperm by the fusion of small membrane vesicles known as epididymosomes. Interestingly, Belleannée and coll. (Belleannee et al., 2013) showed that these vesicles can transport miRNA, and hypothesized that via this route miRNA synthesized and secreted in one epididymal region could modulate the function of epididymal cells in another region. Since these epididymosomes can fuse with sperm, they could also provide new ncRNAs to sperm. To verify this hypothesis, several types of experiments were performed.

First, the composition of ncRNA in sperm was measured using RNA sequencing on immature sperm (testicular sperm) and maturing sperm located in different regions of the epididymis. These analyses showed that the ncRNA composition of sperm changes dramatically, with loss and acquisition of ncRNA, mostly in the distal part of the epididymis (Nixon et al., 2015). A study tracking the composition of the ncRNA in the testis from pachytene spermatocytes to immature sperm cells, and in the epididymis from caput sperm to cauda sperm indicated that the predominant ncRNA in testis are piRNA, and that transit through the epididymis is associated with a loss of almost all piRNAs and a remarkable increase in tRFs (Sharma et al., 2018). The results of this study also confirmed a notable qualitative and quantitative increase in miRNAs during transit through the caput epididymis (Fig. 7A).

Second, to demonstrate that these changes were due to uptake of epididymosomes, the concentration of ncRNA was measured in immature sperm before and after co-incubation with caput epididymosomes. Reilly and coll. (Reilly et al., 2016) showed that this co-incubation actually increased the RNA copy numbers for miR-191, miR-375, miR-467a, miR-467d, miR-467e demonstrating that the sperm RNA payload is strongly influenced by secretions in the epididymis. Similarly, another comparison of ncRNA content between testicular sperm and testicular sperm incubated with caput epididymosomes indicated that incubation with caput epididymosomes changes the composition of ncRNA, with notable increases in miRNA, tRFs and a decrease in piRNA (Sharma et al., 2016, 2018).

Epididymosomes not only provide new epididymal ncRNA to sperm but also increase the copy number of ncRNA in sperm. These observations reinforce the overall potential epigenetic influence of sperm after fertilization. The composition of sperm ncRNA and their evolution from the testis to the cauda epididymis is shown in Fig. 7A.

6. Functions of sperm-borne ncRNA

6.1. Role of sperm-borne ncRNA in embryonic development

Although the presence of several types of ncRNA, including tRFs, miRNA, siRNA, and piRNA was clearly demonstrated in mature cauda epididymis sperm, the function of the sperm ncRNA upon fertilization and early embryo development may not be so clear-cut because (i) the quantity of sperm-borne ncRNA delivered at fertilization into the oocyte remains very low compared to the amount already present within the oocyte, (ii) the most abundant sperm miRNA are also present in the oocyte before fertilization (Amanai et al., 2006), (iii) oocyte maturation and preimplantation embryonic development are not affected by complete depletion of maternal miRNA, as demonstrated by Dgcr8 oocyte-deficient females, (of note, this observation suggests that the miRNA-dependent gene silencing pathway is not activated at these stages (Suh et al., 2010)) and (iv) In several species including mouse and Human, injection of round spermatids and testicular sperm, with a very different miRNA contents than fully mature sperm, permits to obtain live healthy offspring (Tanaka et al., 2015) Altogether, these results raise questions about any role of sperm-borne ncRNA, and in particular miRNA function in the development of mammalian zygotes and embryos.

To address these questions, several approaches were used to

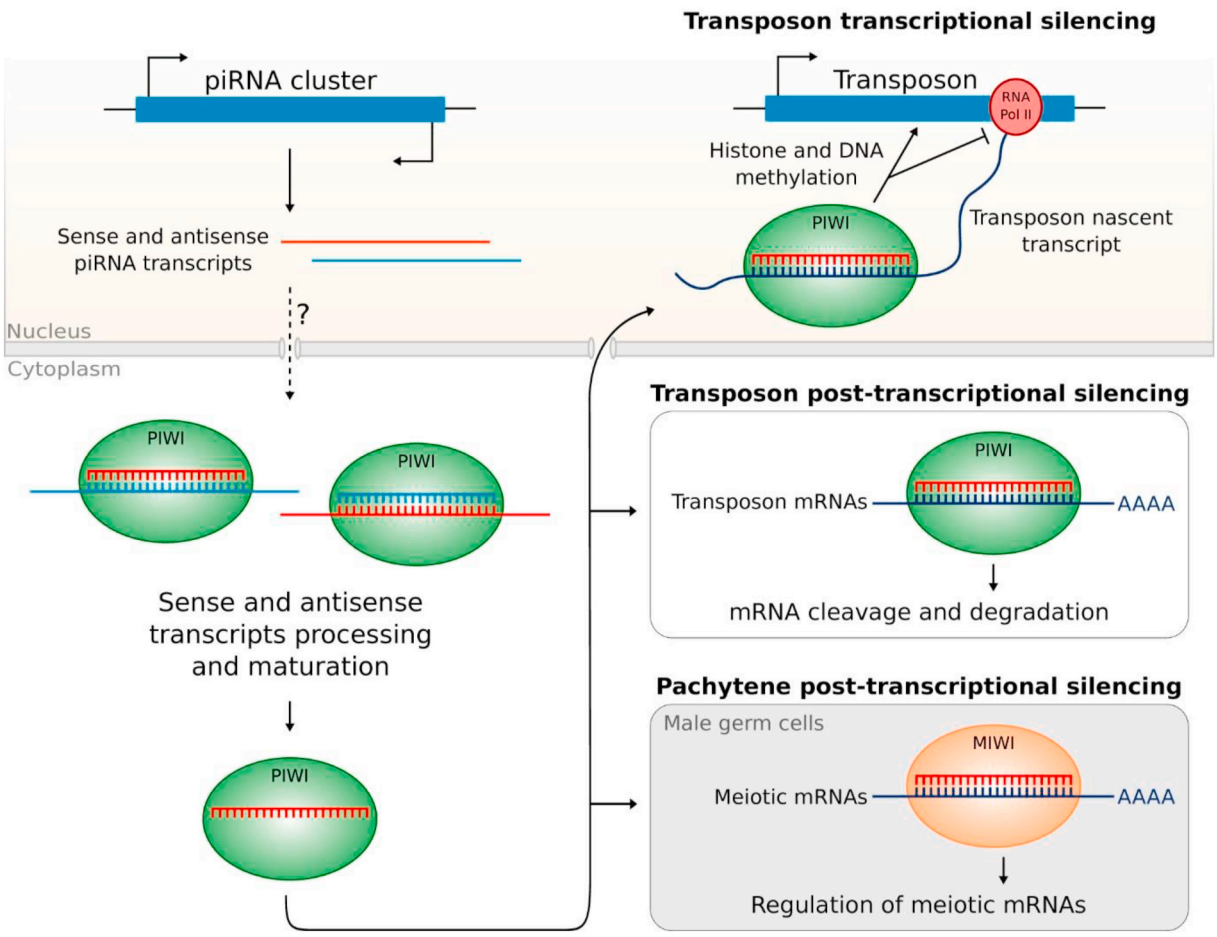

Fig. 6. A simplified mechanism of piRNA biosynthesis and function. OR The mechanism of piRNA biosynthesis and function. Mammalian piRNAs derive from distinct transposon sequences known as piRNA clusters. They can be transcribed in the sense or antisense direction, and give rise to single-stranded long non-coding RNA transcripts. The precursors are transported into the cytoplasm by an unknown mechanism and processed in a Dicer-independent manner. Sense and antisense transcripts are in turn loaded onto PIWI clade proteins and trimmed to the length of mature piRNA, their 5′ and 3′ ends are modified, and they are used in an amplification loop to generate other complementary mature sense and antisense piRNAs. Mature piRNAs are mainly involved in transposon silencing by repressing their transcription or by cleaving their mRNAs. Transposon transcriptional silencing is thought to occur when a piRNA-guided PIWI protein recognizes a nascent transposon transcript in the nucleus and recruits a DNA and histone methylation machinery to the transposon locus, which silences transcription. In the cytoplasm, piRNA induces post-transcriptional silencing of target transposon transcripts in an RNAi-like manner. In mouse spermatocytes, pachytene piRNAs are depleted of transposon sequences, and these piRNAs are thought to regulate gene expression during meiosis and late spermiogenesis, but the exact mechanism is unknown. (Adapted from (Meister, 2013; Ozata et al., 2019)).

investigate the role of sperm ncRNAs in fertilization and embryo development:

Although tissue-specific inactivation of DICER or DROSHA in male germ cells leads to infertility, some non-motile and abnormal sperm are produced that can be used for ICSI. Interestingly, embryos generated with sperm lacking DICER or DROSHA and WT oocytes developed poorly in comparison to those generated with WT sperm and oocytes, but their development was improved when KO sperm were co-injected with small amounts of ncRNA from WT sperm (Yuan et al., 2016). The absence of DICER affected around 47% of sperm miRNAs and 8% of sperm siRNAs, and the absence of DROSHA had an impact on around 52% of sperm miRNAs (DROSHA is not involved in siRNA biogenesis), suggesting that some ncRNAs produced during spermatogenesis play a crucial role in embryonic development. Interestingly, DICER and DROSHA-deficient sperm did not perform equally. Embryos generated with DICER-deficient sperm developed poorly at all stages (from 2-cell to blastocyst), whereas those generated with DROSHA-deficient sperm developed almost normally up to the 4-cell stage, from which point they showed marked developmental defects. These results suggest that sperm-borne siRNA plays a role in the early stages of embryonic development, whereas sperm-borne miRNA are more important at later stages, beyond the 4-cell stage. These results also highlight a long-term effect of these sperm-borne ncRNAs, after embryonic gene activation, which occurs at the 2-cell stage in mice. It is interesting to note that the improvement was greater when total WT RNA was injected than with small RNA only, suggesting that sperm not only deliver regulatory RNA molecules but also mRNA.

To assess the importance of the different types of ncRNA in embryo development, and in particular ncRNAs provided by epididymosomes, embryos were generated by ICSI with testicular, caput and cauda sperm, and embryo development was studied. mRNA from embryos were sequenced at various stages (4-cell, 8-cell, morula, and blastocyst). Overexpression of transcripts coding for RNA-binding proteins (Hnrnpab, Hnrnpu, Pcbp1, Eif3b, Yrdc, Ythdf1, Srsf2, and Ybx1) and chromatin-associated factors (Smarcd2, Smarca5, Smarcc1, Trim28, and Ezh2) was observed only in embryos generated with caput sperm and not those generated with cauda sperm (Conine et al., 2018). These changes affected embryo development: 50% of embryos were absent at day 7.5 of gestation, suggesting that their post-implantation development was abnormal, and finally no pups were obtained at term. This result suggests that the ncRNA gained as sperm pass through the caput transiently make sperm unable to sustain embryo development and that

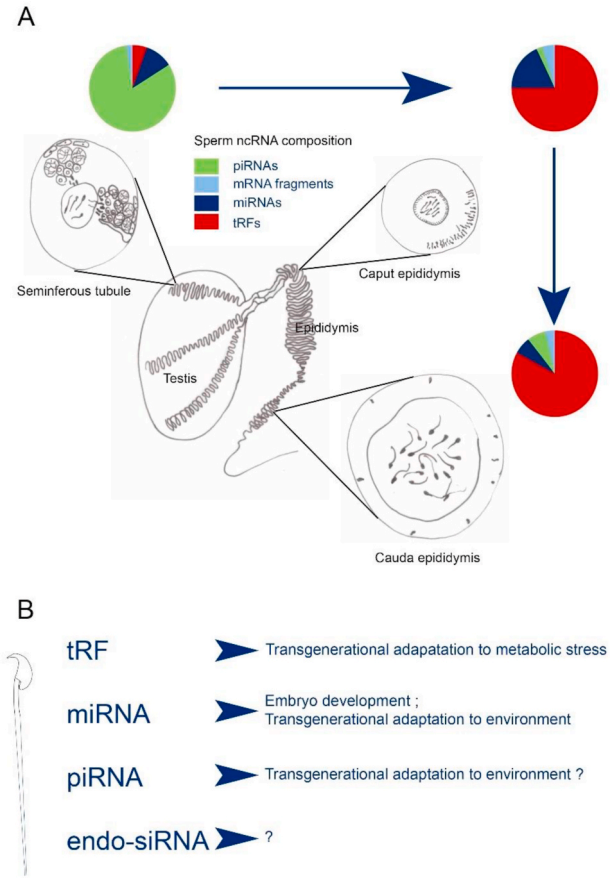

Fig. 7. Origin and functions of sperm ncRNA. A. The composition of sperm ncRNA changes dramatically as cells travel from the testis to the cauda epididymis. In the testis, the most abundant type of ncRNA is piRNA, which plays a crucial role in transposon control. After spermiation, sperm transit through the caput epididymis, where tRFs and miRNAs are gained. piRNAs are no longer present, but how they are eliminated remains unknown. In the cauda epididymis, the miRNA composition is also strongly modified. B. In the absence of miRNAs and tRFs, embryo development is abnormal. The miRNA are also key nucleic acids for transgenerational adaptation in response to paternal environmental stress. Adapted in part from (Sharma et al., 2016, 2018).

the ncRNA payload is drastically modified in the cauda epididymis. Interestingly, co-incubation of caput sperm with epididymosomes purified from the cauda epididymis rescued the level of expression of transcripts for RNA-binding and chromatin-associated factors in embryos, allowing the embryos to develop to term (Conine et al., 2018). Remarkably, only the injection of miRNAs, but not tRFs, purified from cauda sperm restored normal embryo development following fertilization with caput sperm. This observation suggests that miRNAs gained during epididymal transit are involved in embryo development, and that the tRFs acquired play a distinct role. Several sperm-borne miRNAs were identified as crucial for early embryo development, such as miR-34c, which is involved in DNA synthesis and inhibition of Bcl-2 expression in the zygote. Inhibition of miR-34c leads to failure of the first mitosis (Liu et al., 2012).

6.2. Roles of ncRNAs in the environmental stress-response

Environmental injuries suffered by the parents and their impact on phenotypes in the next generation were first discovered by a study monitoring the health of adults whose mothers lived through the Dutch famine during the Second World War. The results showed that the adults exposed to famine in utero during the first trimester of pregnancy had a higher risk of obesity and those exposed in the third trimester had a lower risk (Ravelli et al., 1976). Most early studies on transgenerational effects of parental stress focused on the influence of metabolic stress over the course of pregnancy. The effects of preconceptional stress on female gametes were more difficult to demonstrate since any preconceptional stress that affects oogenesis may also have an impact on the subsequent pregnancy. Nevertheless, a recent study showed that corticotropin releasing factor type 1 (CRF1) mRNA, a key component in the stress response, is increased in eggs harvested from stressed female rats, and that offspring obtained after mating stressed females with control males exhibited higher levels of CRF1 in the brain and behavioral defects (Zaidan et al., 2013). Thus, female germ cells appear to be able to transmit stress-induced traits to their progeny. Similar experiments aiming to demonstrate transgenerational transmission of environmental stress by sperm were easier to carry out since stress suffered by the male impacts neither full embryo development nor the raising of pups, which are mother-dependent.

Obesity is a significant health issue, and several epidemiologists have compared the increase in the rate of obesity in Western countries to an epidemic-like phenomenon, suggesting possible transmission of this condition. The first observations that a father's diet can affect his daughters' health, leading to obesity and diabetes, were reported quite recently (Ng et al., 2010). This paternal diet-induced phenotype is associated with reprogramming of metabolic gene expression in liver due to alteration of epigenetic marks (Carone et al., 2010). These first reports were followed by numerous studies investigating the transgenerational impact of paternal diet on the progeny's susceptibility to metabolic disorders, and seeking to identify the molecular basis for its transgenerational transmission. The transmission of the phenotype was observed up to the third generation. A high-fat diet (HFD) leads to extensive modifications to the ncRNA content in both testis and sperm cells (Fullston et al., 2013) and miRNAs, piRNAs, and tRFs were found to be differentially expressed in sperm from animals consuming the HFD, piRNA being the most likely (de Castro Barbosa et al., 2016). Interestingly, Let-7c, one miRNA that is upregulated in sperm from males fed with HFD, was also upregulated in adipose tissues of their F1 offspring. This miRNA is known to regulate glucose homeostasis and insulin sensitivity, and has been linked to a predisposition for type-2 diabetes. The importance of ncRNA in paternal transmission of obesity and diabetes was also supported by an experiment where ncRNA were injected into zygotes: the injection of spermatic ncRNA from a male fed with the HFD into a control zygote led to metabolic disorders in the progeny, whereas injection of spermatic ncRNA from a male fed with the control diet had no effect (Grandjean et al., 2015). Interestingly, the injection of miR19b into a control zygote mimicked the phenotype observed after injection of ncRNA from the HFD male. It is worth noting that the various reports on miRNAs involved in the paternal transmission of metabolic disorders fail to agree. Even more surprisingly, the change in miRNA content induced by HFD is not observed in sperm from male progeny, despite the fact that they can transmit the metabolic phenotype to their own offspring, the grand-children of HFD males (Fullston et al., 2016). This unexpected result strongly suggests that components other than miRNA are also important for transgenerational paternal effects. This hypothesis was recently confirmed by Sharma and coll. (Sharma et al., 2016), who showed that sperm from males consuming a low-protein diet contains higher levels of tRF-Gly-GCC, that regulates the endogenous retroelement MERVL. Importantly, the long terminal repeat (LTR) in MERVL regulates a subset of genes expressed at high levels in preimplantation embryos. The impact of the low-protein diet on gene expression in preimplantation embryos was reproduced by microinjection of a synthetic tRF-Gly-GCC oligo (Sharma et al., 2016). A HFD also deregulates several thousand long ncRNAs in sperm, and it was thus suggested that these long ncRNA could be involved in paternal heredity (An et al., 2017). Taken together, these results suggest that stress activates the production of numerous ncRNA types in the testis and/or epididymis, and that it consequently affects gene expression in post-fertilization embryos at multiple levels.

It is worth noting the plasticity of ncRNA production. The transgenerational metabolic phenotype can easily be reversed by exercise. Progeny produced from males fed a HFD exhibit metabolic disorders than can be restored when obese fathers engage in low-to moderate-intensity exercise for 2 months (McPherson et al, 2015, 2017). This phenotype reversion following exercise is supported by the fact that physical training modifies sperm ncRNA, and in particular a subset of piRNAs in humans (Ingerslev et al., 2018) as well as a subset of miRNA (miR-19b, miR-455 and miR-133a) and two species of tRF derived from tRNA-Gly and tRNA-Pro in mice (Short et al., 2017). As with diet, there is no consensus on the type and identity of the ncRNA induced in sperm by physical training.

Transgenerational stress transmission by sperm is not restricted to metabolic stress, and several reports suggest that physical stress (loud noises, predator odor, physical constraints, etc.) or hormonal stress (cortisone injection) experienced by the father alters behavioral responses to stress in the progeny, partly due to deregulation of the hypothalamic-pituitary-adrenal axis (Rodgers et al., 2013; Short et al., 2016). Importantly, the stress experienced by the father modifies a specific subset of spermatic miRNAs: nine miRNA (miR-193-5p, miR-204, miR-29c, miR-30a, miR-30c, miR-32, miR-375, miR-532–3p, and miR-698) were determined to be over-expressed by (Rodgers et al., 2013), and three (miR-98, miR-144 and miR-190b) were reported by (Short et al., 2016). Another observation of the transgenerational impact of stress applied early during life reported effects on 73 miRNAs, including miR-375-3p and -5p, miR-200b-3p, miR-672-5p, and miR-466-5p, which were upregulated (Gapp et al., 2014). Yet another report indicated that more than 100 miRNAs were modified in response to hormonal stress (Chan et al., 2020). It is important to highlight that there was no overlap in deregulated miRNA expression in sperm between these reports, although all linked the effects to the hypothalamic-pituitary-adrenal axis. Furthermore, injection of the nine miRNA reported by Rodgers et al. (2013) into a control zygote fully reproduced the disruption of the hypothalamic-pituitary-adrenal axis observed with sperm from stressed fathers, confirming the importance of these miRNAs (Rodgers et al., 2015). Interestingly, injection of just one miRNA partly reproduced the stress phenotype, suggesting that the combination of several miRNAs is important for transgenerational stress adaptation. The injection of the nine miRNAs modified the expression of 75 mRNAs present in oocytes, including genes playing roles in chromatin remodeling. This epigenetic control induced long-term modifications of gene expression in the target tissue, with 298 genes found to have altered expression in the paraventricular nucleus of the hypothalamus (Rodgers et al., 2015). Interestingly, changes to miRNA levels were observed up to 12 weeks after a short initial stress, suggesting that stress has a long-term effect on the transcriptomic program of epididymal cells (Chan et al., 2020). Thus, physical stress experienced by the father induces altered stress responsivity in offspring, but physical exercise produces a compensatory anxiolytic effect in the progeny (Short et al., 2017).

Finally, stress-induced ncRNA modifications of the father's sperm modify the cancer susceptibility of the progeny, in particular for breast cancer following metabolic stress (da Cruz et al., 2018; Fontelles et al., 2016), and medulloblastoma following irradiation (Paris et al., 2015).

In conclusion, the composition of sperm ncRNA is very sensitive to environmental stress, and these changes can have long-term effects on the expression of genes in various tissues, allowing rapid adaptability of the progeny without the need for DNA mutations, which are rare and random and therefore require a large population and many generations to achieve efficient adaptability.

The functions of the different ncRNAs are summarized in Fig. 7B.

7. Importance of sperm DNA methylation in the environmental stress-response

DNA methylation, which consists in the methylation of cytosine residues in CpG dinucleotides to form 5-methylcytosine, is a well-characterized mechanism driving gene expression. DNA methylation of a gene promotor is known to inhibit transcription of the corresponding gene. Consequently, DNA methylation is an important regulator of spermatogenesis, and its deregulation is associated with multiple forms of male infertility (Gunes et al., 2016). DNA methylation of male germ cells is mostly acquired in utero, and is completed by the end of the pachytene spermatocyte stage (Oakes et al., 2007).

There is now some evidence that the sperm methylation profile influences the phenotype of the progeny. First, several researchers modified the level of folate in the paternal diet (Lambrot et al., 2013; Ly et al., 2017). Folate is a precursor of co-enzymes necessary for several synthetic pathways, including those producing purine bases or thymidine monophosphate. These co-enzymes are also methyl donors and are involved in DNA methylation among other things. When the paternal diet lacks folate, a significant change in sperm DNA methylation is observed, with 57 genomic regions showing altered methylation profiles (Lambrot et al., 2013). Notably, these different methylated sites are close to the TSS of genes involved in development. These changes were associated with developmental abnormalities in the progeny, supporting the importance of sperm DNA methylation in the phenotype of the progeny. Second, reproduction in dairy cattle mainly relies on artificial insemination, and the best bull sires can have several thousand offspring. It is thus possible to study any relationship between sperm methylation and complex phenotypes in the offspring. In the study by Liu et al. (2019), the levels of methylation of variably methylated regions (VMRs) in sperm from 19 sires correlated with complex traits in their daughters including reproduction, milk production, and health. A high level of correlation was observed between methylation levels of VMR and reproductive traits, clearly demonstrating the intergenerational transmission of traits through DNA methylation (Liu et al., 2019).

We showed above that ncRNA are involved in the paternal epigenetic legacy, and in particular in the transgenerational transmission of environmental insults. Is there any evidence showing that methylation of sperm DNA also contributes to the paternal legacy? First, the possible role of sperm DNA methylation in the transgenerational transmission of obesity was observed in several studies. Obesity in rats induces a change in the methylation profile of epididymal sperm, and 18 regions were identified as differentially methylated between control rats and rats fed a HFD. Interestingly, the same regions were also differentially methylated in sperm from F1 offspring, but not in control progeny. Some regions were found to be hyper- or hypo-methylated (de Castro Barbosa et al., 2016). Similarly, physical training modified the methylation profile of sperm in humans, and around 300 differentially-methylated regions were identified following a 6-week exercise regimen (Ingerslev et al., 2018). Second, paternal stress can also modify the behavior of offspring in rodents. For instance, males separated from their mothers at an early age showed anxiety in adulthood. This separation anxiety induced a change in the methylation of genes, including *MeCP2*, cannabinoid receptor 1 (*CB1*), and corticotropin releasing factor receptor 2 (*CRFR2*) in sperm. The offspring and grand-offspring of these males, reared normally, also showed anxious behavior and similar alterations of the methylation of these genes in neural tissues (Franklin et al., 2010).

The transgenerational transmission of methylation profiles and their contribution to the phenotype of progeny remain a mystery when considering the two waves of general erasing of methylation marks. The first wave occurs just after fertilization and preserves only imprinted marks (Abdalla et al., 2009; Jenkins and Carrell, 2012)), and the second wave of DNA demethylation occurs before meiosis in PGCs in the developing embryo, corresponding, respectively, to embryonic days E11.5 and E12.5 in mice (Yamaguchi et al., 2012); for review, see (Cantone and Fisher, 2013). It is worth highlighting that in most studies relating to transgenerational transmission of environmental stress through paternal germ cells, simultaneous changes were observed in both methylation profiles and ncRNA content in sperm. It is therefore

difficult to weigh up the respective contributions of DNA methylation and ncRNA in the paternal legacy. Surprisingly, the changes in ncRNA observed in the father are generally not observed in the subsequent generation even though the phenotype is transmitted to the grand-offspring (Gapp et al., 2014). It is therefore possible that the paternal stress-induced ncRNA signal is converted into DNA methylation or histone post-translational modifications. Are ncRNA and DNA methylation two sides of the same coin? If DNA methylation is involved in such a process, it suggests that specific methylation marks made in response to environmental events are protected from the first wave of demethylation occurring within the zygote, in a similar way to imprinted marks, or that the transmitted ncRNA could contribute to apposing these marks after the demethylation wave. In contrast to most of the genome, which is compacted with protamines, imprinted genes remain associated with histones in nucleosomes. The presence of nucleosomes at these loci allows them to escape from the general erasing of marks. The localization of stress-dependent methylation marks in regions of compacted DNA in sperm with nucleosomes, and their escape from the first demethylation wave in zygotes remain to be formally demonstrated. Moreover, it is expected that species such as humans containing a larger proportion of sperm chromatin packaged in nucleosomes are more sensitive to environmental stress than species with a more limited proportion of their DNA compacted in nucleosomes, such as murine or bovine species. This hypothesis deserves further exploration.

8. Histones and other proteins as sperm-borne factors

As indicated in the first paragraph above, nucleosomes retained in sperm are important for paternal genome activation, and subsequent embryo development. Histones play key roles in epigenetics, and their post-translational modifications (PTM) such as methylation, acetylation, crotonylation, …, allow transcription to be adapted by changing the relaxation state of DNA. The histones retained in sperm carry several types of PTM (La Spina et al., 2014; Steilmann et al., 2011), and these histone marks have been described as repressive or active (Brykczynska et al., 2010).

As expected from the localization of the histones retained in the promotors of genes important for development (see above), changing the histone marks in sperm has a negative impact on embryo development. For instance, reducing H3K4 and H3K9 methylation in sperm by overexpression of histone H3 lysine 4 demethylase (*KDM1A*) increased embryo resorption during pregnancy and the rate of morphological defects in live offspring (Perez-Cerezales et al., 2017; Siklenka et al., 2015). More surprisingly, developmental and morphological defects were trans-generationally transmitted from the F1 to the F2 generation, even though germ cells in F1 males lacked *KDM1A* overexpression (Siklenka et al., 2015). This finding suggests that epigenetic marks at the histone level also support transgenerational adaptation to stress. Modification of histone marks was also observed with Vinclozolin, an agricultural fungicide used as a model to study transgenerational inheritance of chemical stress. Vinclozolin is an endocrine disruptor that decreases sperm count and viability, causing decreased male fertility (Anway et al., 2005). In this model, the F1 generation is treated at embryonic stages, and thus the F2 is produced from treated sperm. Studying transgenerational inheritance in this model revealed extra areas of histone H3 retention in sperm from the F3 generation of Vinclozolin-exposed lineages compared to a control lineage (Ben Maamar et al., 2018). Unexpectedly, the number of histone retention sites was normal in sperm from the F2 generation but increased in sperm from the F3 generation and beyond (Skinner et al., 2018), suggesting that histone modifications may be induced by other epigenetic factors. In addition to histone modifications, Vinclozolin treatment induces DNA methylation and alters the ncRNA payload (Skinner et al., 2018), and the various contributions and interactions of these epigenetic modifications to the infertility phenotype remain to be clarified.

Finally, apart from the sperm factor PLCzeta, which triggers oocyte activation and the absence of which leads to human infertility (Escoffier et al., 2016; Parrington et al., 2019), other sperm-borne proteins have been shown to play a role in embryo development. For instance, glutathione-S-transferase omega 2 (GSTO2), localized in the perinuclear theca of the sperm head, in conjunction with GSTO from the oocyte speeds up sperm DNA decondensation. Selective inhibition of GSTO2 in sperm before ICSI delays sperm DNA decondensation, leading to abnormal cleavage timings, and ultimately to a decreased rate of blastocyst formation (Hamilton et al., 2019a).

9. Perspectives and discussion

The discovery of the role of ncRNA in embryo development and adaptation to environmental stress has potentially significant medical consequences and technical applications.

9.1. Medical implications

Several reports indicated that analysis of the ncRNA composition of semen may be predictive of the fertilization competence of sperm (Cui et al., 2015; Munoz et al., 2015; Salas-Huetos et al., 2015). ncRNA profiling of infertile males may therefore be of interest to identify possible epigenetic causes for couples presenting with embryonic development failures after several cycles of ovarian stimulation. Nevertheless, all sperm-borne miRNAs necessary for optimal embryo development in humans remain to be characterized. Because of extensive variability in ncRNA between species, the short list identified so far in mice may not be relevant for human fertility. This identification step is required before any attempt to rescue or optimize embryonic development using synthetic ncRNA can be made.

We have also shown above that environmental insults can modify the ncRNA load in sperm and have dramatic effects on the physiopathology of the progeny, including the emergence of metabolic disorders and stress responses. A transient change in lifestyle, with a balanced diet, physical exercise and stress management approaches will likely modify the sperm ncRNA payload and could be recommended to couples consulting for infertility, to optimize the chances of fertilization, embryo development, and the health of any child born.

Finally, it would be interesting, for ICSI with testicular sperm to co-inject the most important and specific epididymal ncRNAs to improve embryo development. Again, this necessitates to characterize them in the human species because of species variability.

9.2. Technical applications

The most promising application of the discovery of the role of ncRNA in embryo development is in embryo cloning from somatic cells. It is well known that embryos obtained through somatic cell nuclear transfer (SCNT) show abnormal development, with disrupted kinetics of the first cleavage and defects in histone methylation, leading to low live birth rates and overweight offspring. Interestingly, co-injection of purified sperm ncRNAs along with a somatic cell nucleus decreases histone H3 methylation (H3K9me3), and increases K40 acetylation of tubulin, both of which are associated with increased SCNT yields (Qu et al., 2019). Among the classes of miRNAs involved in embryo development, miR-449a seems to be relevant since, when SCNT is performed with co-injection of miR-449a, the cleavage rate increases, epigenetic reprogramming of the embryo is improved, and the apoptotic index of blastocysts decreases (Wang et al., 2017). Sperm ncRNA is also a marker of the quality of sperm and could be used in animal reproduction to select bulls with a high fertility index as, for example, the level of expression of miR-216b in sperm is inversely correlated with the fertility index for bulls (Alves et al., 2019).

10. Conclusion

The data presented in this review show that the spermatozoon not only provides the paternal DNA component, but also a large number of epigenetic regulators, which influence embryonic development and allow rapid adaptation of the offspring to environmental stress. Much remains to be discovered, such as the identity and function of all the ncRNAs involved in embryonic development and stress adaptation. The targets of these ncRNAs and the signaling pathways activated have yet to be characterized, and also need to be investigated.

Acknowledgments

This work was supported by CNRS (to C.A.), the French National Research Agency (Agence Nationale de la Recherche; ANR-LIPAV-2-Consolidation) and by a grant from IMV Technologies to C.A.

References

Abdalla, H., Yoshizawa, Y., Hochi, S., 2009. Active demethylation of paternal genome in mammalian zygotes. J. Reprod. Dev. 55, 356–360.
Ahmad, K., Henikoff, S., 2002. The histone variant H3.3 marks active chromatin by replication-independent nucleosome assembly. Mol. Cell 9, 1191–1200.
Alfonso, P.J., Stephen Kistle, W., 1993. Immunohistochemical localization of spermatid nuclear transition protein 2 in the testes of rats and mice. Biol. Reprod. 48, 522–529.
Allen, M.J., Bradbury, E.M., Balhorn, R., 1997. AFM analysis of DNA-protamine complexes bound to mica. Nucleic Acids Res. 25, 2221–2226.
Allen, M.J., Lee, C., Lee, J.D., Pogany, G.C., Balooch, M., Siekhaus, W.J., Balhorn, R., 1993. Atomic force microscopy of mammalian sperm chromatin. Chromosoma 102, 623–630.
Alves, M.B.R., de Arruda, R.P., De Bem, T.H.C., Florez-Rodriguez, S.A., Sa Filho, M.F., Belleannee, C., Meirelles, F.V., da Silveira, J.C., Perecin, F., Celeghini, E.C.C., 2019. Sperm-borne miR-216b modulates cell proliferation during early embryo development via K-RAS. Sci. Rep. 9, 10358.
Amanai, M., Brahmajosyula, M., Perry, A.C., 2006. A restricted role for sperm-borne microRNAs in mammalian fertilization. Biol. Reprod. 75, 877–884.
An, T., Zhang, T., Teng, F., Zuo, J.C., Pan, Y.Y., Liu, Y.F., Miao, J.N., Gu, Y.J., Yu, N., Zhao, D.D., Mo, F.F., Gao, S.H., Jiang, G., 2017. Long non-coding RNAs could act as vectors for paternal heredity of high fat diet-induced obesity. Oncotarget 8, 47876–47889.
Anuar, N.D., Kurscheid, S., Field, M., Zhang, L., Rebar, E., Gregory, P., Buchou, T., Bowles, J., Koopman, P., Tremethick, D.J., Soboleva, T.A., 2019. Gene editing of the multi-copy H2A.B gene and its importance for fertility. Genome Biol. 20, 1–16.
Anway, M.D., Cupp, A.S., Uzumcu, M., Skinner, M.K., 2005. Epigenetic transgenerational actions of endocrine disruptors and male fertility. Science 308, 1466–1469.
Arpanahi, A., Brinkworth, M., Iles, D., Krawetz, S.A., Paradowska, A., Platts, A.E., Saida, M., Steger, K., Tedder, P., Miller, D., 2009. Endonuclease-sensitive regions of human spermatozoal chromatin are highly enriched in promoter and CTCF binding sequences. Genome Res. 19, 1338–1349.
Balhorn, R., 2007. The protamine family of sperm nuclear proteins. Genome Biol. 8, 227.
Balhorn, R., Corzett, M., Mazrimas, J.A., 1992. Formation of intraprotamine disulfides in vitro. Arch. Biochem. Biophys. 296, 384–393.
Balhorn, R., Gledhill, B.L., Wyrobek, A.J., 1977. Mouse sperm chromatin proteins: quantitative isolation and partial characterization. Biochemistry 16, 4074–4080.
Barral, S., Morozumi, Y., Tanaka, H., Montellier, E., Govin, J., Dieuleveult, Md, Charbonnier, G., Couté, Y., Puthier, D., Buchou, T., Boussouar, F., Urahama, T., Fenaille, F., Curtet, S., Héry, P., Fernandez-Nunez, N., Shiota, H., Gérard, M., Rousseaux, S., Kurumizaka, H., et al., 2017. Histone variant H2A.L.2 guides transition protein-dependent protamine assembly in male germ cells. Mol. Cell 66, 89–101.e108.
Baskaran, R., Rao, M.R., 1990. Interaction of spermatid-specific protein TP2 with nucleic acids, in vitro. A comparative study with TP1. J. Biol. Chem. 265, 21039–21047.
Baskaran, R., Rao, M.R.S., 1991. Mammalian spermatid specific protein, TP2, is a zinc metalloprotein with two finger motifs. Biochem. Biophys. Res. Commun. 179, 1491–1499.
Belleannee, C., Calvo, E., Caballero, J., Sullivan, R., 2013. Epididymosomes convey different repertoires of microRNAs throughout the bovine epididymis. Biol. Reprod. 89, 30.
Ben Maamar, M., Sadler-Riggleman, I., Beck, D., Skinner, M.K., 2018. Epigenetic transgenerational inheritance of altered sperm histone retention sites. Sci. Rep. 8, 5308.
Bench, G., Corzett, M.H., Kramer, C.E., Grant, P.G., Balhorn, R., 2000. Zinc is sufficiently abundant within mammalian sperm nuclei to bind stoichiometrically with protamine 2. Mol. Reprod. Dev. 56, 512–519.
Bench, G.S., Friz, A.M., Corzett, M.H., Morse, D.H., Balhorn, R., 1996. DNA and total protamine masses in individual sperm from fertile mammalian subjects. Cytometry 23, 263–271.
Bianchi, F., Rousseaux-Prevost, R., Sautiere, P., Rousseaux, J., 1992. P2 protamines from human sperm are zinc -finger proteins with one Cys2His2 motif. Biochem. Biophys. Res. Commun. 182, 540–547.
Björndahl, L., Kvist, U., 2010. Human sperm chromatin stabilization: a proposed model including zinc bridges. Mol. Hum. Reprod. 16, 23–29.
Bramlage, B., Kosciessa, U., Doenecke, D., 1997. Differential expression of the murine histone genes H3.3A and H3.3B. Differentiation 62, 13–20.
Brewer, L., Corzett, M., Lau, E.Y., Balhorn, R., 2003. Dynamics of protamine 1 binding to single DNA molecules. J. Biol. Chem. 278, 42403–42408.
Brunner, A.M., Nanni, P., Mansuy, I.M., 2014. Epigenetic marking of sperm by post-translational modification of histones and protamines. Epigenet. Chromatin 7, 1–12.
Brykczynska, U., Hisano, M., Erkek, S., Ramos, L., Oakeley, E.J., Roloff, T.C., Beisel, C., Schubeler, D., Stadler, M.B., Peters, A.H., 2010. Repressive and active histone methylation mark distinct promoters in human and mouse spermatozoa. Nat. Struct. Mol. Biol. 17, 679–687.
Bui, H.-T., Wakayama, S., Mizutani, E., Park, K.-K., Kim, J.-H., Thuan, N.V., Wakayama, T., 2011. Essential role of paternal chromatin in the regulation of transcriptional activity during mouse preimplantation development. Reproduction 141, 67–77.
Caballero, J.N., Frenette, G., Belleannée, C., Sullivan, R., 2013. CD9-Positive microvesicles mediate the transfer of molecules to bovine spermatozoa during epididymal maturation. PLoS One 8.
Calvin, H.I., 1976. Comparative analysis of the nuclear basic proteins in rat, human, guinea pig, mouse and rabbit spermatozoa. Biochim. Biophys. Acta (BBA) Protein Struct. 434, 377–389.
Cantone, I., Fisher, A.G., 2013. Epigenetic programming and reprogramming during development. Nat. Struct. Mol. Biol. 20, 282–289.
Caron, N., Veilleux, S., Boissonneault, G., 2001. Stimulation of DNA repair by the spermatidal TP1 protein. Mol. Reprod. Dev. 58, 437–443.
Carone, B.R., Fauquier, L., Habib, N., Shea, J.M., Hart, C.E., Li, R., Bock, C., Li, C., Gu, H., Zamore, P.D., Meissner, A., Weng, Z., Hofmann, H.A., Friedman, N., Rando, O.J., 2010. Paternally induced transgenerational environmental reprogramming of metabolic gene expression in mammals. Cell 143, 1084–1096.
Carone Benjamin, R., Hung, J.-H., Hainer Sarah, J., Chou, M.-T., Carone Dawn, M., Weng, Z., Fazzio Thomas, G., Rando Oliver, J., 2014. High-resolution mapping of chromatin packaging in mouse embryonic stem cells and sperm. Dev. Cell 30, 11–22.
Carré-Eusèbe, D., Lederer, F., Lê, K.H.D., Elsevier, S.M., 1991. Processing of the precursor of protamine P2 in mouse. Peptide mapping and N-terminal sequence analysis of intermediates. Biochem. J. 277, 39–45.
Chan, J.C., Morgan, C.P., Adrian Leu, N., Shetty, A., Cisse, Y.M., Nugent, B.M., Morrison, K.E., Jasarevic, E., Huang, W., Kanyuch, N., Rodgers, A.B., Bhanu, N.V., Berger, D.S., Garcia, B.A., Ament, S., Kane, M., Neill Epperson, C., Bale, T.L., 2020. Reproductive tract extracellular vesicles are sufficient to transmit intergenerational stress and program neurodevelopment. Nat. Commun. 11, 1499.
Chandler, V.L., 2007. Paramutation: from maize to mice. Cell 128, 641–645.
Chu, C.Y., Rana, T.M., 2007. Small RNAs: regulators and guardians of the genome. J. Cell. Physiol. 213, 412–419.
Cole, K.D., Kistler, W.S., 1987. Nuclear transition protein 2 (TP2) of mammalian spermatids has a very basic carboxyl terminal domain. Biochem. Biophys. Res. Commun. 147, 437–442.
Conine, C.C., Sun, F., Song, L., Rivera-Perez, J.A., Rando, O.J., 2018. Small RNAs gained during epididymal transit of sperm are essential for embryonic development in mice. Dev. Cell 46, 470–480.e473.
Corzett, M., Mazrimas, J., Balhorn, R., 2002. Protamine 1: protamine 2 stoichiometry in the sperm of eutherian mammals. Mol. Reprod. Dev. 61, 519–527.
Cox, L.J., Larman, M.G., Saunders, C.M., Hashimoto, K., Swann, K., Lai, F.A., 2002. Sperm phospholipase Czeta from humans and cynomolgus monkeys triggers Ca2+ oscillations, activation and development of mouse oocytes. Reproduction 124, 611–623.
Cui, L., Fang, L., Shi, B., Qiu, S., Ye, Y., 2015. Spermatozoa micro ribonucleic acid-34c level is correlated with intracytoplasmic sperm injection outcomes. Fertil. Steril. 104, 312–317.e311.
da Cruz, R.S., Carney, E.J., Clarke, J., Cao, H., Cruz, M.I., Benitez, C., Jin, L., Fu, Y., Cheng, Z., Wang, Y., de Assis, S., 2018. Paternal malnutrition programs breast cancer risk and tumor metabolism in offspring. Breast Cancer Res. 20, 99.
Da Ros, V.G., Munoz, M.W., Battistone, M.A., Brukman, N.G., Carvajal, G., Curci, L., Gomez-Ellas, M.D., Cohen, D.B., Cuasnicu, P.S., 2015. From the epididymis to the egg: participation of CRISP proteins in mammalian fertilization. Asian J. Androl. 17, 711–715.
Dadoune, J.P., 2009. Spermatozoal RNAs: what about their functions? Microsc. Res. Tech. 72, 536–551.
de Castro Barbosa, T., Ingerslev, L.R., Alm, P.S., Versteyhe, S., Massart, J., Rasmussen, M., Donkin, I., Sjogren, R., Mudry, J.M., Vetterli, L., Gupta, S., Krook, A., Zierath, J.R., Barres, R., 2016. High-fat diet reprograms the epigenome of rat spermatozoa and transgenerationally affects metabolism of the offspring. Mol. Metab. 5, 184–197.
Delucia, F., Faraonemennella, M.R., Derme, M., Quesada, P., Caiafa, P., Farina, B., 1994. Histone-induced condensation of rat testis chromatin: testis-specific H1t versus somatic H1 variants. Biochem. Biophys. Res. Commun. 198, 32–39.
DeRouchey, J.E., Rau, D.C., 2011. Role of amino acid insertions on intermolecular forces between arginine peptide condensed DNA helices implications for protamine-DNA packaging in sperm. J. Biol. Chem. 286, 41985–41992.
Drabent, B., Bode, C., Bramlage, B., Doenecke, D., 1996. Expression of the mouse testicular histone gene H1t during spermatogenesis. Histochem. Cell Biol. 106, 247–251.
El Fekih, S., Nguyen, M.H., Perrin, A., Beauvillard, D., Morel, F., Saad, A., Ben Ali, H., De Braekeleer, M., 2017. Sperm RNA preparation for transcriptomic analysis: review of the techniques and personal experience. Andrologia 49.

El Kennani, S., Adrait, A., Shaytan, A.K., Khochbin, S., Bruley, C., Panchenko, A.R., Landsman, D., Pflieger, D., Govin, J., 2017. MS_HistoneDB, a manually curated resource for proteomic analysis of human and mouse histones. Epigenet. Chromatin 10, 2.
Erkek, S., Hisano, M., Liang, C.-Y., Gill, M., Murr, R., Dieker, J., Schübeler, D., Jvd, Vlag, Stadler, M.B., Peters, A.H.F.M., 2013. Molecular determinants of nucleosome retention at CpG-rich sequences in mouse spermatozoa. Nat. Struct. Mol. Biol. 20, 868–875.
Escoffier, J., Lee, H.C., Yassine, S., Zouari, R., Martinez, G., Karaouzene, T., Coutton, C., Kherraf, Z.E., Halouani, L., Triki, C., Nef, S., Thierry-Mieg, N., Savinov, S.N., Fissore, R., Ray, P.F., Arnoult, C., 2016. Homozygous mutation of PLCZ1 leads to defective human oocyte activation and infertility that is not rescued by the WW-binding protein PAWP. Hum. Mol. Genet. 25, 878–891.
Fita, I., Campos, J.L., Puigjaner, L.C., Subirana, J.A., Luzzati, V., 1983. X-ray diffraction study of DNA complexes with arginine peptides and their relation to nucleoprotamine structure. J. Mol. Biol. 167, 157–177.
Fol, H., 1873. Le premier développement de l'œuf chez les Géronidés. Arch. Sci. Phys. Nat. 48, 2nd ser.
Fontelles, C.C., Carney, E., Clarke, J., Nguyen, N.M., Yin, C., Jin, L., Cruz, M.I., Ong, T.P., Hilakivi-Clarke, L., de Assis, S., 2016. Paternal overweight is associated with increased breast cancer risk in daughters in a mouse model. Sci. Rep. 6, 28602.
Franklin, T.B., Russig, H., Weiss, I.C., Graff, J., Linder, N., Michalon, A., Vizi, S., Mansuy, I.M., 2010. Epigenetic transmission of the impact of early stress across generations. Biol. Psychiatry 68, 408–415.
Fullston, T., Ohlsson-Teague, E.M., Print, C.G., Sandeman, L.Y., Lane, M., 2016. Sperm microRNA content is altered in a mouse model of male obesity, but the same suite of microRNAs are not altered in offspring's sperm. PLoS One 11, e0166076.
Fullston, T., Ohlsson Teague, E.M., Palmer, N.O., DeBlasio, M.J., Mitchell, M., Corbett, M., Print, C.G., Owens, J.A., Lane, M., 2013. Paternal obesity initiates metabolic disturbances in two generations of mice with incomplete penetrance to the F2 generation and alters the transcriptional profile of testis and sperm microRNA content. FASEB J. 27, 4226–4243.
Ganguly, I., Gaur, G.K., Kumar, S., Mandal, D.K., Kumar, M., Singh, U., Kumar, S., Sharma, A., 2013. Differential expression of protamine 1 and 2 genes in mature spermatozoa of normal and motility impaired semen producing crossbred Frieswal (HF×Sahiwal) bulls. Res. Vet. Sci. 94, 256–262.
Gapp, K., Jawaid, A., Sarkies, P., Bohacek, J., Pelczar, P., Prados, J., Farinelli, L., Miska, E., Mansuy, I.M., 2014. Implication of sperm RNAs in transgenerational inheritance of the effects of early trauma in mice. Nat. Neurosci. 17, 667–669.
Gardiner-Garden, M., Ballesteros, M., Gordon, M., Tam, P.P.L., 1998. Histone- and protamine-DNA association: conservation of different patterns within the β-globin domain in human sperm. Mol. Cell Biol. 18, 3350–3356.
Goh, W.S., Falciatori, I., Tam, O.H., Burgess, R., Meikar, O., Kotaja, N., Hammell, M., Hannon, G.J., 2015. piRNA-directed cleavage of meiotic transcripts regulates spermatogenesis. Genes Dev. 29, 1032–1044.
Gosálvez, J., López-Fernández, C., Fernández, J.L., Gouraud, A., Holt, W.V., 2011. Relationships between the dynamics of iatrogenic DNA damage and genomic design in mammalian spermatozoa from eleven species. Mol. Reprod. Dev. 78, 951–961.
Gou, L.T., Dai, P., Yang, J.H., Xue, Y., Hu, Y.P., Zhou, Y., Kang, J.Y., Wang, X., Li, H., Hua, M.M., Zhao, S., Hu, S.D., Wu, L.G., Shi, H.J., Li, Y., Fu, X.D., Qu, L.H., Wang, E. D., Liu, M.F., 2015. Pachytene piRNAs instruct massive mRNA elimination during late spermiogenesis. Cell Res. 25, 266.
Govin, J., Escoffier, E., Rousseaux, S., Kuhn, L., Ferro, M., Thévenon, J., Catena, R., Davidson, I., Garin, J., Khochbin, S., Caron, C., 2007. Pericentric heterochromatin reprogramming by new histone variants during mouse spermiogenesis. J. Cell Biol. 176, 283–294.
Grandjean, V., Fourre, S., De Abreu, D.A., Derieppe, M.A., Remy, J.J., Rassoulzadegan, M., 2015. RNA-mediated paternal heredity of diet-induced obesity and metabolic disorders. Sci. Rep. 5, 18193.
Grandjean, V., Gounon, P., Wagner, N., Martin, L., Wagner, K.D., Bernex, F., Cuzin, F., Rassoulzadegan, M., 2009. The miR-124-Sox9 paramutation: RNA-mediated epigenetic control of embryonic and adult growth. Development 136, 3647–3655.
Green, G.R., Balhorn, R., Poccia, D.L., Hecht, N.B., 1994. Synthesis and processing of mammalian protamines and transition proteins. Mol. Reprod. Dev. 37, 255–263.
Gunes, S., Arslan, M.A., Hekim, G.N.T., Asci, R., 2016. The role of epigenetics in idiopathic male infertility. J. Assist. Reprod. Genet. 33, 553–569.
Gupta, N., Madapura, M.P., Bhat, U.A., Rao, M.R.S., 2015. Mapping of post-translational modifications of transition proteins, TP1 and TP2, and identification of protein arginine methyltransferase 4 and lysine methyltransferase 7 as methyltransferase for TP2. J. Biol. Chem. 290, 12101–12122.
Hamilton, L.E., Suzuki, J., Aguila, L., Meinsohn, M.C., Smith, O.E., Protopapas, N., Xu, W., Sutovsky, P., Oko, R., 2019a. Sperm-borne glutathione-S-transferase omega 2 accelerates the nuclear decondensation of spermatozoa during fertilization in micedagger. Biol. Reprod. 101, 368–376.
Hamilton, T.R.S., Simões, R., Mendes, C.M., Goissis, M.D., Nakajima, E., Martins, EaL., Visintin, J.A., Assumpção, M.E.O.A., 2019b. Detection of protamine 2 in bovine spermatozoa and testicles. Andrology 7, 373–381.
Hammond, S.M., 2015. An overview of microRNAs. Adv. Drug Deliv. Rev. 87, 3–14.
Hammoud, S.S., Nix, D.A., Zhang, H., Purwar, J., Carrell, D.T., Cairns, B.R., 2009. Distinctive chromatin in human sperm packages genes for embryo development. Nature 460, 473–478.
Hartsoecker, N., 1694. Essay de dioptrique. Paris.
Hertwig, O., 1876. Beiträge zur Kenntniss des Bildung und Theilung des thierischen Eies. In: Morphologisches Jahrbuch, pp. 347–434.
Hess, R.A., Renato de Franca, L., 2008. Spermatogenesis and cycle of the seminiferous epithelium. Adv. Exp. Med. Biol. 636, 1–15.
Hoghoughi, N., Barral, S., Curtet, S., Chuffart, F., Charbonnier, G., Puthier, D., Buchou, T., Rousseaux, S., Khochbin, S., 2020. RNA-guided genomic localization of H2A.L.2 histone variant. Cells 9, 474.
Hombach, S., Kretz, M., 2016. Non-coding RNAs: classification, biology and functioning. Adv. Exp. Med. Biol. 937, 3–17.
Hud, N.V., Allen, M.J., Downing, K.H., Lee, J., Balhorn, R., 1993. Identification of the elemental packing unit of DNA in mammalian sperm cells by atomic force microscopy. Biochem. Biophys. Res. Commun. 193, 1347–1354.
Hud, N.V., Milanovich, F.P., Balhorn, R., 1994. Evidence of novel secondary structure in DNA-bound protamine is revealed by Raman spectroscopy. Biochemistry 33, 7528–7535.
Hutchison, J.M., Rau, D.C., DeRouchey, J.E., 2017. Role of disulfide bonds on DNA packaging forces in bull sperm chromatin. Biophys. J. 113, 1925–1933.
Ihara, M., Meyer-Ficca, M.L., Leu, N.A., Rao, S., Li, F., Gregory, B.D., Zalenskaya, I.A., Schultz, R.M., Meyer, R.G., 2014. Paternal poly (ADP-ribose) metabolism modulates retention of inheritable sperm histones and early embryonic gene expression. PLoS Genet. 10, e1004317.
Ingerslev, L.R., Donkin, I., Fabre, O., Versteyhe, S., Mechta, M., Pattamaprapanont, P., Mortensen, B., Krarup, N.T., Barres, R., 2018. Endurance training remodels sperm-borne small RNA expression and methylation at neurological gene hotspots. Clin. Epigen. 10, 12.
Jenkins, T.G., Carrell, D.T., 2012. Dynamic alterations in the paternal epigenetic landscape following fertilization. Front. Genet. 3, 143.
Jung, Y.H., Sauria, M.E.G., Lyu, X., Cheema, M.S., Ausio, J., Taylor, J., Corces, V.G., 2017. Chromatin states in mouse sperm correlate with embryonic and adult regulatory landscapes. Cell Rep. 18, 1366–1382.
Keam, S.P., Hutvagner, G., 2015. tRNA-derived fragments (tRFs): emerging new roles for an ancient RNA in the regulation of gene expression. Life (Basel) 5, 1638–1651.
Kiani, J., Grandjean, V., Liebers, R., Tuorto, F., Ghanbarian, H., Lyko, F., Cuzin, F., Rassoulzadegan, M., 2013. RNA-mediated epigenetic heredity requires the cytosine methyltransferase Dnmt2. PLoS Genet. 9, e1003498.
Kleene, K.C., Flynn, J.F., 1987. Characterization of a cDNA clone encoding a basic protein, TP2, involved in chromatin condensation during spermiogenesis in the mouse. J. Biol. Chem. 262, 17272–17277.
Kremling, H., Luerssen, H., Adham, I.M., Klemm, U., Tsaousidou, S., Engel, W., 1989. Nucleotide sequences and expression of cDNA clones for boar and bull transition protein 1 and its evolutionary conservation in mammals. Differentiation 40, 184–190.
La Spina, F.A., Romanato, M., Brugo-Olmedo, S., De Vincentiis, S., Julianelli, V., Rivera, R.M., Buffone, M.G., 2014. Heterogeneous distribution of histone methylation in mature human sperm. J. Assist. Reprod. Genet. 31, 45–49.
Lam, J.K., Chow, M.Y., Zhang, Y., Leung, S.W., 2015. siRNA versus miRNA as therapeutics for gene silencing. Mol. Ther. Nucleic Acids 4, e252.
Lambrot, R., Xu, C., Saint-Phar, S., Chountalos, G., Cohen, T., Paquet, M., Suderman, M., Hallett, M., Kimmins, S., 2013. Low paternal dietary folate alters the mouse sperm epigenome and is associated with negative pregnancy outcomes. Nat. Commun. 4, 2889.
Liu, S., Fang, L., Zhou, Y., Santos, D.J.A., Xiang, R., Daetwyler, H.D., Chamberlain, A.J., Cole, J.B., Li, C.J., Yu, Y., Ma, L., Zhang, S., Liu, G.E., 2019. Analyses of inter-individual variations of sperm DNA methylation and their potential implications in cattle. BMC Genom. 20, 888.
Liu, W.M., Pang, R.T., Chiu, P.C., Wong, B.P., Lao, K., Lee, K.F., Yeung, W.S., 2012. Sperm-borne microRNA-34c is required for the first cleavage division in mouse. Proc. Natl. Acad. Sci. U. S. A. 109, 490–494.
Loeb, J., 1913. Artificial parthenogenesis and fertilization. In: Chicago ITUoCP.
Ly, L., Chan, D., Aarabi, M., Landry, M., Behan, N.A., MacFarlane, A.J., Trasler, J., 2017. Intergenerational impact of paternal lifetime exposures to both folic acid deficiency and supplementation on reproductive outcomes and imprinted gene methylation. Mol. Hum. Reprod. 23, 461–477.
Mahadevaiah, S.K., Turner, J.M., Baudat, F., Rogakou, E.P., de Boer, P., Blanco-Rodriguez, J., Jasin, M., Keeney, S., Bonner, W.M., Burgoyne, P.S., 2001. Recombinational DNA double-strand breaks in mice precede synapsis. Nat. Genet. 27, 271–276.
Maier, W.-M., Nussbaum, G., Domenjoud, L., Klemm, U., Engel, W., 1990. The lack of protamine 2 (P2) in boar and bull spermatozoa is due to mutations within the P2 gene. Nucleic Acids Res. 18, 1249–1254.
Martianov, I., Brancorsini, S., Catena, R., Gansmuller, A., Kotaja, N., Parvinen, M., Sassone-Corsi, P., Davidson, I., 2005. Polar nuclear localization of H1T2, a histone H1 variant, required for spermatid elongation and DNA condensation during spermiogenesis. Proc. Natl. Acad. Sci. Unit. States Am. 102, 2808–2813.
Marushige, Y., Marushige, K., 1978. Phosphorylation of sperm histone during spermiogenesis in mammals. Biochim. Biophys. Acta (BBA) Nucleic Acids Protein Synth. 518, 440–449.
Mazrimas, J.A., Corzett, M., Campos, C., Balhorn, R., 1986. A corrected primary sequence for bull protamine. Biochim. Biophys. Acta (BBA) Protein Struct. Mol. Enzymol. 872, 11–15.
McKay, D.J., Renaux, B.S., Dixon, G.H., 1985. The amino acid sequence of human sperm protamine P1. Biosci. Rep. 5, 383–391.
McKAY, D.J., Renaux, B.S., Dixon, G.H., 1986. Human sperm protamines. Eur. J. Biochem. 156, 5–8.
McPherson, N.O., Lane, M., Sandeman, L., Owens, J.A., Fullston, T., 2017. An exercise-only intervention in obese fathers restores glucose and insulin regulation in conjunction with the rescue of pancreatic islet cell morphology and MicroRNA expression in male offspring. Nutrients 9.
McPherson, N.O., Owens, J.A., Fullston, T., Lane, M., 2015. Preconception diet or exercise intervention in obese fathers normalizes sperm microRNA profile and

metabolic syndrome in female offspring. Am. J. Physiol. Endocrinol. Metab. 308, E805–E821.
Meetei, A.R., Ullas, K.S., Rao, M.R.S., 2000. Identification of two novel zinc finger modules and nuclear localization signal in rat spermatidal protein TP2 by site-directed mutagenesis. J. Biol. Chem. 275, 38500–38507.
Meister, G., 2013. Argonaute proteins: functional insights and emerging roles. Nat. Rev. Genet. 14, 447–459.
Meyer-Ficca, M.L., Lonchar, J.D., Ihara, M., Bader, J.J., Meyer, R.G., 2013. Alteration of poly(ADP-ribose) metabolism affects murine sperm nuclear architecture by impairing pericentric heterochromatin condensation. Chromosoma 122, 319–335.
Miescher, F., 1874. Das Protamin, eine neue organische Base aus den Samenfäden des Rheinlachses. Ber. Dtsch. Chem. Ges. 7, 376–379.
Montellier, E., Boussouar, F., Rousseaux, S., Zhang, K., Buchou, T., Fenaille, F., Shiota, H., Debernardi, A., Hery, P., Curtet, S., Jamshidikia, M., Barral, S., Holota, H., Bergon, A., Lopez, F., Guardiola, P., Pernet, K., Imbert, J., Petosa, C., Tan, M., et al., 2013. Chromatin-to-nucleoprotamine transition is controlled by the histone H2B variant TH2B. Genes Dev. 27, 1680–1692.
Munoz, X., Mata, A., Bassas, L., Larriba, S., 2015. Altered miRNA signature of developing germ-cells in infertile patients relates to the severity of spermatogenic failure and persists in spermatozoa. Sci. Rep. 5, 17991.
Ng, S.F., Lin, R.C., Laybutt, D.R., Barres, R., Owens, J.A., Morris, M.J., 2010. Chronic high-fat diet in fathers programs beta-cell dysfunction in female rat offspring. Nature 467, 963–966.
Nixon, B., Stanger, S.J., Mihalas, B.P., Reilly, J.N., Anderson, A.L., Tyagi, S., Holt, J.E., McLaughlin, E.A., 2015. The microRNA signature of mouse spermatozoa is substantially modified during epididymal maturation. Biol. Reprod. 93, 91.
Oakes, C.C., La Salle, S., Smiraglia, D.J., Robaire, B., Trasler, J.M., 2007. Developmental acquisition of genome-wide DNA methylation occurs prior to meiosis in male germ cells. Dev. Biol. 307, 368–379.
Ozata, D.M., Gainetdinov, I., Zoch, A., O'Carroll, D., Zamore, P.D., 2019. PIWI-interacting RNAs: small RNAs with big functions. Nat. Rev. Genet. 20, 89–108.
Padavattan, S., Shinagawa, T., Hasegawa, K., Kumasaka, T., Ishii, S., Kumarevel, T., 2015. Structural and functional analyses of nucleosome complexes with mouse histone variants TH2a and TH2b, involved in reprogramming. Biochem. Biophys. Res. Commun. 464, 929–935.
Papoutsopoulou, S., 1999. SR protein-specific kinase 1 is highly expressed in testis and phosphorylates protamine 1. Nucleic Acids Res. 27, 2972–2980.
Parhad, S.S., Theurkauf, W.E., 2019. Rapid evolution and conserved function of the piRNA pathway. Open Biol. 9, 180181.
Paris, L., Giardullo, P., Leonardi, S., Tanno, B., Meschini, R., Cordelli, E., Benassi, B., Longobardi, M.G., Izzotti, A., Pulliero, A., Mancuso, M., Pacchierotti, F., 2015. Transgenerational inheritance of enhanced susceptibility to radiation-induced medulloblastoma in newborn Ptch1(+)/(-) mice after paternal irradiation. Oncotarget 6, 36098–36112.
Parrington, J., Arnoult, C., Fissore, R.A., 2019. The eggstraordinary story of how life begins. Mol. Reprod. Dev. 86, 4–19.
Peng, H., Shi, J., Zhang, Y., Zhang, H., Liao, S., Li, W., Lei, L., Han, C., Ning, L., Cao, Y., Zhou, Q., Chen, Q., Duan, E., 2012. A novel class of tRNA-derived small RNAs extremely enriched in mature mouse sperm. Cell Res. 22, 1609–1612.
Perez-Cerezales, S., Ramos-Ibeas, P., Lopez-Cardona, A., Pericuesta, E., Fernandez-Gonzalez, R., Pintado, B., Gutierrez-Adan, A., 2017. Elimination of methylation marks at lysines 4 and 9 of histone 3 (H3K4 and H3K9) of spermatozoa alters offspring phenotype. Reprod. Fertil. Dev. 29, 740–746.
Pessot, C.A., Brito, M., Figueroa, J., Concha II, Yanez, A., Burzio, L.O., 1989. Presence of RNA in the sperm nucleus. Biochem. Biophys. Res. Commun. 158, 272–278.
Puglisi, R., Maccari, I., Pipolo, S., Conrad, M., Mangia, F., Boitani, C., 2012. The nuclear form of glutathione peroxidase 4 is associated with sperm nuclear matrix and is required for proper paternal chromatin decondensation at fertilization. J. Cell. Physiol. 227, 1420–1427.
Qu, P., Zuo, Z., Liu, Z., Niu, Z., Zhang, Y., Du, Y., Ma, X., Qiao, F., Wang, M., Zhang, Y., Qing, S., Wang, Y., 2019. Sperm-borne small RNAs regulate alpha-tubulin acetylation and epigenetic modification of early bovine somatic cell nuclear transfer embryos. Mol. Hum. Reprod. 25, 471–482.
Queralt, R., Adroer, R., Oliva, R., Winkfein, R.J., Retief, J.D., Dixon, G.H., 1995. Evolution of protamine P1 genes in mammals. J. Mol. Evol. 40, 601–607.
Rassoulzadegan, M., Grandjean, V., Gounon, P., Vincent, S., Gillot, I., Cuzin, F., 2006. RNA-mediated non-mendelian inheritance of an epigenetic change in the mouse. Nature 441, 469–474.
Rathke, C., Baarends, W.M., Awe, S., Renkawitz-Pohl, R., 2014. Chromatin dynamics during spermiogenesis. Biochim. Biophys. Acta (BBA) Gene Regul. Mech. 1839, 155–168.
Ravelli, G.P., Stein, Z.A., Susser, M.W., 1976. Obesity in young men after famine exposure in utero and early infancy. N. Engl. J. Med. 295, 349–353.
Reilly, J.N., McLaughlin, E.A., Stanger, S.J., Anderson, A.L., Hutcheon, K., Church, K., Mihalas, B.P., Tyagi, S., Holt, J.E., Eamens, A.L., Nixon, B., 2016. Characterisation of mouse epididymosomes reveals a complex profile of microRNAs and a potential mechanism for modification of the sperm epigenome. Sci. Rep. 6, 31794.
Rodgers, A.B., Morgan, C.P., Bronson, S.L., Revello, S., Bale, T.L., 2013. Paternal stress exposure alters sperm microRNA content and reprograms offspring HPA stress axis regulation. J. Neurosci. 33, 9003–9012.
Rodgers, A.B., Morgan, C.P., Leu, N.A., Bale, T.L., 2015. Transgenerational epigenetic programming via sperm microRNA recapitulates effects of paternal stress. Proc. Natl. Acad. Sci. U. S. A. 112, 13699–13704.
Rossi, P., Sette, C., Dolci, S., Geremia, R., 2000. Role of c-kit in mammalian spermatogenesis. J. Endocrinol. Invest. 23, 609–615.
Royo, H., Stadler, M.B., Peters, A.H.F.M., 2016. Alternative computational analysis shows no evidence for nucleosome enrichment at repetitive sequences in mammalian spermatozoa. Dev. Cell 37, 98–104.
Salas-Huetos, A., Blanco, J., Vidal, F., Godo, A., Grossmann, M., Pons, M.C., F-Fernández, S., Garrido, N., Anton, E., 2015. Spermatozoa from patients with seminal alterations exhibit a differential micro-ribonucleic acid profile. Fertil. Steril. 104, 591–601.
Samans, B., Yang, Y., Krebs, S., Sarode Gaurav, V., Blum, H., Reichenbach, M., Wolf, E., Steger, K., Dansranjavin, T., Schagdarsurengin, U., 2014. Uniformity of nucleosome preservation pattern in mammalian sperm and its connection to repetitive DNA elements. Dev. Cell 30, 23–35.
Saowaros, W., Panyim, S., 1979. The formation of disulfide bonds in human protamines during sperm maturation. Experientia 35, 191–192.
Sato, H., Taketomi, Y., Isogai, Y., Miki, Y., Yamamoto, K., Masuda, S., Hosono, T., Arata, S., Ishikawa, Y., Ishii, T., Kobayashi, T., Nakanishi, H., Ikeda, K., Taguchi, R., Hara, S., Kudo, I., Murakami, M., 2010. Group III secreted phospholipase A2 regulates epididymal sperm maturation and fertility in mice. J. Clin. Invest. 120, 1400–1414.
Saunders, C.M., Larman, M.G., Parrington, J., Cox, L.J., Royse, J., Blayney, L.M., Swann, K., Lai, F.A., 2002. PLC zeta: a sperm-specific trigger of Ca(2+) oscillations in eggs and embryo development. Development 129, 3533–3544.
Schlüter, G., Kremling, H., Engel, W., 1992. The gene for human transition protein 2: nucleotide sequence, assignment to the protamine gene cluster, and evidence for its low expression. Genomics 14, 377–383.
Schuster, A., Tang, C., Xie, Y., Ortogero, N., Yuan, S., Yan, W., 2016. SpermBase: a database for sperm-borne RNA contents. Biol. Reprod. 95, 99.
Selvaraju, S., Parthipan, S., Somashekar, L., Kolte, A.P., Krishnan Binsila, B., Arangasamy, A., Ravindra, J.P., 2017. Occurrence and functional significance of the transcriptome in bovine (Bos taurus) spermatozoa. Sci. Rep. 7, 42392.
Sendler, E., Johnson, G.D., Mao, S., Goodrich, R.J., Diamond, M.P., Hauser, R., Krawetz, S.A., 2013. Stability, delivery and functions of human sperm RNAs at fertilization. Nucleic Acids Res. 41, 4104–4117.
Sharma, U., Conine, C.C., Shea, J.M., Boskovic, A., Derr, A.G., Bing, X.Y., Belleannee, C., Kucukural, A., Serra, R.W., Sun, F., Song, L., Carone, B.R., Ricci, E.P., Li, X.Z., Fauquier, L., Moore, M.J., Sullivan, R., Mello, C.C., Garber, M., Rando, O.J., 2016. Biogenesis and function of tRNA fragments during sperm maturation and fertilization in mammals. Science 351, 391–396.
Sharma, U., Sun, F., Conine, C.C., Reichholf, B., Kukreja, S., Herzog, V.A., Ameres, S.L., Rando, O.J., 2018. Small RNAs are trafficked from the epididymis to developing mammalian sperm. Dev. Cell 46, 481–494.e486.
Shiraishi, K., Shindo, A., Harada, A., Kurumizaka, H., Kimura, H., Ohkawa, Y., Matsuyama, H., 2018. Roles of histone H3.5 in human spermatogenesis and spermatogenic disorders. Andrology 6, 158–165.
Shirley, C.R., Hayashi, S., Mounsey, S., Yanagimachi, R., Meistrich, M.L., 2004. Abnormalities and reduced reproductive potential of sperm from Tnp1- and Tnp2-null double mutant mice. Biol. Reprod. 71, 1220–1229.
Short, A.K., Fennell, K.A., Perreau, V.M., Fox, A., O'Bryan, M.K., Kim, J.H., Bredy, T.W., Pang, T.Y., Hannan, A.J., 2016. Elevated paternal glucocorticoid exposure alters the small noncoding RNA profile in sperm and modifies anxiety and depressive phenotypes in the offspring. Transl. Psychiatry 6, e837.
Short, A.K., Yeshurun, S., Powell, R., Perreau, V.M., Fox, A., Kim, J.H., Pang, T.Y., Hannan, A.J., 2017. Exercise alters mouse sperm small noncoding RNAs and induces a transgenerational modification of male offspring conditioned fear and anxiety. Transl. Psychiatry 7, e1114.
Siklenka, K., Erkek, S., Godmann, M., Lambrot, R., McGraw, S., Lafleur, C., Cohen, T., Xia, J., Suderman, M., Hallett, M., Trasler, J., Peters, A.H., Kimmins, S., 2015. Disruption of histone methylation in developing sperm impairs offspring health transgenerationally. Science 350, aab2006.
Sillaste, G., Kaplinski, L., Meier, R., Jaakma, Ü., Eriste, E., Salumets, A., 2017. A novel hypothesis for histone-to-protamine transition in Bos taurus spermatozoa. Reproduction 153, 241–251.
Singh, J., Rao, M.R., 1987. Interaction of rat testis protein, TP, with nucleic acids in vitro. Fluorescence quenching, UV absorption, and thermal denaturation studies. J. Biol. Chem. 262, 734–740.
Skinner, M.K., Ben Maamar, M., Sadler-Riggleman, I., Beck, D., Nilsson, E., McBirney, M., Klukovich, R., Xie, Y., Tang, C., Yan, W., 2018. Alterations in sperm DNA methylation, non-coding RNA and histone retention associate with DDT-induced epigenetic transgenerational inheritance of disease. Epigenet. Chromatin 11, 8.
Soboleva, T.A., Nekrasov, M., Pahwa, A., Williams, R., Huttley, G.A., Tremethick, D.J., 2012. A unique H2A histone variant occupies the transcriptional start site of active genes. Nat. Struct. Mol. Biol. 19, 25–30.
Soboleva, T.A., Parker, B.J., Nekrasov, M., Hart-Smith, G., Tay, Y.J., Tng, W.-Q., Wilkins, M., Ryan, D., Tremethick, D.J., 2017. A new link between transcriptional initiation and pre-mRNA splicing: the RNA binding histone variant H2A.B. PLoS Genet. 13, e1006633.
Song, R., Hennig, G.W., Wu, Q., Jose, C., Zheng, H., Yan, W., 2011. Male germ cells express abundant endogenous siRNAs. Proc. Natl. Acad. Sci. U. S. A. 108, 13159–13164.
Soon, L.L., Ausio, J., Breed, W.G., Power, J.H., Muller, S., 1997. Isolation of histones and related chromatin structures from spermatozoa nuclei of a dasyurid marsupial, *Sminthopsis crassicaudata*. J. Exp. Zool. 278, 322–332.
Steger, K., 1999. Transcriptional and translational regulation of gene expression in haploid spermatids. Anat. Embryol. 199, 471–487.
Steilmann, C., Paradowska, A., Bartkuhn, M., Vieweg, M., Schuppe, H.C., Bergmann, M., Kliesch, S., Weidner, W., Steger, K., 2011. Presence of histone H3 acetylated at lysine

9 in male germ cells and its distribution pattern in the genome of human spermatozoa. Reprod. Fertil. Dev. 23, 997–1011.
Suh, N., Baehner, L., Moltzahn, F., Melton, C., Shenoy, A., Chen, J., Blelloch, R., 2010. MicroRNA function is globally suppressed in mouse oocytes and early embryos. Curr. Biol. 20, 271–277.
Tachiwana, H., Kagawa, W., Osakabe, A., Kawaguchi, K., Shiga, T., Hayashi-Takanaka, Y., Kimura, H., Kurumizaka, H., 2010. Structural basis of instability of the nucleosome containing a testis-specific histone variant, human H3T. Proc. Natl. Acad. Sci. Unit. States Am. 107, 10454–10459.
Tanaka, A., Nagayoshi, M., Takemoto, Y., Tanaka, I., Kusunoki, H., Watanabe, S., Kuroda, K., Takeda, S., Ito, M., Yanagimachi, R., 2015. Fourteen babies born after round spermatid injection into human oocytes. Proc. Natl. Acad. Sci. U. S. A. 112, 14629–14634.
Tanphaichitr, N., Sobhon, P., Taluppeth, N., Chalermisarachai, P., 1978. Basic nuclear proteins in testicular cells and ejaculated spermatozoa in man. Exp. Cell Res. 117, 347–356.
Thakar, A., Gupta, P., Ishibashi, T., Finn, R., Silva-Moreno, B., Uchiyama, S., Fukui, K., Tomschik, M., Ausio, J., Zlatanova, J., 2009. H2A.Z and H3.3 histone variants affect nucleosome structure: biochemical and biophysical studies. Biochemistry 48, 10852–10857.
Thoma, F., Koller, T., Klug, A., 1979. Involvement of histone H1 in the organization of the nucleosome and of the salt-dependent superstructures of chromatin. J. Cell Biol. 83, 403–427.
Tobita, T., Nomoto, M., Nakano, M., Ando, T., 1982. Isolation and characterization of nuclear basic protein (protamine) from boar spermatozoa. Biochim. Biophys. Acta (BBA) Protein Struct. Mol. Enzymol. 707, 252–258.
Trostle-Weige, P.K., Meistrich, M.L., Brock, W.A., Nishioka, K., 1984. Isolation and characterization of TH3, a germ cell-specific variant of histone 3 in rat testis. J. Biol. Chem. 259, 8769–8776.
Trostle-Weige, P.K., Meistrich, M.L., Brock, W.A., Nishioka, K., Bremer, J.W., 1982. Isolation and characterization of TH2A, a germ cell-specific variant of histone 2A in rat testis. J. Biol. Chem. 257, 5560–5567.
Ueda, J., Harada, A., Urahama, T., Machida, S., Maehara, K., Hada, M., Makino, Y., Nogami, J., Horikoshi, N., Osakabe, A., Taguchi, H., Tanaka, H., Tachiwana, H., Yao, T., Yamada, M., Iwamoto, T., Isotani, A., Ikawa, M., Tachibana, T., Okada, Y., et al., 2017. Testis-specific histone variant H3t gene is essential for entry into spermatogenesis. Cell Rep. 18, 593–600.
Uhlén, M., Hallström, B.M., Lindskog, C., Mardinoglu, A., Pontén, F., Nielsen, J., 2016. Transcriptomics resources of human tissues and organs. Mol. Syst. Biol. 12, 862.
Urahama, T., Harada, A., Maehara, K., Horikoshi, N., Sato, K., Sato, Y., Shiraishi, K., Sugino, N., Osakabe, A., Tachiwana, H., Kagawa, W., Kimura, H., Ohkawa, Y., Kurumizaka, H., 2016. Histone H3.5 forms an unstable nucleosome and accumulates around transcription start sites in human testis. Epigenet. Chromatin 9, 1–16.
van Beneden, E., 1883. Recherches sur la maturation de l'oeuf et la fécondation. Arch. Biol. (Liege) 4, 265–640.
van der Heijden, G.W., Derijck, A.A., Posfai, E., Giele, M., Pelczar, P., Ramos, L., Wansink, D.G., van der Vlag, J., Peters, A.H., de Boer, P., 2007. Chromosome-wide nucleosome replacement and H3.3 incorporation during mammalian meiotic sex chromosome inactivation. Nat. Genet. 39, 251–258.
van der Heijden, G.W., Ramos, L., Baart, E.B., van den Berg, I.M., Derijck, A.A.H.A., van der Vlag, J., Martini, E., de Boer, P., 2008. Sperm-derived histones contribute to zygotic chromatin in humans. BMC Dev. Biol. 8, 34.
van Roijen, H.J., Ooms, M.P., Spaargaren, M.C., Baarends, W.M., Weber, R.F., Grootegoed, J.A., Vreeburg, J.T., 1998. Immunoexpression of testis-specific histone 2B in human spermatozoa and testis tissue. Hum. Reprod. 13, 1559–1566.
Wagner, K.D., Wagner, N., Ghanbarian, H., Grandjean, V., Gounon, P., Cuzin, F., Rassoulzadegan, M., 2008. RNA induction and inheritance of epigenetic cardiac hypertrophy in the mouse. Dev. Cell 14, 962–969.
Wang, M., Gao, Y., Qu, P., Qing, S., Qiao, F., Zhang, Y., Mager, J., Wang, Y., 2017. Sperm-borne miR-449b influences cleavage, epigenetic reprogramming and apoptosis of SCNT embryos in bovine. Sci. Rep. 7, 13403.
Wang, T., Gao, H., Li, W., Liu, C., 2019. Essential role of histone replacement and modifications in male fertility. Front. Genet. 10.
Ward, W.S., 2010. Function of sperm chromatin structural elements in fertilization and development. Mol. Hum. Reprod. 16, 30–36.
Wu, J.Y., Ribar, T.J., Cummings, D.E., Burton, K.A., McKnight, G.S., Means, A.R., 2000. Spermiogenesis and exchange of basic nuclear proteins are impaired in male germ cells lacking Camk4. Nat. Genet. 25, 448–452.
Yamaguchi, K., Hada, M., Fukuda, Y., Inoue, E., Makino, Y., Katou, Y., Shirahige, K., Okada, Y., 2018. Re-evaluating the localization of sperm-retained histones revealed the modification-dependent accumulation in specific genome regions. Cell Rep. 23, 3920–3932.
Yamaguchi, S., Hong, K., Liu, R., Shen, L., Inoue, A., Diep, D., Zhang, K., Zhang, Y., 2012. Tet1 controls meiosis by regulating meiotic gene expression. Nature 492, 443–447.
Yan, W., Ma, L., Burns, K.H., Matzuk, M.M., 2003. HILS1 is a spermatid-specific linker histone H1-like protein implicated in chromatin remodeling during mammalian spermiogenesis. Proc. Natl. Acad. Sci. Unit. States Am. 100, 10546–10551.
Yan, W., Morozumi, K., Zhang, J., Ro, S., Park, C., Yanagimachi, R., 2008. Birth of mice after intracytoplasmic injection of single purified sperm nuclei and detection of messenger RNAs and MicroRNAs in the sperm nuclei. Biol. Reprod. 78, 896–902.
Yelick, P.C., Balhorn, R., Johnson, P.A., Corzett, M., Mazrimas, J.A., Kleene, K.C., Hecht, N.B., 1987. Mouse protamine 2 is synthesized as a precursor whereas mouse protamine 1 is not. Mol. Cell Biol. 7, 2173–2179.
Yoshida, K., Muratani, M., Araki, H., Miura, F., Suzuki, T., Dohmae, N., Katou, Y., Shirahige, K., Ito, T., Ishii, S., 2018. Mapping of histone-binding sites in histone replacement-completed spermatozoa. Nat. Commun. 9, 3885.
Yossefi, S., Oschry, Y., Lewin, L.M., 1994. Chromatin condensation in hamster sperm: a flow cytometric investigation. Mol. Reprod. Dev. 37, 93–98.
Yu, Y.E., Zhang, Y., Unni, E., Shirley, C.R., Deng, J.M., Russell, L.D., Weil, M.M., Behringer, R.R., Meistrich, M.L., 2000. Abnormal spermatogenesis and reduced fertility in transition nuclear protein 1-deficient mice. Proc. Natl. Acad. Sci. Unit. States Am. 97, 4683–4688.
Yuan, S., Schuster, A., Tang, C., Yu, T., Ortogero, N., Bao, J., Zheng, H., Yan, W., 2016. Sperm-borne miRNAs and endo-siRNAs are important for fertilization and preimplantation embryonic development. Development 143, 635–647.
Yuen, B.T.K., Bush, K.M., Barrilleaux, B.L., Cotterman, R., Knoepfler, P.S., 2014. Histone H3.3 regulates dynamic chromatin states during spermatogenesis. Development 141, 3483–3494.
Zaidan, H., Leshem, M., Gaisler-Salomon, I., 2013. Prereproductive stress to female rats alters corticotropin releasing factor type 1 expression in ova and behavior and brain corticotropin releasing factor type 1 expression in offspring. Biol. Psychiatry 74, 680–687.
Zalenskaya, I.A., Bradbury, E.M., Zalensky, A.O., 2000. Chromatin structure of telomere domain in human sperm. Biochem. Biophys. Res. Commun. 279, 213–218.
Zhao, M., Shirley, C.R., Mounsey, S., Meistrich, M.L., 2004. Nucleoprotein transitions during spermiogenesis in mice with transition nuclear protein Tnp1 and Tnp2 mutations. Biol. Reprod. 71, 1016–1025.
Zhao, M., Shirley, C.R., Yu, Y.E., Mohapatra, B., Zhang, Y., Unni, E., Deng, J.M., Arango, N.A., Terry, N.H.A., Weil, M.M., Russell, L.D., Behringer, R.R., Meistrich, M. L., 2001. Targeted disruption of the transition protein 2 gene affects sperm chromatin structure and reduces fertility in mice. Mol. Cell Biol. 21, 7243–7255.

DISCUSSION AND PERSPECTIVES

Infertility is a growing global health problem. It touches approximately 9% of couples and its causes remain unexplained in around 40% of them (Sadeghi 2015). In this work we focused on a particular severe subtype of primary male infertility called the multiple morphological abnormalities of the sperm flagella (MMAF). This syndrome is characterized by a mosaic of flagellar abnormalities including short, coiled, bent, irregular, or absent flagella (Ben Khelifa et al. 2014). Defects in sperm head morphology were also associated with the MMAF syndrome in men harbouring homozygous mutations in genes, including *DNAH2* (Hwang et al. 2021), *CFAP43/44* (Charles Coutton et al. 2018), and *CFAP69* (Dong et al. 2018). The flagellar defects have a negative effect on sperm motility and the syndrome is characterized by asthenozoospermia. It also has a strong genetic component, and it has been associated with more than 40 recessive genes. Our laboratory primarily focuses on the study of male infertility. Among our cohort of 167 MMAF-affected patients, the team had already identified biallelic deleterious variants in 22 genes in 83 subjects.

Among this cohort of MMAF patients, we identified homozygous truncating mutations in gene Coiled coil domain-containing 146 (*CCDC146)* in two men. The primary focus of this thesis was thus to characterize the role of CCDC146 in male fertility. We used a mouse *Ccdc146* knock-out (KO) model to describe the spermatogenic defects caused by the absence of CCDC146 and verified that the model reproduced the MMAF phenotype observed in humans. Our results showed that CCDC146 is centrosome-associated and flagellar protein that is essential for spermiogenesis, including flagellum assembly, manchette formation and proper HTCA connection to the sperm head.

In the first part of the discussion, we will review our results and propose hypotheses about the function of CCDC146. In the following part, we will discuss the prognoses for patients harbouring mutations in MMAF-related genes to conceive with ICSI. And finally, we will talk about other actors that might influence male fertility including oligogenic inheritance.

1 THE FUNCTION OF CCDC146

Characterizing the role of CCDC146 in male fertility was the primary objective of this thesis. We showed that in mice, CCDC146 is essential for correct spermiogenesis, including manchette formation and axoneme assembly. Its absence also led to multiplicated centrioles in spermatids and to an aberrant HTCA attachment to the sperm head. Because the manchette, head shaping, HTCA and flagellum formation are interlinked, it is difficult to distinguish the cause and its consequences only based on defects in these processes. Several experiments could help us gain more insight into the function of CCDC146 in both male germ cells and somatic cells. Below, we will discuss these experiments and hypotheses about the function of CCDC146.

1.1 CCDC146 AND CENTRIOLES

CCDC146 has been previously identified as a centriolar protein in bovine spermatozoa and was also detected at the mother centriole in HeLa and RPE1 cells (Firat-Karalar et al. 2014). We thus wanted to see if CCDC146 was also associated with centrioles in human and mouse spermatogenic cells, and if we could confirm its centriolar localization in another human somatic cell line (HEK293T).

No centriolar signal was observed in neither mouse nor human spermatogenic cells by immunofluorescence (IF), and a CCDC146 signal was only associated with sperm flagella (Article 1, Figures 7, 8). Interestingly, despite the absence of CCDC146 labeling at the HTCA in mouse spermatids, the protein's absence had an impact on the structure. The centriole pair was observed correctly attached to the spermatid head in round spermatids, but it could often be seen in the cytoplasm at various distances from the head in elongating spermatids. Despite the abnormal distance of the HTCA from head, mature *Ccdc146* KO spermatozoa were not decapitated, and centrioles were retained in the cytoplasmic sac. We were unable to say if centriole movement toward the nucleus during spermiogenesis or their attachment were somehow disrupted or whether their connection with the sperm head was too fragile and they detached during spermatid elongation.

Moreover, we observed supernumerary centrioles or multiple pieces of centrioles in elongating spermatids. The last centriole duplication occurs in spermatocytes before they enter meiosis (Avidor-Reiss and Fishman 2019). It could be interesting to observe whether KO spermatogonia

and spermatocytes contain aberrant numbers of centrioles, or whether new centriole duplication occurs in spermatids. Defects in centriole number are generally associated with aneuploidy and cancer (Shin et al. 2021; Bühler and Stolz 2022; J. Z. Zhao et al. 2021). However, even-though we observed a significant increase in apoptosis in KO seminiferous tubules, no specific cell population appeared to be affected, suggesting that if supernumerary centrioles were already present in spermatogonia or spermatocytes, they did not systematically cause severe defects in cell division leading to cell death in most cells. Mice were viable and we did not observe an apparition of tumors or any other phenotype except for male infertility. For instance, aberrant centriole duplication was observed in humans for loss-of-function mutations in *DZIP1*, another MMAF-associated gene (Lv et al. 2020), and mouse *Ccdc42* (Pasek et al. 2016).

In human somatic cells, CCDC146 was associated with both centrioles throughout the cells cycle and with the basal body of primary cilia. We are unsure why our signal was always associated with both centrioles, while Firat-Karalar *et al.* showed that it is only present at the mother centriole (Firat-Karalar et al. 2014).

A precise localization of the protein would allow us to gain a better understanding of its function. In somatic cells, CCDC146 was only partially co-localized with centrin, which is present within the inner scaffold of both centrioles. We could determine the localization of CCDC146 at centrioles (proximal or distal end, distal or subdistal appendages) in somatic cells using conventional IF though the co-localization with proteins belonging only to these subparts, or even more precisely (e.g. within the inner scaffold) using ultrastructure expansion microscopy (Huang et al. 2017; Le Guennec et al. 2020; T. T. Yang et al. 2018). We could also use immunogold labeling coupled with transmission electron microscopy in both somatic cells and spermatogenic cells. When applied to mouse and human testis cross-sections, it could show where CCDC146 accumulates during spermiogenesis. Since CCDC146 is particularly expressed in spermatids and it influences the structure of the manchette, the HTCA and the assembly of the axoneme, it might be associated with these structures.

1.2 CCDC146 AND MITOSIS

During mitosis, CCDC146 was associated with centrioles at the mitotic poles, and it was also positioned at the midbody, suggesting that CCDC146 could be important for cell division and

cytokinesis. As was previously mentioned, centriolar defects including centriole loss and multiplication, can negatively affect cell division and chromosome segregation (Sir et al. 2013; Godinho and Pellman 2014; J. Z. Zhao et al. 2021), and a precise spatio-temporal control of midbody proteins is important for correct separation of daughter cells (Mierzwa and Gerlich 2014).

Interestingly, a primary screen using RNAi against Ccdc146 was available at the Mitocheck website (Cai et al. 2018; "MitoCheck" n.d.). The Mitocheck database is based on large-scale RNAi screens, and automated microscopy and analysis. The knock-down of *CCDC146* in HeLa cells did not seem to affect cell division in a very severe manner, but some cells could be seen dividing into 3 daughter cells, suggesting that CCDC146 might play a minor role in mitosis. The regulation of centriole number could also be compromised in these cells and remains to be investigated.

1.3 CCDC146 AS A CENTRIOLAR SATELLITE

The IF signal for CCDC146 at the centriole was only partially co-localizing with the centriolar protein centrin, and showed a larger punctiform signal that was concentrated around both centrioles/ basal body (Article 1, Figure 4). The punctiform signal highly resembled centriolar satellites. To verify whether CCDC146 could be a centriolar satellite, we performed an IF co-localization study with PCM1 that is believed to be the marker of the majority of centriolar satellites (Article 1, Supplementary figure 4). Again, we only observed a partial co-localization with PCM1, and CCDC146 was not identified as an interactor of PCM1 in proteomics studies (Quarantotti et al. 2019; Gheiratmand et al. 2019), suggesting that CCDC146 is not a centriolar satellite.

1.4 CCDC146 AS A MICROTUBULE-ASSOCIATED PROTEIN

We proposed that CCDC146 is a microtubule-associated protein (MAP), and our hypothesis is based on several observations in both human somatic cells and spermatogenic cells from WT and *Ccdc146* KO mice. In human somatic cells undergoing mitosis, the localization of CCDC146 was dynamic. As was mentioned before, a part of the CCDC146 protein pool remained associated with the centrioles, but another part was mobile. A punctiform signal for CCDC146 concentrated on astral MTs in the proximity of the centrioles. During metaphase, CCDC146 relocated to microtubule tips, possibly to the kinetochores, but this interaction remains to be confirmed.

Subsequently, it was found co-localizing with MTs of the midzone/ central spindle, and then remained associated with this region and was seen at the midbody during cytokinesis. In spermatogenic cells, CCDC146 was present in the flagellum of both human and mouse spermatozoa. Its absence in the mouse also influenced MT-based structures: the axoneme, the manchette, and the HTCA. These results suggested that CCDC146 could be a MAP.

We showed that CCDC146 is present in the sperm flagellum of humans and mice and appeared to be associated with outer microtubule doublets. To more accurately localize the protein within the sperm flagellum, we could use super-resolution microscopy with STORM and reconstruct a cross-sectional view of the flagellum as was previously shown (Gervasi et al. 2018).

1.5 CCDC146 AS A MICROTUBULE INNER PROTEIN

Then, we hypothesized whether CCDC146 could also be a microtubule inner protein (MIP). The *Chlamydomonas* orthologue of CCDC146 called MBO2 was also shown to be a flagellar protein (Tam and Lefebvre 2002). In the absence of MBO2, microtubule doublets 5 and 6 lack "beak-like projections" in the B-tubule. These projections are MIPs that are present in MT doublets 1, 5 and 6 in the proximal and central regions of the axoneme. They are important for correct flagellar beating, but their composition is unknown (Ma et al. 2019). Moreover, we had difficulties solubilizing CCDC146 and sarkosyl, a known detergent that destabilizes microtubules, was efficient to solubilize the protein. Based on these results, we hypothesized that CCDC146 could be a MIP in the sperm axoneme. Sarkosyl has been shown to disrupt axonemal microtubule doublets in isolated *Chlamydomonas* axonemes, where a concentration >0.3% dissolved most B-tubules while singlet A-tubules remained, and a treatment with sarkosyl for 1h at 0.7% disrupted A-tubules (Kirima and Oiwa 2018). A treatment with 0.2% showed that some unknown proteins dissociated from the axoneme. An overnight treatment with 0.7% sarkosyl cleaved microtubule doublets and resulted in the formation of a sarkosyl-insoluble ribbon composed of tubulin and two MIPs, Rib72 and Rib43 (Kirima and Oiwa 2018; Ma et al. 2019). In our case, CCDC146 was already solubilized at 0.2% sarkosyl concentration from mouse flagella and we wondered whether mouse sperm flagella were more fragile and susceptible to the treatment that *Chlamydomonas* axonemes. These hypotheses could be verified by treating mouse (or human) sperm flagella with increasing sarkosyl concentrations and observing the structure of microtubule doublets by electron

microscopy. SDS-PAGE would reveal the presence and molecular weight of proteins that would be released from the MT doublets. If we knew the MIP composition of mouse and human sperm axonemes, which is largely unknown, we could detect specific B-tubule- or A-tubule-associated MIPs by western blotting as they were being released. Further confirmation that CCDC146 is located on the inside of MT doublets could be performed by immunogold labelling of sperm axonemes that were lightly treated by sarkosyl in order to partially splay open some microtubule doublets. Immunogold labelling might localize the protein in these regions, as was shown for an a *Chlamydomonas* MIP called FAP85 (Kirima and Oiwa 2018). If CCDC146 is a MIP, it could also co-immunoprecipitate with tubulin. To our knowledge, no MIPs were yet described to cause male infertility in mice or humans.

1.6 THE INTERACTOME OF CCDC146

The identification of CCDC146's molecular partners could give key insights into its function. Since the protein's localization is dynamic, we could use co-immunoprecipitation coupled with mass spectrometry to investigate its molecular partners in both spermatids and somatic cells. It would be interesting to see whether and how the molecular partners would differ in these cell types and in the different locations within the cells (centrioles, midbody, axoneme).

Based on the human interactome of CCDC146 on the STRING website, human CCDC146 has 2 physical interactors (Figure 70): Geminin (GMNN) and Rab-3A-interacting protein (RAB3IP) also known as Rabin8 ("STRING: Functional Protein Association Networks" n.d.; Szklarczyk et al. 2021; Huttlin et al. 2017). The interactome of CCDC146 in the mouse was not available at the time of writing. Figure 70 shows other physical interactors (purple) of Geminin and Rabin8. These proteins are associated with the centriole (violet; CCDC146, CEP164, RAB8A), the centrosome (yellow; BBS1, RAB3IP, CEP164, RAB8A, RAB11A, RAB11FIP3), the ciliary basal body (red; RAB3IP, BBS1, RAB8A) and the midbody (green; EXOC6, RAB11FIP3).

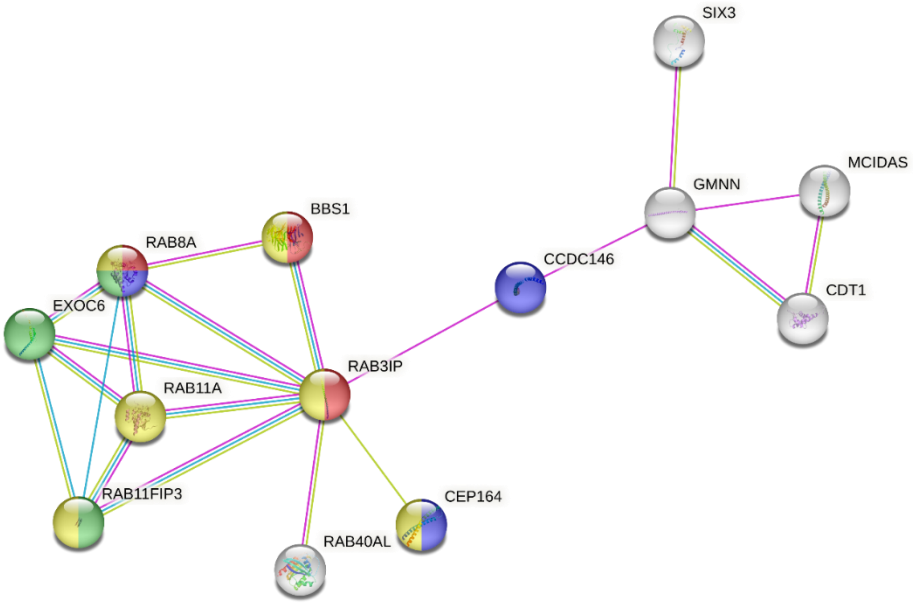

Figure 70: The interactome of human CCDC146 based on physical interactions from STRING. *The colors are associated with protein localization or function in cellular structures including the centriole (violet), the centrosome (yellow), the ciliary basal body (red), and the midbody (green). From "STRING: Functional Protein Association Networks" n.d.; Szklarczyk et al. 2021; Huttlin et al. 2017.*

Geminin is a multifunctional coiled-coil protein that ensures that genome replication only occurs once per cell cycle (McGarry and Kirschner 1998) and is linked to cell fate decisions (Patmanidi et al. 2017). Geminin also plays a role in pre-meiotic DNA replication and its absence results in infertility due to undifferentiated spermatogonia, a sharp decrease in the number of spermatocytes, and DNA damage and low motility of elongating spermatids (Yue Yuan et al. 2017). In embryos, Geminin is essential during the first embryonic divisions and knock-out blastocysts fail to develop the inner cell mass. Geminin family members GemC1 and McIdas form heterodimers with Geminin *in vitro* and *in vivo*. GemC1 and McIdas act as transcriptional co-regulators of genes involved in centriole amplification and (multi)ciliogenesis and are inhibited by Geminin (Arbi et al. 2018). Geminin is a nuclear protein that relocates to the cytoplasm during a part of the G1 phase and is returned back to the nucleus by Cdt1 (Dimaki et al. 2013). The possible association(s) of Geminin and CCDC146 remain unclear.

RAB3IP/Rabin8 is a guanine nucleotide-exchange factor that activates the Rab8/Rab8a GTPase. Rabin8 stimulates an ejection of guanosine diphosphate (GDP) and loading of guanosine triphosphate (GTP) onto Rab8. The Ras-related protein (Rab) GTPase family proteins cycle

between a soluble GDP-bound state and a membrane-associated GTP-bound state. In the GTP-bound state, the proteins directly recruit effector proteins (Frémont and Echard 2018). The Rab family has regulatory roles in vesicle formation, trafficking, and fusion. Rabin8 and Rab8 are also involved in multiple steps of ciliogenesis (Blacque, Scheidel, and Kuhns 2018).

A signaling cascade of Rabin8, Rab8 and Rab11 is involved in vesicular trafficking in primary ciliogenesis where they are believed to regulate the delivery and docking of secretory vesicles to the cilium membrane (Figure 34). When the cell exits from mitosis, Rabin8 is recruited by Rab11 to small cytoplasmic vesicles (preciliary vesicles) originating from the *trans*-Golgi and the recycling endosomes. The vesicles are transported via a dynein-mediated transport along microtubules. They accumulate around distal appendages of the mother centriole, where they appear to dock, and form the primary ciliary vesicle (Sorokin 1962). At the mother centriole, Rabin8 interacts with a distal appendage protein CEP164 and is believed to participate in vesicle docking. Rab11-GTP activates Rabin8 towards Rab8-GDP, forming Rab8-GTP (Knödler et al. 2010; Sánchez and Dynlacht 2016). An actin motor Myosin-Va is also associated with preciliary vesicles which may be derived from the *trans*-Golgi and are transported to the pericentriolar region. A branched actin filament network is formed around the distal end of the mother centriole. Near the distal end, myosin-Va moves along the actin filaments is believed to transport the associated preciliary vesicles to the distal appendages for docking (C.-T. Wu, Chen, and Tang 2018). Following the recruitment of Rabin8 to the centriole, Rab8-GFP starts to accumulate in the membrane of forming and elongating primary cilia (Westlake et al. 2011). Rab8 is involved in ciliary membrane biogenesis through vesicle- and non-vesicle-mediated mechanisms (Figure 71A) (Blacque, Scheidel, and Kuhns 2018; L. Lu and Madugula 2018; Morthorst, Christensen, and Pedersen 2018; Knödler et al. 2010; Chiba et al. 2013).

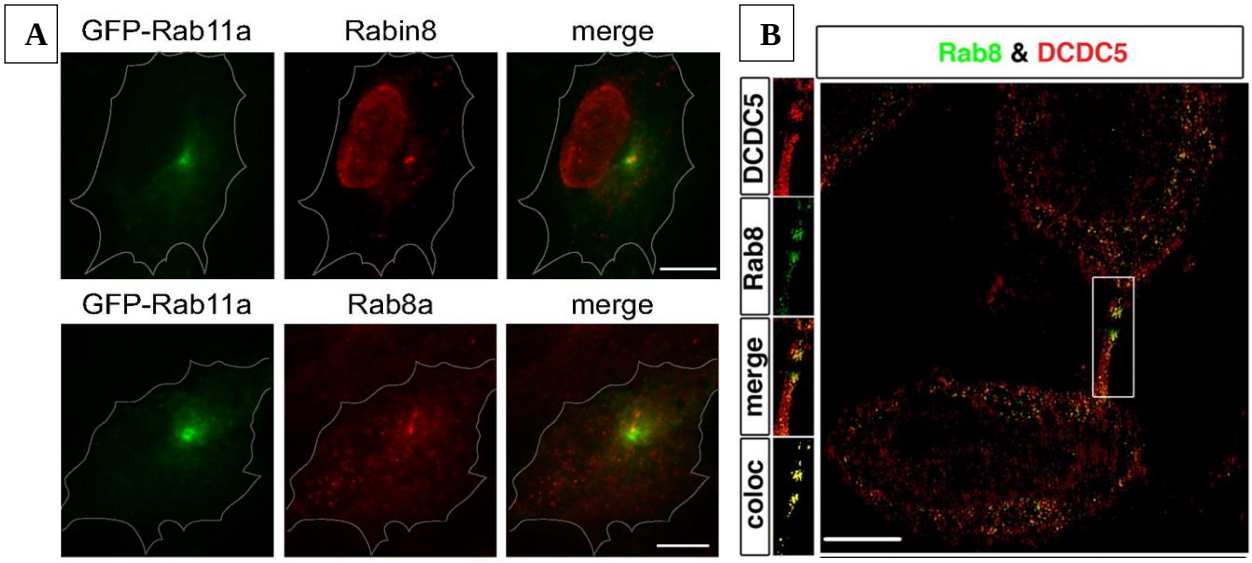

Figure 71: Cellular localization of Rab11, Rab8 and Rabin8 in hTERT-RPE1 cells (A) and co-localization of Rab8 and DCDC5 in HeLa cells (B). *(A) Rab11a accumulates at the base of primary cilia where it co-localizes with Rabin8 present at the centrosome. Rab8a marks the ciliary membrane. Scale bars: 10 µm. From Knödler et al., 2010. (B) Rab8 and DCDC5, a mitotic MAP, co-localize at the midbody during cytokinesis. Scale bars: 30 µm. From Kaplan and Reiner 2011.*

Rabin8 and Rab8 also interact with the BBSome, a complex of Bardet-Biedl syndrome proteins that are essential for ciliogenesis. The BBSome complex is a cargo adaptor for the IFT machinery that promotes the export of signalling receptors and membrane proteins from the cilium. The IFT machinery is docked at the distal appendages of the mother centriole. Rabin8 is thought to interact with BBS1 and recruit the BBSome from centriolar satellites to the centrosome/ basal body (Nachury et al. 2007; Morthorst, Christensen, and Pedersen 2018).

Rab8, and therefore possibly also Rabin8, Rab11 and its effector FIP3 also participate in midbody formation and cytokinesis. Rab8 and Rab11 are associated with endosomal vesicles and Rab8 vesicles are thought to participate in targeted delivery of membrane components to the midbody ring (Figure 61) (Pohl and Jentsch 2008; Frémont and Echard 2018). Rab8 and Rabin8 also interact with DCDC5, a mitotic MAP present at metaphase and midbody microtubules, that appears to mediate dynein-dependent transport of Rab8 vesicles during cytokinesis (Figure 71B). Cargos of Rab8-associated endosomes are unknown but they are believed to promote the stability of the intercellular bridge before abscission (Kaplan and Reiner 2011).

In male germ cells, some Rab proteins (Rab2A, Rab3A) participate in acrosome biogenesis and the acrosomal reaction. In mouse sperm, Rab8 (Rab8a isoform) is present at the acrosome and the signal reduces after capacitation (Bae et al. 2019). The double knock-out of Rab8 (Rab8a and Rab8b isoforms) in mice is lethal by 3 weeks after birth and the knock-out of Rab8a is lethal by 4 post-natal weeks, however the Rab8b knock-out is viable. The double knock-out did not lead to a ciliogenesis phenotype in studied organs (liver, kidneys, cerebellum, small intestine) (Sato et al. 2013) and the fertility status was not investigated or discussed.

1.7 CCDC146 AND VESICLE TRAFFICKING

The Mitocheck screen also showed severe secretion defects following the knock-down of CCDC146 (Cai et al. 2018; "MitoCheck" n.d.). The test was based on following the transport of a CFP-tagged cargo molecule tsO45G from the endoplasmic reticulum, via the Golgi and endosomal system, to the cell surface in a period of one hour. As was previously mentioned, human CCDC146 was shown to interact with Rabin8, a guanine nucleotide exchange factor, which activates the Rab GTPase Rab8 ("STRING: Functional Protein Association Networks" n.d.; Szklarczyk et al. 2021). Rabin8, Rab8 and Rab11 participate in vesicle trafficking from the *trans*-Golgi to the plasma membrane, the basal body in early steps of ciliogenesis and to the midbody during cell division. Similarly, Rab8 and Rab11 endosomes also accumulate at the midbody and Rab8 vesicles are thought to promote the stability of the intercellular bridge (Kaplan and Reiner 2011; Blacque, Scheidel, and Kuhns 2018; C.-T. Chen, Hehnly, and Doxsey 2012; Frémont and Echard 2018). The knock-down of CCDC146 might have a negative impact on vesicle transport mediated by Rab8, Rabin8 or Rab11 and could disrupt cell division by destabilizing the midbody.

Moreover, CCDC146 signal resembled Rab11a around the basal body and Rab8 at the midbody (Figure 71). A co-localization with Rab11, as well as Rab8 and Rabin8 might reveal whether CCDC146 is implicated in vesicle trafficking in these pathways.

1.8 CONCLUSION

To conclude, these results suggest additional and complementary hypotheses about the function of CCDC146. Similar spermiogenic defects as in *Ccdc146* KO mice, including manchette and axoneme malformations, were observed in IFT/ IMT proteins (M S Lehti and Sironen 2016) and

MT-regulatory proteins (Dunleavy et al. 2017; O'Donnell et al. 2012). The absence of CCDC146 in mice caused defects in MT-based organelles and processes, and CCDC146 was positioned along microtubules in somatic cells, suggesting that CCDC146 could be a MAP or possibly a MIP. The aforementioned similarities in localization with Rabin8, Rab8 and Rab11 and secretion defects due to the knock-down of CCDC146 also suggest that it could be implicated in vesicle trafficking. Could CCDC146 mediate vesicle transport along microtubules? Could it be a cargo, a MAP that regulates microtubule dynamics at centrioles and at spindle microtubules? Or a MIP that is transported as cargo into sites of microtubule polymerization and is necessary for the stability of sperm axonemal microtubules? These questions remain to be answered.

2 PROGNOSIS OF ICSI IN MMAF PATIENTS

In the previous part, we discussed the implication of CCDC146 in male fertility and hypothesized about its function. The homozygous loss-of-function of mutations in *CCDC146* led to MMAF, a syndrome that is characterized by a severely decreased sperm motility due to flagellar defects. *CCDC146* is one among more than 40 MMAF-related genes that have been identified. Spermatozoa from MMAF patients are typically immotile and require ICSI to conceive.

Currently, the only treatment for fertility issues is the use of assisted-reproductive technologies (ART). Despite their availability, about half of all couples fail to achieve pregnancy (C. Coutton et al. 2015). ICSI prognoses of MMAF patients are mainly favorable (Touré et al. 2021). Positive outcomes were reported in cases with *DNAH1*, *CFAP43* and *CFAP44* (Wambergue et al. 2016; Yan-Wei Sha, Wang, Su, et al. 2019) that represent the most common MMAF-related mutations. Favorable results were also observed with variants in *CCDC39* (Antony et al. 2013), *CFAP47* (C. Liu et al. 2021), *CFAP54* (Tian et al. 2023), *CFAP58* (Yankun Sha et al. 2021), *CFAP74* (Yanwei Sha, Wei, Ding, Ji, et al. 2020), *CFAP251* (J. Wang, Zhang, et al. 2022), *WDR63* (S. Lu et al. 2021), *SPAG6* (Xu et al. 2022), *ARMC2* (J. Wang, Liu, et al. 2022), *DNAH2* (Y. Gao et al. 2021; Y. Li et al. 2019), and *DNAH8* (C. Liu et al. 2020), while poor outcomes were associated with *CEP128* (Xueguang Zhang et al. 2022), CEP135 (Yan-Wei Sha et al. 2017), *DNAH17* (Whitfield et al. 2019; R. Zheng et al. 2021), *AK7* (Xiang et al. 2022), and *AKAP3* (C. Liu et al. 2022). ICSI results were variable among patients with mutations in *TTC29* (Dai et al. 2022; C. Liu et al. 2019)

and *FSIP2* (Yuan Yuan et al. 2022; W. Liu et al. 2019), possibly due to the presence of variants that had different impact at the protein level.

Understanding of the chances of successful ICSI are important factors for medical counseling for couples that consider ART. Undergoing IVF or ICSI are lengthy and expensive processes, especially when multiple rounds are necessary, and are associated with physical difficulties due to invasive processes and hormonal treatments (A. Sharma and Shrivastava 2022). When the procedures are not working, and especially in cases of idiopathic infertility, couples can find themselves in states of distress, hopelessness and depression. Therefore, in the case of poor prognosis, obtaining counseling and a diagnosis might be psychologically beneficial for couples who might opt for other solutions such as adoption or sperm donation to fulfill their wish to have a child.

For the moment, most of the abovementioned studies report results from only one or several patients for each mutation. Larger cohorts are difficult to obtain but are necessary to confidently predict the most probable outcome of ICSI, and to know when the presence of a specific mutation is very likely not compatible with embryo development. Despite some differences in spermatogenesis and embryo development, studies using knock-out mice for the different MMAF genes could be highly beneficial and allow us to gain more information about the ICSI outcome.

3 IDENTIFICATION OF NEW ACTORS IN MALE FERTILITY

In the previous part, we discussed our results on the implication of a single gene that was found to be important for male fertility. Spermatogenesis is a highly complex process, and it involves hundreds to thousands of genes that contribute to proper sperm formation. Identification of new genes involved in male fertility has been on the rise in the recent years due to an increased use of massive parallel sequencing technologies, especially of whole-exome sequencing (WES) (Houston et al. 2021). The identification and functional characterization of these genes is important for our fundamental comprehension of spermatogenesis as well as for improving medical diagnostic, counselling, and infertility treatment.

In about half of MMAF patients, however, a biallelic pathogenic variant in a single gene cannot be identified using WES (Touré et al. 2021). Some of these negative results might be linked to technological and analytical limitations due to the presence of variants in deep intronic regions,

copy number variations, complex structural chromosomal rearrangements, and due to bioinformatics pipelines used for analysis that might not be able to confidently distinguish deleterious variants from genetic diversity. Whole-genome sequencing might be an alternative to WES for patients with negative WES results that could overcome some of these difficulties (Meienberg et al. 2016; Hoffman-Andrews 2017). Moreover, the identification of pathogenic variants, improved statistical and bioinformatic analysis as well as functional validation of genes, has been the focus of the international groups of researchers and clinicians called the International Male Infertility Genomics Consortium (Houston et al. 2021; "IMIGC | Male Infertility Consortium" n.d.).

Studies usually focus on finding monogenic biallelic variants in rare and severe diseases including male infertility. However, patients with the same mutation(s) in various other diseases can also show different phenotypes (Messaoud et al. 2021). Emerging evidence shows that some cases in many different diseases might be oligogenic, including ciliopathies such as the Bardet-Biedl syndrome; obesity; neurodevelopmental disorders such as schizophrenia, autism and epilepsy; and endocrine, cardiac and renal disorders. Oligogenism is poorly understood and highly complex. It postulates that two or several genes are functionally linked and participate in a similar pathway or a cellular process, and specific gene variants must be inherited together to allow a disease phenotype to arise. In other words, one gene or an allele can influence the phenotypic outcome of a second gene/ locus (Kousi and Katsanis 2015). These variants can be homozygous or heterozygous. An interaction between two genes might be complex and also involve genetic modifiers that can impact the penetrance and/ or expressivity of specific alleles.

In our second study (*Chapter Results: Paper 2*), we focused on heterozygous oligogenic inheritance in genes whose proteins are important for a correct assembly of sperm flagella and their absence leads to the MMAF syndrome. We showed that an accumulation of heterozygous loss-of-function mutations in these genes was inversely correlated with sperm head morphology and led to a decrease in sperm motility. These results suggest that various types of oligogenic inheritance might also play a role in male infertility and could explain some cases of idiopathic infertility where a monogenic cause could not be identified. New studies could identify new specific combinations of genes and their variants that could lead to (male) infertility.

Effort in the study of oligogenic diseases led to the formation of the Oligogenic Disease Database (OLIDA) that will hopefully continue to be updated to serve as a useful tool to deepen our understanding of oligogenic diseases (Nachtegael et al. 2022).

CONCLUSION

In this work, we discussed multiple factors that can affect male fertility and were associated with the multiple morphological abnormalities with the flagella (MMAF) syndrome. We identified a new monogenic cause of male infertility due to the biallelic disruption of *Ccdc146* that leads to MMAF in both humans and mice. We have also shown that an accumulation of rare heterozygous variants in genes that are important for proper axoneme assembly (*Ccdc146, Armc2, Cfap43,* and *Cfap44*) leads to a progressive degradation of sperm head morphology and has an impact on sperm motility, suggesting that oligogenic inheritance could be implicated in some cases of idiopathic male infertility. Finally, in our review article, we discussed several aspects of the sperm epigenome, the importance of non-coding RNAs on sperm formation, embryo development, and their potential roles in inter- and transgenerational inheritance that could mediate the adaptation of the progeny to the environment.

REFERENCES

Abbasi, Ferheen, Haruhiko Miyata, Keisuke Shimada, Akane Morohoshi, Kaori Nozawa, Takafumi Matsumura, Zoulan Xu, Putri Pratiwi, and Masahito Ikawa. 2018. "Radial Spoke Head 6 Homolog a Is Required for Sperm Flagellum Formation and Male Fertility in Mice." *Journal of Cell Science*, January, jcs.221648. https://doi.org/10.1242/jcs.221648.

Adams, G M, B Huang, G Piperno, and D J Luck. 1981. "Central-Pair Microtubular Complex of Chlamydomonas Flagella: Polypeptide Composition as Revealed by Analysis of Mutants." *Journal of Cell Biology* 91 (1): 69–76. https://doi.org/10.1083/jcb.91.1.69.

Agarwal, Ashok, Aditi Mulgund, Alaa Hamada, and Michelle Renee Chyatte. 2015. "A Unique View on Male Infertility around the Globe." *Reproductive Biology and Endocrinology* 13 (1): 37. https://doi.org/10.1186/s12958-015-0032-1.

Ahmed, Emad A., and Dirk G. de Rooij. 2009. "Staging of Mouse Seminiferous Tubule Cross-Sections." In *Meiosis*, edited by Scott Keeney, 558:263–77. Methods in Molecular Biology. Totowa, NJ: Humana Press. https://doi.org/10.1007/978-1-60761-103-5_16.

Akhmanova, Anna, and Lukas C. Kapitein. 2022. "Mechanisms of Microtubule Organization in Differentiated Animal Cells." *Nature Reviews Molecular Cell Biology* 23 (8): 541–58. https://doi.org/10.1038/s41580-022-00473-y.

Almeida, Filipe, Maria P. Luís, Inês Serrano Pereira, Sara V. Pais, and Luís Jaime Mota. 2018. "The Human Centrosomal Protein CCDC146 Binds Chlamydia Trachomatis Inclusion Membrane Protein CT288 and Is Recruited to the Periphery of the Chlamydia-Containing Vacuole." *Frontiers in Cellular and Infection Microbiology* 8 (July): 254. https://doi.org/10.3389/fcimb.2018.00254.

Amos, Linda A. 2008. "The Tektin Family of Microtubule-Stabilizing Proteins." *Genome Biology* 9 (7): 229. https://doi.org/10.1186/gb-2008-9-7-229.

Antony, Dinu, Anita Becker-Heck, Maimoona A. Zariwala, Miriam Schmidts, Alexandros Onoufriadis, Mitra Forouhan, Robert Wilson, et al. 2013. "Mutations in *CCDC 39* and *CCDC 40* Are the Major Cause of Primary Ciliary Dyskinesia with Axonemal Disorganization and Absent Inner Dynein Arms." *Human Mutation* 34 (3): 462–72. https://doi.org/10.1002/humu.22261.

Arbi, Marina, Dafni-Eleftheria Pefani, Stavros Taraviras, and Zoi Lygerou. 2018. "Controlling Centriole Numbers: Geminin Family Members as Master Regulators of Centriole Amplification and Multiciliogenesis." *Chromosoma* 127 (2): 151–74. https://doi.org/10.1007/s00412-017-0652-7.

Austin, C. R. 1952. "The 'Capacitation' of the Mammalian Sperm." *Nature* 170 (4321): 326–326. https://doi.org/10.1038/170326a0.

Avasthi, Prachee, Jan Frederik Scheel, Guoxin Ying, Jeanne M. Frederick, Wolfgang Baehr, and Uwe Wolfrum. 2013. "Germline Deletion of *Cetn1* Causes Infertility in Male Mice." *Journal of Cell Science*, January, jcs.128587. https://doi.org/10.1242/jcs.128587.

Avidor-Reiss, Tomer, and Emily L Fishman. 2019. "It Takes Two (Centrioles) to Tango." *Reproduction* 157 (2): R33–51. https://doi.org/10.1530/REP-18-0350.

Avidor-Reiss, Tomer, Andrew Ha, and Marcus L. Basiri. 2017. "Transition Zone Migration: A Mechanism for Cytoplasmic Ciliogenesis and Postaxonemal Centriole Elongation." *Cold Spring Harbor Perspectives in Biology* 9 (8): a028142. https://doi.org/10.1101/cshperspect.a028142.

Avidor-Reiss, Tomer, Atul Khire, Emily L. Fishman, and Kyoung H. Jo. 2015. "Atypical Centrioles during Sexual Reproduction." *Frontiers in Cell and Developmental Biology* 3 (April). https://doi.org/10.3389/fcell.2015.00021.

Bae, Jeong-Won, So-Hye Kim, Dae-Hyun Kim, Jae Jung Ha, Jun Koo Yi, Seongsoo Hwang, Buom-Yong Ryu, Myung-Geol Pang, and Woo-Sung Kwon. 2019. "Ras-Related Proteins (Rab) Are Key Proteins Related to Male Fertility Following a Unique Activation Mechanism." *Reproductive Biology* 19 (4): 356–62. https://doi.org/10.1016/j.repbio.2019.10.001.

Balashova, E. E., P. G. Lokhov, and V. B. Bystrevskaya. 2009. "Distribution of Tyrosinated and Acetylated Tubulin in Centrioles during Mitosis of 3T3 and SV40-3T3 Cells." *Cell and Tissue Biology* 3 (4): 359–68. https://doi.org/10.1134/S1990519X09040087.

Balhorn, Rod, B. L. Gledhill, and A. J. Wyrobek. 1977. "Mouse Sperm Chromatin Proteins: Quantitative Isolation and Partial Characterization." *Biochemistry* 16 (18): 4074–80. https://doi.org/10.1021/bi00637a021.

Bedoni, Nicola, Lonneke Haer-Wigman, Veronika Vaclavik, Viet H. Tran, Pietro Farinelli, Sara Balzano, Beryl Royer-Bertrand, et al. 2016. "Mutations in the Polyglutamylase Gene *TTLL5* , Expressed in Photoreceptor Cells and Spermatozoa, Are Associated with Cone-Rod Degeneration and Reduced Male Fertility." *Human Molecular Genetics*, August, ddw282. https://doi.org/10.1093/hmg/ddw282.

Bellve, Ar, Jc Cavicchia, Cf Millette, Da O'Brien, Ym Bhatnagar, and M Dym. 1977. "Spermatogenic Cells of the Prepuberal Mouse: Isolation and Morphological Characterization." *Journal of Cell Biology* 74 (1): 68–85. https://doi.org/10.1083/jcb.74.1.68.

Bench, G.S., A.M. Friz, M.H. Corzett, D.H. Morse, and R. Balhorn. 1996. "DNA and Total Protamine Masses in Individual Sperm from Fertile Mammalian Subjects." *Cytometry* 23 (4): 263–71. https://doi.org/10.1002/(SICI)1097-0320(19960401)23:4<263::AID-CYTO1>3.0.CO;2-I.

Ben Khelifa, Mariem, Charles Coutton, Raoudha Zouari, Thomas Karaouzène, John Rendu, Marie Bidart, Sandra Yassine, et al. 2014. "Mutations in DNAH1, Which Encodes an Inner Arm Heavy Chain Dynein, Lead to Male Infertility from Multiple Morphological Abnormalities of the Sperm Flagella." *The American Journal of Human Genetics* 94 (1): 95–104. https://doi.org/10.1016/j.ajhg.2013.11.017.

Bernabé-Rubio, Miguel, Germán Andrés, Javier Casares-Arias, Jaime Fernández-Barrera, Laura Rangel, Natalia Reglero-Real, David C. Gershlick, et al. 2016. "Novel Role for the Midbody in Primary Ciliogenesis by Polarized Epithelial Cells." *Journal of Cell Biology* 214 (3): 259–73. https://doi.org/10.1083/jcb.201601020.

Bernhard, W., and E. de Harven. 1960. "L'ultrastructure du centriole et d'autres éléments de l'appareil achromatique." In *Verhandlungen Band II / Biologisch-Medizinischer Teil*, edited by W. Bargmann, D. Peters, and C. Wolpers, 217–27. Berlin, Heidelberg: Springer Berlin Heidelberg. https://doi.org/10.1007/978-3-662-22058-0_42.

Bessis, M., and J. Breton-Gorius. 1958. "[On an pericentral inframicroscopic structure; electron microscopy of mammalian leukocytes]." *Comptes Rendus Hebdomadaires Des Seances De l'Academie Des Sciences* 246 (8): 1289–91.

Beurois, Julie, Caroline Cazin, Zine-Eddine Kherraf, Guillaume Martinez, Tristan Celse, Aminata Touré, Christophe Arnoult, Pierre F. Ray, and Charles Coutton. 2020. "Genetics of

Teratozoospermia: Back to the Head." *Best Practice & Research Clinical Endocrinology & Metabolism* 34 (6): 101473. https://doi.org/10.1016/j.beem.2020.101473.

Bhogaraju, Sagar, Lukas Cajanek, Cécile Fort, Thierry Blisnick, Kristina Weber, Michael Taschner, Naoko Mizuno, et al. 2013. "Molecular Basis of Tubulin Transport Within the Cilium by IFT74 and IFT81." *Science* 341 (6149): 1009–12. https://doi.org/10.1126/science.1240985.

Blacque, Oliver E., Noemie Scheidel, and Stefanie Kuhns. 2018. "Rab GTPases in Cilium Formation and Function." *Small GTPases* 9 (1–2): 76–94. https://doi.org/10.1080/21541248.2017.1353847.

Blanchon, Sylvain, Marie Legendre, Bruno Copin, Philippe Duquesnoy, Guy Montantin, Esther Kott, Florence Dastot, et al. 2012. "Delineation of *CCDC39/CCDC40* Mutation Spectrum and Associated Phenotypes in Primary Ciliary Dyskinesia." *Journal of Medical Genetics* 49 (6): 410–16. https://doi.org/10.1136/jmedgenet-2012-100867.

"BLAST | UniProt." n.d. Accessed February 21, 2023. https://www.uniprot.org/blast.

Bobinnec, Y., M. Moudjou, J.P. Fouquet, E. Desbruyères, B. Eddé, and M. Bornens. 1998. "Glutamylation of Centriole and Cytoplasmic Tubulin in Proliferating Non-Neuronal Cells." *Cell Motility and the Cytoskeleton* 39 (3): 223–32. https://doi.org/10.1002/(SICI)1097-0169(1998)39:3<223::AID-CM5>3.0.CO;2-5.

Bodakuntla, Satish, A.S. Jijumon, Cristopher Villablanca, Christian Gonzalez-Billault, and Carsten Janke. 2019. "Microtubule-Associated Proteins: Structuring the Cytoskeleton." *Trends in Cell Biology* 29 (10): 804–19. https://doi.org/10.1016/j.tcb.2019.07.004.

Boitani, Carla, Sara Di Persio, Valentina Esposito, and Elena Vicini. 2016. "Spermatogonial Cells: Mouse, Monkey and Man Comparison." *Seminars in Cell & Developmental Biology* 59 (November): 79–88. https://doi.org/10.1016/j.semcdb.2016.03.002.

Boitrelle, Florence, Rupin Shah, Ramadan Saleh, Ralf Henkel, Hussein Kandil, Eric Chung, Paraskevi Vogiatzi, Armand Zini, Mohamed Arafa, and Ashok Agarwal. 2021. "The Sixth Edition of the WHO Manual for Human Semen Analysis: A Critical Review and SWOT Analysis." *Life* 11 (12): 1368. https://doi.org/10.3390/life11121368.

Boivin, Jacky, Laura Bunting, John A. Collins, and Karl G. Nygren. 2007. "International Estimates of Infertility Prevalence and Treatment-Seeking: Potential Need and Demand for Infertility Medical Care." *Human Reproduction* 22 (6): 1506–12. https://doi.org/10.1093/humrep/dem046.

Bolcun-Filas, Ewelina, and Mary Ann Handel. 2018. "Meiosis: The Chromosomal Foundation of Reproduction." *Biology of Reproduction* 99 (1): 112–26. https://doi.org/10.1093/biolre/ioy021.

Bower, Raqual, Douglas Tritschler, Kristyn VanderWaal, Catherine A. Perrone, Joshua Mueller, Laura Fox, Winfield S. Sale, and M. E. Porter. 2013. "The N-DRC Forms a Conserved Biochemical Complex That Maintains Outer Doublet Alignment and Limits Microtubule Sliding in Motile Axonemes." Edited by Erika Holzbaur. *Molecular Biology of the Cell* 24 (8): 1134–52. https://doi.org/10.1091/mbc.e12-11-0801.

Braschi, Bryony, Heymut Omran, George B. Witman, Gregory J. Pazour, K. Kevin Pfister, Elspeth A. Bruford, and Stephen M. King. 2022. "Consensus Nomenclature for Dyneins and Associated Assembly Factors." *Journal of Cell Biology* 221 (2): e202109014. https://doi.org/10.1083/jcb.202109014.

Brokaw, C. J., and R. Kamiya. 1987. "Bending Patterns OfChlamydomonas Flagella: IV. Mutants with Defects in Inner and Outer Dynein Arms Indicate Differences in Dynein Arm

Function." *Cell Motility and the Cytoskeleton* 8 (1): 68–75. https://doi.org/10.1002/cm.970080110.

Brown, Paula R., Kiyoshi Miki, Deborah B. Harper, and Edward M. Eddy. 2003. "A-Kinase Anchoring Protein 4 Binding Proteins in the Fibrous Sheath of the Sperm Flagellum." *Biology of Reproduction* 68 (6): 2241–48. https://doi.org/10.1095/biolreprod.102.013466.

Bühler, Miriam, and Ailine Stolz. 2022. "Estrogens—Origin of Centrosome Defects in Human Cancer?" *Cells* 11 (3): 432. https://doi.org/10.3390/cells11030432.

Bui, Khanh Huy, Hitoshi Sakakibara, Tandis Movassagh, Kazuhiro Oiwa, and Takashi Ishikawa. 2008. "Molecular Architecture of Inner Dynein Arms in Situ in Chlamydomonas Reinhardtii Flagella." *Journal of Cell Biology* 183 (5): 923–32. https://doi.org/10.1083/jcb.200808050.

Burgoyne, R. D., M. A. Cambray-Deakin, S. A. Lewis, S. Sarkar, and N. J. Cowan. 1988. "Differential Distribution of Beta-Tubulin Isotypes in Cerebellum." *The EMBO Journal* 7 (8): 2311–19. https://doi.org/10.1002/j.1460-2075.1988.tb03074.x.

Cai, Yin, M. Julius Hossain, Jean-Karim Hériché, Antonio Z. Politi, Nike Walther, Birgit Koch, Malte Wachsmuth, et al. 2018. "Experimental and Computational Framework for a Dynamic Protein Atlas of Human Cell Division." *Nature* 561 (7723): 411–15. https://doi.org/10.1038/s41586-018-0518-z.

Calvi, Alessandra, Arnette Shi Wei Wong, Graham Wright, Esther Sook Miin Wong, Tsui Han Loo, Colin L. Stewart, and Brian Burke. 2015. "SUN4 Is Essential for Nuclear Remodeling during Mammalian Spermiogenesis." *Developmental Biology* 407 (2): 321–30. https://doi.org/10.1016/j.ydbio.2015.09.010.

Campbell, Patrick K, Katrina G Waymire, Robb L Heier, Catherine Sharer, Diane E Day, Heike Reimann, J Michael Jaje, et al. 2002. "Mutation of a Novel Gene Results in Abnormal Development of Spermatid Flagella, Loss of Intermale Aggression and Reduced Body Fat in Mice." *Genetics* 162 (1): 307–20. https://doi.org/10.1093/genetics/162.1.307.

Carbajal-González, Blanca I., Thomas Heuser, Xiaofeng Fu, Jianfeng Lin, Brandon W. Smith, David R. Mitchell, and Daniela Nicastro. 2013. "Conserved Structural Motifs in the Central Pair Complex of Eukaryotic Flagella." *Cytoskeleton* 70 (2): 101–20. https://doi.org/10.1002/cm.21094.

Carone, Benjamin R., Lucas Fauquier, Naomi Habib, Jeremy M. Shea, Caroline E. Hart, Ruowang Li, Christoph Bock, et al. 2010. "Paternally Induced Transgenerational Environmental Reprogramming of Metabolic Gene Expression in Mammals." *Cell* 143 (7): 1084–96. https://doi.org/10.1016/j.cell.2010.12.008.

Carr, Ian M., Sanjeev Bhaskar, James O' Sullivan, Mohammed A. Aldahmesh, Hanan E. Shamseldin, Alexander F. Markham, David T. Bonthron, Graeme Black, and Fowzan S. Alkuraya. 2013. "Autozygosity Mapping with Exome Sequence Data." *Human Mutation* 34 (1): 50–56. https://doi.org/10.1002/humu.22220.

Castaneda, Julio M., Rong Hua, Haruhiko Miyata, Asami Oji, Yueshuai Guo, Yiwei Cheng, Tao Zhou, et al. 2017. "TCTE1 Is a Conserved Component of the Dynein Regulatory Complex and Is Required for Motility and Metabolism in Mouse Spermatozoa." *Proceedings of the National Academy of Sciences* 114 (27). https://doi.org/10.1073/pnas.1621279114.

Castleman, Victoria H., Leila Romio, Rahul Chodhari, Robert A. Hirst, Sandra C.P. de Castro, Keith A. Parker, Patricia Ybot-Gonzalez, et al. 2009. "Mutations in Radial Spoke Head Protein Genes RSPH9 and RSPH4A Cause Primary Ciliary Dyskinesia with Central-

Microtubular-Pair Abnormalities." *The American Journal of Human Genetics* 84 (2): 197–209. https://doi.org/10.1016/j.ajhg.2009.01.011.

Castro Barbosa, Thais de, Lars R. Ingerslev, Petter S. Alm, Soetkin Versteyhe, Julie Massart, Morten Rasmussen, Ida Donkin, et al. 2016. "High-Fat Diet Reprograms the Epigenome of Rat Spermatozoa and Transgenerationally Affects Metabolism of the Offspring." *Molecular Metabolism* 5 (3): 184–97. https://doi.org/10.1016/j.molmet.2015.12.002.

Cauvin, Clothilde, and Arnaud Echard. 2015. "Phosphoinositides: Lipids with Informative Heads and Mastermind Functions in Cell Division." *Biochimica et Biophysica Acta (BBA) - Molecular and Cell Biology of Lipids* 1851 (6): 832–43. https://doi.org/10.1016/j.bbalip.2014.10.013.

Chaigne, Agathe, and Thibaut Brunet. 2022. "Incomplete Abscission and Cytoplasmic Bridges in the Evolution of Eukaryotic Multicellularity." *Current Biology* 32 (8): R385–97. https://doi.org/10.1016/j.cub.2022.03.021.

Chang, Paul, and Tim Stearns. 2000. "δ-Tubulin and ε-Tubulin: Two New Human Centrosomal Tubulins Reveal New Aspects of Centrosome Structure and Function." *Nature Cell Biology* 2 (1): 30–35. https://doi.org/10.1038/71350.

Chen, Chun-Ting, Heidi Hehnly, and Stephen J. Doxsey. 2012. "Orchestrating Vesicle Transport, ESCRTs and Kinase Surveillance during Abscission." *Nature Reviews Molecular Cell Biology* 13 (8): 483–88. https://doi.org/10.1038/nrm3395.

Chen, Daijuan, Yan Liang, Juan Li, Xueguang Zhang, Rui Zheng, Xiaodong Wang, Heng Zhang, and Ying Shen. 2021. "A Novel CCDC39 Mutation Causes Multiple Morphological Abnormalities of the Flagella in a Primary Ciliary Dyskinesia Patient." *Reproductive BioMedicine Online* 43 (5): 920–30. https://doi.org/10.1016/j.rbmo.2021.07.005.

Chen, Zhen, Garrett A. Greenan, Momoko Shiozaki, Yanxin Liu, Will M. Skinner, Xiaowei Zhao, Shumei Zhao, et al. 2023. "In Situ Cryo-Electron Tomography Reveals the Asymmetric Architecture of Mammalian Sperm Axonemes." *Nature Structural & Molecular Biology*, January. https://doi.org/10.1038/s41594-022-00861-0.

Chianese, C., M. G. Fino, A. Riera Escamilla, O. López Rodrigo, S. Vinci, E. Guarducci, F. Daguin, et al. 2015. "Comprehensive Investigation in Patients Affected by Sperm Macrocephaly and Globozoospermia." *Andrology* 3 (2): 203–12. https://doi.org/10.1111/andr.12016.

Chiba, Shuhei, Yuta Amagai, Yuta Homma, Mitsunori Fukuda, and Kensaku Mizuno. 2013. "NDR2-Mediated Rabin8 Phosphorylation Is Crucial for Ciliogenesis by Switching Binding Specificity from Phosphatidylserine to Sec15." *The EMBO Journal* 32 (6): 874–85. https://doi.org/10.1038/emboj.2013.32.

Clavijo, Raul I. 2020. "Finding of Parental Consanguinity in Men with Infertility Facilitates the Discovery of Specific Genetic Causes for Nonobstructive Azoospermia." *F&S Reports* 1 (3): 173. https://doi.org/10.1016/j.xfre.2020.08.006.

Clermont, Y. 1972. "Kinetics of Spermatogenesis in Mammals: Seminiferous Epithelium Cycle and Spermatogonial Renewal." *Physiological Reviews* 52 (1): 198–236. https://doi.org/10.1152/physrev.1972.52.1.198.

Cohen, P. E., S. E. Pollack, and J. W. Pollard. 2006. "Genetic Analysis of Chromosome Pairing, Recombination, and Cell Cycle Control during First Meiotic Prophase in Mammals." *Endocrine Reviews* 27 (4): 398–426. https://doi.org/10.1210/er.2005-0017.

Condò, Ivano. 2022. “Rare Monogenic Diseases: Molecular Pathophysiology and Novel Therapies.” *International Journal of Molecular Sciences* 23 (12): 6525. https://doi.org/10.3390/ijms23126525.

Conine, Colin C., Fengyun Sun, Lina Song, Jaime A. Rivera-Pérez, and Oliver J. Rando. 2018. “Small RNAs Gained during Epididymal Transit of Sperm Are Essential for Embryonic Development in Mice.” *Developmental Cell* 46 (4): 470-480.e3. https://doi.org/10.1016/j.devcel.2018.06.024.

Consolati, Tanja, Julia Locke, Johanna Roostalu, Zhuo Angel Chen, Julian Gannon, Jayant Asthana, Wei Ming Lim, et al. 2020. “Microtubule Nucleation Properties of Single Human ΓTuRCs Explained by Their Cryo-EM Structure.” *Developmental Cell* 53 (5): 603-617.e8. https://doi.org/10.1016/j.devcel.2020.04.019.

Courtens, J. L., M. Loir, Bernadette Delaleu, and Jitka Durand. 1981. “The Spermatid Manchette of Mammals : Formation and Relations with the Nuclear Envelope and the Chromatin.” *Reproduction Nutrition Développement* 21 (3): 467–77. https://doi.org/10.1051/rnd:19810312.

Coutton, C., J. Escoffier, G. Martinez, C. Arnoult, and P. F. Ray. 2015. “Teratozoospermia: Spotlight on the Main Genetic Actors in the Human.” *Human Reproduction Update* 21 (4): 455–85. https://doi.org/10.1093/humupd/dmv020.

Coutton, Charles, Guillaume Martinez, Zine-Eddine Kherraf, Amir Amiri-Yekta, Magalie Boguenet, Antoine Saut, Xiaojin He, et al. 2019. “Bi-Allelic Mutations in ARMC2 Lead to Severe Astheno-Teratozoospermia Due to Sperm Flagellum Malformations in Humans and Mice.” *The American Journal of Human Genetics* 104 (2): 331–40. https://doi.org/10.1016/j.ajhg.2018.12.013.

Coutton, Charles, Alexandra S. Vargas, Amir Amiri-Yekta, Zine-Eddine Kherraf, Selima Fourati Ben Mustapha, Pauline Le Tanno, Clémentine Wambergue-Legrand, et al. 2018. “Mutations in CFAP43 and CFAP44 Cause Male Infertility and Flagellum Defects in Trypanosoma and Human.” *Nature Communications* 9 (1): 686. https://doi.org/10.1038/s41467-017-02792-7.

Craft, Julie M., J. Aaron Harris, Sebastian Hyman, Peter Kner, and Karl F. Lechtreck. 2015. “Tubulin Transport by IFT Is Upregulated during Ciliary Growth by a Cilium-Autonomous Mechanism.” *Journal of Cell Biology* 208 (2): 223–37. https://doi.org/10.1083/jcb.201409036.

Cruz, Raquel Santana da, Elissa J. Carney, Johan Clarke, Hong Cao, M. Idalia Cruz, Carlos Benitez, Lu Jin, et al. 2018. “Paternal Malnutrition Programs Breast Cancer Risk and Tumor Metabolism in Offspring.” *Breast Cancer Research* 20 (1): 99. https://doi.org/10.1186/s13058-018-1034-7.

Cunningham, Fiona, James E Allen, Jamie Allen, Jorge Alvarez-Jarreta, M Ridwan Amode, Irina M Armean, Olanrewaju Austine-Orimoloye, et al. 2022a. “Ensembl 2022.” *Nucleic Acids Research* 50 (D1): D988–95. https://doi.org/10.1093/nar/gkab1049.

———. 2022b. “Ensembl 2022.” *Nucleic Acids Research* 50 (D1): D988–95. https://doi.org/10.1093/nar/gkab1049.

Dai, Siyu, Yan Liang, Mohan Liu, Yanting Yang, Hongqian Liu, and Ying Shen. 2022. “Novel Biallelic Mutations in *TTC29* Cause Asthenoteratospermia and Male Infertility.” *Molecular Genetics & Genomic Medicine* 10 (12). https://doi.org/10.1002/mgg3.2078.

Dammermann, Alexander, and Andreas Merdes. 2002. "Assembly of Centrosomal Proteins and Microtubule Organization Depends on PCM-1." *Journal of Cell Biology* 159 (2): 255–66. https://doi.org/10.1083/jcb.200204023.

Darszon, Alberto, Takuya Nishigaki, Chris Wood, Claudia L. Treviño, Ricardo Felix, and Carmen Beltrán. 2005. "Calcium Channels and Ca2+ Fluctuations in Sperm Physiology." In *International Review of Cytology*, 243:79–172. Elsevier. https://doi.org/10.1016/S0074-7696(05)43002-8.

Deane, James A., Douglas G. Cole, E.Scott Seeley, Dennis R. Diener, and Joel L. Rosenbaum. 2001. "Localization of Intraflagellar Transport Protein IFT52 Identifies Basal Body Transitional Fibers as the Docking Site for IFT Particles." *Current Biology* 11 (20): 1586–90. https://doi.org/10.1016/S0960-9822(01)00484-5.

Delgehyr, Nathalie, James Sillibourne, and Michel Bornens. 2005. "Microtubule Nucleation and Anchoring at the Centrosome Are Independent Processes Linked by Ninein Function." *Journal of Cell Science* 118 (8): 1565–75. https://doi.org/10.1242/jcs.02302.

Dimaki, Maria, Georgia Xouri, Ioanna-Eleni Symeonidou, Chaido Sirinian, Hideo Nishitani, Stavros Taraviras, and Zoi Lygerou. 2013. "Cell Cycle-Dependent Subcellular Translocation of the Human DNA Licensing Inhibitor Geminin." *Journal of Biological Chemistry* 288 (33): 23953–63. https://doi.org/10.1074/jbc.M113.453092.

Ding, Xu, Rener Xu, Juehua Yu, Tian Xu, Yuan Zhuang, and Min Han. 2007. "SUN1 Is Required for Telomere Attachment to Nuclear Envelope and Gametogenesis in Mice." *Developmental Cell* 12 (6): 863–72. https://doi.org/10.1016/j.devcel.2007.03.018.

Djureinovic, D., L. Fagerberg, B. Hallström, A. Danielsson, C. Lindskog, M. Uhlén, and F. Pontén. 2014. "The Human Testis-Specific Proteome Defined by Transcriptomics and Antibody-Based Profiling." *MHR: Basic Science of Reproductive Medicine* 20 (6): 476–88. https://doi.org/10.1093/molehr/gau018.

Dong, Frederick N., Amir Amiri-Yekta, Guillaume Martinez, Antoine Saut, Julie Tek, Laurence Stouvenel, Patrick Lorès, et al. 2018. "Absence of CFAP69 Causes Male Infertility Due to Multiple Morphological Abnormalities of the Flagella in Human and Mouse." *The American Journal of Human Genetics* 102 (4): 636–48. https://doi.org/10.1016/j.ajhg.2018.03.007.

Dooher, G. B., and D. Bennett. 1973. "Fine Structural Observations on the Development of the Sperm Head in the Mouse." *American Journal of Anatomy* 136 (3): 339–61. https://doi.org/10.1002/aja.1001360307.

Doxsey, Stephen. 2001. "Re-Evaluating Centrosome Function." *Nature Reviews Molecular Cell Biology* 2 (9): 688–98. https://doi.org/10.1038/35089575.

Dunleavy, Jessica E M, Moira K O'Bryan, Peter G Stanton, and Liza O'Donnell. 2019. "The Cytoskeleton in Spermatogenesis." *Reproduction* 157 (2): R53–72. https://doi.org/10.1530/REP-18-0457.

Dunleavy, Jessica E. M., Hidenobu Okuda, Anne E. O'Connor, D. Jo Merriner, Liza O'Donnell, Duangporn Jamsai, Martin Bergmann, and Moira K. O'Bryan. 2017. "Katanin-like 2 (KATNAL2) Functions in Multiple Aspects of Haploid Male Germ Cell Development in the Mouse." Edited by Martin M. Matzuk. *PLOS Genetics* 13 (11): e1007078. https://doi.org/10.1371/journal.pgen.1007078.

Dutcher, Susan K. 2020. "Asymmetries in the Cilia of *Chlamydomonas*." *Philosophical Transactions of the Royal Society B: Biological Sciences* 375 (1792): 20190153. https://doi.org/10.1098/rstb.2019.0153.

Echard, Arnaud. 2012. "Connecting Membrane Traffic to ESCRT and the Final Cut." *Nature Cell Biology* 14 (10): 983–85. https://doi.org/10.1038/ncb2598.

Eddy, Edward M., Kiyotaka Toshimori, and Deborah A. O'Brien. 2003. "Fibrous Sheath of Mammalian Spermatozoa." *Microscopy Research and Technique* 61 (1): 103–15. https://doi.org/10.1002/jemt.10320.

Egydio de Carvalho, Carlos, Hiromitsu Tanaka, Naoko Iguchi, Sami Ventelä, Hiroshi Nojima, and Yoshitake Nishimune. 2002. "Molecular Cloning and Characterization of a Complementary DNA Encoding Sperm Tail Protein SHIPPO 11." *Biology of Reproduction* 66 (3): 785–95. https://doi.org/10.1095/biolreprod66.3.785.

Elkis, Yoav, Shai Bel, Roni Rahimi, Tali Lerer-Goldstein, Smadar Levin-Zaidman, Tatiana Babushkin, Sally Shpungin, and Uri Nir. 2015. "TMF/ARA160 Governs the Dynamic Spatial Orientation of the Golgi Apparatus during Sperm Development." Edited by Sidney Yu. *PLOS ONE* 10 (12): e0145277. https://doi.org/10.1371/journal.pone.0145277.

Erzurumluoglu, A. Mesut, Hashem A. Shihab, Santiago Rodriguez, Tom R. Gaunt, and Ian N.M. Day. 2016. "Importance of Genetic Studies in Consanguineous Populations for the Characterization of Novel Human Gene Functions: Consanguineous Populations and Genetics." *Annals of Human Genetics* 80 (3): 187–96. https://doi.org/10.1111/ahg.12150.

Escalier, Denise, Xi-Yuan Bai, Derek Silvius, Pin-Xian Xu, and Xin Xu. 2003. "Spermatid Nuclear and Sperm Periaxonemal Anomalies in the MouseUbe2b Null Mutant." *Molecular Reproduction and Development* 65 (3): 298–308. https://doi.org/10.1002/mrd.10290.

Escoffier, Jessica, Sandra Yassine, Hoi Chang Lee, Guillaume Martinez, Julie Delaroche, Charles Coutton, Thomas Karaouzène, et al. 2015. "Subcellular Localization of Phospholipase Cζ in Human Sperm and Its Absence in DPY19L2-Deficient Sperm Are Consistent with Its Role in Oocyte Activation." *MHR: Basic Science of Reproductive Medicine* 21 (2): 157–68. https://doi.org/10.1093/molehr/gau098.

Esteves, Sandro C., Matheus Roque, Giuliano Bedoschi, Thor Haahr, and Peter Humaidan. 2018. "Intracytoplasmic Sperm Injection for Male Infertility and Consequences for Offspring." *Nature Reviews Urology* 15 (9): 535–62. https://doi.org/10.1038/s41585-018-0051-8.

Fan, Jun, and Kenneth A. Beck. 2004. "A Role for the Spectrin Superfamily Member Syne-1 and Kinesin II in Cytokinesis." *Journal of Cell Science* 117 (4): 619–29. https://doi.org/10.1242/jcs.00892.

Fawcett, Don W. 1975. "The Mammalian Spermatozoon." *Developmental Biology* 44 (2): 394–436. https://doi.org/10.1016/0012-1606(75)90411-X.

Fawcett, Don W., Edward M. Eddy, and David M. Phillips. 1970. "Observations on the Fine Structure and Relationships of the Chromatoid Body in Mammalian Spermatogenesis1." *Biology of Reproduction* 2 (1): 129–53. https://doi.org/10.1095/biolreprod2.1.129.

Fawcett, Don W., and David M. Phillips. 1969. "The Fine Structure and Development of the Neck Region of the Mammalian Spermatozoon." *The Anatomical Record* 165 (2): 153–83. https://doi.org/10.1002/ar.1091650204.

Fayomi, Adetunji P., and Kyle E. Orwig. 2018. "Spermatogonial Stem Cells and Spermatogenesis in Mice, Monkeys and Men." *Stem Cell Research* 29 (May): 207–14. https://doi.org/10.1016/j.scr.2018.04.009.

Feng, Ruizhi, Qing Sang, Yanping Kuang, Xiaoxi Sun, Zheng Yan, Shaozhen Zhang, Juanzi Shi, et al. 2016. "Mutations in *TUBB8* and Human Oocyte Meiotic Arrest." *New England Journal of Medicine* 374 (3): 223–32. https://doi.org/10.1056/NEJMoa1510791.

Ferlin, Alberto, Savina Dipresa, Andrea Delbarba, Filippo Maffezzoni, Teresa Porcelli, Carlo Cappelli, and Carlo Foresta. 2019. "Contemporary Genetics-Based Diagnostics of Male Infertility." *Expert Review of Molecular Diagnostics* 19 (7): 623–33. https://doi.org/10.1080/14737159.2019.1633917.

Ferlin, Alberto, and Carlo Foresta. 2020. "Infertility: Practical Clinical Issues for Routine Investigation of the Male Partner." *Journal of Clinical Medicine* 9 (6): 1644. https://doi.org/10.3390/jcm9061644.

Fesahat, Farzaneh, Ralf Henkel, and Ashok Agarwal. 2020. "Globozoospermia Syndrome: An Update." *Andrologia* 52 (2). https://doi.org/10.1111/and.13459.

Firat-Karalar, Elif N., Joshua Sante, Sarah Elliott, and Tim Stearns. 2014. "Proteomic Analysis of Mammalian Sperm Cells Identifies New Components of the Centrosome." *Journal of Cell Science*, January, jcs.157008. https://doi.org/10.1242/jcs.157008.

Fishman, Emily L., Kyoung Jo, Quynh P. H. Nguyen, Dong Kong, Rachel Royfman, Anthony R. Cekic, Sushil Khanal, et al. 2018. "A Novel Atypical Sperm Centriole Is Functional during Human Fertilization." *Nature Communications* 9 (1): 2210. https://doi.org/10.1038/s41467-018-04678-8.

Fitzgerald, Carolyn J., Richard J. Oko, and Frans A. van der Hoorn. 2006. "Rat Spag5 Associates in Somatic Cells with Endoplasmic Reticulum and Microtubules but in Spermatozoa with Outer Dense Fibers." *Molecular Reproduction and Development* 73 (1): 92–100. https://doi.org/10.1002/mrd.20388.

Fouquet, J. 1998. "Gamma-Tubulin during the Differentiation of Spermatozoa in Various Mammals and Man." *Molecular Human Reproduction* 4 (12): 1122–29. https://doi.org/10.1093/molehr/4.12.1122.

França, L. R., R. A. Hess, J. M. Dufour, M. C. Hofmann, and M. D. Griswold. 2016. "The Sertoli Cell: One Hundred Fifty Years of Beauty and Plasticity." *Andrology* 4 (2): 189–212. https://doi.org/10.1111/andr.12165.

Freitas, Maria João, Srinivasan Vijayaraghavan, and Margarida Fardilha. 2017. "Signaling Mechanisms in Mammalian Sperm Motility†." *Biology of Reproduction* 96 (1): 2–12. https://doi.org/10.1095/biolreprod.116.144337.

Frémont, Stéphane, and Arnaud Echard. 2018. "Membrane Traffic in the Late Steps of Cytokinesis." *Current Biology* 28 (8): R458–70. https://doi.org/10.1016/j.cub.2018.01.019.

Fry, Andrew M., Josephina Sampson, Caroline Shak, and Sue Shackleton. 2017. "Recent Advances in Pericentriolar Material Organization: Ordered Layers and Scaffolding Gels." *F1000Research* 6 (August): 1622. https://doi.org/10.12688/f1000research.11652.1.

Fullston, Tod, E. Maria C. Ohlsson Teague, Nicole O. Palmer, Miles J. DeBlasio, Megan Mitchell, Mark Corbett, Cristin G. Print, Julie A. Owens, and Michelle Lane. 2013. "Paternal Obesity Initiates Metabolic Disturbances in Two Generations of Mice with Incomplete Penetrance to the F_2 Generation and Alters the Transcriptional Profile of Testis and Sperm MicroRNA Content." *The FASEB Journal* 27 (10): 4226–43. https://doi.org/10.1096/fj.12-224048.

Gadadhar, Sudarshan, Gonzalo Alvarez Viar, Jan Niklas Hansen, An Gong, Aleksandr Kostarev, Côme Ialy-Radio, Sophie Leboucher, et al. 2021. "Tubulin Glycylation Controls Axonemal Dynein Activity, Flagellar Beat, and Male Fertility." *Science* 371 (6525): eabd4914. https://doi.org/10.1126/science.abd4914.

Gadadhar, Sudarshan, Tatjana Hirschmugl, and Carsten Janke. 2023. "The Tubulin Code in Mammalian Sperm Development and Function." *Seminars in Cell & Developmental Biology* 137 (March): 26–37. https://doi.org/10.1016/j.semcdb.2021.12.003.

Gan, Haiyun, Lu Wen, Shangying Liao, Xiwen Lin, Tingting Ma, Jun Liu, Chun-xiao Song, et al. 2013. "Dynamics of 5-Hydroxymethylcytosine during Mouse Spermatogenesis." *Nature Communications* 4 (1): 1995. https://doi.org/10.1038/ncomms2995.

Gao, Qian, Ranjha Khan, Changping Yu, Manfred Alsheimer, Xiaohua Jiang, Hui Ma, and Qinghua Shi. 2020. "The Testis-Specific LINC Component SUN3 Is Essential for Sperm Head Shaping during Mouse Spermiogenesis." *Journal of Biological Chemistry* 295 (19): 6289–98. https://doi.org/10.1074/jbc.RA119.012375.

Gao, Yang, Shixiong Tian, Yanwei Sha, Xiaomin Zha, Huiru Cheng, Anyong Wang, Chunyu Liu, et al. 2021. "Novel Bi-Allelic Variants in DNAH2 Cause Severe Asthenoteratozoospermia with Multiple Morphological Abnormalities of the Flagella." *Reproductive BioMedicine Online* 42 (5): 963–72. https://doi.org/10.1016/j.rbmo.2021.01.011.

Garanina, Anastasiia S., Irina B. Alieva, Elizaveta E. Bragina, Emmanuelle Blanchard, Brigitte Arbeille, Fabrice Guerif, Svetlana Uzbekova, and Rustem E. Uzbekov. 2019. "The Centriolar Adjunct–Appearance and Disassembly in Spermiogenesis and the Potential Impact on Fertility." *Cells* 8 (2): 180. https://doi.org/10.3390/cells8020180.

Gatewood, J. M., G. R. Cook, R. Balhorn, C. W. Schmid, and E. M. Bradbury. 1990. "Isolation of Four Core Histones from Human Sperm Chromatin Representing a Minor Subset of Somatic Histones." *The Journal of Biological Chemistry* 265 (33): 20662–66.

Gervasi, María Gracia, Xinran Xu, Blanca Carbajal-Gonzalez, Mariano G. Buffone, Pablo E. Visconti, and Diego Krapf. 2018. "The Actin Cytoskeleton of the Mouse Sperm Flagellum Is Organized in a Helical Structure." *Journal of Cell Science*, January, jcs.215897. https://doi.org/10.1242/jcs.215897.

Gheiratmand, Ladan, Etienne Coyaud, Gagan D Gupta, Estelle MN Laurent, Monica Hasegan, Suzanna L Prosser, João Gonçalves, Brian Raught, and Laurence Pelletier. 2019. "Spatial and Proteomic Profiling Reveals Centrosome-independent Features of Centriolar Satellites." *The EMBO Journal* 38 (14). https://doi.org/10.15252/embj.2018101109.

Giordano, Tiziana, Sudarshan Gadadhar, Satish Bodakuntla, Jonas Straub, Sophie Leboucher, Guillaume Martinez, Walid Chemlali, et al. 2019. "Loss of the Deglutamylase CCP5 Perturbs Multiple Steps of Spermatogenesis and Leads to Male Infertility." *Journal of Cell Science*, January, jcs.226951. https://doi.org/10.1242/jcs.226951.

Girardet, Laura, Céline Augière, Marie-Pier Asselin, and Clémence Belleannée. 2019. "Primary Cilia: Biosensors of the Male Reproductive Tract." *Andrology*, May, andr.12650. https://doi.org/10.1111/andr.12650.

Glotzer, Michael. 2009. "The 3Ms of Central Spindle Assembly: Microtubules, Motors and MAPs." *Nature Reviews Molecular Cell Biology* 10 (1): 9–20. https://doi.org/10.1038/nrm2609.

Göb, Eva, Johannes Schmitt, Ricardo Benavente, and Manfred Alsheimer. 2010. "Mammalian Sperm Head Formation Involves Different Polarization of Two Novel LINC Complexes." Edited by Mary Bryk. *PLoS ONE* 5 (8): e12072. https://doi.org/10.1371/journal.pone.0012072.

Godinho, S. A., and D. Pellman. 2014. "Causes and Consequences of Centrosome Abnormalities in Cancer." *Philosophical Transactions of the Royal Society B: Biological Sciences* 369 (1650): 20130467. https://doi.org/10.1098/rstb.2013.0467.

Gönczy, Pierre. 2012. "Towards a Molecular Architecture of Centriole Assembly." *Nature Reviews Molecular Cell Biology* 13 (7): 425–35. https://doi.org/10.1038/nrm3373.

Goodenough, U W, and J E Heuser. 1985. "Substructure of Inner Dynein Arms, Radial Spokes, and the Central Pair/Projection Complex of Cilia and Flagella." *The Journal of Cell Biology* 100 (6): 2008–18. https://doi.org/10.1083/jcb.100.6.2008.

Goodson, Holly V., and Erin M. Jonasson. 2018. "Microtubules and Microtubule-Associated Proteins." *Cold Spring Harbor Perspectives in Biology* 10 (6): a022608. https://doi.org/10.1101/cshperspect.a022608.

Goto, M., D. A. O'Brien, and E. M. Eddy. 2010. "Speriolin Is a Novel Human and Mouse Sperm Centrosome Protein." *Human Reproduction* 25 (8): 1884–94. https://doi.org/10.1093/humrep/deq138.

Gou, Lan-Tao, Peng Dai, Jian-Hua Yang, Yuanchao Xue, Yun-Ping Hu, Yu Zhou, Jun-Yan Kang, et al. 2014. "Pachytene PiRNAs Instruct Massive MRNA Elimination during Late Spermiogenesis." *Cell Research* 24 (6): 680–700. https://doi.org/10.1038/cr.2014.41.

Greco, Ermanno, Katarzyna Litwicka, Maria Giulia Minasi, Elisabetta Cursio, Pier Francesco Greco, and Paolo Barillari. 2020. "Preimplantation Genetic Testing: Where We Are Today." *International Journal of Molecular Sciences* 21 (12): 4381. https://doi.org/10.3390/ijms21124381.

Green, Christopher Daniel, Qianyi Ma, Gabriel L. Manske, Adrienne Niederriter Shami, Xianing Zheng, Simone Marini, Lindsay Moritz, et al. 2018. "A Comprehensive Roadmap of Murine Spermatogenesis Defined by Single-Cell RNA-Seq." *Developmental Cell* 46 (5): 651-667.e10. https://doi.org/10.1016/j.devcel.2018.07.025.

Greenbaum, M. P., T. Iwamori, G. M. Buchold, and M. M. Matzuk. 2011. "Germ Cell Intercellular Bridges." *Cold Spring Harbor Perspectives in Biology* 3 (8): a005850–a005850. https://doi.org/10.1101/cshperspect.a005850.

Grill, Stephan W., and Anthony A. Hyman. 2005. "Spindle Positioning by Cortical Pulling Forces." *Developmental Cell* 8 (4): 461–65. https://doi.org/10.1016/j.devcel.2005.03.014.

Griswold, Michael D. 2016. "Spermatogenesis: The Commitment to Meiosis." *Physiological Reviews* 96 (1): 1–17. https://doi.org/10.1152/physrev.00013.2015.

Gu, Ni-Hao, Wen-Long Zhao, Gui-Shuan Wang, and Fei Sun. 2019. "Comparative Analysis of Mammalian Sperm Ultrastructure Reveals Relationships between Sperm Morphology, Mitochondrial Functions and Motility." *Reproductive Biology and Endocrinology* 17 (1): 66. https://doi.org/10.1186/s12958-019-0510-y.

Guan, Jikui, Makoto Kinoshita, and Li Yuan. 2009. "Spatiotemporal Association of DNAJB13 with the Annulus during Mouse Sperm Flagellum Development." *BMC Developmental Biology* 9 (1): 23. https://doi.org/10.1186/1471-213X-9-23.

Gudimchuk, Nikita B., and J. Richard McIntosh. 2021. "Regulation of Microtubule Dynamics, Mechanics and Function through the Growing Tip." *Nature Reviews Molecular Cell Biology* 22 (12): 777–95. https://doi.org/10.1038/s41580-021-00399-x.

Gui, Miao, Hannah Farley, Priyanka Anujan, Jacob R. Anderson, Dale W. Maxwell, Jonathan B. Whitchurch, J. Josephine Botsch, et al. 2021. "De Novo Identification of Mammalian Ciliary Motility Proteins Using Cryo-EM." *Cell* 184 (23): 5791-5806.e19. https://doi.org/10.1016/j.cell.2021.10.007.

Gui, Miao, Meisheng Ma, Erica Sze-Tu, Xiangli Wang, Fujiet Koh, Ellen D. Zhong, Bonnie Berger, et al. 2021. "Structures of Radial Spokes and Associated Complexes Important for

Ciliary Motility." *Nature Structural & Molecular Biology* 28 (1): 29–37. https://doi.org/10.1038/s41594-020-00530-0.

Guichard, Paul, Virginie Hamel, and Pierre Gönczy. 2018. "The Rise of the Cartwheel: Seeding the Centriole Organelle." *BioEssays* 40 (4): 1700241. https://doi.org/10.1002/bies.201700241.

Guichard, Paul, Marine H. Laporte, and Virginie Hamel. 2023. "The Centriolar Tubulin Code." *Seminars in Cell & Developmental Biology* 137 (March): 16–25. https://doi.org/10.1016/j.semcdb.2021.12.001.

Gupta, Satish Kumar. 2021. "Human Zona Pellucida Glycoproteins: Binding Characteristics With Human Spermatozoa and Induction of Acrosome Reaction." *Frontiers in Cell and Developmental Biology* 9 (February): 619868. https://doi.org/10.3389/fcell.2021.619868.

Ha, Seungshin, Anna M Lindsay, Andrew E Timms, and David R Beier. 2016. "Mutations in *Dnaaf1* and *Lrrc48* Cause Hydrocephalus, Laterality Defects, and Sinusitis in Mice." *G3 Genes|Genomes|Genetics* 6 (8): 2479–87. https://doi.org/10.1534/g3.116.030791.

Halcrow, Ella F. J., Riccardo Mazza, Anna Diversi, Anton Enright, and Pier Paolo D'Avino. 2022. "Midbody Proteins Display Distinct Dynamics during Cytokinesis." *Cells* 11 (21): 3337. https://doi.org/10.3390/cells11213337.

Hall, Emma A., Margaret Keighren, Matthew J. Ford, Tracey Davey, Andrew P. Jarman, Lee B. Smith, Ian J. Jackson, and Pleasantine Mill. 2013. "Acute Versus Chronic Loss of Mammalian Azi1/Cep131 Results in Distinct Ciliary Phenotypes." Edited by Susan K. Dutcher. *PLoS Genetics* 9 (12): e1003928. https://doi.org/10.1371/journal.pgen.1003928.

Hall, Emma A., Dhivya Kumar, Suzanna L. Prosser, Patricia L. Yeyati, Vicente Herranz Pérez, Jose Manuel García Verdugo, Lorraine Rose, et al. 2022. "Centriolar Satellites Expedite Mother Centriole Remodeling to Promote Ciliogenesis." Preprint. Cell Biology. https://doi.org/10.1101/2022.04.04.486992.

Hall, Nicole A., and Heidi Hehnly. 2021. "A Centriole's Subdistal Appendages: Contributions to Cell Division, Ciliogenesis and Differentiation." *Open Biology* 11 (2): 200399. https://doi.org/10.1098/rsob.200399.

Hamada, Takahiro. 2014. "Microtubule Organization and Microtubule-Associated Proteins in Plant Cells." In *International Review of Cell and Molecular Biology*, 312:1–52. Elsevier. https://doi.org/10.1016/B978-0-12-800178-3.00001-4.

Handel, Mary Ann, and John C. Schimenti. 2010. "Genetics of Mammalian Meiosis: Regulation, Dynamics and Impact on Fertility." *Nature Reviews Genetics* 11 (2): 124–36. https://doi.org/10.1038/nrg2723.

Hausrat, Torben J., Jennifer Radwitz, Franco L. Lombino, Petra Breiden, and Matthias Kneussel. 2021. "Alpha- and Beta-tubulin Isotypes Are Differentially Expressed during Brain Development." *Developmental Neurobiology* 81 (3): 333–50. https://doi.org/10.1002/dneu.22745.

Hayasaka, Shinichi, Yukihiro Terada, Kichiya Suzuki, Haruo Murakawa, Ikuo Tachibana, Tadashi Sankai, Takashi Murakami, Nobuo Yaegashi, and Kunihiro Okamura. 2008. "Intramanchette Transport during Primate Spermiogenesis: Expression of Dynein, Myosin Va, Motor Recruiter Myosin Va, VIIa-Rab27a/b Interacting Protein, and Rab27b in the Manchette during Human and Monkey Spermiogenesis." *Asian Journal of Andrology* 10 (4): 561–68. https://doi.org/10.1111/j.1745-7262.2008.00392.x.

He, Xiaojin, Chunyu Liu, Xiaoyu Yang, Mingrong Lv, Xiaoqing Ni, Qiang Li, Huiru Cheng, et al. 2020. "Bi-Allelic Loss-of-Function Variants in CFAP58 Cause Flagellar Axoneme and

Mitochondrial Sheath Defects and Asthenoteratozoospermia in Humans and Mice." *The American Journal of Human Genetics* 107 (3): 514–26. https://doi.org/10.1016/j.ajhg.2020.07.010.

Heller, C. H., and Y. Clermont. 1964. "KINETICS OF THE GERMINAL EPITHELIUM IN MAN." *Recent Progress in Hormone Research* 20: 545–75.

Henty-Ridilla, Jessica L., Aneliya Rankova, Julian A. Eskin, Katelyn Kenny, and Bruce L. Goode. 2016. "Accelerated Actin Filament Polymerization from Microtubule plus Ends." *Science* 352 (6288): 1004–9. https://doi.org/10.1126/science.aaf1709.

Hess, Rex A., and A. Wayne Vogl. 2015. "Sertoli Cell Anatomy and Cytoskeleton." In *Sertoli Cell Biology*, 1–55. Elsevier. https://doi.org/10.1016/B978-0-12-417047-6.00001-6.

Heuser, Thomas, Milen Raytchev, Jeremy Krell, Mary E. Porter, and Daniela Nicastro. 2009. "The Dynein Regulatory Complex Is the Nexin Link and a Major Regulatory Node in Cilia and Flagella." *Journal of Cell Biology* 187 (6): 921–33. https://doi.org/10.1083/jcb.200908067.

Hibbard, Jaime V. K., Neftali Vazquez, Rohit Satija, and John B. Wallingford. 2021. "Protein Turnover Dynamics Suggest a Diffusion-to-Capture Mechanism for Peri-Basal Body Recruitment and Retention of Intraflagellar Transport Proteins." Edited by Wallace Marshall. *Molecular Biology of the Cell* 32 (12): 1171–80. https://doi.org/10.1091/mbc.E20-11-0717.

Hinsch, Klaus-Dieter, Vito De Pinto, Viviana A. Aires, Xenia Schneider, Angela Messina, and Elvira Hinsch. 2004. "Voltage-Dependent Anion-Selective Channels VDAC2 and VDAC3 Are Abundant Proteins in Bovine Outer Dense Fibers, a Cytoskeletal Component of the Sperm Flagellum." *Journal of Biological Chemistry* 279 (15): 15281–88. https://doi.org/10.1074/jbc.M313433200.

Ho, Han-Chen, and Shiuan Wey. 2007. "Three Dimensional Rendering of the Mitochondrial Sheath Morphogenesis during Mouse Spermiogenesis." *Microscopy Research and Technique* 70 (8): 719–23. https://doi.org/10.1002/jemt.20457.

Hoek, Hugo van den, Nikolai Klena, Mareike A. Jordan, Gonzalo Alvarez Viar, Ricardo D. Righetto, Miroslava Schaffer, Philipp S. Erdmann, et al. 2022. "In Situ Architecture of the Ciliary Base Reveals the Stepwise Assembly of Intraflagellar Transport Trains." *Science* 377 (6605): 543–48. https://doi.org/10.1126/science.abm6704.

Hoffman-Andrews, Lily. 2017. "The Known Unknown: The Challenges of Genetic Variants of Uncertain Significance in Clinical Practice." *Journal of Law and the Biosciences* 4 (3): 648–57. https://doi.org/10.1093/jlb/lsx038.

Hoffmann, Ingrid. 2021. "Centrosomes in Mitotic Spindle Assembly and Orientation." *Current Opinion in Structural Biology* 66 (February): 193–98. https://doi.org/10.1016/j.sbi.2020.11.003.

Horani, Amjad, Steven L. Brody, Thomas W. Ferkol, David Shoseyov, Mollie G. Wasserman, Asaf Ta-shma, Kate S. Wilson, et al. 2013. "CCDC65 Mutation Causes Primary Ciliary Dyskinesia with Normal Ultrastructure and Hyperkinetic Cilia." Edited by Dominik Hartl. *PLoS ONE* 8 (8): e72299. https://doi.org/10.1371/journal.pone.0072299.

Horn, Henning F., Dae In Kim, Graham D. Wright, Esther Sook Miin Wong, Colin L. Stewart, Brian Burke, and Kyle J. Roux. 2013. "A Mammalian KASH Domain Protein Coupling Meiotic Chromosomes to the Cytoskeleton." *Journal of Cell Biology* 202 (7): 1023–39. https://doi.org/10.1083/jcb.201304004.

Hornef, Nada, Heike Olbrich, Judit Horvath, Maimoona A. Zariwala, Manfred Fliegauf, Niki Tomas Loges, Johannes Wildhaber, et al. 2006. "*DNAH5* Mutations Are a Common Cause

of Primary Ciliary Dyskinesia with Outer Dynein Arm Defects." *American Journal of Respiratory and Critical Care Medicine* 174 (2): 120–26. https://doi.org/10.1164/rccm.200601-084OC.

Hosio, Mayu, Viljar Jaks, Heli Lagus, Jyrki Vuola, Rei Ogawa, and Esko Kankuri. 2020. "Primary Ciliary Signaling in the Skin—Contribution to Wound Healing and Scarring." *Frontiers in Cell and Developmental Biology* 8 (November): 578384. https://doi.org/10.3389/fcell.2020.578384.

Hou, Yuqing, Hongmin Qin, John A. Follit, Gregory J. Pazour, Joel L. Rosenbaum, and George B. Witman. 2007. "Functional Analysis of an Individual IFT Protein: IFT46 Is Required for Transport of Outer Dynein Arms into Flagella." *Journal of Cell Biology* 176 (5): 653–65. https://doi.org/10.1083/jcb.200608041.

Hou, Yuqing, and George B. Witman. 2015. "Dynein and Intraflagellar Transport." *Experimental Cell Research* 334 (1): 26–34. https://doi.org/10.1016/j.yexcr.2015.02.017.

Houston, Brendan J, Antoni Riera-Escamilla, Margot J Wyrwoll, Albert Salas-Huetos, Miguel J Xavier, Liina Nagirnaja, Corinna Friedrich, et al. 2021. "A Systematic Review of the Validated Monogenic Causes of Human Male Infertility: 2020 Update and a Discussion of Emerging Gene–Disease Relationships." *Human Reproduction Update* 28 (1): 15–29. https://doi.org/10.1093/humupd/dmab030.

Howe, Katie, and greg fitzharris. 2013. "A Non-Canonical Mode of Microtubule Organization Operates throughout Pre-Implantation Development in Mouse." *Cell Cycle* 12 (10): 1616–24. https://doi.org/10.4161/cc.24755.

Hoyer-Fender, Sigrid. 2022. "Development of the Connecting Piece in ODF1-Deficient Mouse Spermatids." *International Journal of Molecular Sciences* 23 (18): 10280. https://doi.org/10.3390/ijms231810280.

Hruz, Tomas, Oliver Laule, Gabor Szabo, Frans Wessendorp, Stefan Bleuler, Lukas Oertle, Peter Widmayer, Wilhelm Gruissem, and Philip Zimmermann. 2008. "Genevestigator V3: A Reference Expression Database for the Meta-Analysis of Transcriptomes." *Advances in Bioinformatics* 2008 (July): 1–5. https://doi.org/10.1155/2008/420747.

Huang, Ning, Yuqing Xia, Donghui Zhang, Song Wang, Yitian Bao, Runsheng He, Junlin Teng, and Jianguo Chen. 2017. "Hierarchical Assembly of Centriole Subdistal Appendages via Centrosome Binding Proteins CCDC120 and CCDC68." *Nature Communications* 8 (1): 15057. https://doi.org/10.1038/ncomms15057.

Huttlin, Edward L., Raphael J. Bruckner, Joao A. Paulo, Joe R. Cannon, Lily Ting, Kurt Baltier, Greg Colby, et al. 2017. "Architecture of the Human Interactome Defines Protein Communities and Disease Networks." *Nature* 545 (7655): 505–9. https://doi.org/10.1038/nature22366.

Hwang, Jae Yeon, Shoaib Nawaz, Jungmin Choi, Huafeng Wang, Shabir Hussain, Mehboob Nawaz, Francesc Lopez-Giraldez, et al. 2021. "Genetic Defects in DNAH2 Underlie Male Infertility With Multiple Morphological Abnormalities of the Sperm Flagella in Humans and Mice." *Frontiers in Cell and Developmental Biology* 9 (April): 662903. https://doi.org/10.3389/fcell.2021.662903.

Ibtisham, Fahar, Jiang Wu, Mei Xiao, Lilong An, Zachary Banker, Aamir Nawab, Yi Zhao, and Guanghui Li. 2017. "Progress and Future Prospect of *in Vitro* Spermatogenesis." *Oncotarget* 8 (39): 66709–27. https://doi.org/10.18632/oncotarget.19640.

Ichikawa, Muneyoshi, Dinan Liu, Panagiotis L. Kastritis, Kaustuv Basu, Tzu Chin Hsu, Shunkai Yang, and Khanh Huy Bui. 2017. "Subnanometre-Resolution Structure of the Doublet

Microtubule Reveals New Classes of Microtubule-Associated Proteins." *Nature Communications* 8 (1): 15035. https://doi.org/10.1038/ncomms15035.

Iida, Hiroshi, Yoshiko Honda, Takuya Matsuyama, Yosaburo Shibata, and Tetsuichiro Inai. 2006. "Tektin 4 Is Located on Outer Dense Fibers, Not Associated with Axonemal Tubulins of Flagella in Rodent Spermatozoa." *Molecular Reproduction and Development* 73 (7): 929–36. https://doi.org/10.1002/mrd.20486.

Ikawa, Masahito, Naokazu Inoue, Adam M. Benham, and Masaru Okabe. 2010. "Fertilization: A Sperm's Journey to and Interaction with the Oocyte." *Journal of Clinical Investigation* 120 (4): 984–94. https://doi.org/10.1172/JCI41585.

Ikegami, Koji, Showbu Sato, Kenji Nakamura, Lawrence E. Ostrowski, and Mitsutoshi Setou. 2010. "Tubulin Polyglutamylation Is Essential for Airway Ciliary Function through the Regulation of Beating Asymmetry." *Proceedings of the National Academy of Sciences* 107 (23): 10490–95. https://doi.org/10.1073/pnas.1002128107.

"IMIGC | Male Infertility Consortium." n.d. Accessed February 15, 2023. http://www.imigc.org/.

Inaba, K. 2011. "Sperm Flagella: Comparative and Phylogenetic Perspectives of Protein Components." *Molecular Human Reproduction* 17 (8): 524–38. https://doi.org/10.1093/molehr/gar034.

Ingerslev, Lars R., Ida Donkin, Odile Fabre, Soetkin Versteyhe, Mie Mechta, Pattarawan Pattamaprapanont, Brynjulf Mortensen, Nikolaj Thure Krarup, and Romain Barrès. 2018. "Endurance Training Remodels Sperm-Borne Small RNA Expression and Methylation at Neurological Gene Hotspots." *Clinical Epigenetics* 10 (1): 12. https://doi.org/10.1186/s13148-018-0446-7.

Ishikawa, Hiroaki, Takahiro Ide, Toshiki Yagi, Xue Jiang, Masafumi Hirono, Hiroyuki Sasaki, Haruaki Yanagisawa, et al. 2014. "TTC26/DYF13 Is an Intraflagellar Transport Protein Required for Transport of Motility-Related Proteins into Flagella." *ELife* 3 (March): e01566. https://doi.org/10.7554/eLife.01566.

Ito, Chizuru, Hidenori Akutsu, Ryoji Yao, Keiichi Yoshida, Kenji Yamatoya, Tohru Mutoh, Tsukasa Makino, et al. 2019. "Odf2 Haploinsufficiency Causes a New Type of Decapitated and Decaudated Spermatozoa, Odf2-DDS, in Mice." *Scientific Reports* 9 (1): 14249. https://doi.org/10.1038/s41598-019-50516-2.

Jan, Sabrina Z., Geert Hamer, Sjoerd Repping, Dirk G. de Rooij, Ans M.M. van Pelt, and Tinke L. Vormer. 2012. "Molecular Control of Rodent Spermatogenesis." *Biochimica et Biophysica Acta (BBA) - Molecular Basis of Disease* 1822 (12): 1838–50. https://doi.org/10.1016/j.bbadis.2012.02.008.

Janca, Frank C., Lorna K. Jost, and Donald P. Evenson. 1986. "Mouse Testicular and Sperm Cell Development Characterized from Birth to Adulthood by Dual Parameter Flow Cytometry1." *Biology of Reproduction* 34 (4): 613–23. https://doi.org/10.1095/biolreprod34.4.613.

Janke, Carsten, and Maria M. Magiera. 2020. "The Tubulin Code and Its Role in Controlling Microtubule Properties and Functions." *Nature Reviews Molecular Cell Biology* 21 (6): 307–26. https://doi.org/10.1038/s41580-020-0214-3.

Janke, Carsten, and Guillaume Montagnac. 2017. "Causes and Consequences of Microtubule Acetylation." *Current Biology* 27 (23): R1287–92. https://doi.org/10.1016/j.cub.2017.10.044.

Jeanson, Ludovic, Bruno Copin, Jean-François Papon, Florence Dastot-Le Moal, Philippe Duquesnoy, Guy Montantin, Jacques Cadranel, et al. 2015. "RSPH3 Mutations Cause

Primary Ciliary Dyskinesia with Central-Complex Defects and a Near Absence of Radial Spokes." *The American Journal of Human Genetics* 97 (1): 153–62. https://doi.org/10.1016/j.ajhg.2015.05.004.

Jumper, John, Richard Evans, Alexander Pritzel, Tim Green, Michael Figurnov, Olaf Ronneberger, Kathryn Tunyasuvunakool, et al. 2021. "Highly Accurate Protein Structure Prediction with AlphaFold." *Nature* 596 (7873): 583–89. https://doi.org/10.1038/s41586-021-03819-2.

Jungwirth, Andreas, Aleksander Giwercman, Herman Tournaye, Thorsten Diemer, Zsolt Kopa, Gert Dohle, and Csilla Krausz. 2012. "European Association of Urology Guidelines on Male Infertility: The 2012 Update." *European Urology* 62 (2): 324–32. https://doi.org/10.1016/j.eururo.2012.04.048.

Kalebic, Nereo, Simona Sorrentino, Emerald Perlas, Giulia Bolasco, Concepcion Martinez, and Paul A. Heppenstall. 2013. "ATAT1 Is the Major α-Tubulin Acetyltransferase in Mice." *Nature Communications* 4 (1): 1962. https://doi.org/10.1038/ncomms2962.

Kamiya, Ritsu, and Toshiki Yagi. 2014. "Functional Diversity of Axonemal Dyneins as Assessed by in Vitro and in Vivo Motility Assays of *Chlamydomonas* Mutants." *Zoological Science* 31 (10): 633–44. https://doi.org/10.2108/zs140066.

Kanfer, Gil, Martin Peterka, Vladimir K. Arzhanik, Alexei L. Drobyshev, Fazly I. Ataullakhanov, Vladimir A. Volkov, and Benoît Kornmann. 2017. "CENP-F Couples Cargo to Growing and Shortening Microtubule Ends." Edited by Manuel Théry. *Molecular Biology of the Cell* 28 (18): 2400–2409. https://doi.org/10.1091/mbc.e16-11-0756.

Kaplan, Anna, and Orly Reiner. 2011. "Linking Cytoplasmic Dynein and Transport of Rab8 Vesicles to the Midbody during Cytokinesis by the Doublecortin Domain-Containing 5 Protein." *Journal of Cell Science* 124 (23): 3989–4000. https://doi.org/10.1242/jcs.085407.

Kashihara, Hiroka, Shuhei Chiba, Shin-ichiro Kanno, Koya Suzuki, Tomoki Yano, and Sachiko Tsukita. 2019. "Cep128 Associates with Odf2 to Form the Subdistal Appendage of the Centriole." *Genes to Cells* 24 (3): 231–43. https://doi.org/10.1111/gtc.12668.

Kato, Akira, Yuka Nagata, and Kazuo Todokoro. 2004. "δ-Tubulin Is a Component of Intercellular Bridges and Both the Early and Mature Perinuclear Rings during Spermatogenesis." *Developmental Biology* 269 (1): 196–205. https://doi.org/10.1016/j.ydbio.2004.01.026.

Kazarian, Elizabeth, HyunYoung Son, Paulene Sapao, Wei Li, Zhibing Zhang, Jerome Strauss, and Maria Teves. 2018. "SPAG17 Is Required for Male Germ Cell Differentiation and Fertility." *International Journal of Molecular Sciences* 19 (4): 1252. https://doi.org/10.3390/ijms19041252.

Kherraf, Zine-Eddine, Caroline Cazin, Amine Bouker, Selima Fourati Ben Mustapha, Sylviane Hennebicq, Amandine Septier, Charles Coutton, et al. 2022. "Whole-Exome Sequencing Improves the Diagnosis and Care of Men with Non-Obstructive Azoospermia." *The American Journal of Human Genetics* 109 (3): 508–17. https://doi.org/10.1016/j.ajhg.2022.01.011.

Kherraf, Zine-Eddine, Marie Christou-Kent, Thomas Karaouzene, Amir Amiri-Yekta, Guillaume Martinez, Alexandra S Vargas, Emeline Lambert, et al. 2017. "SPINK 2 Deficiency Causes Infertility by Inducing Sperm Defects in Heterozygotes and Azoospermia in Homozygotes." *EMBO Molecular Medicine* 9 (8): 1132–49. https://doi.org/10.15252/emmm.201607461.

Kherraf, Zine-Eddine, Beatrice Conne, Amir Amiri-Yekta, Marie Christou Kent, Charles Coutton, Jessica Escoffier, Serge Nef, Christophe Arnoult, and Pierre F. Ray. 2018. "Creation of

Knock out and Knock in Mice by CRISPR/Cas9 to Validate Candidate Genes for Human Male Infertility, Interest, Difficulties and Feasibility." *Molecular and Cellular Endocrinology* 468 (June): 70–80. https://doi.org/10.1016/j.mce.2018.03.002.

Kierszenbaum, Abraham L. 2002a. "Keratins: Unraveling the Coordinated Construction of Scaffolds in Spermatogenic Cells." *Molecular Reproduction and Development* 61 (1): 1–2. https://doi.org/10.1002/mrd.1124.

———. 2002b. "Intramanchette Transport (IMT): Managing the Making of the Spermatid Head, Centrosome, and Tail." *Molecular Reproduction and Development* 63 (1): 1–4. https://doi.org/10.1002/mrd.10179.

Kierszenbaum, Abraham L., Eugene Rivkin, and Laura L. Tres. 2003. "Acroplaxome, an F-Actin–Keratin-Containing Plate, Anchors the Acrosome to the Nucleus during Shaping of the Spermatid Head." *Molecular Biology of the Cell* 14 (11): 4628–40. https://doi.org/10.1091/mbc.e03-04-0226.

Kierszenbaum, Abraham L., Eugene Rivkin, Laura L. Tres, Bradley K. Yoder, Courtney J. Haycraft, Michel Bornens, and Rosa M. Rios. 2011. "GMAP210 and IFT88 Are Present in the Spermatid Golgi Apparatus and Participate in the Development of the Acrosome-Acroplaxome Complex, Head-Tail Coupling Apparatus and Tail." *Developmental Dynamics* 240 (3): 723–36. https://doi.org/10.1002/dvdy.22563.

Kierszenbaum, Abraham L., and Laura L. Tres. 2004. "The Acrosome-Acroplaxome-Manchette Complex and the Shaping of the Spermatid Head." *Archives of Histology and Cytology* 67 (4): 271–84. https://doi.org/10.1679/aohc.67.271.

Kierszenbaum, A.L., E. Rivkin, and L.L. Tres. 2003. "The Actin-Based Motor Myosin Va Is a Component of the Acroplaxome, an Acrosome-Nuclear Envelope Junctional Plate, and of Manchette-Associated Vesicles." *Cytogenetic and Genome Research* 103 (3–4): 337–44. https://doi.org/10.1159/000076822.

Kiesel, Petra, Gonzalo Alvarez Viar, Nikolai Tsoy, Riccardo Maraspini, Peter Gorilak, Vladimir Varga, Alf Honigmann, and Gaia Pigino. 2020. "The Molecular Structure of Mammalian Primary Cilia Revealed by Cryo-Electron Tomography." *Nature Structural & Molecular Biology* 27 (12): 1115–24. https://doi.org/10.1038/s41594-020-0507-4.

Kim, Jihye, Jun Tae Kwon, Juri Jeong, Jaehwan Kim, Seong Hyeon Hong, Jinyoung Kim, Zee Yong Park, Kyung Hwun Chung, Edward M Eddy, and Chunghee Cho. 2018. "SPATC 1L Maintains the Integrity of the Sperm Head-tail Junction." *EMBO Reports* 19 (9). https://doi.org/10.15252/embr.201845991.

Kim, Kye-Seong, James A. Foster, and George L. Gerton. 2001. "Differential Release of Guinea Pig Sperm Acrosomal Components During Exocytosis1." *Biology of Reproduction* 64 (1): 148–56. https://doi.org/10.1095/biolreprod64.1.148.

Kirima, Junya, and Kazuhiro Oiwa. 2018. "Flagellar-Associated Protein FAP85 Is a Microtubule Inner Protein That Stabilizes Microtubules." *Cell Structure and Function* 43 (1): 1–14. https://doi.org/10.1247/csf.17023.

Kissel, Holger, Maria-Magdalena Georgescu, Sarit Larisch, Katia Manova, Gary R. Hunnicutt, and Hermann Steller. 2005. "The Sept4 Septin Locus Is Required for Sperm Terminal Differentiation in Mice." *Developmental Cell* 8 (3): 353–64. https://doi.org/10.1016/j.devcel.2005.01.021.

Klena, Nikolai, Maeva Le Guennec, Anne-Marie Tassin, Hugo van den Hoek, Philipp S Erdmann, Miroslava Schaffer, Stefan Geimer, et al. 2020. "Architecture of the Centriole Cartwheel-

containing Region Revealed by Cryo-electron Tomography." *The EMBO Journal* 39 (22). https://doi.org/10.15252/embj.2020106246.

Kmonickova, Vera, Michaela Frolikova, Klaus Steger, and Katerina Komrskova. 2020. "The Role of the LINC Complex in Sperm Development and Function." *International Journal of Molecular Sciences* 21 (23): 9058. https://doi.org/10.3390/ijms21239058.

Knödler, Andreas, Shanshan Feng, Jian Zhang, Xiaoyu Zhang, Amlan Das, Johan Peränen, and Wei Guo. 2010. "Coordination of Rab8 and Rab11 in Primary Ciliogenesis." *Proceedings of the National Academy of Sciences* 107 (14): 6346–51. https://doi.org/10.1073/pnas.1002401107.

Knowles, Michael R, Margaret W Leigh, Johnny L Carson, Stephanie D Davis, Sharon D Dell, Thomas W Ferkol, Kenneth N Olivier, et al. 2012. "Mutations of *DNAH11* in Patients with Primary Ciliary Dyskinesia with Normal Ciliary Ultrastructure." *Thorax* 67 (5): 433–41. https://doi.org/10.1136/thoraxjnl-2011-200301.

Kojima, Yoshio. 1994. "Ultrastructure of Goat Testes: Centriolar Adjunct in Spermiogenesis." *Journal of Veterinary Medical Science* 56 (2): 259–67. https://doi.org/10.1292/jvms.56.259.

Konno, Alu, Koji Ikegami, Yoshiyuki Konishi, Hyun-Jeong Yang, Manabu Abe, Maya Yamazaki, Kenji Sakimura, et al. 2016. "Doublet 7 Shortening, Doublet 5-Preferential Poly-Glu Reduction, and Beating Stall of Sperm Flagella in *Ttll9* −/− Mice." *Journal of Cell Science*, January, jcs.185983. https://doi.org/10.1242/jcs.185983.

Kopylow, Kathrein von, and Andrej-Nikolai Spiess. 2017. "Human Spermatogonial Markers." *Stem Cell Research* 25 (December): 300–309. https://doi.org/10.1016/j.scr.2017.11.011.

Korneev, Denis, D. Jo Merriner, Gediminas Gervinskas, Alex de Marco, and Moira K. O'Bryan. 2021. "New Insights Into Sperm Ultrastructure Through Enhanced Scanning Electron Microscopy." *Frontiers in Cell and Developmental Biology* 9 (April): 672592. https://doi.org/10.3389/fcell.2021.672592.

Kothandaraman, Narasimhan, Ashok Agarwal, Muhammad Abu-Elmagd, and Mohammed H Al-Qahtani. 2016. "Pathogenic Landscape of Idiopathic Male Infertility: New Insight towards Its Regulatory Networks." *Npj Genomic Medicine* 1 (1): 16023. https://doi.org/10.1038/npjgenmed.2016.23.

Kott, Esther, Marie Legendre, Bruno Copin, Jean-François Papon, Florence Dastot-Le Moal, Guy Montantin, Philippe Duquesnoy, et al. 2013. "Loss-of-Function Mutations in RSPH1 Cause Primary Ciliary Dyskinesia with Central-Complex and Radial-Spoke Defects." *The American Journal of Human Genetics* 93 (3): 561–70. https://doi.org/10.1016/j.ajhg.2013.07.013.

Kousi, M., and N. Katsanis. 2015. "Genetic Modifiers and Oligogenic Inheritance." *Cold Spring Harbor Perspectives in Medicine* 5 (6): a017145–a017145. https://doi.org/10.1101/cshperspect.a017145.

Krausz, Csilla, and Antoni Riera-Escamilla. 2018. "Genetics of Male Infertility." *Nature Reviews Urology* 15 (6): 369–84. https://doi.org/10.1038/s41585-018-0003-3.

Krisfalusi, Michelle, Kiyoshi Miki, Patricia L. Magyar, and Deborah A. O'Brien. 2006. "Multiple Glycolytic Enzymes Are Tightly Bound to the Fibrous Sheath of Mouse Spermatozoa1." *Biology of Reproduction* 75 (2): 270–78. https://doi.org/10.1095/biolreprod.105.049684.

Kubo, Tomohiro, Haru-aki Yanagisawa, Toshiki Yagi, Masafumi Hirono, and Ritsu Kamiya. 2010. "Tubulin Polyglutamylation Regulates Axonemal Motility by Modulating Activities

of Inner-Arm Dyneins." *Current Biology* 20 (5): 441–45. https://doi.org/10.1016/j.cub.2009.12.058.

Kumar, Naina, and Amit Kant Singh. 2022. "Impact of Environmental Factors on Human Semen Quality and Male Fertility: A Narrative Review." *Environmental Sciences Europe* 34 (1): 6. https://doi.org/10.1186/s12302-021-00585-w.

Kwitny, Susanna, Angela V. Klaus, and Gary R. Hunnicutt. 2010. "The Annulus of the Mouse Sperm Tail Is Required to Establish a Membrane Diffusion Barrier That Is Engaged During the Late Steps of Spermiogenesis1." *Biology of Reproduction* 82 (4): 669–78. https://doi.org/10.1095/biolreprod.109.079566.

Labat-de-Hoz, Leticia, Armando Rubio-Ramos, Javier Casares-Arias, Miguel Bernabé-Rubio, Isabel Correas, and Miguel A. Alonso. 2021a. "A Model for Primary Cilium Biogenesis by Polarized Epithelial Cells: Role of the Midbody Remnant and Associated Specialized Membranes." *Frontiers in Cell and Developmental Biology* 8 (January): 622918. https://doi.org/10.3389/fcell.2020.622918.

———. 2021b. "A Model for Primary Cilium Biogenesis by Polarized Epithelial Cells: Role of the Midbody Remnant and Associated Specialized Membranes." *Frontiers in Cell and Developmental Biology* 8 (January): 622918. https://doi.org/10.3389/fcell.2020.622918.

Lakshmi, R. Bhagya, Vishnu M. Nair, and Tapas K. Manna. 2018. "Regulators of Spindle Microtubules and Their Mechanisms: Living Together Matters: SPINDLE MICROTUBULES AND THEIR MECHANISMS." *IUBMB Life* 70 (2): 101–11. https://doi.org/10.1002/iub.1708.

Le Guennec, Maeva, Nikolai Klena, Davide Gambarotto, Marine H. Laporte, Anne-Marie Tassin, Hugo van den Hoek, Philipp S. Erdmann, et al. 2020. "A Helical Inner Scaffold Provides a Structural Basis for Centriole Cohesion." *Science Advances* 6 (7): eaaz4137. https://doi.org/10.1126/sciadv.aaz4137.

Leaver, Megan, and Dagan Wells. 2020. "Non-Invasive Preimplantation Genetic Testing (NiPGT): The next Revolution in Reproductive Genetics?" *Human Reproduction Update* 26 (1): 16–42. https://doi.org/10.1093/humupd/dmz033.

Leblond, C. P., and Y. Clermont. 1952. "DEFINITION OF THE STAGES OF THE CYCLE OF THE SEMINIFEROUS EPITHELIUM IN THE RAT." *Annals of the New York Academy of Sciences* 55 (4): 548–73. https://doi.org/10.1111/j.1749-6632.1952.tb26576.x.

Lechtreck, Karl F, Yi Liu, Jin Dai, Rama A Alkhofash, Jack Butler, Lea Alford, and Pinfen Yang. 2022. "Chlamydomonas ARMC2/PF27 Is an Obligate Cargo Adapter for Intraflagellar Transport of Radial Spokes." *ELife* 11 (January): e74993. https://doi.org/10.7554/eLife.74993.

Lechtreck, Karl-Ferdinand, and George B. Witman. 2007. "Chlamydomonas Reinhardtii Hydin Is a Central Pair Protein Required for Flagellar Motility." *Journal of Cell Biology* 176 (4): 473–82. https://doi.org/10.1083/jcb.200611115.

Lee, Geun-Shik, Yuanzheng He, Edward J. Dougherty, Maria Jimenez-Movilla, Matteo Avella, Sean Grullon, David S. Sharlin, et al. 2013. "Disruption of Ttll5/Stamp Gene (Tubulin Tyrosine Ligase-like Protein 5/SRC-1 and TIF2-Associated Modulatory Protein Gene) in Male Mice Causes Sperm Malformation and Infertility." *Journal of Biological Chemistry* 288 (21): 15167–80. https://doi.org/10.1074/jbc.M113.453936.

Lee, Lance, Dean R. Campagna, Jack L. Pinkus, Howard Mulhern, Todd A. Wyatt, Joseph H. Sisson, Jacqueline A. Pavlik, Geraldine S. Pinkus, and Mark D. Fleming. 2008. "Primary

Ciliary Dyskinesia in Mice Lacking the Novel Ciliary Protein Pcdp1." *Molecular and Cellular Biology* 28 (3): 949–57. https://doi.org/10.1128/MCB.00354-07.

LeGuennec, Maeva, Nikolai Klena, Gabriel Aeschlimann, Virginie Hamel, and Paul Guichard. 2021. "Overview of the Centriole Architecture." *Current Opinion in Structural Biology* 66 (February): 58–65. https://doi.org/10.1016/j.sbi.2020.09.015.

Lehti, M S, and A Sironen. 2016. "Formation and Function of the Manchette and Flagellum during Spermatogenesis." *REPRODUCTION* 151 (4): R43–54. https://doi.org/10.1530/REP-15-0310.

Lehti, Mari S., Noora Kotaja, and Anu Sironen. 2013. "KIF3A Is Essential for Sperm Tail Formation and Manchette Function." *Molecular and Cellular Endocrinology* 377 (1–2): 44–55. https://doi.org/10.1016/j.mce.2013.06.030.

Lehti, Mari S, and Anu Sironen. 2017. "Formation and Function of Sperm Tail Structures in Association with Sperm Motility Defects†." *Biology of Reproduction* 97 (4): 522–36. https://doi.org/10.1093/biolre/iox096.

Leung, Miguel Ricardo, Marc C Roelofs, Ravi Teja Ravi, Paula Maitan, Heiko Henning, Min Zhang, Elizabeth G Bromfield, et al. 2021. "The Multi-scale Architecture of Mammalian Sperm Flagella and Implications for Ciliary Motility." *The EMBO Journal* 40 (7). https://doi.org/10.15252/embj.2020107410.

Li, Ren-Ke, Jue-Ling Tan, Li-Ting Chen, Jing-Sheng Feng, Wen-Xue Liang, Xue-Jiang Guo, Ping Liu, et al. 2014. "Iqcg Is Essential for Sperm Flagellum Formation in Mice." Edited by Chris D. Wood. *PLoS ONE* 9 (5): e98053. https://doi.org/10.1371/journal.pone.0098053.

Li, Yang, Yanwei Sha, Xiong Wang, Lu Ding, Wensheng Liu, Zhiyong Ji, Libin Mei, et al. 2019. "*DNAH2* Is a Novel Candidate Gene Associated with Multiple Morphological Abnormalities of the Sperm Flagella." *Clinical Genetics* 95 (5): 590–600. https://doi.org/10.1111/cge.13525.

Li, Yan-Ruide, and Wan-Xi Yang. 2016. "Myosin Superfamily: The Multi-Functional and Irreplaceable Factors in Spermatogenesis and Testicular Tumors." *Gene* 576 (1): 195–207. https://doi.org/10.1016/j.gene.2015.10.022.

Li, You-Zhu, Na Li, Wen-Sheng Liu, Yan-Wei Sha, Rong-Feng Wu, Ya-Ling Tang, Xing-Shen Zhu, et al. 2022. "Biallelic Mutations in Spermatogenesis and Centriole-Associated 1 like (SPATC1L) Cause Acephalic Spermatozoa Syndrome and Male Infertility." *Asian Journal of Andrology* 24 (1): 67. https://doi.org/10.4103/aja.aja_56_21.

Li, Zheng-Zheng, Wen-Long Zhao, Gui-Shuan Wang, Ni-Hao Gu, and Fei Sun. 2020. "The Novel Testicular Enrichment Protein Cfap58 Is Required for Notch-Associated Ciliogenesis." *Bioscience Reports* 40 (1): BSR20192666. https://doi.org/10.1042/BSR20192666.

Lin, Jianfeng, Thomas Heuser, Blanca I. Carbajal-González, Kangkang Song, and Daniela Nicastro. 2012. "The Structural Heterogeneity of Radial Spokes in Cilia and Flagella Is Conserved." *Cytoskeleton* 69 (2): 88–100. https://doi.org/10.1002/cm.21000.

Lin, Jianfeng, Weining Yin, Maria C. Smith, Kangkang Song, Margaret W. Leigh, Maimoona A. Zariwala, Michael R. Knowles, Lawrence E. Ostrowski, and Daniela Nicastro. 2014. "Cryo-Electron Tomography Reveals Ciliary Defects Underlying Human RSPH1 Primary Ciliary Dyskinesia." *Nature Communications* 5 (1): 5727. https://doi.org/10.1038/ncomms6727.

Linck, Richard W., Hector Chemes, and David F. Albertini. 2016. "The Axoneme: The Propulsive Engine of Spermatozoa and Cilia and Associated Ciliopathies Leading to Infertility."

Journal of Assisted Reproduction and Genetics 33 (2): 141–56. https://doi.org/10.1007/s10815-016-0652-1.

Lindemann, Charles B., and Kathleen A. Lesich. 2016. "Functional Anatomy of the Mammalian Sperm Flagellum: Mammalian Sperm Mechanics." *Cytoskeleton* 73 (11): 652–69. https://doi.org/10.1002/cm.21338.

Liška, František, Claudia Gosele, Eugene Rivkin, Laura Tres, M. Cristina Cardoso, Petra Domaing, Eliška Krejčí, et al. 2009. "Rat *Hd* Mutation Reveals an Essential Role of Centrobin in Spermatid Head Shaping and Assembly of the Head-Tail Coupling Apparatus1." *Biology of Reproduction* 81 (6): 1196–1205. https://doi.org/10.1095/biolreprod.109.078980.

Liu, Chunyu, Xiaojin He, Wangjie Liu, Shenmin Yang, Lingbo Wang, Weiyu Li, Huan Wu, et al. 2019. "Bi-Allelic Mutations in TTC29 Cause Male Subfertility with Asthenoteratospermia in Humans and Mice." *The American Journal of Human Genetics* 105 (6): 1168–81. https://doi.org/10.1016/j.ajhg.2019.10.010.

Liu, Chunyu, Haruhiko Miyata, Yang Gao, Yanwei Sha, Shuyan Tang, Zoulan Xu, Marjorie Whitfield, et al. 2020. "Bi-Allelic DNAH8 Variants Lead to Multiple Morphological Abnormalities of the Sperm Flagella and Primary Male Infertility." *The American Journal of Human Genetics* 107 (2): 330–41. https://doi.org/10.1016/j.ajhg.2020.06.004.

Liu, Chunyu, Ying Shen, Shuyan Tang, Jiaxiong Wang, Yiling Zhou, Shixiong Tian, Huan Wu, et al. 2022. "Homozygous Variants in *AKAP3* Induce Asthenoteratozoospermia and Male Infertility." *Journal of Medical Genetics*, February, jmedgenet-2021-108271. https://doi.org/10.1136/jmedgenet-2021-108271.

Liu, Chunyu, Chaofeng Tu, Lingbo Wang, Huan Wu, Brendan J. Houston, Francesco K. Mastrorosa, Wen Zhang, et al. 2021. "Deleterious Variants in X-Linked CFAP47 Induce Asthenoteratozoospermia and Primary Male Infertility." *The American Journal of Human Genetics* 108 (2): 309–23. https://doi.org/10.1016/j.ajhg.2021.01.002.

Liu, Hong, Wei Li, Yong Zhang, Zhengang Zhang, Xuejun Shang, Ling Zhang, Shiyang Zhang, et al. 2017. "IFT25, an Intraflagellar Transporter Protein Dispensable for Ciliogenesis in Somatic Cells, Is Essential for Sperm Flagella Formation†." *Biology of Reproduction* 96 (5): 993–1006. https://doi.org/10.1093/biolre/iox029.

Liu, Shuli, Lingzhao Fang, Yang Zhou, Daniel J.A. Santos, Ruidong Xiang, Hans D. Daetwyler, Amanda J. Chamberlain, et al. 2019. "Analyses of Inter-Individual Variations of Sperm DNA Methylation and Their Potential Implications in Cattle." *BMC Genomics* 20 (1): 888. https://doi.org/10.1186/s12864-019-6228-6.

Liu, Wangjie, Huan Wu, Li Wang, Xiaoyu Yang, Chunyu Liu, Xiaojin He, Weiyu Li, et al. 2019. "Homozygous Loss-of-Function Mutations in FSIP2 Cause Male Infertility with Asthenoteratospermia." *Journal of Genetics and Genomics* 46 (1): 53–56. https://doi.org/10.1016/j.jgg.2018.09.006.

Liu, Yan, Kathleen DeBoer, David M. de Kretser, Liza O'Donnell, Anne E. O'Connor, D. Jo Merriner, Hidenobu Okuda, et al. 2015. "LRGUK-1 Is Required for Basal Body and Manchette Function during Spermatogenesis and Male Fertility." Edited by Wei Yan. *PLOS Genetics* 11 (3): e1005090. https://doi.org/10.1371/journal.pgen.1005090.

LoMastro, Gina M., and Andrew J. Holland. 2019. "The Emerging Link between Centrosome Aberrations and Metastasis." *Developmental Cell* 49 (3): 325–31. https://doi.org/10.1016/j.devcel.2019.04.002.

Lopes, Carla A. M., Suzanna L. Prosser, Leila Romio, Robert A. Hirst, Chris O'Callaghan, Adrian S. Woolf, and Andrew M. Fry. 2011. "Centriolar Satellites Are Assembly Points for Proteins Implicated in Human Ciliopathies, Including Oral-Facial-Digital Syndrome 1." *Journal of Cell Science* 124 (4): 600–612. https://doi.org/10.1242/jcs.077156.

López-Jiménez, Pablo, Sara Pérez-Martín, Inés Hidalgo, Francesc R. García-Gonzalo, Jesús Page, and Rocio Gómez. 2022. "The Male Mouse Meiotic Cilium Emanates from the Mother Centriole at Zygotene Prior to Centrosome Duplication." *Cells* 12 (1): 142. https://doi.org/10.3390/cells12010142.

Loreng, Thomas D., and Elizabeth F. Smith. 2017. "The Central Apparatus of Cilia and Eukaryotic Flagella." *Cold Spring Harbor Perspectives in Biology* 9 (2): a028118. https://doi.org/10.1101/cshperspect.a028118.

Losano, João Diego de Agostini, Daniel de Souza Ramos Angrimani, Roberta Ferreira Leite, Bárbara do Carmo Simões da Silva, Valquíria Hyppolito Barnabe, and Marcilio Nichi. 2018. "Spermatic Mitochondria: Role in Oxidative Homeostasis, Sperm Function and Possible Tools for Their Assessment." *Zygote* 26 (4): 251–60. https://doi.org/10.1017/S0967199418000242.

Lu, Lei, and Viswanadh Madugula. 2018. "Mechanisms of Ciliary Targeting: Entering Importins and Rabs." *Cellular and Molecular Life Sciences* 75 (4): 597–606. https://doi.org/10.1007/s00018-017-2629-3.

Lu, Shuai, Yayun Gu, Yifei Wu, Shenmin Yang, Chenmeijie Li, Lanlan Meng, Wenwen Yuan, et al. 2021. "Bi-Allelic Variants in Human WDR63 Cause Male Infertility via Abnormal Inner Dynein Arms Assembly." *Cell Discovery* 7 (1): 110. https://doi.org/10.1038/s41421-021-00327-5.

Luo, Wangxi, Andrew Ruba, Daisuke Takao, Ludovit P. Zweifel, Roderick Y. H. Lim, Kristen J. Verhey, and Weidong Yang. 2017. "Axonemal Lumen Dominates Cytosolic Protein Diffusion inside the Primary Cilium." *Scientific Reports* 7 (1): 15793. https://doi.org/10.1038/s41598-017-16103-z.

Lv, Mingrong, Wangjie Liu, Wangfei Chi, Xiaoqing Ni, Jiajia Wang, Huiru Cheng, Wei-Yu Li, et al. 2020. "Homozygous Mutations in *DZIP1* Can Induce Asthenoteratospermia with Severe MMAF." *Journal of Medical Genetics* 57 (7): 445–53. https://doi.org/10.1136/jmedgenet-2019-106479.

Ma, Meisheng, Mihaela Stoyanova, Griffin Rademacher, Susan K. Dutcher, Alan Brown, and Rui Zhang. 2019. "Structure of the Decorated Ciliary Doublet Microtubule." *Cell* 179 (4): 909-922.e12. https://doi.org/10.1016/j.cell.2019.09.030.

Maekawa, Mamiko, Kyoko Kamimura, and Toshio Nagano. 1996. "Peritubular Myoid Cells in the Testis: Their Structure and Function." *Archives of Histology and Cytology* 59 (1): 1–13. https://doi.org/10.1679/aohc.59.1.

Manandhar, G., C. Simerly, J.L. Salisbury, and G. Schatten. 1999. "Centriole and Centrin Degeneration during Mouse Spermiogenesis." *Cell Motility and the Cytoskeleton* 43 (2): 137–44. https://doi.org/10.1002/(SICI)1097-0169(1999)43:2<137::AID-CM5>3.0.CO;2-7.

Manandhar, G., P. Sutovsky, H.C. Joshi, T. Stearns, and G. Schatten. 1998. "Centrosome Reduction during Mouse Spermiogenesis." *Developmental Biology* 203 (2): 424–34. https://doi.org/10.1006/dbio.1998.8947.

Manfrevola, Francesco, Florian Guillou, Silvia Fasano, Riccardo Pierantoni, and Rosanna Chianese. 2021. "LINCking the Nuclear Envelope to Sperm Architecture." *Genes* 12 (5): 658. https://doi.org/10.3390/genes12050658.

Mao, Bai-ping, Renshan Ge, and C. Yan Cheng. 2020. "Role of Microtubule +TIPs and -TIPs in Spermatogenesis – Insights from Studies of Toxicant Models." *Reproductive Toxicology* 91 (January): 43–52. https://doi.org/10.1016/j.reprotox.2019.11.006.

Mao, Bai-ping, Linxi Li, Renshan Ge, Chao Li, Chris K C Wong, Bruno Silvestrini, Qingquan Lian, and C Yan Cheng. 2019. "CAMSAP2 Is a Microtubule Minus-End Targeting Protein That Regulates BTB Dynamics Through Cytoskeletal Organization." *Endocrinology* 160 (6): 1448–67. https://doi.org/10.1210/en.2018-01097.

Martinez, Guillaume, Zine-Eddine Kherraf, Raoudha Zouari, Selima Fourati Ben Mustapha, Antoine Saut, Karin Pernet-Gallay, Anne Bertrand, et al. 2018. "Whole-Exome Sequencing Identifies Mutations in FSIP2 as a Recurrent Cause of Multiple Morphological Abnormalities of the Sperm Flagella." *Human Reproduction* 33 (10): 1973–84. https://doi.org/10.1093/humrep/dey264.

Mazaheri Moghaddam, Marziyeh, Madiheh Mazaheri Moghaddam, Hamid Hamzeiy, Amir Baghbanzadeh, Fariba Pashazadeh, and Ebrahim Sakhinia. 2021. "Genetic Basis of Acephalic Spermatozoa Syndrome, and Intracytoplasmic Sperm Injection Outcomes in Infertile Men: A Systematic Scoping Review." *Journal of Assisted Reproduction and Genetics* 38 (3): 573–86. https://doi.org/10.1007/s10815-020-02008-w.

Mazo, Gregory, Nadine Soplop, Won-Jing Wang, Kunihiro Uryu, and Meng-Fu Bryan Tsou. 2016. "Spatial Control of Primary Ciliogenesis by Subdistal Appendages Alters Sensation-Associated Properties of Cilia." *Developmental Cell* 39 (4): 424–37. https://doi.org/10.1016/j.devcel.2016.10.006.

McGarry, Thomas J, and Marc W Kirschner. 1998. "Geminin, an Inhibitor of DNA Replication, Is Degraded during Mitosis." *Cell* 93 (6): 1043–53. https://doi.org/10.1016/S0092-8674(00)81209-X.

McKenzie, Casey W., Branch Craige, Tiffany V. Kroeger, Rozzy Finn, Todd A. Wyatt, Joseph H. Sisson, Jacqueline A. Pavlik, et al. 2015. "CFAP54 Is Required for Proper Ciliary Motility and Assembly of the Central Pair Apparatus in Mice." Edited by Stephen Doxsey. *Molecular Biology of the Cell* 26 (18): 3140–49. https://doi.org/10.1091/mbc.e15-02-0121.

McPherson, Nicole, Michelle Lane, Lauren Sandeman, Julie Owens, and Tod Fullston. 2017. "An Exercise-Only Intervention in Obese Fathers Restores Glucose and Insulin Regulation in Conjunction with the Rescue of Pancreatic Islet Cell Morphology and MicroRNA Expression in Male Offspring." *Nutrients* 9 (2): 122. https://doi.org/10.3390/nu9020122.

Mechaussier, Sabrina, Daniel O Dodd, Patricia L Yeyati, Fraser McPhie, Thomas Attard, Amelia Shoemark, Deepesh K Gupta, et al. 2022. "*TUBB4B* Variants Specifically Impact Ciliary Function, Causing a Ciliopathic Spectrum." Preprint. Genetic and Genomic Medicine. https://doi.org/10.1101/2022.10.19.22280748.

Meienberg, Janine, Rémy Bruggmann, Konrad Oexle, and Gabor Matyas. 2016. "Clinical Sequencing: Is WGS the Better WES?" *Human Genetics* 135 (3): 359–62. https://doi.org/10.1007/s00439-015-1631-9.

Meistrich, Marvin L., and Rex A. Hess. 2013. "Assessment of Spermatogenesis Through Staging of Seminiferous Tubules." In *Spermatogenesis*, edited by Douglas T. Carrell and Kenneth I. Aston, 927:299–307. Methods in Molecular Biology. Totowa, NJ: Humana Press. https://doi.org/10.1007/978-1-62703-038-0_27.

Mendoza-Lujambio, I. 2002. “The Hook1 Gene Is Non-Functional in the Abnormal Spermatozoon Head Shape (Azh) Mutant Mouse.” *Human Molecular Genetics* 11 (14): 1647–58. https://doi.org/10.1093/hmg/11.14.1647.

Mennella, Vito, David A. Agard, Bo Huang, and Laurence Pelletier. 2014. “Amorphous No More: Subdiffraction View of the Pericentriolar Material Architecture.” *Trends in Cell Biology* 24 (3): 188–97. https://doi.org/10.1016/j.tcb.2013.10.001.

Messaoud, Olfa, Atanu Kumar Dutta, Mario Reynaldo Cornejo-Olivas, and Zahurul A. Bhuiyan. 2021. “Editorial: Monogenic vs. Oligogenic Reclassification.” *Frontiers in Genetics* 12 (December): 821591. https://doi.org/10.3389/fgene.2021.821591.

Mierzwa, Beata, and Daniel W. Gerlich. 2014. “Cytokinetic Abscission: Molecular Mechanisms and Temporal Control.” *Developmental Cell* 31 (5): 525–38. https://doi.org/10.1016/j.devcel.2014.11.006.

Miki, Kiyoshi, William D. Willis, Paula R. Brown, Eugenia H. Goulding, Kerry D. Fulcher, and Edward M. Eddy. 2002. “Targeted Disruption of the Akap4 Gene Causes Defects in Sperm Flagellum and Motility.” *Developmental Biology* 248 (2): 331–42. https://doi.org/10.1006/dbio.2002.0728.

Milewski, Robert, and Anna Ajduk. 2017. “Time-Lapse Imaging of Cleavage Divisions in Embryo Quality Assessment.” *Reproduction* 154 (2): R37–53. https://doi.org/10.1530/REP-17-0004.

Minhas, Suks, Carlo Bettocchi, Luca Boeri, Paolo Capogrosso, Joana Carvalho, Nusret Can Cilesiz, Andrea Cocci, et al. 2021. “European Association of Urology Guidelines on Male Sexual and Reproductive Health: 2021 Update on Male Infertility.” *European Urology* 80 (5): 603–20. https://doi.org/10.1016/j.eururo.2021.08.014.

Mitchell, M.J., C. Metzler-Guillemain, A. Toure, C. Coutton, C. Arnoult, and P.F. Ray. 2017. “Single Gene Defects Leading to Sperm Quantitative Anomalies: Single Gene Defects Leading to Sperm Quantitative Anomalies.” *Clinical Genetics* 91 (2): 208–16. https://doi.org/10.1111/cge.12900.

Mitchison, Tim, and Marc Kirschner. 1984. “Dynamic Instability of Microtubule Growth.” *Nature* 312 (5991): 237–42. https://doi.org/10.1038/312237a0.

“MitoCheck.” n.d. Accessed February 10, 2023. https://www.mitocheck.org/gene.shtml?gene=ENSG00000135205.

Mochida, Kazuhiko, Laura L. Tres, and Abraham L. Kierszenbaum. 1999. “Structural and Biochemical Features of Fractionated Spermatid Manchettes and Sperm Axonemes of TheAzh/Azh Mutant Mouse.” *Molecular Reproduction and Development* 52 (4): 434–44. https://doi.org/10.1002/(SICI)1098-2795(199904)52:4<434::AID-MRD13>3.0.CO;2-D.

Moreno, Ricardo D., Jaime Palomino, and Gerald Schatten. 2006. “Assembly of Spermatid Acrosome Depends on Microtubule Organization during Mammalian Spermiogenesis.” *Developmental Biology* 293 (1): 218–27. https://doi.org/10.1016/j.ydbio.2006.02.001.

Moreno, Ricardo D., and Gerald Schatten. 2000. “Microtubule Configurations and Post-Translational ?-Tubulin Modifications during Mammalian Spermatogenesis.” *Cell Motility and the Cytoskeleton* 46 (4): 235–46. https://doi.org/10.1002/1097-0169(200008)46:4<235::AID-CM1>3.0.CO;2-G.

Moretti, Charlotte, Daniel Vaiman, Frederic Tores, and Julie Cocquet. 2016. “Expression and Epigenomic Landscape of the Sex Chromosomes in Mouse Post-Meiotic Male Germ Cells.” *Epigenetics & Chromatin* 9 (1): 47. https://doi.org/10.1186/s13072-016-0099-8.

Morgan, Joshua T., Emily R. Pfeiffer, Twanda L. Thirkill, Priyadarsini Kumar, Gordon Peng, Heidi N. Fridolfsson, Gordon C. Douglas, Daniel A. Starr, and Abdul I. Barakat. 2011. "Nesprin-3 Regulates Endothelial Cell Morphology, Perinuclear Cytoskeletal Architecture, and Flow-Induced Polarization." Edited by Robert David Goldman. *Molecular Biology of the Cell* 22 (22): 4324–34. https://doi.org/10.1091/mbc.e11-04-0287.

Morimoto, Kozo, Minako Hijikata, Maimoona A. Zariwala, Keith Nykamp, Atsushi Inaba, Tz-Chun Guo, Hiroyuki Yamada, et al. 2019. "Recurring Large Deletion in *DRC1* (*CCDC164*) Identified as Causing Primary Ciliary Dyskinesia in Two Asian Patients." *Molecular Genetics & Genomic Medicine* 7 (8). https://doi.org/10.1002/mgg3.838.

Moritz, Lindsay, and Saher Sue Hammoud. 2022. "The Art of Packaging the Sperm Genome: Molecular and Structural Basis of the Histone-To-Protamine Exchange." *Frontiers in Endocrinology* 13 (June): 895502. https://doi.org/10.3389/fendo.2022.895502.

Morohoshi, Akane, Haruhiko Miyata, Keisuke Shimada, Kaori Nozawa, Takafumi Matsumura, Ryuji Yanase, Kogiku Shiba, Kazuo Inaba, and Masahito Ikawa. 2020. "Nexin-Dynein Regulatory Complex Component DRC7 but Not FBXL13 Is Required for Sperm Flagellum Formation and Male Fertility in Mice." Edited by Susan K. Dutcher. *PLOS Genetics* 16 (1): e1008585. https://doi.org/10.1371/journal.pgen.1008585.

Morthorst, Stine Kjær, Søren Tvorup Christensen, and Lotte Bang Pedersen. 2018. "Regulation of Ciliary Membrane Protein Trafficking and Signalling by Kinesin Motor Proteins." *The FEBS Journal* 285 (24): 4535–64. https://doi.org/10.1111/febs.14583.

Movassagh, Tandis, Khanh Huy Bui, Hitoshi Sakakibara, Kazuhiro Oiwa, and Takashi Ishikawa. 2010. "Nucleotide-Induced Global Conformational Changes of Flagellar Dynein Arms Revealed by in Situ Analysis." *Nature Structural & Molecular Biology* 17 (6): 761–67. https://doi.org/10.1038/nsmb.1832.

Mruk, Dolores D., and C. Yan Cheng. 2015. "The Mammalian Blood-Testis Barrier: Its Biology and Regulation." *Endocrine Reviews* 36 (5): 564–91. https://doi.org/10.1210/er.2014-1101.

Nachtegael, Charlotte, Barbara Gravel, Arnau Dillen, Guillaume Smits, Ann Nowé, Sofia Papadimitriou, and Tom Lenaerts. 2022. "Scaling up Oligogenic Diseases Research with OLIDA: The Oligogenic Diseases Database." *Database* 2022 (April): baac023. https://doi.org/10.1093/database/baac023.

Nachury, Maxence V. 2018. "The Molecular Machines That Traffic Signaling Receptors into and out of Cilia." *Current Opinion in Cell Biology* 51 (April): 124–31. https://doi.org/10.1016/j.ceb.2018.03.004.

Nachury, Maxence V., Alexander V. Loktev, Qihong Zhang, Christopher J. Westlake, Johan Peränen, Andreas Merdes, Diane C. Slusarski, et al. 2007. "A Core Complex of BBS Proteins Cooperates with the GTPase Rab8 to Promote Ciliary Membrane Biogenesis." *Cell* 129 (6): 1201–13. https://doi.org/10.1016/j.cell.2007.03.053.

Nakamura, Yoshihiro, Hiromitsu Tanaka, Minoru Koga, Yasushi Miyagawa, Naoko Iguchi, Carlos Egydio de Carvalho, Kentaro Yomogida, et al. 2002. "Molecular Cloning and Characterization of Oppo 1: A Haploid Germ Cell-Specific Complementary DNA Encoding Sperm Tail Protein." *Biology of Reproduction* 67 (1): 1–7. https://doi.org/10.1095/biolreprod67.1.1.

Nakata, Hiroki, Tomohiko Wakayama, Yoshimi Takai, and Shoichi Iseki. 2015. "Quantitative Analysis of the Cellular Composition in Seminiferous Tubules in Normal and Genetically

Modified Infertile Mice." *Journal of Histochemistry & Cytochemistry* 63 (2): 99–113. https://doi.org/10.1369/0022155414562045.

Nakayama, Kazuhisa, and Yohei Katoh. 2020. "Architecture of the IFT Ciliary Trafficking Machinery and Interplay between Its Components." *Critical Reviews in Biochemistry and Molecular Biology* 55 (2): 179–96. https://doi.org/10.1080/10409238.2020.1768206.

"National Center for Biotechnology Information." n.d. Accessed February 21, 2023. https://www.ncbi.nlm.nih.gov/.

Navolanic, Patrick M., and Ann O. Sperry. 2000. "Identification of Isoforms of a Mitotic Motor in Mammalian Spermatogenesis1." *Biology of Reproduction* 62 (5): 1360–69. https://doi.org/10.1095/biolreprod62.5.1360.

Netzel-Arnett, Sarah, Thomas H. Bugge, Rex A. Hess, Kay Carnes, Brett W. Stringer, Anthony L. Scarman, John D. Hooper, Ian D. Tonks, Graham F. Kay, and Toni M. Antalis. 2009. "The Glycosylphosphatidylinositol-Anchored Serine Protease PRSS21 (Testisin) Imparts Murine Epididymal Sperm Cell Maturation and Fertilizing Ability1." *Biology of Reproduction* 81 (5): 921–32. https://doi.org/10.1095/biolreprod.109.076273.

Ng, Sheau-Fang, Ruby C. Y. Lin, D. Ross Laybutt, Romain Barres, Julie A. Owens, and Margaret J. Morris. 2010. "Chronic High-Fat Diet in Fathers Programs β-Cell Dysfunction in Female Rat Offspring." *Nature* 467 (7318): 963–66. https://doi.org/10.1038/nature09491.

Nicastro, Daniela, Xiaofeng Fu, Thomas Heuser, Alan Tso, Mary E. Porter, and Richard W. Linck. 2011. "Cryo-Electron Tomography Reveals Conserved Features of Doublet Microtubules in Flagella." *Proceedings of the National Academy of Sciences* 108 (42). https://doi.org/10.1073/pnas.1106178108.

Nicastro, Daniela, J. Richard McIntosh, and Wolfgang Baumeister. 2005. "3D Structure of Eukaryotic Flagella in a Quiescent State Revealed by Cryo-Electron Tomography." *Proceedings of the National Academy of Sciences* 102 (44): 15889–94. https://doi.org/10.1073/pnas.0508274102.

Nicastro, Daniela, Cindi Schwartz, Jason Pierson, Richard Gaudette, Mary E. Porter, and J. Richard McIntosh. 2006. "The Molecular Architecture of Axonemes Revealed by Cryoelectron Tomography." *Science* 313 (5789): 944–48. https://doi.org/10.1126/science.1128618.

Niedenberger, Bryan A., Kenneth Cook, Valentina Baena, Nicholas D. Serra, Ellen K. Velte, Julio E. Agno, Karen A. Litwa, et al. 2018. "Dynamic Cytoplasmic Projections Connect Mammalian Spermatogonia *in Vivo*." *Development*, January, dev.161323. https://doi.org/10.1242/dev.161323.

Nigg, Erich A., and Andrew J. Holland. 2018. "Once and Only Once: Mechanisms of Centriole Duplication and Their Deregulation in Disease." *Nature Reviews Molecular Cell Biology* 19 (5): 297–312. https://doi.org/10.1038/nrm.2017.127.

Nistal, Manuel, Ricardo Paniagua, and Alfonso Herruzo. 1978. "Multi-Tailed Spermatozoa in a Case with Asthenospermia and Teratospermia." *Virchows Archiv B Cell Pathology* 26 (1): 111–18. https://doi.org/10.1007/BF02889540.

Nozawa, Yoko Inès, Erica Yao, Rhodora Gacayan, Shan-Mei Xu, and Pao-Tien Chuang. 2014. "Mammalian Fused Is Essential for Sperm Head Shaping and Periaxonemal Structure Formation during Spermatogenesis." *Developmental Biology* 388 (2): 170–80. https://doi.org/10.1016/j.ydbio.2014.02.002.

Nsamba, Emmanuel T., and Mohan L. Gupta. 2022. “Tubulin Isotypes – Functional Insights from Model Organisms.” *Journal of Cell Science* 135 (9): jcs259539. https://doi.org/10.1242/jcs.259539.

Oakberg, Eugene F. 1956a. “A Description of Spermiogenesis in the Mouse and Its Use in Analysis of the Cycle of the Seminiferous Epithelium and Germ Cell Renewal.” *American Journal of Anatomy* 99 (3): 391–413. https://doi.org/10.1002/aja.1000990303.

———. 1956b. “Duration of Spermatogenesis in the Mouse and Timing of Stages of the Cycle of the Seminiferous Epithelium.” *American Journal of Anatomy* 99 (3): 507–16. https://doi.org/10.1002/aja.1000990307.

Oakley, C. Elizabeth, and Berl R. Oakley. 1989. “Identification of γ-Tubulin, a New Member of the Tubulin Superfamily Encoded by MipA Gene of Aspergillus Nidulans.” *Nature* 338 (6217): 662–64. https://doi.org/10.1038/338662a0.

O’Bryan, Moira K., Kimberly Sebire, Andreas Meinhardt, Kimberly Edgar, Hong-Hooi Keah, Milton T.W. Hearn, and David M. de Kretser. 2001. “Tpx-1 Is a Component of the Outer Dense Fibers and Acrosome of Rat Spermatozoa.” *Molecular Reproduction and Development* 58 (1): 116–25. https://doi.org/10.1002/1098-2795(200101)58:1<116::AID-MRD14>3.0.CO;2-8.

Oda, Toshiyuki, Haruaki Yanagisawa, Ritsu Kamiya, and Masahide Kikkawa. 2014. “A Molecular Ruler Determines the Repeat Length in Eukaryotic Cilia and Flagella.” *Science* 346 (6211): 857–60. https://doi.org/10.1126/science.1260214.

Odabasi, Ezgi, Umut Batman, and Elif Nur Firat-Karalar. 2020. “Unraveling the Mysteries of Centriolar Satellites: Time to Rewrite the Textbooks about the Centrosome/Cilium Complex.” Edited by Matthew Welch. *Molecular Biology of the Cell* 31 (9): 866–72. https://doi.org/10.1091/mbc.E19-07-0402.

Odate, Toru, Sen Takeda, Keishi Narita, and Toru Kawahara. 2016. “9 + 0 and 9 + 2 Cilia Are Randomly Dispersed in the Mouse Node.” *Microscopy* 65 (2): 119–26. https://doi.org/10.1093/jmicro/dfv352.

O’Donnell, Liza, Danielle Rhodes, Stephanie J. Smith, D. Jo Merriner, Brett J. Clark, Claire Borg, Belinda Whittle, et al. 2012. “An Essential Role for Katanin P80 and Microtubule Severing in Male Gamete Production.” Edited by Wayne N. Frankel. *PLoS Genetics* 8 (5): e1002698. https://doi.org/10.1371/journal.pgen.1002698.

Ohuchi, Jun, Toshio Arai, Yasuhiro Kon, Atsushi Asano, Hideto Yamauchi, and Tomomasa Watanabe. 2001. “Characterization of a Novel Gene, Sperm-Tail-Associated Protein (Stap), in Mouse Post-Meiotic Testicular Germ Cells.” *Molecular Reproduction and Development* 59 (4): 350–58. https://doi.org/10.1002/mrd.1041.

Okitsu, Yu, Mamoru Nagano, Takahiro Yamagata, Chizuru Ito, Kiyotaka Toshimori, Hideo Dohra, Wataru Fujii, and Keiichiro Yogo. 2020. “Dlec1 Is Required for Spermatogenesis and Male Fertility in Mice.” *Scientific Reports* 10 (1): 18883. https://doi.org/10.1038/s41598-020-75957-y.

Okutman, Ozlem, Maroua Ben Rhouma, Moncef Benkhalifa, Jean Muller, and Stéphane Viville. 2018. “Genetic Evaluation of Patients with Non-Syndromic Male Infertility.” *Journal of Assisted Reproduction and Genetics* 35 (11): 1939–51. https://doi.org/10.1007/s10815-018-1301-7.

Olbrich, Heike, Carolin Cremers, Niki T. Loges, Claudius Werner, Kim G. Nielsen, June K. Marthin, Maria Philipsen, et al. 2015. “Loss-of-Function GAS8 Mutations Cause Primary

Ciliary Dyskinesia and Disrupt the Nexin-Dynein Regulatory Complex." *The American Journal of Human Genetics* 97 (4): 546–54. https://doi.org/10.1016/j.ajhg.2015.08.012.

Olson, Gary E., and David W. Sammons. 1980. "Structural Chemistry of Outer Dense Fibers of Rat Sperm1." *Biology of Reproduction* 22 (2): 319–32. https://doi.org/10.1095/biolreprod22.2.319.

Ombelet, W., I. Cooke, S. Dyer, G. Serour, and P. Devroey. 2008. "Infertility and the Provision of Infertility Medical Services in Developing Countries." *Human Reproduction Update* 14 (6): 605–21. https://doi.org/10.1093/humupd/dmn042.

Otani, Hiroki, Osamu Tanaka, Kei-Ichiro Kasai, and Takafumi Yoshioka. 1988. "Development of Mitochondrial Helical Sheath in the Middle Piece of the Mouse Spermatid Tail: Regular Dispositions and Synchronized Changes." *The Anatomical Record* 222 (1): 26–33. https://doi.org/10.1002/ar.1092220106.

Ott, Carolyn M. 2016. "Midbody Remnant Licenses Primary Cilia Formation in Epithelial Cells." *Journal of Cell Biology* 214 (3): 237–39. https://doi.org/10.1083/jcb.201607046.

Oura, Seiya, Haruhiko Miyata, Taichi Noda, Keisuke Shimada, Takafumi Matsumura, Akane Morohoshi, Ayako Isotani, and Masahito Ikawa. 2019. "Chimeric Analysis with Newly Established EGFP/DsRed2-Tagged ES Cells Identify HYDIN as Essential for Spermiogenesis in Mice." *Experimental Animals* 68 (1): 25–34. https://doi.org/10.1538/expanim.18-0071.

Owa, Mikito, Takayuki Uchihashi, Haru-aki Yanagisawa, Takashi Yamano, Hiro Iguchi, Hideya Fukuzawa, Ken-ichi Wakabayashi, Toshio Ando, and Masahide Kikkawa. 2019. "Inner Lumen Proteins Stabilize Doublet Microtubules in Cilia and Flagella." *Nature Communications* 10 (1): 1143. https://doi.org/10.1038/s41467-019-09051-x.

Paintrand, Michel, Mohammed Moudjou, Hervé Delacroix, and Michel Bornens. 1992. "Centrosome Organization and Centriole Architecture: Their Sensitivity to Divalent Cations." *Journal of Structural Biology* 108 (2): 107–28. https://doi.org/10.1016/1047-8477(92)90011-X.

Palermo, G. 1992. "Pregnancies after Intracytoplasmic Injection of Single Spermatozoon into an Oocyte." *The Lancet* 340 (8810): 17–18. https://doi.org/10.1016/0140-6736(92)92425-F.

Park, Kwangjin, and Michel R Leroux. 2022. "Composition, Organization and Mechanisms of the Transition Zone, a Gate for the Cilium." *EMBO Reports* 23 (12). https://doi.org/10.15252/embr.202255420.

Pasch, Elisabeth, Jana Link, Carolin Beck, Stefanie Scheuerle, and Manfred Alsheimer. 2015. "The LINC Complex Component Sun4 Plays a Crucial Role in Sperm Head Formation and Fertility." *Biology Open* 4 (12): 1792–1802. https://doi.org/10.1242/bio.015768.

Pasek, Raymond C., Erik Malarkey, Nicolas F. Berbari, Neeraj Sharma, Robert A. Kesterson, Laura L. Tres, Abraham L. Kierszenbaum, and Bradley K. Yoder. 2016. "Coiled-Coil Domain Containing 42 (Ccdc 42) Is Necessary for Proper Sperm Development and Male Fertility in the Mouse." *Developmental Biology* 412 (2): 208–18. https://doi.org/10.1016/j.ydbio.2016.01.042.

Patmanidi, Alexandra L., Spyridon Champeris Tsaniras, Dimitris Karamitros, Christina Kyrousi, Zoi Lygerou, and Stavros Taraviras. 2017. "Concise Review: Geminin—A Tale of Two Tails: DNA Replication and Transcriptional/Epigenetic Regulation in Stem Cells." *Stem Cells* 35 (2): 299–310. https://doi.org/10.1002/stem.2529.

Pazour, Gregory J., Curtis G. Wilkerson, and George B. Witman. 1998. "A Dynein Light Chain Is Essential for the Retrograde Particle Movement of Intraflagellar Transport (IFT)." *Journal of Cell Biology* 141 (4): 979–92. https://doi.org/10.1083/jcb.141.4.979.

Pereira, Cátia D., Joana B. Serrano, Filipa Martins, Odete A. B. da Cruz e Silva, and Sandra Rebelo. 2019. "Nuclear Envelope Dynamics during Mammalian Spermatogenesis: New Insights on Male Fertility: Nuclear Envelope Dynamics during Spermatogenesis." *Biological Reviews* 94 (4): 1195–1219. https://doi.org/10.1111/brv.12498.

Petersen, Christoph, Gerhard Aumüller, Masoud Bahrami, and Sigrid Hoyer-Fender. 2002. "Molecular Cloning of *Odf3* Encoding a Novel Coiled-Coil Protein of Sperm Tail Outer Dense Fibers*†: NOVEL COILED-COIL CYTOSKELETAL PROTEIN OF RAT ODFs." *Molecular Reproduction and Development* 61 (1): 102–12. https://doi.org/10.1002/mrd.1136.

Pfister, K. Kevin, Paresh R Shah, Holger Hummerich, Andreas Russ, James Cotton, Azlina Ahmad Annuar, Stephen M King, and Elizabeth M. C Fisher. 2006. "Genetic Analysis of the Cytoplasmic Dynein Subunit Families." *PLoS Genetics* 2 (1): e1. https://doi.org/10.1371/journal.pgen.0020001.

Pierre, Virginie, Guillaume Martinez, Charles Coutton, Julie Delaroche, Sandra Yassine, Caroline Novella, Karin Pernet-Gallay, Sylviane Hennebicq, Pierre F. Ray, and Christophe Arnoult. 2012. "Absence of Dpy19l2, a New Inner Nuclear Membrane Protein, Causes Globozoospermia in Mice by Preventing the Anchoring of the Acrosome to the Nucleus." *Development* 139 (16): 2955–65. https://doi.org/10.1242/dev.077982.

Pigino, Gaia, Khanh Huy Bui, Aditi Maheshwari, Pietro Lupetti, Dennis Diener, and Takashi Ishikawa. 2011. "Cryoelectron Tomography of Radial Spokes in Cilia and Flagella." *Journal of Cell Biology* 195 (4): 673–87. https://doi.org/10.1083/jcb.201106125.

Piperno, G, B Huang, and D J Luck. 1977. "Two-Dimensional Analysis of Flagellar Proteins from Wild-Type and Paralyzed Mutants of Chlamydomonas Reinhardtii." *Proceedings of the National Academy of Sciences* 74 (4): 1600–1604. https://doi.org/10.1073/pnas.74.4.1600.

Piperno, G, B Huang, Z Ramanis, and D J Luck. 1981. "Radial Spokes of Chlamydomonas Flagella: Polypeptide Composition and Phosphorylation of Stalk Components." *Journal of Cell Biology* 88 (1): 73–79. https://doi.org/10.1083/jcb.88.1.73.

Pleuger, Christiane, Mari S Lehti, Jessica EM Dunleavy, Daniela Fietz, and Moira K O'Bryan. 2020. "Haploid Male Germ Cells—the Grand Central Station of Protein Transport." *Human Reproduction Update* 26 (4): 474–500. https://doi.org/10.1093/humupd/dmaa004.

Pohl, Christian, and Stefan Jentsch. 2008. "Final Stages of Cytokinesis and Midbody Ring Formation Are Controlled by BRUCE." *Cell* 132 (5): 832–45. https://doi.org/10.1016/j.cell.2008.01.012.

Prevo, Bram, Jonathan M. Scholey, and Erwin J. G. Peterman. 2017. "Intraflagellar Transport: Mechanisms of Motor Action, Cooperation, and Cargo Delivery." *The FEBS Journal* 284 (18): 2905–31. https://doi.org/10.1111/febs.14068.

Priyanka, Patra Priyadarshini, and Suresh Yenugu. 2021. "Coiled-Coil Domain-Containing (CCDC) Proteins: Functional Roles in General and Male Reproductive Physiology." *Reproductive Sciences* 28 (10): 2725–34. https://doi.org/10.1007/s43032-021-00595-2.

Prosser, Suzanna L., and Laurence Pelletier. 2017. "Mitotic Spindle Assembly in Animal Cells: A Fine Balancing Act." *Nature Reviews Molecular Cell Biology* 18 (3): 187–201. https://doi.org/10.1038/nrm.2016.162.

———. 2020. “Centriolar Satellite Biogenesis and Function in Vertebrate Cells.” *Journal of Cell Science* 133 (1): jcs239566. https://doi.org/10.1242/jcs.239566.

Puga Molina, Lis C., Guillermina M. Luque, Paula A. Balestrini, Clara I. Marín-Briggiler, Ana Romarowski, and Mariano G. Buffone. 2018. “Molecular Basis of Human Sperm Capacitation.” *Frontiers in Cell and Developmental Biology* 6 (July): 72. https://doi.org/10.3389/fcell.2018.00072.

Pylyp, Larysa Y., Lyudmyla O. Spinenko, Natalia V. Verhoglyad, and Valery D. Zukin. 2013. “Chromosomal Abnormalities in Patients with Oligozoospermia and Non-Obstructive Azoospermia.” *Journal of Assisted Reproduction and Genetics* 30 (5): 729–32. https://doi.org/10.1007/s10815-013-9990-4.

Qin, Hongmin, Dennis R. Diener, Stefan Geimer, Douglas G. Cole, and Joel L. Rosenbaum. 2004. “Intraflagellar Transport (IFT) Cargo.” *Journal of Cell Biology* 164 (2): 255–66. https://doi.org/10.1083/jcb.200308132.

Quarantotti, Valentina, Jia-Xuan Chen, Julia Tischer, Carmen Gonzalez Tejedo, Evaggelia K Papachristou, Clive S D’Santos, John V Kilmartin, Martin L Miller, and Fanni Gergely. 2019. “Centriolar Satellites Are Acentriolar Assemblies of Centrosomal Proteins.” *The EMBO Journal* 38 (14). https://doi.org/10.15252/embj.2018101082.

Rahban, Rita, and Serge Nef. 2020. “CatSper: The Complex Main Gate of Calcium Entry in Mammalian Spermatozoa.” *Molecular and Cellular Endocrinology* 518 (December): 110951. https://doi.org/10.1016/j.mce.2020.110951.

Ramkumar, Amrita, Brigette Y. Jong, and Kassandra M. Ori-McKenney. 2018. “ReMAPping the Microtubule Landscape: How Phosphorylation Dictates the Activities of Microtubule-Associated Proteins: Phosphorylation of Microtubule-Associated Proteins.” *Developmental Dynamics* 247 (1): 138–55. https://doi.org/10.1002/dvdy.24599.

Rathke, Christina, Willy M. Baarends, Stephan Awe, and Renate Renkawitz-Pohl. 2014. “Chromatin Dynamics during Spermiogenesis.” *Biochimica et Biophysica Acta (BBA) - Gene Regulatory Mechanisms* 1839 (3): 155–68. https://doi.org/10.1016/j.bbagrm.2013.08.004.

Rattner, J.B., and B.R. Brinkley. 1972. “Ultrastructure of Mammalian Spermiogenesis.” *Journal of Ultrastructure Research* 41 (3–4): 209–18. https://doi.org/10.1016/S0022-5320(72)90065-2.

Redenbach, D. M., and K. Boekelheide. 1994. “Microtubules Are Oriented with Their Minus-Ends Directed Apically before Tight Junction Formation in Rat Sertoli Cells.” *European Journal of Cell Biology* 65 (2): 246–57.

Redenbach, D. M., and A. W. Vogl. 1991. “Microtubule Polarity in Sertoli Cells: A Model for Microtubule-Based Spermatid Transport.” *European Journal of Cell Biology* 54 (2): 277–90.

Ren, Dejian, Betsy Navarro, Gloria Perez, Alexander C. Jackson, Shyuefang Hsu, Qing Shi, Jonathan L. Tilly, and David E. Clapham. 2001. “A Sperm Ion Channel Required for Sperm Motility and Male Fertility.” *Nature* 413 (6856): 603–9. https://doi.org/10.1038/35098027.

Robay, Amal, Saleha Abbasi, Ammira Akil, Haitham El-Bardisi, Mohamed Arafa, Ronald G. Crystal, and Khalid A. Fakhro. 2018. “A Systematic Review on the Genetics of Male Infertility in the Era of Next-Generation Sequencing.” *Arab Journal of Urology* 16 (1): 53–64. https://doi.org/10.1016/j.aju.2017.12.003.

Roberts, Anthony J. 2018. “Emerging Mechanisms of Dynein Transport in the Cytoplasm versus the Cilium.” *Biochemical Society Transactions* 46 (4): 967–82. https://doi.org/10.1042/BST20170568.

Roll-Mecak, Antonina. 2015. “Intrinsically Disordered Tubulin Tails: Complex Tuners of Microtubule Functions?” *Seminars in Cell & Developmental Biology* 37 (January): 11–19. https://doi.org/10.1016/j.semcdb.2014.09.026.

———. 2019. “How Cells Exploit Tubulin Diversity to Build Functional Cellular Microtubule Mosaics.” *Current Opinion in Cell Biology* 56 (February): 102–8. https://doi.org/10.1016/j.ceb.2018.10.009.

Roostalu, Johanna, and Thomas Surrey. 2017. “Microtubule Nucleation: Beyond the Template.” *Nature Reviews Molecular Cell Biology* 18 (11): 702–10. https://doi.org/10.1038/nrm.2017.75.

Russell, L.D., R.A. Ettlin, A.P.S. Hikim, and E.D. Clegg. 1990. *Histological and Histopathological Evaluation of the Testis*. 1st ed. Cache River Press.

Russell, Lonnie D., Jill A. Russell, Grant R. MacGregor, and Marvin L. Meistrich. 1991. “Linkage of Manchette Microtubules to the Nuclear Envelope and Observations of the Role of the Manchette in Nuclear Shaping during Spermiogenesis in Rodents.” *American Journal of Anatomy* 192 (2): 97–120. https://doi.org/10.1002/aja.1001920202.

Saade, Murielle, Magali Irla, Jérôme Govin, Genevieve Victorero, Michel Samson, and Catherine Nguyen. 2007. “Dynamic Distribution of Spatial during Mouse Spermatogenesis and Its Interaction with the Kinesin KIF17b.” *Experimental Cell Research* 313 (3): 614–26. https://doi.org/10.1016/j.yexcr.2006.11.011.

Sadeghi, Mohammad Reza. 2015. “Unexplained Infertility, the Controversial Matter in Management of Infertile Couples.” *Journal of Reproduction & Infertility* 16 (1): 1–2.

Sahabandu, N., D. Kong, V. Magidson, R. Nanjundappa, C. Sullenberger, M.R. Mahjoub, and J. Loncarek. 2019. “Expansion Microscopy for the Analysis of Centrioles and Cilia.” *Journal of Microscopy* 276 (3): 145–59. https://doi.org/10.1111/jmi.12841.

Samans, Birgit, Yang Yang, Stefan Krebs, Gaurav Vilas Sarode, Helmut Blum, Myriam Reichenbach, Eckhard Wolf, Klaus Steger, Temuujin Dansranjavin, and Undraga Schagdarsurengin. 2014. “Uniformity of Nucleosome Preservation Pattern in Mammalian Sperm and Its Connection to Repetitive DNA Elements.” *Developmental Cell* 30 (1): 23–35. https://doi.org/10.1016/j.devcel.2014.05.023.

Samsel, Zuzanna, Justyna Sekretarska, Anna Osinka, Dorota Wloga, and Ewa Joachimiak. 2021. “Central Apparatus, the Molecular Kickstarter of Ciliary and Flagellar Nanomachines.” *International Journal of Molecular Sciences* 22 (6): 3013. https://doi.org/10.3390/ijms22063013.

San Agustin, Jovenal T., Gregory J. Pazour, and George B. Witman. 2015. “Intraflagellar Transport Is Essential for Mammalian Spermiogenesis but Is Absent in Mature Sperm.” Edited by Wallace Marshall. *Molecular Biology of the Cell* 26 (24): 4358–72. https://doi.org/10.1091/mbc.E15-08-0578.

Sánchez, Irma, and Brian David Dynlacht. 2016. “Cilium Assembly and Disassembly.” *Nature Cell Biology* 18 (7): 711–17. https://doi.org/10.1038/ncb3370.

Sapiro, Rossana, Igor Kostetskii, Patricia Olds-Clarke, George L. Gerton, Glenn L. Radice, and Jerome F. Strauss. 2002. “Male Infertility, Impaired Sperm Motility, and Hydrocephalus in Mice Deficient in Sperm-Associated Antigen 6.” *Molecular and Cellular Biology* 22 (17): 6298–6305. https://doi.org/10.1128/MCB.22.17.6298-6305.2002.

Sato, Takashi, Tomohiko Iwano, Masataka Kunii, Shinji Matsuda, Rumiko Mizuguchi, Yongwook Jung, Haruo Hagiwara, et al. 2013. "Rab8a and Rab8b Are Essential for Multiple Apical Transport Pathways but Insufficient for Ciliogenesis." *Journal of Cell Science*, January, jcs.136903. https://doi.org/10.1242/jcs.136903.

Schalles, Uwe, Xueping Shao, Frans A. van der Hoorn, and Richard Oko. 1998. "Developmental Expression of the 84-KDa ODF Sperm Protein: Localization to Both the Cortex and Medulla of Outer Dense Fibers and to the Connecting Piece." *Developmental Biology* 199 (2): 250–60. https://doi.org/10.1006/dbio.1998.8931.

Schiavo, Giampietro, Linda Greensmith, Majid Hafezparast, and Elizabeth M.C. Fisher. 2013. "Cytoplasmic Dynein Heavy Chain: The Servant of Many Masters." *Trends in Neurosciences* 36 (11): 641–51. https://doi.org/10.1016/j.tins.2013.08.001.

Schultz, Rüdiger, Varpu Elenius, Heikki Lukkarinen, and Tanja Saarela. 2020. "Two Novel Mutations in the DNAH11 Gene in Primary Ciliary Dyskinesia (CILD7) with Considerable Variety in the Clinical and Beating Cilia Phenotype." *BMC Medical Genetics* 21 (1): 237. https://doi.org/10.1186/s12881-020-01171-2.

Schuster, A., C. Tang, Y. Xie, N. Ortogero, S. Yuan, and W. Yan. 2016. "SpermBase: A Database for Sperm-Borne RNA Contents." *Biology of Reproduction* 95 (5): 99–99. https://doi.org/10.1095/biolreprod.116.142190.

Schweizer, Stephanie, and Sigrid Hoyer-Fender. 2009. "Mouse Odf2 Localizes to Centrosomes and Basal Bodies in Adult Tissues and to the Photoreceptor Primary Cilium." *Cell and Tissue Research* 338 (2): 295–301. https://doi.org/10.1007/s00441-009-0861-3.

Schwer, Heinz D, Patrick Lecine, Sanjay Tiwari, Joseph E Italiano, John H Hartwig, and Ramesh A Shivdasani. 2001. "A Lineage-Restricted and Divergent β-Tubulin Isoform Is Essential for the Biogenesis, Structure and Function of Blood Platelets." *Current Biology* 11 (8): 579–86. https://doi.org/10.1016/S0960-9822(01)00153-1.

Segal, R A, B Huang, Z Ramanis, and D J Luck. 1984. "Mutant Strains of Chlamydomonas Reinhardtii That Move Backwards Only." *Journal of Cell Biology* 98 (6): 2026–34. https://doi.org/10.1083/jcb.98.6.2026.

Sha, Yankun, Yanwei Sha, Wensheng Liu, Xingshen Zhu, Mingxiang Weng, Xinzong Zhang, Yifeng Wang, and Huiliang Zhou. 2021. "Biallelic Mutations of *CFAP58* Are Associated with Multiple Morphological Abnormalities of the Sperm Flagella." *Clinical Genetics* 99 (3): 443–48. https://doi.org/10.1111/cge.13898.

Sha, Yan-Wei, Xiong Wang, Zhi-Ying Su, Li-Bin Mei, Zhi-Yong Ji, Hongchu Bao, and Ping Li. 2019. "Patients with Multiple Morphological Abnormalities of the Sperm Flagella Harbouring *CFAP44* or *CFAP43* Mutations Have a Good Pregnancy Outcome Following Intracytoplasmic Sperm Injection." *Andrologia* 51 (1): e13151. https://doi.org/10.1111/and.13151.

Sha, Yan-Wei, Xiong Wang, Xiaohui Xu, Lu Ding, Wen-Sheng Liu, Ping Li, Zhi-Ying Su, et al. 2019. "Biallelic Mutations in *PMFBP1* Cause Acephalic Spermatozoa." *Clinical Genetics* 95 (2): 277–86. https://doi.org/10.1111/cge.13461.

Sha, Yanwei, Xiaoli Wei, Lu Ding, Zhiyong Ji, Libin Mei, Xianjing Huang, Zhiying Su, Wenrong Wang, Xuequan Zhang, and Shaobin Lin. 2020. "Biallelic Mutations of CFAP74 May Cause Human Primary Ciliary Dyskinesia and MMAF Phenotype." *Journal of Human Genetics* 65 (11): 961–69. https://doi.org/10.1038/s10038-020-0790-2.

Sha, Yanwei, Xiaoli Wei, Lu Ding, Libin Mei, Xianjing Huang, Shaobin Lin, Zhiying Su, Lingyuan Kong, Yi Zhang, and Zhiyong Ji. 2020. "*DNAH17* Is Associated with

Asthenozoospermia and Multiple Morphological Abnormalities of Sperm Flagella." *Annals of Human Genetics* 84 (3): 271–79. https://doi.org/10.1111/ahg.12369.

Sha, Yan-Wei, Xiaohui Xu, Li-Bin Mei, Ping Li, Zhi-Ying Su, Xiao-Qin He, and Lin Li. 2017. "A Homozygous CEP135 Mutation Is Associated with Multiple Morphological Abnormalities of the Sperm Flagella (MMAF)." *Gene* 633 (October): 48–53. https://doi.org/10.1016/j.gene.2017.08.033.

Sha, Y.-W., Y.-K. Sha, Z.-Y. Ji, L.-B. Mei, L. Ding, Q. Zhang, P.-P. Qiu, et al. 2018. "*TSGA10* Is a Novel Candidate Gene Associated with Acephalic Spermatozoa." *Clinical Genetics* 93 (4): 776–83. https://doi.org/10.1111/cge.13140.

Shang, Yongliang, Jie Yan, Wenhao Tang, Chao Liu, Sai Xiao, Yueshuai Guo, Li Yuan, et al. 2018. "Mechanistic Insights into Acephalic Spermatozoa Syndrome–Associated Mutations in the Human SUN5 Gene." *Journal of Biological Chemistry* 293 (7): 2395–2407. https://doi.org/10.1074/jbc.RA117.000861.

Shang, Yongliang, Fuxi Zhu, Lina Wang, Ying-Chun Ouyang, Ming-Zhe Dong, Chao Liu, Haichao Zhao, et al. 2017. "Essential Role for SUN5 in Anchoring Sperm Head to the Tail." *ELife* 6 (September): e28199. https://doi.org/10.7554/eLife.28199.

Sharma, Aanchal, and Deepti Shrivastava. 2022. "Psychological Problems Related to Infertility." *Cureus*, October. https://doi.org/10.7759/cureus.30320.

Sharma, Upasna, Colin C. Conine, Jeremy M. Shea, Ana Boskovic, Alan G. Derr, Xin Y. Bing, Clemence Belleannee, et al. 2016. "Biogenesis and Function of TRNA Fragments during Sperm Maturation and Fertilization in Mammals." *Science* 351 (6271): 391–96. https://doi.org/10.1126/science.aad6780.

Sharma, Upasna, Fengyun Sun, Colin C. Conine, Brian Reichholf, Shweta Kukreja, Veronika A. Herzog, Stefan L. Ameres, and Oliver J. Rando. 2018. "Small RNAs Are Trafficked from the Epididymis to Developing Mammalian Sperm." *Developmental Cell* 46 (4): 481-494.e6. https://doi.org/10.1016/j.devcel.2018.06.023.

Shen, Yi-Ru, Han-Yu Wang, Yung-Che Kuo, Shih-Chuan Shih, Chun-Hua Hsu, Yet-Ran Chen, Shang-Rung Wu, Chia-Yih Wang, and Pao-Lin Kuo. 2017. "SEPT12 Phosphorylation Results in Loss of the Septin Ring/Sperm Annulus, Defective Sperm Motility and Poor Male Fertility." Edited by Pablo E. Visconti. *PLOS Genetics* 13 (3): e1006631. https://doi.org/10.1371/journal.pgen.1006631.

Shi, Lin, Ting Zhou, Qian Huang, Shiyang Zhang, Wei Li, Ling Zhang, Rex A Hess, Gregory J Pazour, and Zhibing Zhang. 2019. "Intraflagellar Transport Protein 74 Is Essential for Spermatogenesis and Male Fertility in Mice†." *Biology of Reproduction* 101 (1): 188–99. https://doi.org/10.1093/biolre/ioz071.

Shin, Byungho, Myung Se Kim, Yejoo Lee, Gee In Jung, and Kunsoo Rhee. 2021. "Generation and Fates of Supernumerary Centrioles in Dividing Cells." *Molecules and Cells* 44 (10): 699–705. https://doi.org/10.14348/molcells.2021.0220.

Sir, Joo-Hee, Monika Pütz, Owen Daly, Ciaran G. Morrison, Mark Dunning, John V. Kilmartin, and Fanni Gergely. 2013. "Loss of Centrioles Causes Chromosomal Instability in Vertebrate Somatic Cells." *Journal of Cell Biology* 203 (5): 747–56. https://doi.org/10.1083/jcb.201309038.

Sironen, Anu, Noora Kotaja, Howard Mulhern, Todd A. Wyatt, Joseph H. Sisson, Jacqueline A. Pavlik, Mari Miiluniemi, Mark D. Fleming, and Lance Lee. 2011. "Loss of SPEF2 Function in Mice Results in Spermatogenesis Defects and Primary Ciliary Dyskinesia1." *Biology of Reproduction* 85 (4): 690–701. https://doi.org/10.1095/biolreprod.111.091132.

Sironen, Anu, Amelia Shoemark, Mitali Patel, Michael R. Loebinger, and Hannah M. Mitchison. 2020. "Sperm Defects in Primary Ciliary Dyskinesia and Related Causes of Male Infertility." *Cellular and Molecular Life Sciences* 77 (11): 2029–48. https://doi.org/10.1007/s00018-019-03389-7.

Smirnov, Vasily, Olivier Grunewald, Jean Muller, Christina Zeitz, Carolin D. Obermaier, Aurore Devos, Valérie Pelletier, et al. 2021. "Novel TTLL5 Variants Associated with Cone-Rod Dystrophy and Early-Onset Severe Retinal Dystrophy." *International Journal of Molecular Sciences* 22 (12): 6410. https://doi.org/10.3390/ijms22126410.

Smith, Elizabeth F., and Paul A. Lefebvre. 1997. "The Role of Central Apparatus Components in Flagellar Motility and Microtubule Assembly." *Cell Motility and the Cytoskeleton* 38 (1): 1–8. https://doi.org/10.1002/(SICI)1097-0169(1997)38:1<1::AID-CM1>3.0.CO;2-C.

Smrzka, Oskar W., Nathalie Delgehyr, and Michel Bornens. 2000. "Tissue-Specific Expression and Subcellular Localisation of Mammalian δ-Tubulin." *Current Biology* 10 (7): 413–16. https://doi.org/10.1016/S0960-9822(00)00418-8.

Song, Rui, Grant W. Hennig, Qiuxia Wu, Charlie Jose, Huili Zheng, and Wei Yan. 2011. "Male Germ Cells Express Abundant Endogenous SiRNAs." *Proceedings of the National Academy of Sciences* 108 (32): 13159–64. https://doi.org/10.1073/pnas.1108567108.

Sorokin, Sergei. 1962. "CENTRIOLES AND THE FORMATION OF RUDIMENTARY CILIA BY FIBROBLASTS AND SMOOTH MUSCLE CELLS." *Journal of Cell Biology* 15 (2): 363–77. https://doi.org/10.1083/jcb.15.2.363.

Stathatos, G. Gemma, Jessica E.M. Dunleavy, Jennifer Zenker, and Moira K. O'Bryan. 2021. "Delta and Epsilon Tubulin in Mammalian Development." *Trends in Cell Biology* 31 (9): 774–87. https://doi.org/10.1016/j.tcb.2021.03.010.

Steger, Klaus. 1999. "Transcriptional and Translational Regulation of Gene Expression in Haploid Spermatids." *Anatomy and Embryology* 199 (6): 471–87. https://doi.org/10.1007/s004290050245.

"STRING: Functional Protein Association Networks." n.d. Accessed February 21, 2023. https://string-db.org/.

Suarez, S. S. 2008. "Control of Hyperactivation in Sperm." *Human Reproduction Update* 14 (6): 647–57. https://doi.org/10.1093/humupd/dmn029.

Sugimoto, Ryo, Yo-ichi Nabeshima, and Shosei Yoshida. 2012. "Retinoic Acid Metabolism Links the Periodical Differentiation of Germ Cells with the Cycle of Sertoli Cells in Mouse Seminiferous Epithelium." *Mechanisms of Development* 128 (11–12): 610–24. https://doi.org/10.1016/j.mod.2011.12.003.

Suryavanshi, Swati, Bernard Eddé, Laura A. Fox, Stella Guerrero, Robert Hard, Todd Hennessey, Amrita Kabi, et al. 2010. "Tubulin Glutamylation Regulates Ciliary Motility by Altering Inner Dynein Arm Activity." *Current Biology* 20 (5): 435–40. https://doi.org/10.1016/j.cub.2009.12.062.

Svingen, Terje, Mathias François, Dagmar Wilhelm, and Peter Koopman. 2012. "Three-Dimensional Imaging of Prox1-EGFP Transgenic Mouse Gonads Reveals Divergent Modes of Lymphangiogenesis in the Testis and Ovary." Edited by Moises Mallo. *PLoS ONE* 7 (12): e52620. https://doi.org/10.1371/journal.pone.0052620.

Svitkina, Tatyana M. 2020. "Actin Cell Cortex: Structure and Molecular Organization." *Trends in Cell Biology* 30 (7): 556–65. https://doi.org/10.1016/j.tcb.2020.03.005.

Szklarczyk, Damian, Annika L Gable, Katerina C Nastou, David Lyon, Rebecca Kirsch, Sampo Pyysalo, Nadezhda T Doncheva, et al. 2021. "The STRING Database in 2021:

Customizable Protein–Protein Networks, and Functional Characterization of User-Uploaded Gene/Measurement Sets." *Nucleic Acids Research* 49 (D1): D605–12. https://doi.org/10.1093/nar/gkaa1074.

Tagelenbosch, Ruud A.J., and Dirk G. de Rooij. 1993. "A Quantitative Study of Spermatogonial Multiplication and Stem Cell Renewal in the C3H/101 F1 Hybrid Mouse." *Mutation Research/Fundamental and Molecular Mechanisms of Mutagenesis* 290 (2): 193–200. https://doi.org/10.1016/0027-5107(93)90159-D.

Takao, Daisuke, Liang Wang, Allison Boss, and Kristen J. Verhey. 2017. "Protein Interaction Analysis Provides a Map of the Spatial and Temporal Organization of the Ciliary Gating Zone." *Current Biology* 27 (15): 2296-2306.e3. https://doi.org/10.1016/j.cub.2017.06.044.

Tam, Lai-Wa, and Paul A. Lefebvre. 2002. "The ChlamydomonasMBO2 Locus Encodes a Conserved Coiled-Coil Protein Important for Flagellar Waveform Conversion." *Cell Motility and the Cytoskeleton* 51 (4): 197–212. https://doi.org/10.1002/cm.10023.

Tanaka, Hiromitsu, Naoko Iguchi, Yoshiro Toyama, Kouichi Kitamura, Tohru Takahashi, Kazuhiro Kaseda, Mamiko Maekawa, and Yoshitake Nishimune. 2004. "Mice Deficient in the Axonemal Protein Tektin-t Exhibit Male Infertility and Immotile-Cilium Syndrome Due to Impaired Inner Arm Dynein Function." *Molecular and Cellular Biology* 24 (18): 7958–64. https://doi.org/10.1128/MCB.24.18.7958-7964.2004.

Tang, Elizabeth I., Will M. Lee, and C. Yan Cheng. 2016. "Coordination of Actin- and Microtubule-Based Cytoskeletons Supports Transport of Spermatids and Residual Bodies/Phagosomes During Spermatogenesis in the Rat Testis." *Endocrinology* 2016 (1): 47–62. https://doi.org/10.1210/en.2015-1962.

Tang, Elizabeth I., Ka-Wai Mok, Will M. Lee, and C. Yan Cheng. 2015. "EB1 Regulates Tubulin and Actin Cytoskeletal Networks at the Sertoli Cell Blood-Testis Barrier in Male Rats: An In Vitro Study." *Endocrinology* 156 (2): 680–93. https://doi.org/10.1210/en.2014-1720.

Tanos, Barbara E., Hui-Ju Yang, Rajesh Soni, Won-Jing Wang, Frank P. Macaluso, John M. Asara, and Meng-Fu Bryan Tsou. 2013. "Centriole Distal Appendages Promote Membrane Docking, Leading to Cilia Initiation." *Genes & Development* 27 (2): 163–68. https://doi.org/10.1101/gad.207043.112.

Tapia Contreras, Constanza, and Sigrid Hoyer-Fender. 2019. "CCDC42 Localizes to Manchette, HTCA and Tail and Interacts With ODF1 and ODF2 in the Formation of the Male Germ Cell Cytoskeleton." *Frontiers in Cell and Developmental Biology* 7 (August): 151. https://doi.org/10.3389/fcell.2019.00151.

———. 2021. "The Transformation of the Centrosome into the Basal Body: Similarities and Dissimilarities between Somatic and Male Germ Cells and Their Relevance for Male Fertility." *Cells* 10 (9): 2266. https://doi.org/10.3390/cells10092266.

Tateishi, Kazuhiro, Yuji Yamazaki, Tomoki Nishida, Shin Watanabe, Koshi Kunimoto, Hiroaki Ishikawa, and Sachiko Tsukita. 2013. "Two Appendages Homologous between Basal Bodies and Centrioles Are Formed Using Distinct Odf2 Domains." *Journal of Cell Biology* 203 (3): 417–25. https://doi.org/10.1083/jcb.201303071.

Thawani, Akanksha, and Sabine Petry. 2021. "Molecular Insight into How γ-TuRC Makes Microtubules." *Journal of Cell Science* 134 (14): jcs245464. https://doi.org/10.1242/jcs.245464.

Thé, Guy de-. 1964. "CYTOPLASMIC MICROTUBULES IN DIFFERENT ANIMAL CELLS." *Journal of Cell Biology* 23 (2): 265–75. https://doi.org/10.1083/jcb.23.2.265.

The UniProt Consortium, Alex Bateman, Maria-Jesus Martin, Sandra Orchard, Michele Magrane, Rahat Agivetova, Shadab Ahmad, et al. 2021. "UniProt: The Universal Protein Knowledgebase in 2021." *Nucleic Acids Research* 49 (D1): D480–89. https://doi.org/10.1093/nar/gkaa1100.

Tian, Shixiong, Chaofeng Tu, Xiaojin He, Lanlan Meng, Jiaxiong Wang, Shuyan Tang, Yang Gao, et al. 2023. "Biallelic Mutations in *CFAP54* Cause Male Infertility with Severe MMAF and NOA." *Journal of Medical Genetics*, January, jmg-2022-108887. https://doi.org/10.1136/jmg-2022-108887.

Tokuhiro, Keizo, Ayako Isotani, Sadaki Yokota, Yoshihisa Yano, Shigeru Oshio, Mika Hirose, Morimasa Wada, et al. 2009. "OAZ-t/OAZ3 Is Essential for Rigid Connection of Sperm Tails to Heads in Mouse." Edited by Gregory P. Copenhaver. *PLoS Genetics* 5 (11): e1000712. https://doi.org/10.1371/journal.pgen.1000712.

Torisawa, Takayuki, and Akatsuki Kimura. 2020. "The Generation of Dynein Networks by Multi-Layered Regulation and Their Implication in Cell Division." *Frontiers in Cell and Developmental Biology* 8 (January): 22. https://doi.org/10.3389/fcell.2020.00022.

Touré, Aminata, Guillaume Martinez, Zine-Eddine Kherraf, Caroline Cazin, Julie Beurois, Christophe Arnoult, Pierre F. Ray, and Charles Coutton. 2021. "The Genetic Architecture of Morphological Abnormalities of the Sperm Tail." *Human Genetics* 140 (1): 21–42. https://doi.org/10.1007/s00439-020-02113-x.

Tournaye, Herman, Csilla Krausz, and Robert D Oates. 2017. "Novel Concepts in the Aetiology of Male Reproductive Impairment." *The Lancet Diabetes & Endocrinology* 5 (7): 544–53. https://doi.org/10.1016/S2213-8587(16)30040-7.

Tovey, Corinne A., and Paul T. Conduit. 2018. "Microtubule Nucleation by γ-Tubulin Complexes and Beyond." Edited by James G. Wakefield and Carolyn A. Moores. *Essays in Biochemistry* 62 (6): 765–80. https://doi.org/10.1042/EBC20180028.

Truebestein, Linda, and Thomas A. Leonard. 2016. "Coiled-coils: The Long and Short of It." *BioEssays* 38 (9): 903–16. https://doi.org/10.1002/bies.201600062.

Tu, Chaofeng, Jiangshan Cong, Qianjun Zhang, Xiaojin He, Rui Zheng, Xiaoxuan Yang, Yang Gao, et al. 2021. "Bi-Allelic Mutations of DNAH10 Cause Primary Male Infertility with Asthenoteratozoospermia in Humans and Mice." *The American Journal of Human Genetics* 108 (8): 1466–77. https://doi.org/10.1016/j.ajhg.2021.06.010.

Tüttelmann, Frank, Manuela Simoni, Sabine Kliesch, Susanne Ledig, Bernd Dworniczak, Peter Wieacker, and Albrecht Röpke. 2011. "Copy Number Variants in Patients with Severe Oligozoospermia and Sertoli-Cell-Only Syndrome." Edited by Laszlo Orban. *PLoS ONE* 6 (4): e19426. https://doi.org/10.1371/journal.pone.0019426.

Uehara, Ryota, and Gohta Goshima. 2010. "Functional Central Spindle Assembly Requires de Novo Microtubule Generation in the Interchromosomal Region during Anaphase." *Journal of Cell Biology* 191 (2): 259–67. https://doi.org/10.1083/jcb.201004150.

Uhlén, Mathias, Linn Fagerberg, Björn M. Hallström, Cecilia Lindskog, Per Oksvold, Adil Mardinoglu, Åsa Sivertsson, et al. 2015. "Tissue-Based Map of the Human Proteome." *Science* 347 (6220): 1260419. https://doi.org/10.1126/science.1260419.

Uhlen, Mathias, Per Oksvold, Linn Fagerberg, Emma Lundberg, Kalle Jonasson, Mattias Forsberg, Martin Zwahlen, et al. 2010. "Towards a Knowledge-Based Human Protein Atlas." *Nature Biotechnology* 28 (12): 1248–50. https://doi.org/10.1038/nbt1210-1248.

Ustinova, Monta, Raitis Peculis, Raimonds Rescenko, Vita Rovite, Linda Zaharenko, Ilze Elbere, Laila Silamikele, et al. 2021. "Novel Susceptibility Loci Identified in a Genome-Wide

Association Study of Type 2 Diabetes Complications in Population of Latvia." *BMC Medical Genomics* 14 (1): 18. https://doi.org/10.1186/s12920-020-00860-4.

Uzbekov, Rustem, and Irina Alieva. 2018. "Who Are You, Subdistal Appendages of Centriole?" *Open Biology* 8 (7): 180062. https://doi.org/10.1098/rsob.180062.

Van De Weghe, Julie Craft, J. Aaron Harris, Tomohiro Kubo, George B. Witman, and Karl F. Lechtreck. 2020. "Diffusion Rather than IFT Likely Provides Most of the Tubulin Required for Axonemal Assembly." *Journal of Cell Science*, January, jcs.249805. https://doi.org/10.1242/jcs.249805.

Varadi, Mihaly, Stephen Anyango, Mandar Deshpande, Sreenath Nair, Cindy Natassia, Galabina Yordanova, David Yuan, et al. 2022. "AlphaFold Protein Structure Database: Massively Expanding the Structural Coverage of Protein-Sequence Space with High-Accuracy Models." *Nucleic Acids Research* 50 (D1): D439–44. https://doi.org/10.1093/nar/gkab1061.

Varuzhanyan, Grigor, and David C. Chan. 2020. "Mitochondrial Dynamics during Spermatogenesis." *Journal of Cell Science* 133 (14): jcs235937. https://doi.org/10.1242/jcs.235937.

Vasquez-Limeta, Alejandra, and Jadranka Loncarek. 2021. "Human Centrosome Organization and Function in Interphase and Mitosis." *Seminars in Cell & Developmental Biology* 117 (September): 30–41. https://doi.org/10.1016/j.semcdb.2021.03.020.

Verhey, Kristen J., and Jacek Gaertig. 2007. "The Tubulin Code." *Cell Cycle* 6 (17): 2152–60. https://doi.org/10.4161/cc.6.17.4633.

Vincent, Marie-Claire, Myriam Daudin, Philippe De Mas, Gerard Massat, Roger Mieusset, Francis Pontonnier, Patrick Calvas, Louis Bujan, and Georges Bourrouillou. 2002. "Cytogenetic Investigations of Infertile Men With Low Sperm Counts: A 25-Year Experience." *Journal of Andrology* 23 (1): 18–22. https://doi.org/10.1002/j.1939-4640.2002.tb02597.x.

Vogel, P., G. Hansen, G. Fontenot, and R. Read. 2010. "Tubulin Tyrosine Ligase–Like 1 Deficiency Results in Chronic Rhinosinusitis and Abnormal Development of Spermatid Flagella in Mice." *Veterinary Pathology* 47 (4): 703–12. https://doi.org/10.1177/0300985810363485.

Vogl, A. W., M. Weis, and D. C. Pfeiffer. 1995. "The Perinuclear Centriole-Containing Centrosome Is Not the Major Microtubule Organizing Center in Sertoli Cells." *European Journal of Cell Biology* 66 (2): 165–79.

Volta, Francesco, and Jantje M. Gerdes. 2017. "The Role of Primary Cilia in Obesity and Diabetes: Primary Cilia in Obesity and Diabetes." *Annals of the New York Academy of Sciences* 1391 (1): 71–84. https://doi.org/10.1111/nyas.13216.

Wadsworth, Patricia. 2021. "The Multifunctional Spindle Midzone in Vertebrate Cells at a Glance." *Journal of Cell Science* 134 (10): jcs250001. https://doi.org/10.1242/jcs.250001.

Walton, Travis, Hao Wu, and Alan Brown. 2021. "Structure of a Microtubule-Bound Axonemal Dynein." *Nature Communications* 12 (1): 477. https://doi.org/10.1038/s41467-020-20735-7.

Wambergue, Clémentine, Raoudha Zouari, Selima Fourati Ben Mustapha, Guillaume Martinez, Françoise Devillard, Sylviane Hennebicq, Véronique Satre, et al. 2016. "Patients with Multiple Morphological Abnormalities of the Sperm Flagella Due to *DNAH1* Mutations Have a Good Prognosis Following Intracytoplasmic Sperm Injection." *Human Reproduction* 31 (6): 1164–72. https://doi.org/10.1093/humrep/dew083.

Wang, Jiaxiong, Xiaoran Liu, Ce Zhang, Yongle Xu, Weizhuo Wang, Hong Li, Shenmin Yang, and Jing Zhao. 2022. "Patient with Multiple Morphological Abnormalities of Sperm Flagella Caused by a Novel ARMC2 Mutation Has a Favorable Pregnancy Outcome from Intracytoplasmic Sperm Injection." *Journal of Assisted Reproduction and Genetics* 39 (7): 1673–81. https://doi.org/10.1007/s10815-022-02516-x.

Wang, Jiaxiong, Weizhuo Wang, Liyan Shen, Aiyan Zheng, Qingxia Meng, Hong Li, and Shenmin Yang. 2022. "Clinical Detection, Diagnosis and Treatment of Morphological Abnormalities of Sperm Flagella: A Review of Literature." *Frontiers in Genetics* 13 (November): 1034951. https://doi.org/10.3389/fgene.2022.1034951.

Wang, Jiaxiong, Ce Zhang, Hui Tang, Aiyan Zheng, Hong Li, Shenmin Yang, and Jingjing Xiang. 2022. "Successful Results of Intracytoplasmic Sperm Injection of a Chinese Patient With Multiple Morphological Abnormalities of Sperm Flagella Caused by a Novel Splicing Mutation in CFAP251." *Frontiers in Genetics* 12 (January): 783790. https://doi.org/10.3389/fgene.2021.783790.

Wang, Lingling, Ming Yan, Siwen Wu, Baiping Mao, Chris K C Wong, Renshan Ge, Fei Sun, and C Yan Cheng. 2020. "Microtubule Cytoskeleton and Spermatogenesis—Lesson From Studies of Toxicant Models." *Toxicological Sciences* 177 (2): 305–15. https://doi.org/10.1093/toxsci/kfaa109.

Wang, Liying, Ruidan Zhang, Bingbing Wu, Yang Yu, Wei Li, Shiguo Li, and Chao Liu. 2022. "Autophagy Mediated Tubulobulbar Complex Components Degradation Is Required for Spermiation." *Fundamental Research*, October, S2667325822004186. https://doi.org/10.1016/j.fmre.2022.10.006.

Wang, Mei, Xixi Liu, Gang Chang, Yidong Chen, Geng An, Liying Yan, Shuai Gao, et al. 2018. "Single-Cell RNA Sequencing Analysis Reveals Sequential Cell Fate Transition during Human Spermatogenesis." *Cell Stem Cell* 23 (4): 599-614.e4. https://doi.org/10.1016/j.stem.2018.08.007.

Wang, Tong, Hui Gao, Wei Li, and Chao Liu. 2019. "Essential Role of Histone Replacement and Modifications in Male Fertility." *Frontiers in Genetics* 10 (October): 962. https://doi.org/10.3389/fgene.2019.00962.

Wang, Wei-Li, Chao-Feng Tu, and Yue-Qiu Tan. 2020. "Insight on Multiple Morphological Abnormalities of Sperm Flagella in Male Infertility: What Is New?" *Asian Journal of Andrology* 22 (3): 236. https://doi.org/10.4103/aja.aja_53_19.

Wang, Xiong, Yan-wei Sha, Wen-ting Wang, Yuan-qing Cui, Jie Chen, Wei Yan, Xiao-tao Hou, Li-bin Mei, Cui-cui Yu, and Jiahui Wang. 2019. "Novel *IFT140* Variants Cause Spermatogenic Dysfunction in Humans." *Molecular Genetics & Genomic Medicine* 7 (9). https://doi.org/10.1002/mgg3.920.

Wang, Yipeng, and Eckhard Mandelkow. 2016. "Tau in Physiology and Pathology." *Nature Reviews Neuroscience* 17 (1): 22–35. https://doi.org/10.1038/nrn.2015.1.

Wang, Yu, Ming-Fei Xiang, Na Zheng, Yun-Xia Cao, and Fu-Xi Zhu. 2022. "Genetic Pathogenesis of Acephalic Spermatozoa Syndrome: Past, Present, and Future." *Asian Journal of Andrology* 24 (3): 231. https://doi.org/10.4103/aja202198.

Wang, Zhigang, Wei Liu, Chong Chen, Xiaolin Yang, Yunping Luo, and Bailin Zhang. 2019. "Low Mutation and Neoantigen Burden and Fewer Effector Tumor Infiltrating Lymphocytes Correlate with Breast Cancer Metastasization to Lymph Nodes." *Scientific Reports* 9 (1): 253. https://doi.org/10.1038/s41598-018-36319-x.

Wattanathamsan, Onsurang, and Varisa Pongrakhananon. 2022. "Emerging Role of Microtubule-Associated Proteins on Cancer Metastasis." *Frontiers in Pharmacology* 13 (September): 935493. https://doi.org/10.3389/fphar.2022.935493.

Wen, Qing, Elizabeth I. Tang, Wing-yee Lui, Will M. Lee, Chris K. C. Wong, Bruno Silvestrini, and C. Yan Cheng. 2018. "Dynein 1 Supports Spermatid Transport and Spermiation during Spermatogenesis in the Rat Testis." *American Journal of Physiology-Endocrinology and Metabolism* 315 (5): E924–48. https://doi.org/10.1152/ajpendo.00114.2018.

Wen, Qing, Elizabeth I. Tang, Xiang Xiao, Ying Gao, Darren S. Chu, Dolores D. Mruk, Bruno Silvestrini, and C. Yan Cheng. 2016. "Transport of Germ Cells across the Seminiferous Epithelium during Spermatogenesis—the Involvement of Both Actin- and Microtubule-Based Cytoskeletons." *Tissue Barriers* 4 (4): e1265042. https://doi.org/10.1080/21688370.2016.1265042.

Wen, Qing, Siwen Wu, Will M Lee, Chris K C Wong, Wing-yee Lui, Bruno Silvestrini, and C Yan Cheng. 2019. "Myosin VIIa Supports Spermatid/Organelle Transport and Cell Adhesion During Spermatogenesis in the Rat Testis." *Endocrinology* 160 (3): 484–503. https://doi.org/10.1210/en.2018-00855.

Westlake, Christopher J., Lisa M. Baye, Maxence V. Nachury, Kevin J. Wright, Karen E. Ervin, Lilian Phu, Cecile Chalouni, et al. 2011. "Primary Cilia Membrane Assembly Is Initiated by Rab11 and Transport Protein Particle II (TRAPPII) Complex-Dependent Trafficking of Rabin8 to the Centrosome." *Proceedings of the National Academy of Sciences* 108 (7): 2759–64. https://doi.org/10.1073/pnas.1018823108.

Wheway, Gabrielle, David A Parry, and Colin A Johnson. 2014. "The Role of Primary Cilia in the Development and Disease of the Retina." *Organogenesis* 10 (1): 69–85. https://doi.org/10.4161/org.26710.

Whitfield, Marjorie, Lucie Thomas, Emilie Bequignon, Alain Schmitt, Laurence Stouvenel, Guy Montantin, Sylvie Tissier, et al. 2019. "Mutations in DNAH17, Encoding a Sperm-Specific Axonemal Outer Dynein Arm Heavy Chain, Cause Isolated Male Infertility Due to Asthenozoospermia." *The American Journal of Human Genetics* 105 (1): 198–212. https://doi.org/10.1016/j.ajhg.2019.04.015.

Wieczorek, Michal, Linas Urnavicius, Shih-Chieh Ti, Kelly R. Molloy, Brian T. Chait, and Tarun M. Kapoor. 2020. "Asymmetric Molecular Architecture of the Human γ-Tubulin Ring Complex." *Cell* 180 (1): 165-175.e16. https://doi.org/10.1016/j.cell.2019.12.007.

Wilhelmsen, Kevin, Sandy H.M. Litjens, Ingrid Kuikman, Ntambua Tshimbalanga, Hans Janssen, Iman van den Bout, Karine Raymond, and Arnoud Sonnenberg. 2005. "Nesprin-3, a Novel Outer Nuclear Membrane Protein, Associates with the Cytoskeletal Linker Protein Plectin." *Journal of Cell Biology* 171 (5): 799–810. https://doi.org/10.1083/jcb.200506083.

Woehlke, Günther, and Manfred Schliwa. 2000. "Walking on Two Heads: The Many Talents of Kinesin." *Nature Reviews Molecular Cell Biology* 1 (1): 50–58. https://doi.org/10.1038/35036069.

Wolkowicz, M. J., L. Digilio, K. Klotz, J. Shetty, C. J. Flickinger, and J. C. Herr. 2008. "Equatorial Segment Protein (ESP) Is a Human Alloantigen Involved in Sperm-Egg Binding and Fusion." *Journal of Andrology* 29 (3): 272–82. https://doi.org/10.2164/jandrol.106.000604.

Wong, Vivien, and Lonnie D. Russell. 1983. "Three-Dimensional Reconstruction of a Rat Stage V Sertoli Cell: I. Methods, Basic Configuration, and Dimensions." *American Journal of Anatomy* 167 (2): 143–61. https://doi.org/10.1002/aja.1001670202.

Woodruff, Jeffrey B., Oliver Wueseke, and Anthony A. Hyman. 2014. "Pericentriolar Material Structure and Dynamics." *Philosophical Transactions of the Royal Society B: Biological Sciences* 369 (1650): 20130459. https://doi.org/10.1098/rstb.2013.0459.

Woolley, David M., and Don W. Fawcett. 1973. "The Degeneration and Disappearance of the Centrioles during the Development of the Rat Spermatozoon." *The Anatomical Record* 177 (2): 289–301. https://doi.org/10.1002/ar.1091770209.

World Health Organization. 2010. "WHO laboratory manual for the examination and processing of human semen," 271.

———. 2021. *WHO Laboratory Manual for the Examination and Processing of Human Semen*. 6th ed. Geneva: World Health Organization. https://apps.who.int/iris/handle/10665/343208.

Wu, Bingbing, Hui Gao, Chao Liu, and Wei Li. 2020. "The Coupling Apparatus of the Sperm Head and Tail†." *Biology of Reproduction* 102 (5): 988–98. https://doi.org/10.1093/biolre/ioaa016.

Wu, Chien-Ting, Hsin-Yi Chen, and Tang K. Tang. 2018. "Myosin-Va Is Required for Preciliary Vesicle Transportation to the Mother Centriole during Ciliogenesis." *Nature Cell Biology* 20 (2): 175–85. https://doi.org/10.1038/s41556-017-0018-7.

Wu, Hui-Yuan, Peng Wei, and James I. Morgan. 2017. "Role of Cytosolic Carboxypeptidase 5 in Neuronal Survival and Spermatogenesis." *Scientific Reports* 7 (1): 41428. https://doi.org/10.1038/srep41428.

Wu, Jingchao, and Anna Akhmanova. 2017. "Microtubule-Organizing Centers." *Annual Review of Cell and Developmental Biology* 33 (1): 51–75. https://doi.org/10.1146/annurev-cellbio-100616-060615.

Xavier, M. J., A. Salas-Huetos, M. S. Oud, K. I. Aston, and J. A. Veltman. 2021. "Disease Gene Discovery in Male Infertility: Past, Present and Future." *Human Genetics* 140 (1): 7–19. https://doi.org/10.1007/s00439-020-02202-x.

Xiang, Mingfei, Yu Wang, Weilong Xu, Na Zheng, Hongshi Deng, Jingjing Zhang, Zongliu Duan, et al. 2022. "A Novel Homozygous Missense Mutation in AK7 Causes Multiple Morphological Anomalies of the Flagella and Oligoasthenoteratozoospermia." *Journal of Assisted Reproduction and Genetics* 39 (1): 261–66. https://doi.org/10.1007/s10815-021-02363-2.

Xu, Chuan, Dongdong Tang, Zhongmei Shao, Hao Geng, Yang Gao, Kuokuo Li, Qing Tan, et al. 2022. "Homozygous SPAG6 Variants Can Induce Nonsyndromic Asthenoteratozoospermia with Severe MMAF." *Reproductive Biology and Endocrinology* 20 (1): 41. https://doi.org/10.1186/s12958-022-00916-3.

Yang, Kefei, Andreas Meinhardt, Bing Zhang, Pawel Grzmil, Ibrahim M. Adham, and Sigrid Hoyer-Fender. 2012. "The Small Heat Shock Protein ODF1/HSPB10 Is Essential for Tight Linkage of Sperm Head to Tail and Male Fertility in Mice." *Molecular and Cellular Biology* 32 (1): 216–25. https://doi.org/10.1128/MCB.06158-11.

Yang, Pinfen, Dennis R. Diener, Joel L. Rosenbaum, and Winfield S. Sale. 2001. "Localization of Calmodulin and Dynein Light Chain Lc8 in Flagellar Radial Spokes." *Journal of Cell Biology* 153 (6): 1315–26. https://doi.org/10.1083/jcb.153.6.1315.

Yang, T. Tony, Weng Man Chong, Won-Jing Wang, Gregory Mazo, Barbara Tanos, Zhengmin Chen, Thi Minh Nguyet Tran, et al. 2018. "Super-Resolution Architecture of Mammalian Centriole Distal Appendages Reveals Distinct Blade and Matrix Functional Components." *Nature Communications* 9 (1): 2023. https://doi.org/10.1038/s41467-018-04469-1.

Yassine, Sandra, Jessica Escoffier, Guillaume Martinez, Charles Coutton, Thomas Karaouzène, Raoudha Zouari, Jean-Luc Ravanat, et al. 2015. "Dpy19l2-Deficient Globozoospermic Sperm Display Altered Genome Packaging and DNA Damage That Compromises the Initiation of Embryo Development." *MHR: Basic Science of Reproductive Medicine* 21 (2): 169–85. https://doi.org/10.1093/molehr/gau099.

Yassine, Sandra, Jessica Escoffier, Roland Abi Nahed, Virginie Pierre, Thomas Karaouzene, Pierre F. Ray, and Christophe Arnoult. 2015. "Dynamics of Sun5 Localization during Spermatogenesis in Wild Type and Dpy19l2 Knock-Out Mice Indicates That Sun5 Is Not Involved in Acrosome Attachment to the Nuclear Envelope." Edited by Xuejiang Guo. *PLOS ONE* 10 (3): e0118698. https://doi.org/10.1371/journal.pone.0118698.

Yogo, Keiichiro. 2022. "Molecular Basis of the Morphogenesis of Sperm Head and Tail in Mice." *Reproductive Medicine and Biology* 21 (1). https://doi.org/10.1002/rmb2.12466.

Yoshinaga, Kazuya, and Kiyotaka Toshimori. 2003. "Organization and Modifications of Sperm Acrosomal Molecules during Spermatogenesis and Epididymal Maturation." *Microscopy Research and Technique* 61 (1): 39–45. https://doi.org/10.1002/jemt.10315.

Yu, Che-Hang, Stefanie Redemann, Hai-Yin Wu, Robert Kiewisz, Tae Yeon Yoo, William Conway, Reza Farhadifar, Thomas Müller-Reichert, and Daniel Needleman. 2019. "Central-Spindle Microtubules Are Strongly Coupled to Chromosomes during Both Anaphase A and Anaphase B." Edited by Yixian Zheng. *Molecular Biology of the Cell* 30 (19): 2503–14. https://doi.org/10.1091/mbc.E19-01-0074.

Yu, Yi, Jiaxiong Wang, Liming Zhou, Haibo Li, Bo Zheng, and Shenmin Yang. 2021. "CFAP43-Mediated Intra-Manchette Transport Is Required for Sperm Head Shaping and Flagella Formation." *Zygote* 29 (1): 75–81. https://doi.org/10.1017/S0967199420000556.

Yuan, Shuiqiao, Clifford J. Stratton, Jianqiang Bao, Huili Zheng, Bhupal P. Bhetwal, Ryuzo Yanagimachi, and Wei Yan. 2015. "*Spata6* Is Required for Normal Assembly of the Sperm Connecting Piece and Tight Head–Tail Conjunction." *Proceedings of the National Academy of Sciences* 112 (5). https://doi.org/10.1073/pnas.1424648112.

Yuan, Yuan, Wen-qing Xu, Zi-yi Chen, Ying Chen, Li Zhang, Liping Zheng, Tao Luo, and Hou-yang Chen. 2022. "Successful Outcomes of Intracytoplasmic Sperm Injection–Embryo Transfer Using Ejaculated Spermatozoa from Two Chinese Asthenoteratozoospermic Brothers with a Compound Heterozygous *FSIP2* Mutation." *Andrologia* 54 (3). https://doi.org/10.1111/and.14351.

Yuan, Yue, Xue-Shan Ma, Qiu-Xia Liang, Zhao-Yang Xu, Lin Huang, Tie-Gang Meng, Fei Lin, Heide Schatten, Zhen-Bo Wang, and Qing-Yuan Sun. 2017. "Geminin Deletion in Pre-Meiotic DNA Replication Stage Causes Spermatogenesis Defect and Infertility." *Journal of Reproduction and Development* 63 (5): 481–88. https://doi.org/10.1262/jrd.2017-036.

Zabeo, Davide, Jacob T. Croft, and Johanna L. Höög. 2019. "Axonemal Doublet Microtubules Can Split into Two Complete Singlets in Human Sperm Flagellum Tips." *FEBS Letters* 593 (9): 892–902. https://doi.org/10.1002/1873-3468.13379.

Zakrzewski, Przemysław, Robert Lenartowski, Maria Jolanta Rędowicz, Kathryn G. Miller, and Marta Lenartowska. 2017. "Expression and Localization of Myosin VI in Developing Mouse Spermatids." *Histochemistry and Cell Biology* 148 (4): 445–62. https://doi.org/10.1007/s00418-017-1579-z.

Zakrzewski, Przemysław, Maria Jolanta Rędowicz, Folma Buss, and Marta Lenartowska. 2020. "Loss of Myosin VI Expression Affects Acrosome/Acroplaxome Complex Morphology

during Mouse Spermiogenesis†." *Biology of Reproduction* 103 (3): 521–33. https://doi.org/10.1093/biolre/ioaa071.

Zanetti, Natalia, and Luis S. Mayorga. 2009. "Acrosomal Swelling and Membrane Docking Are Required for Hybrid Vesicle Formation During the Human Sperm Acrosome Reaction1." *Biology of Reproduction* 81 (2): 396–405. https://doi.org/10.1095/biolreprod.109.076166.

Zenker, J., M. D. White, R. M. Templin, R. G. Parton, O. Thorn-Seshold, S. Bissiere, and N. Plachta. 2017. "A Microtubule-Organizing Center Directing Intracellular Transport in the Early Mouse Embryo." *Science* 357 (6354): 925–28. https://doi.org/10.1126/science.aam9335.

Zhang, Guohui, Dongyan Li, Chaofeng Tu, Lanlan Meng, Yueqiu Tan, Zhiliang Ji, Jiao Cheng, et al. 2021. "Loss-of-Function Missense Variant of *AKAP4* Induced Male Infertility through Reduced Interaction with QRICH2 during Sperm Flagella Development." *Human Molecular Genetics* 31 (2): 219–31. https://doi.org/10.1093/hmg/ddab234.

Zhang, Jintao, Xiaojin He, Huan Wu, Xin Zhang, Shenmin Yang, Chunyu Liu, Siyu Liu, et al. 2021. "Loss of DRC1 Function Leads to Multiple Morphological Abnormalities of the Sperm Flagella and Male Infertility in Human and Mouse." *Human Molecular Genetics* 30 (21): 1996–2011. https://doi.org/10.1093/hmg/ddab171.

Zhang, Shiyang, Yunhao Liu, Qian Huang, Shuo Yuan, Hong Liu, Lin Shi, Yi Tian Yap, et al. 2020. "Murine Germ Cell-Specific Disruption of Ift172 Causes Defects in Spermiogenesis and Male Fertility." *Reproduction*, January. https://doi.org/10.1530/REP-17-0789.

Zhang, Teng, Mark W. Murphy, Micah D. Gearhart, Vivian J. Bardwell, and David Zarkower. 2014. "The Mammalian Doublesex Homolog DMRT6 Coordinates the Transition between Mitotic and Meiotic Developmental Programs during Spermatogenesis." *Development* 141 (19): 3662–71. https://doi.org/10.1242/dev.113936.

Zhang, Xiaochang, Kai Lei, Xiaobing Yuan, Xiaohui Wu, Yuan Zhuang, Tian Xu, Rener Xu, and Min Han. 2009. "SUN1/2 and Syne/Nesprin-1/2 Complexes Connect Centrosome to the Nucleus during Neurogenesis and Neuronal Migration in Mice." *Neuron* 64 (2): 173–87. https://doi.org/10.1016/j.neuron.2009.08.018.

Zhang, Xiao-Zhen, Lin-Lin Wei, Hui-Juan Jin, Xiao-Hui Zhang, and Su-Ren Chen. 2022. "The Perinuclear Theca Protein Calicin Helps Shape the Sperm Head and Maintain the Nuclear Structure in Mice." *Cell Reports* 40 (1): 111049. https://doi.org/10.1016/j.celrep.2022.111049.

Zhang, Xin, Jiang Sun, Yonggang Lu, Jintao Zhang, Keisuke Shimada, Taichi Noda, Shuqin Zhao, et al. 2021. "LRRC23 Is a Conserved Component of the Radial Spoke That Is Necessary for Sperm Motility and Male Fertility in Mice." *Journal of Cell Science* 134 (20): jcs259381. https://doi.org/10.1242/jcs.259381.

Zhang, Xueguang, Lingbo Wang, Yongyi Ma, Yan Wang, Hongqian Liu, Mohan Liu, Lang Qin, et al. 2022. "CEP128 Is Involved in Spermatogenesis in Humans and Mice." *Nature Communications* 13 (1): 1395. https://doi.org/10.1038/s41467-022-29109-7.

Zhang, Ying, Chao Liu, Bingbing Wu, Liansheng Li, Wei Li, and Li Yuan. 2021. "The Missing Linker between SUN5 and PMFBP1 in Sperm Head-Tail Coupling Apparatus." *Nature Communications* 12 (1): 4926. https://doi.org/10.1038/s41467-021-25227-w.

Zhang, Ying, Young Ou, Min Cheng, Habib Shojaei Saadi, Jacob C. Thundathil, and Frans A. van der Hoorn. 2012. "KLC3 Is Involved in Sperm Tail Midpiece Formation and Sperm Function." *Developmental Biology* 366 (2): 101–10. https://doi.org/10.1016/j.ydbio.2012.04.026.

Zhang, Yong, Hong Liu, Wei Li, Zhengang Zhang, Shiyang Zhang, Maria E Teves, Courtney Stevens, et al. 2018. "Intraflagellar Transporter Protein 140 (IFT140), a Component of IFT-A Complex, Is Essential for Male Fertility and Spermiogenesis in Mice." *Cytoskeleton* 75 (2): 70–84. https://doi.org/10.1002/cm.21427.

Zhang, Yunfei, Linfei Yang, Lihua Huang, Gang Liu, Xinmin Nie, Xinxing Zhang, and Xiaowei Xing. 2021. "SUN5 Interacting With Nesprin3 Plays an Essential Role in Sperm Head-to-Tail Linkage: Research on Sun5 Gene Knockout Mice." *Frontiers in Cell and Developmental Biology* 9 (June): 684826. https://doi.org/10.3389/fcell.2021.684826.

Zhang, Zhengang, Wei Li, Yong Zhang, Ling Zhang, Maria E. Teves, Hong Liu, Jerome F. Strauss, et al. 2016. "Intraflagellar Transport Protein IFT20 Is Essential for Male Fertility and Spermiogenesis in Mice." Edited by Yukiko Yamashita. *Molecular Biology of the Cell* 27 (23): 3705–16. https://doi.org/10.1091/mbc.e16-05-0318.

Zhang, Zhibing, Igor Kostetskii, Waixing Tang, Lisa Haig-Ladewig, Rossana Sapiro, Zhangyong Wei, Aatish M. Patel, et al. 2006. "Deficiency of SPAG16L Causes Male Infertility Associated with Impaired Sperm Motility1." *Biology of Reproduction* 74 (4): 751–59. https://doi.org/10.1095/biolreprod.105.049254.

Zhao, Ji Zhong, Qin Ye, Lan Wang, and Shao Chin Lee. 2021. "Centrosome Amplification in Cancer and Cancer-Associated Human Diseases." *Biochimica et Biophysica Acta (BBA) - Reviews on Cancer* 1876 (1): 188566. https://doi.org/10.1016/j.bbcan.2021.188566.

Zhao, Lei, Yuqing Hou, Tyler Picariello, Branch Craige, and George B. Witman. 2019. "Proteome of the Central Apparatus of a Ciliary Axoneme." *Journal of Cell Biology* 218 (6): 2051–70. https://doi.org/10.1083/jcb.201902017.

Zheng, Rui, Yongkang Sun, Chuan Jiang, Daijuan Chen, Yihong Yang, and Ying Shen. 2021. "A Novel Mutation in DNAH17 Is Present in a Patient with Multiple Morphological Abnormalities of the Flagella." *Reproductive BioMedicine Online* 43 (3): 532–41. https://doi.org/10.1016/j.rbmo.2021.05.009.

Zhou, Rui, Jingrouzi Wu, Bang Liu, Yiqun Jiang, Wei Chen, Jian Li, Quanyuan He, and Zuping He. 2019. "The Roles and Mechanisms of Leydig Cells and Myoid Cells in Regulating Spermatogenesis." *Cellular and Molecular Life Sciences* 76 (14): 2681–95. https://doi.org/10.1007/s00018-019-03101-9.

Zhu, F., F. Gong, G. Lin, and G. Lu. 2013. "DPY19L2 Gene Mutations Are a Major Cause of Globozoospermia: Identification of Three Novel Point Mutations." *Molecular Human Reproduction* 19 (6): 395–404. https://doi.org/10.1093/molehr/gat018.

Zhu, Fuxi, Chao Liu, Fengsong Wang, Xiaoyu Yang, Jingjing Zhang, Huan Wu, Zhiguo Zhang, et al. 2018. "Mutations in PMFBP1 Cause Acephalic Spermatozoa Syndrome." *The American Journal of Human Genetics* 103 (2): 188–99. https://doi.org/10.1016/j.ajhg.2018.06.010.

Zhu, Fuxi, Fengsong Wang, Xiaoyu Yang, Jingjing Zhang, Huan Wu, Zhou Zhang, Zhiguo Zhang, et al. 2016. "Biallelic SUN5 Mutations Cause Autosomal-Recessive Acephalic Spermatozoa Syndrome." *The American Journal of Human Genetics* 99 (4): 942–49. https://doi.org/10.1016/j.ajhg.2016.08.004.

Zhu, Zi-Jue, Yi-Zhou Wang, Xiao-Bo Wang, Chen-Cheng Yao, Liang-Yu Zhao, Zhen-Bo Zhang, Yu Wu, Wei Chen, and Zheng Li. 2022. "Novel Mutation in ODF2 Causes Multiple Morphological Abnormalities of the Sperm Flagella in an Infertile Male." *Asian Journal of Andrology* 24 (5): 463. https://doi.org/10.4103/aja202183.